UPSCALING OF TWO-PHASE FLOW IN OIL-GAS SYSTEMS

by

Nasir B. Haji Darman

Thesis Submitted for the

Degree of Doctor of Philosophy

Department of Petroleum Engineering

Heriot-Watt University

Edinburgh

April 2000

DECLARATION

I hereby declare that the work presented in this thesis was carried out by myself in the last three years under the direction of Professor Kenneth S. Sorbie and Dr. Gillian E. Pickup at Heriot-Watt University, Edinburgh. It has not been submitted for any other degree.

Nasir B. Haji Darman (Candidate)

Prof. Kenneth S. Sorbie (Supervisor)

Dr. Gillian E. Pickup (Supervisor)

DEDICATION

I dedicated this work to

my wife and children

(Shamsiah Kamaruddin, Nurul Sharina Nasir and Muhammad Nazmi Nasir)

TABLE OF CONTENTS

LIST OF TABLES

LIST OF FIGURES

ACKNOWLEDGEMENTS

Praise be to Allah s.w.t., who blessed me with health and knowledge to carry out this research study.

I would like to take this opportunity to thank my supervisors, Professor Ken Sorbie and Dr. Gillian Pickup, for their excellent encouragement and endless guidance throughout the course of this study. Their enthusiasm towards my work has benefited me immensely in completing this study.

I would also like to thank all the staff and students in this department for their support and help, especially the other members of the Reservoir Heterogeneity Group (HET).

The financial support from Petroliam Nasional Berhad (PETRONAS) is highly appreciated.

Many thanks to the Ex-General Manager of Petronas Research & Scientific Services (PRSS), Dr. Khalid Ngah, and Ex-Senior Manager of Production Research Group (PRSS), Dr. D.M. Anwar Raja, for their moral and administrative support for me to start and complete this study.

Finally, I thank all the members of my family for their encouraging support especially my parents-in-laws, my sisters and my brothers. My sincere thanks to my lovely wife and my wonderful children for their patience and understanding. I love you all!

ABSTRACT

In modern reservoir characterisation, a detailed geological reservoir description may produce a model with millions of grid blocks each with individual geological and petrophysical properties. This high-resolution geological model often exceeds the computational capabilities of currently available fluid flow simulators by a significant margin. The concept of pseudo functions has been developed to upscale this model to a reasonable size while still capturing the effects of small-scale multi-phase fluid mechanics and heterogeneity.

This study explores the idea of using pseudo functions in immiscible two-phase displacement in gas/oil systems. In such cases, the effects of large mobility differences and significant gravitational forces are always encountered. A new pseudo method, known as the Transmissibility Weighted method (TW), has been developed and tested by comparing it with several well-known pseudo generation methods i.e. the Kyte and Berry (1975), the Stone (1991), the Hewett and Archer (1997) and the Vertical Equilibrium (1971) methods. Better performance compared with these well-known pseudo methods was observed especially in the gravity-dominated cases encountered in immiscible gas injection. This is demonstrated using a wide range of test cases in which we investigate the conditions under which this new TW pseudo generation method performs better than existing approaches.

The second part of this thesis centers on the development and validation of a new grid coarsening scheme. This work is motivated by some recent results derived from the averaged saturation equation with gravitational effects included. In addition to the static properties (i.e. porositv permeability etc.) of the fine grid models, this new coarsening technique also takes into account the dynamic properties (i.e. saturation distribution, fluid velocity etc.) of the fluid flow. It is shown that the coarse grid simulation error correlates closely with specific sub-grid quantities involving higher moments of fine grid variables such as the variance of gas saturation (σ^2_S), the velocity-saturation covariance (σ^2_{vS}) and the absolute permeability-saturation covariance (σ^2_{kS}). These sub-grid quantities can also be used in the form of coefficient of variation (the C_v). The specific sub-grid measure that best correlated with the coarse grid error was shown to vary depending on whether rock curves or pseudo functions are used in the coarse grid model. By forming a coarse grid that minimizes the appropriate sub-grid quantity, optimal coarse scale descriptions can be generated. The resulting coarsening scheme might be non-uniform in nature but would fulfill all purposes of using pseudo functions (i.e. to control numerical dispersion, to capture the effect of small-scale heterogeneity etc.) with less error and without any adjustment to the pseudo equations themselves.

The overall coarsening approach is shown to be applicable to coarse scale descriptions using either rock or pseudo relative permeability curves. However, the accuracy of the coarse grid calculations is significantly better when pseudo functions are used. The method can also be applied to determine the optimal number and configuration of

coarse grid layers in more general cases, and it is shown that coarse grid results do not always improve as the number of coarse grid layers is increased. The accuracy of using pseudo functions will also depend on the configuration of the layering scheme adopted for the coarse grid model.

CHAPTER 1

INTRODUCTION

1.1 BACKGROUND

In modern reservoir characterisation, detailed geological reservoir description may produce a model with millions of grid blocks each with individual geological and petrophysical properties. Variability in these properties might occur at many length scales in the reservoir, in some cases down to the smallest scale of lamination (mm). The effects of this small-scale heterogeneity on oil recovery processes has been studied by several authors such as Kortekaas (1985), Corbett *et al.* (1992), Ringrose *et al.* (1993), Huang *et al.* (1995) and Coll *et al.* (1998).

For example, Kortekaas (1985) noted that a considerable amount of movable oil might be left in the high permeability foreset laminae, trapped by the lower permeability bottomsets when he conducted numerical simulation of water-oil displacement perpendicular to the crossbedding. Corbett *et al.* (1992) used a 2D cross-sectional model of the Rannoch formation to show that capillary forces can play an important role, in the presence of small-scale heterogeneity, in the performance of large-scale fluid flow simulation results. Ringrose *et al.* (1993) realised the importance of the interplay between gravitational, viscous and capillary forces with small-scale

heterogeneity in their study using laminated and cross-bedded sandstone models. Furthermore, Huang *et al.* (1995) showed the same results as mentioned above in their laboratory experimental work of water flood behaviour using water-wet laminated rocks. Coll et al. (1998) also examined the effects of small-scale geological structure on upscaled pseudo properties. In general, the findings from these studies suggested that incorporation of this small-scale heterogeneity in fluid flow simulation may be important in certain cases to obtain a reliable simulation prediction.

In contrast to the fine grid geological models that only involve the manipulation of static data, fluid flow simulations for such models at the full-field scale are very costly and often exceed the computational capabilities of currently available computers. These detailed geological models must be upscaled in some way before they can be used practically for fluid flow simulation (Kossack *et al.*, 1990; Lake *et al.*, 1990). Both the concept and practice of using pseudo functions have been developed for this purpose. When successfully applied, pseudo functions will incorporate the interaction between small-scale multi-phase fluid mechanics and heterogeneity, as well as correcting for the numerical dispersion in the coarse grid model.

In general, pseudo functions which are derived from the various upscaling methods can be divided into three broad categories as follows (Figure 1.1):

(i) vertical equilibrium pseudo functions,

(ii) steady-state pseudo functions, and

(iii) dynamic pseudo functions.

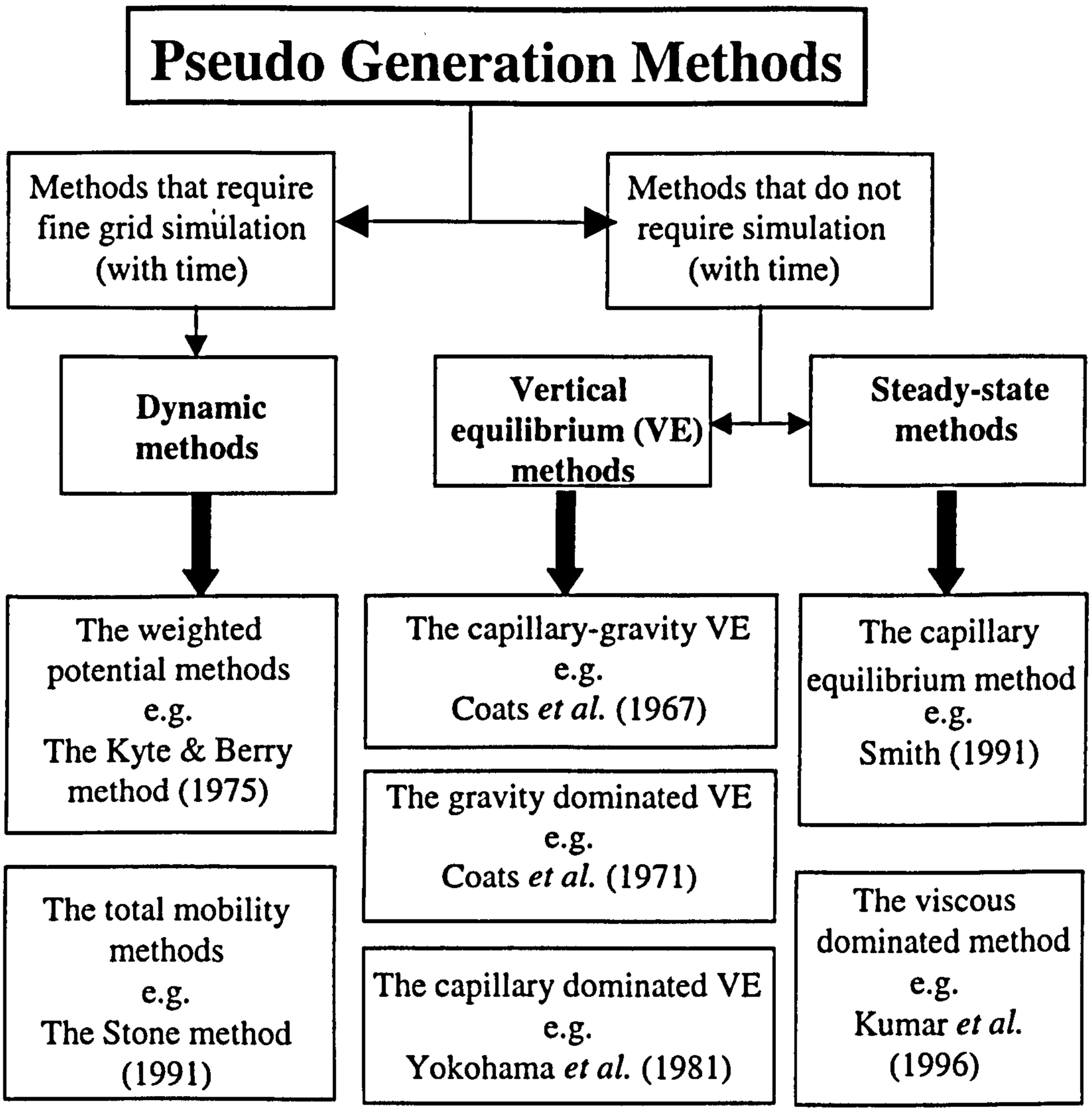

Figure 1.1: Summary of pseudo generation methods showing the three categories of the pseudo functions.

In vertical equilibrium (VE) conditions, the vertical distribution of fluid is purely determined by the balance of forces between gravity and capillary pressure in all the grid blocks and time steps in the simulation model. The viscous force must be negligible in the vertical direction. Under these assumptions, the resulting pseudo functions, will be independent of the initial conditions and production history. These pseudo functions are solely a function of averaged saturation only; or in other words, they are intrinsic properties of the rock-fluid system. Many authors like Coats *et al.*

(1967 and 1971), Spivak (1974) and Lake (1989) have investigated the validity of the assumptions made by the VE method, but none so far is accepted to be universal. One disadvantage of using these VE methods is that they are not applicable for reservoirs that do not reach equilibrium conditions due to poor vertical communication or high lateral velocities.

When a reservoir simulation calculation is in a steady-state condition, steady-state upscaling methods can be used. A steady-state condition is achieved when the saturations in each of the grid blocks are constant with time (or, in practice, are slowly varying with time). In general, there are two types of steady-state pseudo generation methods that depend on the balance of capillary and viscous forces in the model. In a capillary dominated model, it is assumed that the system has come to capillary equilibrium. In this case, in order to calculate the effective phase permeabilities, several steady-state simulations are performed at different capillary pressure levels. Several authors, such as Smith (1991), Pickup and Sorbie (1996) and Lemouzy *et al.* (1993), have described examples of this method.

In viscous dominated floods, it can be assumed that the capillary pressure gradient is negligible compared with the viscous pressure gradient. In addition, it is also assumed that the capillary pressure itself is negligible, so that the pressures in both of the fluid phases are equal. For this case, at steady-state conditions the fractional flow of fluid is constant throughout the system, which may be compared with the capillary equilibrium steady-state method where capillary pressure is constant in the system. In order to calculate the effective phase permeabilities in viscous steady-state conditions, steady-

state simulations are performed at different fractional flow levels. A more detailed discussion of these two steady-state methods will be given in Chapter 2.

All dynamic pseudo generation methods involve performing and then using the results of fine grid flow simulations. Basically, there are two major steps in generating dynamic pseudo functions. Firstly, all the single phase fluid flow properties such as porosity (pore volume) and absolute permeability (transmissibility) must be upscaled. For porosity (pore volume) averaging, it is very straightforward because only the total pore volume needs to be conserved. On the other hand, permeability (transmissibility) averaging can be obtained using methods as simple as applying the arithmetic or harmonic averages through more sophisticated methods involving solving Laplace's equation. Guzman *et al.* (1994) noted that the accuracy of the permeability averaging was increased by solving Laplace's equation compared to carrying out simple harmonic or arithmetic averaging. Generally, the scaleup of these single-phase properties was not an issue in generating pseudo functions since both of them are only functions of the porosity/permeability distribution and coarse grid geometry alone (Hewett 1997).

The second issue in dynamic upscaling is that the multi-phase flow properties such as the relative permeability and capillary pressure also need to be upscaled. There are many methods that have been published in the literature for this purpose. The most widely used methods are the Kyte and Berry (1975), the Stone (1991) and the pore volume weighted (see *Schlumberger Geoquest Pseudo* reference manual, 1995). In the Kyte and Berry method, Darcy's law is solved to obtain the pseudo relative

permeability whereas in the Stone method, a fractional flow formulation is used. A more detailed discussion of these two methods will be given in Chapter 2.

Recently, Hewett and Archer (1997) have also published a new method utilising a conceptual streamtube approach. In this method, capillary pressure is accounted for by the introduction of an effective capillary pressure defined by associating the capillary pressure at the coarse grid blocks centres with the average saturations of the coarse grid blocks. In addition, gravity is accounted for by using the conventional gravity terms based on the actual phase density differences and the difference in elevation of the coarse grid blocks centres. A more detailed discussion of this method will also be given in Chapter 2.

1.2 STATEMENT OF THE PROBLEM

In our study of a range of scaleup techniques, it is evident that the application of these methods to the upscaling of gas/oil systems is more difficult than in water/oil systems. This may be expected due the large mobility differences and the increased effect of the gravitational forces. Because of this increased difficulty, we may turn the problem round and use gas/oil immiscible displacements as "difficult" problems, which will help us to perform more rigorous testing of the various upscaling methods.

Furthermore, all of the three dynamic pseudo methods mentioned above, the Kyte and Berry, the Stone and the Hewett and Archer, have been applied principally to oil-water displacements where gravity may not have a dominant effect and displacement mobility ratios are not so unfavourable. The use and validity of these three pseudo

methods is investigated in this thesis for gas-oil displacements. This will provide a more stringent series of tests of the various upscaling methods due to the large effect of gravity forces and problems with gas channelling/fingering due to the difference in fluid densities and unfavourable mobility ratio, respectively.

There are limitations in all of the types of upscaling approaches mentioned above i.e. the VE methods, the steady-state methods and the dynamic methods. Stone (1991) discussed the limitations of the application of vertical equilibrium pseudo functions. Recently, several authors have shown that dynamic pseudo functions are also subject to certain limitations. For example, the Stone method has some inconsistencies in handling gravity in both fine and coarse gridblock simulations (Guzman, 1994; Barker and Thibeau, 1996) which may be a severe limitation on the use of this approach for gas injection cases.

Another problem that we focus on this thesis is the issue of designing an optimal grid coarsening scheme. By "optimal" we mean that the coarse grid is chosen to give the best agreement with the fine grid results whether rock curves or pseudos are used at the coarse grid scale. Conventional coarsening schemes take into account only the static properties of the fine grid models such as the porosity and/or permeability distribution, net-to-gross ratio etc. These coarsening schemes ignore the dynamic properties of the fine grid model such as the flood pattern, pressure and saturation distribution. This in turn can lead to inaccurate predictions of important quantities such as total oil recovery and gas-oil ratio when pseudo functions are applied. This situation motivates us to find a better coarsening approach for the scaleup of reservoir models.

The development of our optimal grid coarsening scheme was motivated from a volume averaged analysis of the fine scale saturation equations. Starting with the initial work of Durlofsky (1998) who used single-phase simulation in viscous dominated models to design a non-uniform coarsening for the coarse grid model, we expand and validate the idea of using the volume averaged saturation equation in models with gravity. It is shown that the coarse grid simulation error correlates closely with specific sub-grid quantities involving higher moments of fine grid variables such as the variance of gas saturation (σ^2_s), the velocity-saturation covariance (σ^2_{vS}) and the absolute permeability-saturation covariance (σ^2_{kS}). These sub-grid quantities can also be used in the form of coefficient of variation (the C_v). The specific sub-grid measure that best correlated with the coarse grid error was shown to vary depending on whether rock curves or pseudo functions are used in the coarse grid model. By forming a coarse grid that minimizes the appropriate sub-grid quantity, optimal coarse scale descriptions can be generated. A detailed discussion on this subject will be given later in Chapters 5 and 6.

At this point, reasonable questions might be:

- *Knowing that most of the existing pseudo-isation methods such as the Kyte and Berry and the Stone were derived using water-oil systems, can we still use them in gas-oil displacements where gravity might be a dominant force?*

- *Can we use these pseudo methods at highly adverse mobility ratios ($M >> 1$), which also normally occur in gas - oil systems?*

- *Can we develop an alternative method that will be more successful in both of the aspects mentioned above?*

- *Can we quantify the strengths and the weaknesses of each of the pseudo methods?*

- *Can we develop a more optimal grid coarsening scheme using dynamic fluid flow properties that will minimise the resulting error in gas-oil displacements?*

Addressing these questions forms the main tasks of this thesis. A description of the research associated with this study is presented in the following sections.

1.3 OBJECTIVES

The central task of this thesis is to address the questions raised in the previous section.

The objectives of this thesis are as follows:

1. To review and assess currently available pseudo-isation techniques.

2. To validate currently available pseudo methods in gas-oil displacements where significant gravitational effects and unfavourable mobility ratios provide a very stringent test of each of the various pseudo methods.

3. To develop a new pseudo method which can provide more accurate upscaling results in gas-oil displacements.

4. To quantify the strengths and weaknesses of each of the pseudo methods and the reasons behind its success or failure for various type of problems.

5. To develop a new optimal grid coarsening scheme ("intelligent" coarsening) which will produce less error when pseudo functions or fine grid relative permeabilities are applied directly in the coarse grid models.

1.4 THESIS OUTLINE

There is an extensive literature in petroleum reservoir engineering that deals with the determination and generation of pseudo functions. This research project started with a literature search and review. Several of the most widely used pseudo methods such as the Kyte and Berry, the Stone, the Hewett and Archer, the vertical equilibrium methods and the steady-state methods were thoroughly reviewed. A detailed presentation of this phase of the work is given in Chapter 2.

The research project then turned to the development of a new pseudo generation method called the "Transmissibility Weighted" method (TW). This method is based on the information derived from the fine grid simulation results and is specifically designed to handle large gravitational effects. This method follows the same approach as the Kyte and Berry method where the pseudo functions are obtained by solving Darcy's law at the coarse grid level, but with some modifications. The TW method averages pressure *gradients* rather than the pressure itself in order to reduce the potentially large error in averaging the individual coarse grid block pressures and then

calculating the pressure gradient. This helps to prevent the accumulation of errors due to averaging individual pressure points. Furthermore, a new set of weighting factors for calculating the respective fluid potential difference was introduced. A detailed description of the TW pseudo method is presented in Chapter 3.

To validate this TW method, results of seven test models using this technique were compared with the results of the other existing pseudo methods; viz the Kyte and Berry, Stone, Hewett and Archer and the Vertical Equilibrium methods. The results from this exercise show significant improvements when using the TW method especially in the gravity dominated cases. Detailed discussion on this subject is also presented in Chapter 3.

Having established the very good performance of this new method, the research effort was then focussed on investigating why the TW method performs better than other existing pseudo methods. A step by step investigation of the reason for the difference between these pseudo methods was carefully carried out and the detailed work in this area is presented in Chapter 4.

Chapters 5 and 6 focus on the development of an average saturation equation with the gravity effect included. Using this new equation as the framework, we developed a new optimal grid coarsening scheme that takes into account not only the static properties of the fine grid models (i.e. porosity, permeability, net-to-gross ratio etc.) but also the dynamic properties of the fluid flow. It is shown that the coarse grid simulation error correlates closely with specific sub-grid quantities involving higher

moments of fine grid variables, which can be computed from the fine scale simulations. The resulting coarsening scheme might be non-uniform in nature but would fulfill all purposes of using pseudo function (i.e. to control numerical dispersion, to capture small-scale heterogeneity etc) with less error and without any adjustment to the pseudo equations themselves.

This new coarsening technique was validated using a wide range of test cases. We prove that this approach is applicable to coarse-scale descriptions using either the original rock curves or the pseudo relative permeability curves. The accuracy of the coarse grid calculations is, however, significantly better when pseudo functions are used. It is shown that it is not necessarily true that, when we increase the number of coarse grid layers, the performance of the pseudo functions will improve. The accuracy in applying the TW pseudo method (or rock curves) will also depend on the configuration of the layering scheme adopted for the coarse grid models. By forming a coarse grid that minimises the appropriate sub-grid quantity, optimal coarse scale descriptions can be generated.

Chapter 7 is a summary of the major findings and conclusions of this research. The direction of possible future investigations is then discussed at the end of this chapter.

1.5 SPECIAL NOTES

The fluid flow simulations in this work were all carried out using the ECLIPSE-100 black oil simulator of *Schlumberger Geoquest.* For the calculation of the Kyte and Berry and the Stone pseudo methods, the *PSEUDO* program supplied by *Schlumberger*

Geoquest was used. The pseudo relative permeability curves for the TW method, the Hewett and Archer method and sub-grid fluctuating moments were calculated using FORTRAN programs developed by the author and presented in Appendices 3 and 4.

All of the work referring to the validation, derivation and testing of all the pseudo-isation methods that are discussed in the next few chapters (the Kyte and Berry, the Stone, the Hewett and Archer and the Vertical Equilibrium) are presented in the context of immicible two-phase displacement processes of oil-gas systems. In all cases, capillary pressure was ignored. Ignoring capillary pressure in these cases is acceptable considering the dimension of our grid blocks of 10s of metres (upscaling from the scale of geological models to fluid flow simulation model), although we note that we may have to derive the "rock" curves from a capillary equilibrium upscaling calculation in some cases (Pickup *et al.*, 1998).

CHAPTER 2

LITERATURE REVIEW

2.1 GENERAL REMARKS

The purpose of this chapter is to review the main pseudo-isation techniques that are currently available to the oil industry. There are two main reasons for using pseudo functions in reservoir simulation. Firstly, they can be used to capture the effect of interaction between multi–phase fluid flow and small-scale variability and secondly, they can also be used for correcting the effect of numerical dispersion in the coarse grid models. However, this latter issue will not be analysed in this chapter. This review will be concentrated on the generation of pseudo functions to capture the effect of interaction between multi–phase fluid flow and smaller scale variability only.

2.2 LITERATURE BACKGROUND OF PSEUDO FUNCTIONS

In general, pseudo functions which are derived from the various upscaling methods can be divided into three broad categories as shown in Figure 1.1. Among the earliest approaches used to generate pseudo functions are the two vertical equilibrium (VE) methods of Coats et al. (1967 and 1971) for the capillary-gravity vertical equilibrium and gravity dominated cases respectively. Historically, the introduction of the vertical equilibrium concept was motivated by the need to simulate a three-dimensional two-

phase flow model with a two-dimensional fluid flow simulator in which the vertical effects are included. For this case, viscous force must be negligible in the vertical direction. Also, the models must have excellent vertical communication to allow fluids to segregate even during the production period. One advantage of using these VE methods is that they do not require any fine grid simulation in order to derive the pseudo functions needed for the coarse grid models.

When the simulation run is in a steady-state condition, steady-state upscaling methods can be used. By "steady-state" we mean that the saturations in each of the grid blocks are constant with time. In general, there are two types of steady-state pseudo generation methods that depend on the balance of capillary and viscous forces in the models. This technique normally simplifies the problems (eliminate the necessity to do two-phase simulation on the fine grid models) but does not reduce the dimensionality of the models as the VE methods discussed above.

When both of the gravitational and viscous forces are significant, dynamic pseudo functions must be used. In this case, the pseudo functions are flow rate dependent and are derived from the information obtained from the fine grid simulation. One of the earliest methods using this concept is the work reported by Jacks *et al.* (1973). In their method, all the fine grid potential differences are assumed to be equal and equate to the pseudo potential difference. In other word, the authors assume that a vertical equilibrium condition exists in each of the coarse grid columns. The assumption of constant potential differences leads to a constant flow rate between grid blocks. This is

a very restrictive assumption and as a result, this method clearly cannot be applied to fully dynamic cases.

Kyte and Berry (1975) improved the Jacks *et al.* (1973) method by eliminating the assumption of equal potential differences. In their method, Kyte and Berry used the fine grid pressures to calculate the coarse grid pressures and then use them to calculate the coarse grid fluid potential differences. Subsequently, these coarse grid potential differences were used to calculate the pseudo relative permeability from Darcy's law. In addition to coarsening the fine grid model in the vertical direction, this method also has the capability to coarsen the fine grid model in the areal plane (horizontal direction). This was a significant contribution by the authors. Furthermore, by considering only the most down stream blocks in calculating the total flow rate while computing the pseudo saturation as a pore volume weighted averages over the entire fine grid system lying within a coarse grid block, the authors introduced a viable method of controlling numerical dispersion. One disadvantage of using this method is that it requires the use of directional pseudo relative permeability if the coarse grid block model has more than one dimension. In addition, the weighting factors used by this technique were derived empirically, and as a consequence, they may not work in all the cases. For a detailed explanation on this subject, refer to Chapter 4.

The idea of adopting the fractional flow formulation is an important contribution by Stone (1991). By using this procedure, the need to estimate the potential difference (as required by Darcy's law) is eliminated. Stone suggested computing an average total mobility and a net fractional flow from which the pseudo relative permeability can

easily be calculated. However, as shown by several authors such as Guzman *et al.* (1996), this method has some inconsistency when capillary pressure and/or gravity are included. Also, this method is less accurate if there are significant variations in total mobility of the fluids (Barker and Fayers, 1994).

Both methods of the Kyte and Berry (1975) and the Stone (1991) were derived at a time when the two-dimensional model was coarsened to a one-dimensional model (flow in a single direction at the coarse grid scale). However, flow in "real" reservoirs is normally anisotropic and the flow direction dependency of the pseudo functions generated by these methods is one of the weaknesses that need to be considered. In this case, the use of directional pseudo functions is unavoidable and analogous to the use of directional absolute permeability in the single-phase flow.

It is obvious that using directional permeabilities is more accurate than using isotropic scalar permeabilities. This phenomenon motivated the work by Pickup *et al.* (1994) who showed that tensor based effective permeability may be necessary for accurate single phase scaleup, and in most cases, the same findings should be adopted for the two-phase pseudo functions. They also noted significant improvement of this method (tensor based pseudo functions) compared to the Kyte and Berry method when gravitational cross flow is important.

Recently, Hewett and Archer (1997) published a new method utilizing conceptual streamtubes, whose geometry is defined by the fine grid cells at the outlet face of the coarse grid blocks to calculate the pseudo functions. In this method, capillary pressure

is accounted for by the introduction of an effective capillary pressure defined by associating the capillary pressure at the coarse grid blocks centers with the average saturations of the coarse grid blocks. In addition, gravity is accounted for using the conventional gravity terms based on the actual phase density differences and the difference in elevation of the coarse grid blocks centres.

Some other pseudo generation methods have also been published in the literature, such as the works reported by Hales (1983), Christie *et al.* (1995) and Guzman *et al.* (1996). In the next two sections, a literature review will be carried out and then the mathematical derivation of some of the most widely used pseudo-isation techniques will be discussed in detail. We will start the discussion by considering the concept of (i) the vertical equilibrium, (ii) the steady-state upscaling and (iii) the dynamic pseudo methods in the following sections.

2.3 VERTICAL EQUILIBRIUM (VE) METHODS

The VE method is one of the earliest pseudo-isation techniques available. The use of this pseudo concept is motivated by the need to simulate 3D two-phase flow with a 2D reservoir simulator in which vertical effects are included. Viscous forces must be negligible in the vertical direction. Also, the reservoir must have sufficient vertical permeability to allow fluids to segregate completely and instantaneously. The main condition for VE is achieved when the viscous to gravity ratio is low enough that the vertical potential gradient of each fluid phase is essentially zero.

$$\frac{\partial \Phi_p}{\partial z} = 0.0 \qquad (2.1)$$

where p = oil, water or gas. From Equation (2.1) above and the definition of capillary pressure, we can deduce that:

$$P_c(x,y,z) = P_c(x,y,z_{ref}) - \int_{z_{ref}}^{z} (\rho_o - \rho_g) g_z .dz \qquad (2.2)$$

where $P_c(x,y,z_{ref})$ is the capillary pressure for a given point (x,y) on a reference surface z_{ref}. z_{ref} is usually taken at the oil-water contact or mid-point of the reservoir. The above two equations apply to all points within the three-dimensional medium. Thus, by adopting these equations, 3D fluid flow models can be represented by only 2D areal model with properties variation in the vertical direction are accounted for.

Dake (1978) defined the favorable conditions for the VE methods to be applied as follows:

- *small reservoir thickness*
- *low fluid viscosities*
- *low injection rates*
- *low lateral velocities*
- *large vertical permeabilities*
- *high gravity and/or capillary forces.*

There are three types of VE and they are categorized according to the relative importance of gravity and capillary forces (Ahmadi *et al.*, 1996). The categories are as follows:

(i) *Gravity-capillary VE*, which refers to a situation where the vertical viscous force is small, and there is a balance between gravity and capillary forces.

(ii) *Gravity segregated VE*, which refers to a situation where capillary forces are low or negligible as might occur in thick reservoir with relatively small transition zone.

(iii) *Capillary dominated VE*, which refers to a situation where the capillary force is dominant.

2.3.1 Capillary-Gravity Vertical Equilibrium

In the case of capillary-gravity equilibrium, the two forces of capillary pressure and gravity are balanced along the vertical direction of the model and are about the same order of magnitude. Subsequently, as shown in Figure 2.1, the thickness of the capillary transition zone should be about the same order as the reservoir thickness. For this specific case,

$$h \approx h_c, \tag{2.3}$$

where h is the reservoir thickness and h_c is the thickness of the capillary transition zone.

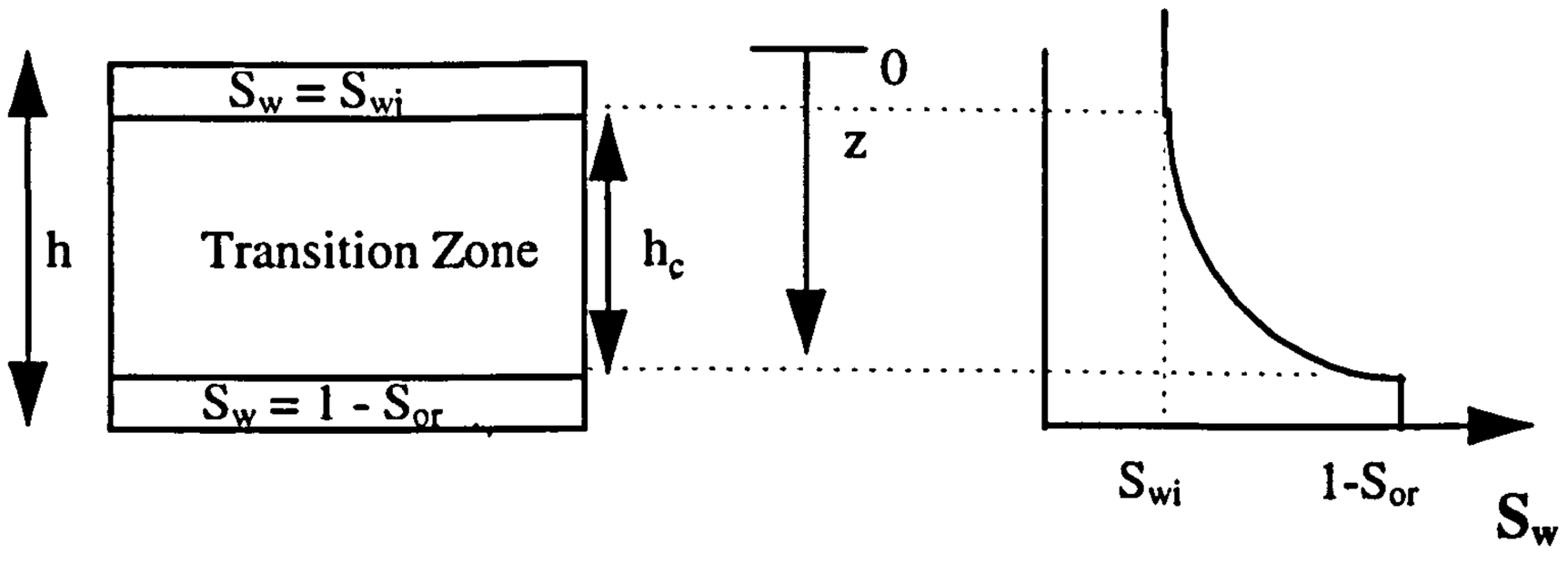

Figure 2.1: Model under capillary-gravity vertical equilibrium and the saturation profile.

The first concept and model of this technique was published by Coats *et al.* (1967). By assuming that the vertical potential difference of the two fluids is essentially zero, Coat *et al.* have integrated the 3 dimensional partial differential equations governing 2-phase fluid flow along the vertical axis. By doing this, they could simplify a 3D reservoir simulation model as a 2D model without losing the distribution and variation of fluid flow properties in the vertical direction. Assuming the origin is set at the bottom of the model, the averaged water saturation is defined as:

$$\overline{S_w} = \frac{\int_0^h \phi . S_w . dz}{\int_0^h \phi . dz} \tag{2.4}$$

and assuming that the absolute permeability to be isotropic in the horizontal plane the pseudo relative permeability is defined as:

$$\overline{k_{rp}} = \frac{\int_0^h k . k_{rp} . dz}{\int_0^h k . dz} \tag{2.5}$$

An over bar (¯) will be used to denote quantities evaluated at the coarse grid scale. The finite difference approximation of these two integrals in the vertical column of blocks

are shown in Equations (2.6) and (2.7) (Stone, 1991) for a system with nz vertical blocks:

$$\overline{S_w} = \frac{\sum_{k=1}^{nz}(PV.S_w)_k}{\sum_{k=1}^{nz}(PV)_k} \qquad (2.6)$$

for the pseudo water saturation and

$$\overline{k_{rp}} = \frac{\sum_{k=1}^{nz}(T_x.k_{rp})_k}{\sum_{k=1}^{nz}(T_x)_k} \qquad (2.7)$$

for the pseudo relative permeability. In these two equations, T_x is the transmissibility in the horizontal direction, PV is a pore volume and k is the number of fine grid layers. The authors noted that when there exists absolute permeability anisotropy in the horizontal plane ($k_x \neq k_y$), then separate calculation must be done in each of the dimensions. In other words, directional pseudo relative permeability must be used.

An example of the successful application of this method in a fluid flow simulation was reported by Killough *et al.* (1979). They used this method in the simulation of the Empire Abo Field. A three-layer model with capillary-gravity equilibrium is used instead of the 22-layer fine grid model. By introducing the directional relative permeabilities, an acceptable result was obtained between the fine grid model and the coarse grid model.

2.3.2 Gravity Segregated Vertical Equilibrium

The model of Coats *et al.* (1971) is one of the pioneering studies in this category. In this case, the vertical distribution of fluids is due to gravity only. The capillary pressure (transition zone) must be small or negligible. Coats *et al.* (1971) mentioned that the capillary transition zone should be less than 10 % of the total reservoir thickness. This assumption is particularly suited to the problem that we are considering (gas-oil displacements) where the density difference between the two fluids is expected to be large enough for them to segregate instantaneously.

Figure 2.2 below shows the concept of gravity segregated VE and its related water saturation distribution. Since the reservoir is under VE conditions, the existence of distinct fluid contacts can be considered. For the example of a water displacement process, the water saturation in the invaded zone will be at one minus residual oil saturation ($S_w = 1 - S_{or}$) whereas, in the non-invaded zone, the water saturation will be at its initial value (S_{wi}). In the transition zone, the water saturation will vary between these two values. For this specific case, water and oil pressures are equal at every point ($P_c = 0$).

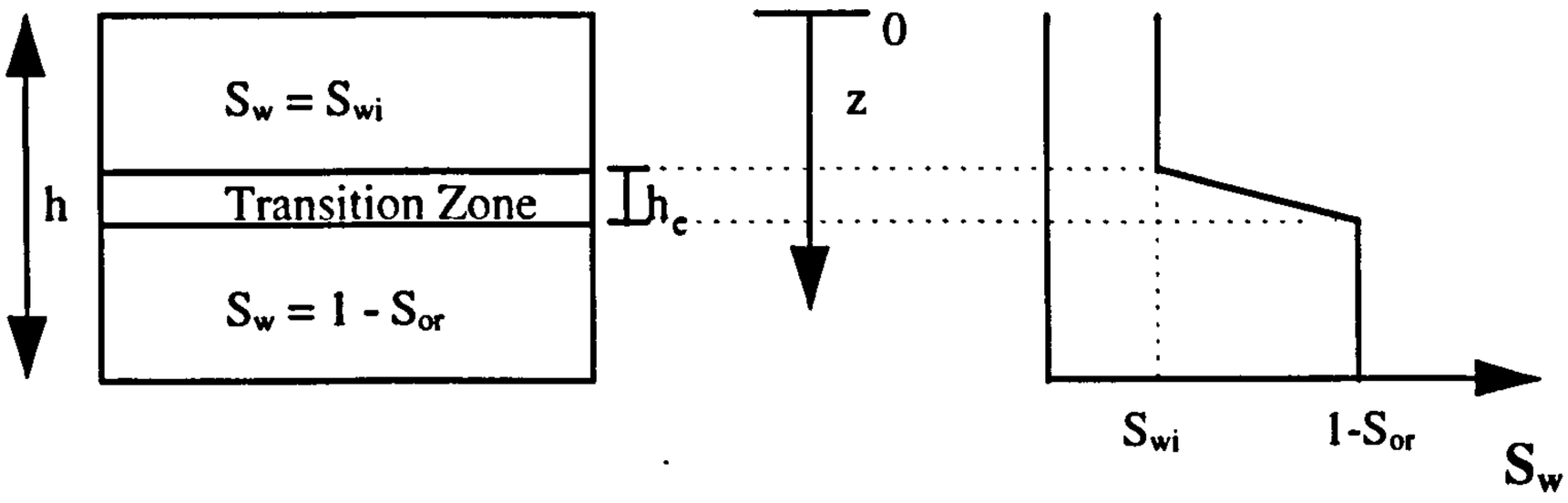

Figure 2.2: A 2D cross-sectional model under gravity segregated flow and the saturation profile (capillary transition zone should be small or negligible).

For the purpose of deriving the mathematical equations of gravity segregated VE, we will ignore the transition zone ($P_c = 0$) and consider a homogenous cross sectional model of a water-gas system with an initial gas-water contact (GWC) at $z = z_{ci}$ as shown in Figure 2.3 below.

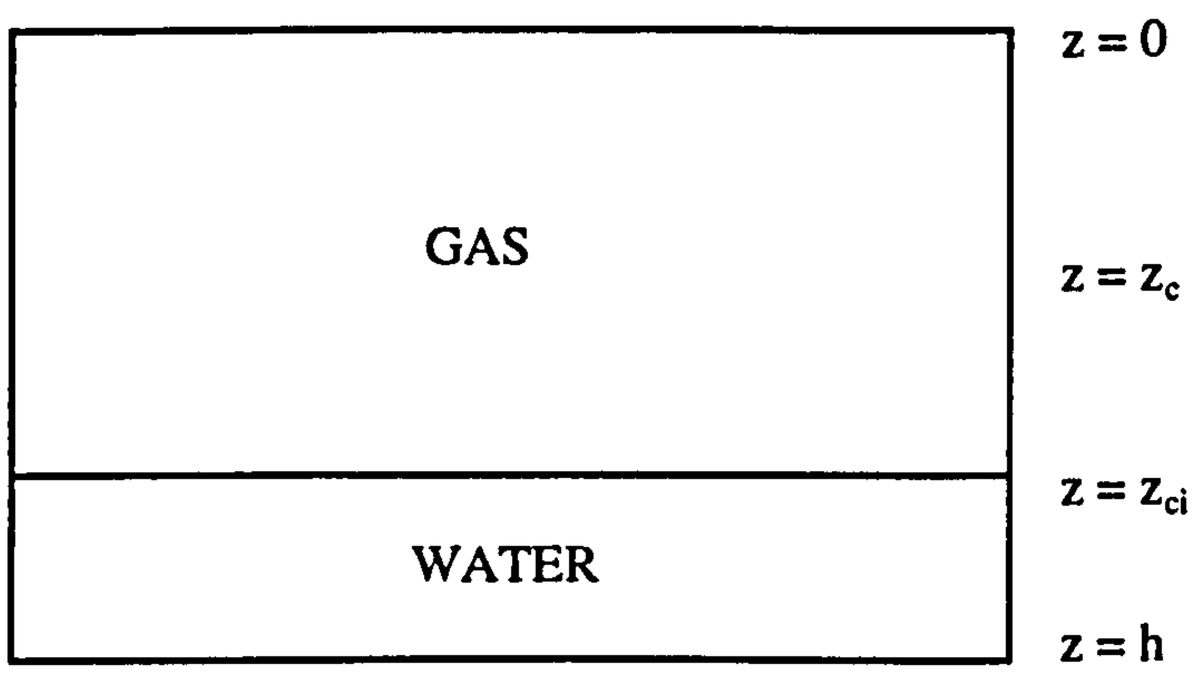

Figure 2.3: Homogenous horizontal reservoir for a water-gas system under gravity-segregated VE

In this method, the averaged properties of $\overline{S_w}$, $\overline{P_c}$ and $\overline{k_{rp}}$ are defined such that correct flows and mass balance are obtained.

2.3.2.1 Averaged Water Saturation

The average saturation of this model is initially uniform and is given by Equation (2.8) below (assuming that $S_w = 1$ in the water zone):

$$\overline{S_{wi}} = \frac{z_{ci}.S_{wi} + h - z_{ci}}{h} \tag{2.8}$$

The assumption of instantaneous fluid segregation by gravity (even during production and/or injection) means that the averaged water saturation can be calculated for a given point x and at a given time t using depth averaging as follows:

$$\overline{S_w} = \frac{z_c . S_{wi} + (z_{ci} - z_c)(1 - S_{gr}) + h - z_{ci}}{h} \qquad \text{for } z_c < z_{ci} \qquad (2.9)$$

and

$$\overline{S_w} = \frac{z_c . S_{wi} + h - z_c}{h} \qquad \text{for } z_c > z_{ci} \qquad (2.10)$$

where S_{gr} is the residual gas saturation and S_{wi} is the irreducible water saturation.

2.3.2.2 Pseudo Capillary Pressure

The averaged water and gas pressures ($\overline{P_o}$ and $\overline{P_g}$) are assumed to be at the reference plane of z = 0. At the fluid interface ($z = z_c$), we have an equal pressure in both gas and water phase since capillary pressure is zero at this point.

$$P_w(z_c) = P_g(z_c) \qquad (2.11)$$

When $z \neq z_c$ and $z \neq 0$, the pressures in the two fluid phases are :

$$P_p(z) = P_p(z_c) + \rho_p g(z - z_c) \qquad (2.12)$$

where subscript p = gas or water. The difference in the two pressures at the reference point is by definition the pseudo capillary pressure and is given by the following equation:

$$P_g(0) - P_w(0) = \overline{P}_c = (\rho_w - \rho_g).g.z_c \qquad (2.13)$$

Substituting z_c from Equation (2.13) into Equation (2.9) and (2.10), we derive a relationship between pseudo capillary pressure and the averaged water saturations.

$$\overline{\overline{S_w}} = -\frac{(1 - S_{wi} - S_{gr})\overline{P}_c}{h(\rho_w - \rho_g)g} + 1 - \frac{S_{gr}.z_{ci}}{h} \qquad \text{when } z_C < z_{Ci} \qquad (2.14)$$

and

$$\overline{\overline{S_w}} = 1 - \frac{1 - S_{wi}}{h(\rho_w - \rho_g)g}\overline{P}c \qquad \text{when } z_C > z_{Ci} \qquad (2.15)$$

2.3.2.3 Pseudo Relative Permeability

The pseudo relative permeabilities are derived by averaging over the entire section of the reservoir. In our example of a homogenous model, with an assumption of $k_{rw} = 1$ in the water zone, this gives

$$\overline{\overline{k_{rw}}} = \frac{k_{rwrg}(z_{ci} - z_c) + (h - z_{ci})}{h} \qquad \text{when } z_C < z_{Ci} \qquad (2.16)$$

and

$$\overline{k_{rw}} = \frac{h - z_c}{h} \qquad \text{when } z_c > z_{ci} \qquad (2.17)$$

where k_{rwrg} is the water relative permeability at the residual gas saturation.

Using Equations (2.9) and (2.10), z_c can be eliminated from Equations (2.16) and (2.17) which gives the pseudo relative permeability with respect to $\overline{S_w}$. If the GWC rises to z_c ($z_c < z_{ci}$) the equation is as follow:

$$\overline{k_{rw}} = \frac{k_{rwrg}.\overline{S_w}}{(1-S_{gr}-S_{wi})} + \frac{k_{rwrg}[z_{ci}(1-S_{gr}-S_{wi})-h+S_{gr}.z_{ci}]}{h(1-S_{gr}-S_{wi})} + \frac{(h-z_{ci})(1-S_{gr}-S_{wi})}{h(1-S_{gr}-S_{wi})} \qquad (2.18)$$

If instead the gas-water contact (GWC) drops below its initial location ($z_c > z_{ci}$), the equation is given by the following:

$$\overline{k_{rw}} = \frac{S_w - S_{wi}}{1-S_{wi}} \qquad (2.19)$$

A similar calculation gives the following gas relative permeabilities:

$$\overline{k_{rg}} = \frac{k_{rgcw}}{1 - S_{gr} - S_{wi}}\left[1 - \frac{S_{gr}.z_{ci}}{h} - \overline{S}_w\right] \qquad \text{when } z_c < z_{ci} \qquad (2.20)$$

$$\overline{k_{rg}} = \frac{k_{rgcw}}{1 - S_{wi}}\left[1 - \overline{S}_w\right] \qquad \text{when } z_c > z_{ci} \qquad (2.21)$$

where k_{rgcw} is the gas relative permeability at irreducible water saturation (S_{wi})

2.3.3 Capillary Dominated Vertical Equilibrium

Capillary dominated VE is the situation where gravity effects are negligible compared to the capillary pressure. In this case, the capillary pressure and also saturation are uniform over the whole thickness of the reservoir as shown in Figure 2.4 below:

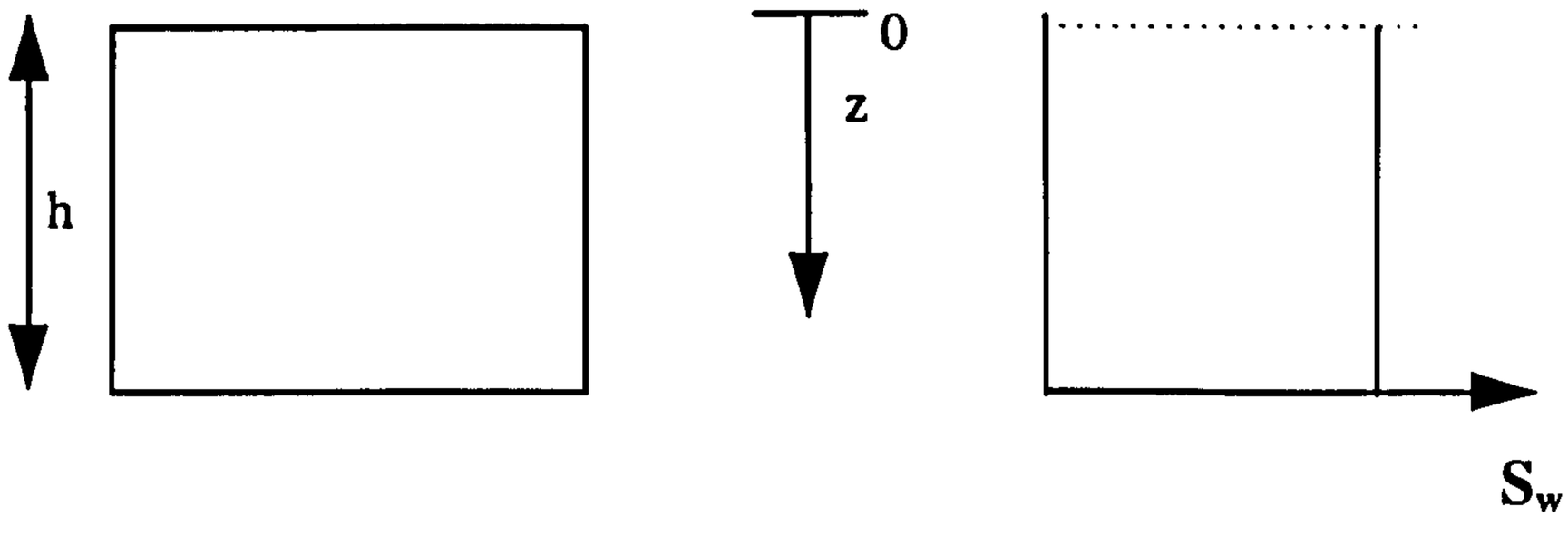

Figure 2.4: Model under capillary dominated VE and the saturation profile.

The idea of using this VE model was developed by Yokohama and Lake (1981) using water-oil displacement in a stratified medium. They suggested the following procedures to calculate the pseudo functions for a model with *nz* layers of grid blocks:

1. Choose a water saturation S_w for an arbitrary layer and determine the capillary pressure from the capillary pressure-water saturation $P_c(S_w)$ curve. Consider this capillary pressure as the averaged $\overline{P_c}$.

2. Determine the water saturations of other layers from the value of $\overline{P_c}$ obtained above.

3. Calculate the average water saturation $\overline{S_w}$ as follow:

$$\overline{S_w} = \frac{\sum_{k=1}^{nz} \phi_k h_k S_{wk}}{\sum_{k=1}^{nz} \phi_k h_k} \quad \text{(porosity-thickness weighted)} \tag{2.22}$$

4. Determine k_{rwj} and k_{roj} ($k = 1 \ldots nz$) from the local relative permeability vs. water saturation curves of each layer corresponding to local S_{wj} (obtained from procedure 2).

5. Calculate the pseudo relative permeability as follow:

$$\overline{k_{ro}} = \frac{\sum_{k=1}^{nz} k_{xk} h_k k_{rok}}{\sum_{k=1}^{nz} k_{xk} . h_k} \quad \text{(for pseudo oil relative permeability)} \tag{2.23}$$

and

$$\overline{k_{rw}} = \frac{\sum_{k=1}^{nz} k_{xk} h_k k_{rwk}}{\sum_{k=1}^{nz} k_{xk} . h_k} \qquad \text{(for pseudo water relative permeability)} \qquad (2.24)$$

6. Repeat procedure 1 to 5 for other values of S_w and establish the pseudo curves.

   Pseudo relative permeability curves for oil and water phases are given as $\overline{k_{ro}}$ vs. $\overline{S_w}$ and $\overline{k_{rw}}$ vs. $\overline{S_w}$ respectively, and the pseudo capillary pressure curves is given as $\overline{P_c}$ vs. $\overline{S_w}$.

However, as mentioned in the introductory chapter (Chapter 1), we will only focus our attention on oil-gas displacements where gravity is a dominant force although viscous forces are also significant. For simplicity, we will ignore the capillary pressure in all of the cases that we consider. Neglecting capillary pressure is reasonable in this context because capillary effects are typically small for the length scale (from geological model to fluid flow simulation model) and the fluid flow processes (gas-oil displacements) that we considered. As such, we will limit our subsequent discussion to the second VE method discussed above i.e. *the Gravity Segregated VE* (Section 2.3.2).

2.4 STEADY-STATE UPSCALING METHODS

A number of people, such as Smith (1991), Lemouzy et al. (1993), Pickup and Sorbie (1996) and Kumar and Jerauld (1996), have developed methods for upscaling which assume that the flood is in steady-state conditions. It has been systematically proved that it is possible to apply a capillary dominated steady-state upscaling method when the fluids are in capillary equilibrium. This limit may be assumed at small scale (30 cm

or less), when the flood velocity is low. At high flow rate and larger scales, a viscous dominated steady-state method can be applied which assumes constant fractional flow throughout the upscaled regions.

2.4.1 Steady-State Capillary Equilibrium Pseudo Functions

The concept of steady-state capillary equilibrium should be distinguished from the capillary dominated VE mentioned in section 2.3.3. This method can be seen as an extension (or generalization) to the capillary dominated VE method where it normally simplifies the problem (eliminates the need to do the full two-phase simulation on the fine grid model) but does not reduce the dimensionality of the fine grid model. If the injection rate is low, the fluids will come to capillary pressure equilibrium and the saturation can be determined from the capillary pressure curves. The capillary equilibrium method has been presented in several papers such as Smith (1991), Lemouzy et al. (1993) and Pickup and Sorbie (1996). In general, the method can be outlined as follows (for water-oil systems):

a) Select a capillary pressure value;

b) Using the capillary pressure curves for each region, determine the corresponding water saturation;

c) Calculate the average water saturation for the coarse grid block using pore volume weighted of S_w obtained above (step b);

d) Use the fine grid relative permeability tables to determine the relative permeabilities to oil and water for the saturation values above (step b). Then

calculate the phase permeabilities by multiplying them by the absolute permeabilities;

e) Perform single-phase steady-state simulations separately on the oil and water phase permeability, and then calculate the effective phase permeabilities to oil and water.

f) Calculate the effective relative permeabilities by dividing the effective phase permeabilities by the effective absolute permeabilities.

g) Select another capillary pressure value, and repeat step b) to f).

2.4.2 Viscous Dominated Steady-State Pseudo Functions

A flood can be considered to be in a steady-state condition if the saturations in each grid blocks are constant with time. In the viscous dominated case (negligible capillary pressure and gravity), the fractional flow is constant with time and this can be used to determine the water saturation. A step-by-step technique on how to calculate pseudo functions for the coarse grid block using this method is shown below:

a) Select a fractional flow value;

b) Determine the corresponding water saturation in each region using this value;

c) Calculate the average water saturation for the coarse grid block using pore volume weighted of S_w obtained above (step b);

d) Determine the relative permeabilities in each region, and then calculate the total mobility in each region;

$$\lambda_t = k_{abs}\left(\frac{k_{rw}}{\mu_w} + \frac{k_{ro}}{\mu_o}\right) \tag{2.25}$$

e) Perform single-phase steady-state simulations using the total mobility, and then calculate the effective total mobility;

f) Use the fractional flow of water to determine the effective relative permeabilities:

$$\overline{k_{rw}} = \frac{\mu_w . \overline{\lambda_t} . \overline{f_w}}{\overline{k_{abs}}} \qquad (2.26)$$

$$\overline{k_{ro}} = \frac{\mu_o . \overline{\lambda_t} . (1 - \overline{f_w})}{\overline{k_{abs}}} \qquad (2.27)$$

g) Select another fractional flow value, and repeat step b) to f).

However, since both of the steady-state methods that are mentioned above ignore the effect of gravitational force which is important in the cases that we consider (gas displacements), we do not attempt to use these methods in our work.

2.5 DYNAMIC PSEUDO FUNCTIONS

The word "dynamic" applies to the calculation of pseudo functions that are based on the results of fine grid simulations (Barker and Thibeau, 1996). In this case, the saturation distribution is not a unique average as found in the VE methods, but also depends on several aspects of the displacements processes e.g. boundary condition, flow rate, heterogeneity etc.

In general, there are two approaches for calculating dynamic pseudo functions as follows:

(i) *The weighted potential approach* where the potential in the coarse grid block is calculated using the average of the fine grid values of the potential. Examples of this type of method include those of Kyte and Berry (1975), the Pore volume weighted method (*Geoquest's Eclipse Pseudos*, 1995), Guzman's method (1996), the Thomas method (1983) etc.

(ii) *The total mobility approach* that solves the problem by adopting a fractional flow formulation. Examples of this approach are those of Stone (1991), Zhang and Sorbie (1995), Christie *et al.* (1995) etc.

In this section, we will focus on the use of two of the most widely known pseudo-isation methods; vis the Kyte and Berry method (weighted potential) and the Stone method (total mobility) as representatives of each of the two approaches discussed above. In addition, we also discuss a method proposed by Hewett and Archer (weighted potential) which utilizes the idea of using a conceptual streamtube. All of these upscaling methods are described schematically by considering a 2D fine grid model of 10 x 1 x 5 grid blocks that is to be coarsened to a 1D model of 2 x 1 x 1 grid blocks; see Figure 2.5 below. The pseudo function is calculated for the upstream coarse gridblock only.

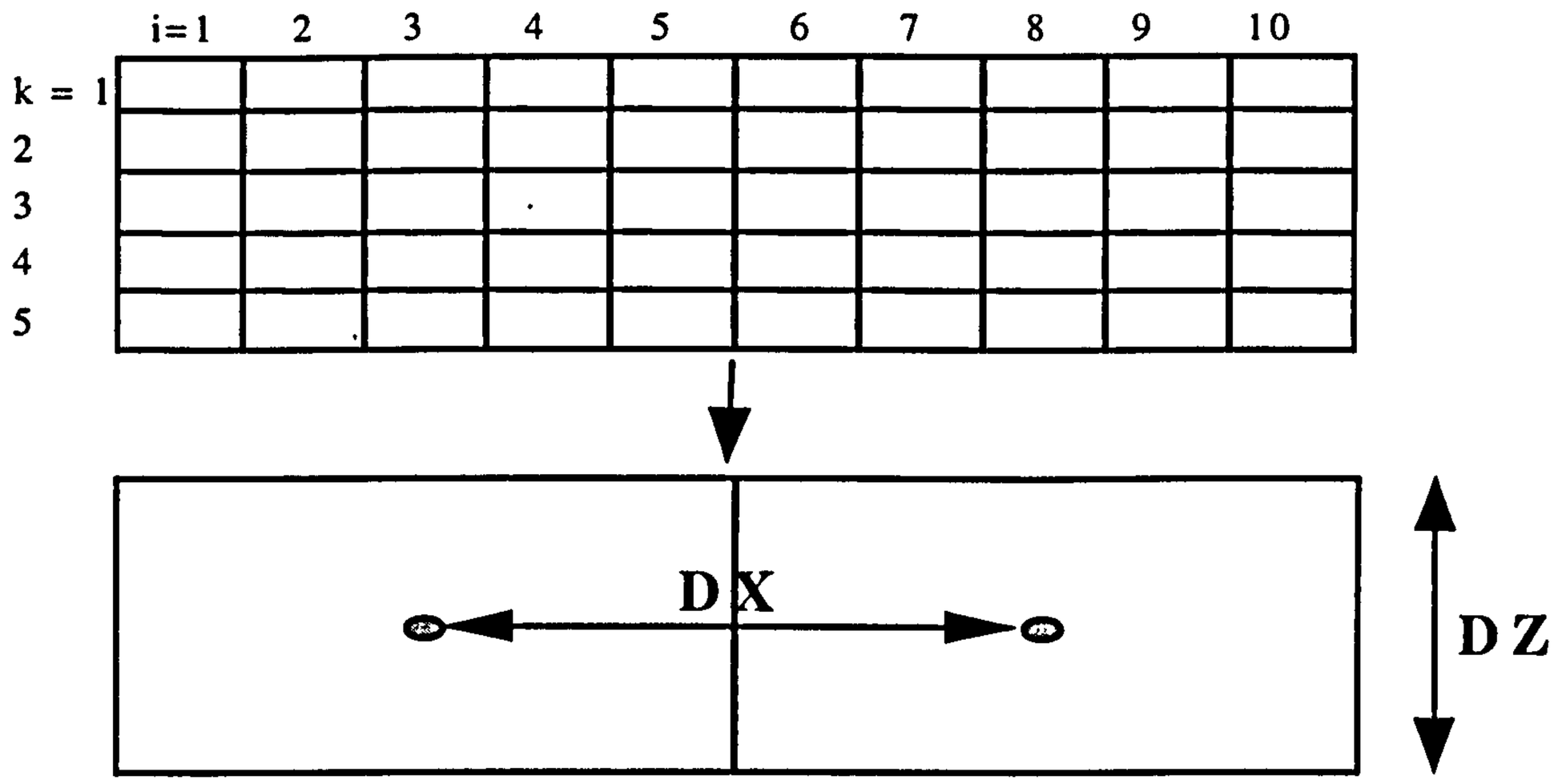

Figure 2.5: Coarsening scheme of the fine grid model in the case of x-direction flow in the 2D vertical cross-sectional model.

2.5.1 The Kyte and Berry Method

In the Kyte and Berry method, the flow rate, q_p, of phase p in the fine and the coarse grid blocks was matched by summing the respective phase fluid flow rates over the fine grid blocks located at the coarse grid block boundary; see Figure 2.5 above.

$$\overline{q_p} = \sum_{k=1}^{5} [q_{pk}]_{i=5} \tag{2.28}$$

Furthermore, the coarse grid pressures are estimated from the fine grid pressures and then used to calculate the fluid potential difference between the coarse grid blocks. Note that the potential gradient was found by *first* taking the average potentials in the coarse blocks and *then* taking the difference to calculate the $\overline{\Delta\Phi_p}$. This phase potential difference was then used to solve Darcy's Law in order to obtain the (pseudo)

relative permeability function for each fluid phase in the coarse grid blocks as shown as follows:

$$\overline{k_{r_p}} = \frac{-\overline{\mu_p}.\overline{q_p}.\Delta X}{\Delta Z.\Delta Y.\overline{k_x}.\overline{\Delta\Phi_p}} \qquad (2.29)$$

The pseudo potential difference was given by the following equations

$$\overline{\Delta\Phi_p} = \overline{\Delta P_p} - g.\rho_p.\Delta D \qquad (2.30)$$

where the averaged pseudo phase pressure is :

$$\overline{P_p} = \frac{\sum_{k=1}^{5}\left[k_k.krp_k.dz_k(P_{pk} - g.\rho_p.(D_k - D))\right]_{i=3}}{\sum_{k=1}^{5}[k_k.krp_k.dz_k]_{i=3}} \qquad (2.31)$$

From Equation (2.31), we can see that the Kyte and Berry method uses the product of phase relative permeability times the absolute permeability times layer thickness as a weighting factor to average the respective fluid pressures.

To be meaningful, the derived pseudo relative permeability must be related to the averaged saturation in the coarse block. In this case, the saturation was averaged using pore volume weighting over the entire fine grid blocks to give the following value in a coarse gridblock.

$$\overline{S_p} = \frac{\sum_{k=1}^{5}\sum_{i=1}^{5} S_{pik}.PV_{ik}}{\sum_{k=1}^{5}\sum_{i=1}^{5} PV_{ik}} \qquad (2.32)$$

By summing the respective flow rate of each fluid only at the downstream boundary grid blocks of the coarse grid while averaging the saturation over the entire coarse grid block, numerical dispersion is minimized. This is one of the most important ideas that Kyte and Berry introduced in their method, as the actual title of their paper implies.

2.5.1.1 The Modified Kyte and Berry Method Used in the Pseudo Program

As mentioned in the introductory chapter, the *Schlumberger Geoquest's Pseudo* program was used to generate the Kyte and Berry pseudo relative permeability and capillary pressure throughout this research study. In this software, the Kyte and Berry method is modified. To avoid problems related to the generation of pseudo capillary pressure even when the fine grid capillary pressure is zero (Barker and Dupouy, 1999), two distinct pressure averages are defined.

To calculate the pseudo relative permeability, the original pseudo phase pressure equation is used as shown in Equation (2.31). However, to calculate the pseudo capillary pressure this equation was modified to be:

$$\overline{P_p} = \frac{\sum_{k=1}^{5}\left[PV_k\left(P_{pk} - g.\rho_p.(D_k - D)\right)\right]_{i=3}}{\sum_{k=1}^{5}[PV_k]_{i=3}} \tag{2.33}$$

where PV is the pore volume and pseudo capillary pressure is defined by:

$$P_c = P_{nw} - P_w \tag{2.34}$$

From these two equations, it is obvious that the *Geoquest's Pseudo* program will set the pseudo capillary pressure to zero if the fine grid capillary pressure is zero.

2.5.2 The Stone Method

In the method proposed by Stone (1991), the average fluid flow rates and saturations were determined in the same way as in the Kyte and Berry method using Equations (2.28) and (2.32) respectively. However, instead of solving Darcy's equation which requires the determination of the fluid potential difference at the coarse grid level, the Stone method uses a fractional flow formulation that requires (i) the averaged fractional flow, $\overline{f_p}$ and (ii) the averaged total pseudo mobility, $\overline{\lambda_t}$. These two quantities were found using the following equations:

$$\overline{f_p} = \frac{\overline{q_p}}{\overline{q_t}} = \frac{\sum_{k=1}^{5}[q_t.f_p]_{i=5}}{\sum_{k=1}^{5}[q_t]_{i=5}} \tag{2.35}$$

$$\overline{\lambda_t} = \frac{\sum_{k=1}^{5}[T_{xk}.\lambda_{tk}]_{i=5}}{\sum_{k=1}^{5}[T_{xk}]_{i=5}} \tag{2.36}$$

From the above, the Stone pseudo relative permeability for phase p was then calculated using Equation (2.37) below:

$$\overline{k_{rp}} = \overline{\mu_p}.\overline{f_p}.\overline{\lambda_t} \tag{2.37}$$

2.5.2.1 The Modified Stone Method Used in the Pseudo Program

Again, the *Geoquest's Pseudo* program was used to generate the Stone pseudo functions throughout this research study. As we can see in the original Stone method, Equation (2.35) is solved in order to obtain the average fractional flow. In this equation, the fine grid fractional flow is defined using the mobility terms as $f_p = \lambda_p / \lambda_t$, with $\lambda_p = k_{rp}/\mu_p$. Using this equation, the resulting pseudo functions are constrained to be in the range of 0 to 1.

One of the weakness of constraining the calculated pseudos to be in the range of 0 to 1 is that it will result in insufficient oil phase pseudo relative permeability prior to breakthrough (Suzuki, 1999). Realizing this weakness, this program adjusts Equation (2.35) to be:

$$\overline{f_p} = \frac{\overline{q_p}}{\overline{q_t}} = \frac{\sum_{k=1}^{5}[q_p]_{i=5}}{\sum_{k=1}^{5}[q_t]_{i=5}} \tag{2.38}$$

Although Equations (2.38) and (2.35) are the same by the definition of fractional flow, their usage can lead to a different answer. Using Equation (2.38), the resulting pseudo functions can yield out of range pseudos (pseudos that are more than 1) if counterflow

exists between phases. By adopting this equation, it will guarantee sufficient oil phase mobility prior to breakthrough in the coarse grid models.

2.5.3 The Hewett and Archer (HA) Method

This method also solves Darcy's equation to obtain the pseudo relative permeability as shown in these two equations.

$$\overline{q_o} = \frac{\overline{T_x}.\overline{k_{ro}}}{\overline{\mu_o}}.\overline{\Delta\Phi_o} \tag{2.39}$$

$$\overline{q_g} = \frac{\overline{T_x}.\overline{k_{rg}}}{\overline{\mu_g}}.\left[\overline{\Delta\Phi_o} + \overline{\Delta P_c} - \Delta\rho g\,\overline{\Delta h}\right] \tag{2.40}$$

where overbar indicates the averaged properties for the coarse grid blocks.

Conceptually, this method computes individual phase mobilities in each streamtube segment whose geometry is defined by the fine grid cells at the coarse grid block outlet face. One streamtube is defined for each of the fine grid cells comprising the coarse grid block outlet face and each streamtube consists of all streamlines passing through one fine grid block outlet face. These streamtubes are based on the total volumetric flowrate, since this is the only conserved quantity in unsteady multi-phase flow. The individual phase mobilities for each of these streamtubes are then calculated in the segments which are between the iso-potential lines running through the centers of the coarse grid block n and the one next to it, (n+1).

However in the real calculation of the pseudo functions, they never actually calculate the geometry of these streamtubes or define the location of the iso-potential lines except at the coarse grid blocks centers. Indeed, the HA method simply takes the potential in the fine grid block located at the center of the coarse grid block. Thus, what are required from the fine grid solutions are only:

(i) the phase fluxes from each of the fine grid cells comprising the outlet face of the coarse grid blocks,

(ii) the oil phase potentials in the fine grid cells containing the coarse grid block centers,

(iii) the capillary pressure in the same fine grid cells,

(iv) the elevation difference in the coarse grid cell centers, and

(v) the porosity weighted averaged saturation of the coarse grid blocks.

Having all the required fine grid information above, the respective fluid flow rates were obtained using the same equation as the previous two methods (Equation 2.28). The only difference between this method and the Kyte and Berry method is the way they defined the averaged fluid potential difference. In this method, the oil potential differences were simply taken as the difference in oil phase potential of the fine grid cell located at the coarse grid centers. On the other hand, the gas potential difference was calculated using Equation (2.41) below:

$$\overline{\Delta\Phi_g} = \overline{\Delta\Phi_o} + \overline{\Delta P_c} - \Delta\rho g\overline{\Delta h} \qquad (2.41)$$

where $\overline{\Delta P_c}$ is the difference in capillary pressure between grid block n and n+1, and $\overline{\Delta h}$ is the difference in elevation between these two grid blocks. Both of these values are taken at the fine grid block located at the center of the coarse grid blocks.

2.6 SUMMARY AND CONCLUSIONS

The gravity dominated vertical equilibrium pseudo functions are based on the assumption of rapid vertical segregation of fluids by gravity compared with the changes in fluid saturation due to horizontal fluid movement (i.e. there is a low viscous to gravity ratio). This assumption may be valid in the gas displacement processes that we consider. The resulting pseudo functions using this technique are independent from initial and boundary conditions: they are intrinsic properties of the rock-fluid system i.e. true "effective properties".

When the simulation run is in a steady-state condition, steady-state upscaling methods can be used. By "steady-state" we mean that the saturations in each of the grid blocks are constant with time. In general, there are two types of steady-state pseudo generation methods that depend on the balance of capillary and viscous forces in the models. However, since both of the steady-state methods that are mentioned above ignore the effect of gravitational force which is important in the cases that we consider (gas displacement processes), we do not attempt to use these methods in our work.

Unlike the VE methods, dynamic pseudo functions have been developed to upscale models where there are sufficiently high viscous forces that vertical equilibrium assumptions do not apply, although the gravitational force is also important. Summary

of the methodologies and formulae used by the Kyte and Berry (1975), the Stone (1991) and the Hewett and Archer (1997) methods are presented in Table 2.1 through Table 2.3 respectively. The mathematical derivation for all the three methods was actually performed in oil-water displacement where gravity may not be the dominant effect. The investigation on the use and validity of these three widely used pseudo-isation methods (together with the vertical equilibrium pseudo functions) in a gas-oil displacement is the prime objective for the following chapter. This will provide a more stringent test of the various upscaling methods due to the large effect of gravity forces and problems with gas channelling and/or fingering due to the difference in fluid densities and unfavorable mobility ratio.

Furthermore, in the following chapter, we will propose a novel method that is specifically designed to be used in high gravity cases (gas-oil displacements). It will be shown that this new method will out-perform the two widely used dynamic pseudo-isation methods of Kyte and Berry and Stone as well as the Vertical Equilibrium option in this specific environment.

Method	Methodology	Formulae
The Kyte and Berry method	• The averaged coarse grid flow is equal to the summation of fine grid flows.	$\overline{q_p} = \sum_{k=1}^{5} q_{pk}$ **(2.28)**
	• In calculating the pseudo phase pressure, the product of absolute permeability times respective fluid relative permeability times layer thickness are used as a weighting factors.	$\overline{P_p} = \frac{\sum_{k=1}^{5}\left[k_k.k_{rpk}.dz_k.(P_{pk} - g.\rho_p.(D_k - D))\right]_{i=3}}{\sum_{k=1}^{5}[k_k.k_{rpk}.dz_k]_{i=3}}$ **(2.31)**
	• The averaged fluid potential gradient is obtained by using the derived pseudo phase pressures.	$\overline{\Delta\Phi_p} = \overline{\Delta P_p} - g.\rho_p.\Delta D$ **(2.30)**
	• The pseudo relative permeability is obtained by solving Darcy's equation.	$\overline{k_{rp}} = \frac{-\overline{\mu_p}.\overline{q_p}.\Delta X}{\Delta Y.\Delta Z.\overline{k_x}.\overline{\Delta\Phi_p}}$ **(2.29)**
	• The averaged saturation is obtained by using pore volume weighted averaged over the entire fine grid blocks that correspond to the coarse grid blocks.	$\overline{S_p} = \frac{\sum_{k=1}^{5}\sum_{i=1}^{5} S_{pik}.PV_{ik}}{\sum_{k=1}^{5}\sum_{i-1}^{5} PV_{ik}}$ **(2.32)**

Table 2.1: Summary of the mathematical formulae used by the Kyte and Berry method

Method	Methodology	Formulae
The Stone method	• The averaged flow rates and saturation are defined the same way as the Kyte and Berry method. (Eq. 2.28 and Eq. 2.32 respectively) • Compute the fractional flow in the coarse grid model.	$\overline{f_p} = \frac{\overline{q_p}}{\overline{q_t}} = \frac{\sum_{k=1}^{5}[q_p]_{i=5}}{\sum_{k=1}^{5}[q_t]_{i=5}}$ **(2.38)**
	• Compute the total pseudo mobility using the transmissibility as a weighting factor.	$\overline{\lambda_t} = \frac{\sum_{k=1}^{5}[T_{xk}.\lambda_{tk}]_{i=5}}{\sum_{k=1}^{5}[T_{xk}]_{i=5}}$ **(2.36)**
	• Solve fractional flow formulation to obtain the pseudo relative permeability.	$\overline{k_{rp}} = \overline{\mu_p}.\overline{f_p}.\overline{\lambda_t}$ **(2.37)**

Table 2.2: Summary of the mathematical formulae used by the Stone method

Method	Methodology	Formulae
The Hewett and Archer method	• The averaged flow rates and saturation are defined the same way as the Kyte and Berry method (Eq.2.28 and Eq. 2.32 respectively) • Compute the pseudo oil potential gradients using fine grid oil potential located at the centre of the coarse grid domain (2.41a). • The gas potential gradients were calculated using equation (2.41) where $\overline{\Delta P_c}$ is the difference in capillary pressure between grid block n and n+1, and $\overline{\Delta h}$ is the difference in elevation between these two grid blocks. Both of these values are taken at the fine grid block located at the centre of the coarse grid blocks. • Solve Darcy's law to obtain the pseudo relative permeability. (Eq. 2.29)	$\Delta\Phi_o = [\Phi_o]_{i=8,k=3} - [\Phi_o]_{i=3,k=3}$ **(2.41a)** $\overline{\Delta\Phi_g} = \overline{\Delta\Phi_o} + \overline{\Delta P_c} - \Delta\rho g\overline{\Delta h}$ **(2.41)**

Table 2.3: Summary of the mathematical formulae used by the Hewett and Archer method

CHAPTER 3

DEVELOPMENT AND VALIDATION OF THE NEW TW METHOD

3.1 GENERAL REMARKS

This chapter centers on the development and validation of a new alternative method for calculating dynamic pseudo functions known as the Transmissibility Weighted (TW) method. This novel method has been specifically formulated to handle cases with high gravity, which are normally encountered in gas displacement processes. In our study of a range of upscaling techniques, it is evident that the application of these methods to upscale gas-oil systems is more difficult than for water-oil systems. This may be expected due the large mobility differences and the increased gravitational force. Because of this increased difficulty, we may turn the problem round and use gas-oil immiscible displacements as "difficult" problems, which can help us to carry out more rigorous testing of the various upscaling methods.

Pseudo functions do have costs and limitations associated with them. For example, Stone (1991) discussed the limitations of using vertical equilibrium pseudo functions. Several other authors have also recently shown that dynamic pseudo functions may

also have problems. Guzman *et al.* (1994) and Barker and Thibeau (1996) discussed some inconsistencies in the Stone method for handling gravity terms in both the fine and the coarse grid blocks which may be a severe limitation on the use of this approach for the gas injection cases. Barker and Thibeau (1996) also discussed several other problems in using dynamic pseudo methods relating to other pseudo generation methods. Among others, the problems that were discussed by Barker and Thibeau (1996) include the need to use (i) directional pseudo relative permeability if the coarse grid models have more than a single dimension, (ii) non realistic pseudo relative permeability, e.g. pseudos that are bigger than one or smaller than zero, and (iii) non-monotonic pseudos, etc.

Furthermore, most of the recently reported works on dynamic upscaling methods, such as the Kyte and Berry (1975), the Stone (1991) and the Hewett and Archer (1997) methods, have been performed using oil-water displacements where gravity may not be the dominant effect. The use and validity of these pseudo methods is investigated in this chapter for gas-oil displacements. This is expected to provide a more stringent test of the various upscaling methods due to the large effect of gravity forces and problems with gas channeling and/or fingering due to the difference in fluid densities and unfavorable mobility ratios.

The results reported in this chapter show that the Kyte and Berry method produces larger errors compared with the Stone method in non-dipping, gas-oil systems. The Stone method is found to be very poor in dipping systems. An alternative modified

Kyte and Berry approach (the Transmissibility Weighted - TW method) is proposed and tested for a range of gas-oil displacements where it is compared with the performance of the Kyte and Berry, the Stone, the Hewett and Archer and the VE methods. In almost all cases, the TW method out-performs (or performs equally well as) the other more commonly used pseudo function methods; only in one case does the Kyte and Berry method performs slightly better than the TW approach.

Comparing the results of the TW method and the Hewett and Archer method show a number of similarities. A detailed discussion of these two methods is presented in the following chapter.

3.2 DEVELOPMENT OF THE TW METHOD

A new method known as the Transmissibility Weighted (TW) method is proposed in this section. This method follows exactly the same approach as the Kyte and Berry method (Section 2.5.1) except in the averaging of the fluid potential difference at the coarse grid level. Using the same notation as in Figure 2.5, Darcy's law was applied in order to obtain the pseudo relative permeability for each of the fluid phases in the coarse grid blocks. As usual, an over bar will be used to denote the quantities evaluated at the coarse grid scale:

$$\overline{k_{rp}} = \frac{-\overline{\mu_p}.\overline{q_p}.\Delta X}{\Delta Y.\Delta Z.\overline{k_x}.\overline{\Delta\Phi_p}} \qquad (3.1)$$

where $\overline{\mu_p}$, $\overline{q_p}$ and $\overline{\Delta\Phi_p}$ are the average phase viscosity, total phase flow rate and fluid potential difference of phase p, respectively; ΔX, ΔY and ΔZ are the coarse grid block dimensions in the x-, y- and z-directions. The flow rates of individual fluid phases in the fine and the coarse grid blocks were matched by summing the respective phase flow rates over the fine grid blocks located at the coarse grid block boundary as shown below:

$$\overline{q_p} = \sum_{k=1}^{5} [q_{pk}]_{i=5} \tag{3.2}$$

The averaged potential difference, $\overline{\Delta\Phi_p}$ in the TW method is defined as:

$$\overline{\Delta\Phi_p} = \frac{\sum_{k=1}^{5} [T_{xk} . \Delta\Phi_{pk}]_{i=3}}{\sum_{k=1}^{5} [T_{xk}]_{i=3}} \tag{3.3}$$

where $\Delta\Phi_{pk}$ is given by the following equation

$$\Delta\Phi_{pk} = [\Phi_{pk}]_{i=8} - [\Phi_{pk}]_{i=3} . \tag{3.4}$$

As a technique to control numerical dispersion, we adopt the same strategy as the Kyte and Berry method. We make the summation of each respective fluid flow rates only at fine grid blocks located at the coarse grid block down-stream boundary (Equation 3.2), but the averaged saturation was obtained from the entire domain of the coarse grid block using pore volume weighted as shown below:

$$\overline{S_p} = \frac{\sum_{k=1}^{5}\sum_{i=1}^{5} S_{pik} . PV_{ik}}{\sum_{k=1}^{5}\sum_{i=1}^{5} PV_{ik}} \tag{3.5}$$

This again minimizes the numerical dispersion in our coarse grid model.

The rationale for the TW method is that we do not want to average the fluid potential differences in the coarse grid blocks by first calculating the average fluid potentials in each of the coarse grid blocks and then taking the difference between them. Rather, we calculate a weighted average of the fluid potential gradients between the coarse blocks directly from the fine grid gradients. In this context, when these pressure gradients are the same (or similar), this method will give results which are the same as (or close to) the Kyte and Berry approach. It is only when there are significantly different potential gradients in the various grid layers that differences are seen. Furthermore, it appears that the selection of transmissibility as the weighting factor in averaging the fluid potential gradients is more appropriate compared to the selection of relative permeability times layer thickness times absolute permeability as in the Kyte and Berry method especially in the gravity dominated cases.

3.3 NUMERICAL TESTING OF THE METHODS

At this stage, we go on to validate the TW method and compare it with the four most widely used pseudo generation methods namely:

i. the Kyte and Berry method,

ii. the Stone method,

iii. the Hewett and Archer method, and

iv. the vertical equilibrium (VE) method.

Cross sectional models of 100 x 1 x 5 were used to evaluate these upscaling methods. These fine grid models were then upscaled to a 1D model with a grid dimension of 20 x 1 x 1, which meant that every coarse grid block contained 25 fine grid blocks as shown in Figure 3.1 below:

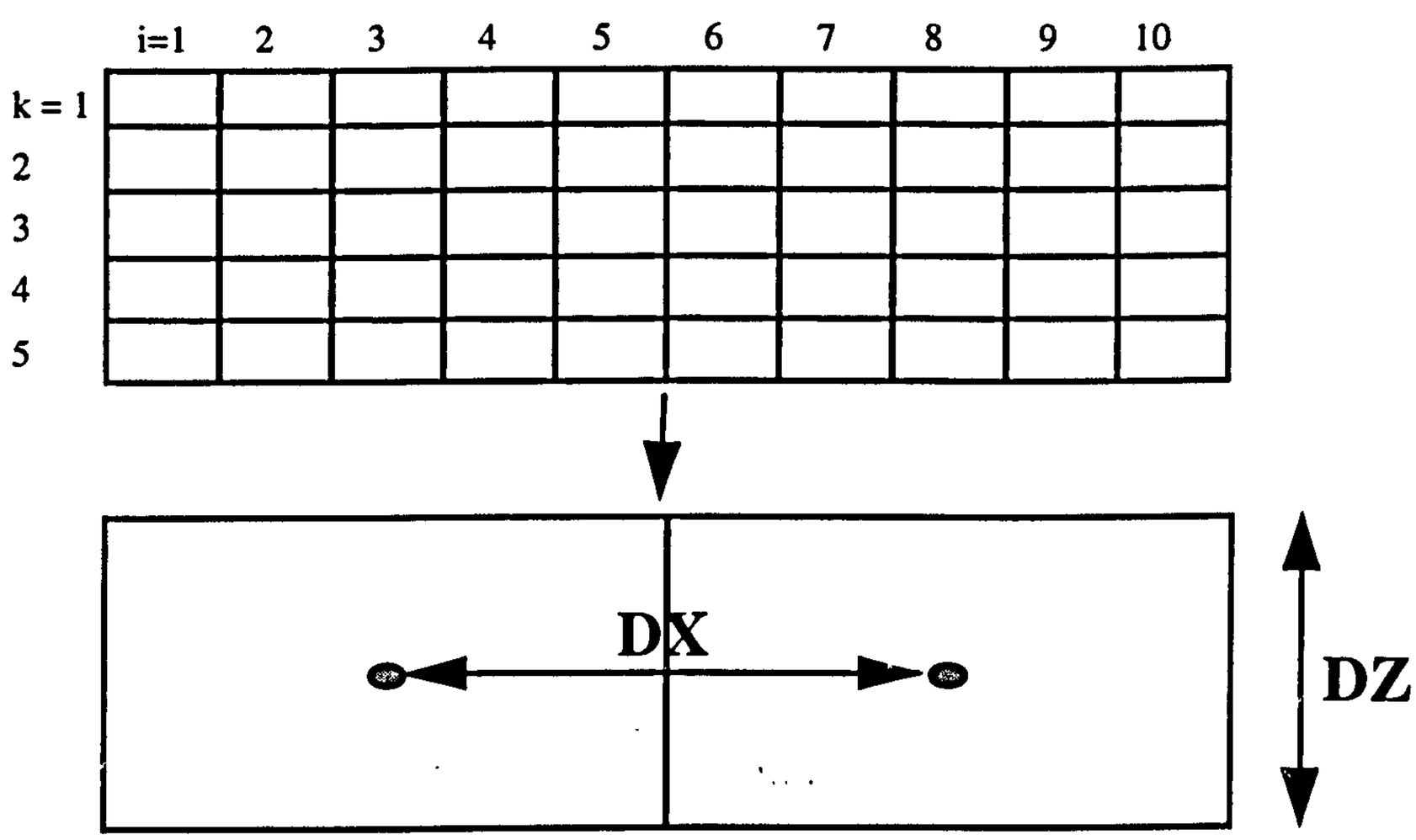

Figure 3.1: Schematic diagrams showing the fine and the coarse grid models for the first two coarse grid blocks.

The initial properties of the fine grid blocks are as follows:

Porosity, $\phi = 0.2$;
Grid block sizes, DX = DY = DZ = 25 ft. (7.63 m)
Viscosities, $\mu_o = 10$ cp ; $\mu_g = 0.1$ cp
Densities, Oil, $\rho_o = 43.68$ lb/ft^3 (700 Kg/m^3);
Gas $\rho_g = 0.06243$ lb/ft^3 (1.0 Kg/m^3)

The fluids were assumed to be incompressible and immiscible. The rock relative permeabilities were power law curves, given by the following two equations from Guzman *et al.* (1994):

$$k_{ro} = ((1-S_g - S_{org} - S_{wc}) / (1 - S_{wc} - S_{org}))^{2.7}$$

$$k_{rg} = ((S_g - S_{gc}) / (1 - S_{gc} - S_{wc}))^{5.0}$$

where S_{wc} = 0.15 (connate water saturation), S_{gc} = 0.05 (connate gas saturation) and S_{org} = 0.1 (residual oil saturation relative to gas). Figure 3.2 shows these curves graphically. Gas was injected from an injector located at the left of the model and dead oil was produced from a well on the right of the model. Both wells were completed vertically throughout the model and the injection rate was set to give a frontal velocity of 0.3 m/d.

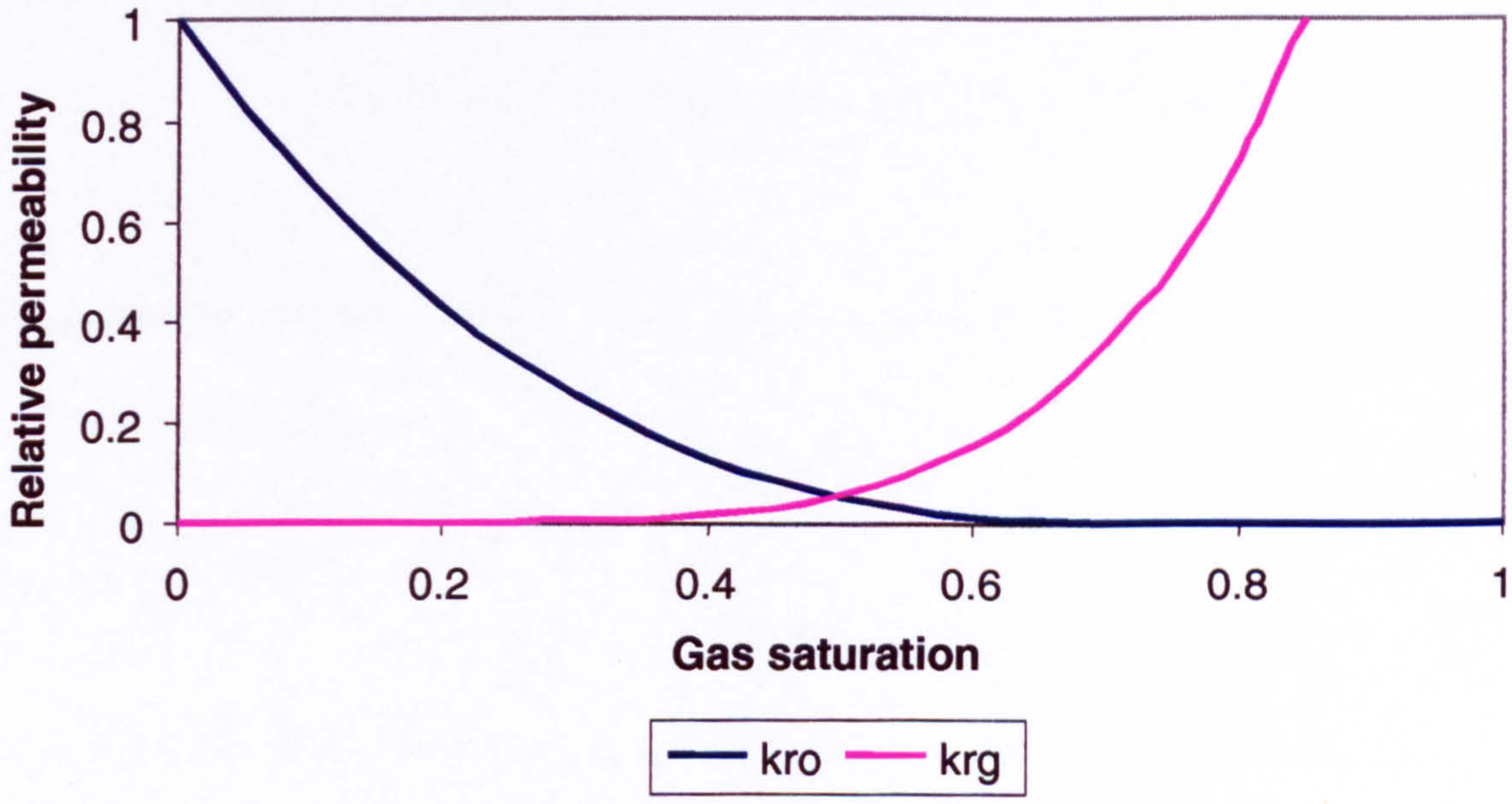

Figure 3.2: Relative permeability used in the fine grid models

To test and evaluate the five upscaling methods discussed above (the VE, the Kyte and Berry, the Stone, the Hewett and Archer and the TW), seven cases were developed as summarized in Table 3.1. Cases 1 and 2 were designed to evaluate the five pseudo methods in models with free crossflow between layers. Cases 3 and 4 are used to

examine models where the crossflow between layers was restricted by barriers. Furthermore, Cases 5, 6 and 7 were constructed to test the performance of the upscaling methods in a dipping reservoir, with low gravity (high viscous forces) and high gravity (low viscous forces) cases, respectively.

Cases	Perm layer 1-2 (mD)	Perm layer 3-5 (mD)	k_v/k_h	Dip	Mobility ratio	$\Delta\rho$ (Kg/m^3)	N_{gv}
Case1	500	10	1	0	100	699	0.0958
Case2	10	500	1	0	100	699	0.0649
Case3	500	10	0	0	100	699	0.0
Case4	10	500	0	0	100	699	0.0
Case5	500	500	1	15°	100	699	-
Case6	500	500	1	0	100	≈ 0	0.0003
Case7	500	500	1	0	10	≈ 700	19.754

Table 3.1: Case description for Case 1 to Case 7

The gravity to viscous ratio (N_{gv}) was calculated using the equation given by Zhou *et al.* (1993) as follows:

$$N_{gv} = \frac{\Delta\rho g L k_{av}}{H q \mu_o} \tag{3.6}$$

where $\Delta\rho$ is the difference in the fluid densities, g is the gravitational constant, L is the reservoir length, k_{av} is the average vertical permeability, H is the reservoir thickness, q is the total Darcy flow velocity and μ_o is the oil viscosity.

These cases were developed to test a range of flow conditions from viscous to gravity dominated along with cases where both forces are significant. The test objective of each case is summarized in Table 3.2 below:

CASE	OBJECTIVES / ENVIRONMENTS
CASE 1	Case where gravity crossflow is not restricted. The flow is expected to be segregated due to poor vertical sweep efficiency.
CASE 2	Reverse of *Case 1*. The flow is more diffused due to improved vertical sweep efficiency.
CASE 3	Gravity crossflow is negligible ($k_v/k_h \sim 0.0$) with gas flowing more at the top of the model due to permeability distribution.
CASE 4	Gravity crossflow is negligible ($k_v/k_h \sim 0.0$) with gas flowing more at the bottom of the model due to permeability distribution
CASE 5	To test the ability of the various upscaling methods in handling a dipping model.
CASE 6	Viscous dominated flow. The flow is expected to be very diffuse (sharp vertical front).
CASE 7	To investigate the ability of the various upscaling methods to handle cases with higher gravity.

Table 3.2: The flow regimes examined by each of the test cases (Case 1 to case 7)

As a quality index, we will use the normalized rms error in oil recovery factor as well as in the produced gas-oil ratio. The normalized rms errors were calculated from the difference in oil recovery factor or the produced gas-oil ratio (using normalized

curves) between the coarse and the fine grid models, over a range of pore volume injected. The equation to calculate rms error is shown below:

$$rms = \sqrt{\frac{\sum_{i=1}^{n}(Rc_i - Rf_i)^2}{n}} \qquad (3.7)$$

where *Rc* is the normalized oil recovery factor (or produced gas-oil ratio) for the coarse grid model, *Rf* is the normalized oil recovery (or produced gas-oil ratio) for the fine grid model and n is the total number of calculated timesteps.

3.4 DISCUSSION OF THE RESULTS

Depending on the reservoir type, it is possible to have a very good recovery as a result of gravity stabilized flow in the reservoir model. On the other hand, it is also possible to have a very poor recovery due to gas channeling through a high permeability streak (unstable front). For gas-oil systems, unfavorable mobility ratio displacements are normally encountered and this type of displacement is liable to both gravity and viscous fingering. The combined effect of these two forces will frequently result in a gravity tongue, travelling along the top of the model and by passing the oil.

3.4.1 Models with Free Crossflow (CASE 1 and CASE 2)

Considering first the cases with good vertical communication (Case 1 and Case 2), the recovery of the model is directly proportional to the vertical sweep efficiency between the two permeability regions. In general, the better the vertical sweep between the regions, the higher the recovery will be. In Case 1, the combined effect of the large

density difference between the oil and the injected gas and the permeability distribution of the model (increasing upwards) will cause the injected gas to crossflow to the top of the model very near to the injector. This effect will definitely reduce the efficiency of the vertical sweep, thus reducing the recovery. It is also worth emphasizing that this will normally result in a segregated flow.

On the other hand, fluid flow in Case 2 (permeability decreasing upwards) is more diffuse since more gas is allowed to flow horizontally at the bottom of the model before being "uplifted" to the top due to gravity. This effect will increase the efficiency of the vertical sweep and thus increase the recovery.

From the plots of the oil recovery factor, the gas-oil ratio and the gas saturation for these two models (Figures 3.3a – 3.3d and 3.4a – 3.4d), the observations can be summarized as follows:

Model	**Recoveries**	**Vertical Sweep Efficiency**	**Flow Pattern**	**Quality of Scaleup Method**
Case 1: Highkup	Low	Low	Segregated	Poor
Case 2: Lowkup	High	High	Diffused	Good

Table 3.3: Summary of performance for Case 1 and Case 2.

Both of the dynamic pseudo methods of the Kyte and Berry and the Stone perform better in Case 2 compared to Case 1. This phenomenon is consistent with our finding regarding the influence of sub-grid properties and the averaged saturation equation, where we found that low variability in gas saturation (diffuse flow) will result in more accurate usage of the pseudo functions. We will discuss this issue in great detail later in Chapter 5. Also, it is interesting to observe that the Stone method performs far better than the Kyte and Berry method especially in matching the fine grid gas-oil ratio performance for these two cases. We will discuss the reason behind the superiority of the Stone method even when the fluid crossflow is not restricted (relatively higher N_{gv}) as shown in these cases in the following chapter.

It is very encouraging to observe that the new TW method also performs better in terms of the produced gas-oil ratio and oil recoveries compared to the Kyte and Berry method although both of them were using the same type of equations (except in averaging the fluid potential difference). On the other hand, the performance of the TW method is equally good when compared to the Stone method for these two cases. In addition, the performance of the Hewett and Archer method also tracks very closely to the TW method.

Although the fluid flow in the vertical direction is not constrained in these two cases (crossflow is essential for gravity segregation of fluids), the VE pseudo functions still failed completely to duplicate the performance of the fine grid model. The strength and weakness of the VE method will be discussed later in Chapter 4.

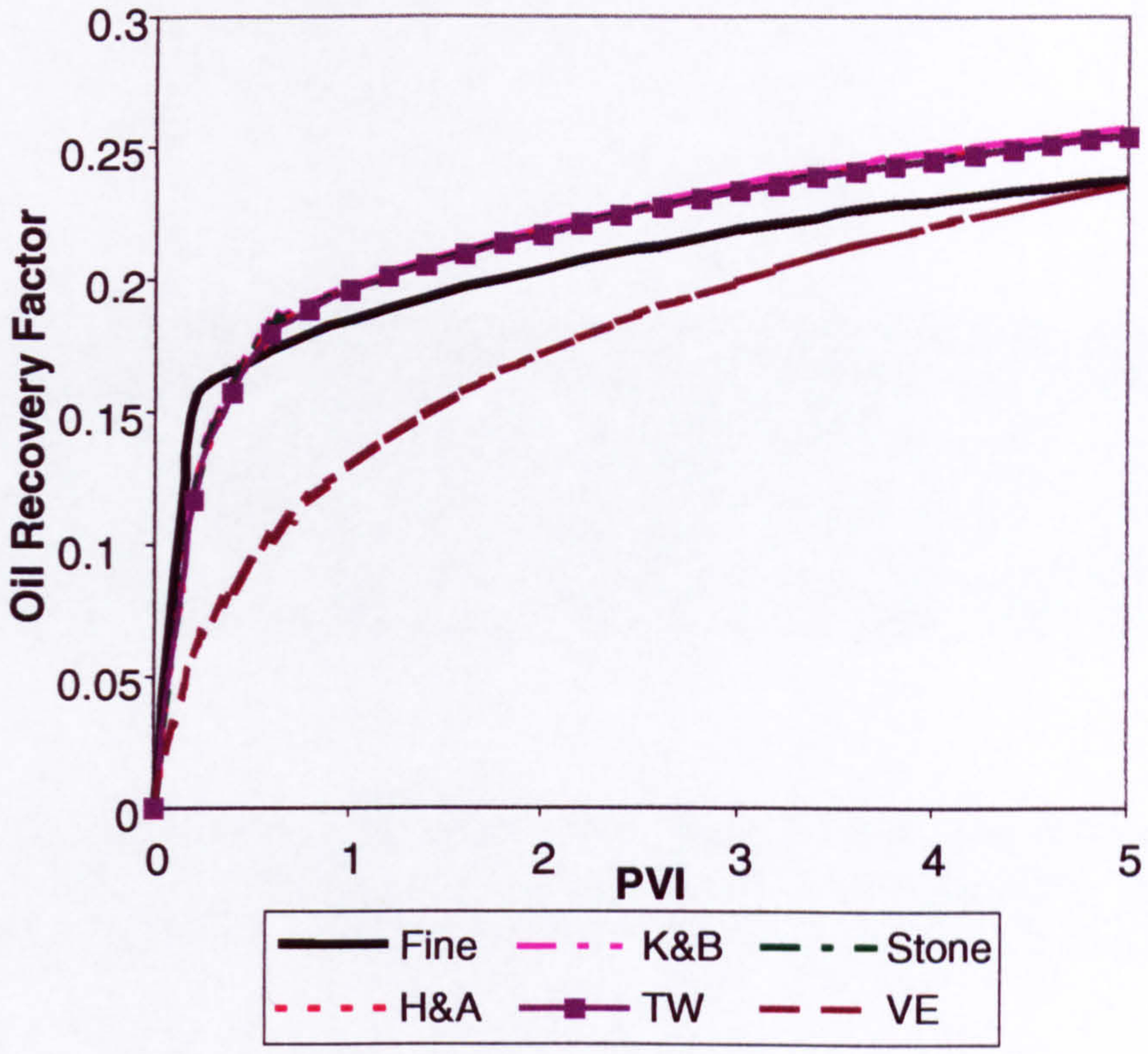

Figure 3.3a: Oil Recovery Factor versus Pore Volume Injected for Case 1: comparison between several upscaling methods

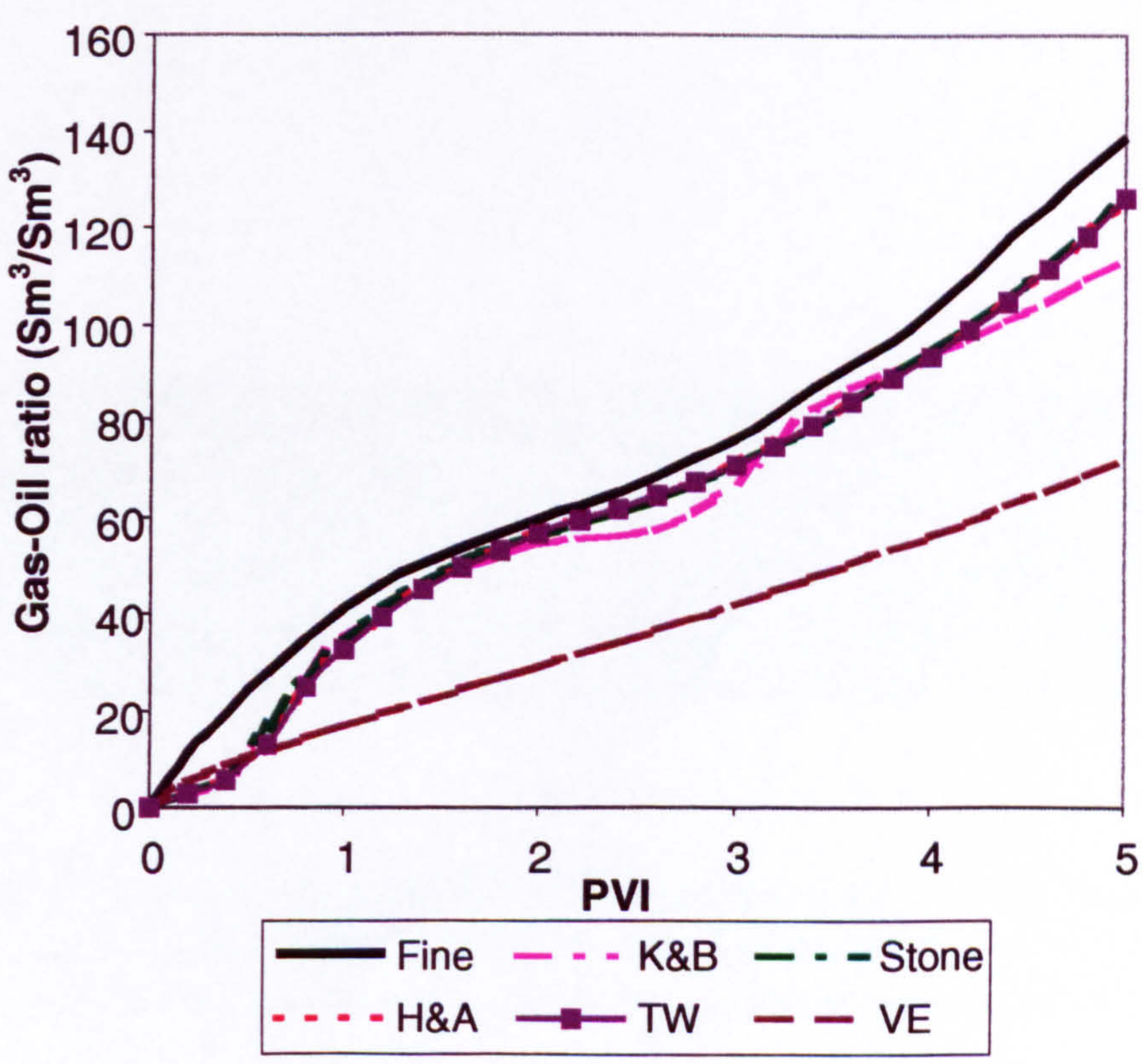

Figure 3.3b: Gas-Oil Ratio versus Pore Volume Injected for Case 1: comparison between several upscaling methods

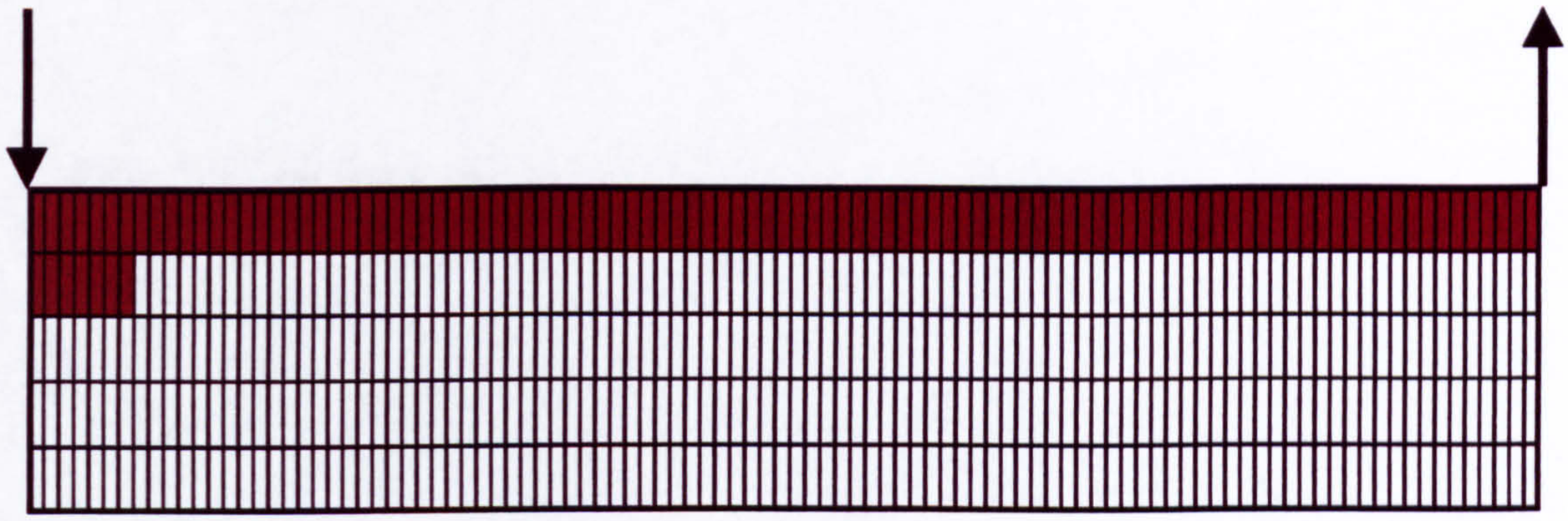

Figure 3.3c: Gas saturation plot after 1 PV injected (Case 1, coarsening upwards model with k_v/k_h equal 1.0); lighter coloured region shows gas saturation between 0.0 to 0.5 whereas darker coloured region shows gas saturation between 0.5 to 0.85.

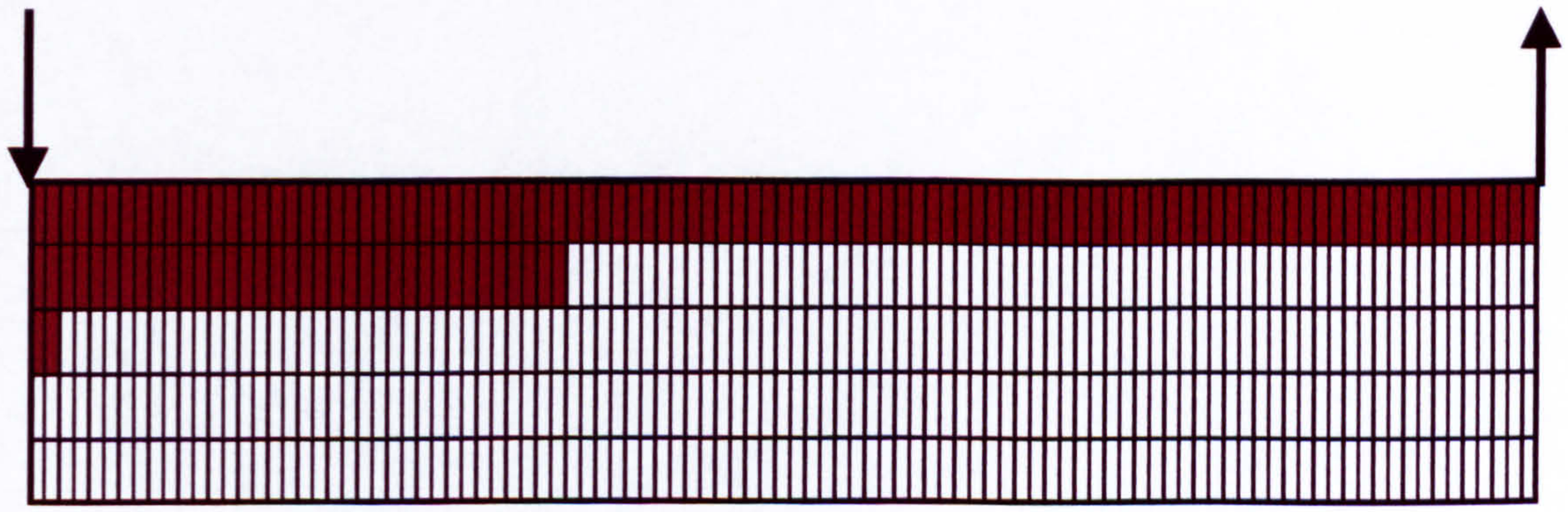

Figure 3.3d: Gas saturation plot after 5 PV injected (Case 1, coarsening upwards model with k_v/k_h equal 1.0)); lighter coloured region shows gas saturation between 0.0 to 0.5 whereas darker coloured region shows gas saturation between 0.5 to 0.85.

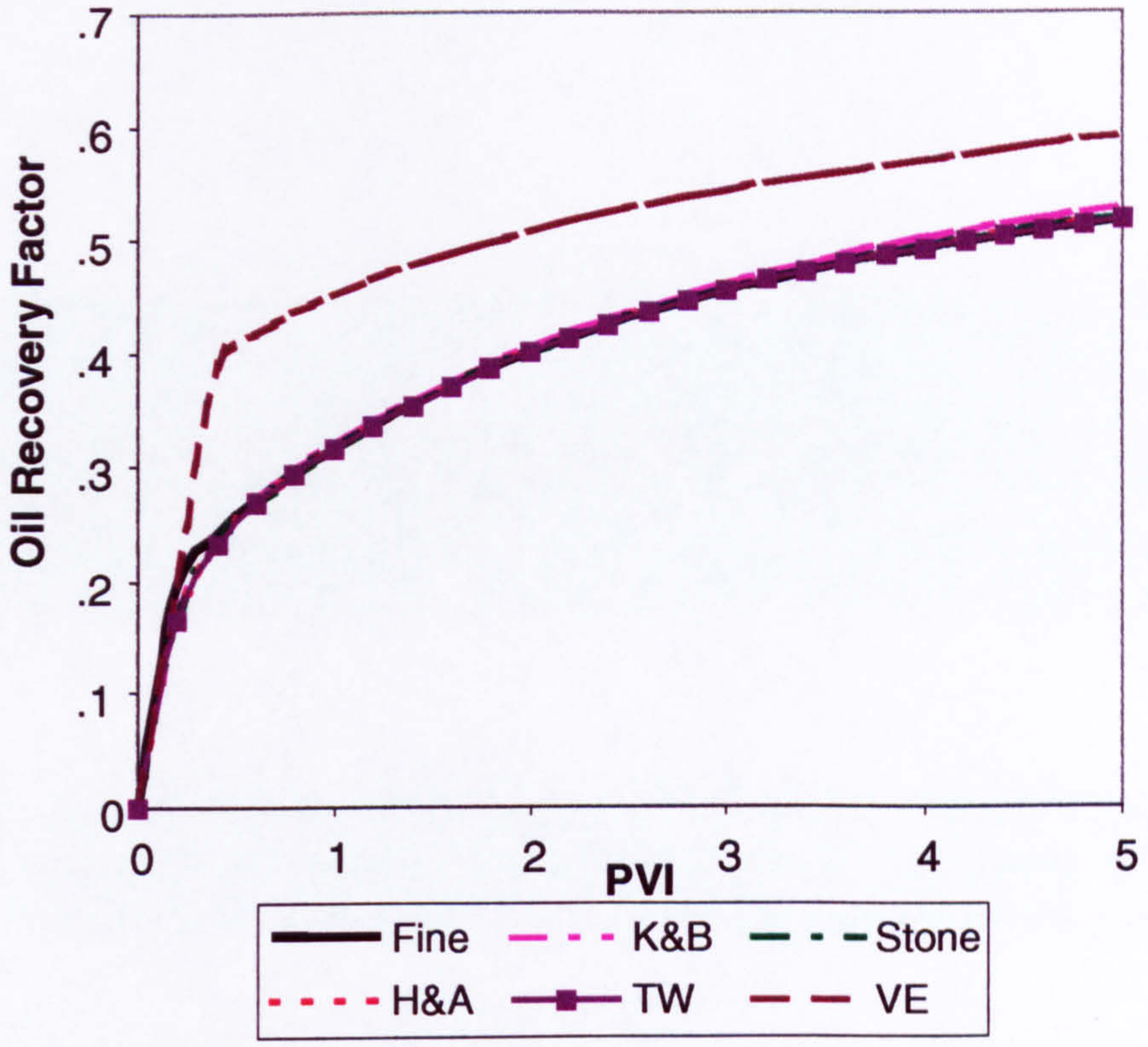

Figure 3.4a: Oil Recovery Factor versus Pore Volume Injected for Case 2: comparison between several upscaling methods

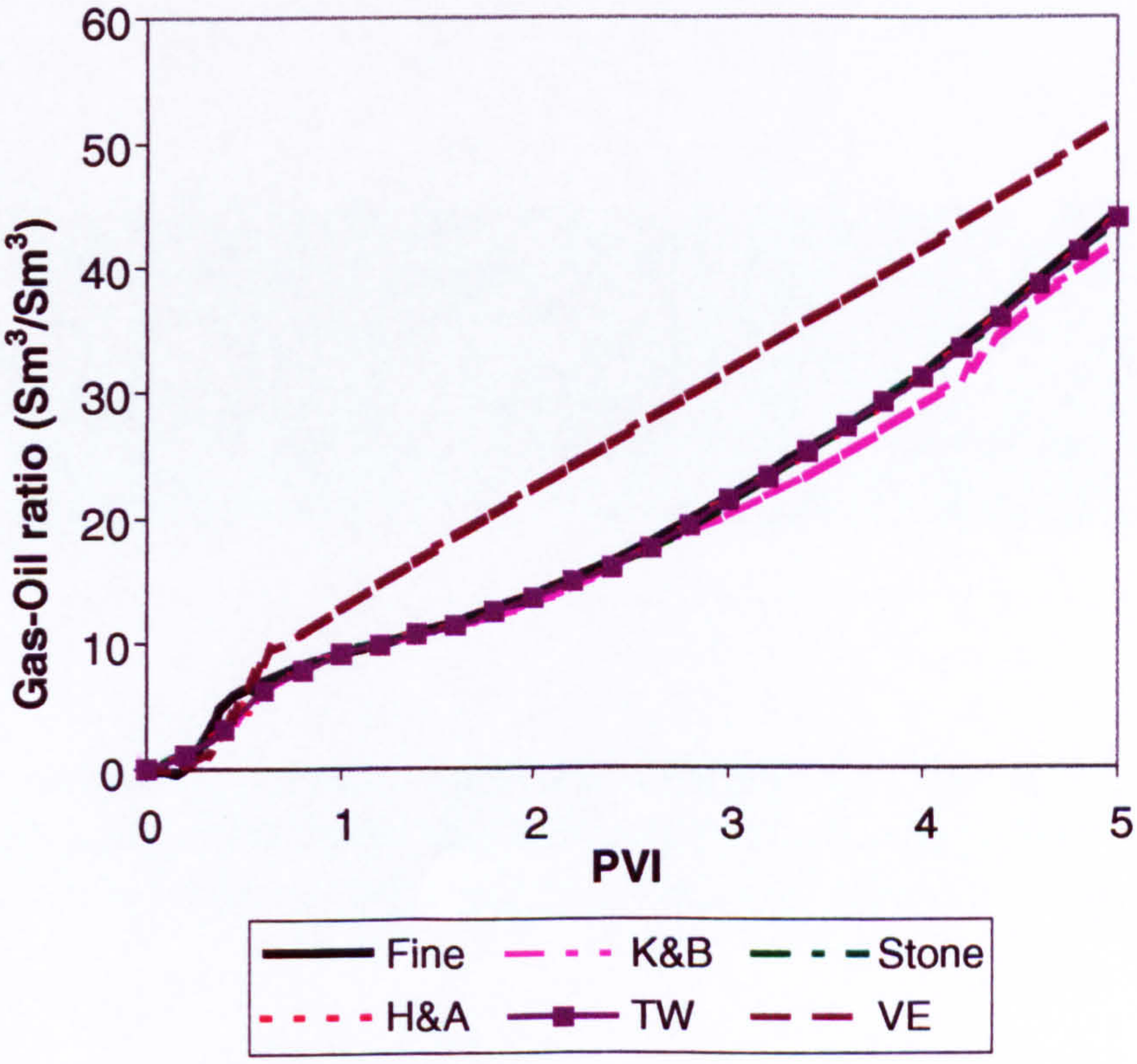

Figure 3.4b: Gas-Oil Ratio versus Pore Volume Injected for Case 2: comparison between several upscaling methods

Figure 3.4c: Gas saturation plot after 1 PV injected (Case 2, fining upwards model with k_v/k_h equal 1.0); lighter coloured region shows gas saturation between 0.0 to 0.5 whereas darker coloured region shows gas saturation between 0.5 to 0.85.

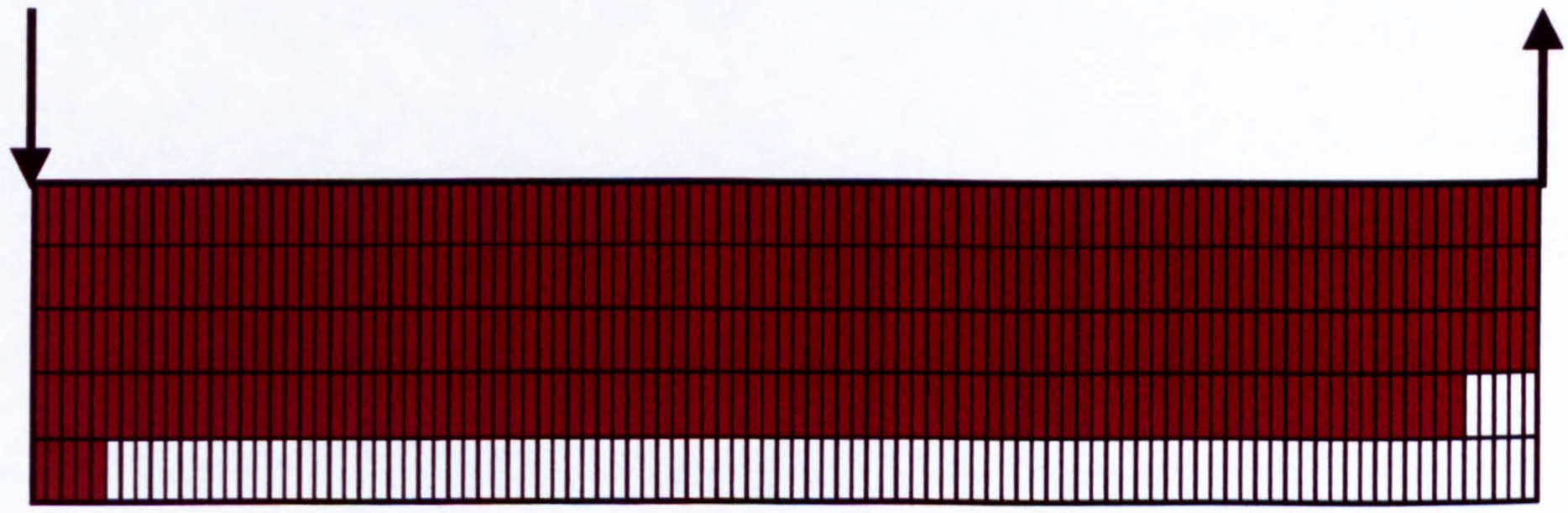

Figure 3.4d: Gas saturation plot after 5 PV injected (Case 2, fining upwards model with k_v/k_h equal 1.0); lighter coloured region shows gas saturation between 0.0 to 0.5 whereas darker coloured region shows gas saturation between 0.5 to 0.85.

3.4.2 Models with Restricted Crossflow (CASE 3 and CASE 4)

Case 3 and Case 4 were designed to further investigate the validity of the upscaling methods in gas-oil systems. Case 3 was designed to produce a segregated flow with more gas flowing at the top while Case 4 was used to test the methods with more gas is flowing at the bottom of the model. In both of these cases, k_v/k_h is set to zero so as to prevent crossflow between the layers. Saturation plots in Figures 3.5c and 3.5d for Case 3 and Figures 3.6c and 3.6d for Case 4 confirmed these conditions.

Comparison made on the oil recovery factor and the produced gas-oil ratio of each of the methods as shown in Figures 3.5a and 3.5b for Case 3 and Figures 3.6a and 3.6b for Case 4 suggest the following:

In Case 3, where more gas is flowing at the top of the model (gas over-riding), the new TW method shows some improvement in matching the produced gas-oil ratio compared to the Stone, the Kyte and Berry and the VE methods. In terms of the normalized rms error in oil recovery factor for this case, all the three dynamic pseudo functions perform rather similarly. As expected, the VE pseudo method again fails in reproducing the fine grid performance. On the other hand, in Case 4 where gas is under-running, the Kyte and Berry method performs better than the Stone or TW methods especially in predicting the produced gas-oil ratio as shown in Figure 3.6b. The same performance trends as in Case 3 were observed in comparing these pseudo methods in terms of oil recovery factor i.e. all the three dynamic pseudo functions show a rather similar performance.

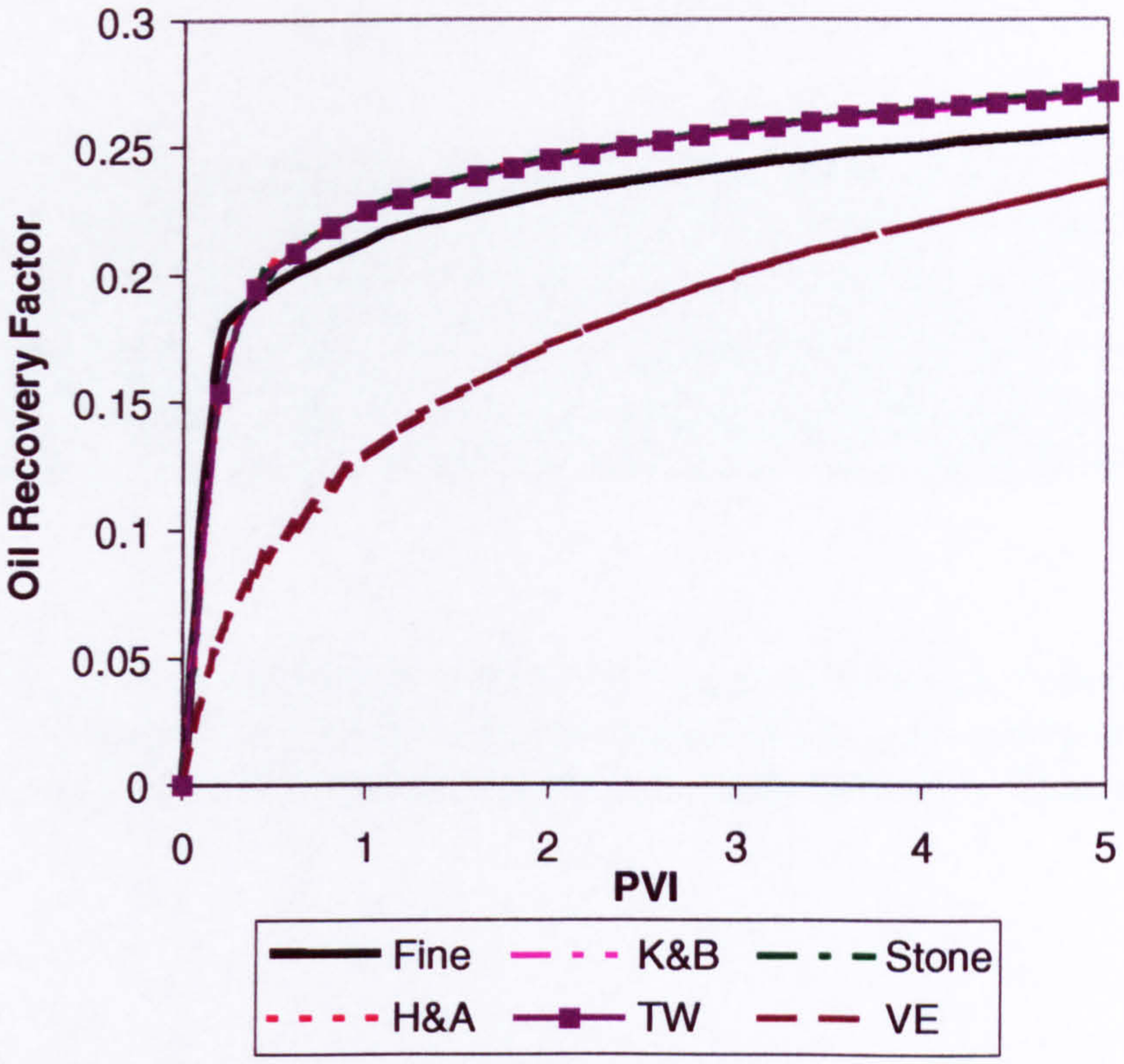

Figure 3.5a: Oil Recovery Factor versus Pore Volume Injected for Case 3: comparison between several upscaling methods

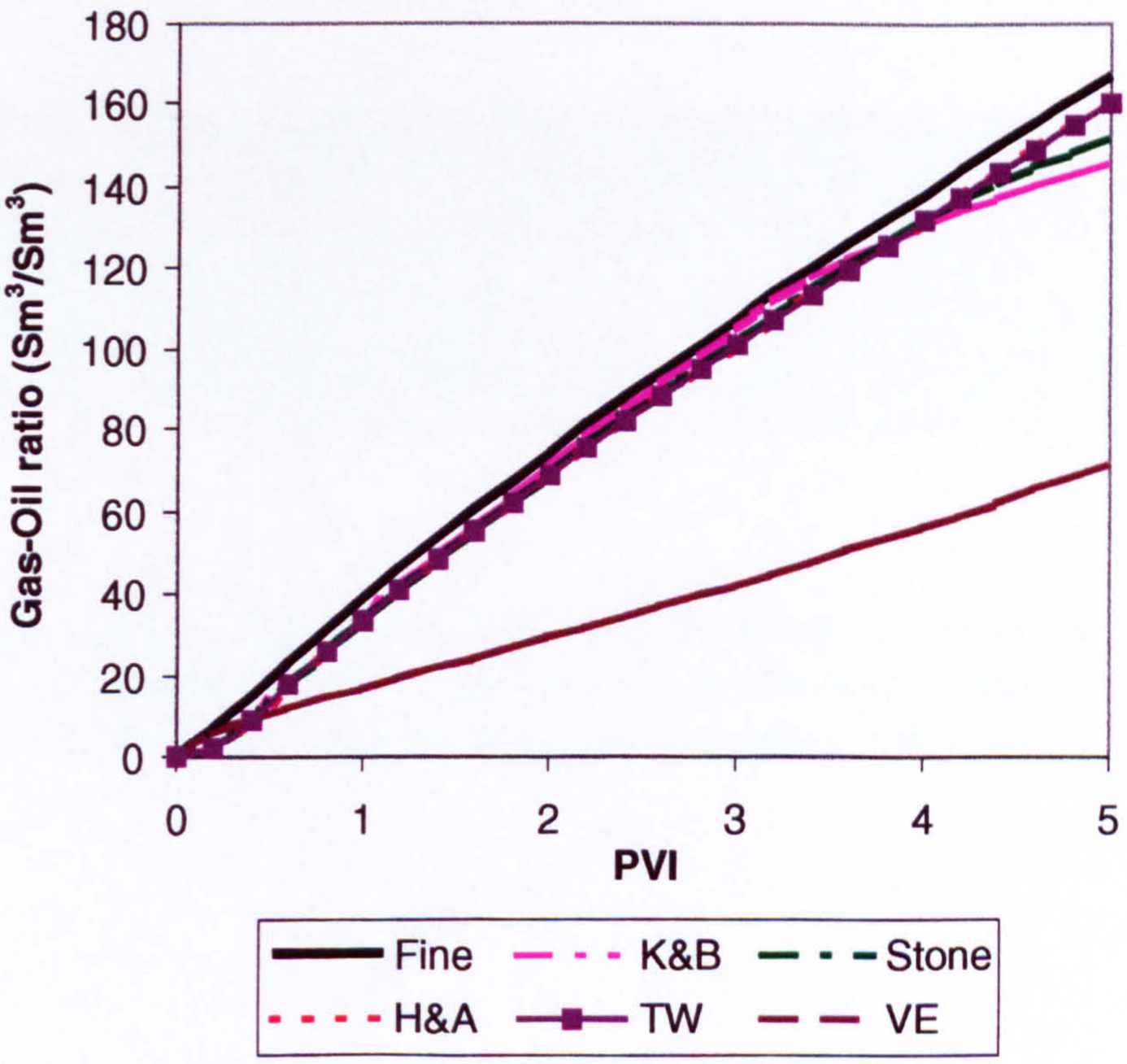

Figure 3.5b: Gas-Oil Ratio versus Pore Volume Injected for Case 3: comparison between several upscaling methods

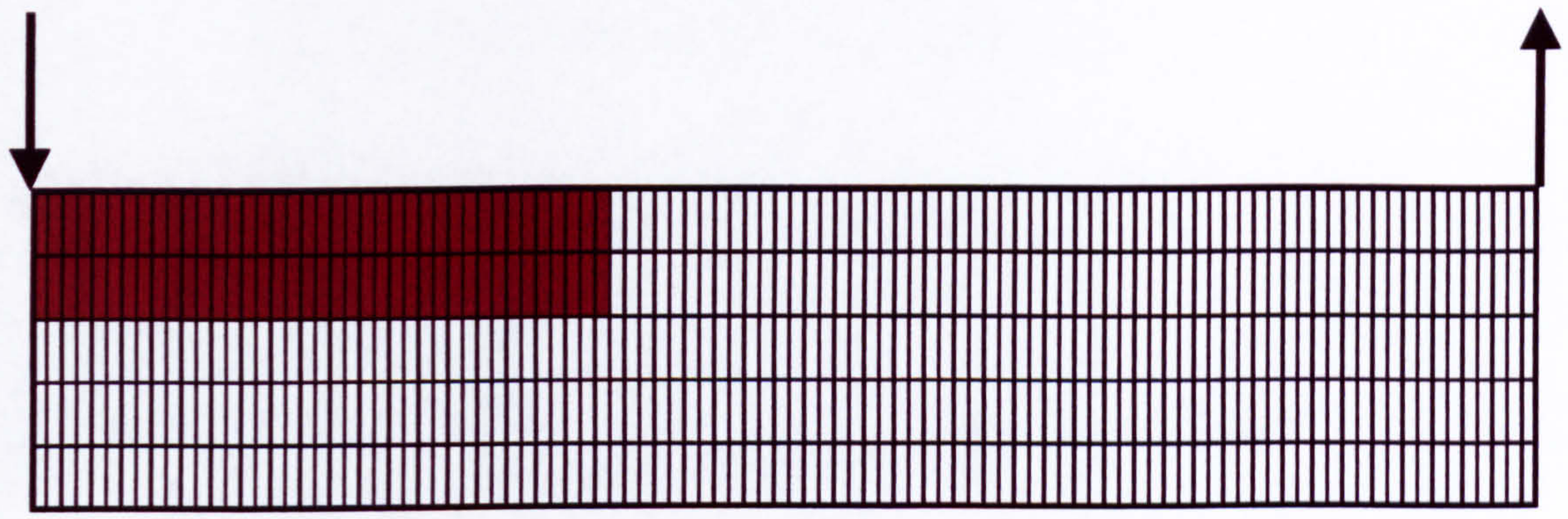

Figure 3.5c: Gas saturation plot after 1 PV injected (Case 3, coarsening upwards model with k_v/k_h equal 0.0); lighter coloured region shows gas saturation between 0.0 to 0.5 whereas darker coloured region shows gas saturation between 0.5 to 0.85.

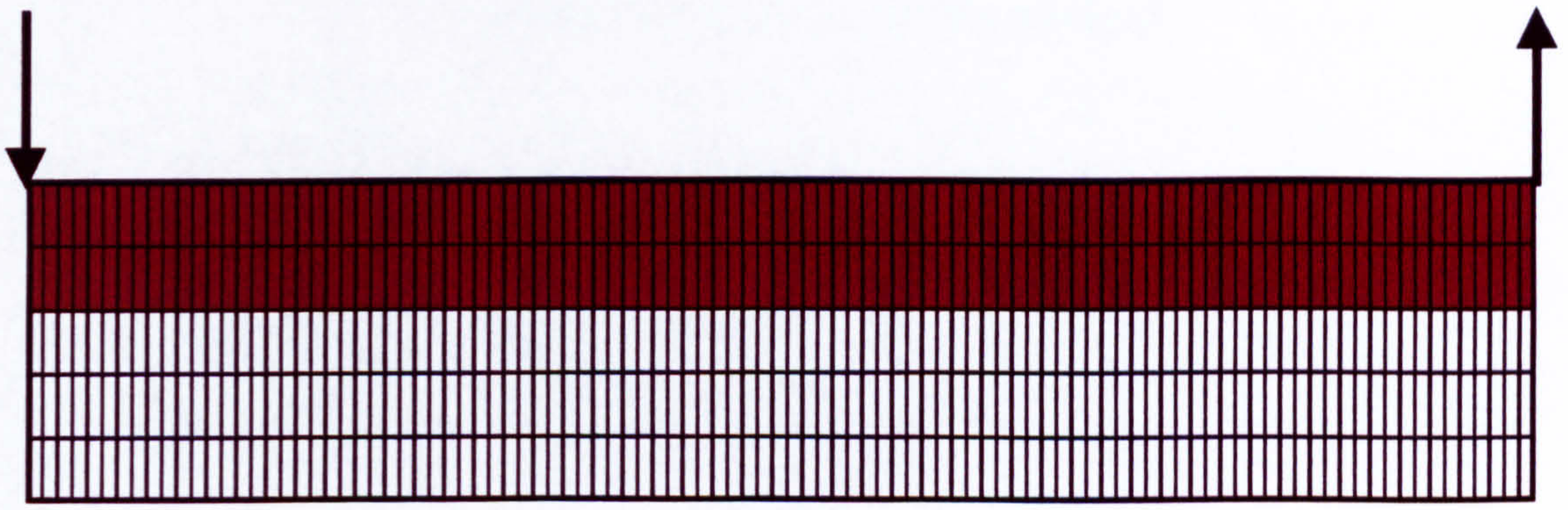

Figure 3.5d: Gas saturation plot after 5 PV injected (Case 3, coarsening upwards model with k_v/k_h equal 0.0); lighter coloured region shows gas saturation between 0.0 to 0.5 whereas darker coloured region shows gas saturation between 0.5 to 0.85.

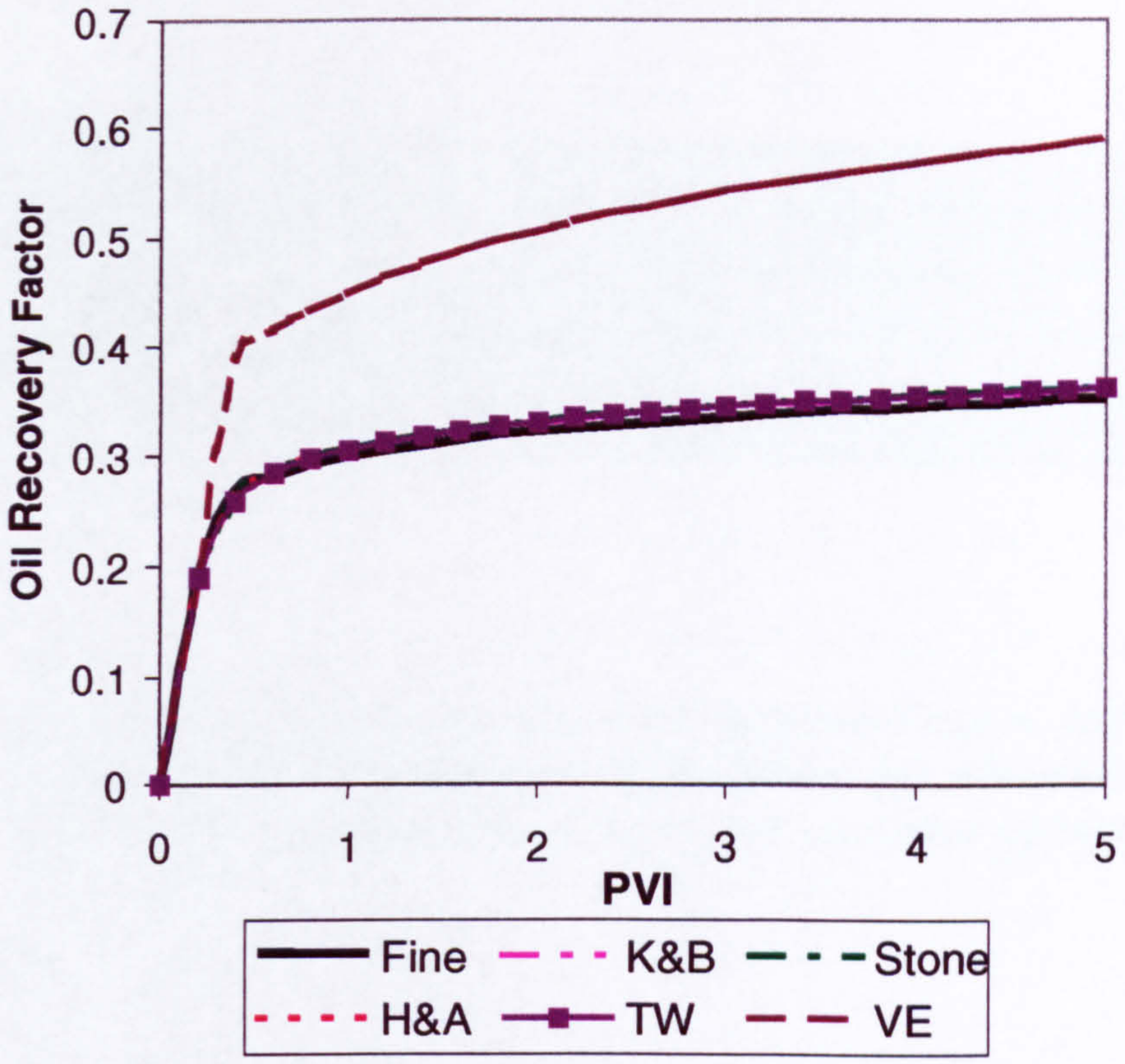

Figure 3.6a: Oil Recovery Factor versus Pore Volume Injected for Case 4: comparison between several upscaling methods

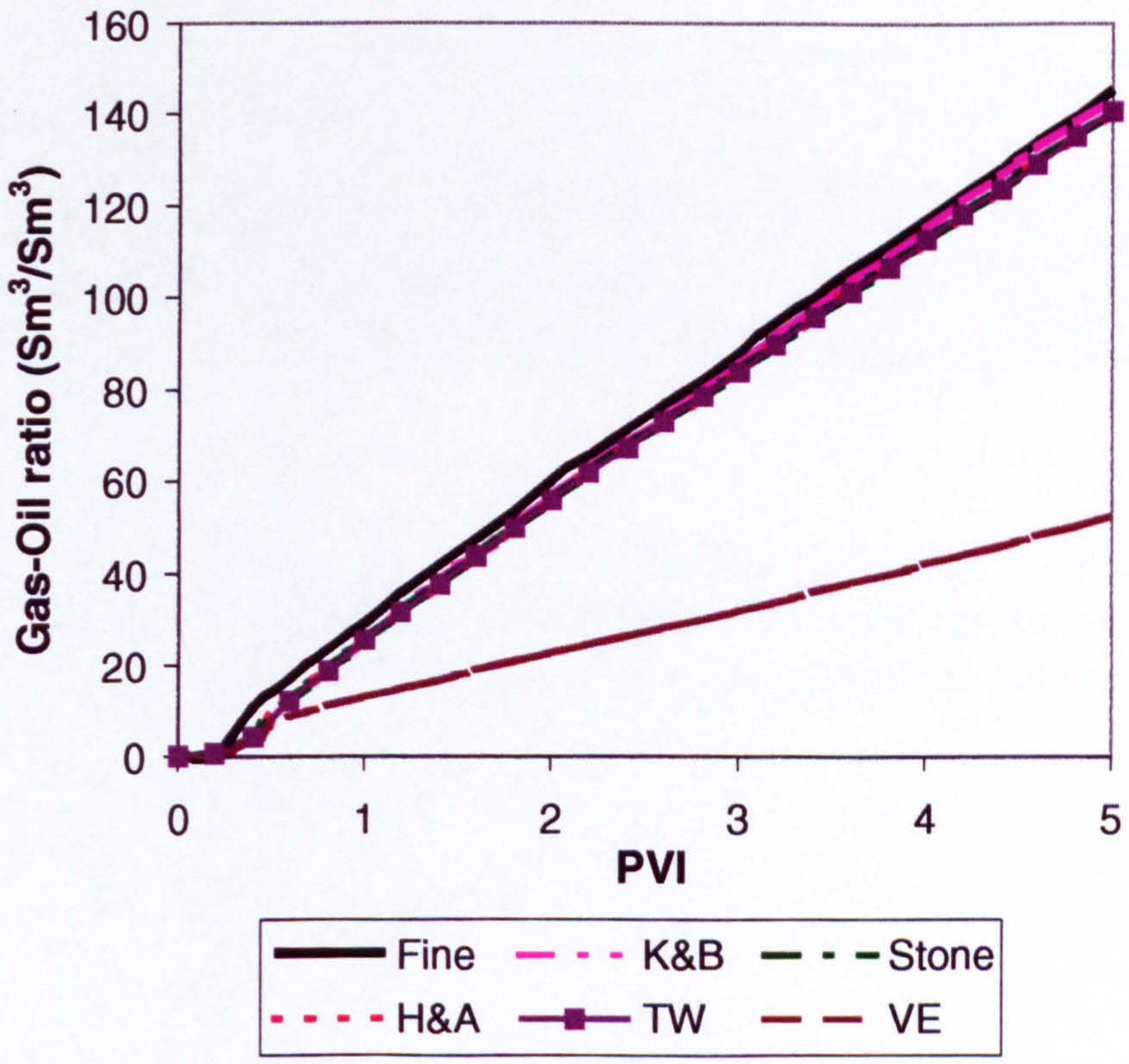

Figure 3.6b: Gas-Oil Ratio versus Pore Volume Injected for Case 4: comparison between several upscaling methods

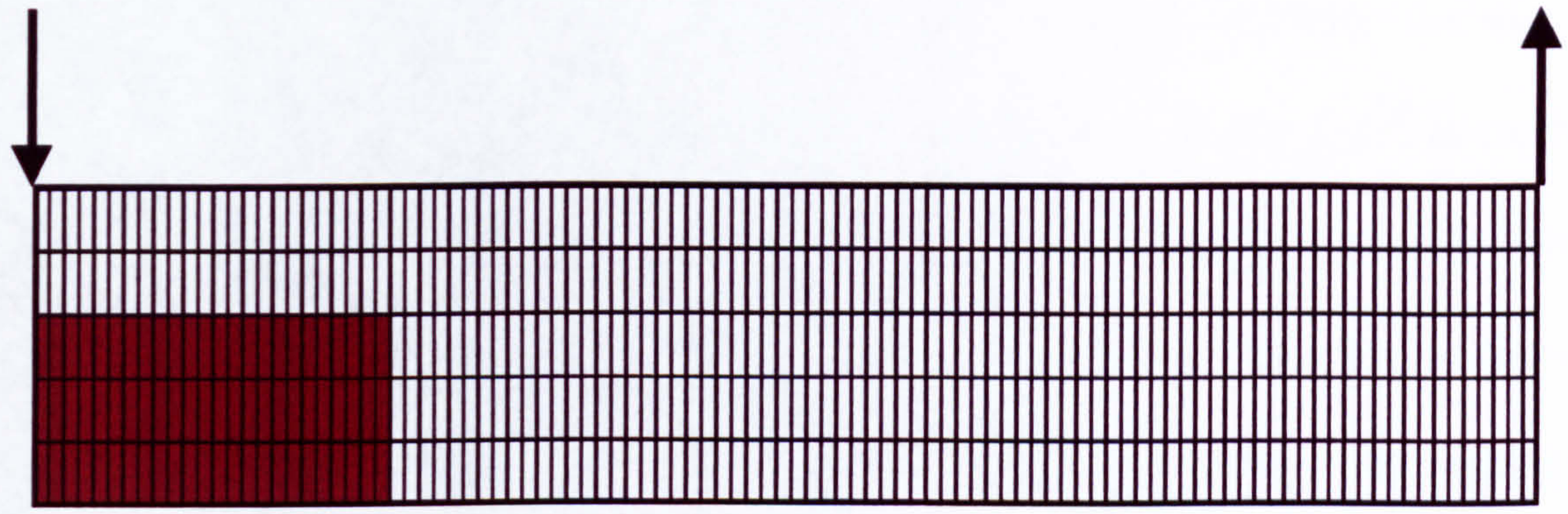

Figure 3.6c: Gas saturation plot after 1 PV injected (Case 4, fining upwards model with k_v/k_h equal 0.0); lighter coloured region shows gas saturation between 0.0 to 0.5 whereas darker coloured region shows gas saturation between 0.5 to 0.85.

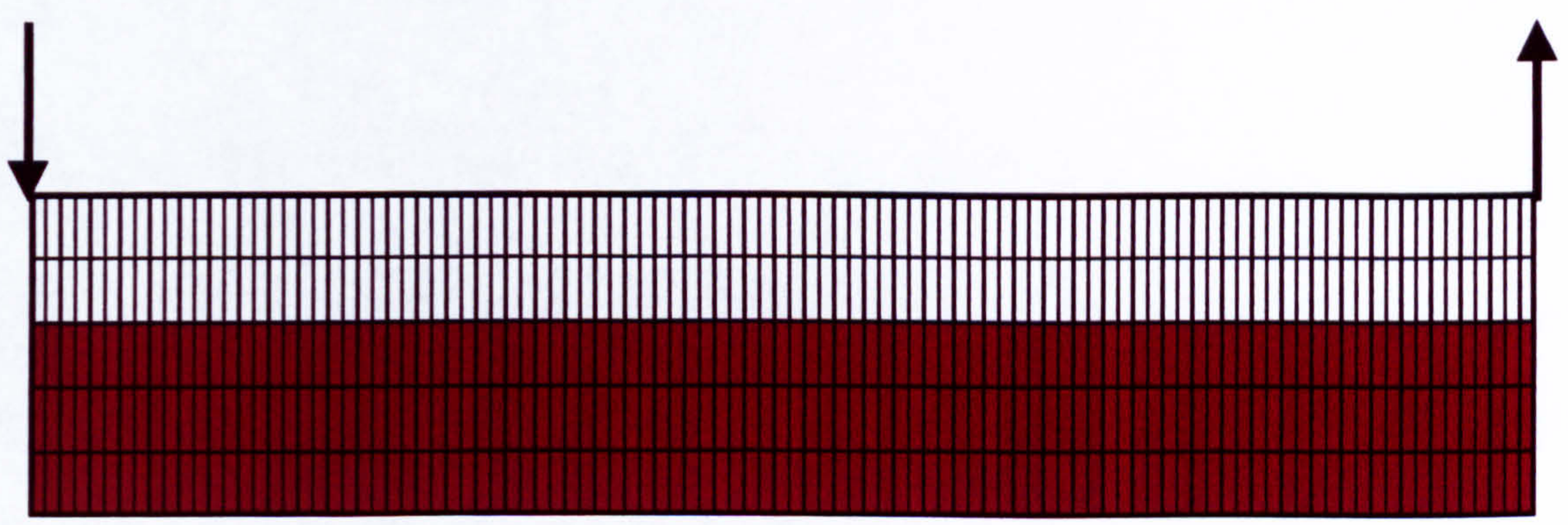

Figure 3.6d: Gas saturation plot after 5 PV injected (Case 4, fining upwards model with k_v/k_h equal 0.0); lighter coloured region shows gas saturation between 0.0 to 0.5 whereas darker coloured region shows gas saturation between 0.5 to 0.85.

Comparing Case 3 to Case 1 and Case 4 to Case 2, we can clearly see that when crossflow between model layers is restricted, the error in using the VE method is increased significantly, as we would expect. As mentioned before, crossflow between the model layers is essential for gravity segregation; and this condition is one of the pre-requisites for using the VE method. As the vertical permeability is decreased (k_v/k_h is set to zero for Cases 3 and 4), the crossflow between layers is decreased and this phenomenon will invalidate the assumption made by the VE method. This decreases the accuracy of the VE method to reproduce the fine grid performance. The performance of the Hewett and Archer method again tracks very closely to the TW method in these two cases.

3.4.3 Model with Dip (CASE 5)

Case 5 was constructed to evaluate the performance of upscaling techniques in a dipping reservoir. The inconsistency of the Stone method in handling gravity is very obvious in this case. A mathematical explanation of why the Stone method produces a large error in this particular case is presented in the following chapter.

In general, the Stone method gave a poor match to the GOR as well as the oil recoveries compared to the Kyte and Berry and the TW methods (refer to Figures 3.7a and 3.7b). The TW method, in this case, predicts the GOR a little better than the Kyte and Berry method especially in the later stages of the run as shown in Figure 3.7b. The performance of the Hewett and Archer method is rather similar to the TW method for this test case. In addition, Figures 3.7c and 3.7d show the saturation plot for this case.

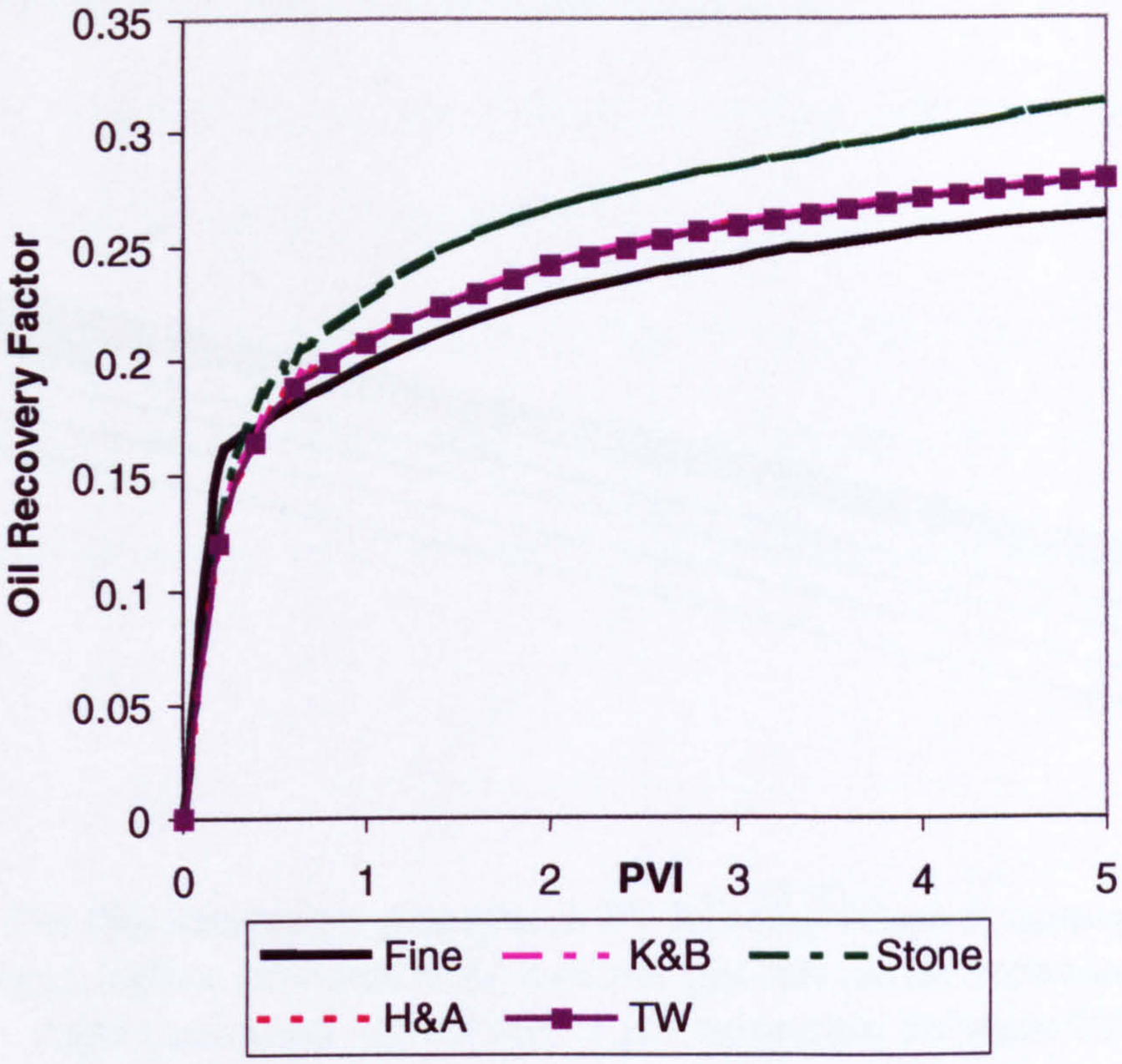

Figure 3.7a: Oil recovery Factor versus Pore Volume Injected for Case 5: comparison between several upscaling methods

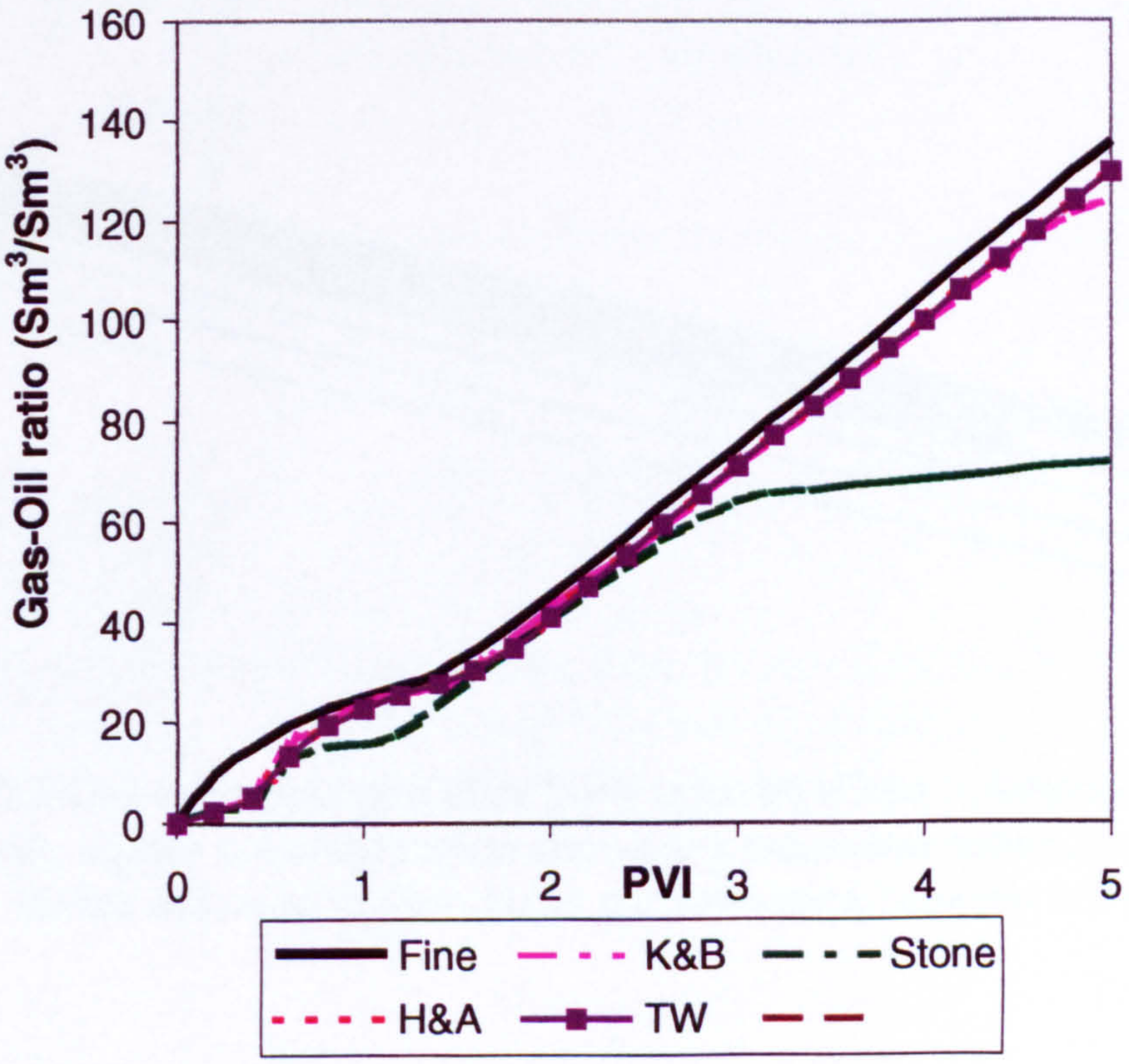

Figure 3.7b: Gas-Oil Ratio versus Pore Volume Injected for Case 5: comparison between several upscaling methods

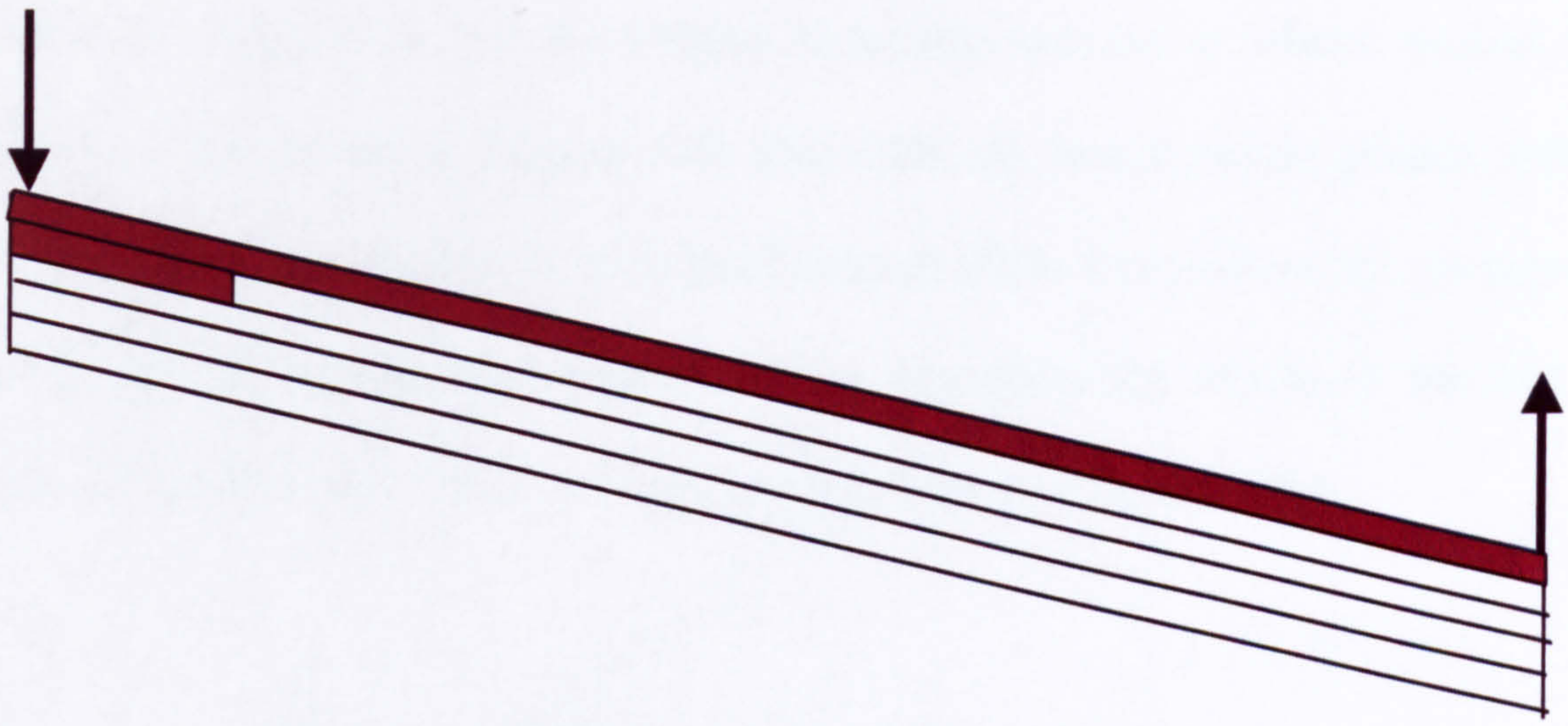

Figure 3.7c: Gas saturation plot after 1 PV injected (Case 5, homogenous model with 15° dipping); lighter coloured region shows gas saturation between 0.0 to 0.5 whereas darker coloured region shows gas saturation between 0.5 to 0.85.

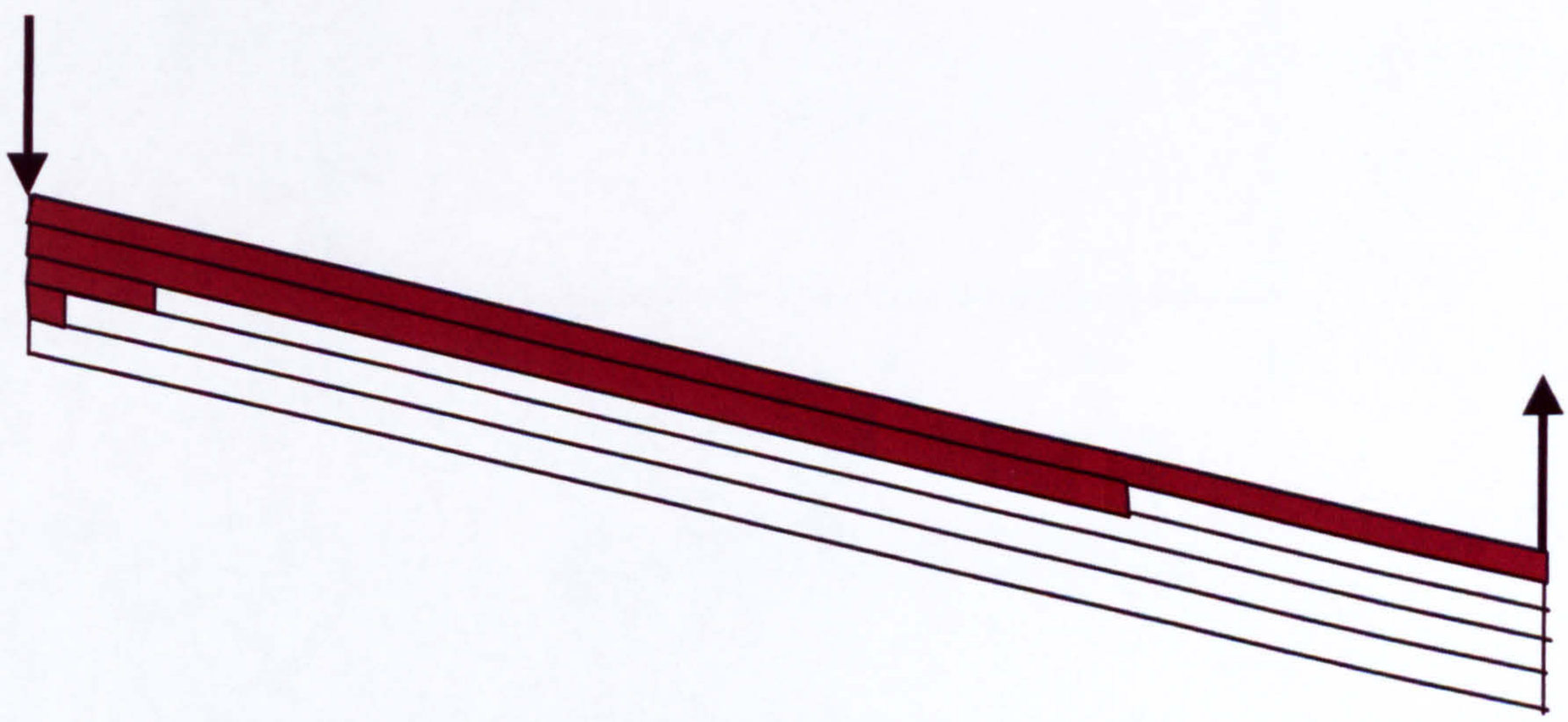

Figure 3.7d: Gas saturation plot after 5 PV injected (Case 5, homogenous model with 15° dipping); lighter coloured region shows gas saturation between 0.0 to 0.5 whereas darker coloured region shows gas saturation between 0.5 to 0.85.

3.4.4 Model with NO Gravity Effect (CASE 6)

Case 6 is designed to test the various upscaling techniques where viscous force dominate. As shown in Figures 3.8a and 3.8b, all four dynamic pseudo methods perform equally well in matching the performance of the fine grid model. As expected, the VE pseudo method once again failed to reproduce the results of the fine grid model. Saturation plots for Case 6 are shown in Figures 3.8c and 3.8d.

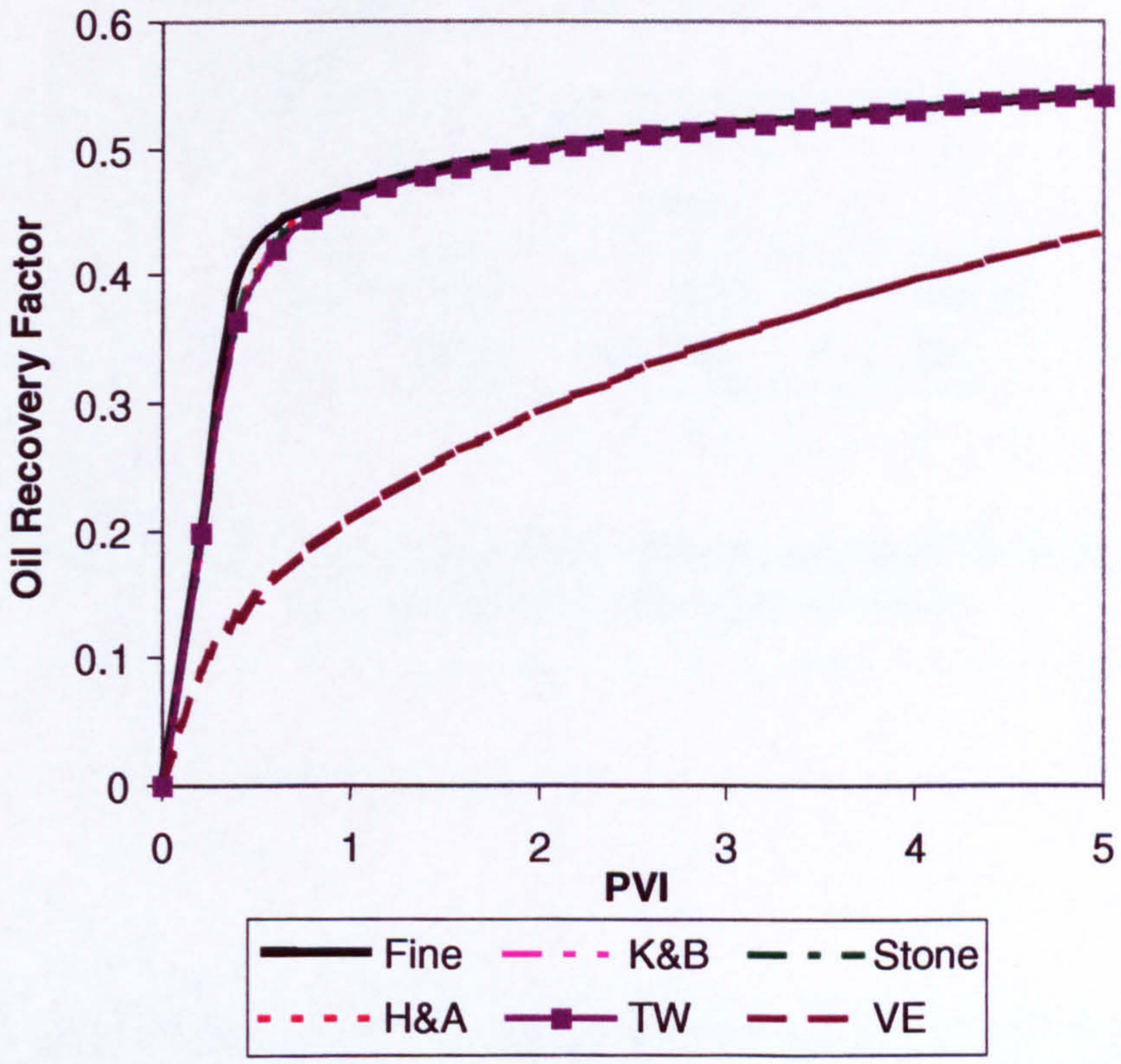

Figure 3.8a: Oil Recovery Factor versus Pore Volume Injected for Case 6: comparison between several upscaling methods

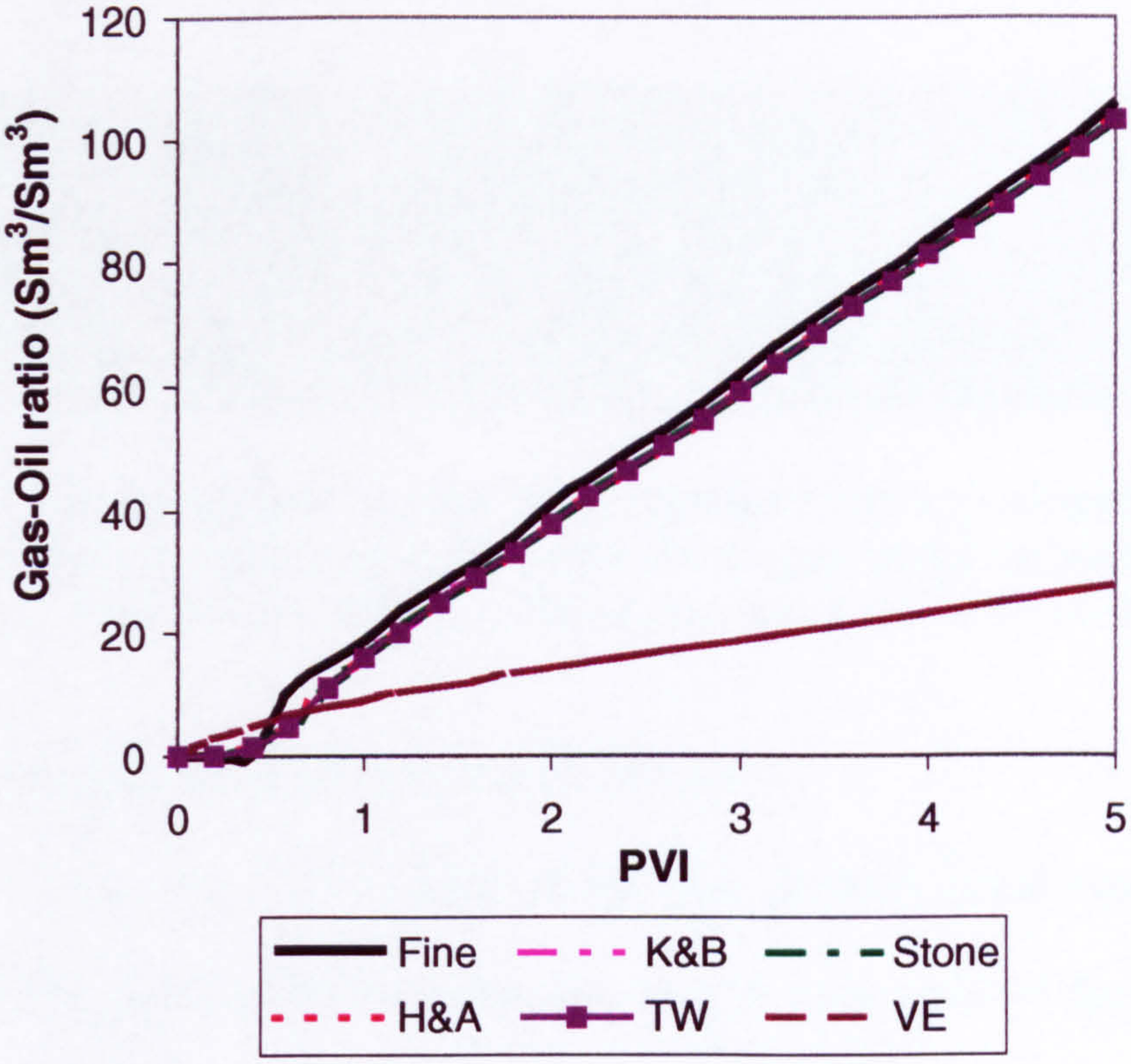

Figure 3.8b: Gas-Oil Ratio versus Pore Volume Injected for Case 6: comparison between several upscaling methods

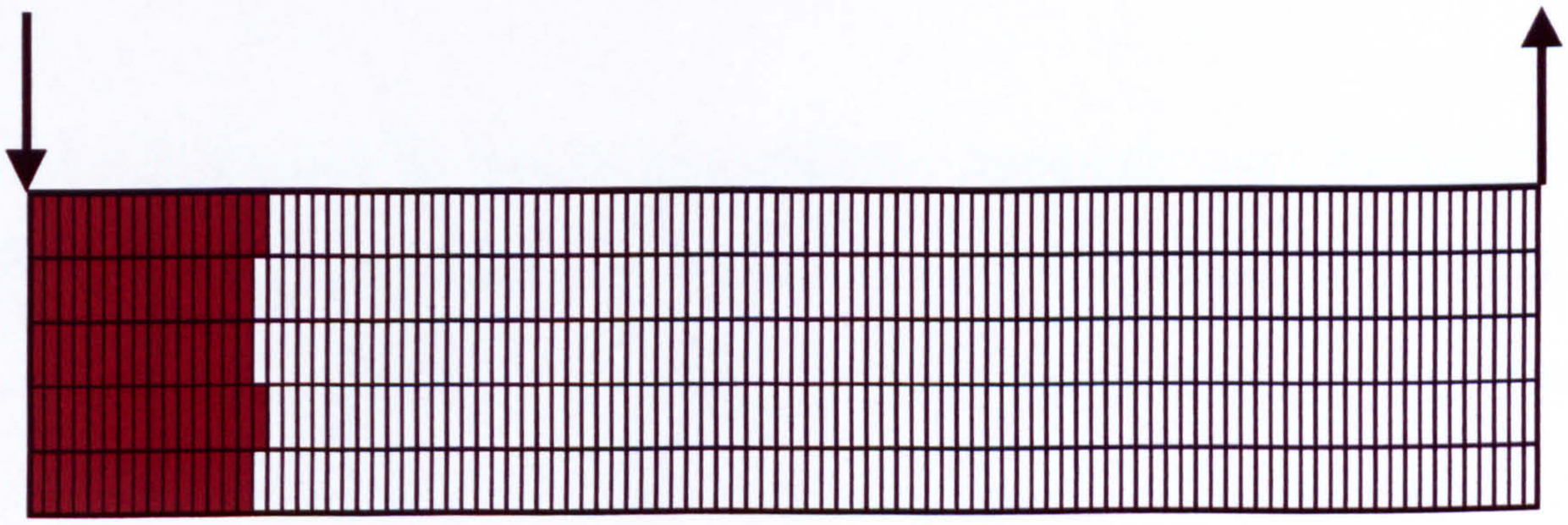

Figure 3.8c: Gas saturation plot after 1 PV injected (Case 6, homogenous model with low gravity force); lighter coloured region shows gas saturation between 0.0 to 0.5 whereas darker coloured region shows gas saturation between 0.5 to 0.85.

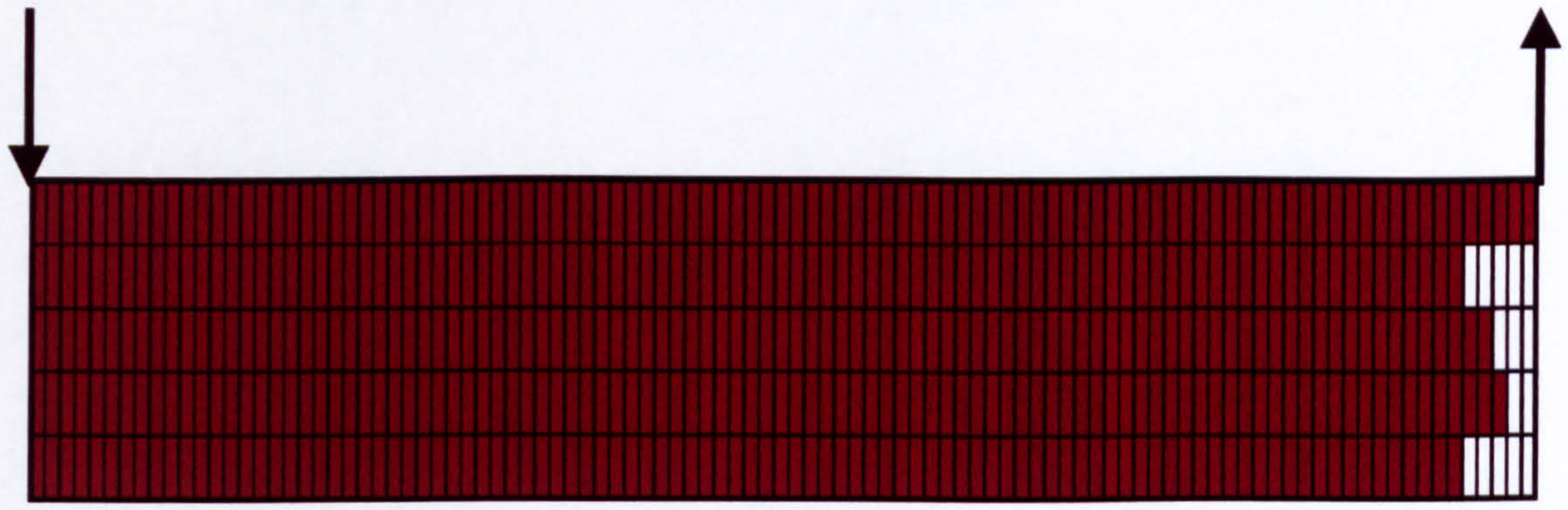

Figure 3.8d: Gas saturation plot after 5 PV injected (Case 6, homogenous model with low gravity force); lighter coloured region shows gas saturation between 0.0 to 0.5 whereas darker coloured region shows gas saturation between 0.5 to 0.85.

3.4.5 Model with High Gravity Effect (CASE 7)

Lastly, Case 7 was run to test which of the four methods could best model a larger gravity force compared with the viscous forces. The superiority of the TW method was clearly shown in this case as shown in Figures 3.9a and 3.9b. The TW method predicts the oil recoveries as well as the GOR much better than the Kyte and Berry, the Stone or the VE methods. Again, the performance of the Hewett and Archer method tracks very closely to the TW method in this case.

It also worth emphasizing that the Kyte and Berry method produced the biggest error compared to the other dynamic pseudo method for this case. This finding is consistent with the results of Guzman *et al.* (1994) who found that the Kyte and Berry method was unsuitable to be used in models with strong gravity segregation (high N_{gv}). A detailed discussion of why the Kyte and Berry method failed in gravity dominated flow (segregated flow) will be discussed later in Chapter 4.

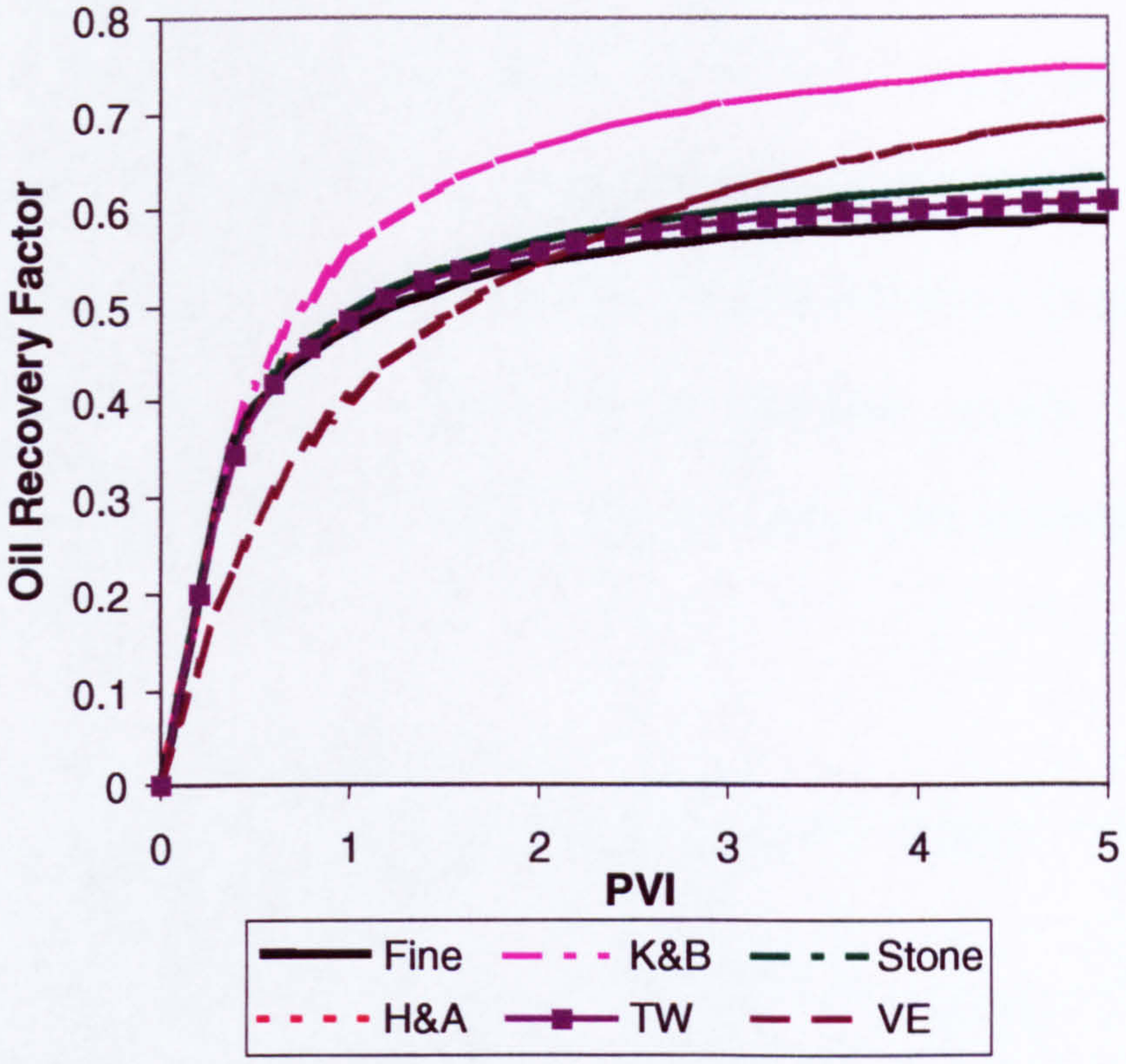

Figure 3.9a: Oil Recovery Factor versus Pore Volume Injected for Case 7: comparison between several upscaling methods

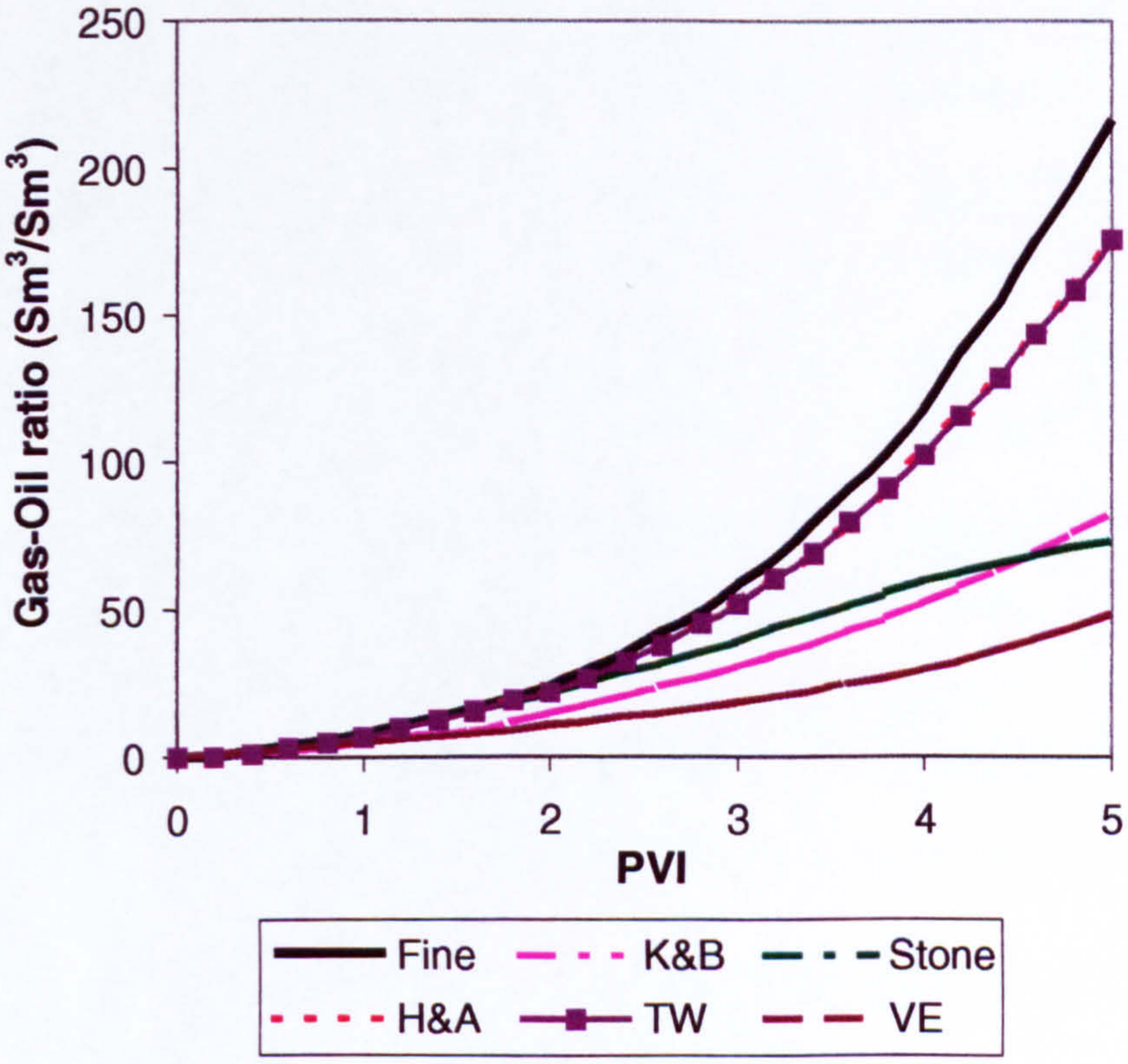

Figure 3.9b: Gas-Oil Ratio versus Pore Volume Injected for Case 7: comparison between several upscaling methods

3.4.6 Overall results

The results of all the cases can be summarized in the following two tables (Table 3.4 and 3.5) for the normalised rms errors in oil recovery factor and the gas-oil ratio, respectively. The rms errors were calculated from the difference in oil recovery factor (or gas-oil ratio) between the coarse and the fine-scale models, at different pore volumes injected. Numbers in brackets show the normalized rms errors relative to the TW method.

CASES	KYTE & BERRY	STONE	HEWETT & ARCHER	TW	VE
CASE 1	**0.0142 (1.1007)**	0.0128 (0.9953)	0.0130 (1.0078)	0.0129 (1.0000)	**0.0339 (2.6252)**
CASE 2	**0.0034 (1.2029)**	0.0026 (0.9428)	0.0028 (1.0000)	0.0028 (1.0000)	**0.0407 (14.5422)**
CASE 3	0.0101 (0.9812)	0.0106 (1.0294)	0.0102 (0.9903)	0.0103 (1.0000)	**0.0478 (4.6414)**
CASE 4	0.0043 (0.9415)	0.0046 (0.9980)	0.0047 (1.0174)	0.0046 (1.0000)	**0.1077 (23.4061)**
CASE 5	0.0114 (1.0309)	**0.0291 (2.6195)**	0.0109 (0.9820)	0.0111 (1.0000)	**0.1757 (15.8285)**
CASE 6	0.0032 (1.0001)	0.0032 (0.9935)	0.0032 (1.0013)	0.0032 (1.0000)	**0.0715 (22.3371)**
CASE 7	**0.0447 (7.9864)**	**0.0101 (1.7982)**	0.0059 (1.0536)	0.0056 (1.0000)	**0.0261 (4.6678)**

Table 3.4: The normalised rms errors for each case in terms of oil recovery factor (Case 1 to Case 7)

CASES	KYTE & BERRY	STONE	HEWETT & ARCHER	TW	VE
CASE 1	**0.0170 (1.3007)**	0.0122 (0.9339)	0.0139 (1.0611)	0.0131 (1.0000)	**0.0579 (4.4177)**
CASE 2	**0.0077 (2.7394)**	0.0027 (0.9807)	0.0027 (0.9643)	0.0028 (1.0000)	**0.0390 (13.9332)**
CASE 3	**0.0104 (1.3864)**	**0.0089 (1.1870)**	0.0076 (1.0133)	0.0075 (1.0000)	**0.0753 (10.0402)**
CASE 4	**0.0043 (0.7219)**	0.0058 (0.9629)	0.0059 (0.9833)	0.0060 (1.0000)	**0.0776 (12.9309)**
CASE 5	**0.0086 (1.1595)**	**0.0422 (5.7039)**	0.0079 (1.0676)	0.0074 (1.0000)	-
CASE 6	0.0053 (1.0000)	0.0053 (0.9934)	0.0053 (1.0003)	0.0053 (1.0000)	**0.0836 (15.7680)**
CASE 7	**0.0464 (3.4913)**	**0.0457 (3.4358)**	0.0128 (0.9624)	0.0133 (1.0000)	**0.0601 (4.5186)**

Table 3.5: The normalised rms errors for each case in terms of gas-oil ratio (Case 1 to Case 7)

Taking a 10% cut-off as our differentiating criterion, the numbers in brackets in Table 3.4 and 3.5 show the relative weakness (or strength) of each method compared to the TW method. This criterion suggests that a value of less than 0.9 assumes that particular method perform better than the TW method and a value larger than 1.1 indicates that the method is poorer. In general, the results show that the Kyte and Berry method produces larger errors compared to the Stone method in non-dipping, gas-oil systems. On the other hand, the Stone method is found to be very poor in dipping systems, as expected since gravity was neglected in deriving these equations

(Guzman *et al.*, 1994). In all the cases investigated, the VE pseudo approach is the least acceptable (even in Case 7, where the effect of gravity is high). The reasons behind this apparent weakness of the VE method are further investigated and are presented in the following chapter.

The TW method shows promising results both in dipping and in non-dipping systems. In all cases investigated, there is only one instance where the TW method does not perform best: this was in Case 4 where the GOR was more accurately predicted by the Kyte and Berry method. In all other scenarios, the TW method performs equally well or far better than the Kyte and Berry, the Stone or the VE methods in handling immiscible gas-oil systems. It is also evident that the TW method gives far better results in Case 7 where the gravity effect is dominant compared with the other pseudo methods. Further analysis of the conditions under which this new method performs better than the Kyte and Berry, the Stone and the VE method is presented the following chapter.

Comparing the results of the TW method and the Hewett and Archer method show a lot of similarities. It turns out that there is a very good reason for this and this is presented in the following chapter.

3.5 SUMMARY AND CONCLUSIONS

In this chapter, we have introduced and validated a new dynamic pseudo method known as the Transmissibility Weighted (TW) method. This method has been

specifically formulated to handle cases with a high gravity effect, which is normally encountered in gas displacement processes. The main findings on the use of various pseudo functions in a range of reservoir flow situations can be summarized as follow:

1. There is no pseudo generation method that is perfect for all the conditions i.e. produces zero error. However, it is shown that the TW method gives more accurate results in applying pseudo functions where gravity effects are significant than the Kyte and Berry, the Stone and the VE methods.

2. The Stone method performs very badly in a dipping model. A detailed mathematical explanation of this weakness of the Stone method is presented the following chapter.

3. When fluid flow is in the viscous-dominated regime, all the dynamic pseudo function methods perform rather similarly with high accuracy. As expected, the VE method will definitely fail in this case.

4. In all the cases that we investigate, the VE method is the least acceptable (even in Case 7, where the effect of gravity is very high). The reasons behind this apparent weakness of the VE method are further investigated and are presented in the following chapter.

5. The performance of the Hewett and Archer method is rather similar to the TW method in all of the test cases. This observation will be investigated further and explained in detail in Chapter 4.

CHAPTER 4

FURTHER ANALYSIS OF PSEUDO FUNCTIONS

4.1 GENERAL REMARKS

A number of methods for calculating dynamic pseudo functions have been developed over the years. Each method has its advantages and disadvantages, and it is well known that using an inappropriate method can lead to inaccurate results. However, there is a lack of understanding as to why a certain method will succeed in some cases but fail in others. In this chapter, we will discuss some of the similarities and limitations of the five pseudo methods that we discussed in Chapter 3 namely:

(i) the Stone method,

(ii) the Kyte and Berry method,

(iii) the Hewett and Archer method,

(iv) the TW method and

(v) the VE method.

4.2 WEAKNESS OF THE STONE METHOD

In Chapter 3, we saw that the Stone method performed very badly when the model was dipping compared to when the model was horizontal. It is our intention in this section

to investigate the reason behind this finding. Two new simulation models, with and without dip, will be used for this purpose.

4.2.1 Description of the Test Models

Two cross sectional models each with 200 x 1 x 100 fine grid blocks were used in this study. The initial properties of the fine grid models are as follows:

Porosity, $\phi = 0.2$;

Grid block sizes, $\Delta X = 15.24$ metres, $\Delta Y = 7.62$ metres and $\Delta Z = 0.762$ metres;

Viscosities, $\mu_o = 1$ cp, $\mu_g = 0.1$ cp

Densities, $\rho_o = 43.68$ lb/ft^3 or 700 Kg/m^3,

$\rho_g = 0.0624$ lb/ft^3 or 1.0 Kg/m^3.

The absolute permeabilities in these two test models are set to vary exponentially increasing upwards from 10 mD at the bottom layer to about 1462 mD at the top of the models. The same rock relative permeabilities were used as before (see Chapter 3). Gas was injected from an injector located at the left of the model and dead oil was produced from a well on the right of the model. Both wells were completed vertically throughout the model and the injection rate was set to give a frontal velocity of 0.6 m/d (about 2 feet/day).

In the first model (Case A), the model is taken to be horizontal with the calculated gravity to viscous ratios (N_{gv}) of about 1.84, whereas in the second model (Case B), the model is tilted with a 15° dipping angle. In Case B, gas is injected in the first up-dip grid block.

4.2.2 Governing Equations

In the fine grid model, Darcy's equations are solved in order to obtain the fluid flow rates as follows (for simplicity, we will only consider 1-D flow in the x-direction):

$$q_o = \frac{T_x.k_{ro}}{\mu_o}.\Delta\Phi_o \tag{4.1}$$

$$q_g = \frac{T_x.k_{rg}}{\mu_g}.\Delta\Phi_g \tag{4.2}$$

where q_o and q_g are the volumetric flow rate of oil and gas respectively, T_x is the single-phase transmissibility (which is a function of permeability and grid block geometry alone), k_{ro} and k_{rg} are the oil and gas relative permeability, μ_o is the oil viscosity, μ_g is the gas viscosity, and $\Delta\Phi_o$ and $\Delta\Phi_g$ are the oil and gas potential differences between this particular grid block at the one next to it (down-stream).

From the definition of capillary pressure and fluid potential, the gas potential for each of the fine gridblocks can be written in terms of oil potential as follow:

$$\Phi_g = \Phi_o + P_c - \Delta\rho g h \tag{4.3}$$

where $P_c = P_g - P_o$, and P_o and P_g are oil and gas phase pressures, $\Delta\rho = \rho_o - \rho_g$, and h is the height above some datum.

Therefore, from Equation (4.3), the difference in fluid potential between two adjacent blocks can be calculated as:

$$\Delta\Phi_g = \Delta\Phi_o + \Delta P_c - \Delta\rho g \Delta h \tag{4.4}$$

where ΔP_c is the difference in capillary pressure between grid block n and n+1, and Δh is the difference in elevation between these two grid blocks (normally taken at their centres).

At the coarse scale, it is assumed that the same set of equations can be solved but with averaged properties of the coarse grid blocks. Thus, Equation (4.1) and (4.2) can be written as:

$$\overline{q_o} = \frac{\overline{T_x}.\overline{k_{ro}}}{\overline{\mu_o}}.\overline{\Delta\Phi_o} \tag{4.5}$$

$$\overline{q_g} = \frac{\overline{T_x}.\overline{k_{rg}}}{\overline{\mu_g}}.[\overline{\Delta\Phi_g}] = \frac{\overline{T_x}.\overline{k_{rg}}}{\overline{\mu_g}}.\left[\overline{\Delta\Phi_o} + \overline{\Delta P_c} - \Delta\rho g\,\overline{\Delta h}\right] \tag{4.6}$$

where the overbar (-) indicates the averaged properties for the coarse grid blocks.

4.2.2.1 Governing Equations for the 2D Horizontal Cross-Sectional Model (CASE A)

For this case, since the model is horizontal and has zero capillary pressure, Equation (4.6) can be simplified as follow:

$$\overline{q_g} = \frac{\overline{T_x}.\overline{k_{rg}}}{\overline{\mu_g}}.\boxed{\Delta\Phi_o} \tag{4.7}$$

From Equations (4.6) and (4.7), we can see that for this specific case, the $\overline{\Delta\Phi_g}$ will always be equal to $\overline{\Delta\Phi_o}$, although the local absolute values of Φ_o and Φ_g can be quite different. Because of these two assumptions (zero capillary pressure and horizontal model), the only information that are needed from the fine grid model in order to

preserve the fractional flow in the fine and coarse grid models are the fluid flow rates. From these two fine grid properties (q_o and q_g), it is possible to correctly construct the fractional flow needed for the coarse grid blocks regardless of any other descriptions of the fine grid models.

Since for this case the $\Delta\Phi_g$ is equal to the $\Delta\Phi_o$, the fractional flow for the coarse grid blocks can be calculated as follows:

$$\overline{f_g} = \frac{\overline{q_g}}{\overline{q_g} + \overline{q_o}} = \frac{\dfrac{\overline{T_x}\,\overline{k_{rg}}}{\overline{\mu_g}}\,\overline{\Delta\Phi_o}}{\left(\dfrac{\overline{T_x}\,\overline{k_{rg}}}{\overline{\mu_g}}\right)\overline{\Delta\Phi_o} + \left(\dfrac{\overline{T_x}\,\overline{k_{ro}}}{\overline{\mu_o}}\right)\overline{\Delta\Phi_o}} \tag{4.8}$$

which can be factored out to be:

$$\overline{f_g} = \frac{\overline{q_g}}{\overline{q_g} + \overline{q_o}} = \frac{1}{1 + \dfrac{\overline{k_{ro}}\,\overline{\mu_g}}{\overline{k_{rg}}\,\overline{\mu_o}}} \tag{4.9}$$

Assuming we know the values of $\overline{\mu_o}$, $\overline{\mu_g}$, $\overline{q_o}$ and $\overline{q_g}$ from the fine grid run, we can set one of the phase pseudo relative permeability (either $\overline{k_{ro}}$ or $\overline{k_{rg}}$) arbitrarily – e.g. as a straight line - and adjust the other curve so that the fractional flow is honoured. The resulting pseudo curves might be very non-monotonic, but they will still reproduce the fine grid results perfectly satisfactorily (since we conserve the fractional flow). It should be noted that while conserving the fractional flow will guarantee the correct calculation of fluid flow rates in the simulation models, the pressure distribution will not be reproduced unless the total mobility of the fluids is also conserved. Since our

quality index concentrates on the reproduction of the fine grid total oil recovery factor and GOR only, we can see from Equation (4.9) that the issue of how we average the fluid potential difference (or mobility) is irrelevant for this case. We will discuss the issue of capturing the right pressure distribution of the fine grid model in the coarse grid model in Section 4.5 when we compare the performance of the TW method to that of the Hewett and Archer method.

4.2.2.2 Governing Equations for the 2D Cross-Sectional Model with the Dipping (Case B)

For this case, only capillary pressure is ignored since the model is dipping. Therefore, Equation (4.6) now becomes:

$$\overline{q_g} = \frac{\overline{T_x}.\overline{k_{rg}}}{\overline{\mu_g}}.\left[\overline{\Delta\Phi_o} + \Delta\rho g\overline{\Delta h}\right] \tag{4.10}$$

From Equations (4.6) and (4.10), it is evident that for the case of a dipping reservoir, then $\overline{\Delta\Phi_g}$ will not be equal to $\overline{\Delta\Phi_o}$ (i.e. the "$\Delta\rho g\overline{\Delta h}$" term cannot be ignored).

4.2.3 Discussion of the Results

Figures 4.1 and 4.2 show the relative performance (in terms of oil recovery factor) of the four dynamic pseudo generation methods for Case A and Case B respectively. From these figures, we can see that the Kyte and Berry method produced the worst results for Case A (horizontal model), whereas the Stone, the Hewett and Archer and the TW methods produce a rather similar performance.

For Case B (dipping model), it now appears that there are some differences between these various methods. From Figure 4.2, we can see that the worst result is produced by the Stone method and this is due to the fact that it says nothing about the potentials in the presence of gravity. The other three methods, the Kyte and Berry, the Hewett and Archer and the TW methods, are somewhat better than that of Stone.

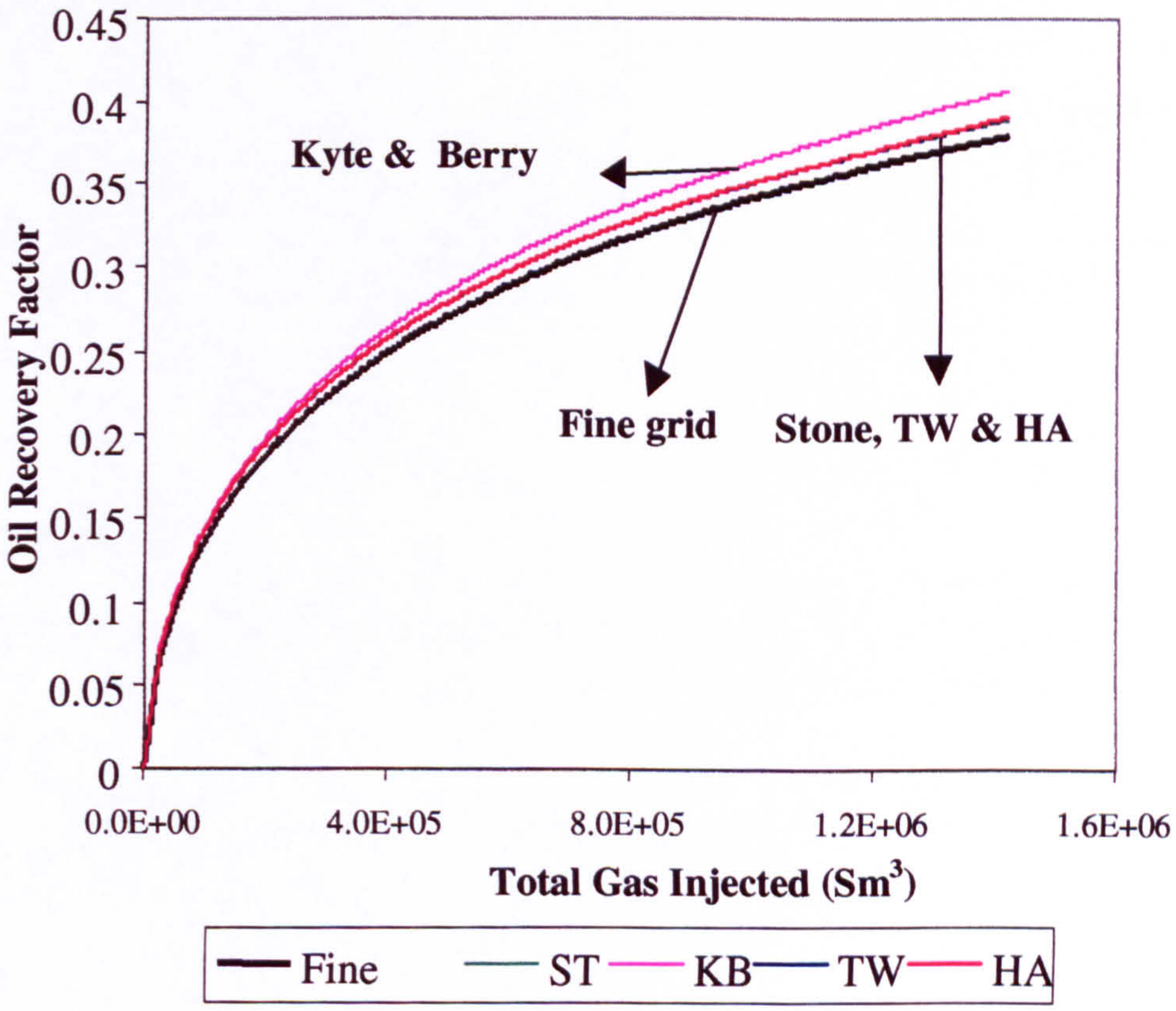

Figure 4.1: Oil recovery factor versus total gas injected showing the performance of the four dynamic pseudo methods (the KB, the Stone, the TW and the HA) relative to the fine grid model for Case A (Horizontal model).

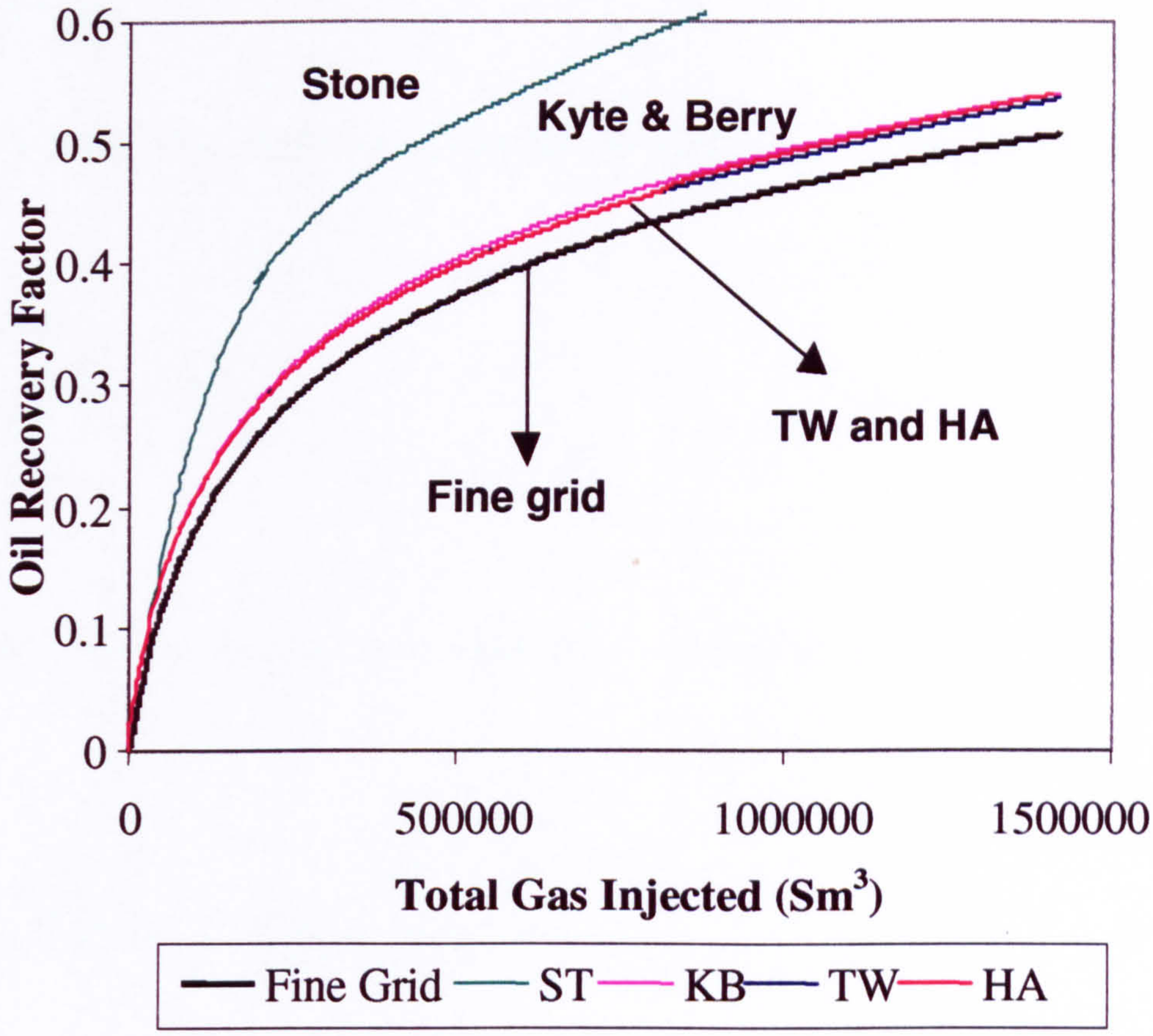

Figure 4.2: Oil recovery factor versus total gas injected showing the performance of the four dynamic pseudo methods (the KB, the Stone, the TW and the HA) relative to the fine-grid model for Case B (Dipping model).

4.2.3.1 Performance of the Stone Method in Case A (Horizontal Model)

The Stone method uses total mobility as a way of avoiding the problems associated with estimating the fluid potential differences. From Guzman *et al.* (1994) it is known that the Stone method equates the coarse grid fluid potentials by setting:

$$\overline{T_x}.\overline{\lambda_t}.\overline{\Delta\Phi_p} = \sum_k (T_x.\lambda_t.\Delta\Phi_p)_k \ . \tag{4.11}$$

The pseudo phase mobility can be calculated as:

$$\overline{\lambda_p} = -\frac{\overline{q_p}}{\overline{T_x}.\overline{\Delta\Phi_p}} \tag{4.12}$$

and the averaged total mobility is equal to the sum of all the phase mobilities.

$$\overline{\lambda_t} = \frac{\sum_k (T_x.\lambda_t)_k}{\sum T_x} = \sum_p \overline{\lambda_p} \tag{4.13}$$

Substitution of Equation (4.12) into Equation (4.13) gives the following equation:

$$1 = -\left(\frac{\overline{q_o}}{\sum_k (T_x.\lambda_t.\Delta\Phi_o)} + \frac{\overline{q_g}}{\sum_k (T_x.\lambda_t.\Delta\Phi_g)} \right) \tag{4.14}$$

From Equation (4.14) we can see that Stone method will always assume that $\Delta\Phi_g$ be equal to $\Delta\Phi_o$ for the equations to be consistent (subsequently, $\overline{\Delta\Phi_g} = \overline{\Delta\Phi_o}$). For this particular case, this apparently severe limitation is valid and that is the reason why we can see Stone method performs better than the Kyte and Berry in a horizontal case although the overall gravity to viscous number (N_{gv}) for this model is relatively big. This same assumption also makes the performance of the Stone method rather similar to that of the Hewett and Archer and the TW methods since all of them set the $\Delta\Phi_g$ value to be same as the $\overline{\Delta\Phi_o}$. This might not be the case when we have dip in our model (Case B) as we will discuss in the following section below.

4.2.3.2 Performance of the Stone Method in Case B (Dipping Model)

As we can see from Equation (4.14), the Stone method will always assume that $\Delta\Phi_g = \Delta\Phi_o$ for the equations to be consistent (subsequently, $\overline{\Delta\Phi_g} = \overline{\Delta\Phi_o}$). For Case B i.e. the dipping model, this severe assumption ignores the effect of the gravity term ($\Delta\rho g\overline{\Delta h}$). As such, whenever the fine grid model is dipping, some error related to the gravity term will always be introduced by the Stone method in its current form. This is the reason why we can see in Figure 4.2 that the Stone method produced the worst results compared to the other methods.

4.3 THE TW VERSUS THE KYTE AND BERRY METHODS

In order to investigate the relative strengths of the TW and the Kyte and Berry methods, we extended our analysis from the previous chapter (Chapter 3) to include an additional fourteen cases which cover a much wider spectrum of mobility ratio, k_v/k_h ratio and N_{gv}. The description of the models for the new cases (Case 8 through Case 21) is presented in Table 4.1. For each of the cases, the quality index (the normalized rms error in oil recovery factor) and the gravity to viscous ratio (N_{gv}) were calculated using Equation (3.6).

Cases	Perm layer 1 (mD)	Perm layer 2 (mD)	Perm layer 3 (mD)	Perm layer 4 (mD)	Perm layer 5 (mD)	k_v/k_h	Mobility ratio	Density ratio	N_{gv}
Case 8	500	500	500	500	500	1.0	100	700	1.9729
Case 9	500	500	500	500	500	1.0	100	70000	197.56
Case 10	500	500	500	500	500	1.0	10	700	19.728
Case 11	500	500	500	500	500	1.0	100	1.01	0.01
Case 12	500	500	500	500	500	1.0	100	1.05	0.1
Case 13	500	500	500	500	500	1.0	100	2.06	1.0
Case 14	500	10	500	10	500	1.0	100	700	0.0958
Case 15	500	250	500	250	500	1.0	100	700	1.4092
Case 16	500	500	500	10	10	0.1	100	700	0.0096
Case 17	10	10	10	500	500	0.1	100	700	0.0065
Case 18	500	10	500	10	500	0.1	100	700	0.0096
Case 19	500	10	500	10	500	0.0	100	700	0.0
Case 20	500	250	500	250	500	0.1	100	700	0.1409
Case 21	500	250	500	250	500	0.0	100	700	0.0

Table 4.1: Case descriptions for Case 8 to Case 21

4.3.1 Strength of the TW method over the Kyte and Berry method

We start our investigation by analysing when the TW method performs better than the Kyte and Berry method. We split the twenty-one test cases that we described above into two groups. In the first group, we collect all the homogenous models to simplify our findings, whereas in the second group we generalised our finding by analysing all the test cases simultaneously.

4.3.1.1 Homogenous Models

Grouping all of the homogenous models together (Case 6, 7, 8, 9, 10, 11, 12 and 13), the percentage difference[a] between these two methods was plotted against the calculated N_{gv}[b] on a log-log scale. A clear correlation between these quantities was evident with a coefficient of determination (R^2) of more than 0.84, as shown in Figure 4.3. Thus, it was concluded that the strength of the TW over the Kyte and Berry method was in the high gravity scenarios.

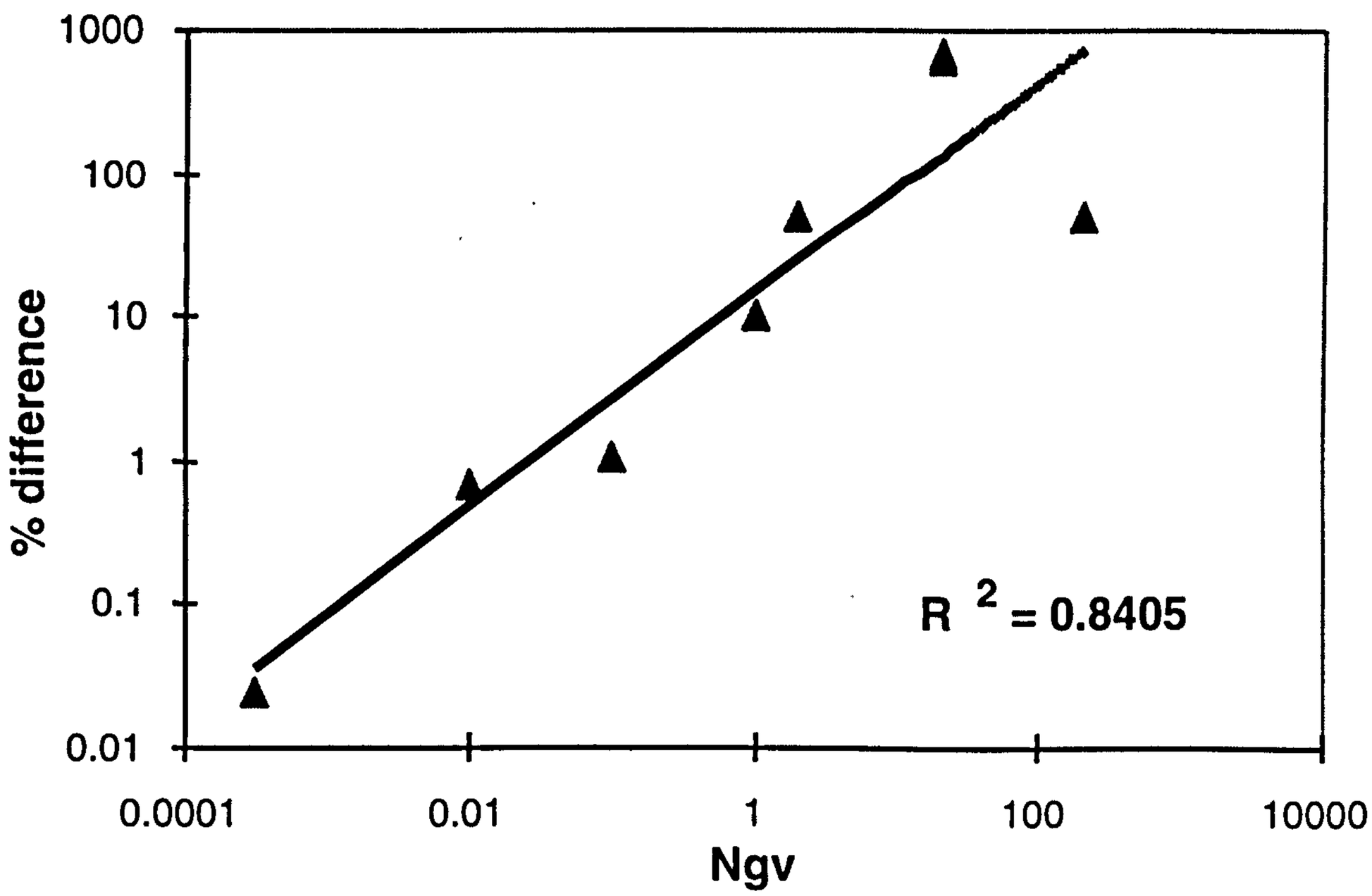

Figure 4.3: Percentage difference between the Kyte and Berry method and the TW method versus the gravity to viscous number for homogeneous models (Case 6, 7, 8, 9, 10, 11, 12 and 13)

---

[a] Percentage differences were calculated by first calculating the error in each of the cases and then calculate the difference in error between the Kyte and Berry and the TW methods using the TW method as a base case. A positive number means that TW method produces less error compared to the Kyte and Berry method, whereas a negative number implies the opposite.

[b] All N_{gv} values of 0.0 (due to k_v/k_h of zero) were ignored.

4.3.1.2 All Models

Now, extending the above finding using all the 21 models (Cases 1 - 21), the same percentage difference[c] between these two methods vs. N_{gv} is plotted in Figure 4.4. The same trend is observed in this figure with an R^2 of ~0.69 thus confirming our previous finding using the homogenous model results only.

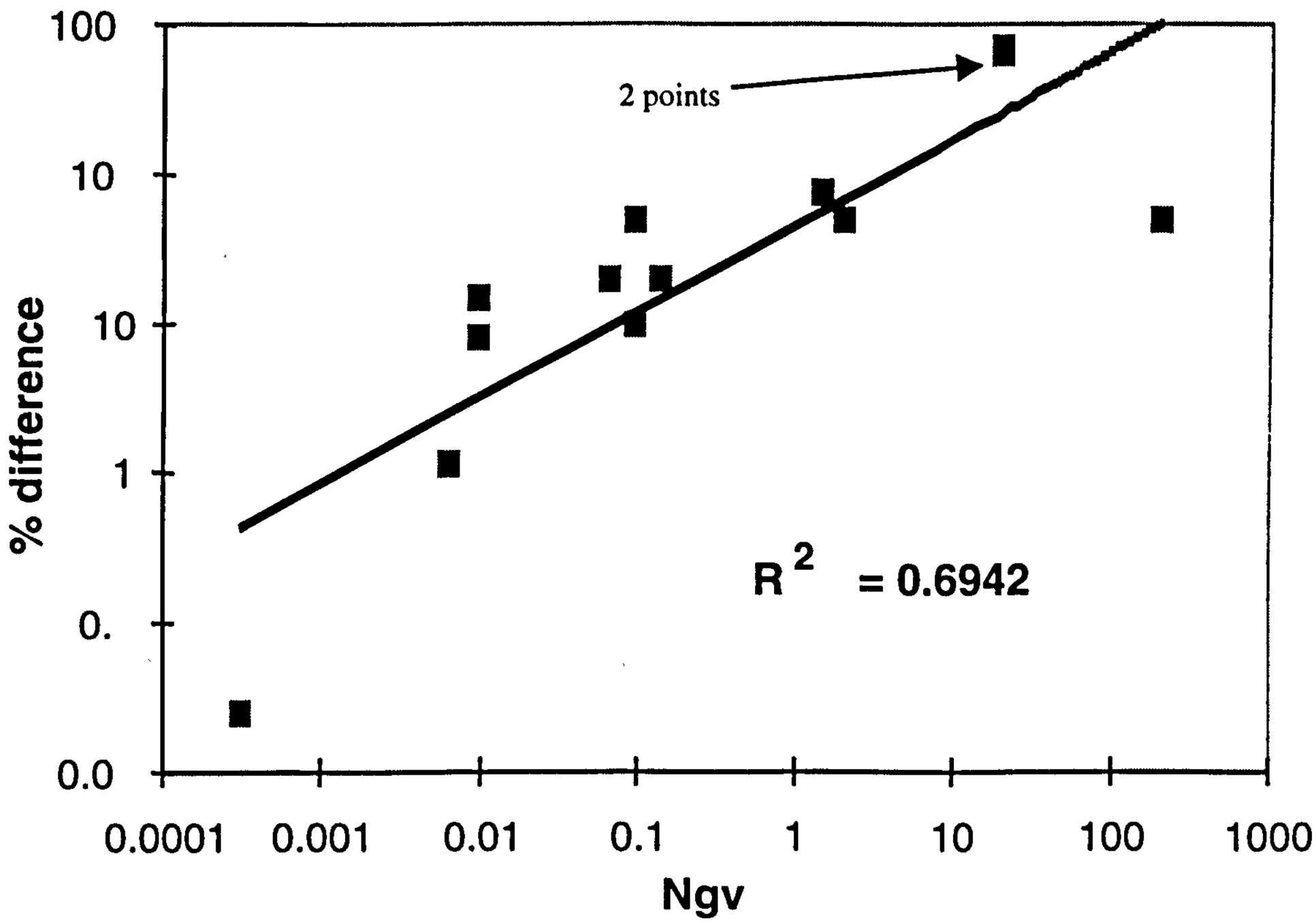

Figure 4.4: Percentage difference between the Kyte and Berry method and the TW method versus the gravity to viscous number for all the 21 models.

[c] Only two cases produced small negative numbers (Case 11 and Case 12). Both of the points were ignored because they cannot be plotted on a log-log graph.

4.3.2 Analysis of the Differences Between the TW and the Kyte and Berry Methods

There are two main differences between the TW and the Kyte and Berry methods. First, as seen in Equation (3.3), the TW method uses the transmissibility as its weighting factor in calculating the averaged fluid potential difference at the coarse grid level. On the other hand, the Kyte and Berry method uses the product of absolute permeability, relative permeability and grid block thickness as its weighting factors. All of the weighting parameters for both of the pseudo methods are evaluated at the coarse grid block centers. The second difference between these two methods is that the TW method averages the fluid potential difference directly between two coarse grid blocks whereas the Kyte and Berry method first averages the fluid potential in each individual coarse grid block then takes the difference between them to calculate the potential gradient.

4.3.2.1 Evaluation of the Averaging Method

The question that must be answered now is: which of these differences contribute to the improved performance of the TW method? Two runs were made to evaluate the relative effects of these differences, denoted as STEP 1 and STEP 2. Run STEP 1 was performed to evaluate the two differences mentioned above i.e. different weighting factors and different averaging techniques used by each of the methods. Case 7 was used as a comparison case since in this case, the difference in the quality indicator (the normalised rms error) between the two methods is almost the greatest.

Case STEP 1 uses a method that is basically the same as the Kyte and Berry method except that the run used the TW style of averaging the fluid potential difference (the weighting parameters were kept the same i.e. the product of absolute permeability times relative permeability times grid block thickness). Thus, the difference between STEP 1 and the TW method will reflect the importance of the weighting factor used and the difference between STEP 1 and the Kyte and Berry method will reflect the importance of the averaging method for calculating the fluid potential difference used by each of the pseudo techniques.

The results in Figure 4.5 show that the curves for the Kyte and Berry method and STEP 1 are barely distinguishable. This implies that the techniques for averaging the fluid potential difference between the two pseudo methods produce the same results (at least for this particular case). On the other hand, the difference in the result between STEP 1 and the TW method is very large which implies that most of the difference between the Kyte and Berry method and the TW method is caused by the different weighting factors used by each of the methods. Thus, we conclude that the weighting factor used in the TW method is the main cause of the improvement of the TW method over the Kyte and Berry method.

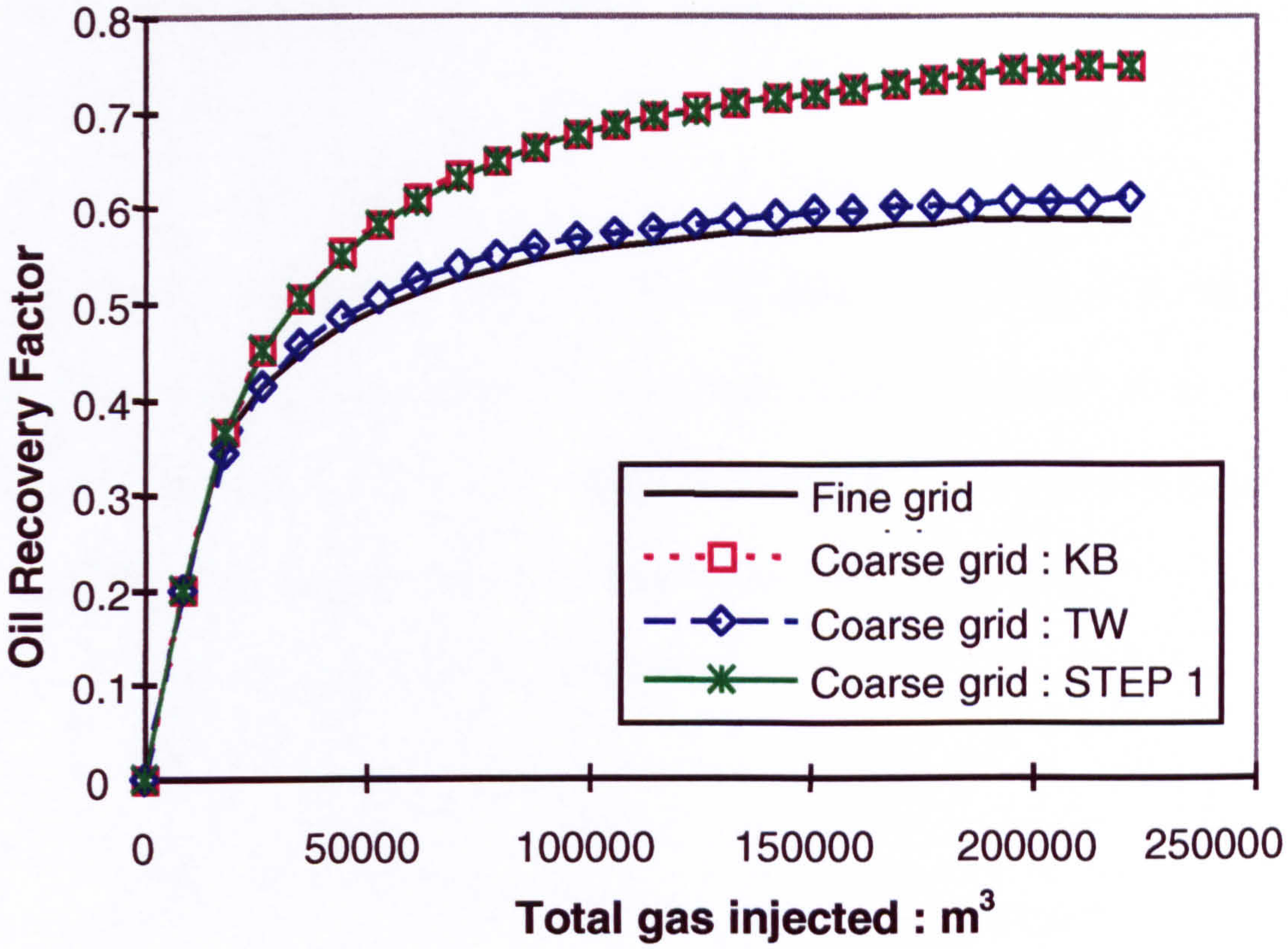

Figure 4.5: Oil recovery factor versus total gas injected showing the effect of the difference in averaging method used by the Kyte and Berry and the TW pseudo methods.

4.3.2.2 Evaluation of the Weighting Parameters

The previous result leads immediately to the next question: which of these weighting factors is good and which one is inappropriate? Run STEP 2 was performed to evaluate which of the weighting parameters used in the Kyte and Berry equations made the method less accurate compared with the TW method. Again, Case 7 was

used as a reference case for the same reasons as above. STEP 2 used a method that is basically the same as the Kyte and Berry method except that the run eliminates the use of relative permeability as a weighting parameter (only permeability times layer thickness is used).

The results as shown in Figure 4.6 clearly demonstrate that it is the relative permeability which is inappropriate as a weighting factor, especially when the flow is gravity dominated (as in Case 7). After eliminating it as a weighting factor, the performance of the Kyte and Berry method tracks very closely to the TW method and shows a considerably improved performance.

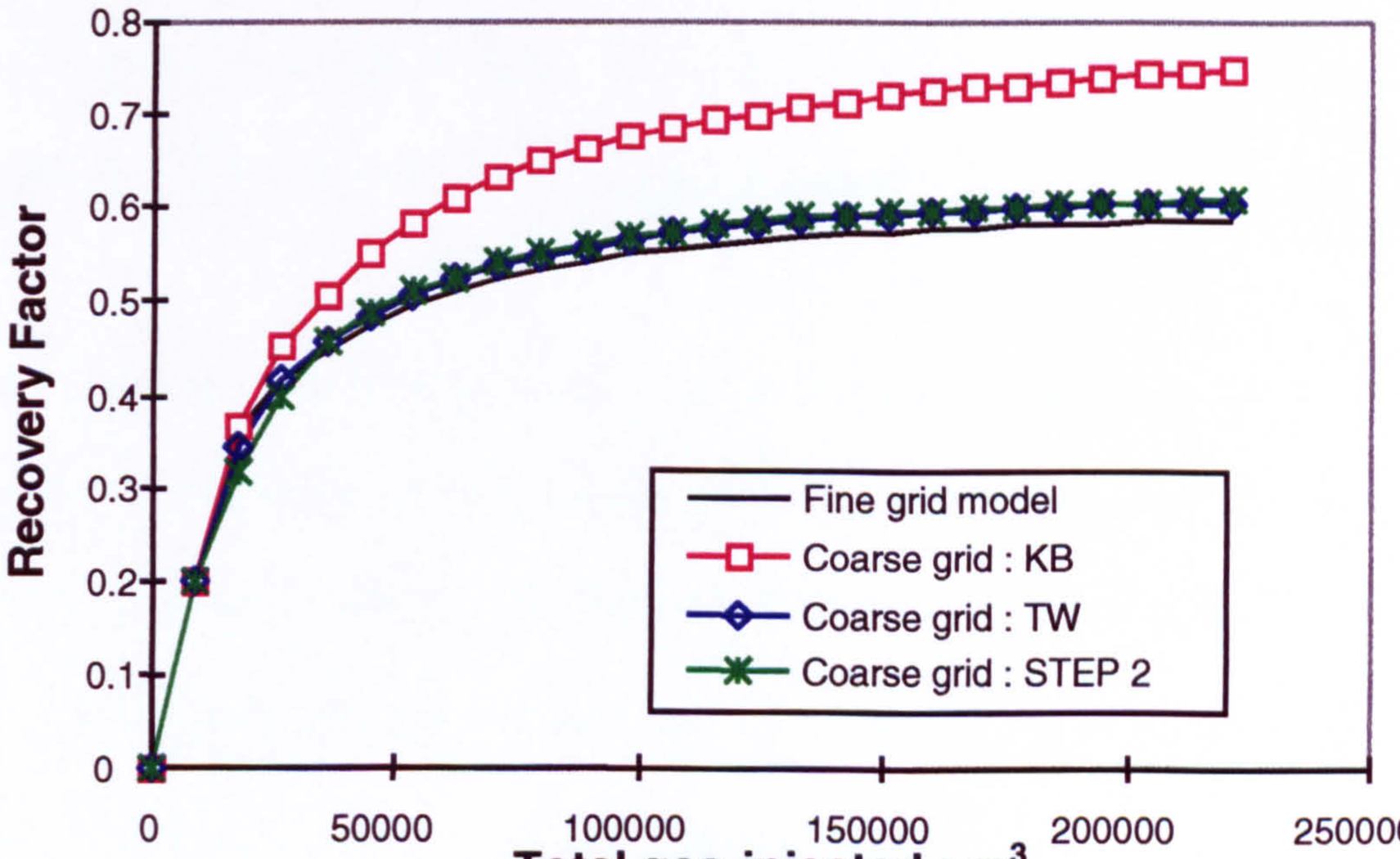

Figure 4.6: Oil recovery factor versus total gas injected showing the effect of the difference in weighting factors used by the Kyte and Berry and the TW pseudo methods.

The same results as above can also be derived using different approach. As we mentioned in Chapter 2, the Kyte and Berry method uses the following equations to define the fluid potential difference:

$$\overline{\Delta\Phi_p} = \overline{\Delta P_p} - g.\rho_p.\Delta D, \tag{4.15}$$

and the averaged pseudo phase pressure in Equation (4.15) is defined as:

$$\overline{P_p} = \frac{\sum_{k=1}^{5}\left[k_k.k_{rpk}.dz_k(P_{pk} - g.\rho_p.(D_k - D))\right]_{i=3}}{\sum_{k=1}^{5}[k_k.krpk.dz_k]_{i=3}} \tag{4.16}$$

where dz_k is the thickness of fine grid cell k. D_k is the depth of the cell, and D is the depth of the gridblock centre. From Equation (4.16), we can see that the Kyte and Berry method uses the product of phase relative permeability x the absolute permeability x layer thickness as a weighting factor.

For this case, the selection of k_{rp} as a weighting factor (which is also a function of saturation) in averaging the fluid pseudo pressures and subsequently the fluid potential difference, will set the $\overline{\Delta\Phi_g}$ to be different from the $\overline{\Delta\Phi_o}$. As we described in Section 4.2, for the horizontal model it is necessary to set the $\overline{\Delta\Phi_g}$ to be equal to $\overline{\Delta\Phi_o}$. If this is not the case then the coarse grid will produce large errors in relation to the fine grid performance. Therefore, as the gravity number becomes larger, the segregation of the two fluids will become more apparent and this method will become less accurate due to variation in fluid saturation vertically which will then affect the k_{rp} values used in the weighting factor.

4.4 THE TW VERSUS THE VE METHODS

In this section, we want to compare the performance of the TW method in relation to the VE method and we will focus our attention on two of the cases that we discussed in Chapter 3. The cases were Case 6 representing cases with low gravity to viscous ratio and Case 7 representing cases with high N_{gv}. In both of the cases, we used the normalized rms error in the total oil recovery factor as our quality index. It is reasonable to expect the VE method to fail in low gravity cases, such as Case 6. However, when the VE method failed in Case 7 (high N_{gv}), it was clear that further investigation was required. Summary of the performance for these two cases is tabulated in Table 4.2 below:

CASE	N_{gv}	TW	VE
Case 6	0.0003	0.0032 (1.0000)	**0.0715** **(22.3371)**
Case 7	19.754	0.0056 (1.0000)	**0.0261** **(4.6678)**

Table 4.2: Normalised rms error in terms of oil recovery factor for Case 6 and 7. The numbers in brackets show the normalised rms error of each method relative to the TW method.

4.4.1 Grid block Sensitivity of the VE Method

From the mathematics of the VE method, it is known that, for the homogenous models of Cases 6 and 7, the resulting pseudo functions produced by the VE method *do not depend on the number of fine grid blocks*. They depend only on the coarse grid blocks or the overall model dimensions. Figure 4.7 shows the plot of recovery factor versus the pore volume injected for the 5, 25, 50 and 200 layer models using Case 7 as the base case (high N_{gv}).

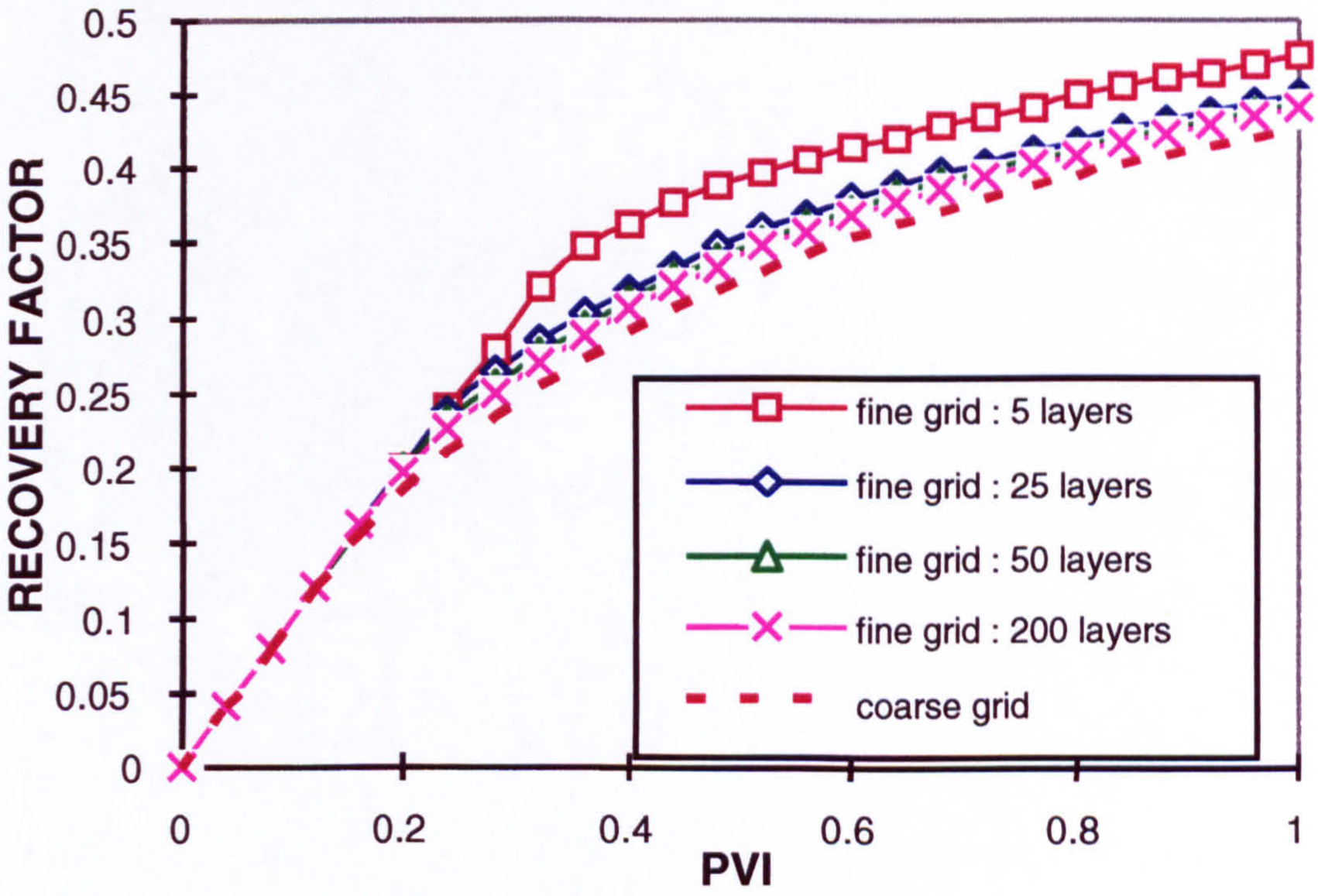

Figure 4.7: Oil recovery factor versus the pore volume injected for Case 7 (model with high gravity) showing the sensitivity of fine grid layer thickness to the oil recovery factor when VE pseudo functions are used.

The recovery profiles of the models are converging towards the coarse grid VE results with increasing numbers of layers in the fine grid block models. We conclude that the fine grid model dimension of 25 feet that we used in our previous test cases did not

resolve the segregation of fluid sufficiently accurately for the VE method to be applied. This is the reason why we surprisingly see that the VE method "fails" (in the sense that it does not reproduce the fine 5 layer grid model) in Case 7 even though the N_{gv} number is relatively high. In other words, the VE method did give the true physical answer but our 5-layer fine grid model did not reproduce this. Clearly, for Case 6 (low N_{gv}), the VE method will not work regardless of the number of layers used in the fine grid models.

4.4.2 Grid Block Sensitivity of the TW Method

In contrast to the VE method discussed above, the equations of all the dynamic pseudo methods, such as the TW method, are designed *primarily to capture the fine grid performance from which they were derived.* Figures 4.8 and 4.9 show the results for the 5 and 50 layer models using the TW method in gravity dominated and viscous dominated flows respectively. As we can see from these two figures, the results for the coarse grids using TW method are dependent on their respective fine grid simulation results only.

In summary, as long as the fine grid is accurately reproducing the physical system, which may be viscous dominated, gravity dominated or in a flow regime where all forces are significant, the TW will give accurate upscaled answers. However, if the system is actually *at* the VE limit but the fine grid cannot resolve this, then the TW will give the same (inaccurate) answer on the coarse grid as on the fine grid.

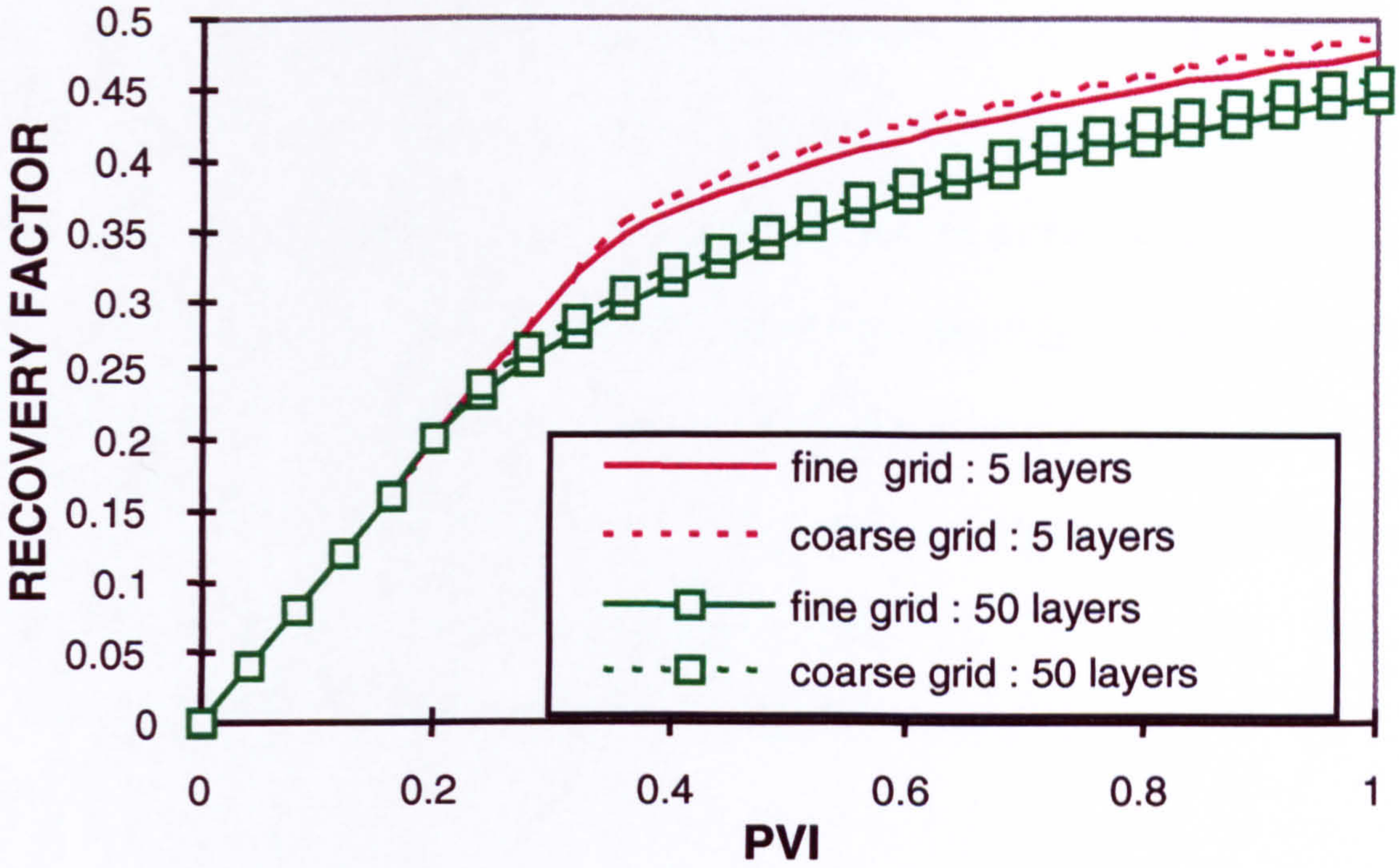

Figure 4.8: Oil recovery factor versus pore volume injected for Case 7 (model with high gravity) showing the sensitivity of fine grid layer thickness to the accuracy of pseudo functions when the TW pseudo method was used.

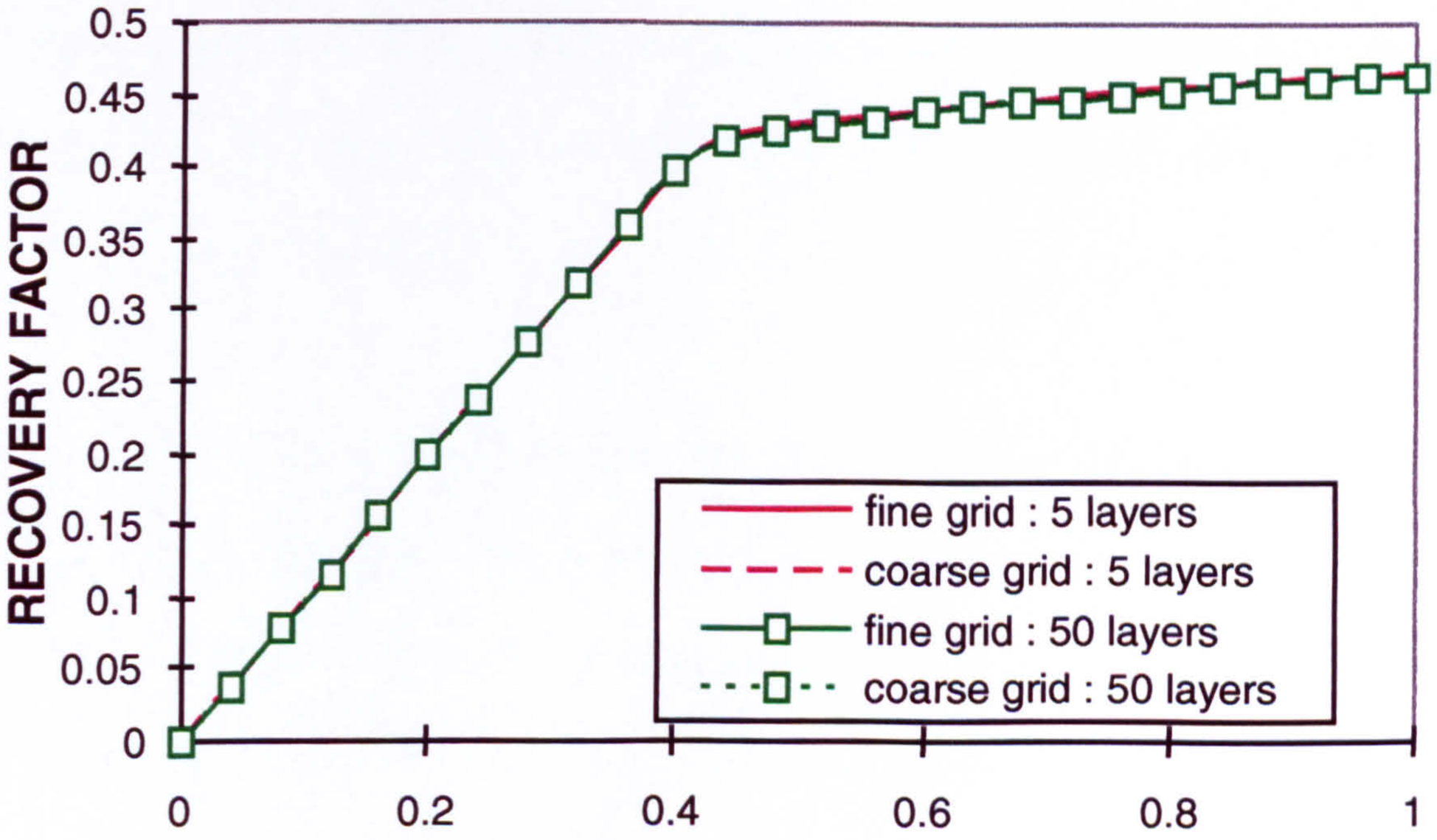

Figure 4.9: Oil recovery factor versus pore volume injected for Case 6 (model with low gravity) showing the sensitivity of fine grid layer thickness to the accuracy of pseudo functions when the TW pseudo method was used.

4.5 THE TW VERSUS THE HEWETT AND ARCHER (HA) METHODS

In Chapter 3, we can see that both of these pseudo methods produce results that are very similar in all of the test cases. This section is therefore intended to further investigate the similarities (or differences) between these two pseudo methods. In this section, we have two objectives. Firstly, we want to investigate the effect of preserving fractional flow between the fine and the coarse grid models generated by these two pseudo methods. Secondly, we also want to investigate the effect of different averaging methods of fluid potential to capture the fine-grid fluid mobility and pressure distributions in the coarse grid models.

For the first objective, we will again use two cases that we discussed in Section 4.2 to explain our findings. In the first model (Case A), the model is taken to be horizontal, whereas in the second model (Case B), the model is dipping with a 15° angle and gas is injected in the up-dip grid blocks. For the second objective, will use one of the cross-sectional models described above (Case A) as well as a quarter 5-spot model with 3D → 2D upscaling (Case C).

The descriptions of the quarter 5-spot model are as follows: The fluid viscosities, fluid densities, fine grid relative permeability, porosity and injection velocity were the same as the two previous cross-sectional models described above (Case A and Case B). This quarter 5-spot model has 100 x 100 x 3 fine grid blocks that are going to be coarsened to a 2D areal model of 20 x 20 x 1grid blocks.

Each of the fine grid blocks has a dimension of 20 meters in x-, y- and z-directions respectively and no dip is included. Permeability in the x- and z-directions is set constant at 500 md whereas permeability in the y-direction is set to 250 md. Gas was injected from an injector located at one of the four corners of the model and dead oil was produced from a well on the diagonally opposite side of the injector. Both wells were completed vertically throughout the model.

4.5.1 Effect of Preserving Fractional Flow

The first objective of this section is to investigate the effect of different fluid potential averaging methods on preserving fractional flow in the coarse grid models. As we mentioned before, we will use two cross-sectional models, each with and without dipping to illustrate our findings (Case A and Case B). Detail explanations of our results for both of the models are listed below.

4.5.1.1 CASE A (Horizontal model)

In the TW method, the averaged fluid potential difference is given by Equation (4.17) below:

$$\overline{\Delta\Phi_p} = \frac{\sum_k (T_x . \Delta\Phi_p)_k}{\sum T_x} \qquad (4.17)$$

As we can see in Equation (4.17), the same weighting factor was used for both of the fluid phases. Since the $\Delta\Phi_g$ is equal to the $\Delta\Phi_o$ for this horizontal case, the $\overline{\Delta\Phi_g}$ will

also be equal to $\overline{\Delta\Phi_o}$, although the real value of Φ_g and Φ_o can be totally different. This is the reason why this method produces very similar results to that of the Stone method as well as to the Hewett and Archer method as shown in Figure 4.1.

In the Hewett and Archer method, the averaged oil potential difference is obtained from the difference in oil potential of the two fine grid blocks located at the centre of that coarse grid block domain:

$$\overline{\Delta\Phi_o} = \Phi_{o,n} - \Phi_{o,n+1} \tag{4.18}$$

and the $\overline{\Delta\Phi_g}$ is set to be equal to $\overline{\Delta\Phi_o}$ based on the assumption that $\overline{\Delta\Phi_g} = \left[\overline{\Delta\Phi_o} + \overline{\Delta P_c} - \Delta\rho g\overline{\Delta h}\right]$ where $\overline{\Delta P_c}$ and $\Delta\rho g\overline{\Delta h}$ were zero (horizontal model). For this pseudo method, note that no information of $\Delta\Phi_g$ is required from the fine grid run.

Comparison between this method and the TW method shows that although these two methods produce a totally different shape of $\overline{k_{ro}}$ and $\overline{k_{rg}}$ as shown in Figure 4.10, the resulting fractional flows are identical as shown in Figure 4.11. Both methods produce exactly the same fractional flow curves for the coarse grid model (Figure 4.11) because $\overline{\Delta\Phi_g} = \overline{\Delta\Phi_o}$.

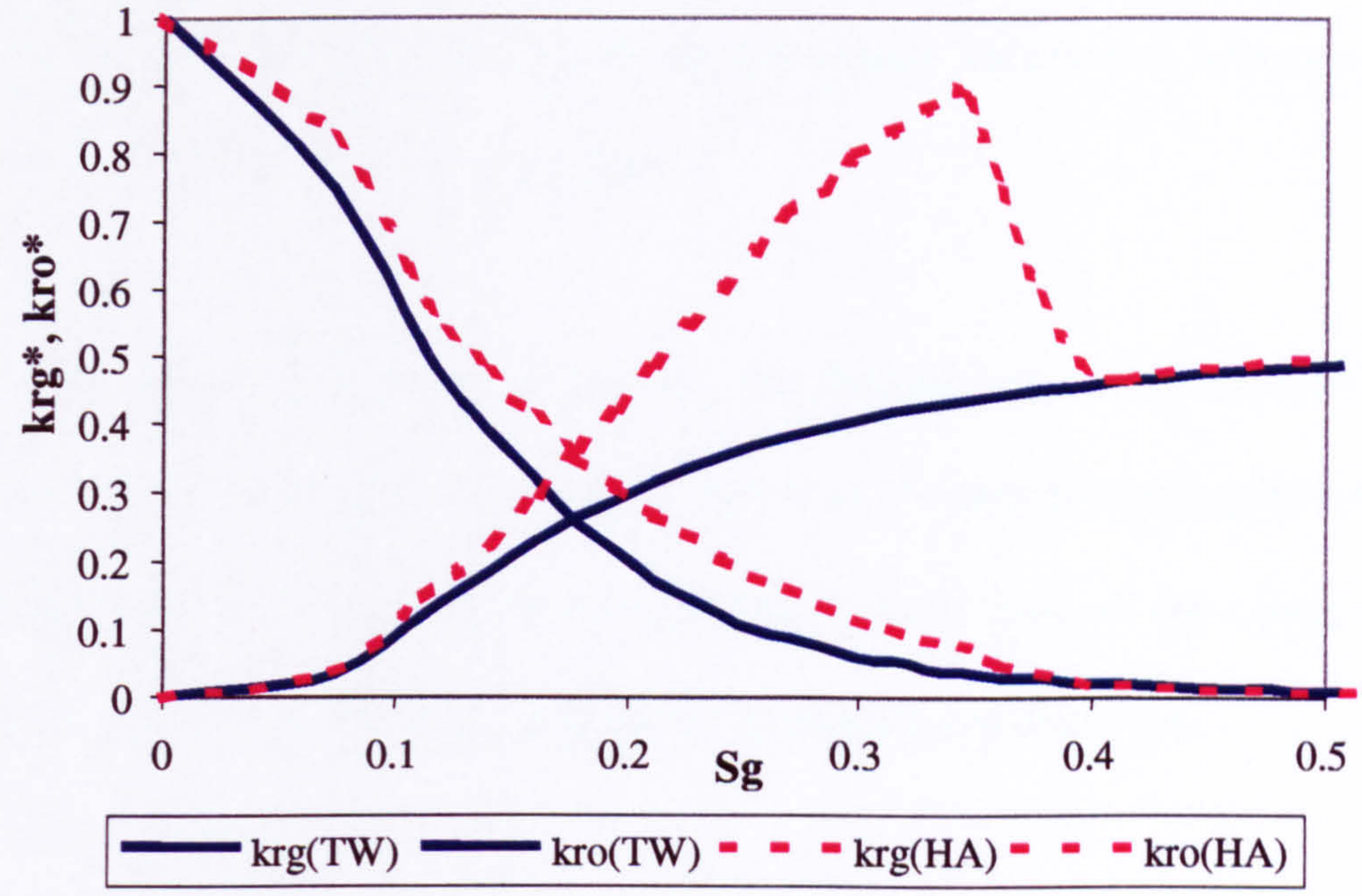

Figure 4.10: Pseudo relative permeability versus gas saturation for Case A (2D horizontal cross-sectional model) showing the totally different pseudo relative permeability derived by the TW and HA pseudo methods.

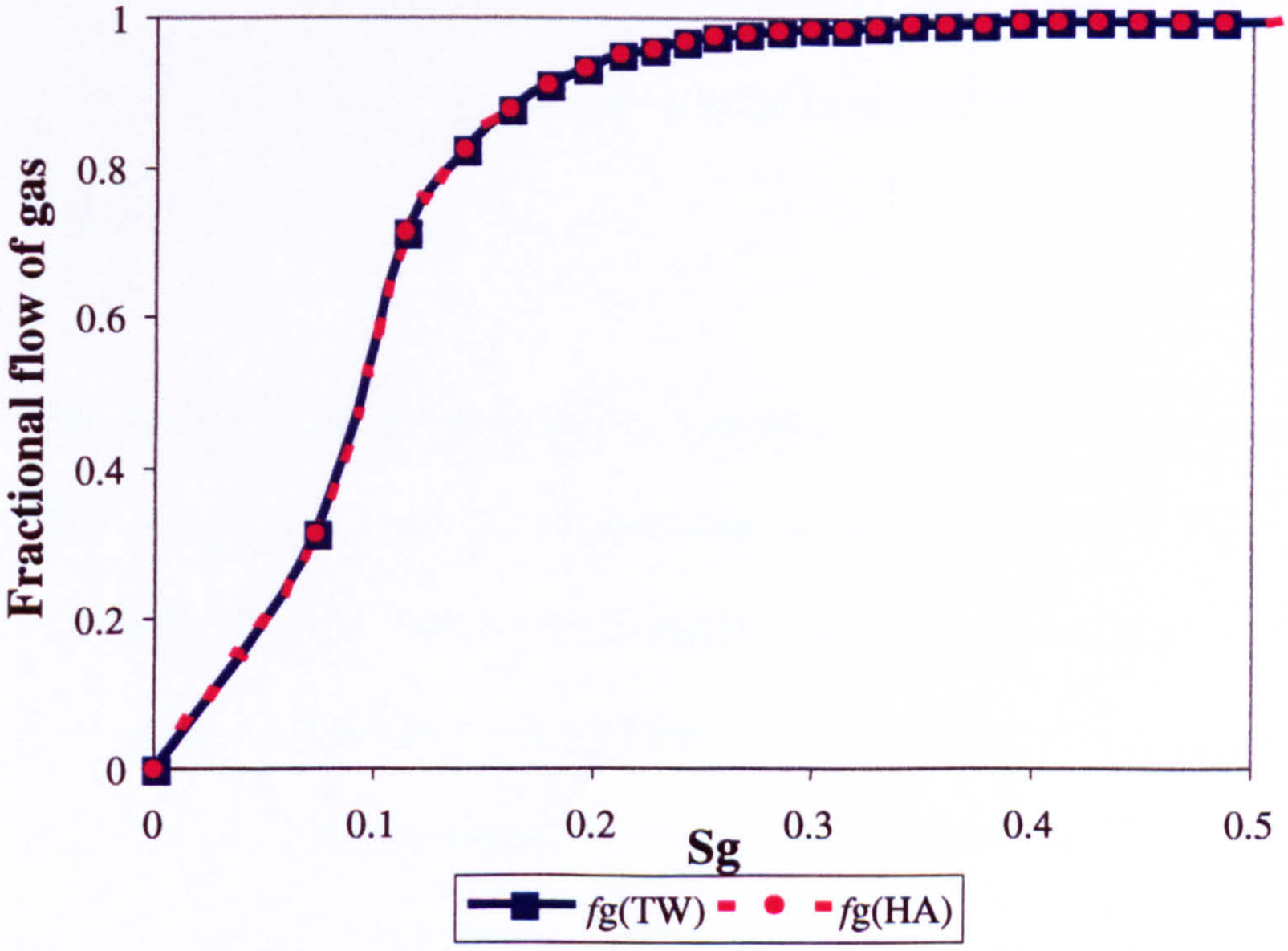

Figure 4.11: Gas fractional flow versus gas saturation for Case A (2D horizontal cross-sectional model) showing the same f_g derived by the TW and HA pseudo methods.

4.5.1.2 Case B (Dipping model)

For the case of a dipping model, there are two major differences between these two pseudo methods (HA and TW). They are:

i) For the averaged oil potential difference, the Hewett and Archer method uses only the difference in oil potential between the centre of the two coarse gridblock domains. On the other hand, the TW method uses the $\Delta\Phi_o$ derived from all the layers ($k = 1, nz$) using transmissibility as the weighting factor in calculating this value.

ii) For the averaged gas potential difference, the Hewett and Archer method uses the value derived above and then adds the gravity term ($\Delta\rho g\overline{\Delta h}$) to it. No information regarding the $\Delta\Phi_g$ is needed from the fine grid run. Alternatively, the TW method adopts the same technique as used in the calculation of the $\overline{\Delta\Phi_o}$ in calculating the $\overline{\Delta\Phi_g}$ (information derived using all the layers were used, and transmissibility was used as the weighting factor).

It appears that these two differences do not contribute to the difference in the overall results as shown in Figure 4.14. It is impossible to say one method is any better than the other from these results. There is clear margin for improvement in both methods in matching the fine grid results for Case B. Note also from Figure 4.12, that although the Hewett and Archer method produces pseudo curves (especially the k_{rg} curve) that are rather "strange" in shape, the resulting fractional flows for these two methods were almost identical as shown in Figure 4.13. Subsequently, the overall results (in terms of

the oil recovery factor) look very much the same except at the later stage of the run, where the Hewett and Archer method deviates marginally from the correct trend for this particular case as shown in Figure 4.14.

It should be noted that in this test model the dip angle was set to be 15°. In a more realistic case, this already small difference between the TW and the HA methods should become even smaller. As such, generally speaking we could expect the results between these two pseudo methods to be very similar in terms of their recovery performance at least.

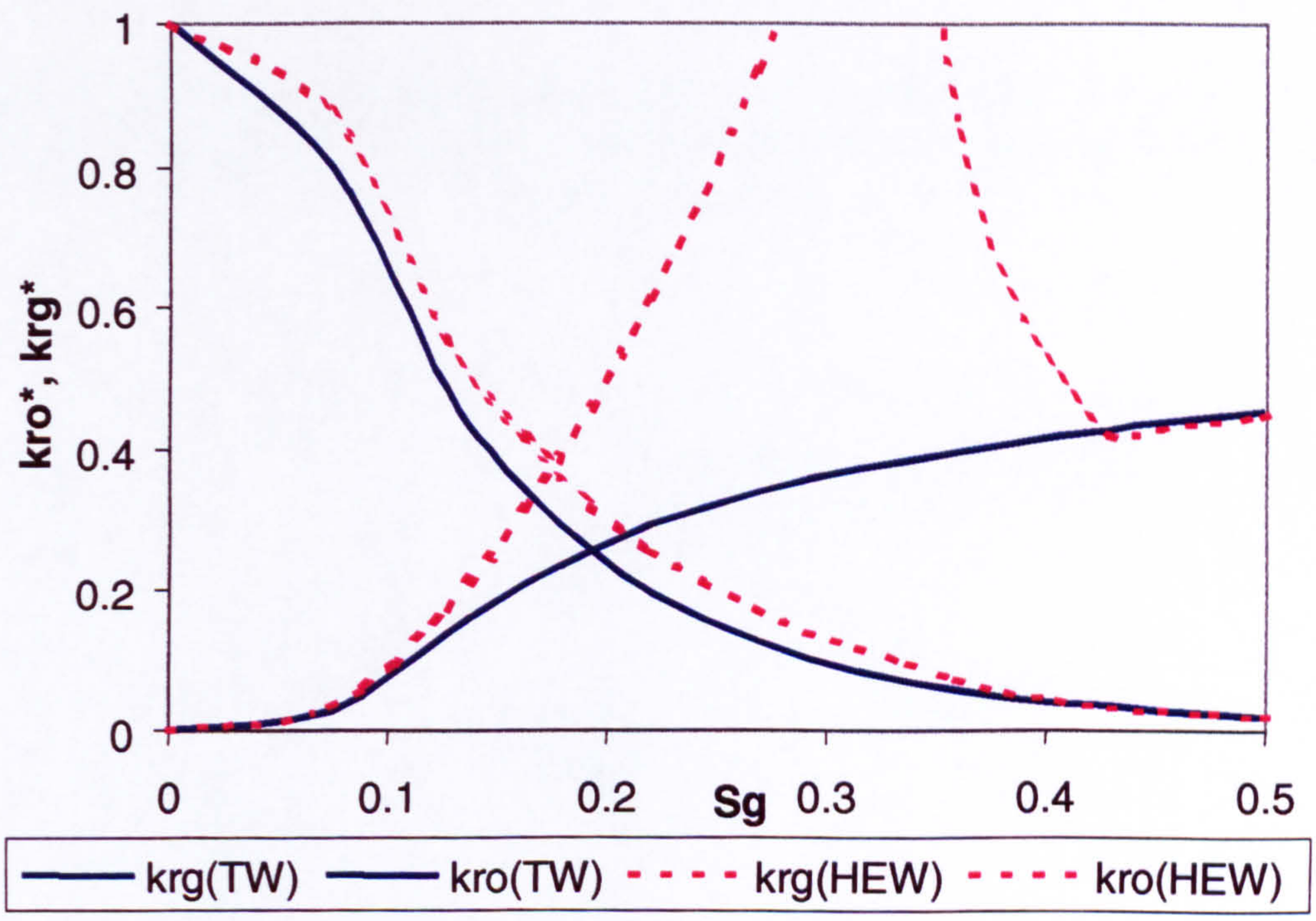

Figure 4.12: Pseudo relative permeability versus gas saturation for Case B (2D cross-sectional model with 15° dipping) showing the totally different pseudo relative permeability derived by the TW and HA pseudo methods.

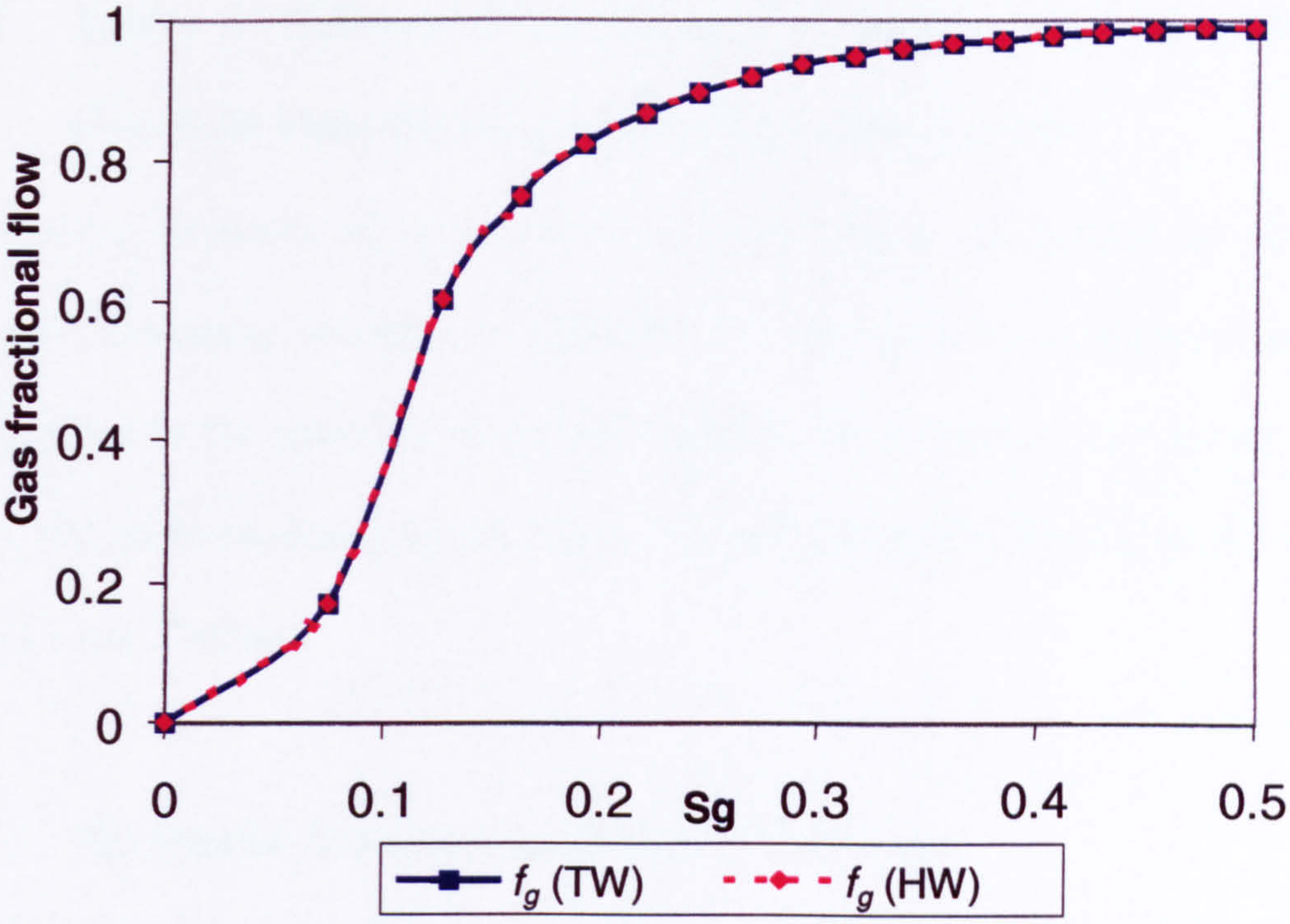

Figure 4.13: Gas fractional flow versus gas saturation for Case B (2D cross-sectional model with 15° dipping) showing the minor difference of f_g derived by the TW and HA pseudo methods.

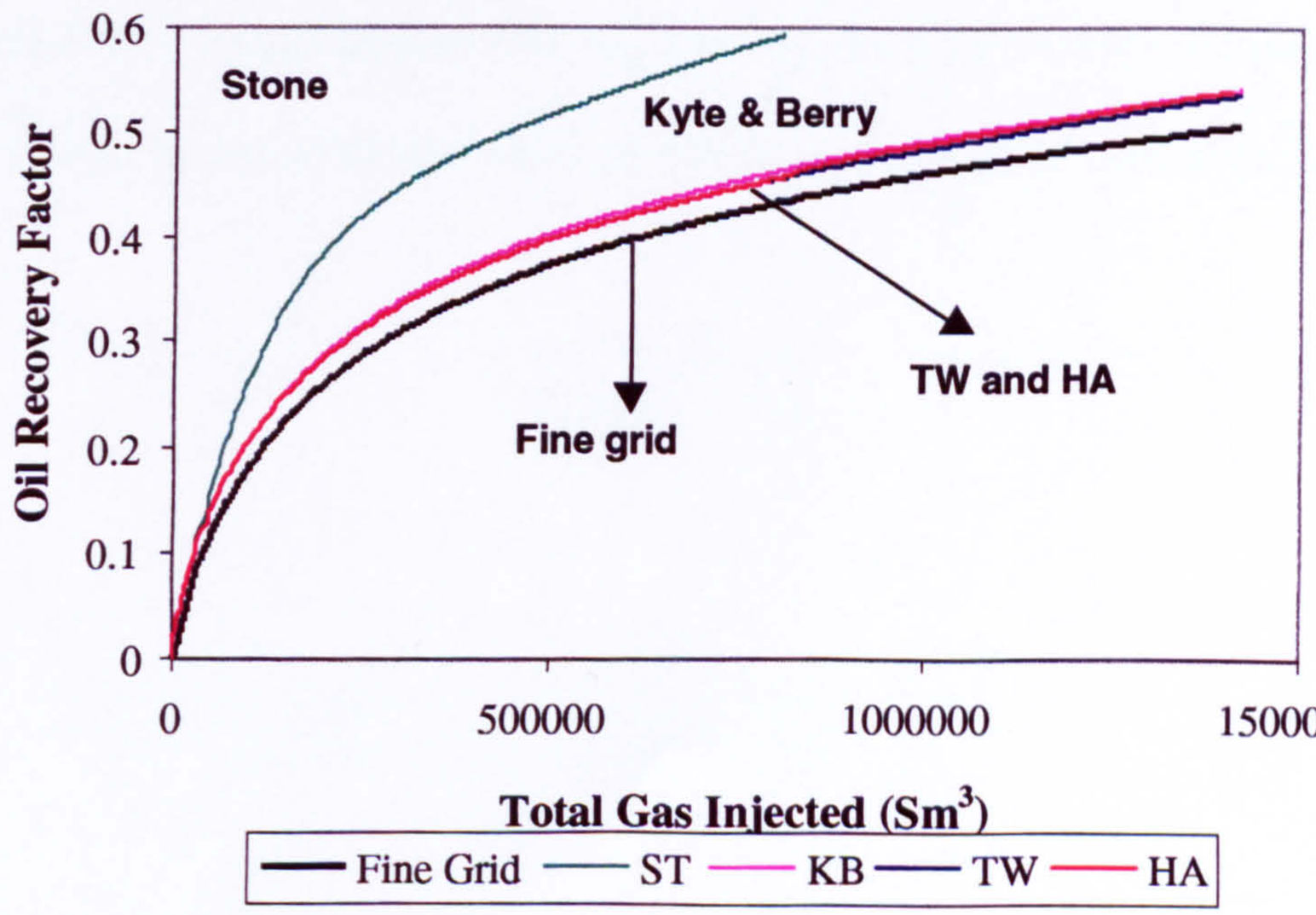

Figure 4.14: Oil recovery factor versus total gas injected showing the performance of the four dynamic pseudo methods (the KB, the Stone, the TW and the HA) relative to the fine grid model for Case B (2D cross-sectional model with 15° dipping).

4.5.2 Ability of Different Fluid Potential Averaging Methods to Preserve the Fine-Grid Fluid Mobility and Pressure Distributions

The second objective of this section is to investigate the ability of different fluid potential averaging methods to preserve the fine-grid fluid mobility and pressure distributions in the upscaled coarse grid models. As mentioned previously, we use our horizontal cross-sectional model (Case A) and our quarter 5-spot model (Case C) to illustrate our findings.

4.5.2.1 Horizontal Cross-Sectional Model (CASE A)

We first investigate which of these two pseudo methods (HA or TW) reproduce the "correct" pressure distribution of the fine grid model. Figures 4.15a to 4.15c show the trend of fluid potential difference between the centre of one particular grid block (n) to the centre of the next downstream coarse block (n+1). We show this for the first, second and fifth coarse grid blocks respectively. In each of these figures, there are six different lines as described below (illustrated using the first coarse grid block, Figure 4.15a):

Name of the lines	Description
Fine(z=1)	This is the line of the **fine-grid** fluid potential difference at the top of the model. $\Rightarrow \Phi_{(3,1,1)} - \Phi_{(8,1,1)}$
Fine(z=50)	This is the line of the **fine-grid** fluid potential difference at the middle of the model. $\Rightarrow \Phi_{(3,1,50)} - \Phi_{(8,1,50)}$
Fine(z=100)	This is the line of the **fine-grid** fluid potential difference at the bottom of the model. $\Rightarrow \Phi_{(3,1,100)} - \Phi_{(8,1,100)}$
Arit. Ave	This is the line of the **arithmetic average of the fine-grid** fluid potential difference. $\Rightarrow \frac{\sum_{z=1}^{100} \Phi_{(3,1,z)} - \Phi_{(8,1,z)}}{100}$
Trans. Ave	This is the line of the **Transmissibility weighted average of the fine-grid** fluid potential difference. $\Rightarrow \frac{\sum_{z=1}^{100} Tx_{(3,1,z)} \cdot [\Phi_{(3,1,z)} - \Phi_{(8,1,z)}]}{\sum_{z=1}^{100} Tx_{(3,1,z)}}$
TW	This is the line of the **coarse-grid** fluid potential difference when TW pseudo functions are used. $\Rightarrow \Phi_{(1,1,1)} - \Phi_{(2,1,1)}$
HA	This is the line of the **coarse-grid** fluid potential difference when HA pseudo functions are used. $\Rightarrow \Phi_{(1,1,1)} - \Phi_{(2,1,1)}$

Table 4.3: Description of the lines used in Figure 4.15a. Lines for Figure 4.15b and 4.15c were defined analogously to Figure 4.15a described above.

From these three figures, we can see that the difference between the six lines described above became smaller as we moved away from the injector. In the fifth coarse grid block (Figure 4.15c), the difference is so small that it does not matter at which layer

we are taking the measurement (i.e. top, middle, bottom, arithmetic average or transmissibility weighted average). At this coarse grid block (and subsequent coarse grid blocks away from the injector), all the lines of fine-grid $\Delta\Phi$ are almost identical to the two coarse-grid $\Delta\Phi$ calculated by the TW and HA pseudo methods.

However, as we show in Figures 4.15a and 4.15b, there are some differences for the first few grid blocks near the injector. In Figure 4.15a, we can see that there are large differences in $\Delta\Phi$ measured at the top, middle and bottom of the fine grid blocks. These different $\Delta\Phi$ values will then differentiate the $\Delta\Phi$ calculated by different averaging schemes (arithmetic or transmissibility weighted). Plotting the coarse-grid $\Delta\Phi$ on the same figure reveals one interesting observation. The coarse grid $\Delta\Phi$ calculated by the HA method tracks very closely to the fine-grid $\Delta\Phi$ measured at the middle of the fine grid model. On the other hand, the coarse-grid $\Delta\Phi$ calculated by the TW method tracks closely to the transmissibility weighted averaged of the fine-grid $\Delta\Phi$. These results are expected since they follow exactly the mathematics behind the two pseudo equations. Refer to Equations (4.17) and (4.18) on how the TW and HA methods calculate the $\overline{\Delta\Phi}$ quantities, respectively.

Knowing that the fluctuation of the fine-grid $\Delta\Phi$ is significant especially at the coarse grid blocks near the injector, one important question arises. ***Which one of these fine-grid $\Delta\Phi$ values is correct and should be reproduced by the coarse grid model?*** At this point, we will treat any method that reproduces the correct fractional flow and results in a $\overline{\Delta\Phi}$ that falls within a "tolerance limit" as a good pseudo method. As such, we

conclude that both HA and TW pseudo methods perform equally well in matching the fine grid fractional flow as well as the fluid mobility compared to the other two well-known pseudo methods of the Kyte and Berry and the Stone as well as the VE method in this specific case.

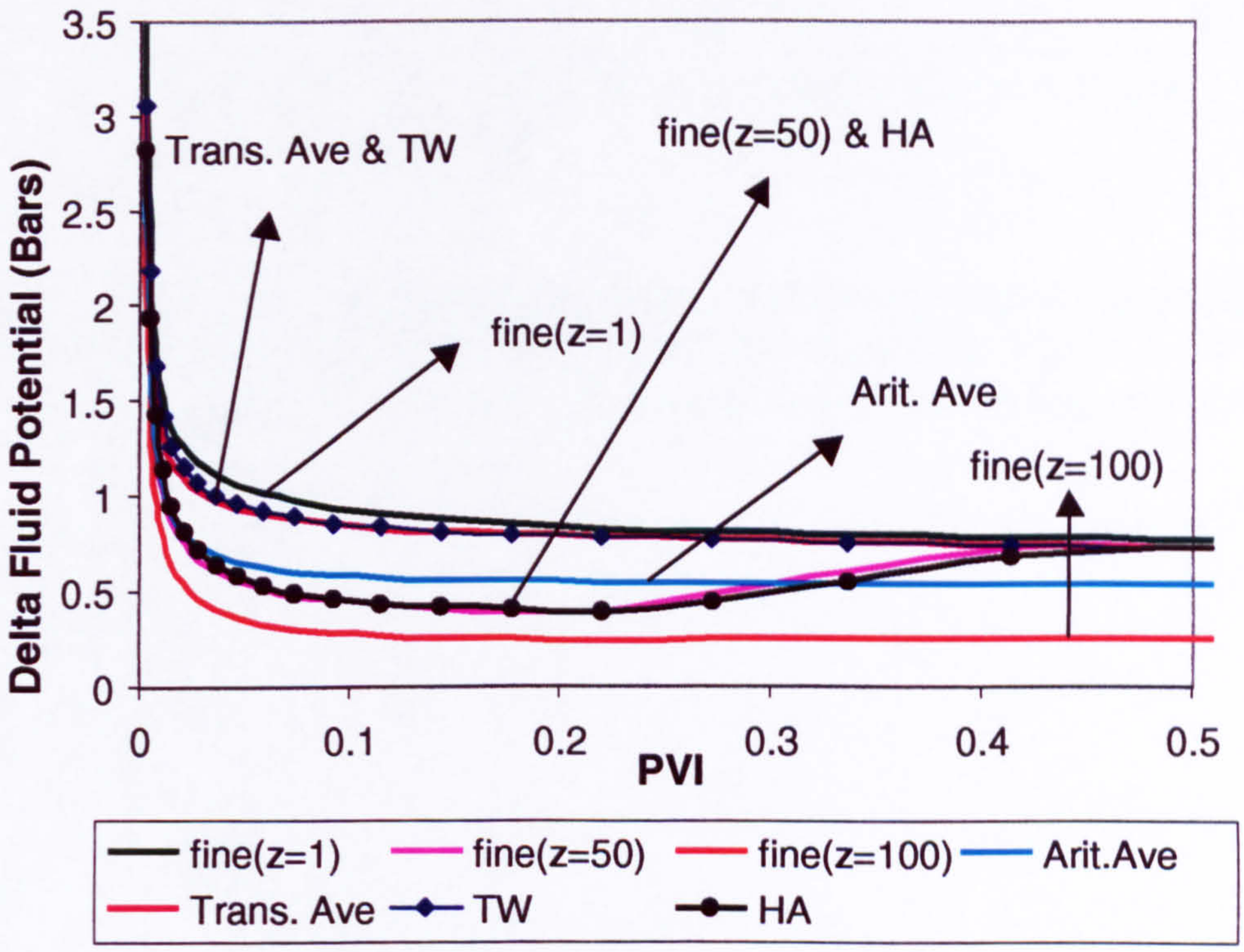

Figure 4.15a: Difference in fluid potential versus pore volume injected for the first coarse grid block (Case A) showing big variation of $\Delta\Phi$ measured at the top, middle and bottom of the fine grid model.

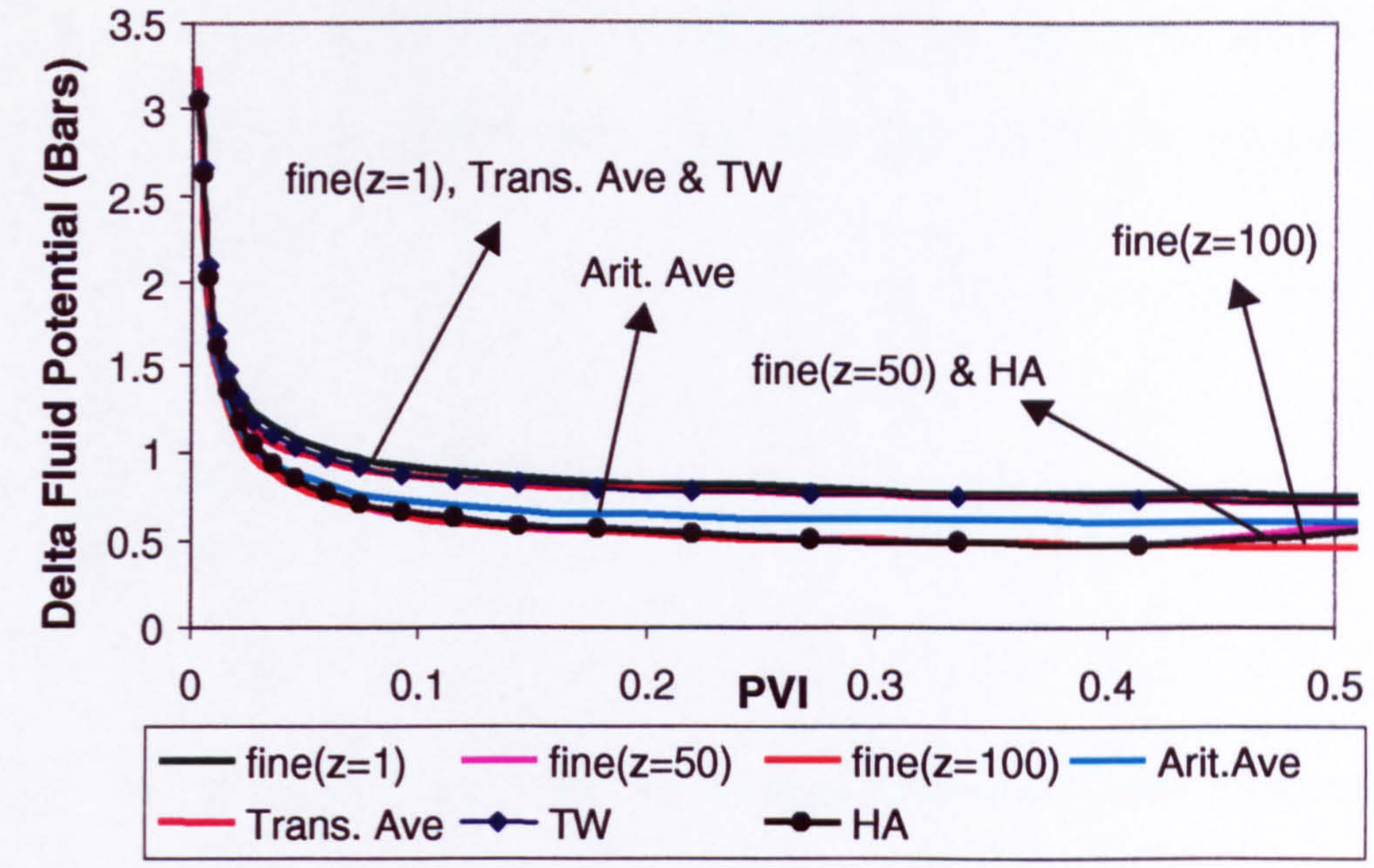

Figure 4.15b: Difference in fluid potential versus pore volume injected for the second coarse grid block (Case A) showing smaller (compared to Figure 4.15a) variation of $\Delta\Phi$ measured at the top, middle and bottom of the fine grid model.

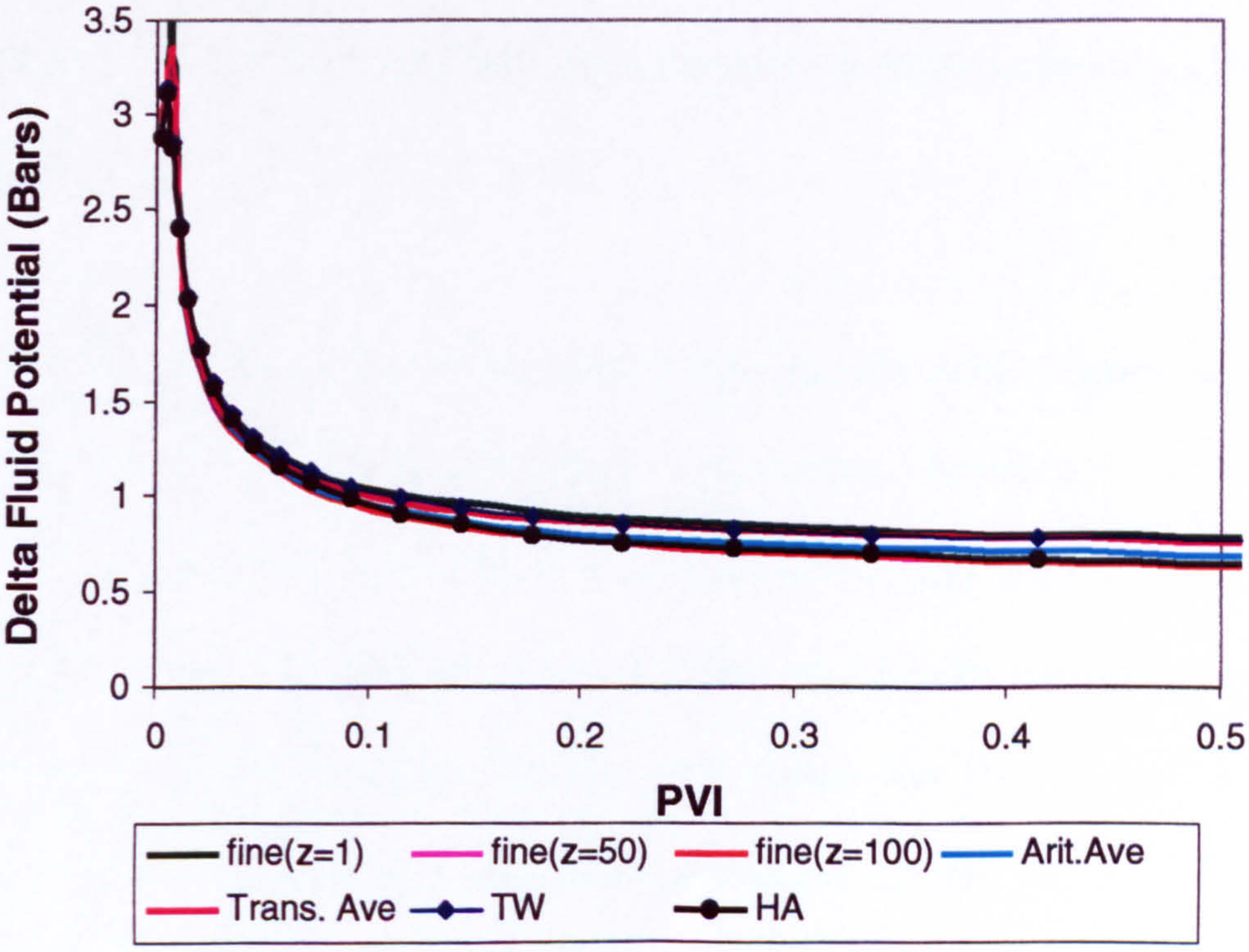

Figure 4.15c: Difference in fluid potential versus pore volume injected for the fifth coarse grid block (Case A) showing small variation of $\Delta\Phi$ measured at the top, middle and bottom of the fine grid model.

However, as shown in Figure 4.10, the different shape of the pseudo relative permeability will set the total mobility derived by these two pseudo methods to be different in the coarse grid models. The total fluid mobility at the coarse grid scale is defined as follows:

$$\overline{M_t} = \frac{\overline{k_{ro}}}{\overline{\mu_o}} + \frac{k_{rg}}{\overline{\mu_g}} \tag{4.19}$$

As we can see in Figure 4.10, the HA method produces a coarse grid model that has a larger (or equal) total mobility compared to the TW method. This is because at any given saturation, the HA method produces pseudo relative permeability that is equal to or larger than that the TW method (for both the k_{ro} and k_{rg}). The question that must be answered now is: how will this result affect the overall performance of the coarse grid model?

In order to obtain the respective fluid phase pseudo relative permeability, both of the pseudo methods basically solve Darcy's equation as shown in Equation (3.1). From the mathematics of the HA method, it is known that this method will utilise the fluid potential difference obtained from the fine grid blocks located at the centre of the coarse grid block boundary. On the other hand, the TW method will more closely honour the fluid potential difference measured at the top of the model since the permeability distribution is set to be exponentially increasing upwards in this model. From Figure 4.15, it can be shown that the HA method is actually using $\Delta\Phi$ that is smaller (or equal) compared to the TW method at least for first few coarse grid blocks

near the injector. This is the reason why the derived pseudo relative permeability for the HA method is larger (or equal) than the TW method, which can then be translated to having a larger total mobility.

However, when the coarse grid models are run, the same Darcy equation is solved. Since the injection rate is set constant as in the fine grid model, the smaller magnitude of $\overline{\Delta\Phi}$ in the HA method will roughly cancel out the larger value of $\overline{k_{rp}}$ (or mobility) as shown in Figure 4.15a. In contrast, the larger value of $\overline{\Delta\Phi}$ used in the TW method will cancel out the smaller $\overline{k_{rp}}$ produced by the TW method. This is the reason why these two pseudo methods still produce the same results although the total mobility for the two methods are different from each other.

This result leads immediately to the next question: what happen if the constant injection rate boundary condition used in this model is changed to constant pressure drop across the whole model? This later boundary condition will now set the injection rate to be different with time and so the previous argument of $\overline{\Delta\Phi}$ and $\overline{k_{rp}}$ cancelling each other due to constant injection rate may not be valid anymore.

4.5.2.2 Horizontal Cross-Sectional Model (CASE A) with Constant Pressure Drop Boundary Condition.

Case A was re-run, but this time the model was set to be controlled by constant pressure drop across the entire model. Figures 4.16 and 4.17 show the performance of the two pseudo methods in reproducing the fine grid total flow rate (versus time) and

fractional flow (versus gas saturation) for the first coarse grid block respectively. From these two figures, it is conclude that although the boundary condition is now changed, the results are still more or less the same as discussed in the previous section (both of the pseudo methods perform rather similarly). The reason for this finding is that although the simulation is controlled by constant pressure drop across the whole model, it cannot guarantee a constant $\Delta\Phi$ for each of the layer as confirmed by Figure 4.18. In this figure, it is shown that the HA method still follows the $\Delta\Phi$ calculated at the middle of the model, whereas the TW method honours more $\Delta\Phi$ calculated at the top of the model and the value of $\overline{\Delta\Phi}$ and $\overline{k_{rp}}$ still roughly cancels each other. In fact, if the model is set at constant $\Delta\Phi$ for each of the layer, the HA and TW methods will both produce identical pseudo functions.

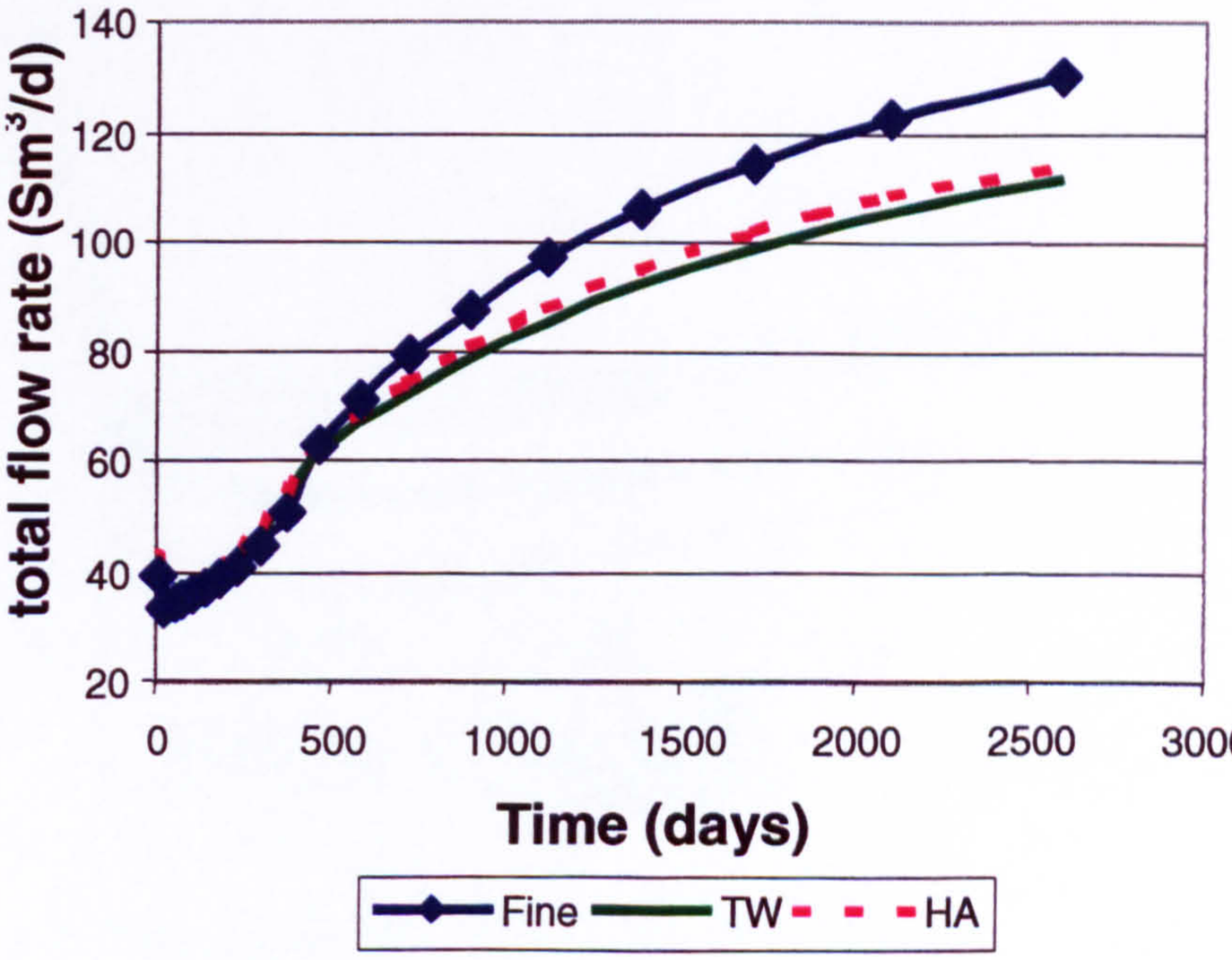

Figure 4.16: Total flow rate versus time for Case A with constant pressure drop across the whole model.

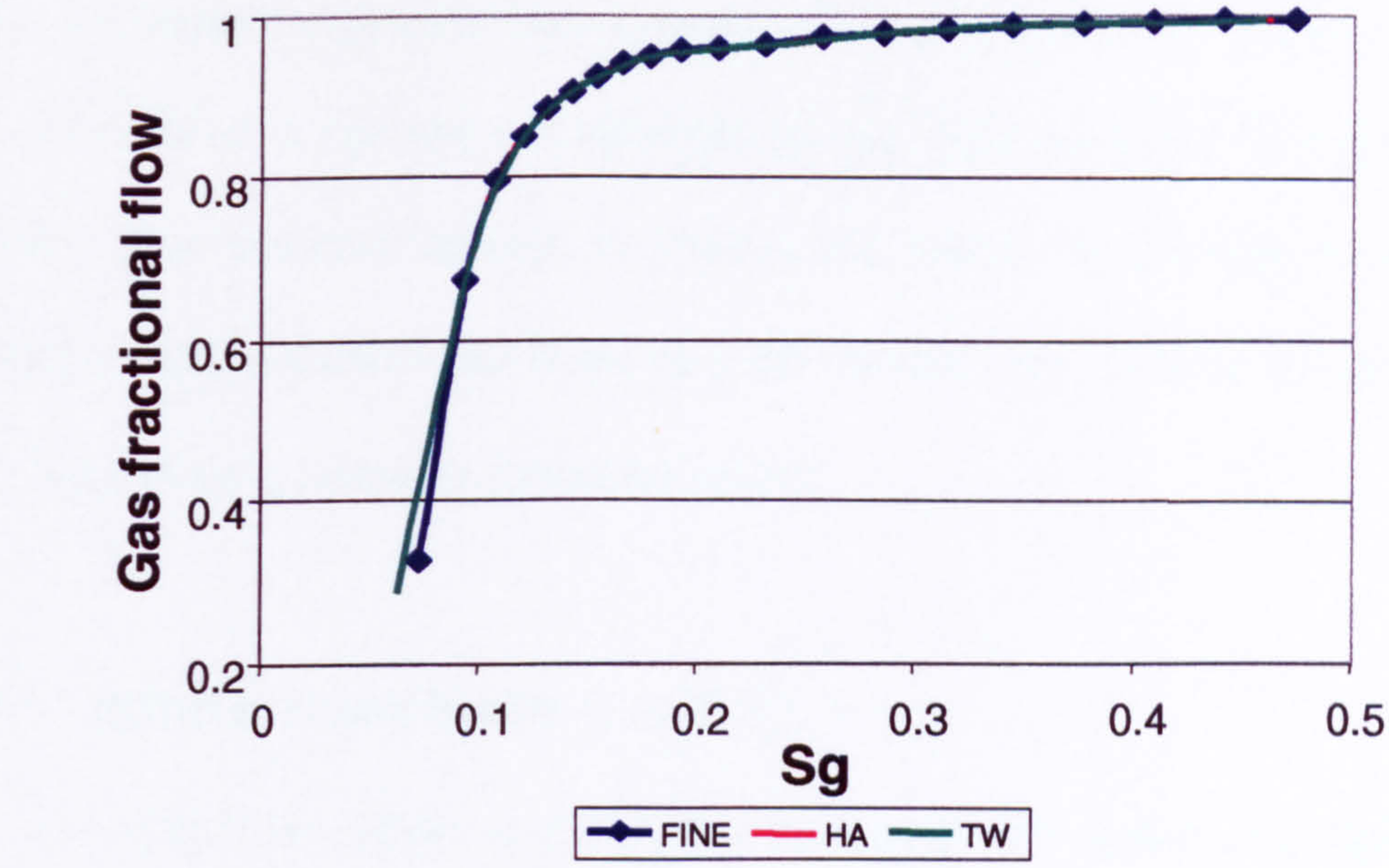

Figure 4.17: Gas fractional flow versus gas saturation for Case A with constant pressure drop across the whole model.

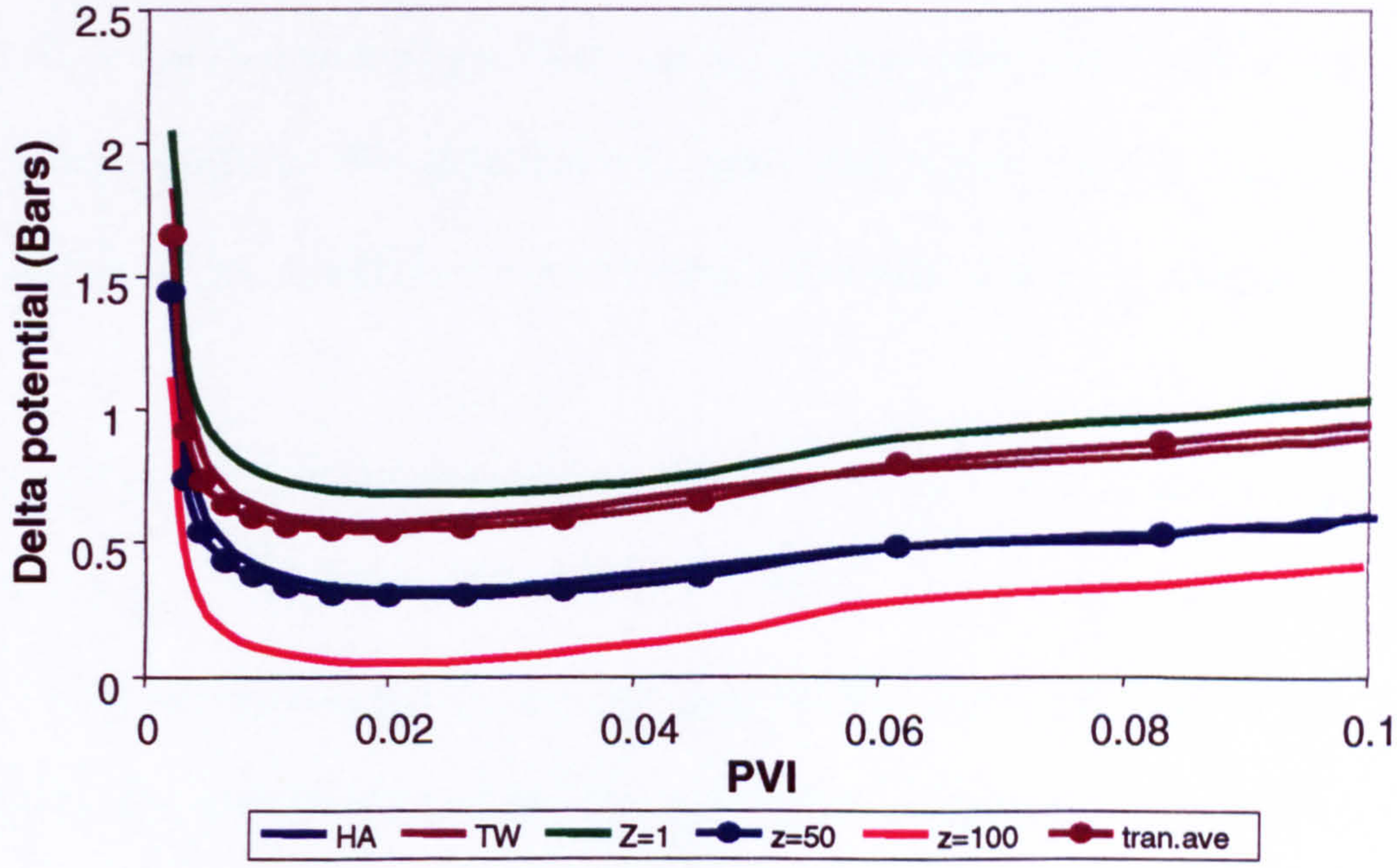

Figure 4.18: Difference in fluid potential versus pore volume injected for Case A with constant pressure drop across the whole model.

Hence, a straight comparison between the coarse grid potential and that on the fine grid does not resolve things since it depends on our view of which fine grid potential is "correct". We therefore attempt to resolve the matter by deriving a case where the resulting mobilities affect the flows in a 2D system. This is done by developing a 3D → 2D upscaling problem as described below.

4.5.2.3 Quarter 5-spot Model (CASE C)

We believed that the effect of different coarse grid $\overline{\Delta\Phi}$ values calculated by the two pseudo methods would become more apparent in 3D → 2D scaleup especially if the fluid flow and pressure distributions in each of the x-, y- and z- directions was totally different. As such, we developed a quarter 5-spot model with different permeability values in the x- and y- directions to simulate this condition (PERMY = 0.5 PERMX). Figure 4.19 shows a plot of gas flow rate versus gas saturation for the first coarse grid block which confirms this phenomenon. From this figure, we can clearly see that the gas flow rate in the x-direction is much larger than that in the y-direction.

Figure 4.20 shows the performance in terms of oil recovery factor of the coarse grid models using HA pseudos, TW pseudos and by direct usage of fine grid relative permeability in comparison to the fine grid model. From this figure, we can hardly distinguish the performance of the fine grid model from the two pseudo methods. On the other hand, the performance of the coarse grid model using fine grid relative permeability shows quite a large deviation from the fine grid results. Figures 4.21 and 4.22 show the comparison of the coarse-grid gas flow rate and fractional flow to the fine grid results respectively. We show this separately for the x- and y- directions.

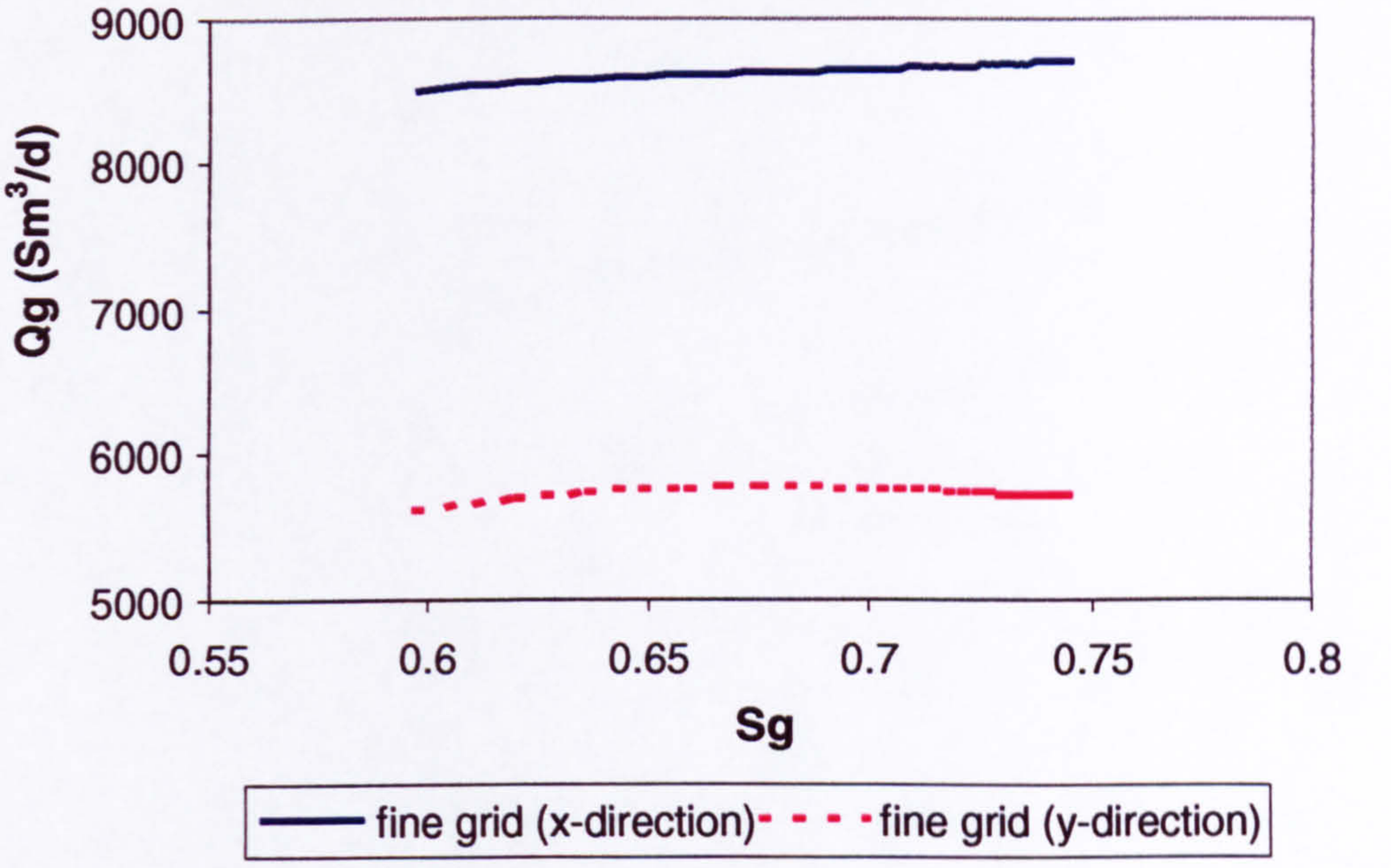

Figure 4.19: Gas flow rate versus Gas saturation for the quarter 5-spot model showing the different flow rate in the x- and y-directions.

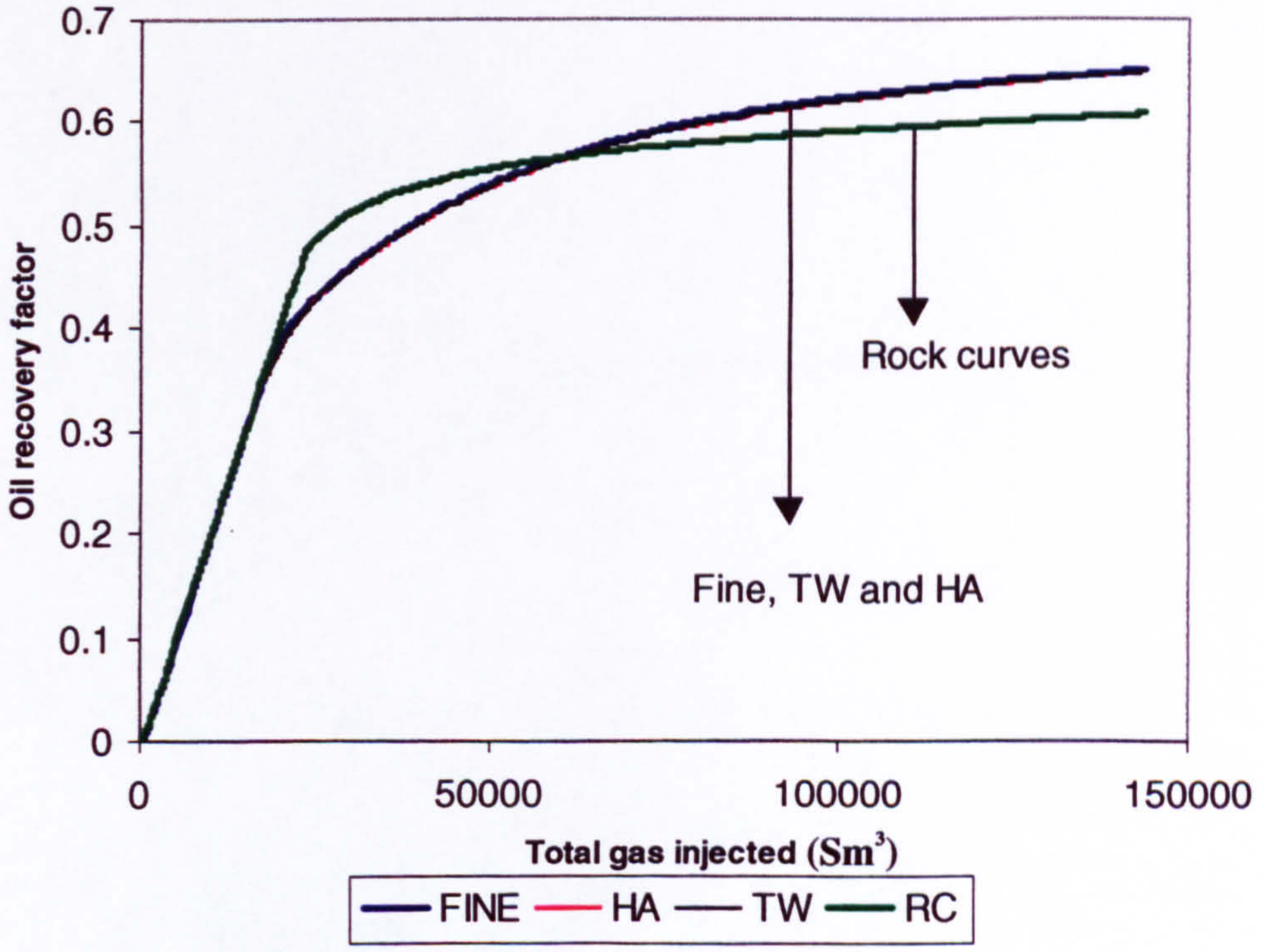

Figure 4.20: Oil recovery factor versus total gas injected showing the performance of the four dynamic pseudo methods (KB, Stone, TW and HA) relative to the fine grid model for Case C (Quarter 5-spot model).

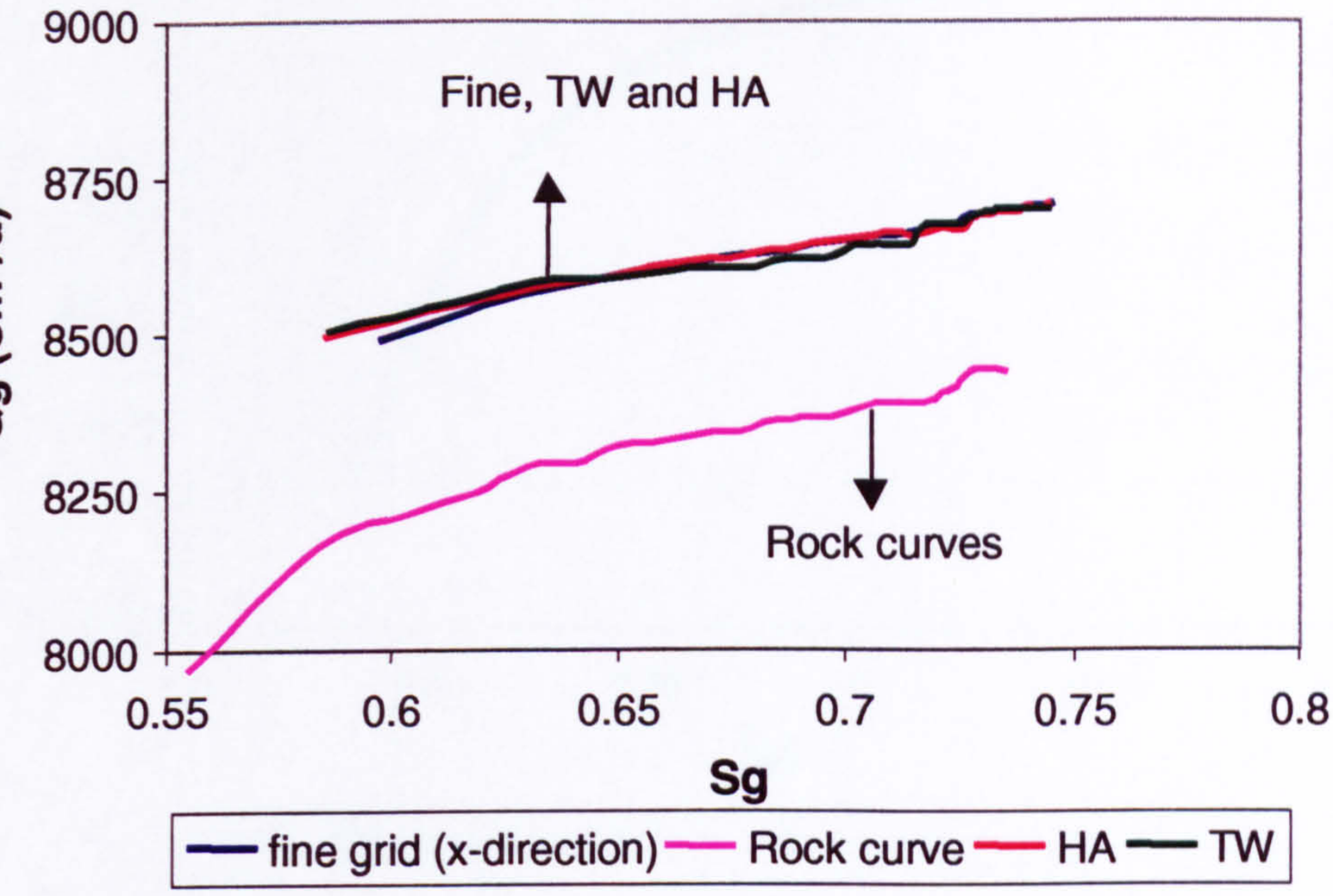

Figure 4.21a: Gas flow rate in the x-direction versus gas saturation for the quarter 5-spot model showing the similarity between the Q_g produced from the coarse grid models using pseudos and the fine grid model.

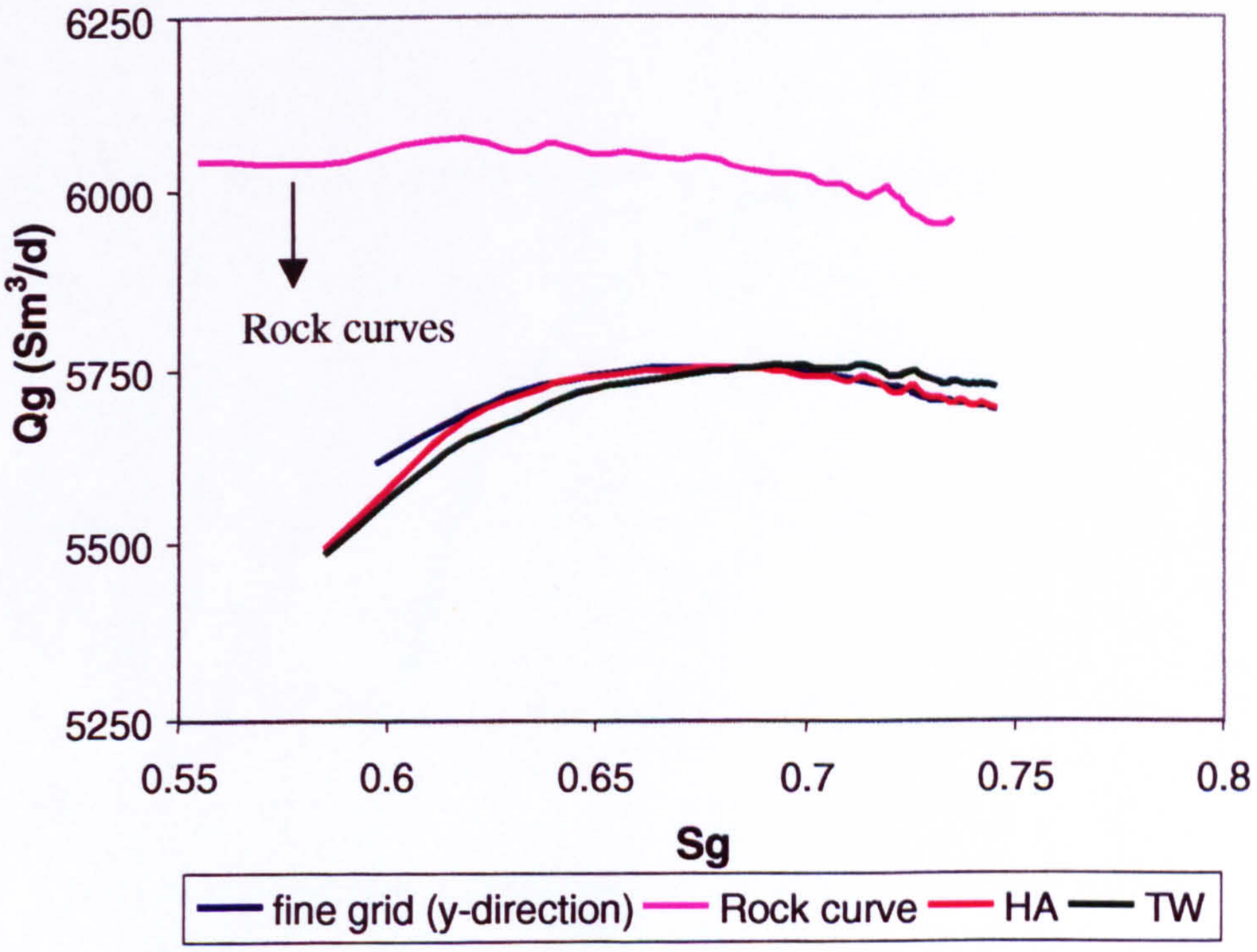

Figure 4.21b: Gas flow rate in the y-direction versus gas saturation for the quarter 5-spot model showing the similarity between the Q_g produced from the coarse grid models using pseudos and the fine grid models.

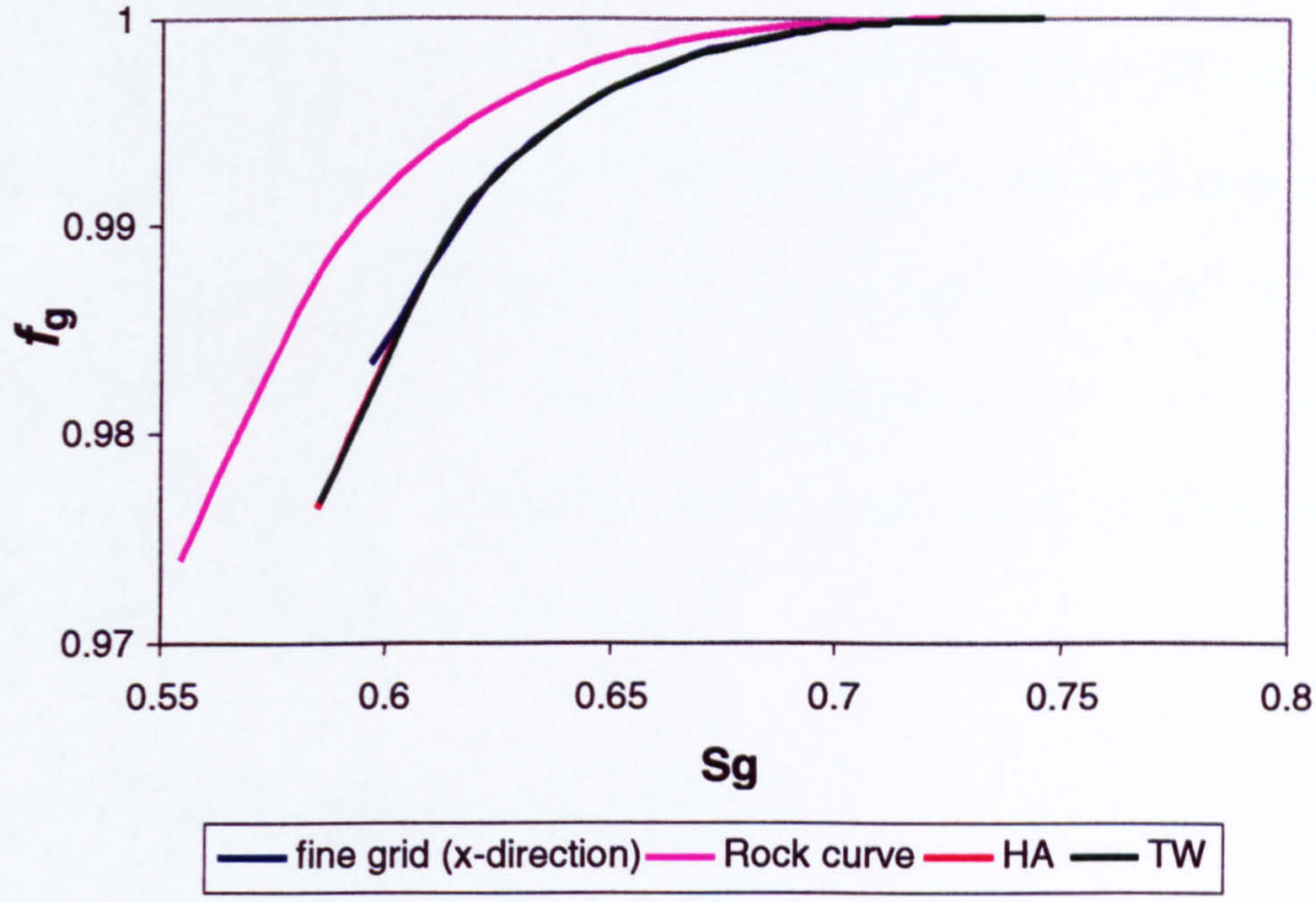

Figure 4.22a: Fractional flow in the x-direction versus gas saturation for the quarter 5-spot model showing the similarity between the f_g produced from the coarse grid models using pseudos and the fine grid model.

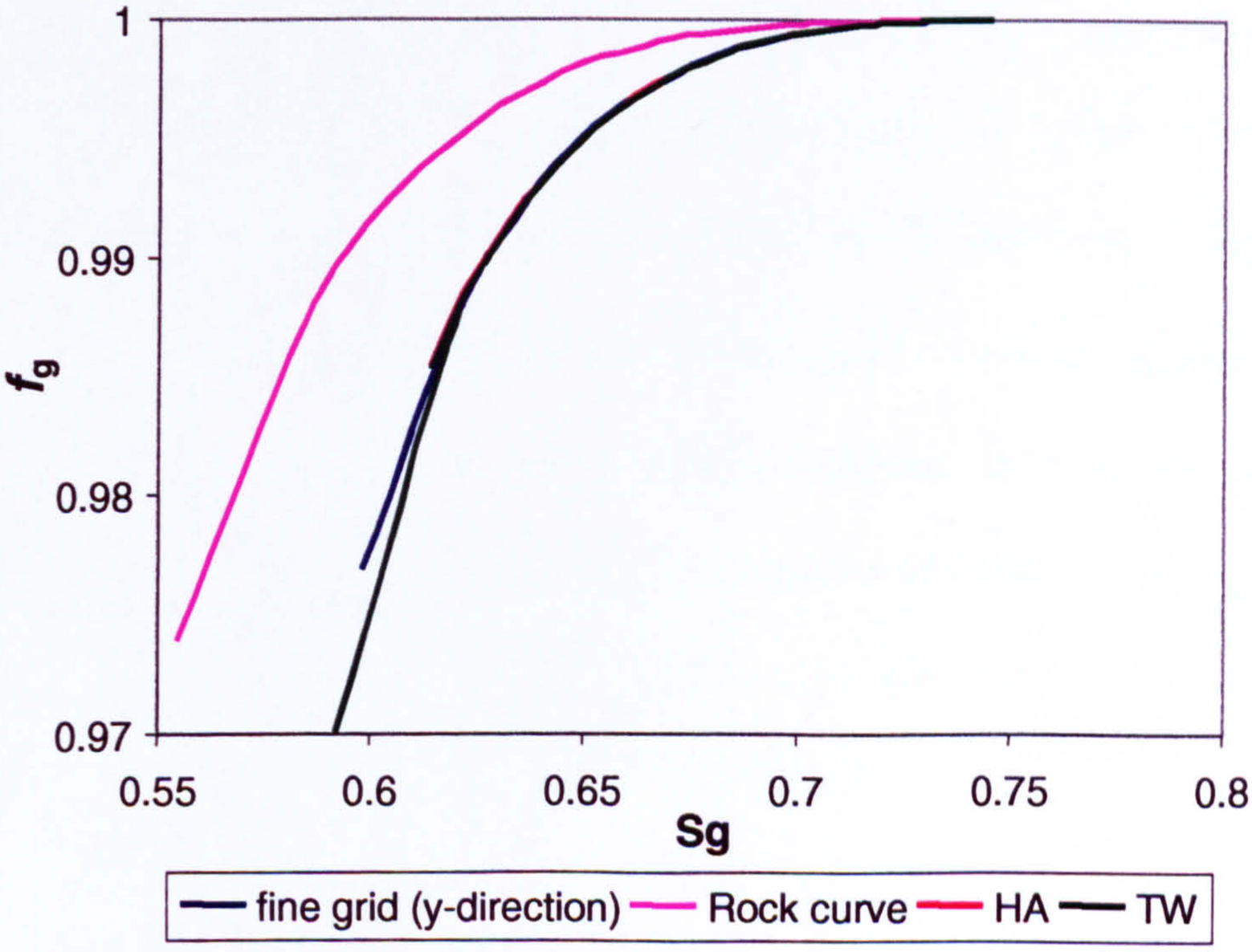

Figure 4.22b: Fractional flow in the y-direction versus gas saturation for the quarter 5-spot model showing the similarity between the f_g produced from the coarse grid models using pseudos and the fine grid model.

From these figures, we can see that, although the flow and pressure properties are different in the x- and y-directions, the use of pseudo functions will guarantee the exact reproduction of the fine grid results in the coarse grid models as long as the pseudos are calculated *independently* in each of the directions (directional pseudos). By adopting the directional pseudos, each of the dimensions in the coarse grid model will be treated like a separate "1D model" and the same results as discussed above (2D cross-sectional models) can be expected.

4.6 SUMMARY AND CONCLUSION

In this chapter, we have made a detailed comparison of the TW pseudo method in relation to several other well-known pseudo methods. The main findings are as follows:

1. For purely **horizontal** models and **negligible capillary pressure**, the exact weighting of the fluid potential difference (and mobility) in the averaging process is quite irrelevant since $\overline{\Delta\Phi_g}$ will always equal to $\overline{\Delta\Phi_o}$ *and can be factored out in the fractional flow calculation*. Hence, for this case, the Stone method will lead to the same fractional flows as other pseudo methods such as the TW and HA methods although gravity was ignored in the Stone method. Thus, as long as we know the respective fluid flow rates from the fine grid runs, the fractional flow of the coarse grid models can be correctly reproduced.

For this case, the Kyte and Berry method may give a different fractional flow since the selection of k_{rp} as a weighting factor in averaging the fluid pressure (which is

also a function of respective fluid saturation) will set the $\overline{\Delta\Phi_g}$ to be different from the $\overline{\Delta\Phi_o}$. A comparison between the TW and the Kyte and Berry methods shows that the difference between these two methods is due to the different weighting factors used in the pseudo equations. The relative permeability weighting used in the Kyte and Berry method is particularly inappropriate in cases where gravitational effects are significant.

The VE method, in this case, will always fail if the gravity to viscous ratio is not high enough for the two fluids to segregate instantaneously.

2. For dipping models, the gravity term of $\Delta\rho g\overline{\Delta h}$ cannot be ignored in averaging the fluid potential differences i.e. $\Delta\Phi_g \neq \Delta\Phi_o$. Therefore, the selection of the weighting factor and different style of averaging these values can be seen as essentially an attempt to correct for the gravity term. As long as one particular method takes into account the gravity term ($\Delta\rho g\overline{\Delta h}$) in its calculation, the results will be a better than methods that ignore it. This is the reason why the Stone method failed in a dipping model.

3. It is very hard to identify which pseudo method reproduces the correct fine-grid fluid mobility and pressure distribution since the vertical fluctuation in fine-grid fluid potential difference is quite large especially at the block near the injector. However, at this point, we will treat any method that reproduces the correct fractional flow, and result in a $\overline{\Delta\Phi}$ that falls within a "tolerance limit" as a good

pseudo method. As such, we conclude that both HA and TW pseudo methods perform equally well in matching the fine grid fractional flow as well as the fluid mobility compared to the other well-known pseudo methods of the Kyte and Berry, the Stone or the VE.

4. In a 3D → 3D or 3D → 2D upscaling, we found out that as long as the required pseudos are calculated *independently* in each of the coarse-grid dimensions they will guarantee the exact reproduction of the fine grid results in the coarse grid models. By adopting the directional pseudos, each of the dimensions in the coarse grid model will be treated like a separate 1D model and the same results as the 2D cross-sectional models can be expected.

5. If the fine grid accurately reproduces reservoir flows, which may be viscous dominated, gravity dominated or in a flow regime where all forces are significant, the TW will give accurate upscaled answers compared to the VE method. However, if the system is actually *at* the VE limit but the fine grid fails to resolve this, then the TW (or any other dynamic pseudo methods) will give the same (inaccurate) answer as the fine grid. In the VE limit, the VE pseudo method is shown to be very accurate and robust since it does not require any fine grid calculation.

CHAPTER 5

DERIVATION OF AVERAGED SATURATION EQUATIONS AND THE DEVELOPMENT OF OPTIMAL GRID COARSENING SCHEMES

5.1 GENERAL REMARKS

In the previous two chapters (Chapters 3 and 4), we have developed and validated a new Transmissibility-Weighted (TW) method for generating pseudo functions. The TW method is found to be most appropriate when applied to models that are highly affected by gravity and/or when the mobility ratio is very unfavourable. For the second part of the study, we extended our research by developing a new optimal grid coarsening scheme ("intelligent" coarsening) which will further reduce the amount of error when certain upscaling techniques are used.

The objective of this chapter is to develop an optimal grid coarsening scheme which uses more than the static properties of the fine grid models, such as permeability distribution, net-to-gross ratio etc. Such a coarsening scheme should use the *dynamic* properties of the fine grid model such as the flood pattern, pressure and saturation distributions. It is hoped that this approach will result in more accurate predictions of important quantities such as total oil recovery and gas-oil ratio in coarse grid models.

The development of our optimal grid coarsening scheme was motivated from a volume-averaged analysis of the fine scale saturation equation. It is shown that the errors produced by the coarse grid models correlate with specific sub-grid quantities involving higher moments of the fine grid variables, which can be computed from the fine grid simulation results. The basic idea of this coarsening method is to identify regions of the fine grid models where there is low variability of certain fluctuating fine grid parameters, and to take such regions as the corresponding coarse grid blocks. As a result, the final composite coarse grid model may include both finely gridded and coarsely gridded regions.

We proceed by first discussing some of the previous works by Durlosky (1998) and Darman *et al.* (1999) that lead to the development of the new volume averaged saturation equation. We will then explain the detailed derivation of the averaged saturation equations in the following section of this chapter. The numerical validation of this new idea will then be presented in Chapter 6.

5.2 PREVIOUS WORKS

The first step in achieving our objective was to identify which dynamic parameters should be used in characterizing the coarsening scheme. There are two previous pieces of work related to this matter. Firstly, Darman *et al.* (1999) investigated the use of several fluctuating fine grid parameters as an error predictor for the coarse grid models. They empirically found that the averaged C_v in S_g is the best higher moment to be used compared to other fine grid parameters in the sense that the coarse grid

should be chosen in order to minimize this quantity on the underlying fine grid. The averaged C_v in S_g is defined as (for uniform size of coarse gridblocks):

$$C_v in S_g = \frac{\sum_{T=1}^{T} \sum_{N=1}^{N} \frac{\sqrt{\overline{S_g}^2 - \overline{S_g}^2}}{\overline{S_g}}}{T.N} \qquad (5.1)$$

where overbar is the average property of one particular coarse gridblock, N is the number of the coarse gridblocks in that particular model and T is the number of calculated timesteps. Secondly, Durlofsky (1998) who used purely viscous dominated models found that coarse grid error could be also correlated to other fluctuating higher moments of the fine grid models. The specific higher moments that appear in his works are the variance of saturation[a] (σ^2_S) and the velocity-saturation covariance[a] (σ_{vS}). The details of these two techniques are discussed below.

5.2.1 The Use of C_v in S_g (Darman et al, 1999)

As the quality indicator in this chapter, we used the correlation of determination (R^2) of the normalised rms error on oil recovery factor versus the fluctuating moments of the fine grid. The higher the value of this quality index, the better the result will be in terms of its ability to be used as an error predictor, i.e. we could formulate our coarsening strategy so that these fluctuating moments are reduced, hence reducing the error simultaneously.

[a] Durlofsky used S_w instead of S_g

Using all of the twenty-one 5-layer cross sectional test models that we described in Chapters 3 and 4 (Case 1 through Case 21), we investigated several fine-grid fluctuating quantities which might correlate with the averaged rms errors of the oil recovery factor. These included: (i) the average coefficient of variation (C_v) in the pressure distribution; (ii) the average C_v in the fluid potential difference, (iii) the average C_v in the total flow rate, (iv) the average C_v in the gas flow rate; and (v) the gravity to viscous ratio, N_{gv}. All of these quantities failed to give a satisfactory coefficient of determination, R^2, as shown in Figures 5.1a-5.1e (R^2 - in the range of 0.0257 to 0.4233).

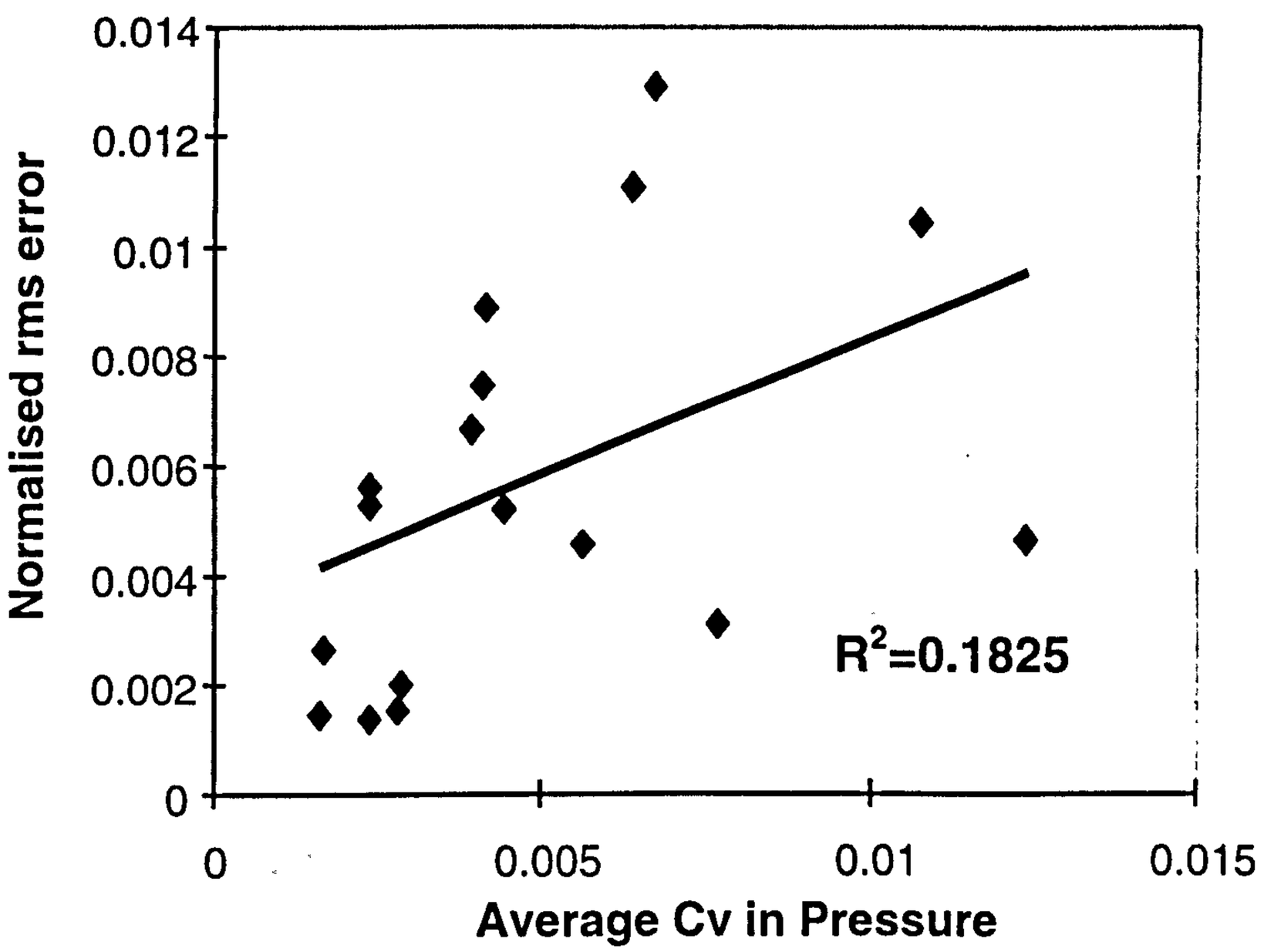

Figure 5.1a: Normalised rms error versus coefficient of variation in the fine grid pressure distribution, using all the twenty-one 5-layer cross-sectional models (Case 1 to Case 21)

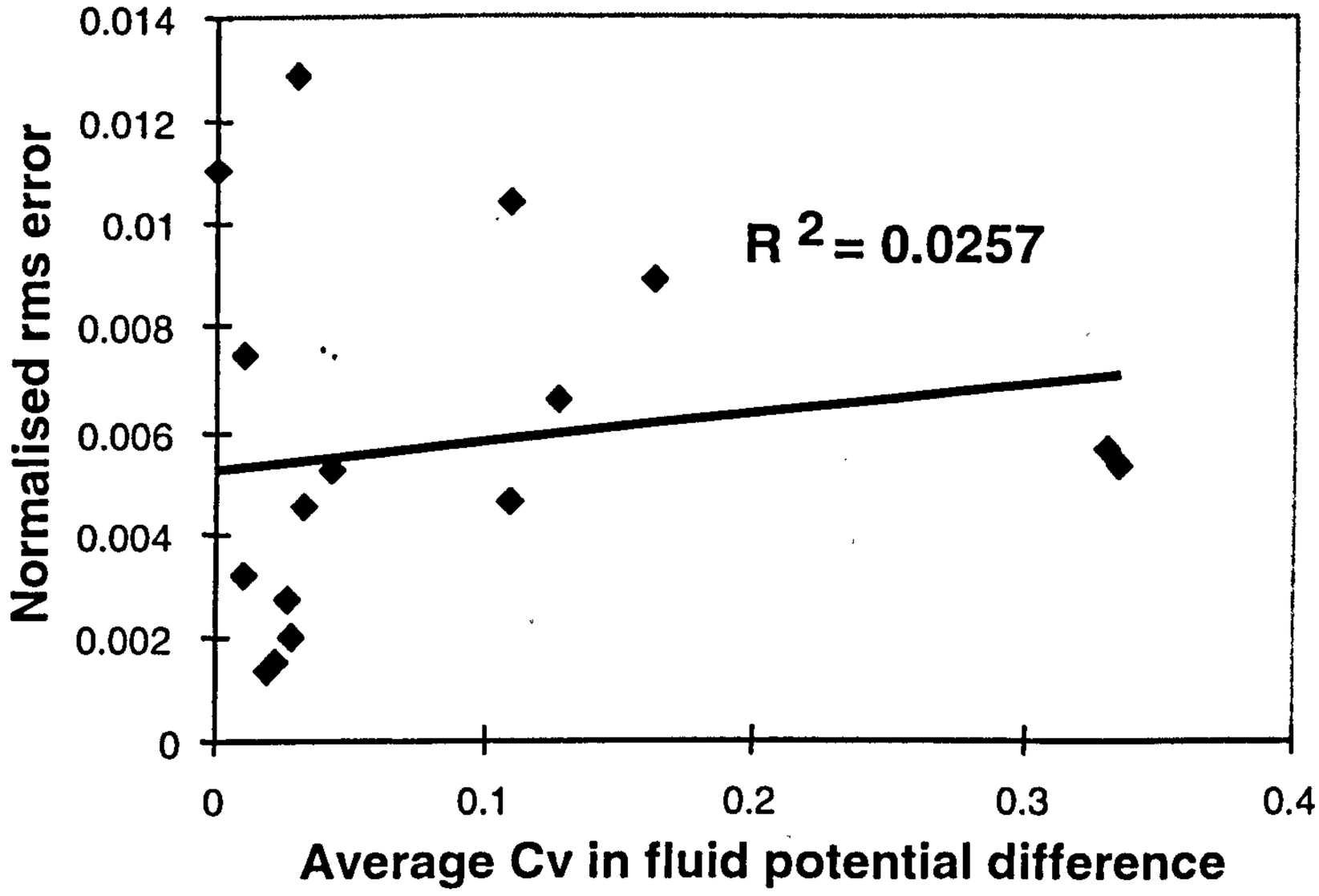

Figure 5.1b: Normalised rms error versus coefficient of variation in the fine grid fluid potential difference, using all the twenty-one 5-layer cross-sectional models (Case 1 to Case 21)

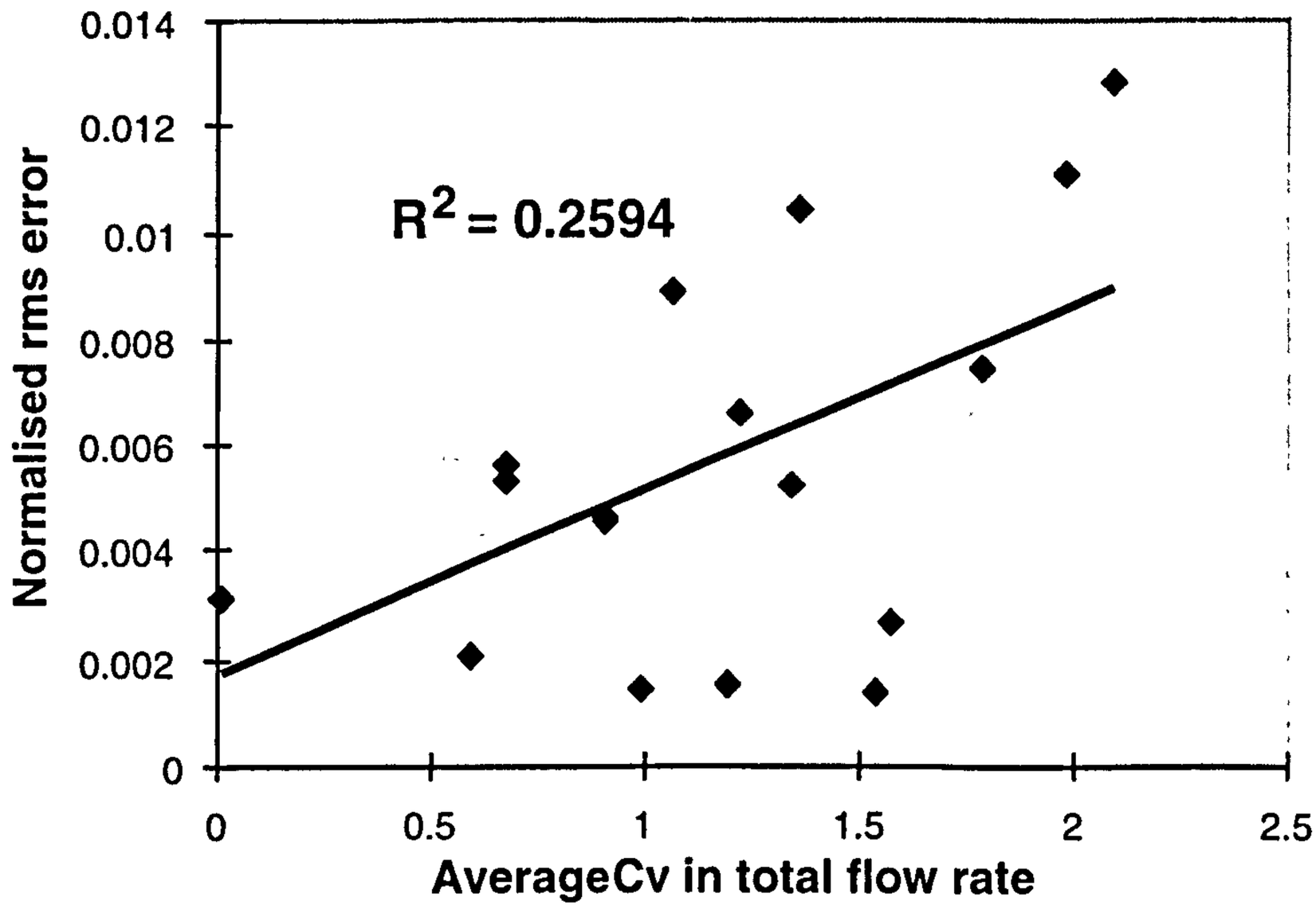

Figure 5.1c: Normalised rms error versus coefficient of variation in the fine grid total flow rate, using all the twenty-one 5-layer cross-sectional models (Case 1 to Case 21)

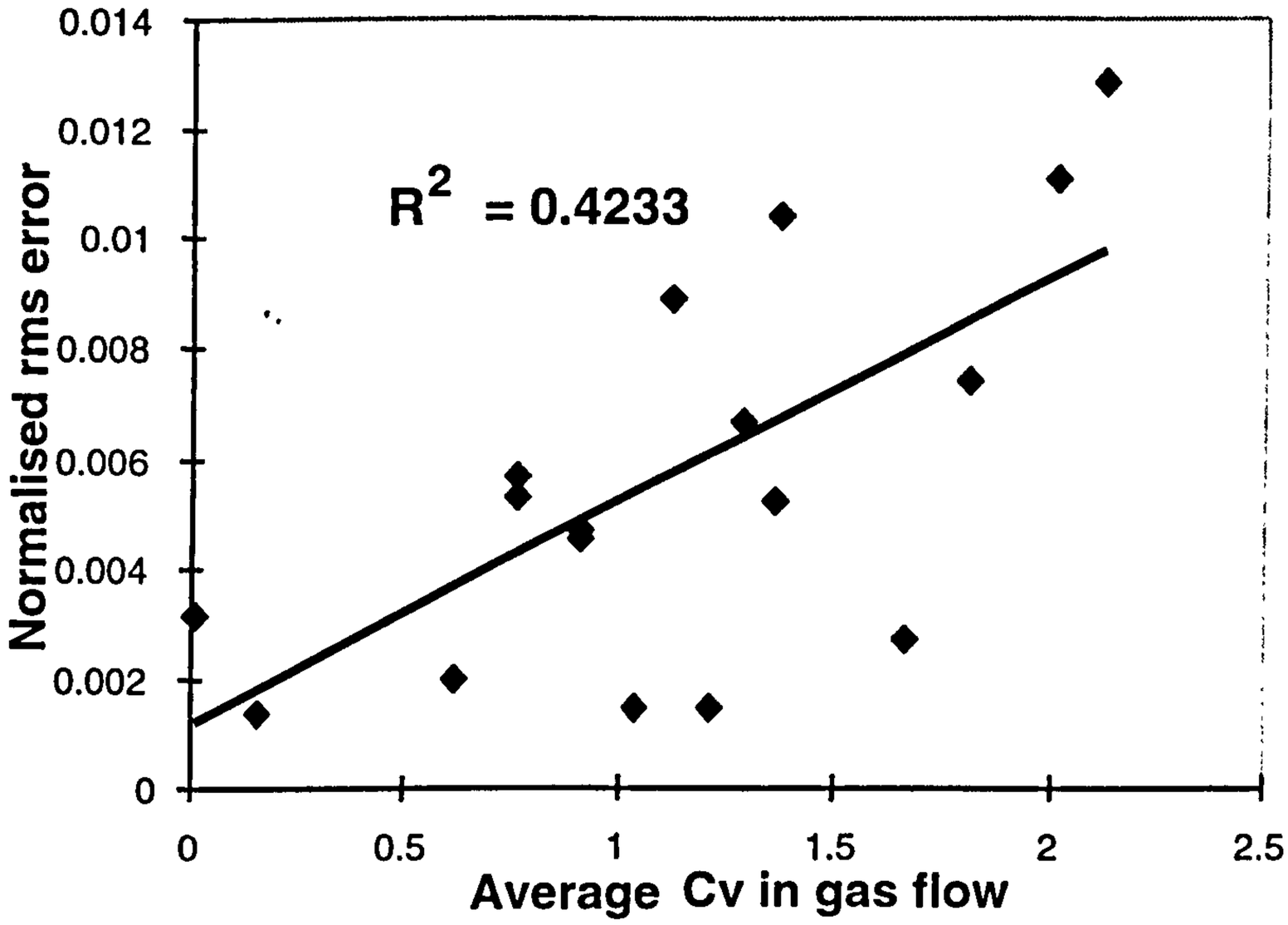

Figure 5.1d: Normalised rms error versus coefficient of variation in the fine grid gas flow rate, using all the twenty-one 5-layer cross-sectional models (Case 1 to Case 21)

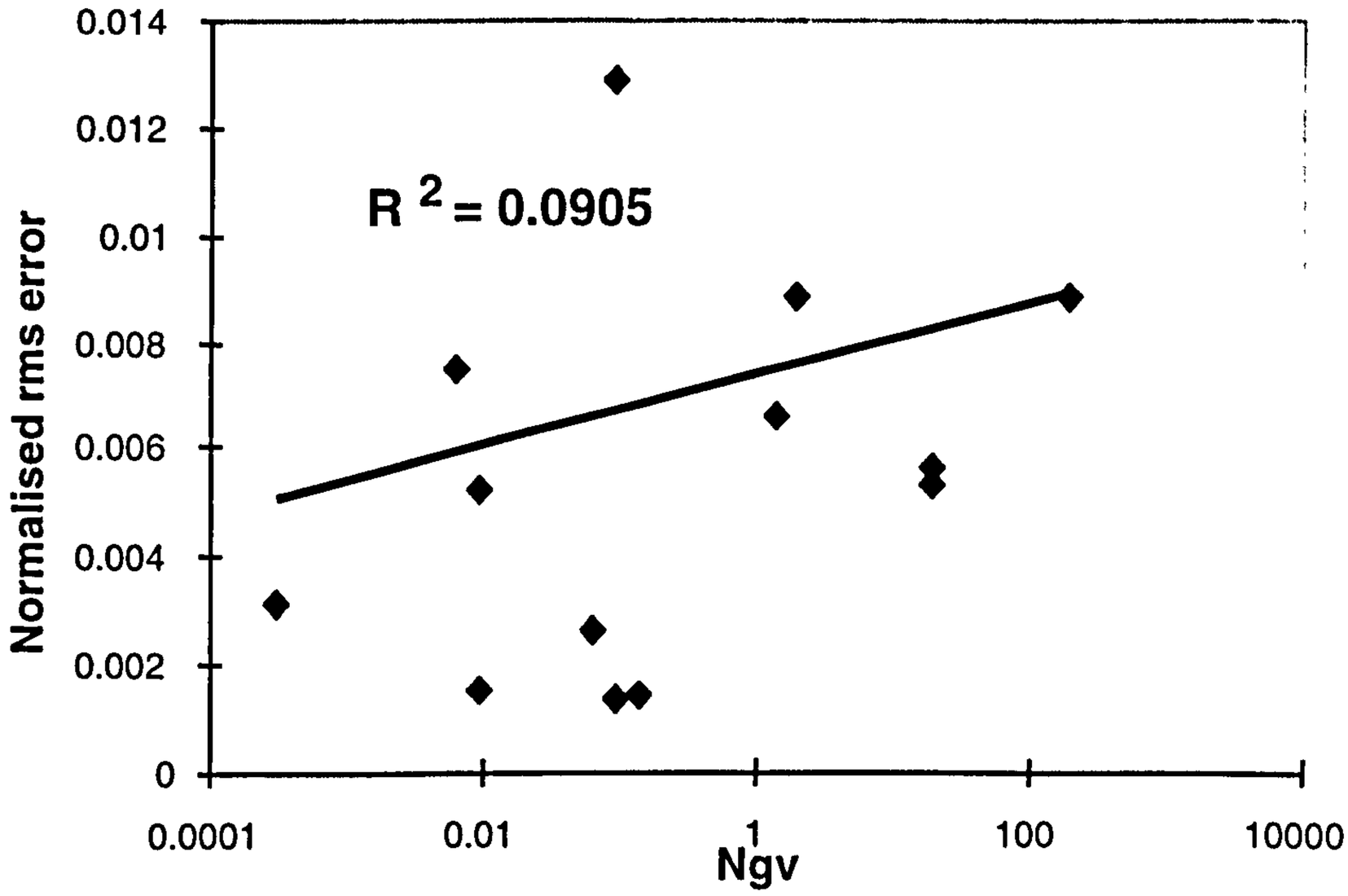

Figure 5.1e: Normalised rms error versus gravity to viscous ratio (N_{gv}), using all the twenty-one 5-layer cross-sectional models (Case 1 to Case 21)

However, the rms error correlates very well with the averaged coefficient of variation in the gas saturation (i.e. C_v in S_g), as shown in Figure 5.2a for the homogenous models ($R^2 = 0.926$) and in Figure 5.2b for all of the models ($R^2 = 0.7697$). Thus, we may conclude that a model with a lower coefficient of variation in gas saturation will produce less error in duplicating the fine grid performance and that this will provide a good basis for the proposed coarsening scheme.

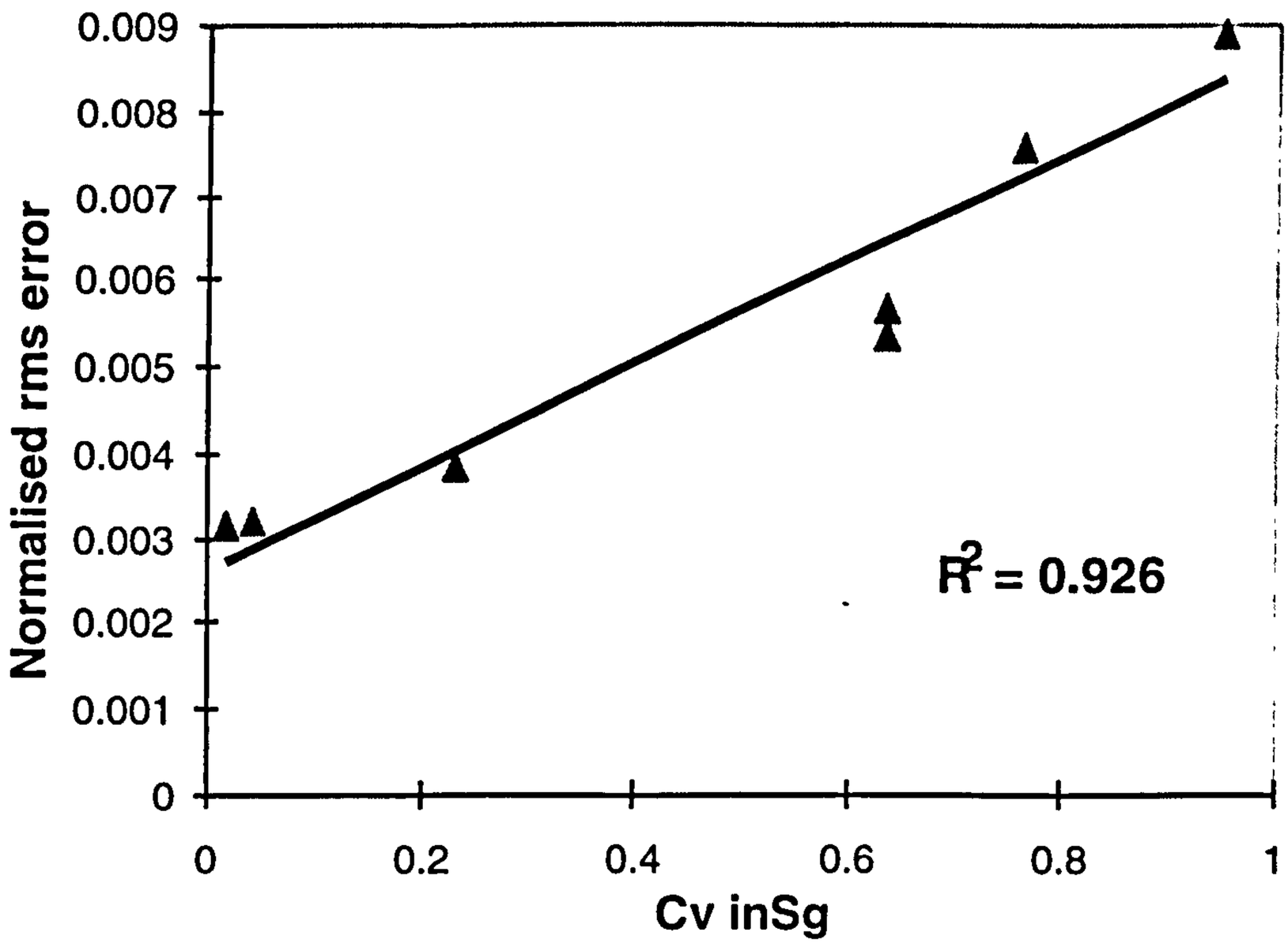

Figure 5.2a: Normalised rms error versus coefficient of variation in gas saturation, using nine homogenous 5-layer cross-sectional models (Case 5 through 13)

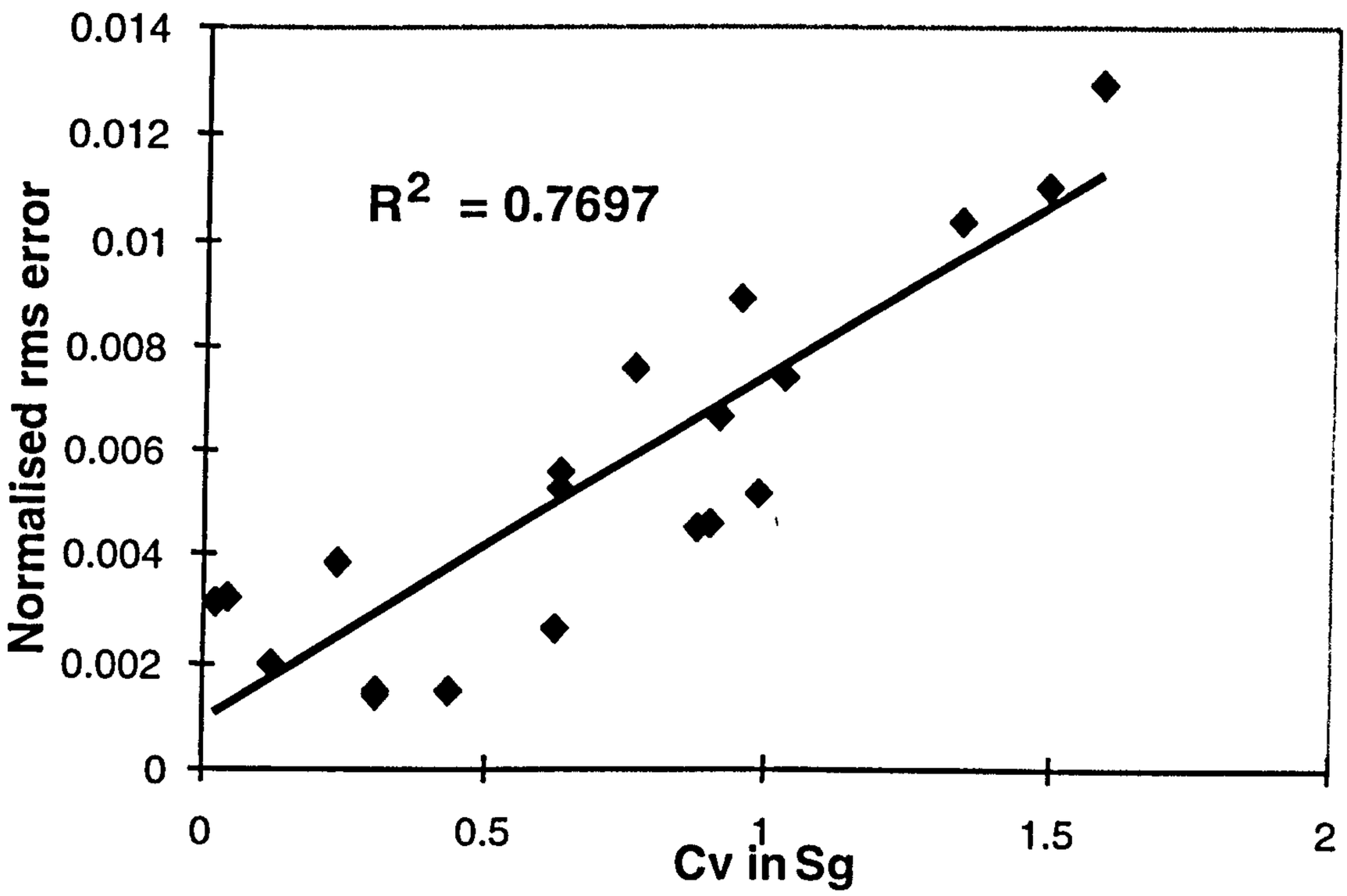

Figure 5.2b: Normalised rms error versus coefficient of variation in the fine-grid gas flow rate, using 21 5-layer cross-sectional models (Case 1 to Case 21)

The summary of the quality index for all the twenty-one cases is shown in table 5.1 below:

Fluctuating properties of the fine grid	**R^2**
Averaged C_v in pressure	0.1825
Averaged C_v in fluid potential difference	0.0257
Averaged C_v in total flow rates	0.2594
Averaged C_v in gas flow rates	0.4233
Gravity to viscous number (N_{gv})	0.0905
Averaged C_v in S_g (for homogenous models – Case 5 through Case 13)	**0.9260**
Averaged C_v in S_g for all the twenty-one test cases.	**0.7697**

Table 5.1: Coefficient of determination (R^2) of fluctuating moments versus normalized rms error.

5.2.2 Viscous Dominated Averaged Saturation Equations (Durlofsky, 1998)

This criterion (minimizing the C_v in S_g), is not the only one that might be applied in developing the grid coarsening scheme. In previous work by Durlofsky (1998), he developed volume averaged saturation equations for viscous dominated immiscible displacements (i.e. gravity and capillary pressure effects were absent). There, it was shown that the coarse grid volume averaged equations contained terms involving higher moments of certain fine grid quantities. The specific higher moments that

appeared were the variance of saturation (σ^2_S) and the velocity-saturation covariance (σ_{vS}) given by the following two equations:

$$\sigma_S^2 = \langle S_g{}^2 \rangle - \langle S_g \rangle^2 = \overline{S'S'} = \langle S'S' \rangle \,, \tag{5.2}$$

$$\sigma_{vS} = \langle vS_g \rangle - \langle v \rangle \langle S_g \rangle = \overline{v'S'} = \langle v'S' \rangle \,. \tag{5.2a}$$

where S_g or S (we use the two interchangeably) represents gas saturation, v represents the component of the total velocity in the dominant flow direction, the prime denotes a spatially fluctuating quantity and an overbar indicates a volume averaged quantity.

Because these higher moments are not explicitly modelled in coarse grid simulations, it might be expected that coarse grid errors could be reduced by minimising the terms containing these higher moments. This could be accomplished by forming the coarse grid such that σ^2_S and σ_{vS} are minimised within these coarse blocks. This expectation is quite consistent with previous results using a non-uniform coarsening procedure for viscous dominated displacements (Durlofsky, 1998).

There is clearly a close link between the numerical findings of Darman *et al.* (1999) and the viscous dominated volume averaging of the fine grid saturation equation results of Durlofsky (1998) in that both have identified sub-grid variability in saturation as an important quantity to consider in forming the coarse grid. However, to apply predictions from volume averaging to coarse scale simulations of immiscible gas displacements more directly, it is necessary to introduce gravitational effects into the

volume averaged saturation equation. This will then allow a direct comparison to be made between the theoretical predictions and the numerical experiments.

A detailed derivation of the volume averaged saturation equation with gravity term included is presented below and follows the idea and equations developed by Durlofsky and published with the author in Darman *et al.* (2000).

5.3 DERIVATION OF THE AVERAGED SATURATION EQUATIONS WITH GRAVITY EFFECT INCLUDED

We start by considering an incompressible two-phase system of gas and oil. With gravitational effects included, the fine scale saturation equation can be written as:

$$\frac{\partial S}{\partial t} + \mathbf{v} \cdot \nabla f - \frac{g \Delta \rho}{\mu_o} \nabla \cdot (\eta \, \mathbf{k} \cdot \mathbf{i}_z) = 0, \tag{5.3}$$

where the functions f and η are defined as:

$$f(S) = \frac{k_{rg}/\mu_g}{k_{rg}/\mu_g + k_{ro}/\mu_o}\ , \tag{5.4}$$

$$\eta(S) = k_{ro} f\ . \tag{5.5}$$

In Equations 5.3 – 5.5, S represents gas saturation, t is time, $\mathbf{v}$ is the total Darcy velocity, $\Delta\rho=\rho_g - \rho_o$ (ρ_g is gas density and ρ_o is the oil density), g is gravitational acceleration (acting in the z-direction), μ_o is the oil viscosity, μ_g is the gas viscosity, $\mathbf{k}$ is the local permeability tensor, $\mathbf{i}_z$ is the unit vector in the z-direction, k_{ro} is the relative permeability to oil and k_{rg} is the relative permeability to gas.

In order to develop the volume averaged equations, we express the saturation, velocity and permeability in Equation (5.3) in terms of averaged and fluctuating quantities. Averages in this context are volume averages (area averages in two dimensions) over the fine grid region to be coarsened into a single coarse grid block. We define averaged and fluctuating quantities via:

$$\Phi(x,z) = \overline{\Phi} + \Phi'(x,z) \ , \tag{5.6}$$

where Φ represents any variable in this case (not necessarily be the fluid potential). The overbar indicates a volume averaged quantity (constant throughout the averaging region) and the prime denotes a spatially varying fluctuating quantity. The volume average in two dimensions is defined as

$$\overline{\Phi} = \frac{1}{A}\int_D \Phi(x,z)dA \ , \tag{5.7}$$

where D denotes the region within the coarse grid block and A is the area. Introducing the fine scale variables as the sum of averaged and fluctuating components into Equation (5.3) gives:

$$\begin{aligned} &\frac{\partial \overline{S}}{\partial t} + \frac{\partial S'}{\partial t} + \overline{\mathbf{v}}\cdot\nabla\overline{f} + \overline{\mathbf{v}}\cdot\nabla f' + \mathbf{v}'\cdot\nabla\overline{f} + \mathbf{v}'\cdot\nabla f' \\ &-\frac{g\Delta\rho}{\mu_o}\nabla\cdot\left\{(\overline{\mathbf{k}}\,\overline{\eta} + \overline{\mathbf{k}}\eta' + \mathbf{k}'\overline{\eta} + \mathbf{k}'\eta')\cdot\mathbf{i}_z\right\} = 0 \ . \end{aligned} \tag{5.8}$$

Averaging Equation (5.8), and noting that averages of singly primed terms are zero, gives the equation for $\overline{S}$,

$$\frac{\partial \overline{S}}{\partial t} + \overline{\mathbf{v}}\cdot\nabla\overline{f} + \overline{\mathbf{v}'\cdot\nabla f'} - \frac{g\Delta\rho}{\mu_o}\nabla\cdot\left\{(\overline{\mathbf{k}}\,\overline{\eta} + \overline{\mathbf{k}'\eta'})\cdot\mathbf{i}_z\right\} = 0 \ . \tag{5.9}$$

We wish to express the averaged terms involving f and η in terms of $\overline{S'S'}$, $\overline{v'S'}$ and $\overline{k'S'}$. We proceed by expanding $f(S)$ in a Taylor series about $\bar{S}$; i.e.

$$f(S) \approx f(\bar{S}) + f_s(\bar{S})(S-\bar{S}) + \frac{1}{2} f_{ss}(\bar{S})(S-\bar{S})^2 + \ldots \tag{5.10}$$

where $f_s(\bar{S}) = df/dS$ evaluated at $\bar{S}$ and $f_{ss}(\bar{S}) = d^2 f/dS^2$ evaluated at $\bar{S}$. Now, neglecting higher order terms, identifying $S' = S - \bar{S}$, and averaging, we can obtain the following expression for $\bar{f}$:

$$\bar{f} \approx f(\bar{S}) + \frac{1}{2} f_{ss}(\bar{S})\overline{S'S'} \; . \tag{5.11}$$

where f_s and f_{ss} are the first and second order derivative of the fractional flow function (f) with respect to the gas saturation S_g. Since $f' = f - \bar{f}$, f' can be computed as

$$f' \approx f_s(\bar{S})S' + \frac{1}{2} f_{ss}(\bar{S})(S'S' - \overline{S'S'}) \; . \tag{5.12}$$

From Equation (5.12), we can approximate $\overline{v'f'}$ as:

$$\overline{v'f'} \approx f_s(\bar{S})\overline{v'S'} + \frac{1}{2} f_{ss}(\bar{S})\overline{v'S'S'} \; . \tag{5.13}$$

We can express $\bar{\eta}$ using a similar approach. This allows us to write:

$$\bar{\eta} \approx \eta(\bar{S}) + \frac{1}{2}\eta_{ss}(\bar{S})\overline{S'S'}, \tag{5.14}$$

$$\eta' \approx \eta_s(\bar{S})S' + \frac{1}{2}\eta_{ss}(\bar{S})(S'S' - \overline{S'S'}) \; . \tag{5.15}$$

where η_s and η_{ss} are the first and second order derivative of η with respect to the gas saturation S_g.

Introducing the above expressions into the averaged saturation Equation (5.9) and retaining terms to first order in fluctuating quantities (i.e. we neglect terms involving the products of three fluctuating quantities) gives the following equation:

$$\begin{aligned}&\frac{\partial \bar{S}}{\partial t}+\bar{\mathbf{v}}\cdot\nabla f(\bar{S})+\frac{1}{2}\bar{\mathbf{v}}\cdot\nabla\left\{f_{ss}(\bar{S})\overline{S'S'}\right\}+\nabla\cdot\left\{f_{s}(\bar{S})\overline{\mathbf{v}'S'}\right\}\\&-\frac{g\Delta\rho}{\mu_{o}}\nabla\cdot\left\{(\bar{\mathbf{k}}\eta(\bar{S})+\frac{1}{2}\eta_{ss}(\bar{S})\bar{\mathbf{k}}\,\overline{S'S'}+\eta_{s}(\bar{S})\overline{\mathbf{k}'S'})\cdot\mathbf{i}_{z}\right\}=0.\end{aligned}\tag{5.16}$$

This equation is the averaged saturation equation for the coarse grid block expressed in terms of the moments $\overline{S'S'}$, $\overline{\mathbf{v}'S'}$ and $\overline{\mathbf{k}'S'}$ that we are interested in.

5.4 DISCUSSIONS

There are several interesting aspects to Equation (5.16). First, we note that the fine scale functions f and η appear explicitly in the coarse scale equation. These functions are not modified for use in the coarse scale models; i.e. the f and η have the same functional forms on both the fine and coarse scales. Secondly, the coarse scale equation is seen to contain three additional terms involving higher moments that account for the sub-grid effects. The moments that appear explicitly are $\overline{S'S'}$, $\overline{\mathbf{v}'S'}$ and $\overline{\mathbf{k}'S'}$, and these terms are always multiplied by derivatives of f or η. The moments appearing in the gravitational terms (the terms multiplied by $g\Delta\rho/\mu_o$) are $\overline{S'S'}$ and $\overline{\mathbf{k}'S'}$ only; $\overline{\mathbf{v}'S'}$ does not appear. From Equation (5.16), we can determine the form of the error that will result from using rock curves (and neglecting the higher moment terms) on the coarse scale. Specifically, because such a scheme neglects all terms involving

higher moments, the error can be expected to correlate with the magnitudes of the neglected terms, i.e. with $\overline{S'S'}$, $\overline{\mathbf{v}'S'}$ and $\overline{\mathbf{k}'S'}$.

Note that pseudo functions do not appear in Equation (5.16). Were we to use pseudo functions, the coarse scale equation would be of the same form as the fine grid equation but with upscaled (pseudo) parameters, computed from fine grid simulations, appearing in place of the fine scale f and η functions; i.e.

$$\frac{\partial \bar{S}}{\partial t} + \bar{\mathbf{v}} \cdot \nabla f^*(\bar{S}) - \frac{g\Delta\rho}{\mu_o} \nabla \cdot (\eta^*(\bar{S})\, \bar{\mathbf{k}} \cdot \mathbf{i}_z) = 0, \tag{5.17}$$

where the * superscript indicates functions derived from pseudo relative permeability. Comparing Equation (5.17) with Equation (5.16), we see that the pseudo functions attempt to capture sub-grid variability (which involves the higher moments $\overline{S'S'}$, $\overline{\mathbf{v}'S'}$ and $\overline{\mathbf{k}'S'}$) through use of coarse grid functions that depend on $\bar{S}$ only. Because the functional dependence of the pseudo functions is limited relative to the actual sub-grid effect (i.e. the pseudo functions depend on $\bar{S}$ only but the sub-grid effect additionally involves $\overline{S'S'}$, $\overline{\mathbf{v}'S'}$ and $\overline{\mathbf{k}'S'}$), this procedure will in general introduce some error. The magnitude of this error is expected to correlate with the magnitude of the sub-grid terms themselves, i.e. with the higher moment terms.

Thus, we see that the error using either the rock curves (and neglecting the higher order moment terms) or pseudo functions (where the pseudo functions approximately account for the sub-grid effects) will be related to the moments $\overline{S'S'}$, $\overline{\mathbf{v}'S'}$ and $\overline{\mathbf{k}'S'}$. However, because the pseudo functions are specifically introduced to capture the sub-grid effect, we expect that the error using pseudo functions will be considerably less

than that using rock curves for the highly coarsened models that we will consider. Further, we also expect that the exact functional dependence of the coarse grid error on the higher moments will vary depending on whether we use rock curves or pseudo functions in the coarse grid model. We will test these speculations through detailed numerical calculations below.

We note that, in all the calculations below, fine grid simulations are required to compute the sub-grid quantities that will ultimately be used to determine the 'optimal' coarse grid structure. Thus, the need for a coarse scale description might be questioned in such cases; i.e. why do we need a coarse scale model if the fine scale result is already known. Because our intent in this chapter is to understand the relationship between the accuracy of the coarse scale model and sub-grid terms, we are not particularly concerned with this issue here. We note finally that this issue is analogous to that surrounding the use of global fine scale simulations to compute coarse scale pseudo functions.

5.5 SUMMARY AND CONCLUSIONS

In this chapter, we reviewed two previous sets of results that lead to the development of a proposed new optimal coarsening scheme utilizing certain dynamic fluctuating properties of the fine grid flow data. In the first work, Darman *et al.* (1999) suggested using a minimization of C_v in S_g as the criteria in order to minimize the coarse grid error. On the other hand, Durlosky (1998) who used a purely viscous flow model, suggested the use of the variance in saturation and/or velocity-saturation covariance as

the way to minimize the error when upscaling. Detailed comparison between the two methods will be presented in the next chapter.

In this chapter, we also used the work of Durlofsky to present a new averaged saturation equation with gravity included (Equation 5.16). There are several interesting observations from this new equation:

1. We note that the fine scale functions f and η appear explicitly in the coarse scale equation. These functions are not modified for use in the coarse scale models; i.e. the f and η have the same functional forms on both the fine and coarse scales.

2. The coarse scale equation is seen to contain three additional terms involving higher moments that account for the sub-grid effects. The moments that appear explicitly are $\overline{S'S'}$, $\overline{\mathbf{v}'S'}$ and $\overline{\mathbf{k}'S'}$, and these terms are always multiplied by derivatives of f or η. The moments appearing in the gravitational terms (the terms multiplied by $g\Delta\rho/\mu_o$) are $\overline{S'S'}$ and $\overline{\mathbf{k}'S'}$ only; $\overline{\mathbf{v}'S'}$ does not appear; whereas in the viscous term only $\overline{S'S'}$ and $\overline{\mathbf{v}'S'}$ appear.

CHAPTER 6

VALIDATION OF THE NEW OPTIMAL GRID COARSENING SCHEMES

6.1 GENERAL REMARKS

In this chapter, we will validate the concepts developed in the previous chapter i.e. developing optimal grid coarsening schemes based on the quantitative use of fine scale two-phase flow information. The basic approach is motivated from a volume average analysis of the fine scale saturation equation including gravitational effects (Equation 5.16). This validation exercise will be done using several layered fine grid systems. It is shown that coarse grid simulation error correlates closely with specific sub-grid quantities involving higher moments of fine grid variables, which can be computed from the fine scale simulations.

By forming a coarse grid that minimizes the appropriate sub-grid quantity, optimal coarse scale descriptions can be generated. The resulting coarsening schemes may be non-uniform, but they fulfil all of the main purposes of using pseudo functions (i.e. to control numerical dispersion and to capture the effects of small-scale heterogeneity) with less error and without any adjustment to the pseudo equations themselves.

The overall approach is shown to be applicable to coarse scale descriptions using not only pseudo relative permeability curves but also with direct inclusion of the rock curves as suggested by the average saturation equation itself. The accuracy of the coarse grid calculations is, however, significantly improved when pseudo functions are used. In any case, all of the data are there to calculate the pseudos since the fine grid calculation is performed.

This grid coarsening method is then applied to determine the optimal number and configuration of coarse grid layers in more general cases i.e. coarse grid models that have more than 2 layers. Using these general models, it is shown that coarse grid results do not always improve as the number of coarse layers is increased. The accuracy in applying this method will also depend on the configuration of the layering scheme adopted for the coarse grid models.

Our intention in this chapter is to explore the relationship between the volume averaged saturation equation and coarse scale numerical simulations for several model problems. We will also study the performance of several coarse grid models developed using our new coarsening scheme in more general cases. This chapter proceeds towards these goals as follows. We consider many different aggregations of 20-layer systems to equivalent 2-layer systems and study the relationship of sub-grid variability to error in the coarse scale simulation results. We assess the use of both pseudo relative permeabilities and rock curves in these coarse scale simulations and determine which measure of sub-grid variability is most appropriate for use with each of these approaches.

In the second part of this chapter, we apply these findings to more general multi-layered cases (i.e. where the coarse grid contains more than 2 layers). In addition, we apply our coarsening method in association with both the TW and the Kyte and Berry methods to study the effect of using other pseudo generation methods with our coarsening technique. It is shown that this new coarsening scheme continues to provide accurate coarse grid results in these more general cases.

6.2 NUMERICAL TESTINGS

As shown in the previous chapter, the final form of the averaged saturation equation can be re-written as:

$$\begin{aligned}&\frac{\partial \bar{S}}{\partial t}+\bar{\mathbf{v}}\cdot\nabla f(\bar{S})+\frac{1}{2}\bar{\mathbf{v}}\cdot\nabla\left\{f_{ss}(\bar{S})\overline{S'S'}\right\}+\nabla\cdot\left\{f_s(\bar{S})\overline{\mathbf{v}'S'}\right\}\\&-\frac{g\Delta\rho}{\mu_o}\nabla\cdot\left\{(\bar{\mathbf{k}}\eta(\bar{S})+\frac{1}{2}\eta_{ss}(\bar{S})\bar{\mathbf{k}}\,\overline{S'S'}+\eta_s(\bar{S})\overline{\mathbf{k}'S'})\cdot\mathbf{i}_z\right\}=0.\end{aligned}\tag{6.1}$$

As mentioned in Chapter 5, the coarse scale equation is seen to contain three additional terms involving higher moments that account for the sub-grid effects. The moments that appear explicitly are $\overline{S'S'}$, $\overline{\mathbf{v}'S'}$ and $\overline{\mathbf{k}'S'}$, and these terms are always multiplied by derivatives of f or η. It is also discussed in Chapter 5 that Darman *et al.* (1999) have found that higher moments such as the C_v in S_g correlates well with the error in the upscaling method.

6.2.1 Description of the Numerical Models

In this section, we investigate the relationship between the volume averaged saturation equations and coarse scale numerical simulations for several model problems. We

want to know which form of the higher moments is appropriate to each of the coarsening strategies i.e. when pseudo functions are used or when rock curves are applied directly in the coarse grid models. For this purpose, four cross sectional models with $100 \times 1 \times 20$ fine grid blocks were developed and used to compare the effectiveness of the sub-grid moments discussed above in different flow scenarios. The permeability trends for these four models are shown in Figure 6.1 (these values vary from 10 mD to 1462 mD).

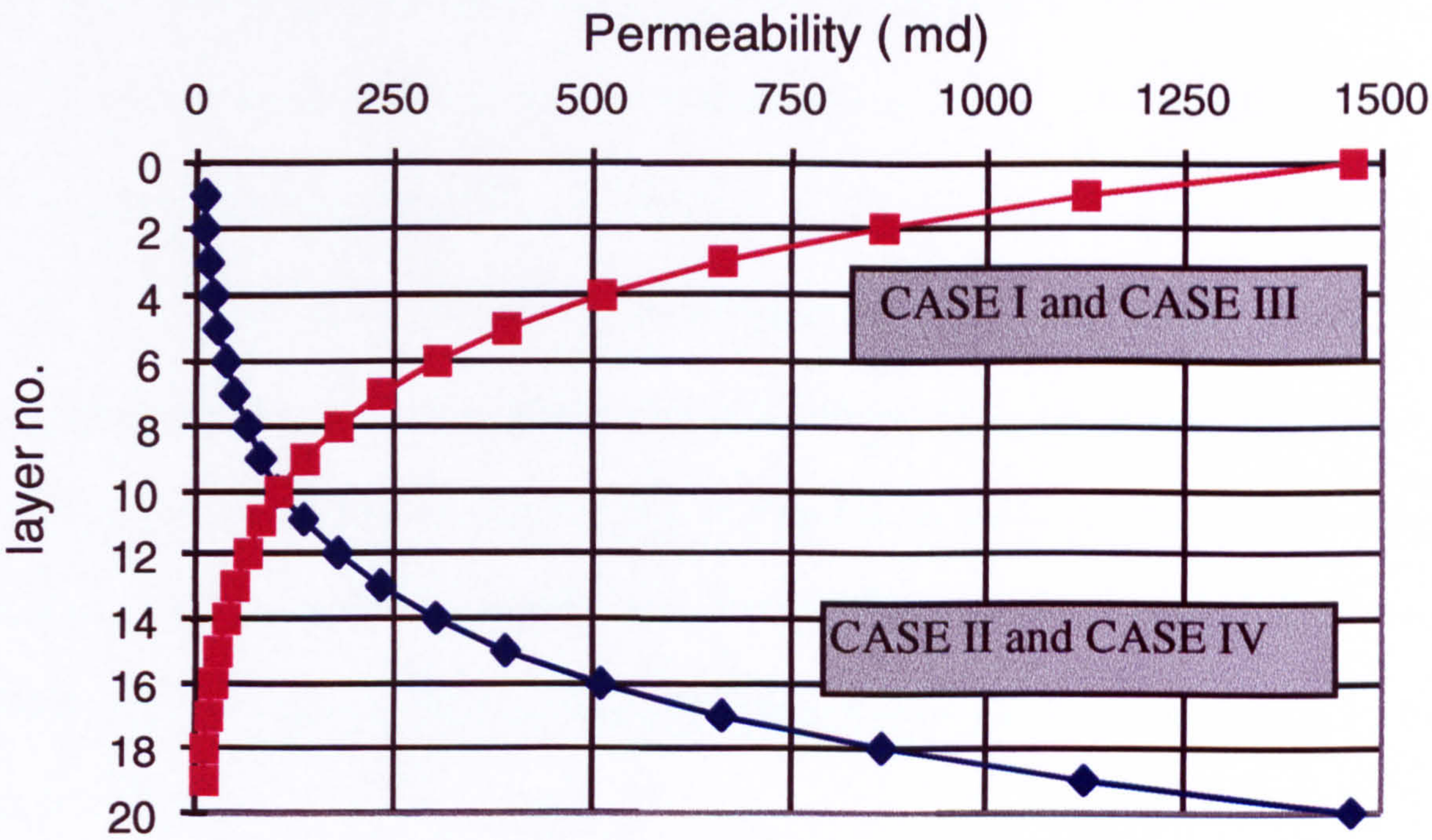

Figure 6.1: Permeability distribution for Case I to Case IV.

Cases I and II were chosen to provide models with no crossflow between the fine grid layers. On the other hand, Cases III and IV were used to evaluate scenarios with free crossflow between the fine grid layers. The properties of the fine grid models are as follows:

Grid block sizes, $\Delta x = \Delta y = \Delta z = 25$ ft or 7.63 m;

Viscosities, $\mu_o = 10$ cp, $\mu_g = 0.1$ cp

Injection velocity, $v = 0.3$ m/d or about 1 ft/day

The fluid densities, fine grid relative permeability and porosity distribution are the same as in the previous chapter.

6.2.2 Coarsening Schemes

The four test cases described above (Cases I - IV) were run to establish the correlation between coarse grid error and C_v in S_g, C_v in vS, C_v in kS, $\overline{S'S'}$, $\overline{\mathbf{v}'S'}$ and $\overline{\mathbf{k}'S'}$. We note that C_v in vS and C_v in kS are defined analogously to C_v in S_g. We further note that we will subsequently refer to $\overline{S'S'}$, $\overline{\mathbf{v}'S'}$ and $\overline{\mathbf{k}'S'}$ as σ^2_S, σ_{vS} and σ_{kS}. In computing σ_{vS} and C_v in vS, we use the x-component of velocity; for σ_{kS} and C_v in kS, we use the z-component of absolute permeability. Error is computed as the normalized root mean square (rms) error in oil recovery factor as stated in Equation (3.7). For each sub-grid quantity, we determine the coefficient of determination (R^2) between the sub-grid quantity and the coarse grid rms error in oil recovery factor. Three upscaling scenarios are considered:

- The coarse grid models are run using the "rock" curves.
- The coarse grid models are run with pseudo functions generated using the TW method.

- The fine grid models are run using the coarse grid absolute permeabilities together with the rock relative permeabilities. This is done to quantify the effects of numerical dispersion in our models.

Our assessment proceeds as follows. For a given model, we first simulate the 20-layer fine grid model. We then consider the generation of equivalent 2-layer coarse grid models. With a 20-layer fine grid model, there are 19 different coarsening combinations that provide 2-layer models (plus one option for 2D → 1D, upscaling by amalgamation the entire fine grid layers). The possible coarsening schemes are listed in Table 6.1 below:

Option	Coarse grid layer 1 is from fine grid :	Coarse grid layer 2 is from fine grid :
1	Layer 1 through 1	Layer 2 through 20
2	Layer 1 through 2	Layer 3 through 20
:	:	:
18	Layer 1 through 18	Layer 19 through 20
19	Layer 1 through 19	Layer 20 through 20
20	Fine grid layer 1 through 20	

Table 6.1: Possible options in 20-layer → 2-layer coarsening

In order to reduce the number of runs required, only coarsening options 5, 7, 9, 10, 11, 13, 15, 17 and 20 were considered. In the x-direction, we uniformly coarsen the 100

fine grid blocks to 20 coarse blocks. The dimensions of our coarse grid models are then $20 \times 1 \times 2$.

Before each of these options was run, the values of the six sub-grid quantities were calculated based on the saturation, velocity and permeability distributions of the fine grid model. Each of the 2-layer coarse models was then run and the results were compared with the fine grid performance to quantify the error. The results for the four cases are discussed below.

6.2.3 Coarse Grid Models Using Rock Curves

The results in Table 6.2 summarize the performance of each coarsening method (using rock curves) for each of the test cases. Figures 6.2 through 6.5 present graphically the performance for representative Case 1 through IV respectively.

Cases	σ^2_S	σ_{vS}	σ_{kS}	C_v in S_g	C_v in vS	C_v in kS
Case I	0.9899	0.9406	-	0.4848	0.9583	-
Case II	0.6447	0.9099	-	0.3965	0.3600	-
Case III	0.8161	0.8109	0.9058	0.9856	0.9755	0.9547
Case IV	0.8254	0.8711	0.9503	0.5176	0.6474	0.3776
Average Performance	**0.8190**	**0.8831**	**0.9281**	**0.5961**	**0.7353**	**0.6662**

Table 6.2: Coefficient of determination (R^2) between rms error and sub-grid quantities using rock curves in the coarse grid models.

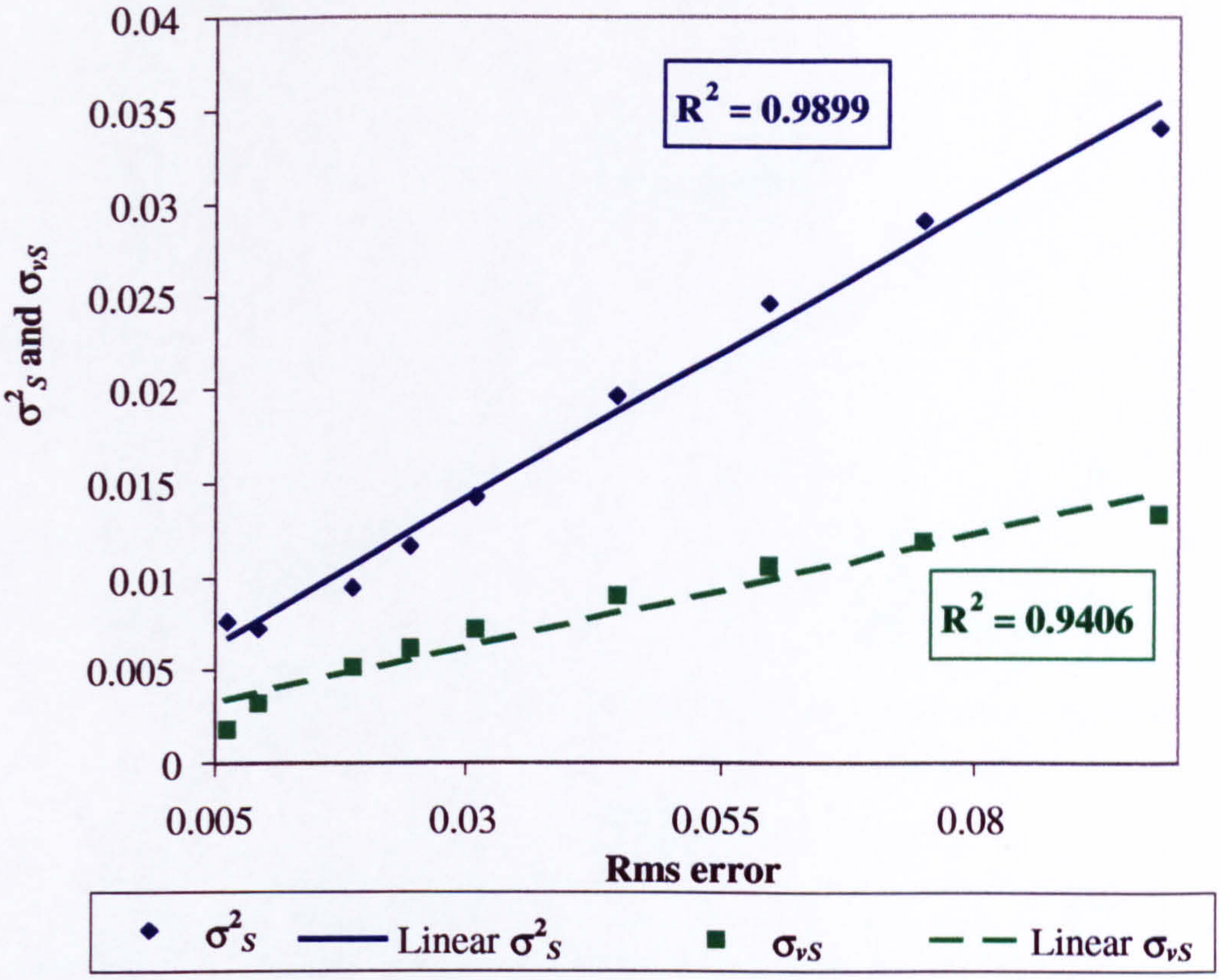

Figure 6.2a: Fluctuating moments in the form of σ versus normalized rms error (Case I, using rock curves)

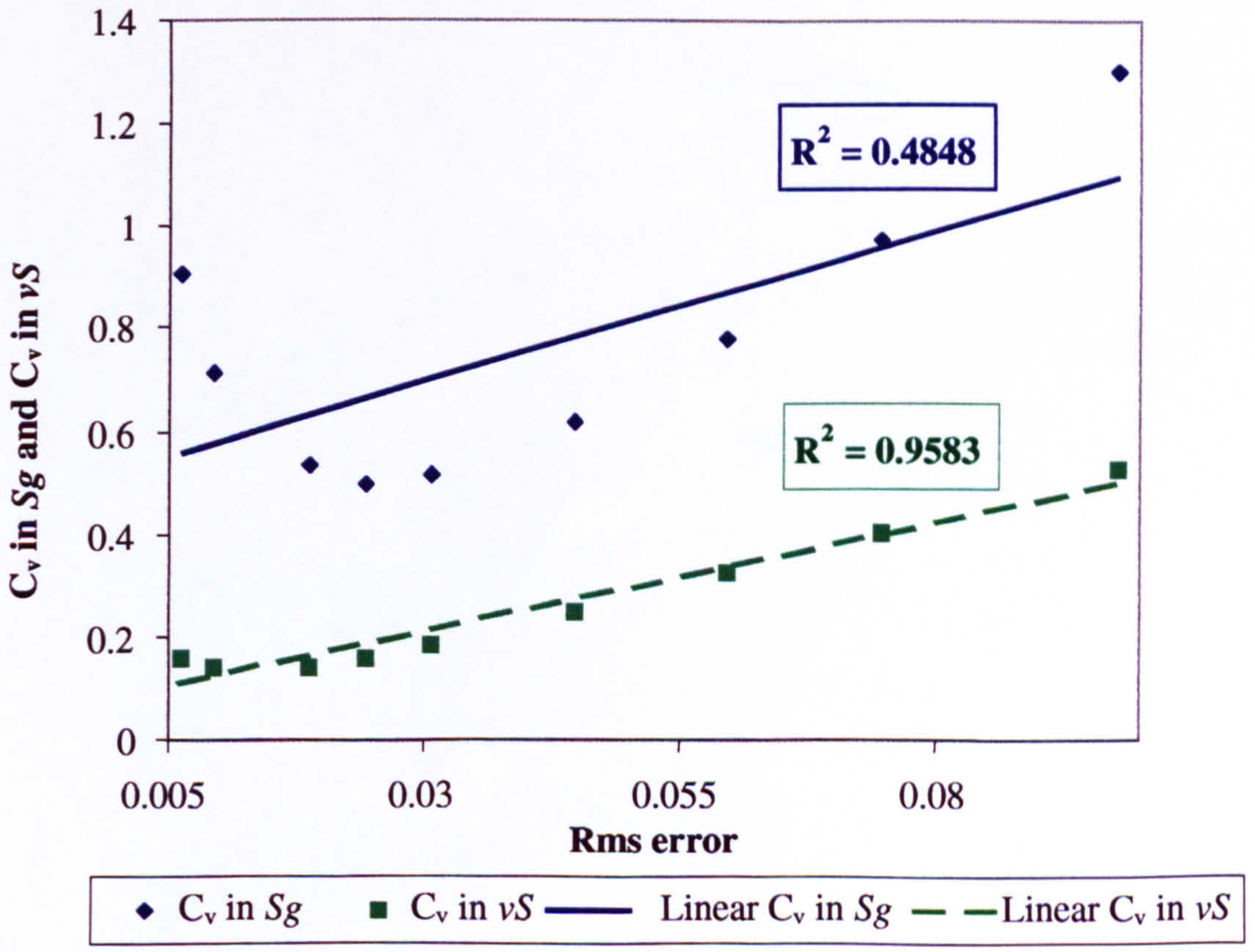

Figure 6.2b: Fluctuating moments in the form of C_v versus normalized rms error (Case I, using rock curves)

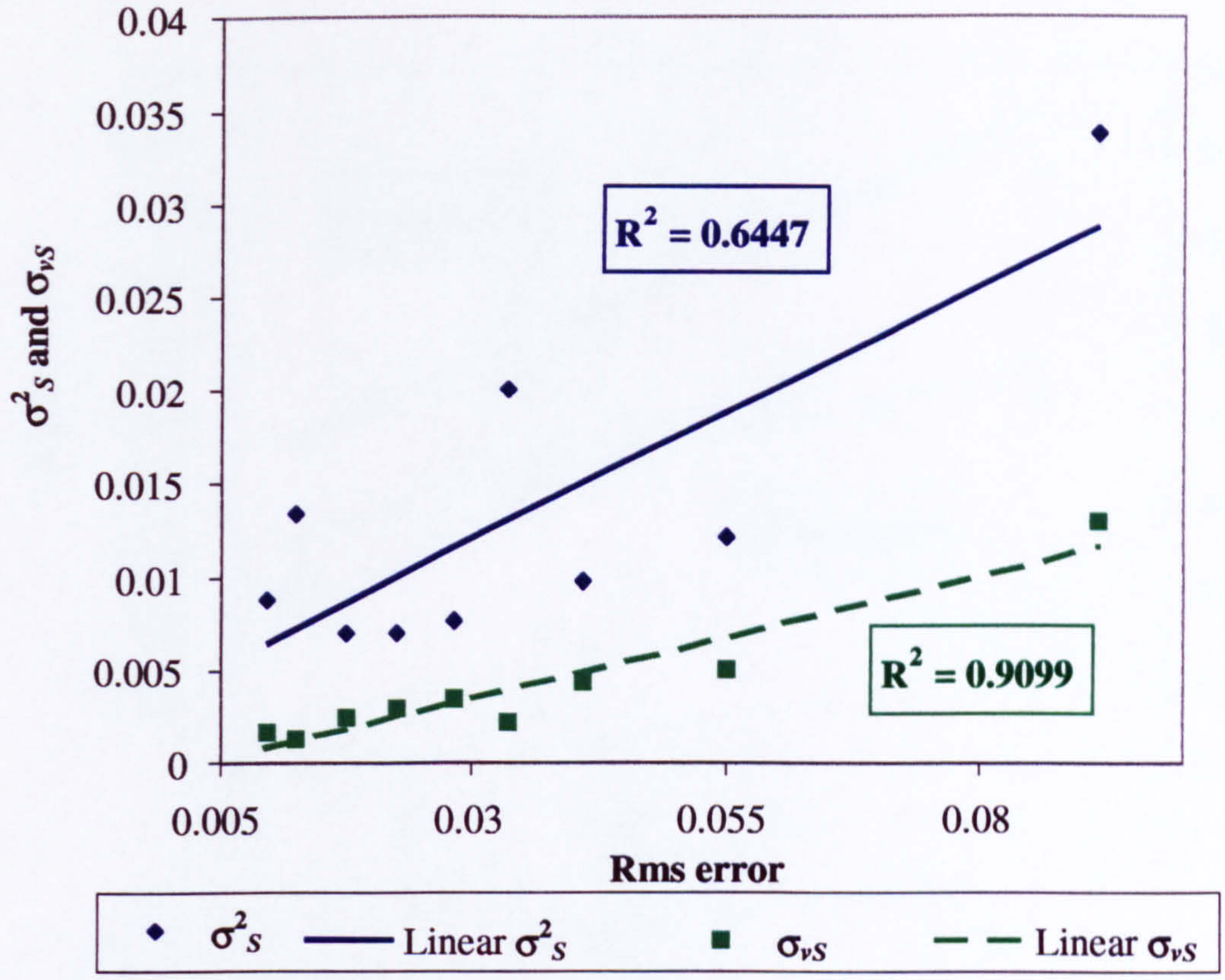

Figure 6.3a: Fluctuating moments in the form of σ versus normalized rms error (Case II, using rock curves)

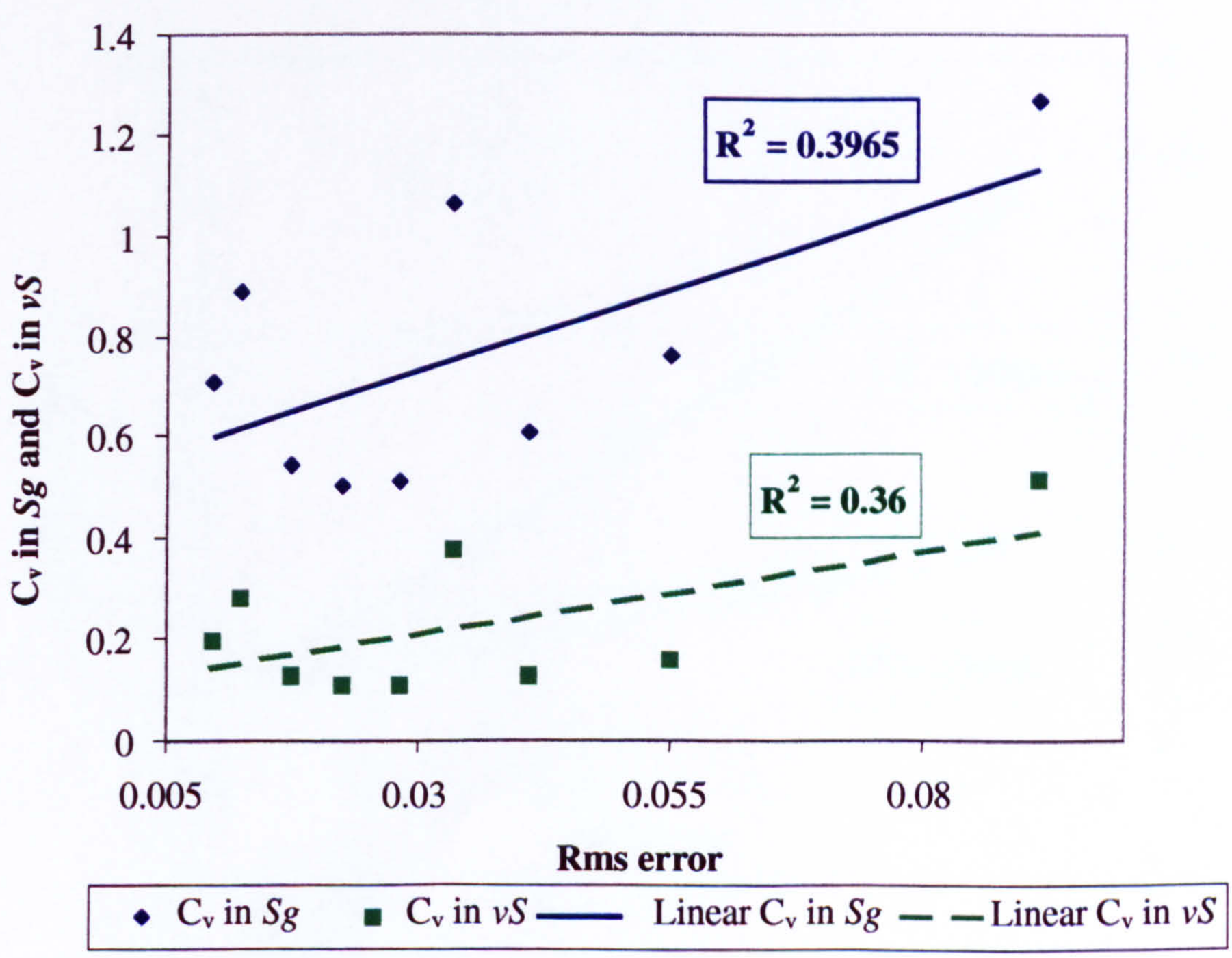

Figure 6.3b: Fluctuating moments in the form of C_v versus normalized rms error (Case II, using rock curves)

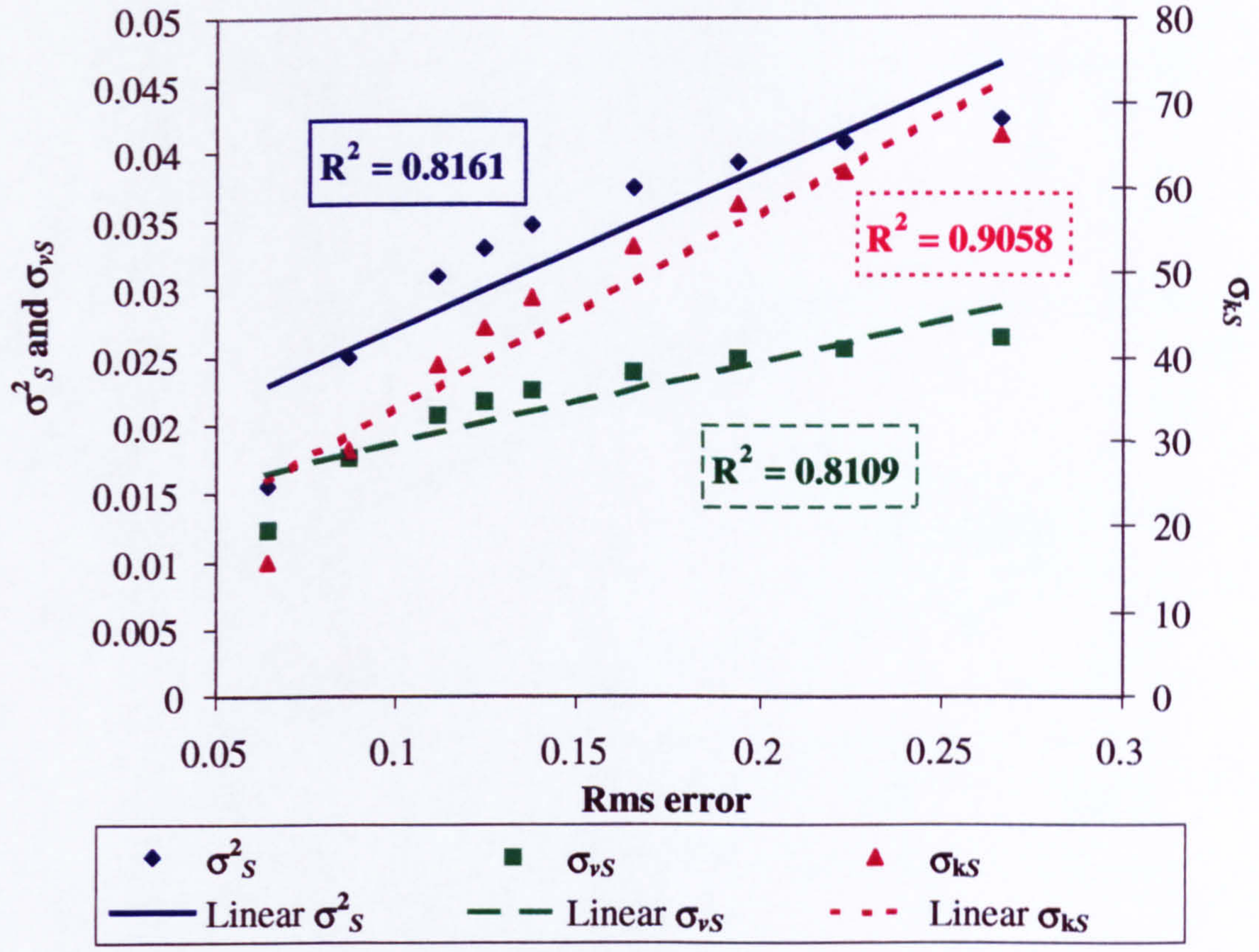

Figure 6.4a: Fluctuating moments in the form of σ versus normalized rms error (Case III, using rock curves)

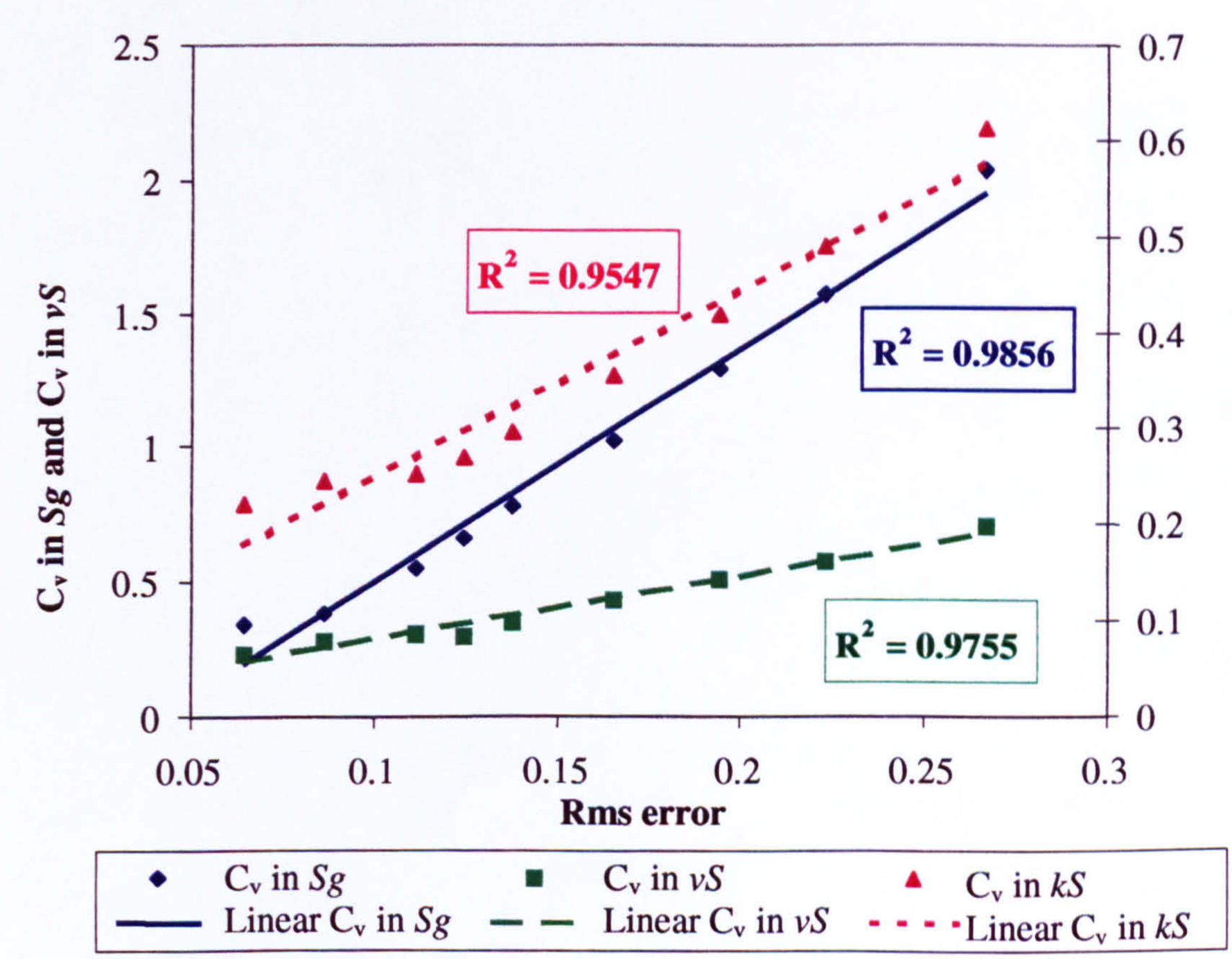

Figure 6.4b: Fluctuating moments in the form of C_v versus normalized rms error (Case III, using rock curves)

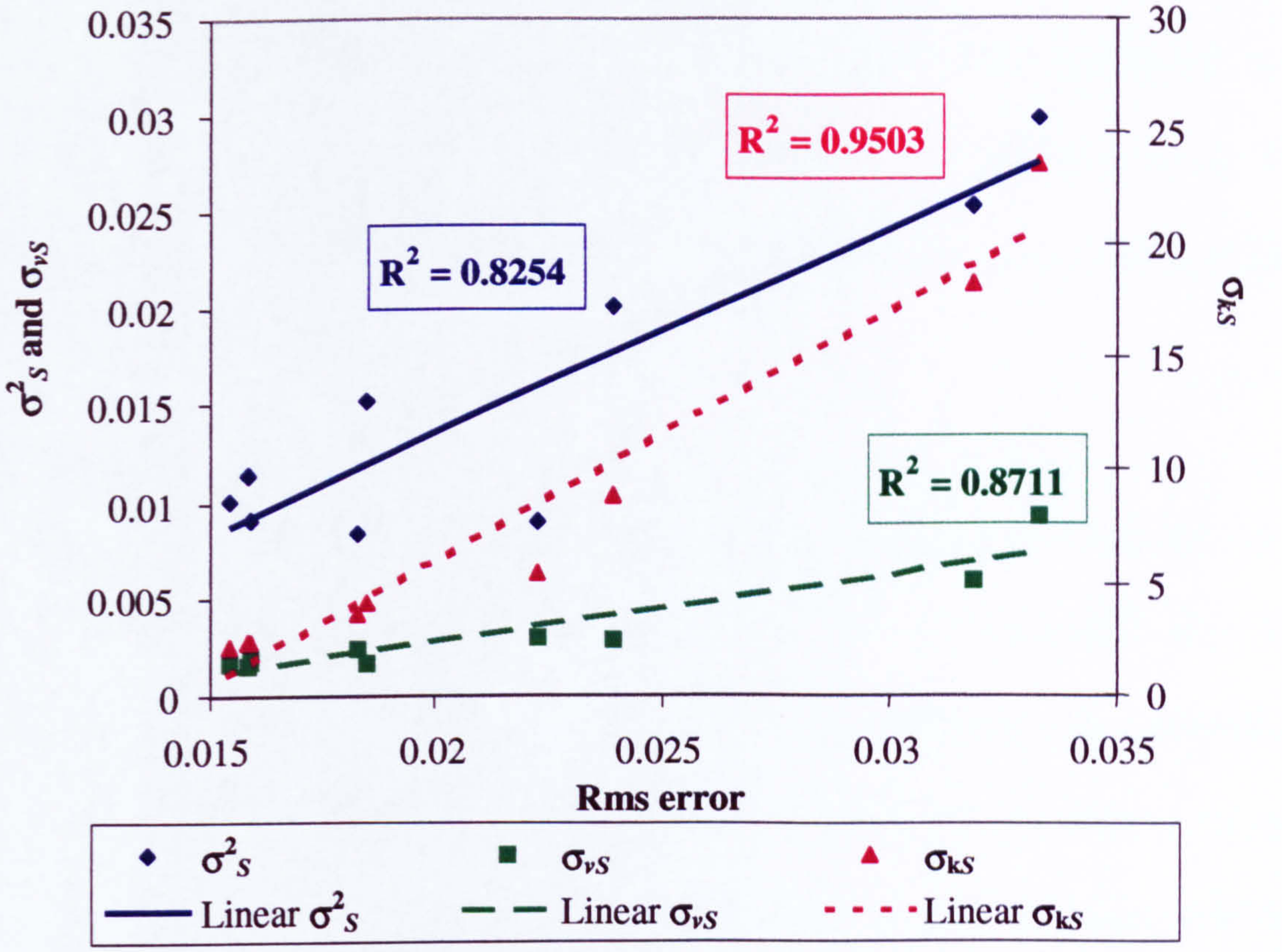

Figure 6.5a: Fluctuating moments in the form of σ versus normalized rms error (Case IV, using rock curves)

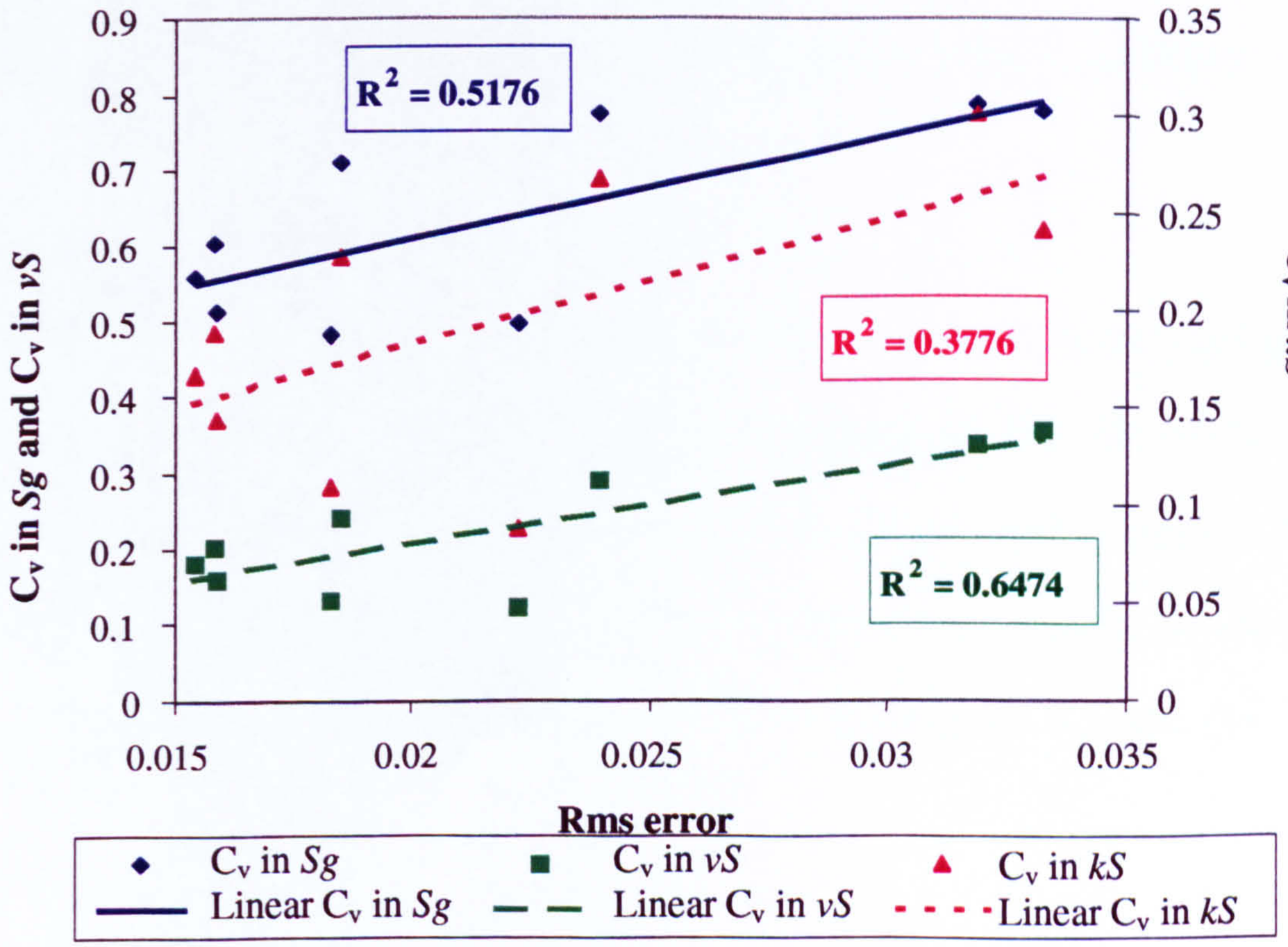

Figure 6.5b: Fluctuating moments in the form of C_v versus normalized rms error (Case IV, using rock curves)

In Cases I and II, $k_z = 0$, and hence gravitational effects are absent. The correlations between rms error and sub-grid quantities (R^2) for these cases are for the most part higher for σ_{vS} and σ^2_S ($\sigma_{kS}= 0$ in these cases) than for C_v in vS and C_v in S_g. The high correlations observed for σ_{vS} and σ^2_S are consistent with previous results of Durlosky (1997 and 1998).

The tendencies observed for Cases I and II are less apparent in Cases III and IV. In fact, Case III shows higher correlations with the C_v quantities than for the corresponding quantities computed in terms of σ. However, the differences are relatively slight (average R^2 of 0.97 versus 0.84). For Case IV, we observe the opposite behavior; namely, the error shows higher correlations with σ quantities than with C_v quantities. In this case, the differences in R^2 for the measures are more significant; 0.88 versus 0.51. Taken in total, we can conclude from Cases I-IV that the error in general correlates more closely with σ_{vS}, σ^2_S and σ_{kS} than with the C_v quantities.

6.2.4 Coarse Grid Models Using Pseudo Functions

The procedure here is the same as that applied in the previous section except that the coarse grid models now use pseudo functions generated by the TW method. The results in Table 6.3 summarise the performance of the six sub-grid measures for each of the test cases and Figures 6.6 and 6.9 show the same results graphically for Case I through Case IV, respectively. Several interesting observations emerge from these data.

Cases	σ^2_S	σ_{vS}	σ_{kS}	C_v in S_g	C_v in vS	C_v in kS
Case I	0.8757	0.6792	-	0.7754	0.9518	-
Case II	0.8774	0.3723	-	0.9691	0.8883	-
Case III	0.8725	0.8673	0.9470	0.9604	0.9443	0.9127
Case IV	0.2274	0.0001	0.0451	0.6017	0.3975	0.7059
Average Performance	**0.7133**	**0.4797**	**0.4961**	**0.8267**	**0.7955**	**0.8093**

Table 6.3: Coefficient of determination (R^2) between rms error and sub-grid quantities using pseudo functions in the coarse grid models.

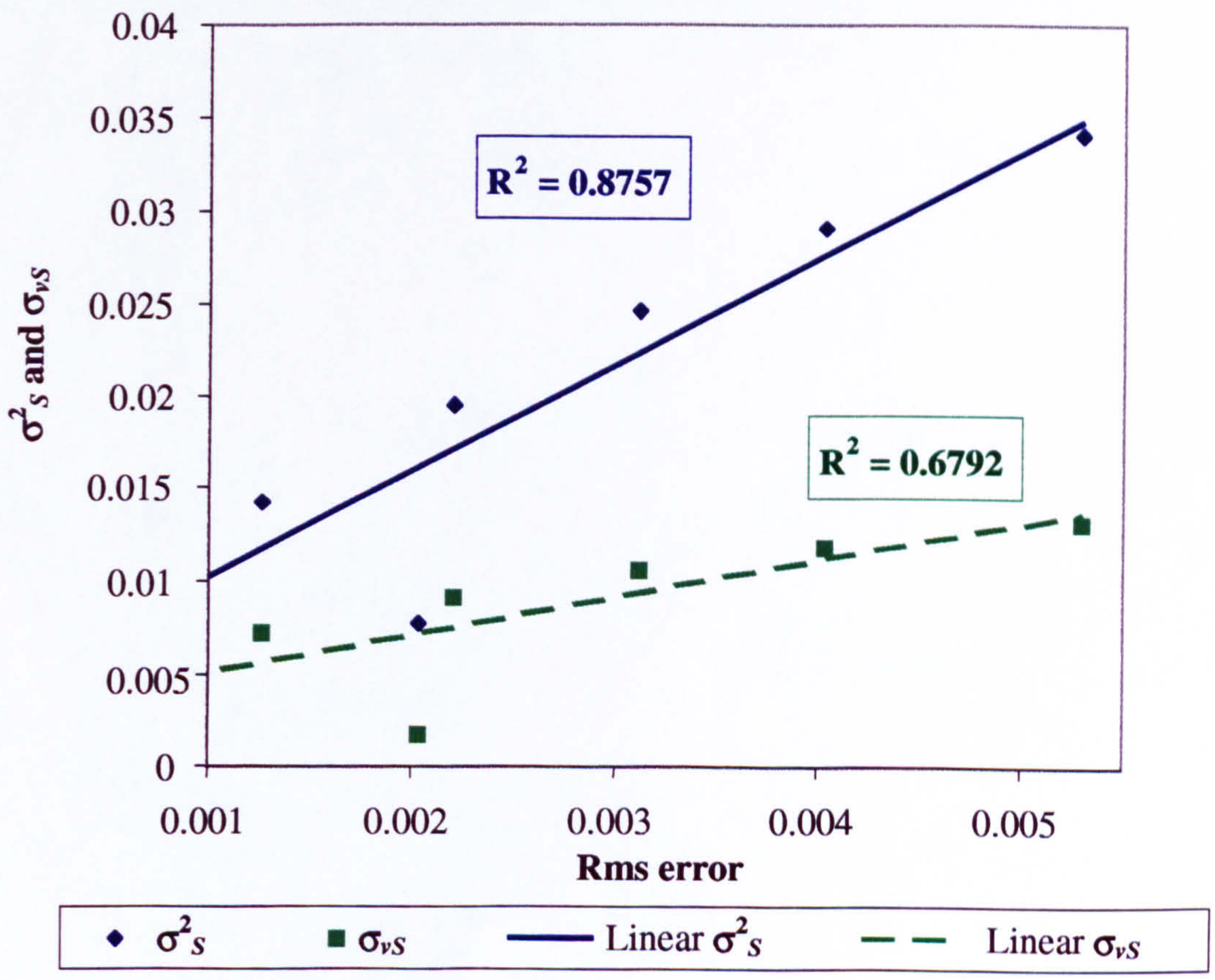

Figure 6.6a: Fluctuating moments in the form of σ versus normalized rms error (Case I, using TW pseudo functions)

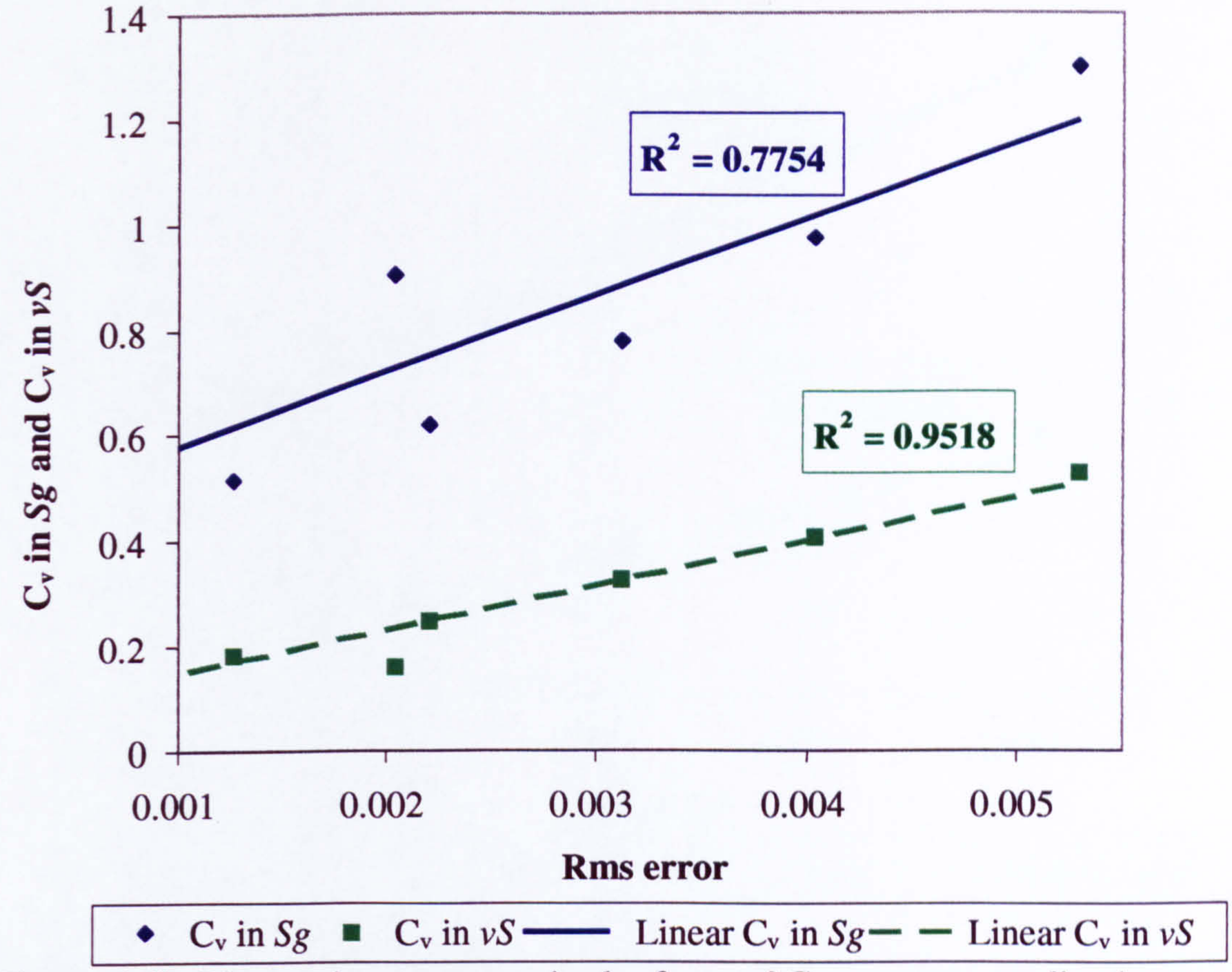

Figure 6.6b: Fluctuating moments in the form of C_v versus normalized rms error (Case I, using TW pseudo functions)

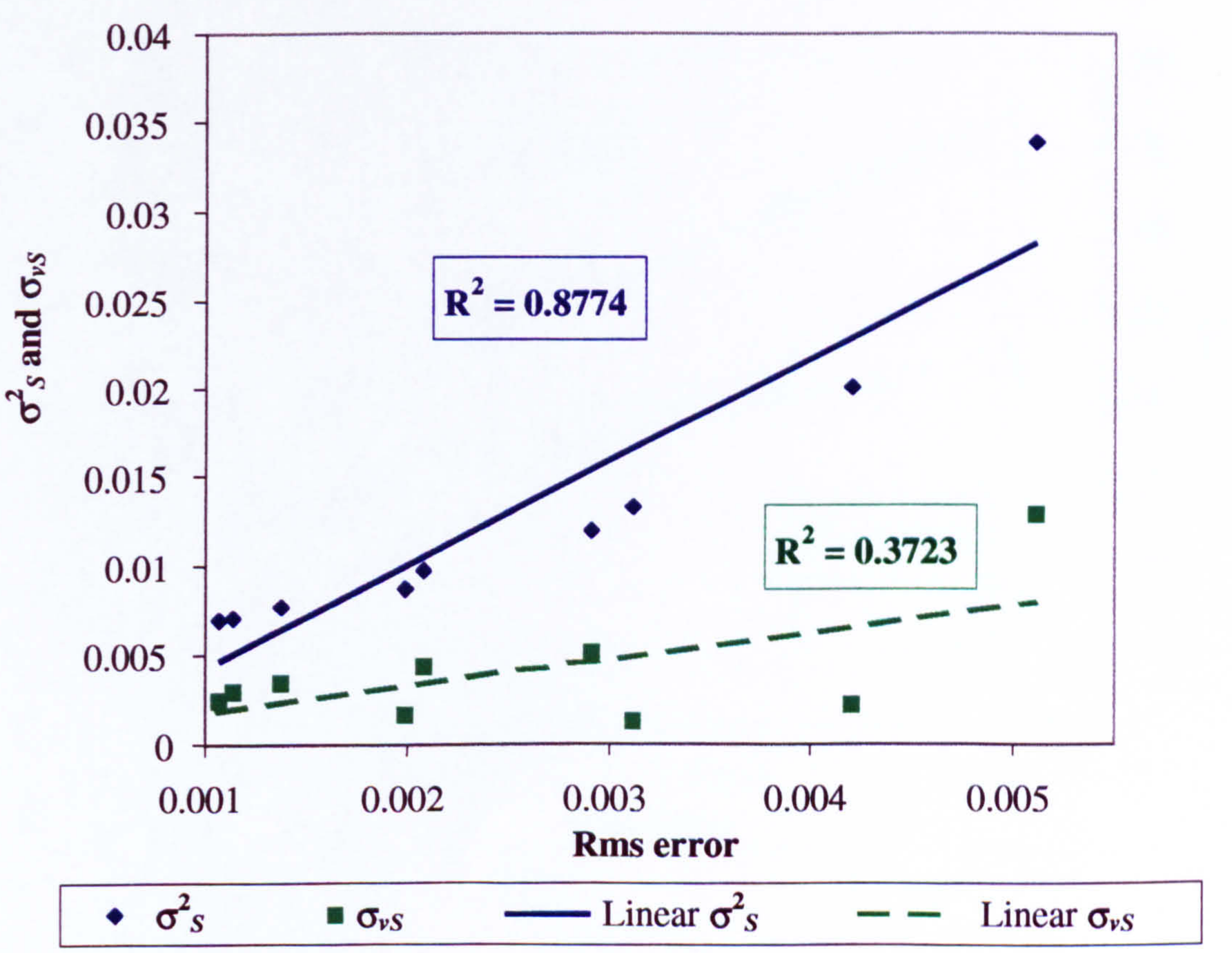

Figure 6.7a: Fluctuating moments in the form of σ versus normalized rms error (Case II, using TW pseudo functions)

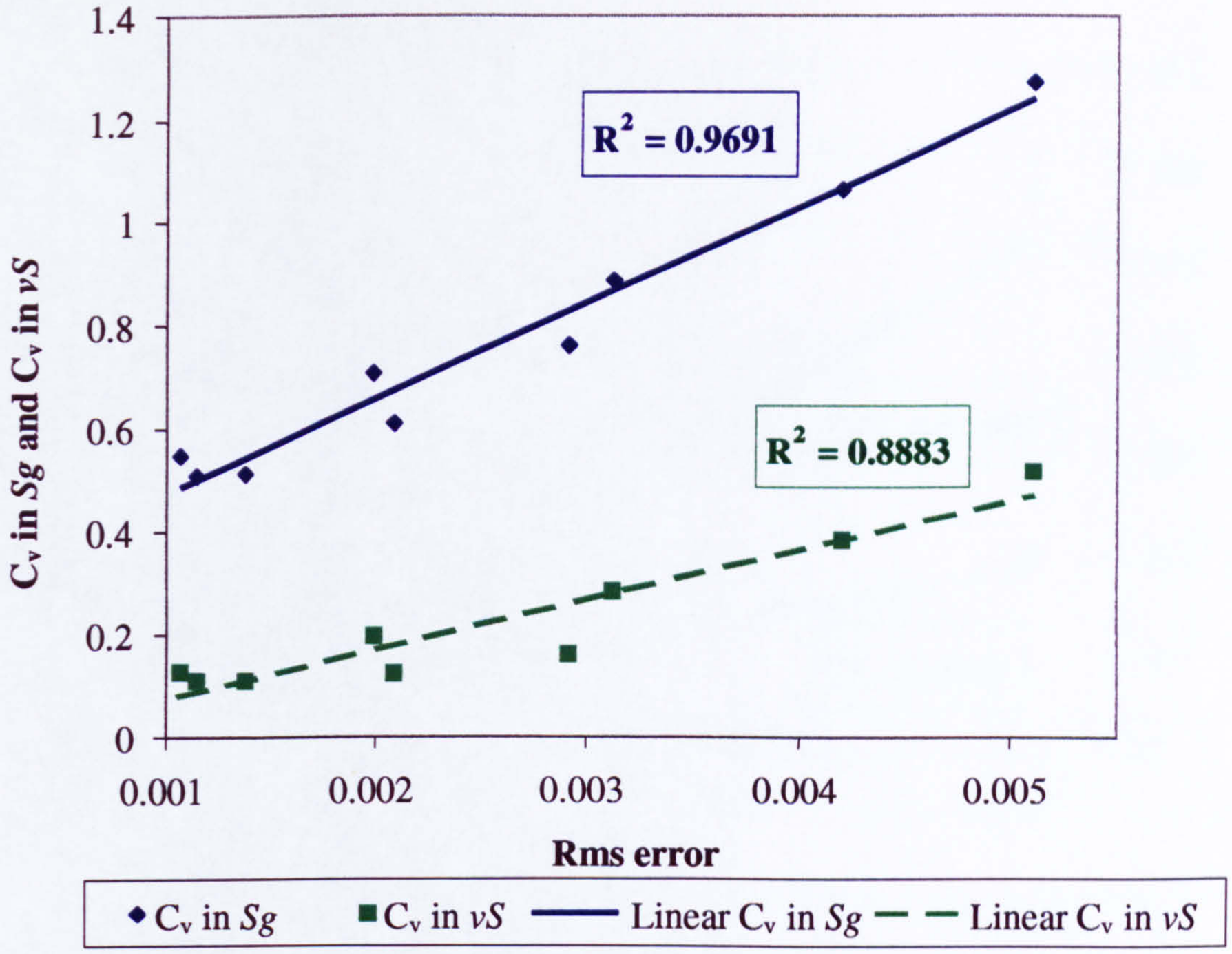

Figure 6.7b: Fluctuating moments in the form of C_v versus normalized rms error (Case II, using TW pseudo functions)

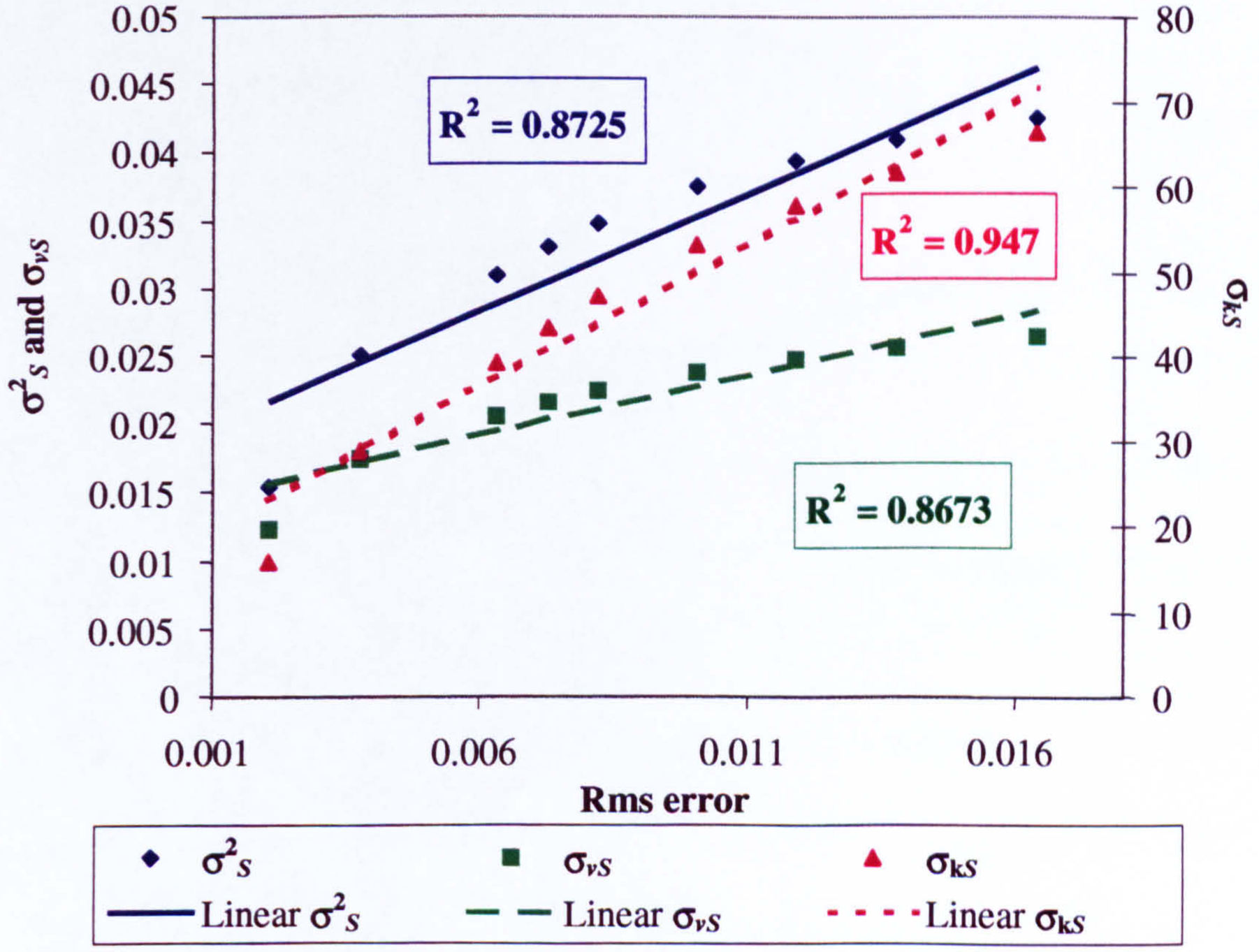

Figure 6.8a: Fluctuating moments in the form of σ versus normalized rms error (Case III, using TW pseudo functions)

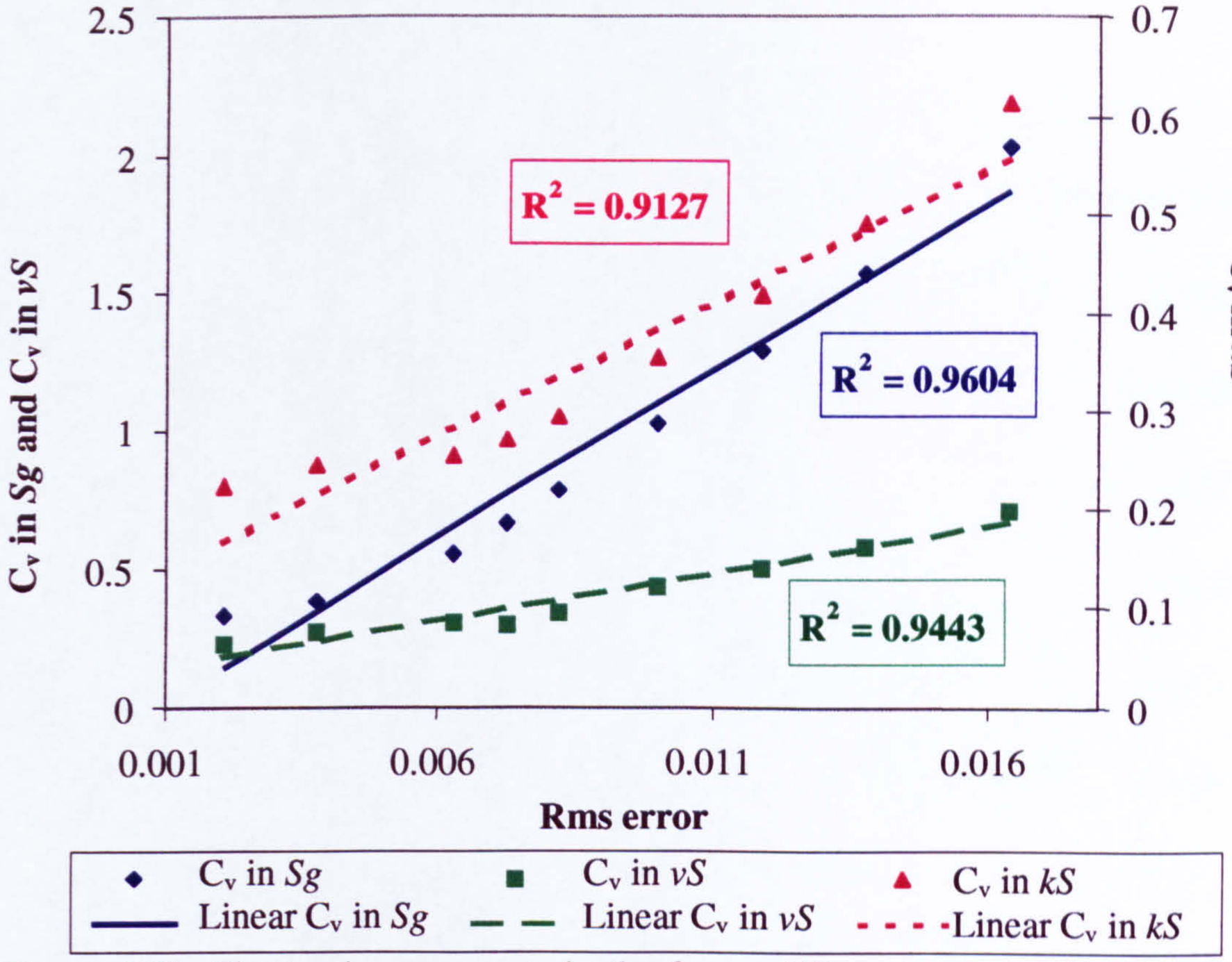

Figure 6.8b: Fluctuating moments in the form of C_v versus normalized rms error (Case III, using TW pseudo functions)

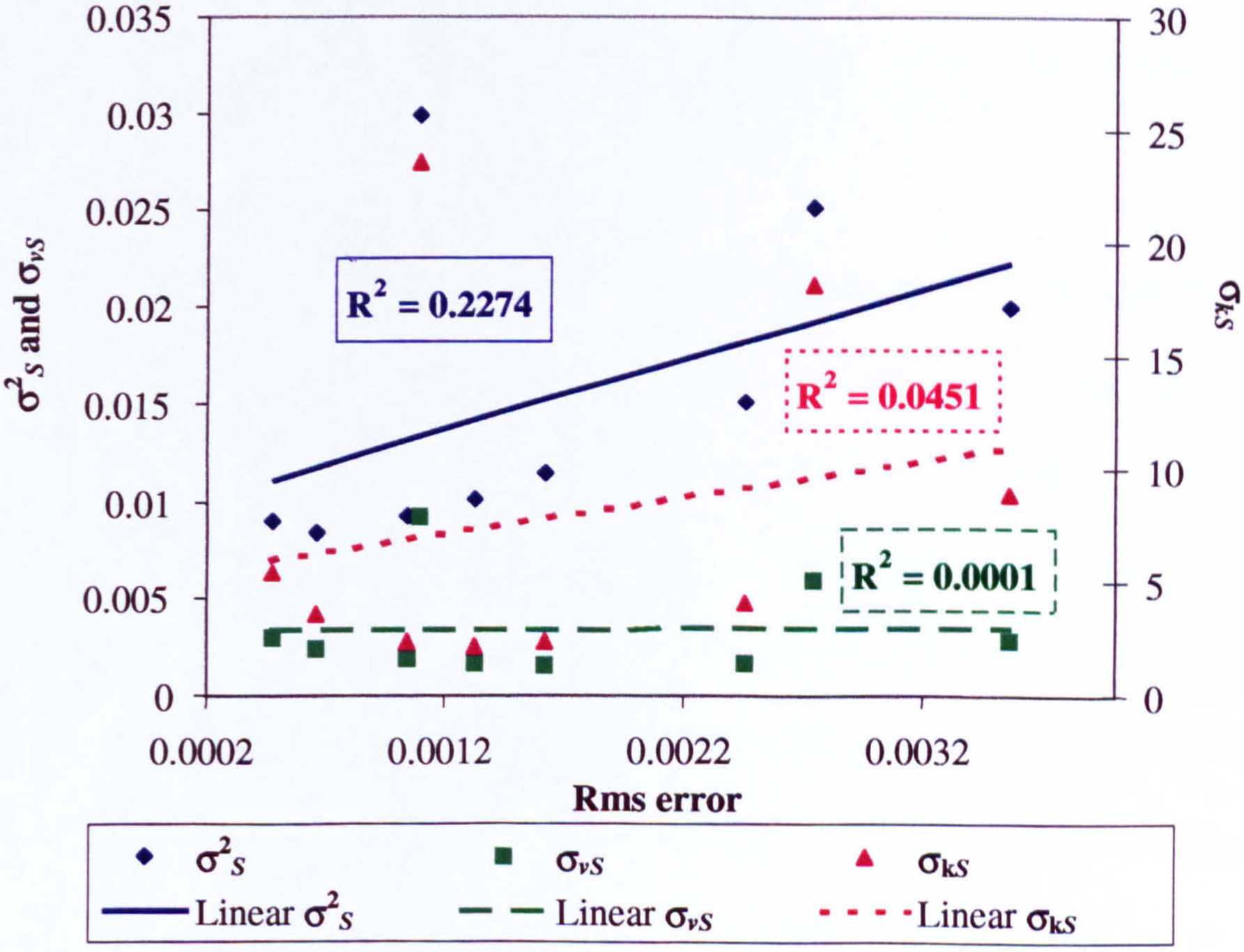

Figure 6.9a: Fluctuating moments in the form of σ versus normalized rms error (Case IV, using TW pseudo functions)

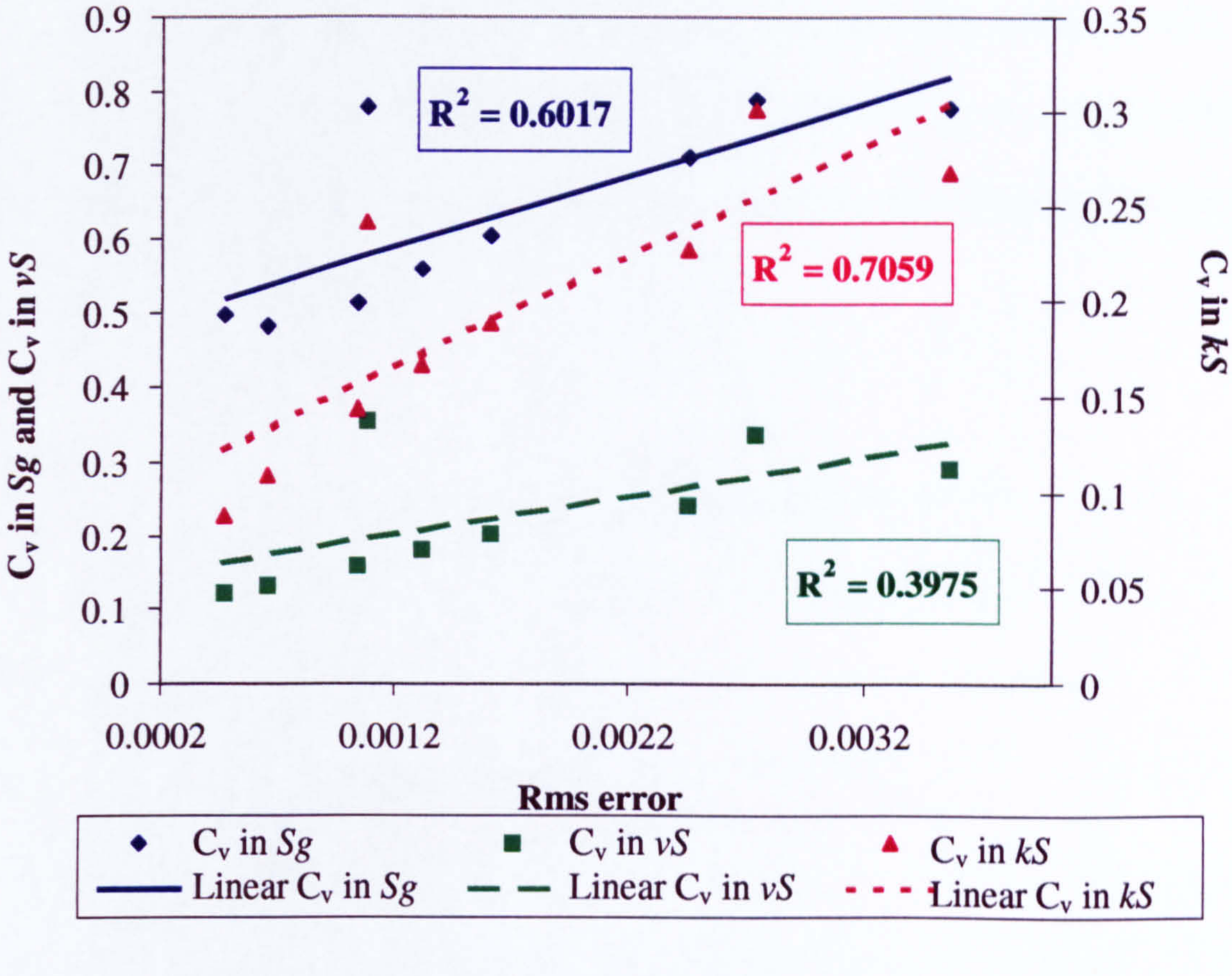

Figure 6.9b: Fluctuating moments in the form of C_v versus normalized rms error (Case IV, using TW pseudo functions)

Most notably, the magnitude of the error produced using the TW pseudo functions is less in all cases than that observed when using the rock curves directly. In fact, the error using pseudo relative permeabilities for any coarsening of the 20-layer system to a 2-layer coarse grid model is less than the error in the best case using rock curves. This is illustrated graphically in Figure 6.10 for representative Case III. The results in Figure 6.10 below clearly demonstrate the sensitivity of the coarse scale simulation results to the grid structure when rock curves are used. However, when pseudo functions are used, the magnitude of the error is much smaller. This might be expected, since the pseudo functions are computed for each specific grid from global fine scale

simulations. This finding is consistent with the results of Wallstrom *et al.* (1999) who found that the use of non-uniform coarsening methods (Durlofsky *et al.*, 1997) together with renormalised relative permeabilities (Christie *et al.*, 1995), that were computed from local fine scale problems, gave better results compared to the use of non-uniform coarsening alone.

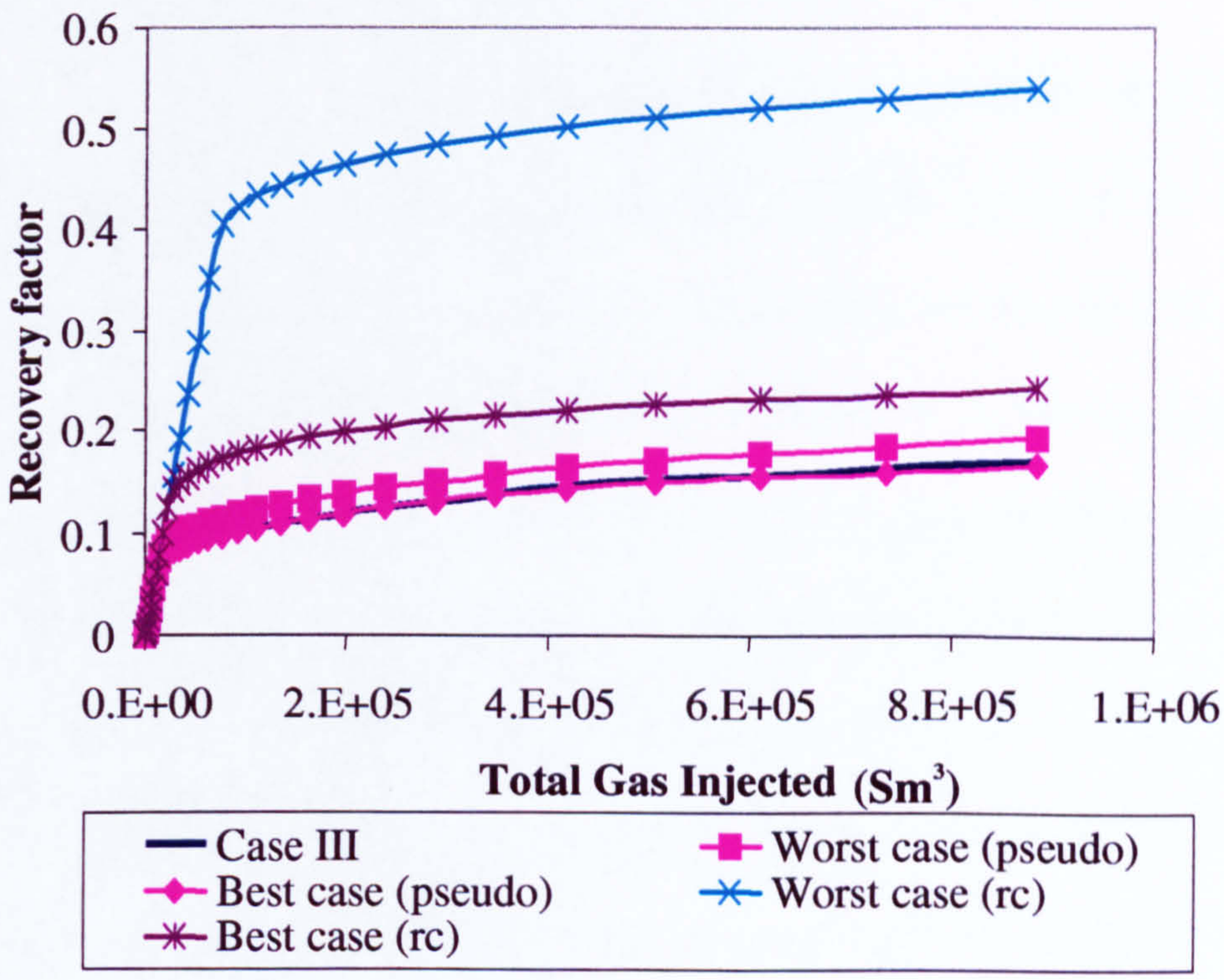

Figure 6.10: Oil recovery factor versus total gas injected for Case III, showing the magnitude of the error produced using the TW pseudo functions is less than that observed when using the rock curves directly.

In Figure 6.10, the worst and the best cases are represented by coarsening option number 20 (2D $\rightarrow$ 1D coarsening) and option number 5 (the first coarse grid layer consists of the first 5 top layers of the fine grid block model), respectively. Having demonstrated that the error using pseudo functions is relatively small, we now consider the correlation of this error with the C_v and σ quantities. A summary of these results is

shown in Table 6.3. Although there are a few exceptions, errors using pseudo functions correlate more closely in general with the C_v quantities than with the σ quantities. This is most apparent for Case IV, for which the σ quantities display particularly low R^2 values. This observation is in contrast to the results using rock curves presented above.

The reason why the error correlates more closely with σ quantities when rock curves are used but more closely with C_v quantities when pseudo functions are used is not clear. It is however quite reasonable that the precise forms of the sub-grid effects that best correlate with the error change when we go from rock curves to pseudo relative permeabilities. This is because pseudo functions are specifically designed to capture sub-grid effects, so the exact form of the error using pseudo functions would be expected to differ from that observed when sub-grid effects are not modeled at all. Graphical illustration of the proposed coarsening schemes for the four cases are shown in Figures 6.11a though 6.11b below for Case I through Case IV respectively.

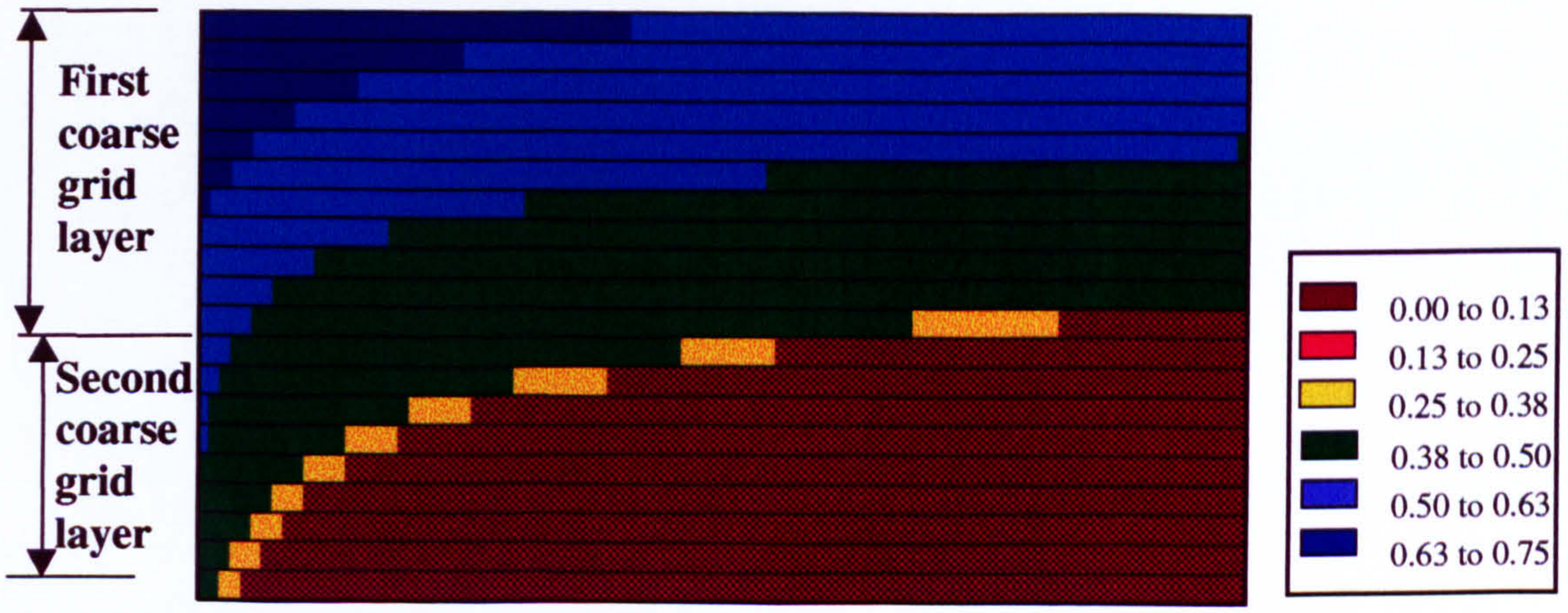

Figure 6.11a: Saturation plot at 4 PVI showing the proposed coarsening scheme for Case I (coarsening upward models with $k_v/k_h = 0.0$)

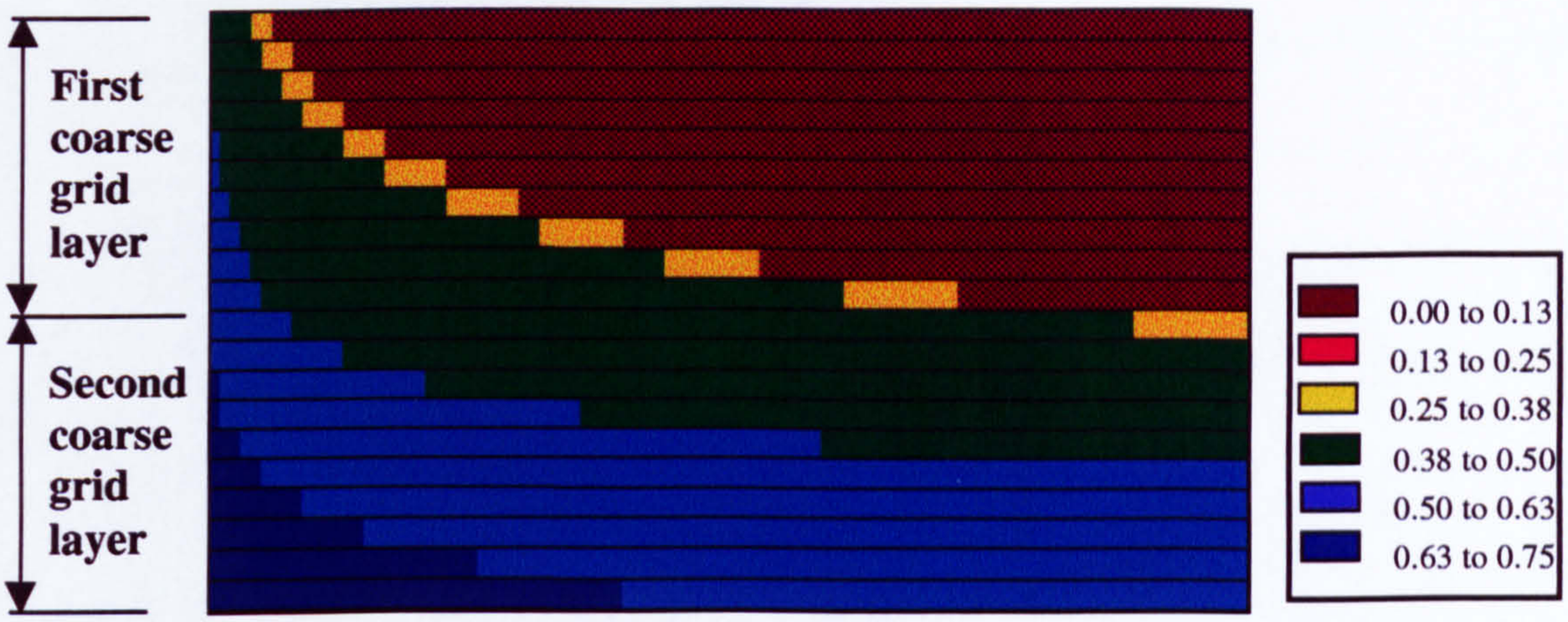

Figure 6.11b: Saturation plot at 4 PVI showing the proposed coarsening scheme for Case II (fining upward models with $k_v/k_h = 0.0$)

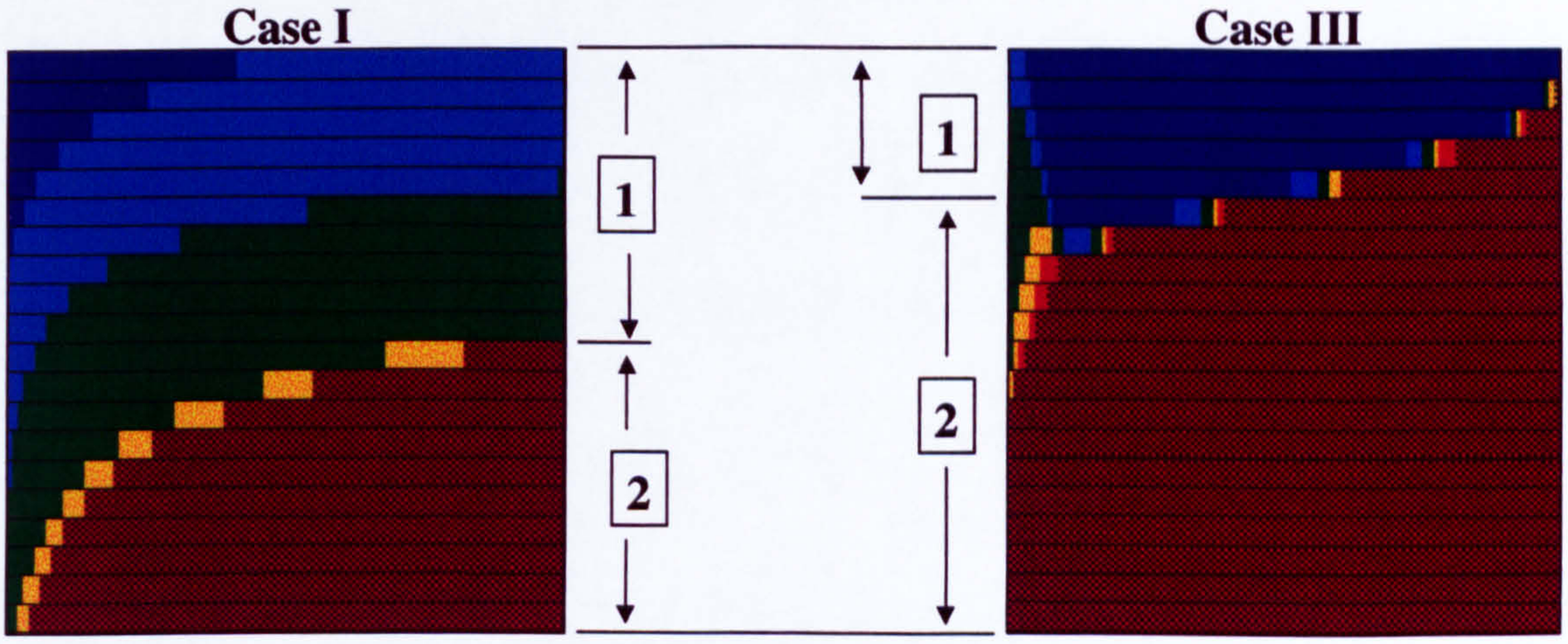

Figure 6.11c: Saturation plot at 4 PVI showing the proposed coarsening scheme for Case III in comparison with Case I (coarsening upward models with $k_v/k_h = 1.0$)

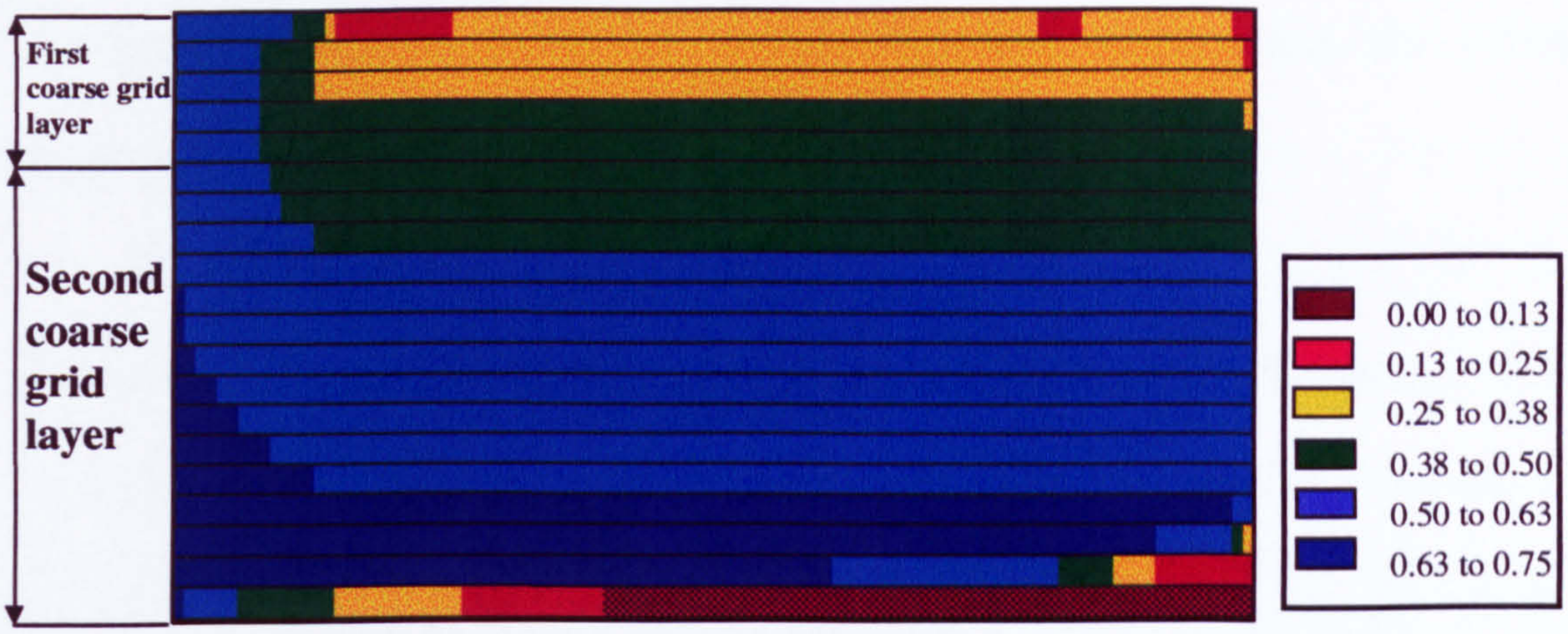

Figure 6.11d: Saturation plot at 4 PVI showing the proposed coarsening scheme for Case IV (fining upward models with $k_v/k_h = 1.0$)

6.2.5 Fine Grid Models Using Coarse Grid Permeabilities and Rock Curves

As discussed in the previous chapter, pseudo functions act both to capture the effects of sub-grid heterogeneity on the fluid flow and to correct for numerical dispersion. In this section, we will evaluate and quantify the effects of numerical dispersion in our coarse grid models.

This is accomplished as follows. For each coarsening scheme, we make an additional run of fine grid models using coarse scale absolute permeability (defined over the same regions as in the coarse models) and the rock curve relative permeabilities. The difference in the results between these models and the coarse grid models using rock curves described above will reflect the effect of numerical dispersion. On the other hand, the difference between these models and the coarse-scale models using pseudo functions will quantify the effect of sub-grid heterogeneity on two-phase flow. Thus, from these results we can distinguish the extent to which the pseudo functions correct

for numerical dispersion versus the degree to which they capture the effects of heterogeneity.

Detailed results comparing the errors due to numerical dispersion to the errors caused by using rock curves rather than pseudo functions are listed in Table 6.4 below:

Coarsening options		5	7	9	11	13	15	17	20
Coarse grid With rock Curve (row 1)	Case I	6.23e-3	9.38e-3	1.87e-2	3.08e-2	4.46e-2	5.95e-2	7.49e-2	9.80e-2
	Case II	5.50e-2	4.10e-2	2.83e-2	1.74e-2	9.53e-3	1.23e-2	3.35e-2	9.16e-2
	Case III	6.45e-2	8.66e-2	1.11e-1	1.38e-1	1.65e-1	1.94e-1	2.23e-1	2.67e-1
	Case IV	2.23e-2	1.83e-2	1.59e-2	1.58e-2	1.85e-2	2.39e-2	3.19e-2	3.33e-2
Coarse grid With pseudo Functions (row 2)	Case I	2.04e-3	5.91e-4	9.34e-4	1.26e-3	2.21e-3	3.12e-3	4.03e-3	5.29e-3
	Case II	2.91e-3	2.08e-3	1.37e-3	1.06e-3	1.99e-3	3.12e-3	4.20e-3	5.11e-3
	Case III	2.07e-3	3.77e-3	6.28e-3	8.20e-3	1.00e-2	1.19e-2	1.37e-2	1.64e-2
	Case IV	4.69e-4	6.56e-4	1.05e-3	1.62e-3	2.46e-3	3.56e-3	2.74e-3	1.09e-3
Fine grid with Averaged Absolute Perm. (row 3)	Case I	9.13e-3	1.05e-2	2.00e-2	3.24e-2	4.64e-2	6.14e-2	7.70e-2	1.00e-1
	Case II	5.67e-2	4.26e-2	2.96e-2	1.84e-2	1.06e-2	1.55e-2	3.77e-2	9.40e-2
	Case III	5.47e-2	7.93e-2	1.07e-1	1.36e-1	1.65e-1	1.95e-1	2.25e-1	2.71e-1
	Case IV	1.93e-2	1.38e-2	1.15e-2	1.50e-2	2.17e-2	2.78e-2	2.96e-2	3.49e-2
Effect of Numerical Dispersion (absolute %)[a]	Case I	29.00	10.51	6.58	5.04	4.00	3.17	2.87	2.58
	Case II	3.08	3.74	4.40	5.37	11.10	20.41	11.19	2.67
	Case III	15.61	8.81	4.54	1.71	0.006	0.70	1.00	1.75
	Case IV	13.41	25.24	29.58	5.71	14.29	13.86	7.81	4.52
Effect of sub-grid Heterogeneity on 2-phase flow (absolute %)[b]	Case I	71.00	89.49	93.42	94.96	96.00	96.83	97.13	97.42
	Case II	96.92	96.26	95.60	94.63	88.90	79.59	88.81	97.33
	Case III	84.39	91.19	95.46	98.29	99.94	93.30	99.00	98.25
	Case IV	86.59	74.76	70.42	94.29	85.71	86.14	92.19	95.48

Table 6.4: Rms error and quantification of effects of using pseudo functions for all the test cases

[a] The effect of numerical dispersion is calculated as [abs (row3 – row1) / (abs (row3 – row2) + abs (row3-row1))] x 100

[b] The effect of heterogeneity is calculated as [abs (row3 – row2) / (abs (row3 – row2) + abs (row3-row1))] x 100

The results in Table 6.4 show quite clearly that numerical dispersion plays a relatively minor role in these test models. Most of the improvement is due to the ability of pseudo functions to capture the interactions between the small-scale multi-phase fluid flow and the heterogeneity of the porous media. This point is illustrated in Figure 6.12 for representative Case I (for the 2D → 1D coarsening scheme). From this figure, we see that there is only a slight difference between the performance of the coarse grid model using rock relative permeability curves and the fine grid model using the averaged absolute permeability and rock relative permeability curves. However, if we use pseudo functions in the coarse grid model, significant improvement is observed.

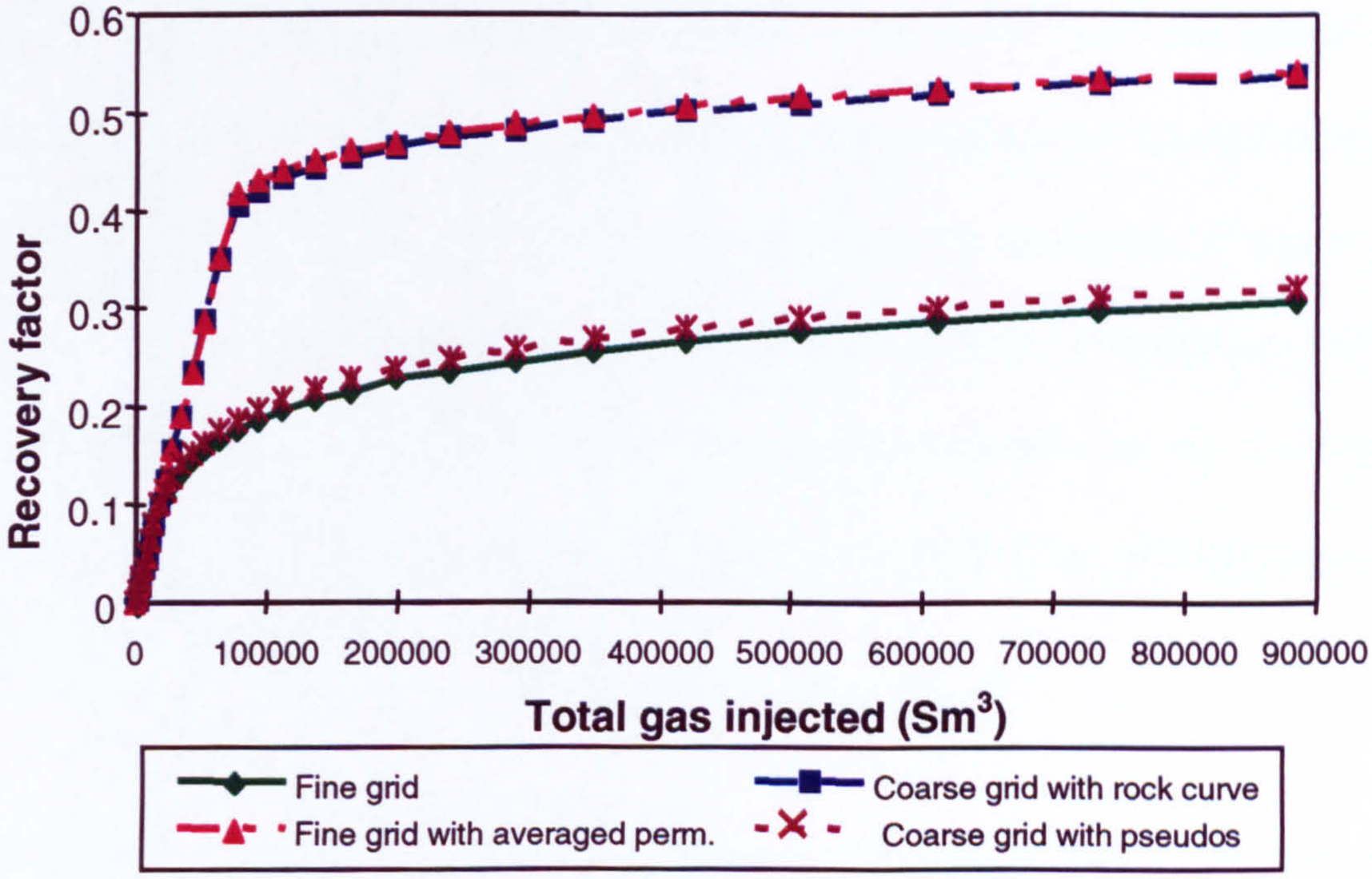

Figure 6.12: Oil recovery factor versus total gas injected for Case I, showing the magnitude of the error caused by numerical dispersion is less than the error by not capturing the appropriate interaction between small-scale heterogeneity and multi-phase flow.

6.3 APPLICATION OF THE OPTIMAL GRID COARSENING SCHEME IN MULTI-LAYERED 2D → 2D UPSCALING

In the previous section, we considered the coarsening of 20-layer (fine grid) models to 2-layer (coarse grid) models, using both rock curves and pseudo functions on the coarse scale. In this section, we will consider coarsening these same 20-layer models to systems containing more than 2 layers. Our intent here is to determine if the coarsening approach used in the previous section applies equally to multi-layer systems. We consider only the use of pseudo functions at the coarse scale in this part of the study.

The results of the previous section (Table 6.3) demonstrate, in general, reasonably good correlations of rms error with C_v in vS, C_v in S_g and, in cases involving gravitational effects, C_v in kS. The use of all three of these quantities together would probably provide the most accurate estimation of rms error. However, rather than form a correlation involving all three quantities, for present purposes we will simply use C_v in S_g to estimate error. We choose C_v in S_g because it is applicable in cases both with and without gravity and because it always provides at least a moderate coefficient of determination (minimum R^2 of 0.60 for the cases considered). In this section, we will test the conjecture that C_v in S_g can be used to correlate error in more general multi-layer cases.

Our approach here is to use C_v in S_g, determined from fine grid simulations, to guide the choice of the number of coarse grid layers as well as their configuration. We assess the applicability and accuracy of this approach through detailed numerical calculations. In order to investigate the compatibility of this coarsening scheme with other dynamic pseudo generation methods, both the TW and the Kyte and Berry methods are used.

6.3.1 Coarsening Scheme

The same four test models described in the previous section were used for this purpose. A simple computer programme was developed to determine every possible layering combination of the fine grid model, given the number of layers specified for the coarse grid model. Based on a single fine grid calculation, this program also calculated the corresponding C_v in S_g for each of the coarsening options and then sorted these values to obtain the maximum and the minimum. The number of possible coarsening options can be obtained using the following expression:

$$\text{No. of possible coarsening options} = \frac{(n-1)!}{(m-1)!(n-m)!}, \tag{6.3}$$

where m is the number of the coarse grid layers and n is the number of the fine grid layers (in all of these cases, $n = 20$). It is clear from Eq. (6.3) that the number of possible coarsening options increases sharply (from both directions) toward a maximum at $m = 10$. Therefore, to reduce the total number of simulations, no attempt was made to verify the new coarsening method using more than seven layers in the coarse grid model. The results for all the test models are discussed below.

6.3.2 Discussion of the Results

Tables 6.5 and 6.6 summarise the layer combinations that produce the minimum and the maximum C_v in S_g, respectively, for each of the test cases (for 2, 3 and 4 coarse grid layers). In these two tables, s1 denotes the number of the fine grid layer at the start of the first coarse grid layer, e1 denotes the number of the fine grid layer at the end of the first coarse grid layer, and so on. For comparative purposes, we will refer to the gas saturation plots for all of the fine grid runs (Case I to Case IV) that are shown in Figures 6.11a to 6.11d.

For Cases III and IV, where $k_v/k_h > 0$, no attempt was made to coarsen the fine grid models into 3-layer (or 5-layer) coarse models. This was because these coarsening schemes produce at least one coarse grid layer containing an even number of fine grid layers, but both pseudo generation methods require an odd number of layers in calculating pseudo functions in the vertical direction. Although the methods could be modified to handle these situations, the required averaging process may introduce an additional source of error. We note that in Cases I and II, where $k_v/k_h = 0$, pseudo functions are not required in the vertical direction, so coarse grids with even numbers of layers were considered.

	2-layer coarse grid models				3-layer coarse grid models						4-layer coarse grid models							
	s1	e1	s2	e2	S 1	e1	s2	e2	s3	e3	s1	e1	s2	e2	s3	e3	s4	e4
Case I	1	9	10	20	1	4	5	10	11	20	1	3	4	7	8	11	12	20
Case II	1	8	9	20	1	6	7	11	12	20	1	5	6	9	10	13	14	20
Case III	1	5	6	20	-	-	-	-	-	-	1	3	4	4	5	7	8	20
Case IV	1	5	6	20	-	-	-	-	-	-	1	1	2	4	5	9	10	20

Table 6.5: The best coarsening options
(configurations that produce the minimum C_v in S_g)

	2-layer coarse grid models				3-layer coarse grid models						4-layer coarse grid models							
	s1	e1	s2	e2	S 1	e1	s2	e2	s3	e3	s1	e1	s2	E 2	s3	e3	s4	e4
Case I	1	19	20	20	1	18	19	19	20	20	1	17	18	18	19	19	20	20
Case II	1	19	20	20	1	18	19	19	20	20	1	17	18	18	19	19	20	20
Case III	1	19	20	20	-	-	-	-	-	-	1	17	18	18	19	19	20	20
Case IV	1	17	18	20	-	-	-	-	-	-	1	17	18	18	19	19	20	20

Table 6.6: The worst coarsening options
(configurations that produce the maximum C_v in S_g)

To illustrate our results, we plot two figures for each of the test cases i.e. Figures 6.13a through 6.16b. In the first figure, we plot the average C_v in S_g together with the normalized rms error in oil recovery factor using the Kyte and Berry (KB) and the TW pseudo generation methods versus the number of coarse grid layers. This is shown using two examples of possible coarsening schemes. Specifically, we use the layer combinations that produce the maximum and the minimum values of C_v in S_g; i.e. the

predicted worst and best layer combinations for upscaling. In the second figure, we plot the rms error calculated using both of the pseudo methods (KB and TW) versus their respective C_v in S_g for both of the coarsening options. Results for the other three cases are summarized and tabulated in Table 6.7 below.

Cases	Kyte and Berry	TW
Case I	0.9145	0.9873
Case II	0.7392	0.9843
Case III	0.9897	0.9916
Case IV	0.4763	0.6297

Table 6.7: The R^2 of rms error vs. C_v in S_g for Case I through Case IV

Detailed discussions on each of the test case will be presented below.

6.3.2.1 Case I, $k_v/k_h = 0.0$

This case was selected to show more gas is flowing at the top of the model due to permeability distribution (Figure 6.11a) but no cross flow between the 20 fine grid layers. Figure 6.13a shows the C_v in S_g and the rms error versus the number of coarse grid layers for the best and worst grouping of layers in the coarse grid calculations. These results show that the performance of the pseudo functions does not necessarily improve as the number of the coarse grid layers is increased. The accuracy of both of the pseudo methods (KB and TW) in this 2D → 2D coarsening scheme will also depend on the configuration of the layering scheme adopted for the coarse grid models.

For this particular case, the performance of the 2-layer coarse grid model using the layering scheme with the minimum value of C_v in S_g is far better than the 7-layer coarse grid model with the maximum value of C_v in S_g (i.e. the worst choice of 7-layer model we can take based on this criterion). The performance trend versus the number of coarse grid layers for both of the pseudo methods is very similar.

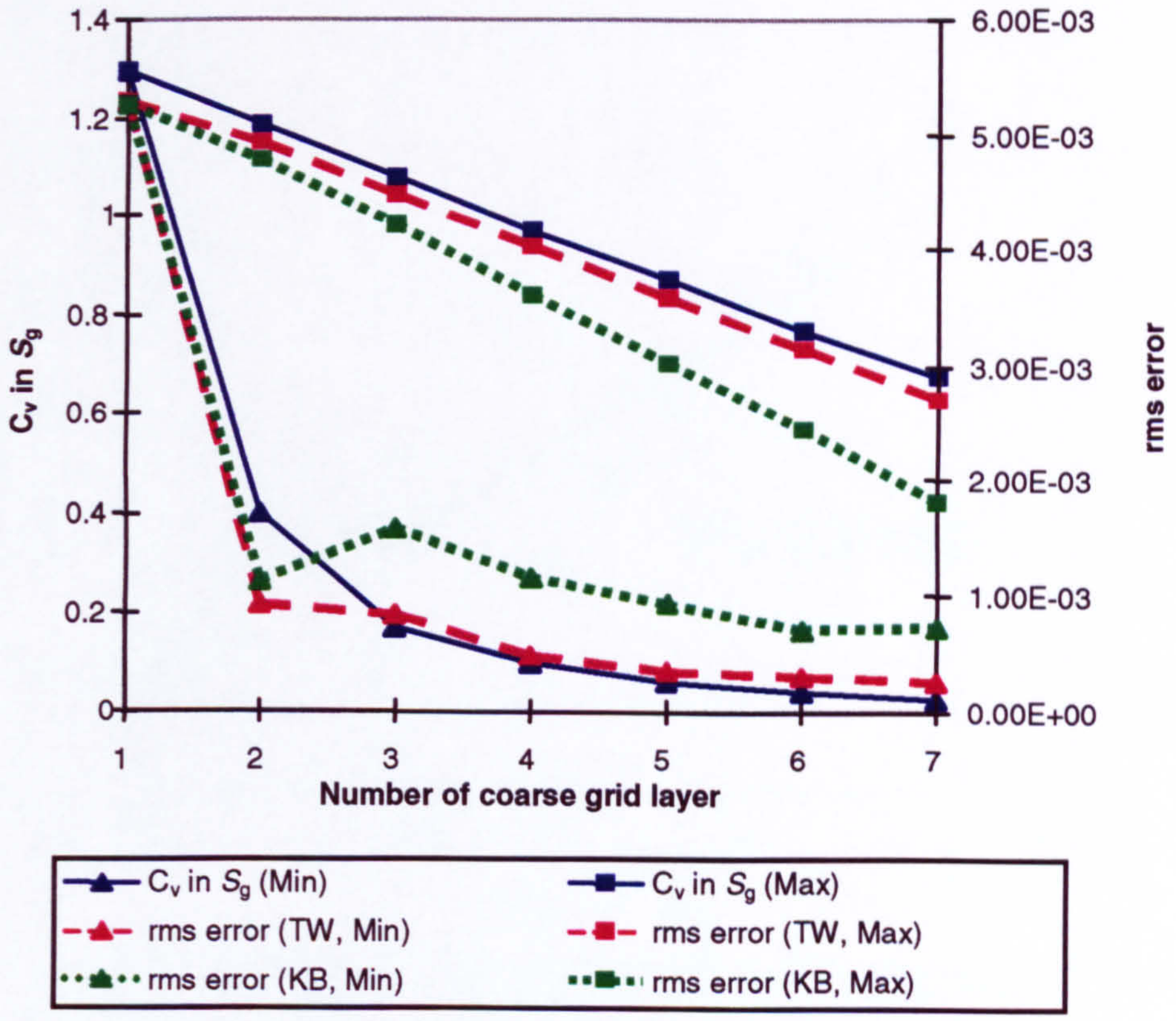

Figure 6.13a: C_v in S_g and rms error versus number of coarse grid layers (Case I, coarsening upwards with $k_v/k_h = 0.0$)

The results can be seen from another perspective as shown in Figure 6.13b where the rms error versus the C_v in S_g is plotted. This figure demonstrates that both of the pseudo methods produce errors that correlate directly with the calculated C_v in S_g. In this case, both of the pseudo methods produced an R^2 of more than 0.9; the TW method produces a slightly better R^2 (0.99) compared to the Kyte and Berry method

($R^2 = 0.91$). Therefore, we can conclude that this new dynamic grid coarsening scheme can be used in conjunction not only with the TW method but also with the Kyte and Berry method (with slightly less accuracy).

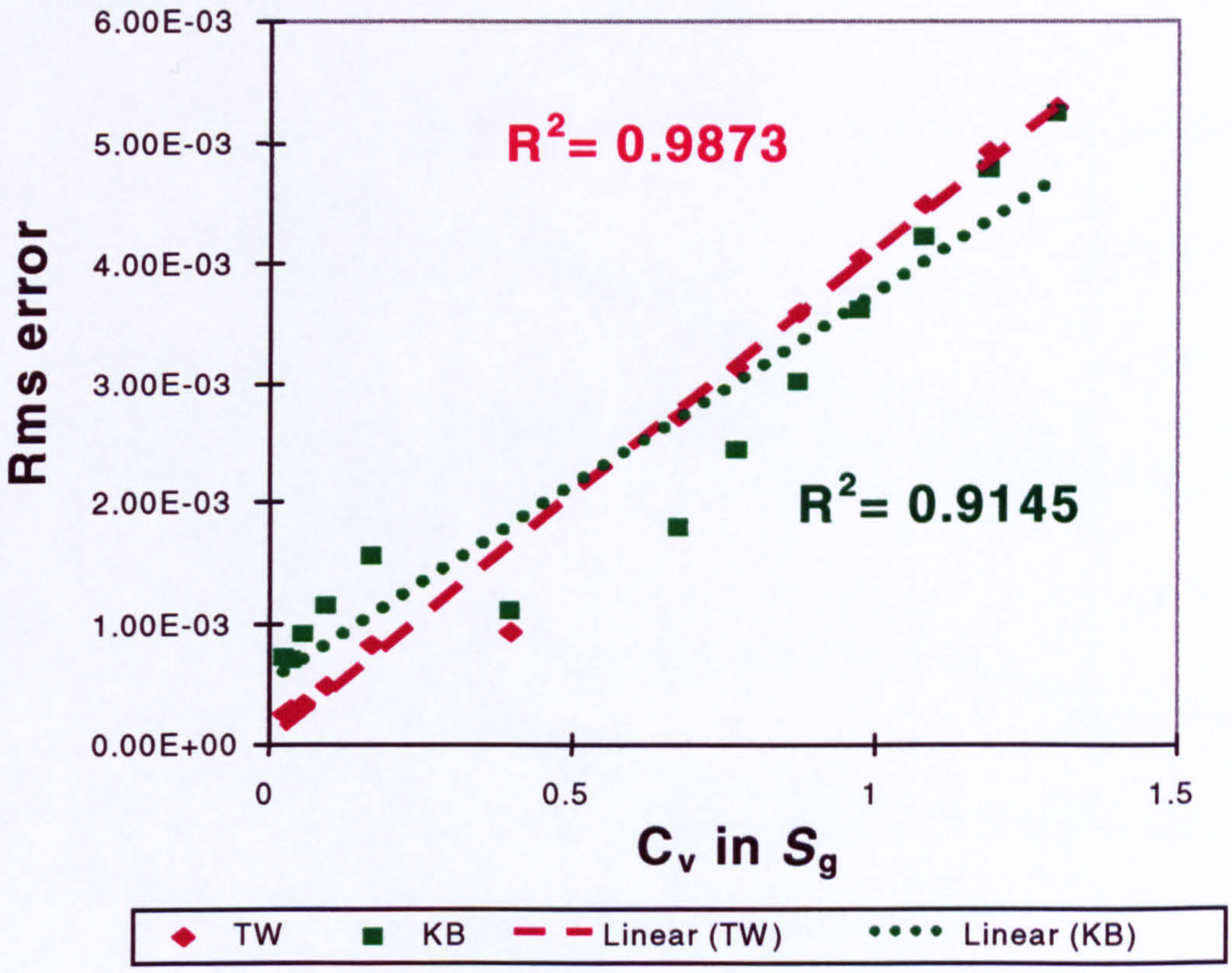

Figure 6.13b: Rms error versus C_v in S_g
(Case I, coarsening upwards with $k_v/k_h = 0.0$)

6.3.2.2 Case II, $k_v/k_h = 0.0$

This case shows more gas is flowing at the bottom of the model (Figure 6.11b) with no cross flow between the 20 fine grid layers. As above, the results indicate that the accuracy of the coarse grid model depends not only on the number of coarse grid layers but also on the configuration of the layering scheme. The actual values of the

rms error calculated using the Kyte and Berry method are again quite comparable to those calculated using the TW method. Table 6.7 shows that the Kyte and Berry method produced an R^2 of about 0.74 (an acceptable number) compared to the TW method of 0.98. The results from this case are therefore consistent with our conclusions for Case I. For a graphical illustration of this case, refer to Figures 6.14a and 6.14b.

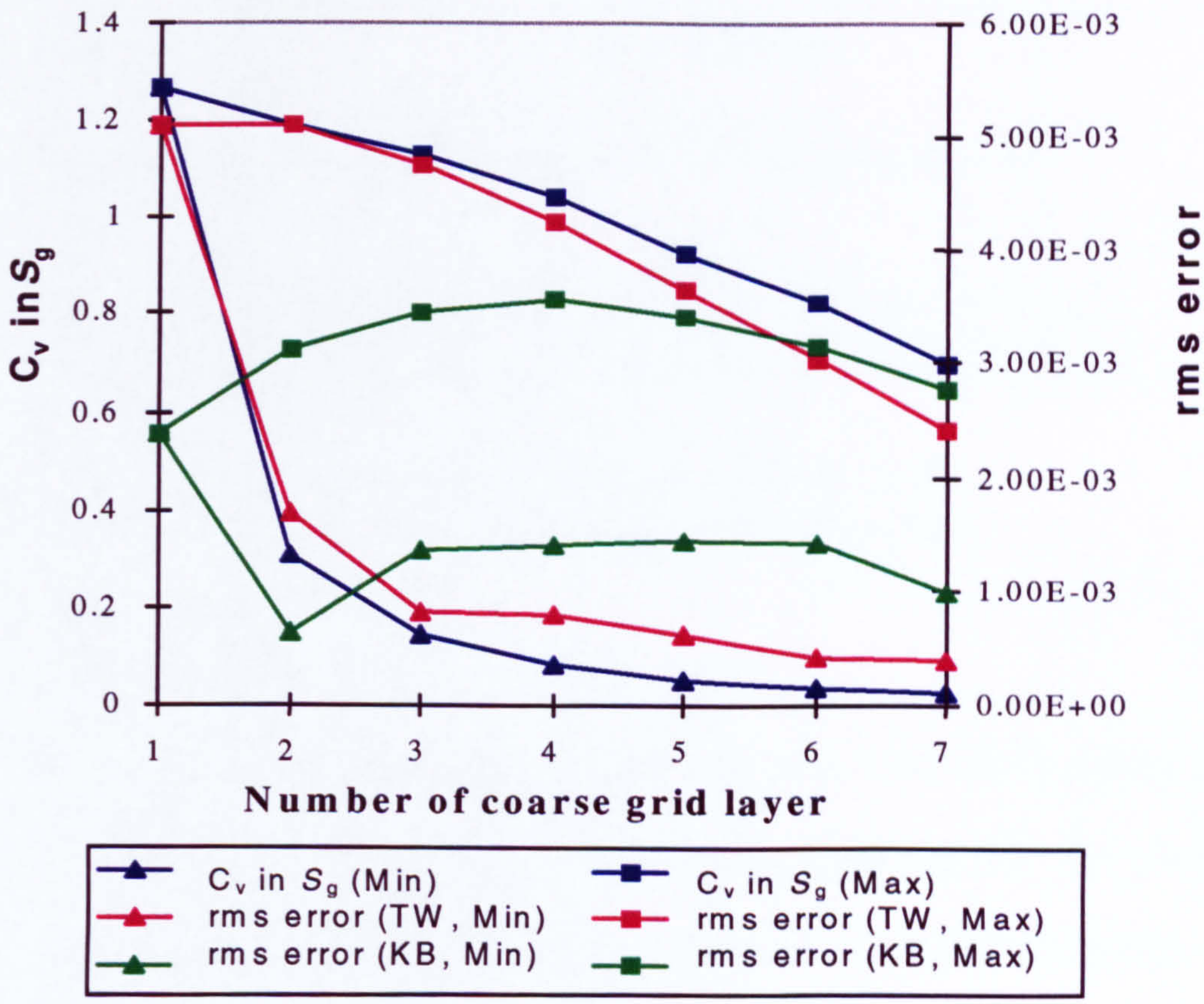

Figure 6.14a: C_v in S_g and rms error versus number of coarse grid layers (Case II, fining upwards with $k_v/k_h = 0.0$)

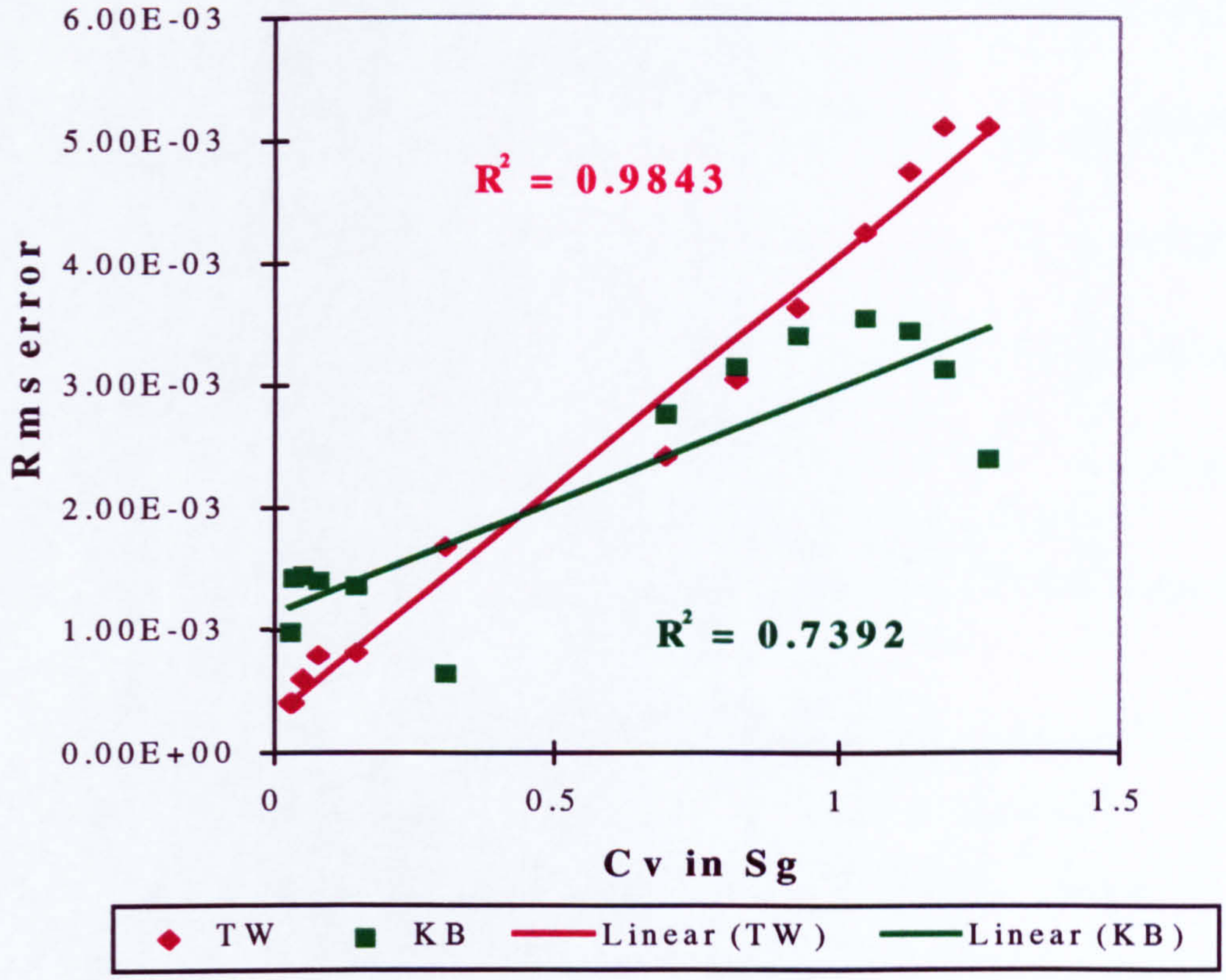

Figure 6.14b: Rms error versus C_v in S_g
(Case II, fining upwards with $k_v/k_h = 0.0$)

6.3.2.3 *Case III, $k_v/k_h = 1.0$*

This model is similar to Case I except that the k_v/k_h ratio is increased to unity. Therefore, gravity cross-flow will reinforce the tendency of the permeability distribution to segregate the injected gas from the reservoir fluid (oil). In this case, the performance of both of the pseudo methods follows a similar trend. The R^2 value of about 0.99 for both methods, as shown in Table 6.7, indicates again that C_v in S_g can provide excellent estimates of rms error for both methods. Figures 6.15a and 6.15b illustrate these findings graphically.

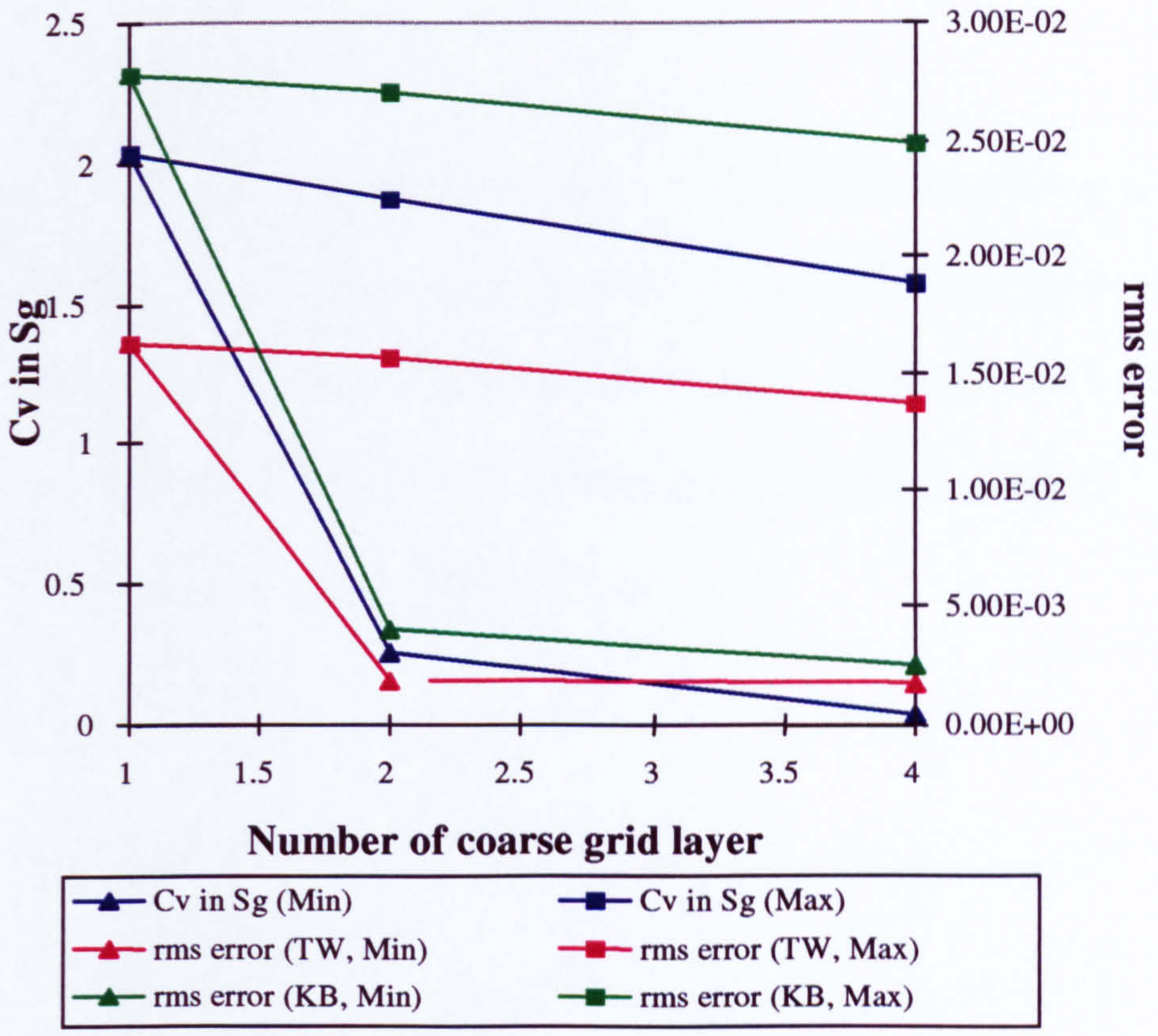

Figure 6.15a: C_v in S_g and rms error versus number of coarse grid layers (Case III, coarsening upwards with $k_v/k_h = 1.0$)

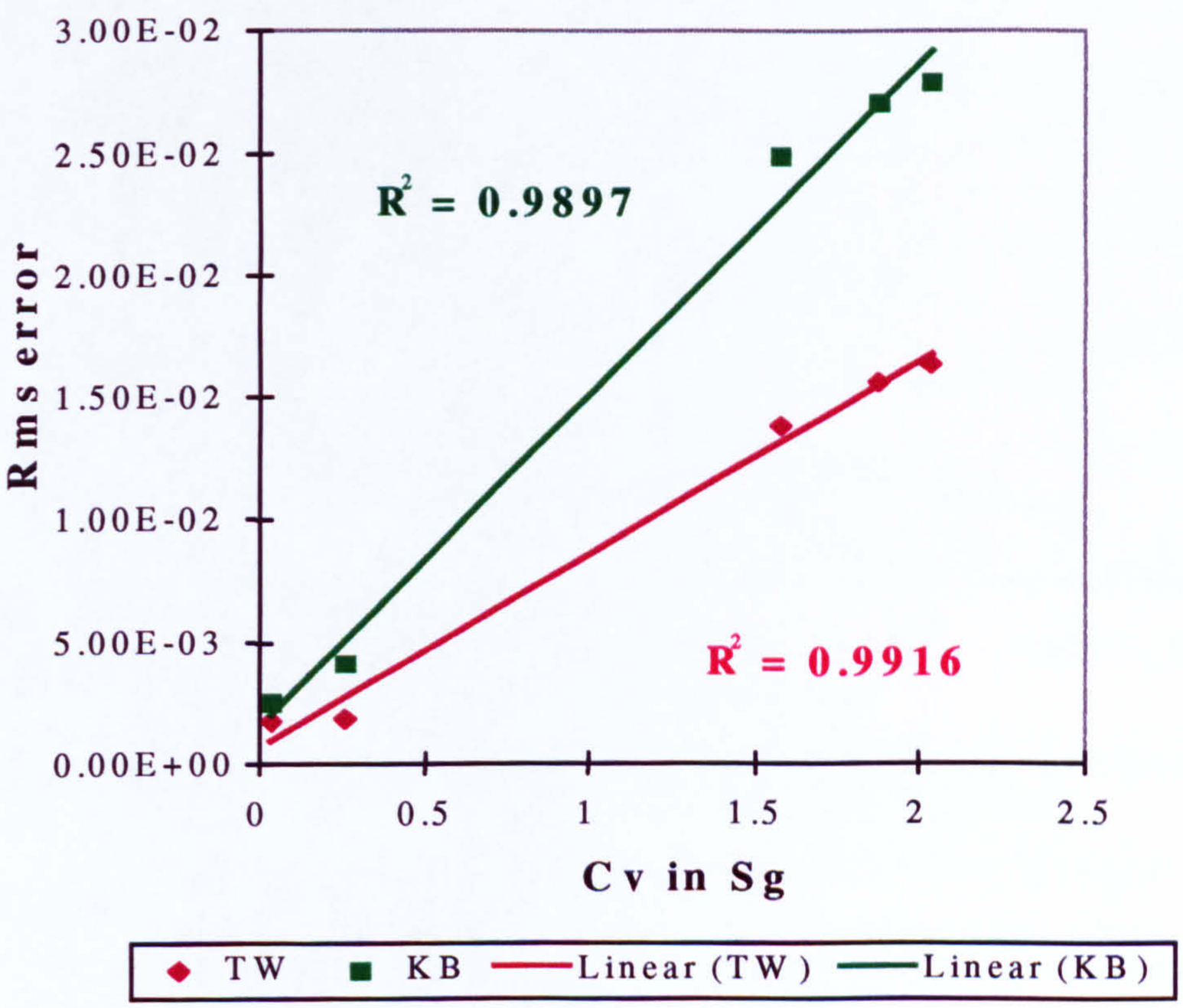

Figure 6.15b: Rms error versus C_v in S_g (Case III, coarsening upwards with $k_v/k_h = 1.0$)

6.3.2.4 Case IV, $k_v/k_h = 1.0$

This is a "difficult" case because the flow here is controlled by the opposing effects of the permeability distribution (decreasing upward) and gravity segregation due to the large difference in fluid densities. The R^2 values for both of the methods are relatively low; for the TW method, $R^2 = 0.63$ and for the Kyte and Berry method, $R^2 = 0.48$. Figures 6.16 a and 6.16 b illustrate these findings.

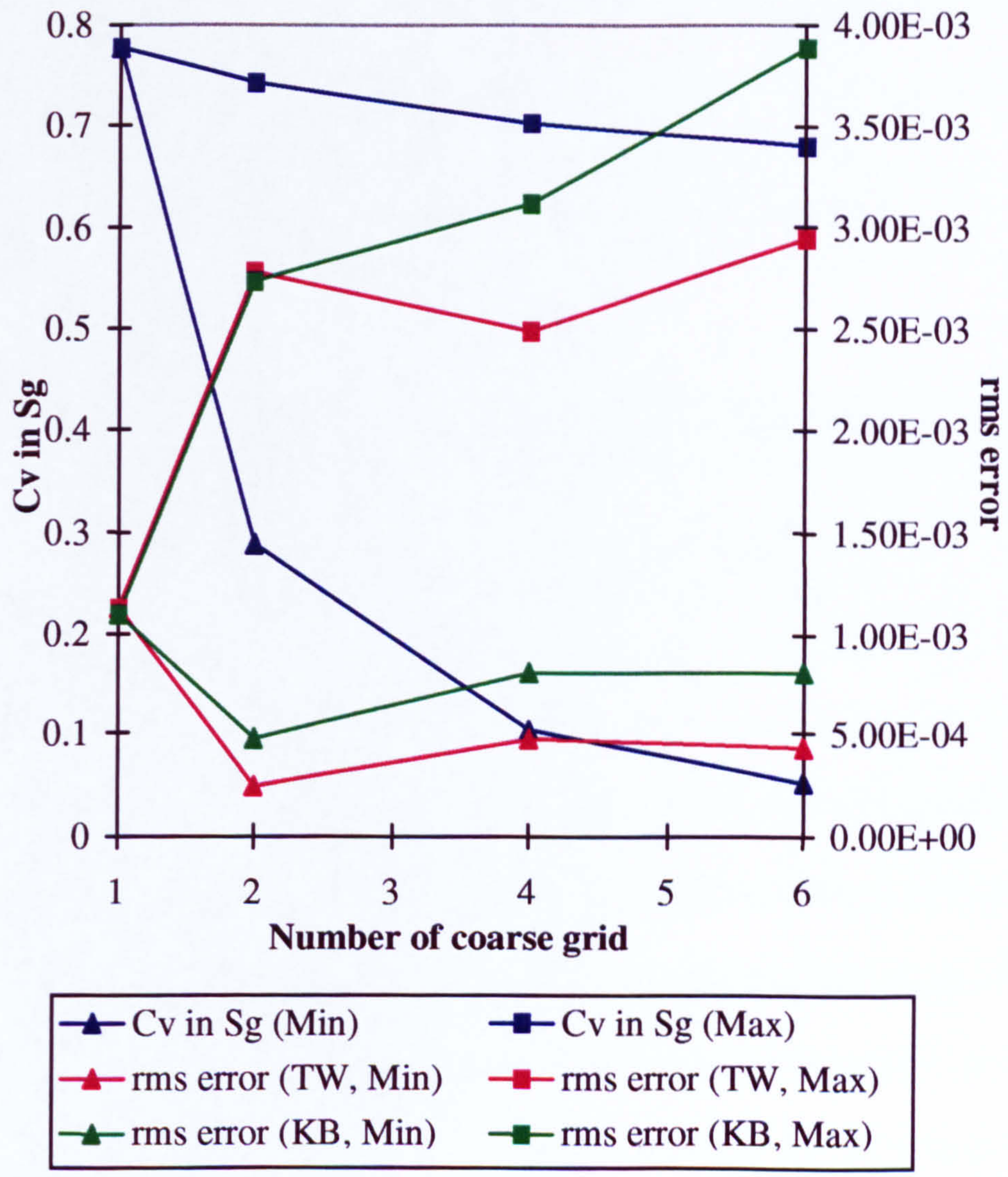

Figure 6.16a: C_v in S_g and rms error versus number of coarse grid layers (Case IV, fining upwards with $k_v/k_h = 1.0$)

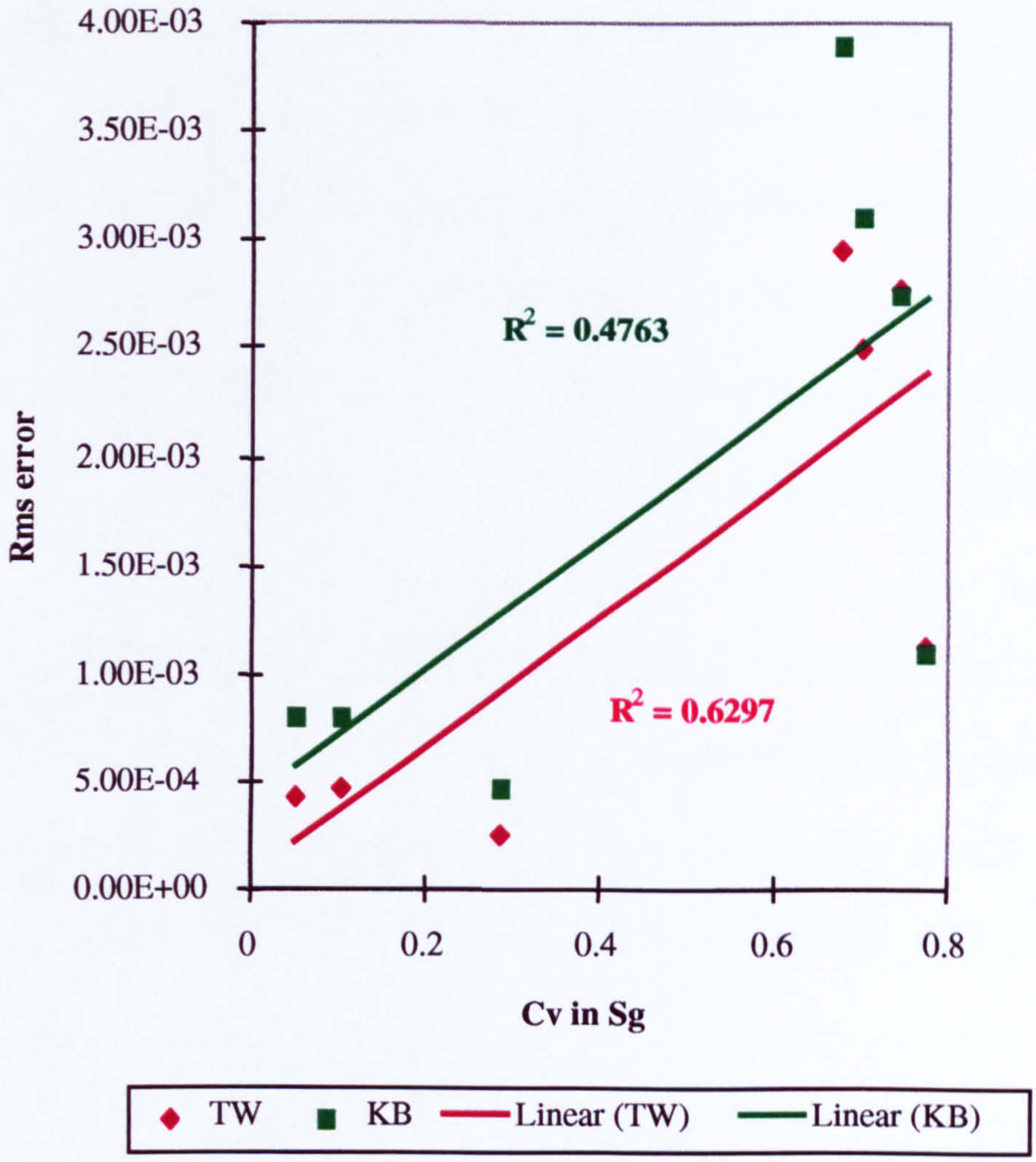

Figure 6.16b: Rms error versus C_v in S_g
(Case IV, fining upwards with $k_v/k_h = 1.0$)

However, if we compare the performance of Case IV to that of Case III above (in terms of the rms error), we see that the overall results are actually better for Case IV. Refer to Table 6.4 for further detail, where the rms error in Case IV is seen to be a factor of 3 to 6 times less than that for Case III (for the 2-layer coarse grid models). This occurs because the combined effect of the permeability distribution and the difference in fluid densities causes the front to be much more uniform in Case IV compared to Case III (see Figures 6.11c and 6.11d).

6.4 SUMMARY AND CONCLUSIONS

In this chapter, we studied the relationship between sub-grid effects and the accuracy of coarse scale simulation models for layered systems. The actual sub-grid measures considered represent higher moments of fine scale variables (C_v in S_g, C_v in vS, C_v in kS, σ^2_S, σ_{kS} and σ_{vS}) and were derived from a volume averaging of the fine grid saturation equation. The coarse scale simulation results, taken in total, demonstrate that the volume averaging procedure can be used to model the form of the coarse grid error.

Further, we showed that the coarse grid error could be minimized by designing the coarse grid models such that certain of these higher moments are minimized. The specific sub-grid measure that best correlated with the coarse grid error was shown to vary depending on whether rock curves or pseudo functions were used in the coarse grid model.

The use of pseudo functions together with the new grid coarsening scheme provides results of significantly better accuracy than does the use of rock curves alone for the cases considered. The effects of numerical dispersion in the coarse grid models were found to be relatively small, indicating that the effectiveness of the pseudo functions results from their ability to capture the effects of fine scale heterogeneity. It is not surprising that the pseudo functions provide accurate coarse grid results for the problems considered. This is because the pseudo functions were generated through the solution of a global fine grid problem and the global boundary conditions imposed on the coarse scale problem were identical to those for the fine scale problem. It would be of interest to assess the accuracy of the pseudo functions in other cases; e.g. for coarse

grid boundary conditions that differ from those used on the fine grid or in the case where the pseudo functions are computed from local (rather than global) fine scale simulations.

We also demonstrated the applicability of the new grid coarsening scheme in more general cases, where we coarsened 20 layer systems to models containing more than 2 layers. For this part of the study, both the TW and Kyte and Berry methods were considered. We showed that the accuracy of the coarse grid descriptions for these problems depended on both the number and configuration of the layers and that the coarse grid error continued to correlate with C_v in S_g (as in the 2-layer cases). The performance of the pseudo functions for these problems did not always improve as we increased the number of coarse grid layers. The results from this part of the study suggest that a user could optimally select the number and configuration of the coarse scale layers from a single fine grid solution. This means that the various coarse grid models need not all be simulated to determine the optimum coarse grid representation.

CHAPTER 7

CONCLUSIONS AND FUTURE DIRECTIONS

7.1 SUMMARY AND CONCLUSIONS

In this thesis, we investigate the use of pseudo functions in immiscible two-phase displacements of oil-gas systems, where the effects of large mobility differences and gravitational forces are normally encountered. For this specific reason, a new pseudo-isation scheme known as the Transmissibility Weighted (TW) method has been developed and tested against several well-known pseudo methods such as the Kyte and Berry, the Stone, the Hewett and Archer and the Vertical Equilibrium (VE) methods. Better performance relative to the other well-known pseudo methods was found especially in the gravity-dominated cases encountered in immiscible gas injection.

As we have shown in this thesis, each pseudo method has its advantages and disadvantages, and it is well known that using an inappropriate method can lead to inaccurate results. However, there is a lack of understanding as to why a certain method will succeed in some cases but fail in others. Focusing on this problem, we dedicated a specific chapter (Chapter 4) to discuss some of the similarities and limitations of the five pseudo methods that we mentioned above.

In this thesis, we also proposed a new optimal grid coarsening scheme based on the quantitative use of fine scale two-phase flow information. The basic approach is motivated by a new volume average analysis of the fine scale saturation equation including gravitational effects. It is shown that coarse grid simulation error correlates closely with specific sub-grid quantities involving higher moments of fine grid variables, which can be computed from the fine scale simulations. By forming a coarse grid that minimizes the appropriate sub-grid quantity, optimal coarse scale descriptions can be generated. The overall approach is shown to be applicable to coarse scale descriptions using either rock or pseudo relative permeability curves. The accuracy of the coarse grid calculations is, however, significantly better when pseudo functions are used.

In general, as mentioned in Chapter 1, this thesis had five primary objectives as follows:

1. To conduct a literature search of currently available pseudo techniques, which include the Vertical Equilibrium pseudo methods as well as the dynamic pseudo methods.

2. To validate currently available pseudo methods in gas-oil system where high gravity effects and unfavourable mobility ratios provide a very stringent test to the assumption made in each of the pseudo methods.

3. To develop a new method which will provide more accurate pseudo functions for gas-oil displacements.

4. To quantify the strengths and weaknesses of each of the pseudo methods and the reasons behind it success or failure.

5. To develop a new optimal grid coarsening scheme which will produce less error when pseudo functions or fine grid relative permeabilities are applied directly into the coarse grid models.

Below we address the main conclusions and findings from the work presented in this thesis.

1. There is no pseudo generation method that is perfect for all the conditions (i.e. produces zero error for all simulation problems). However, it is shown that the TW method gives more accurate results in applying pseudo functions where gravity effects are significant than the Kyte and Berry, Stone and VE methods.

2. The performance of the Hewett and Archer method is rather similar to the TW method in all of the test cases and the reason of this emerged in the course of this work.

3. The Stone method performs very badly in a dipping model compared to when the model is horizontal. In a horizontal model, a high value of gravity to viscous ratio

will have negligible impact to the Stone method although this method ignores the gravity terms altogether. Refer to conclusions nos. 6 and 7 below for further details.

4. When fluid flow is under the viscous-dominated regime, all the dynamic pseudo functions perform quite similarly with high accuracy. The VE method will definitely fail in this case.

5. If the fine grid accurately reproduces reservoir flows, which may be viscous dominated, gravity dominated or in a flow regime where all forces are significant, the TW will give accurate upscaled answers compared to the VE method. However, if the system is actually *at* the VE limit but the fine grid fails to resolve this, then the TW (or any other dynamic pseudo methods) will give the same (inaccurate) answer as the fine grid. In the VE limit, the VE pseudo method is shown to be very accurate and robust since it does not require any fine grid calculation.

6. For purely horizontal models and negligible capillary pressure, the exact weighting of the fluid potential difference in the averaging process is quite irrelevant since $\overline{\Delta\Phi_g}$ will always equal to $\overline{\Delta\Phi_o}$ and can be factored out in the fractional flow calculation. That is, all potential weighted methods are guaranteed to get the correct fractional flow in a horizontal case by summing the respective fluid flow rate only. Hence, for this case, the Stone method will lead to the same fractional flows as other pseudo method such as the TW and HA methods although the gravity terms are ignored in the calculations of the Stone method. Thus, as long as we know the

respective fluid flow rates from the fine grid runs, the fractional flow of the coarse grid models can be correctly reproduced.

For this case, the Kyte and Berry method may give a different fractional flow since the selection of k_{rj} as a weighting factor in averaging the fluid pressure (which is also a function of respective fluid saturation) will set the $\overline{\Delta\Phi_g}$ to be different from the $\overline{\Delta\Phi_o}$. A comparison between the TW and the Kyte and Berry methods shows that the difference between these two methods is due to the different weighting factors used in the pseudo equations. The relative permeability weighting used in the Kyte and Berry method is particularly inappropriate in cases where gravitational effects are significant.

7. For dipping models, the gravity term, $\Delta\rho g\overline{\Delta h}$, cannot be ignored in averaging the fluid potential differences i.e. $\Delta\Phi_g \neq \Delta\Phi_o$. Therefore, the selection of the weighting factor and other style of averaging these values can be seen as essentially an attempt to correct for the gravity term. As long as one particular method takes into account the gravity term ($\Delta\rho g\overline{\Delta h}$) in its calculation, the results will be a better than methods that ignore it. This is the reason why the Stone method failed in a dipping model.

8. It is difficult to establish which pseudo method reproduces the "correct" fine-grid fluid mobility and pressure distributions since the vertical fluctuation in fine-grid fluid potential difference is rather large especially at the coarse block nearest to the

injector. However, at this point, we will treat any method that reproduces the correct fractional flow and results in a $\overline{\Delta\Phi}$ that fall within certain "tolerable limit" as a good pseudo method. As such, we conclude that both HA and TW pseudo methods perform equally well in matching the fine grid fractional flow as well as the fluid mobility compared to the other well-known pseudo methods of the Kyte and Berry, the Stone or the VE.

9. In a 3D → 3D or 3D → 2D upscaling, we found out that as long as the required pseudos are calculated *independently* in each of the coarse-grid dimension it will guarantee the very accurate reproduction of the fine grid results in the coarse grid models. By adopting such directional pseudos, each of the dimensions in the coarse grid model will be treated like a separate 1D model and the same results as the 2D cross-sectional models can be expected.

10. We have also applied the results from Durlofsky of a new averaged saturation equation with gravity effect included. In this new equation, we make several interesting features:

    - We note that the fine scale functions f (fine –scale fractional flow) and η (fine-scale oil relative permeability times fractional flow) appear explicitly in the coarse scale equation. These functions are not modified for use in the coarse scale models; i.e. the f and η have the same functional forms on both the fine and coarse scales.

- The coarse scale equation is seen to contain three additional terms involving higher moments that account for the sub-grid effects. The moments that appear explicitly are $\overline{S'S'}$, $\overline{\mathbf{v}'S'}$ and $\overline{\mathbf{k}'S'}$, and these terms are always multiplied by derivatives of f or η. The moments appearing in the gravitational terms (the terms multiplied by $g\Delta\rho/\mu_o$) are $\overline{S'S'}$ and $\overline{\mathbf{k}'S'}$ only; $\overline{\mathbf{v}'S'}$ does not appear; whereas in the viscous term only $\overline{S'S'}$ and $\overline{\mathbf{v}'S'}$ appear.

11. We have demonstrated that the volume averaging procedure can be used to model the form of the coarse grid error. We showed that the coarse grid error could be minimized by designing the coarse grid models such that certain of these higher moments are minimized. The specific sub-grid measure that best correlated with the coarse grid error was shown to vary depending on whether rock curves or pseudo functions were used in the coarse grid model.

When rock curves were used in the coarse grid model, the fluctuating moments in the form of variance is recommended. However, when pseudo functions are applied in the coarse grid model, the moments should be in the form of the C_v expressions.

12. The use of pseudo functions together with the new optimal grid coarsening scheme provides results of significantly better accuracy than does the use of rock curves

alone for the cases considered. The effects of numerical dispersion in the specific coarse grid models were found to be relatively small, indicating that the effectiveness of the pseudo functions results from their ability to capture the effects of fine scale heterogeneity and not from correcting the numerical dispersion in the coarse grid models.

13. We also have demonstrated the applicability of the new optimal grid coarsening scheme in more general cases, where we coarsened the 20-layer systems to models containing more than 2 layers. Both the TW and Kyte and Berry pseudo methods were considered. We showed that the accuracy of the coarse grid descriptions for these problems depended on both the number and configuration of the layers and that the coarse grid error continued to correlate well with the sub-grid properties as in the 2-layer cases.

The performance of the pseudo functions for these problems did not always improve as we increased the number of coarse grid layers. The results from this part of the study suggest that a user could optimally select the number and configuration of the coarse scale layers from a single fine grid solution. This means that the various possible combinations of the coarse grid models need not all be simulated to determine the optimum coarse grid representation for a given case.

7.2 DIRECTIONS OF FUTURE RESEARCH

Several possible future directions could be pursued following the work in this thesis as follows:

1. To test and validate the TW pseudo equations and the new optimal coarsening approach with a wider spectrum of realistic geological models (e.g. cross-bedded, rippled etc).

2. To test and validate the TW method and the new optimal coarsening schemes at a range of different length scales (e.g. from lamina scale to core plug scale and/or from core plug scale to geological model scale).

3. To incorporate the effects of capillary pressure and compressibility in the TW pseudo equations.

4. To study the effects of different boundary conditions between the fine grid and the coarse grid models. In other words, applying the TW method and optimal grid coarsening schemes in coarse grid models without the need to run the fine grid model.

REFERENCES

Ahmadi, A. and Quintard, M., 1996, "Large-Scale Properties for Two-Phase Flow in Random Porous Media", J. Hydrology, 183, pp 66-99.

Alder, H.L., and Roessler, E.B., 1975, *Introduction to Probability and Statistics*, W.H. Freeman and Company, San Francisco.

Aziz, K, and Settari, A., 1990, *Petroleum Reservoir Simulation*, Elsevier Applied Science, London and New York.

Barker J.W. and Dupouy P., 1999, "An analysis of Dynamic Pseudo Relative Permeability Methods for Oil-Water Flow", *Petroleum Geoscience*, Vol. 5, 1999, pp. 385-394.

Barker, J.W. and Fayers, F.J., 1994, "Transport Coefficients for Compositional Simulation with Coarse Grids in Heterogeneous Media", SPE 22591, *SPE Advanced Technology Series*, Volume 2, No. 2, April 1994.

Barker, J.W. and Thibeau, S., 1996. " A Critical Review of the Use of Pseudo Relative Permeabilities for Upscaling", SPE 35491, presented at the European 3-D Modelling Conference, Stavanger, Norway, 16-17 April, 1996.

Bech, N., Jensen, O.K., and Nielsen, B., 1989, "Modeling of Gravity-Imbibition and Gravity-Drainage Processes : Analytic and Numerical Solutions", SPE 18428, presented at the SPE Symposium on reservoir Simulation, Houston, Feb. 6-8, 1989.

Beier, R.A., 1992, "Pseudorelative Permeabilities From Fractal Distributions", SPE 24371, presented at the SPE Rocky Mountain Regional Meeting, Casper, Wyoming, May 18-21, 1992.

Chang, Y.C. and Mohanty, K.K., 1994, "Stochastic Description of Multiphase Flow in Heterogeneous Porous Media", SPE 28443, presented at the 1994 Annual Technical Conference and Exhibition, New Orleans, Sept. 25-28 1994.

Christie, M.A., "Upscaling for Reservoir Simulation", JPT, 48, 1004-1010, Nov. 1996.

Christie, M. A., Mansfield M., King P.R., Barker J.W. and Culverwell I.D., 1995. "A Renormalisation-Based Upscaling Technique for WAG Floods in Heterogeneous Reservoir", SPE 29127, presented at the 13th Symposium on Reservoir Simulation, San Antonio, Texas, 12-15 February 1995.

Civan., F, and Evans, R.D., 1993, "Relative Permeability and Capillary Pressure Data From Non-Darcy Flow of Gas/Brine System in Laboratory Cores", SPE 26151, presented at the SPE GAs Technology Symposium, Calgary, Canada, 28-30 June 1993.

Coats K.H., Dempsey J.R., Henderson J.H., 1971. "The Use of Vertical Equilibrium in Two-Dimension Simulation of Three-Dimensional Reservoir Performance", SPEJ, March, 1971.

Coats K.H., Nielsen R.L., Terhune M.H., 1967. "Simulation of Three-Dimensional Two-phase Flow in Oil and Gas Reservoirs", SPEJ, December, 1967.

Coll, C., Muggeridge, A.H. and Jing, X.D., 1998, "The Impact of Flow Regime on the Upscaling of Heterogeneous Reservoirs", 6th European Conference on the Mathematics of Oil Recovery (ECMOR VI), 8-11 September 1998, Edinburgh, Scotland.

Corbett, P.W.M., Ringrose, P.S., Jensen, J.L. and Sorbie, K.S., 1992. "Laminated Clastic Reservoirs - The Interplay of Capillary Pressure and Sedimentary Architecture", SPE 24699, presented at the 67th Annual Technical Conference of the SPE, Washington DC, 4-7 October 1992.

Corey, A.T. and Rathjens, C.H., 1956, "Effect of Stratification on Relative Permeability", AIME Pet. Trans., 207, pp 358-360.

Dake, L.P. 1978, :*Fundamentals of Reservoir Engineering*, Elsevier, Amsterdam.

Darman, N.H., Sorbie, K.S. and Pickup, G.E.: "The Development of Pseudo Functions for Gravity-Dominated Immiscible Gas Displacements", SPE 51941, Proceedings of the 15th SPE Reservoir Simulation Symposium, Houston, TX, 14-17 February 1999.

Darman, N.H., Durlofsky, L.J., Sorbie, K.S. and Pickup, G.E.: "Upscaling Immiscible Gas Displacements: Quantitative Use of Fine Grid Flow Data in Grid Coarsening Schemes", SPE 59452, Proceedings of the 2000 SPE Asia Pacific Conference on Integrated Modeling for Asset Management, Yokohama, Japan, 25-26 April 2000.

Dietz, D.N., 1953: A Theoretical Approach to the Problem of Encroaching and By-Passing Edge Water. Akad. Van Wetenschappen, Amsterdam. Proc. V.56-B: 83.

Dupouy P., Barker, J.W., Volois, J.P. 1998. "Grouping Pseudo Relative Permeability Curves", In Situ - A Journal of Earth Resource Utilization, Volume 22, Number 1, 1998.

Durlofsky, L.J. 1998, "Coarse Scale Models of Two Phase Flow in Heterogeneous Reservoirs: Volume Averaged Equations and Their Relationships to Existing Upscaling Techniques", Computational Geosciences, 2, pp 73-92.

Durlofsky, L.J. 1997. "Use of Higher Moments for the Description of Upscaled, Process Independent Relative Permeabilities", SPE 37989, presented at the 1997 Reservoir Simulation Symposium, Dallas, 8-11 June 1997.

Durlofsky, L.J., Behren, R.A., Jones, R.C. and Bernath, A., 1996, "Scale Up of Heterogeneous Three Dimensional Reservoir Descriptions", SPEJ, 1, pp 313-236, Sept. 1996.

Durlofsky, L.J., Jones, R.C., and Milliken, W.J., " A New Method for the Scale Up of the Displacement Processes in Heterogeneous Reservoirs", 1994, Proceedings of the 4th European Conference on the Mathematics of Oil Recovery, Roros, Norway, June 1994.

Fayers, F.J., and Newley, T.M.J., 1987, "Detailed Validation of an Empirical Model for Viscous Fingering With Gravity Effect", SPE 15993, presented at the 9th SPE Symposium on Reservoir Simulation, San Antonio, February 1-4, 1987.

Guzman, R.E., Giordano, D., Fayers, J., Godi, A., Aziz, K., 1994. "The Use of Dynamic Pseudo Functions in Reservoir Simulation", presented at the fifth International Forum on Reservoir Simulation Muscat, Oman, December 10-14, 1994.

Hewett, T.A. and Archer, R.A. 1997. "Scale-Averaged Effective Flow Properties for Coarse-Grid Reservoir Simulation", SPE 37988, presented at the 1997 SPE Reservoir Simulation Symposium, Dallas, Texas, 8-11 June 1997.

Hewett, T.A. and Behrens, R.A., 1993, "Consideration Affecting the Scaling of Displacements in Heterogeneous Permeability Distributions", SPE Formation Evaluation, *, pp 258-266.

Hornarpour, M.M., Cullick, A.S., Saad, N., and Humphreys, N.V., " Effect of Rock Heterogeneity on Relative Permeability : Implications for Scaleup", SPE 29311, presented at the SPE Asia Pacific Oil and Gas Conference, Kuala Lumpur, Journal of Petroleum Technology, 47(11), pp 980-987.

Huang, Y., Ringrose, P.S., and Sorbie, K.S., 1995, "Capillary Trapping Mechanism in Water-Wet Laminated Rocks", *SPE Reservoir Engineering, November 1995*, pp 287-292.

Huang, Y., Ringrose, P.S., and Sorbie, K.S., 1995, "The Effects of Heterogeneity and Wettability on Oil Recovery from Laminated Sedimentary Structures", SPE 30781, presented at the SPE Annual Conference, Dallas, 22-25 Oct., 1995.

Jacks, H.H., Smith, O.J.E., and Mattax, C.C., 1973, "The Modelling of a Three-dimensional Reservoir With a Two-dimensional Reservoir Simulator - the Use of Dynamic Pseudo Functions", *SPEJ*, August 1973, pp 175-183.

Jones, A., Doyle, J., Jacobsen, T., and Kjonsvik, D., 1993, "Which Sub-Seismic Heterogeneity Influence Waterflood Performance ? A Case Study of a Low Net-to-Gross Fluvial Reservoir", presented at the 7th European IOR Symposium, Moscow.

Killough J.E., Foster H.P. Jr., 1979, "Reservoir Simulation of the Empire ABO Field – The Use of Pseudos in a Multilayered Systems", SPEJ, October 1979, pp 279-291.

Kortekaas, T.F.M., 1985, "Water-Oil Displacement Characteristics in Crossbedded reservoir Zones", *SPEJ*, December 1985, pp 917-926.

Kossack, C.A., Aasen, J.O. and Opdal, S.T., 1990, "Scaling up Heterogeneity with Pseudofunctions", *SPE Formation Evaluation*, September 1990. pp 226-232.

Kumar, A.T.A and Jerauld, G.R., 1996, "Impacts of Scale-up on Fluid Flow from Plug to Gridblock Scale in Reservoir Rock", SPE/DOE 35452, presented at the 1996 Symposium on Improved Oil Recovery, Tulsa, April 21-24 1996.

Kyte, J.R. and Berry, D.W., 1975. "New Pseudo Functions to Control Numerical Dispersion", SPEJ (August 1975), 269-275.

Lake, L.W., 1989: *Enhanced Oil Recovery, Prentice Hall,* Englewood Cliffs, N.J.

Lake, L.W., Kasap, E. and Shook, M., 1990, "Pseudofunctions - The Key to Practical Use of Reservoir Description", *North Sea Oil and Gas Reservoir - II,* Norw. Inst. of Technology Graham and Trotman, London.

Land, C.S., 1988: *Reservoir Rock Properties*, Texas Tech University, Lubbock.

Lantz, R.B., 1969, "Rigorous Calculation of Miscible Displacement Using Immiscible Reservoir Simulators", SPE 2594, presented at the SPE 44th Annual Fall Meeting, Denver, Sept. 28 - Oct. 1, 1969.

Lantz, R.B., 1970, "Quantitative Evaluation of Numerical Diffusion (Truncation Error)", SPE 2811, presented at the 2nd SPE Symposium on Numerical Simulation of Reservoir Performance, Dallas, Feb. 5-6, 1970.

Lemouzy P., Kruel Romeu L., Morelan I., 1993, "A New Scaling-up Method to Compute Relative Permeability and Capillary Pressure for Simulation of Heterogeneous Reservoirs", SPE 26660, presented at the 69th Ann. Tech. Conf. Exhib., Houston, Oct. 3-6, 1993.

Mattax, C.C., and Dalton, R.L., 1990: *Reservoir Simulation. SPE Monograph 13.*

Pickup, G.E., Ringrose, P.S., Corbett, P.W.M., Jensen, J.L. and Sorbie, K.S., 1995, "Geology, Geometry and Effective Flow", Petroleum Geoscience, 1(1), pp 37-42.

Pickup, G.E., Ringrose, P.S., Jensen, J.L. and Sorbie, K.S., 1994, "Permeability Tensors for Sedimentary Structures", *Mathematical Geology*, 26(2), pp. 227-250.

Pickup, G.E. and Stephen, K.D., 1998. "Steady-State Scale-up Method", presented at the 6th European Conference on the Mathematics of Oil Recovery, Peebles, Scotland, 8-11 September 1998.

Pickup, G. E. and Sorbie, K. S., 1994. "The scaleup of Two-Phase Flow in Porous Media Using Phase Permeability Tensors", SPE 28586, presented at the SPE Annual Technical Conference & Exhibition, New Orleans, U.S.A., 25-28 September 1994.

Pseudo (1995): *Reference manual, Schlumberger-Geoquest.*

Quintard, M. and Whitaker, S., 1990, "Tow-Phase Flow in Heterogeneous Porous Media I: The Influence of Large Spatial and Temporal Gradient", Transport in Porous Media, 5, pp 341-379.

Ringrose, P.S., Jensen, J.L., and Sorbie, K.S. 1996, "The Use of Geology in the Interpretation of Core-Scale Relative Permeability Data", SPE Formation Evaluation, Sept. 1996.

Ringrose, P.S., Sorbie, K.S., Corbett, P.W.M., and Jensen, J.L. "Immiscible Flow Behaviour in Laminated and Cross-Bedded Sandstones", J. Petroleum Science and Engineering, 9(2), pp 103-124.

Saad, N., Cullick A.S., and Honarpour, M.M., 1995, "Effective Relative Permeability in Scale-Up and Simulation", SPE 29592, presented at the SPE Rocky Mountain Regional Low-Permeability Reservoir Symposium, Denver, 20-22 March, 1995.

Smith E.H., "The Influence of Small-Scale Heterogeneity on Average relative Permeability", Reservoir Characterisation II, Academic Press. pp 52-76.

Sorbie, K.S., Sheb, M., Hosseini, A. and Wat, R.M.S., 1990, "Scaled Miscible Floods in Layered Beadpacks Investigating Viscous Cross flow, the Effect of Gravity and the Dynamics of Viscous Slug Breakdown", SPE 20520, 65th Annual Conference and Exhibition of the Society of Petroleum Engineers, New Orleans. Sept. 23-26. pp 465-500.

Spivak A., 1974, "Gravity Segregation in Two-Phase Displacement Process", *SPEJ*, December 1974, pp. 619-632.

Stern, D. and Dawson, A.G., 1999, "A Technique for Generating Reservoir Simulation Grids to Preserve Geologic Heterogeneity", SPE 51942, Proceedings of the 15th SPE Reservoir Simulation Symposium, Houston, TX, 14-17 February 1999.

Stone, H.L. 1991. "Rigorous Black Oil Pseudo Functions", SPE 21207, presented at the 11th SPE Symposium on Reservoir Simulation, Anaheim, California, February 17-20, 1991.

Suzuki, K., 1999, "Scale-up of Relative Permeabilities of Isolated Gridblocks Accounting for Boundary Effects", PhD Dissertation, Stanford University.

Suzuki, K.and Hewett, T.A., 1999, "Scale-up of Relative Permeabilities of Isolated Gridblocks Accounting for Boundary Effects", SPE 51938, Proceedings of the 15th SPE Reservoir Simulation Symposium, Houston, TX, 14-17 February 1999.

Taggart, I.J., Soedarmo, E., and Paterson, L., 1995, "Limitations in the Use of Pseudo functions for Up-scaling Reservoir simulation Models", SPE 29126, presented at the 13th SPE Symposium on Reservoir Simulation, San Antonio, 12-15 Feb., 1995.

Tan, T.B., 1995, " Estimating Two and Three Dimensional Pseudo-Relative Permeability With Non-Linear Regression", SPE 29129, presented at the 13th SPE Symposium on Reservoir Simulation, San Antonio, 12-15 Feb., 1995.

Thomas, G.W., 1983, "An Extension of Pseudo function Concepts", SPE 12274, presented at the Reservoir Simulation Symposium, San Francisco, Nov. 15-18 1983.

Wallstrom, T.C., Hou, S., Christie, M.A., Durlofsky, L.J. and Sharp, D.H.: "Application of a New Two-Phase Upscaling Technique to Realistic Reservoir Cross Sections", SPE 51939, Proceedings of the 15th SPE Reservoir Simulation Symposium, Houston, TX, 14-17 February 1999.

Woods, E.G., and Khurana, A.K., 1977, "Pseudo functions for Water Coning in a Three-Dimensional Reservoir Simulator", SPEJ, August 1977, pp 251-262.

Yokohama, Y., and Lake, L.W., 1981, "The Effect of Capillary Pressure on Immiscible Displacement in Stratified Porous Media", SPE 10109, presented at the 56th Annual Fall Meeting of the SPE, San Antonio, Oct. 5-7 1981.

Zhang H.R. and Sorbie K.S. 1995. "The Upscaling of Miscible and Immiscible Displacement Processes in Porous Media", SPE 29931, presented at the International Meeting on Petroleum Engineering, Beijing, PR China, 14-17 November, 1995.

Zhou, D., Fayers, F.J. and Orr Jr., F.M. 1993. "Scaling of Multiphase Flow in Simple Heterogeneous Porous Media", SPE/DOE 27833, presented at the ASME Winter Meeting, New Orleans, November 28 - December 3, 1993.

APPENDIX I

SPE 51941

The Development of Pseudo Functions for Gravity-Dominated Immiscible Gas Displacements

N.H.Darman, SPE, Petronas Research, K.S. Sorbie, SPE, and G.E. Pickup, SPE, Heriot-Watt University

This paper was prepared for presentation at the 1999 SPE Reservoir Simulation Symposium held in Houston, Texas, 14—17 February 1999.

This paper was selected for presentation by an SPE Program Committee following review of information contained in an abstract submitted by the author(s). Contents of the paper, as presented, have not been reviewed by the Society of Petroleum Engineers and are subject to correction by the author(s). The material, as presented, does not necessarily reflect any position of the Society of Petroleum Engineers, its officers, or members. Papers presented at SPE meetings are subject to publication review by Editorial Committees of the Society of Petroleum Engineers. Electronic reproduction, distribution, or storage of any part of this paper for commercial purposes without the written consent of the Society of Petroleum Engineers is prohibited. Permission to reproduce in print is restricted to an abstract of not more than 300 words; illustrations may not be copied. The abstract must contain conspicuous acknowledgment of where and by whom the paper was presented. Write Librarian, SPE, P.O. Box 833836, Richardson, TX 75083-3836, U.S.A., fax 01-972-952-9435.

Abstract

In this paper, we investigate the use of pseudo functions in immiscible two phase displacements in oil-gas systems, where the effects of large mobility differences and gravitational forces are normally encountered. For this specific reason, a new pseudo-isation scheme known as the Transmissibility-Potential-Weighted (TPW) method has been developed and tested against several well-known pseudo methods such as the Kyte and Berry[1], the Stone[2] and the Vertical Equilibrium[3] (VE) methods. Better performance relative to the other well-known pseudo methods was found especially in the gravity-dominated cases encountered in immiscible gas injection. This is shown for a wide range of cases. In addition, a detailed discussion on the limits and applicability of the VE method is also included.

Based on results from the TPW method, a new grid coarsening scheme for pseudo-isation has been developed and validated. This technique takes into account not only the static properties (i.e. permeability, porosity etc.) of the fine grid models, but also the dynamic properties of the fluid flow. The idea of this coarsening scheme is to identify regions (possibly layers) of the fine grid where there is low *variability* of gas saturation, and to take such regions as the corresponding coarse grid blocks. The measure of variability used is the coefficient of variation of the gas saturation. The resulting coarsening scheme may be non-uniform, but fulfils the purposes of using pseudo functions (i.e. to control numerical dispersion, to capture the effects of small scale heterogeneity, to reduce the number of grid blocks etc.) with less error and without any adjustment to the pseudo equations themselves.

Introduction

In modern reservoir characterisation, a detailed geological reservoir description may produce a model with millions of grid blocks each with individual geological and petrophysical properties. These properties, such as permeability and relative permeability, may vary significantly within the reservoir and their effective values depend on the length scale being considered. For example, variability in permeability can be observed in reservoir facies down to the smallest scale of lamination (mm)[4-6].

Fluid flow simulation using such full-field geological models directly is very costly and often exceeds the computational capabilities which are practically available. Such fine scale models need to be scaled up before they can be used easily. This process may be a simple averaging/ collapsing of the grid or might involve the application of a full dynamic upscaling method. When successfully applied, the pseudo functions produced in a dynamic upscaling method will incorporate the interaction between small scale multi-phase fluid flow and heterogeneity, as well as correcting for the numerical dispersion in the coarse grid model. Several techniques for generating pseudo functions have been reported in the literature[1-3,7-14]. However, most of these existing approaches have been tested using water-oil systems where gravity effects may not be very important. The use and validity of these pseudo-isation methods is investigated in this paper for oil-gas immiscible displacements. Such cases should provide a more stringent test of the various upscaling algorithms since they involve both significant gravitational effects as well as the effects of gas channelling / fingering due to unfavourable mobility ratios.

In general, the objectives of this paper are three-fold. Firstly, we propose a new dynamic pseudo-isation algorithm known as the Transmissibility-Potential-Weighted (TPW) method that has been developed specifically to handle cases where there is a significant effect of gravity in the simulation models. This new method is tested and validated against several well-known pseudo approaches such as the Kyte and Berry[1], the Stone[2] and the Vertical Equilibrium (VE)[3] methods. Better performance relative to the other well-known pseudo methods was observed for the TPW method, especially in the high gravity cases. Secondly, we investigate the conditions under which the new TPW method performs

better than the existing approaches, especially the Kyte and Berry method, in immiscible gas injection processes. In this context, a detailed analysis of grid block sensitivity to the accuracy of the pseudo-isation techniques is presented. This in turn explains the limit and applicability of the VE method. Thirdly, we propose a new (2D → 2D) coarsening scheme that reduces the amount of error in duplicating the performance of the fine grid models.

Development and Validation of the TPW Method

Development of the TPW method. The new TPW method follows exactly the same approach as the Kyte and Berry method except in the averaging the fluid potential difference at the coarse grid level. Using the notation in Figure 1, Darcy's law was applied in order to obtain the pseudo relative permeability for each of the fluid phases in the coarse grid blocks as follows (an over bar, $\overline{X}$, will be used to denote quantities evaluated at the coarse grid scale):

$$\overline{kr_p} = \frac{-\overline{\mu_p}.\overline{q_p}.\Delta X}{\Delta Y.\Delta Z.\overline{kx}\overline{\Delta\Phi_p}} \qquad (1)$$

where $\overline{\mu_p}$, $\overline{q_p}$ and $\overline{\Delta\Phi_p}$ are the average phase viscosity, flow rate and fluid potential difference of phase p, respectively; ΔX, ΔY and ΔZ are the coarse grid block dimensions in the x-, y- and z-directions. The flow rates of individual fluid phases in the fine and the coarse grid blocks were matched by summing the respective phase flow rates over the fine grid blocks located at the coarse grid block boundary as shown below :

$$\overline{q_p} = \sum_{j=1}^{5} [q_{pj}]_{i=5} \qquad (2)$$

and the averaged potential difference, $\overline{\Delta\Phi_p}$ in the TPW method is defined as:

$$\overline{\Delta\Phi_p} = \frac{\sum_{j=1}^{5} [T_{xj}.\Phi_{pj}.\Delta\Phi_{p_j}]_{i=3}}{\sum_{j=1}^{5} [T_{xj}.\Phi_{pj}]_{i=3}} \qquad (3)$$

where $\Delta\Phi_{pj}$ is given by the following equation

$$\Delta\Phi_{pj} = [\Phi_{pj}]_{i=8} - [\Phi_{pj}]_{i=3}. \qquad (4)$$

To be meaningful, the derived pseudo relative permeability must be related to the average saturation in the coarse grid block. In this case, the saturation was averaged using pore volume weighting over the fine grid blocks to give the following value in a coarse grid block:

$$\overline{S_p} = \frac{\sum_{j=1}^{5}\sum_{i=1}^{5} S_{pij}.PV_{ij}}{\sum_{j=1}^{5}\sum_{i=1}^{5} PV_{ij}} \qquad (5)$$

The rationale for the TPW method is that we do not want to average the fluid potential differences in the coarse grid blocks by first calculating the average fluid potentials in each of the coarse grid blocks and then taking the difference between them. Rather, we *calculate a weighted average of the fluid potential gradients* between the coarse blocks directly from the fine grid gradients. In this context, when these pressure gradients are the same (or similar), this method will give results which are the same as (or close to) the Kyte and Berry approach. It is only when there are significantly different potential *gradients* in the various grid layers that differences are seen. Furthermore, it appears that the selection of the product of transmissibility and the fluid potential as the weighting factor in averaging the fluid potential gradients is more appropriate especially in the high gravity dominated environments.

Numerical Testing of the TPW Method. The new TPW method was validated against the three most widely used pseudo generation methods: viz. the Kyte and Berry[1], the Stone[2] and the vertical equilibrium (VE)[3] methods. Cross sectional models of 100 x 1 x 5 were used to evaluate these upscaling methods. These fine grid models were scaled up to a 1D model with a grid dimension of 20 x 1x 1, which meant that every coarse grid block contained 25 fine grid blocks. The initial properties of the fine grid blocks are as follows:

Porosity,	$\phi = 0.2$;
Grid block sizes	DX = DY = DZ = 25 ft. (7.63 m)
Viscosities,	$\mu_o = 10$ cp ; $\mu_g = 0.1$ cp
Densities,	Oil, $\rho_o = 43.68$ lb/ft^3 (700 Kg/m^3);
	Gas $\rho_g = 0.06243$ lb/ft^3 (1.0 Kg/m^3)

The fluids were assumed to be incompressible and immiscible. The rock relative permeabilities were power law curves, given by the following equations from Guzman et al[9]:

$$K_{ro} = ((1-S_g - S_{org} - S_{wc}) / (1 - S_{wc} - S_{org}))^{2.7}$$

$$K_{rg} = ((S_g - S_{gc}) / (1 - S_{gc} - S_{wc}))^{5.0}$$

where $S_{wc} = 0.15$, $S_{gc} = 0.05$ and $S_{org} = 0.1$. In all cases, capillary pressure was ignored, although we may have to derive the "rock" curves from a capillary equilibrium upscaling calculation in some cases[15]. Gas was injected from an injector located at the left of the model and dead oil was produced from a well on the right of the model. Both wells were completed vertically throughout the model and the injection rate was set to give a frontal velocity of 0.3 m/d.

To test and evaluate the four methods discussed above (VE, Kyte and Berry, Stone and TPW), seven cases were developed as shown in Table 1. Cases 1 and 2 were designed to evaluate the four methods in models with free cross flow between layers; Cases 3 and 4 examined models where the cross flow between layers was restricted by barriers; Cases 5, 6 and 7 were constructed to test the performance of the upscaling methods in a dipping reservoir with low gravity (high viscous forces) and high gravity (low viscous forces) cases, respectively.

The conventional gravity to viscous ratio (N_{gv}) was calculated using the equation given by Zhou et al[16] as follows:

$$N_{gv} = \frac{\Delta\rho g L k_{av}}{H q \mu_o} \qquad (6)$$

where $\Delta\rho$ is the difference in the fluid densities, g is the gravitational constant, L is the reservoir length, k_{av} is the average vertical permeability, H is the reservoir thickness, q is the total Darcy flow velocity and μ_o is the oil viscosity.

Discussion of the Results. The results of all the test cases are summarised in the Table 2, where the normalised rms error in total oil recovery is used as our quality index. The normalised rms errors were calculated from the difference in oil recovery (using normalised curves) between the coarse and the fine-scale models, over a range of pore volumes injected. The numbers in brackets in Table 2 show the normalised rms error of each method relative to the TPW method. Taking a 10% cut-off as our differentiating criterion, the numbers in bold in Table 2 show the relative weakness of each method compared to the TPW method; i.e. this criterion is that < 0.9 suggests that the method performs better than the TPW method and > 1.1 indicates that the method is poorer. In general, the results show that the Kyte and Berry method produces larger errors compared to the Stone method in non-dipping, gas-oil systems. On the other hand, the Stone method is found to be very poor in dipping systems, as expected since gravity was neglected in deriving these equations (Guzman et. al, 1994)[9]. In all the cases investigated, the VE pseudo approach is the least acceptable (even in Case 7, where the effect of gravity is high). The reasons behind this apparent weakness of the VE method are further investigated and are presented in the following section.

The TPW method shows promising results both in dipping and in non-dipping systems. In all scenarios, the TPW method performs equally well or far better than the Kyte and Berry, the Stone or the VE methods in handling immiscible gas-oil systems. It is also evident that the TPW method gives far better results in Case 7 where the gravity effect is dominant compared with the other pseudo methods. Further analysis of the conditions under which this new method performs better than the Kyte and Berry method is presented below.

Further Analysis of the Scaleup Methods

Comparison of the TPW and Kyte and Berry Methods. In order to investigate the relative strengths of the TPW and the Kyte and Berry methods, we extended our analysis to include an additional fourteen cases which covered a much wider spectrum of mobility ratio, density difference, k_v/k_h ratio and N_{gv}. The description of the models for the new cases (Case A through Case N) are presented in Table 3. For each of the cases, the quality index (the normalised rms error) and the gravity to viscous ratio (N_{gv}) were calculated.

Homogenous Models. Grouping all of the homogenous models together (Case 6, 7, A, B, C, D, E and F), the percentage difference[a] between these two methods was plotted against the calculated N_{gv}[b] on a log-log scale. A clear correlation between these quantities was evident with a coefficient of determination (R^2) of more than 0.84, as shown in Figure 2. Thus, it was concluded that the strength of the TPW over the Kyte and Berry method was in the high gravity scenarios.

All Models. Now, extending the above finding using all the 21 models (Cases 1 - 7 and Cases A - N), the same percentage difference[c] between these two methods vs. N_{gv} was plotted in Figure 3. The same trend was observed in this figure with an R^2 of ~0.69 thus confirming our previous finding using the homogenous models.

Analysis of Differences Between the TPW and the Kyte and Berry Methods. There are two main differences between the TPW and the Kyte and Berry methods. First, as seen in Equation 3, the TPW method uses the product of two parameters as its weighting factor in calculating the averaged fluid potential difference at the coarse grid level. The parameters used are the transmissibility and the fluid potential. On the other hand, the Kyte and Berry method uses the product of absolute permeability, relative permeability and grid block thickness as its weighting factors. All of the weighting parameters for both of the pseudo methods are evaluated at the centre grid blocks. The second difference between these two methods is that the TPW method averages the fluid potential difference directly between two coarse grid blocks whereas the Kyte and Berry method first averages the fluid potential in each individual coarse grid block then takes the difference between them.

Evaluation of the Averaging Method. The question that must be answered now is: which of these differences contribute to the improved performance of the TPW method? Two runs were made to evaluate the relative effects of these differences, denoted STEP 1 and STEP 2. Run STEP 1 was performed to evaluate the two differences mentioned above i.e. different weighting factors and different averaging

[a] Percentage differences were calculated using the TPW method as a base case. A positive number means that TPW method produces less error compared to the Kyte and Berry method, whereas a negative number implies the opposite.

[b] All Ngv values of 0.0 (due to kv/kh of zero) were ignored.

[c] Only two cases produced small negative numbers (Case D and Case E). Both of the points were ignored because they cannot be plotted on a log-log graph.

techniques used by each of the methods. Case 7 was used as a comparison case since, in this case, the difference in the quality indicator (the normalised rms error) between the two methods is among the greatest. Case STEP 1 uses a method that is basically the same as the Kyte and Berry method except that the run used the TPW style of averaging the fluid potential difference (the weighting parameters were kept the same i.e. the product of absolute permeability times relative permeability times grid block thickness). Thus, the difference between STEP 1 and the TPW method will reflect the importance of the weighting factor used and the difference between STEP 1 and the Kyte and Berry method will reflect the importance of the averaging method for calculating the fluid potential difference used by each of the pseudo techniques.

The results in Figure 4 show that the curves for the Kyte and Berry method and STEP 1 are barely distinguishable. This implies that the techniques for averaging the fluid potential difference between the two pseudo methods produce the same results (at least for this particular case). On the other hand, the difference in the result between STEP 1 and the TPW method is very large which implies that most of the difference between the Kyte and Berry method and the TPW method is caused by the different weighting factors used by each of the methods. Thus, we conclude that the weighting factor used in the TPW method is the main cause of the improvement of the TPW method over the Kyte and Berry method.

Evaluation of the Weighting Parameters. The previous result leads immediately to the question: which of these weighting factors is good and which one is inappropriate? Run STEP 2 was performed to evaluate which of the weighting parameters used in the Kyte and Berry equations made the method less accurate compared with the TPW method. Again, Case 7 was used as a reference case for the same reasons as above. STEP 2 used a method that is basically the same as the Kyte and Berry method except that the run eliminates the use of relative permeability as a weighting parameter (only permeability times layer thickness is used).

The results as shown in Figure 5 clearly demonstrate that the relative permeability is inappropriate as a weighting factor, especially when the flow is gravity dominated (as in Case 7). After eliminating it as a weighting factor, the performance of the Kyte and Berry method tracks very closely to the TPW method and shows a considerably improved performance.

Grid Block Sensitivity of the VE Method. It is reasonable to expect the VE method to fail in low gravity cases, such as Case 6. However, when the VE method failed in Case 7 (high N_{gv}) we decided that further investigation was required. From the mathematics of the VE method, it is known that, for the homogenous models of Cases 6 and 7, the resulting pseudo functions produced by the VE method *do not depend on the number of fine grid blocks*. They depend only on the coarse grid blocks or the overall model dimensions. Figure 6 shows the plot of recovery factor versus the pore volume injected for the 5, 25, 50 and 200 layer models using Case 7 as the base case (high N_{gv}). The recovery profiles of the models are converging towards the coarse grid VE results with increasing numbers of layers in the fine grid block models. We conclude that the fine grid model dimension of 25 feet that we used in our previous test cases did not resolve the segregation of fluid sufficiently accurately for the VE method to be applied. This is the reason why we surprisingly see that the VE method "fails" (in the sense that it does not reproduce the fine 5 layer grid model) in Case 7 even though the N_{gv} number is relatively high. Clearly, for Case 6 (low N_{gv}), the VE method will not work regardless of the number of layers used in the fine grid models.

Grid Block Sensitivity of the TPW Method. In contrast to the VE method discussed above, the equations of all the dynamic pseudo function methods, such as the TPW method, are designed *primarily to capture the fine grid performance from which they were derived.* Figures 7 and 8 show the results for the 5 and 50 layer models using the TPW method in gravity dominated and viscous dominated flows respectively. As we can see from these two figures, the results for the coarse grids using TPW method are dependent on their respective fine grid simulation results only.

In summary, as long as the fine grid is accurately reproducing the physical system, which may be viscous dominated, gravity dominated or in a flow regime where all forces are significant, the TPW will give accurate upscaled answers. However, if the system is actually *at* the VE limit but the fine grid cannot resolve this, then the TPW will give the same (inaccurate) answer as the fine grid. In contrast, the Kyte and Berry method does not accurately reproduce the results on the coarse grid when gravitational forces become significant.

Improved Dynamic Grid Coarsening Scheme for Scaleup in High Gravity Cases

The objective of this part of our study is to suggest a grid coarsening scheme which uses more than the static properties of the fine grid models, such as permeability distribution, net-to-gross ratio etc. Such a coarsening scheme should use the *dynamic* properties of the fine grid model such as the flood pattern, pressure and saturation distribution. It is hoped that this approach will result in more accurate predictions of important quantities such as total oil recovery and gas-oil ratio when pseudo functions are applied.

The first step in achieving this objective was to identify which dynamic parameters should be used in characterising the coarsening scheme. We take as the quality indicator of a particular coarsening scheme, the normalised rms error on recovery factor (RF) profile; the lower this quantity the better the model. We therefore investigated several quantities which might correlate with this quality indicator, including: (i) the average coefficient of variation[d] (C_v) in the pressure distribution; (ii) the average C_v in the fluid potential difference, (iii) the average C_v in the total flow rate, (iv) the average C_v in the gas flow rate; and (v) the gravity to viscous

[d] The average coefficient of variation is a pore volume average of the Cv in each of the coarse grid blocks, for all the calculated time steps. (Cv is equal to standard deviation divided by mean).

ratio, N_{gv}. All of these quantities failed to give a satisfactory coefficient of determination, R^2, as shown in Figures 9a-9e (R^2 - in the range of 0.0257 to 0.4233).

However, the quality indicator correlates very well with the averaged coefficient of variation in the gas saturation (i.e. C_v in S_g), as shown in Figure 10a for homogenous models (R^2 = 0.926) and in Figure 10b for all of the models (R^2 = 0.7697). Thus, we may conclude that a model with a lower coefficient of variation in gas saturation will produce less error in duplicating the fine grid performance and that this will provide a good basis for the coarsening scheme.

We then apply this idea to our 2D → 2D coarsening scheme where we wish to separate the layers with high gas saturation from those with low saturations based on the statistics of averaged C_v in S_g. Pore volume was used as a weighting factor in combining the C_v in S_g for all of the coarse grid layers.

Grid Coarsening Methods. We adopt the same test models as above except that the number of fine grid layers was increased to 20 (100 x 1 x 20). All of the fine grid models were scaled up to a 2D model with a grid dimension of 20 x 1 x 2. To test and evaluate these ideas, five test models using three different permeability scenarios were run as shown in Figure 11 viz. CASES I - V. To simplify the problem, the 20-layer fine grid models were coarsened only to 2-layer models. All the resulting pseudo relative permeabilities both in the x- and the z-directions for each of the coarse grid blocks were kept and used. Since the number of layers in our fine grid model is twenty, there are only 19 possible coarsening schemes to be considered in our 2D → 2D scenario and one coarsening scheme in 2D → 1D scenario. The possible coarsening schemes are listed in Table 4.

In order to reduce the number of runs needed for all the five test models (CASES I-V), only coarsening options 5, 7, 9, 10, 11, 13, 15, 17 and 20 were considered. Before each of these options was run, the values of C_v in S_g were calculated based on the gas saturation distribution of the fine grid models. Each of the coarsening options was then run and the results were compared with the fine grid performance. The results for each of the test models are discussed below.

Discussion of the Results. For each of the five cases (CASES I-V), three figures are presented. The first shows the averaged C_v in S_g together with the averaged normalised rms error in total oil recovery (the quality index) for each of the coarsening options. In the second and third figures, the averaged C_v in S_g (for each of the coarsening options) is plotted against the averaged normalised rms error in oil recovery and cumulative gas produced respectively. Each case is discussed below.

Case I , k_v/k_h = ***0.0.*** This case was designed to show gas over-ride with no cross flow between the 20 fine grid layers. Figure 12a suggests that the best coarsening scheme for this particular case should be around the middle of the model i.e. layer 1 of the coarse grid layer should be taken from fine grid layer 1 through 8. By adopting this coarsening scheme, the quality index is reduced from 0.0054 for a 2D → 1D coarsening scheme to less than 0.001, a significant improvement.

The results in Figures 12b and 12c confirm the view that we can reduce the error in calculating pseudo functions if we can segregate the coarse grid layers according to the minimum C_v in S_g. These figures show the results in terms of the total oil recovery and the cumulative gas produced vs. the quality indicator, respectively. The correlations (R^2 ~0.78, in each case) are reasonably good.

Case II, k_v/k_h = ***0.0.*** This case was chosen to have gas under-running with no cross flow between the 20 fine grid layers. As above, Figure 13a suggests that the best coarsening scheme for this case should also be around the middle of the model; layer 1 of the coarse grid layer is from fine grid layer 1 through 8. It is evident that a significant improvement can be achieved by adopting this coarsening scheme. Figures 13b and 13c, show the results in terms of total oil recovery and cumulative gas produced vs. quality indicator, respectively. The R^2 values in these figures (> 0.96) further support the idea of splitting the coarse grid layers according to the minimum value of C_v in S_g.

Case III, k_v/k_h = ***1.0.*** This test model is exactly the same as Case I discussed above except that the k_v/k_h ratio is increased to unity and hence gravity cross flow will reinforce the tendency of the permeability distribution to segregate the injected gas and the reservoir fluid (oil). The results in Figure 14a indicate that the best coarsening scheme for this case is shifted from the middle of the model (as seen in Case I) to the top of the model, i.e. that layer 1 of the coarse grid model should be from fine grid layer 1 through 5 only. Again, the R^2 values (>0.96) in Figures 14b and 14c support the main thesis of the coarsening scheme.

Case IV, k_v/k_h = ***1.0.*** This test model is the same as Case II except that the k_v/k_h ratio is increased to unity. This is a difficult case since the fluid flow in this model is strongly controlled by the opposing effects of the permeability distribution (decreasing upward) and the gravity force due to large differences in fluid densities. The rms error of this test model increases when the coarsening scheme goes down the model from layer 1 to approximately layer 15; it then decreases to a very small value for the rest of the fine grid layers as shown in Figure 15a. For this case, the 2D → 1D coarsening scheme is essentially the best option for such a scheme. R^2 values for this case (• 0.6) are reasonable but are not quite as good as for the previous cases as shown in Figures 15b and 15c.

Case V, Homogenous model. In this case, the permeability distribution is set to be isotropic and uniform with a value of 500 md. As shown in Figure 16a, the splitting scheme of the coarse grid layers should take place slightly below the middle of the model (layer 1 of the coarse grid layer should be from fine grid layer 1 through 11). By adopting this layer grouping, the normalised rms error is reduced from 0.0046 for a 2D → 1D coarsening scheme to ~ 0.0018. Again, the resulting R^2 values (0.82 - 0.84) show an good correlation of total oil recovery and cumulative gas

produced vs. quality indicator as shown in Figures 16b and 16c.

Summary and Conclusion

In this work, the main findings on the use of pseudo functions in reservoir flow situations where gravitational effects are significant are as follows:

1. It is shown that the TPW method gives more accurate results in applying pseudo functions where gravity effects are significant than the Kyte and Berry, Stone and VE methods.

2. A comparison between the TPW and the Kyte and Berry methods shows that the difference between these two methods is due to the different weighting factors used in the pseudo equations. The relative permeability weighting used in the Kyte and Berry method is particularly inappropriate in cases where gravitational effects are significant.

3. If the fine grid accurately reproduces the reservoir flows, which may be viscous dominated, gravity dominated or in a flow regime where all forces are significant, the TPW will give accurate upscaled answers. However, if the system is actually *at* the VE limit but the fine grid fails to resolve this, then the TPW will give the same (inaccurate) answer as the fine grid.

4. The error in applying the TPW equation in a (2D → 2D) grid coarsening scheme can be reduced if we separate the regions (layers) within which the variability in gas saturation is as low as possible (based on the average coefficient of variation in gas saturation, C_v of S_g). The resulting coarsening scheme may be non uniform but will fulfil the purpose of using pseudo functions with less error and without any adjustment to the pseudo equations.

Acknowledgements

The authors would like thank members of the Imperial College - BP - Heriot-Watt University informal discussion group on Upscaling for many helpful and stimulating discussions, particularly Peter King (BP) and Ann Muggeridge (IC).

References

1. Kyte, J.R. and Berry, D.W., 1975. "New Pseudo Functions to Control Numerical Dispersion", SPEJ (August 1975), 269-275.
2. Stone, H.L. 1991. "Rigorous Black Oil Pseudo Functions", SPE 21207, presented at the 11th SPE Symposium on Reservoir Simulation, Anaheim, California, February 17-20, 1991.
3. Coats K.H., Dempsey J.R., Henderson J.H., 1971. "The Use of Vertical Equilibrium in Two-Dimension Simulation of Three-Dimensional Reservoir Performance", SPEJ, March, 1971.
4. Corbett, P.W.M., Ringrose, P.S., Jensen, J.L. and Sorbie, K.S., 1992. "Laminated Clastic Reservoirs - The Interplay of Capillary Pressure and Sedimentary Architecture", SPE 24699, presented at the 67th Annual Technical Conference of the SPE, Washington DC, 4-7 October 1992.
5. Ringrose, P.S., Sorbie, K.S., Corbett, P.W.M., and Jensen, J.L. 1993, "Immiscible Flow Behaviour in Laminated and Cross-Bedded Sandstones", J. Petroleum Science and Engineering, 9(2), pp 103-124.
6. Huang, Y., Ringrose, P.S., and Sorbie, K.S., 1995, "The Effects of Heterogeneity and Wettability on Oil Recovery from Laminated Sedimentary Structures", SPE 30781, presented at the SPE Annual Conference, Dallas, 22-25 Oct., 1995.
7. Coats K.H., Nielsen R.L., Terhune M.H., 1967. "Simulation of Three-Dimensional Two-phase Flow in Oil and Gas Reservoirs", SPEJ, December, 1967.
8. Durlofsky, L.J., Jones, R.C., and Milliken, W.J., " A New Method for the Scale Up of the Displacement Processes in Heterogeneous Reservoirs", 1994, Proceedings of the 4th European Conference on the Mathematics of Oil Recovery, Roros, Norway, June 1994.
9. Guzman, R.E., Giordano, D., Fayers, J., Godi, A., Aziz, K., 1994. "The Use of Dynamic Pseudo Functions in Reservoir Simulation", presented at the fifth International Forum on Reservoir Simulation Muscat, Oman, December 10-14, 1994.
10. Zhang H.R. and Sorbie K.S. 1995. "The Upscaling of Miscible and Immiscible Displacement Processes in Porous Media", SPE 29931, presented at the International Meeting on Petroleum Engineering, Beijing, PR China, 14-17 November, 1995.
11. Christie, M. A., Mansfield M., King P.R., Barker J.W. and Culverwell I.D., 1995. "A Renormalisation-Based Upscaling Technique for WAG Floods in Heterogeneous Reservoir", SPE 29127, presented at the 13th Symposium on Reservoir Simulation, San Antonio, Texas, 12-15 February 1995.
12. Pickup, G. E. and Sorbie, K. S., 1996. "The scaleup of Two-Phase Flow in Porous Media Using Phase Permeability Tensors", SPEJ, 1(4), 369-381.
13. Durlofsky L.J. 1997. "Use of Higher Moments for the Description of Upscaled, Process Independent Relative Permeabilities", SPE 37989, presented at the 1997 Reservoir Simulation Symposium, Dallas, 8-11 June 1997.
14. Hewett, T.A. and Archer, R.A. 1997. "Scale-Averaged Effective Flow Properties for Coarse-Grid Reservoir Simulation", SPE 37988, presented at the 1997 SPE Reservoir Simulation Symposium, Dallas, Texas, 8-11 June 1997.
15. Pickup, G.E. and Stephen, K.D., 1998. "Steady-State Scale-up Method", presented at the 6th European Conference on the Mathematics of Oil Recovery, Peebles, Scotland, 8 -11 September 1998.
16. Zhou, D., Fayers, F.J. and Orr Jr., F.M. 1993. "Scaling of Multiphase Flow in Simple Heterogeneous Porous Media", SPE/DOE 27833, presented at the ASME Winter Meeting, New Orleans, November 28 - December 3, 1993.

Cases	Perm layer 1-2	Perm layer 3-5	k_v/k_h	Dip	Mobil-ity ratio	Density ratio	N_{gv}
Case1	500	10	1	0	100	700	0.0958
Case2	10	500	1	0	100	700	0.0649
Case3	500	10	0	0	100	700	0.0
Case4	10	500	0	0	100	700	0.0
Case5	500	500	1	15°	100	700	-
Case6	500	500	1	0	100	1.001	0.0003
Case7	500	500	1	0	10	7000	19.754

Table 1: Case descriptions for Case 1 to Case 7

Cases	Kyte & Berry	Stone	TPW	VE
Case 1	**0.01419 (1.1007)**	0.01283 (0.9953)	0.01289 (1.0000)	**0.03384 (2.6252)**
Case 2	**0.00321 (1.2029)**	0.00252 (0.9428)	0.00267 (1.0000)	**0.03883 (14.5422)**
Case 3	0.01019 (0.9812)	0.01069 (1.0294)	0.01039 (1.0000)	**0.04822 (4.6414)**
Case 4	0.004378 (0.9415)	0.00464 (0.9980)	0.00465 (1.0000)	**0.10884 (23.4061)**
Case 5	0.0114 (1.0309)	**0.02902 (2.6195)**	0.01108 (1.0000)	**0.1754 (15.8285)**
Case 6	0.00315 (1.0001)	0.00313 (0.9935)	0.00315 (1.0000)	**0.07036 (22.3371)**
Case 7	**0.04241 (7.9864)**	**0.00955 (1.7982)**	0.00531 (1.0000)	**0.02479 (4.6678)**

Table 2: The rms errors in oil recovery factor for each of the cases; Cases 1 to 7; results normalised to the TPW case with worst cases >1.1

Cases	Perm layer 1	Perm layer 2	Perm layer 3	Perm layer 4	Perm layer 5	k_v/k_h	Mobility ratio	Density ratio	N_{gv}
Case A	500	500	500	500	500	1.0	100	700	1.9729
Case B	500	500	500	500	500	1.0	100	70000	197.56
Case C	500	500	500	500	500	1.0	10	700	19.7286
Case D	500	500	500	500	500	1.0	100	1.01	0.01
Case E	500	500	500	500	500	1.0	100	1.05	0.1
Case F	500	500	500	500	500	1.0	100	2.06	1.0
Case G	500	10	500	10	500	1.0	100	700	0.0958
Case H	500	250	500	250	500	1.0	100	700	1.4092
Case I	500	500	500	10	10	0.1	100	700	0.0096
Case J	10	10	10	500	500	0.1	100	700	0.0065
Case K	500	10	500	10	500	0.1	100	700	0.0096
Case L	500	10	500	10	500	0.0	100	700	0.0
Case M	500	250	500	250	500	0.1	100	700	0.1409
Case N	500	250	500	250	500	0.0	100	700	0.0

Table 3: Case descriptions for Case A to Case N

Option	Coarse grid layer 1 is from fine grid :	Coarse grid layer 2 is from fine grid :
1	layer 1 through 1	layer 2 through 20
2	layer 1 through 2	layer 3 through 20
3	layer 1 through 3	layer 4 through 20
4	layer 1 through 4	layer 5 through 20
5	layer 1 through 5	layer 6 through 20
6	layer 1 through 6	layer 7 through 20
7	layer 1 through 7	layer 8 through 20
8	layer 1 through 8	layer 9 through 20
9	layer 1 through 9	layer 10 through 20
10	layer 1 through 10	layer 11 through 20
11	layer 1 through 11	layer 12 through 20
12	layer 1 through 12	layer 13 through 20
13	layer 1 through 13	layer 14 through 20
14	layer 1 through 14	layer 15 through 20
15	layer 1 through 15	layer 16 through 20
16	layer 1 through 16	layer 17 through 20
17	layer 1 through 17	layer 18 through 20
18	layer 1 through 18	layer 19 through 20
19	layer 1 through 19	layer 20 through 20
20	Fine grid layer 1 through 20	

Table 4: Possible options in 20 layer → 2 layer coarsening.

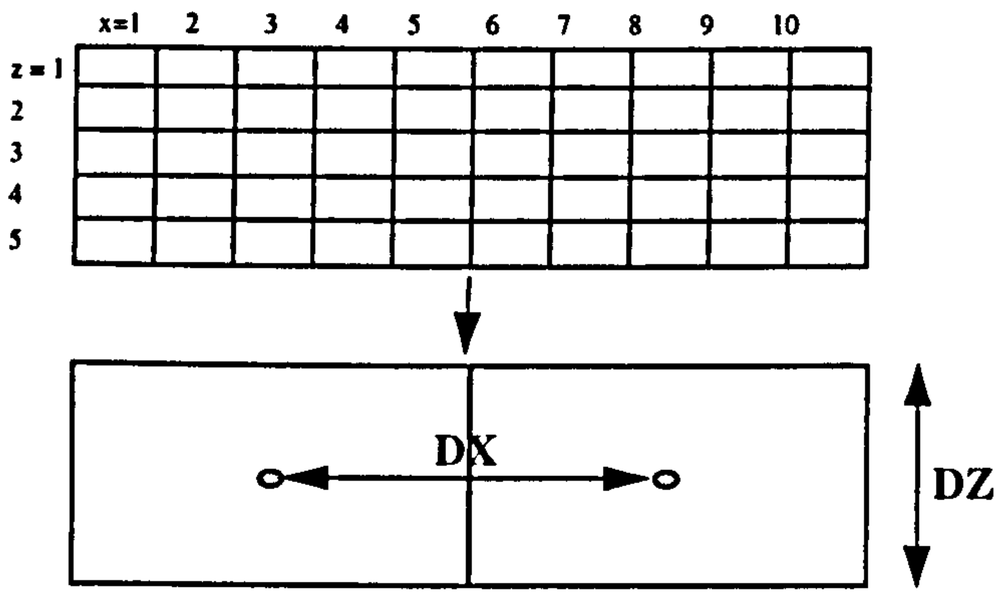

Figure 1: Grid coarsening scheme for upscaling methods

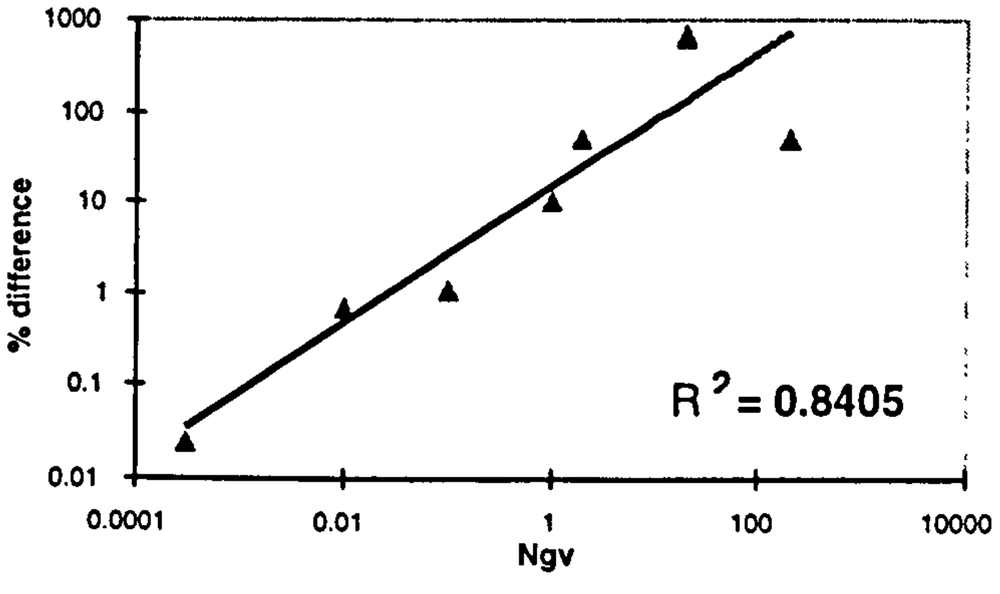

Figure 2: Percentage differences in normalised rms error between the K&B and TPW methods vs. N_{gv} ; Homogenous models.

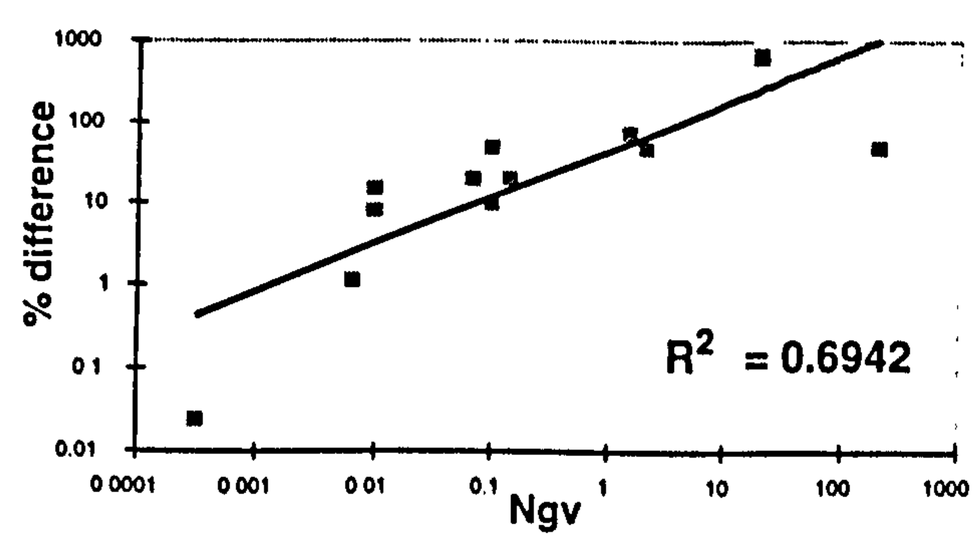

Figure 3: Percentage differences in normalised rms error between the K&B and TPW methods vs. N_{gv} ; All models.

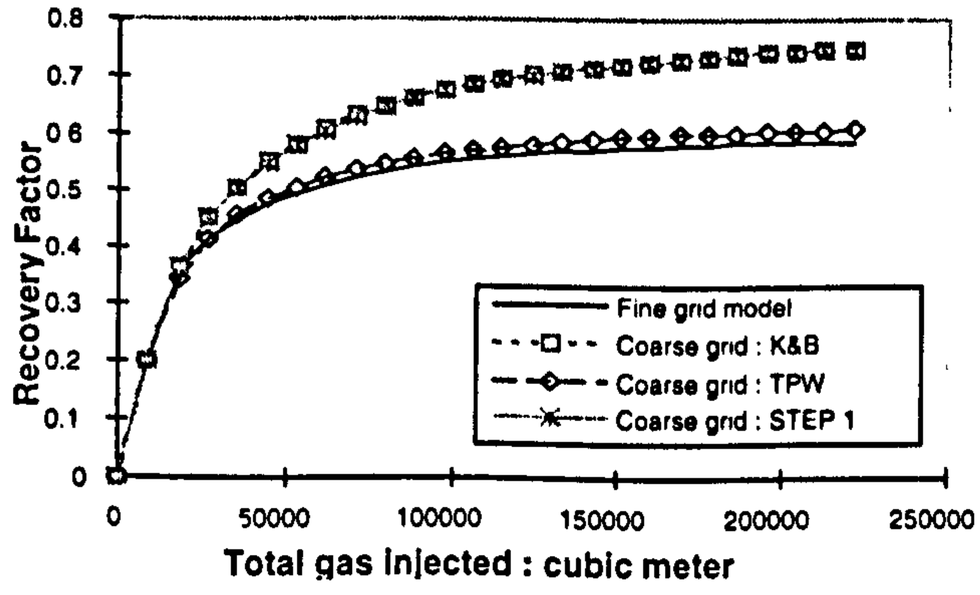

Figure 4: Recovery factor vs. total gas injected (STEP 1)

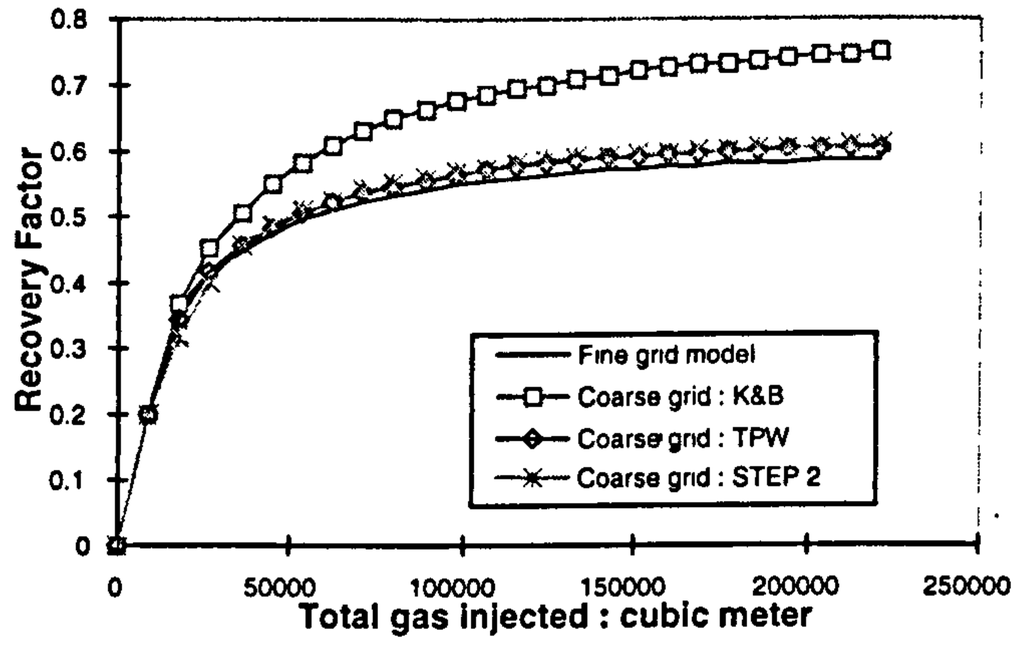

Figure 5: Recovery factor vs. total gas injected (STEP 2)

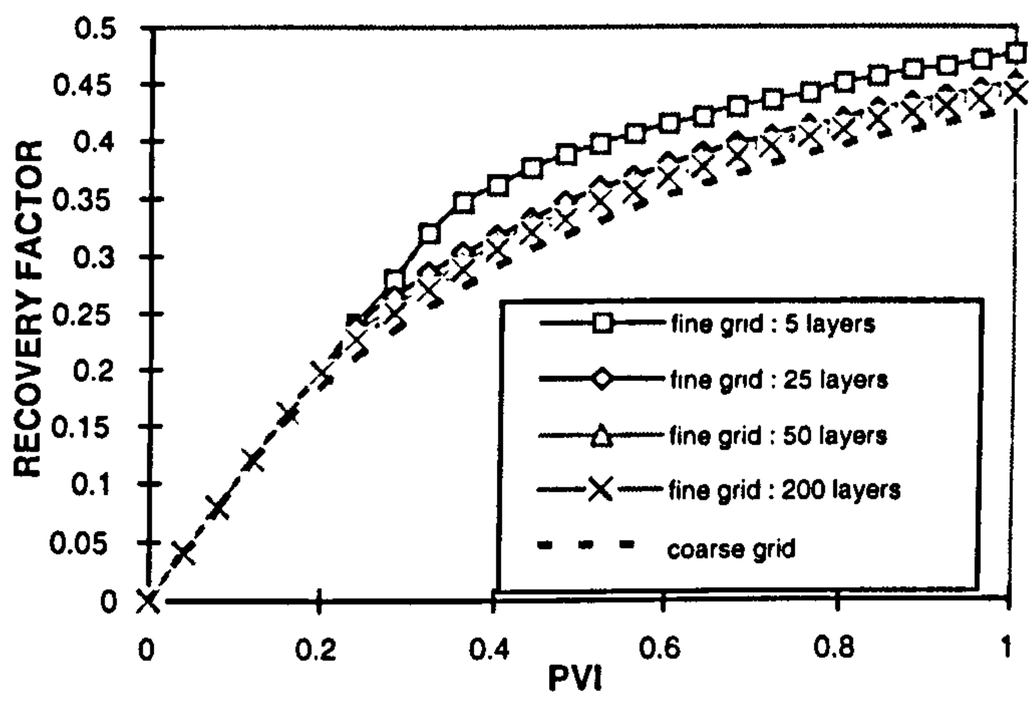

Figure 6: Recovery factor vs. pore volume injected (VE method: Fine grid: High N_{gv})

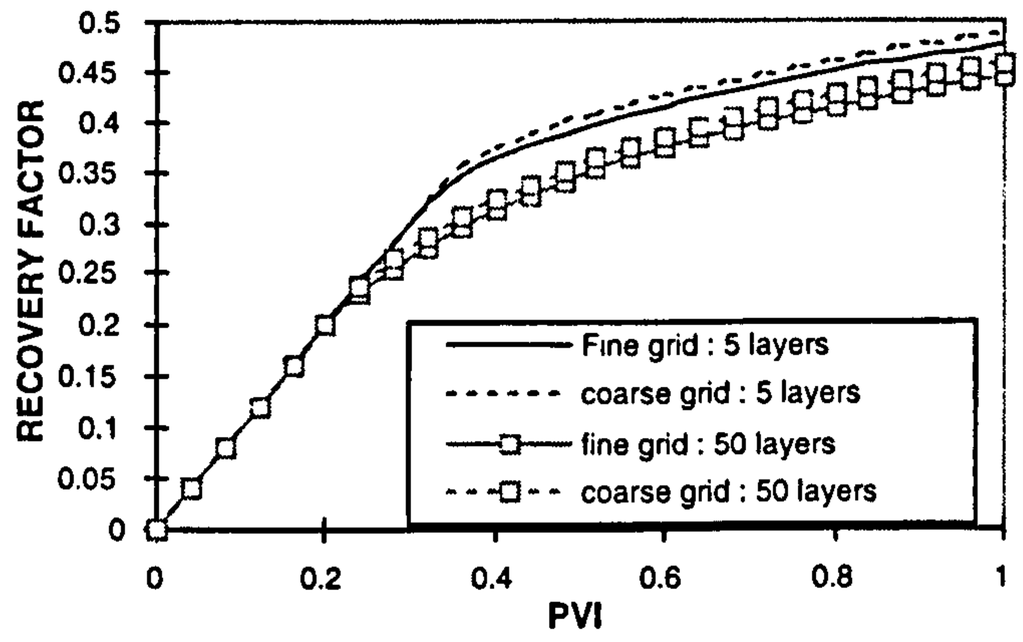

Figure 7: Recovery factor vs. pore volume injected (TPW method: High N_{gv})

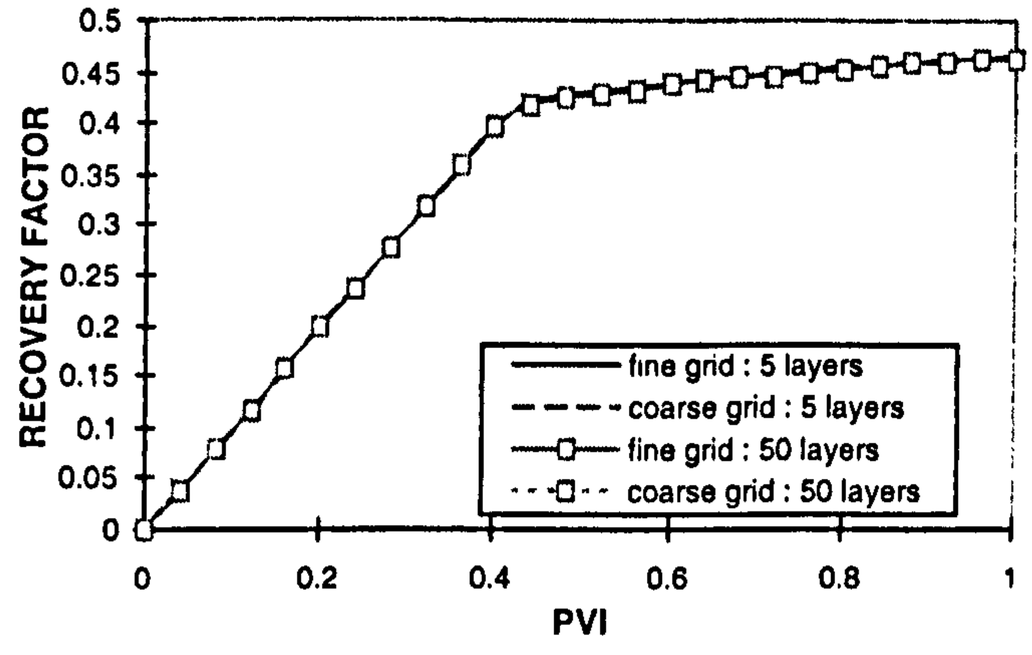

Figure 8: Recovery factor vs. pore volume injected (TPW method: Low N_{gv})

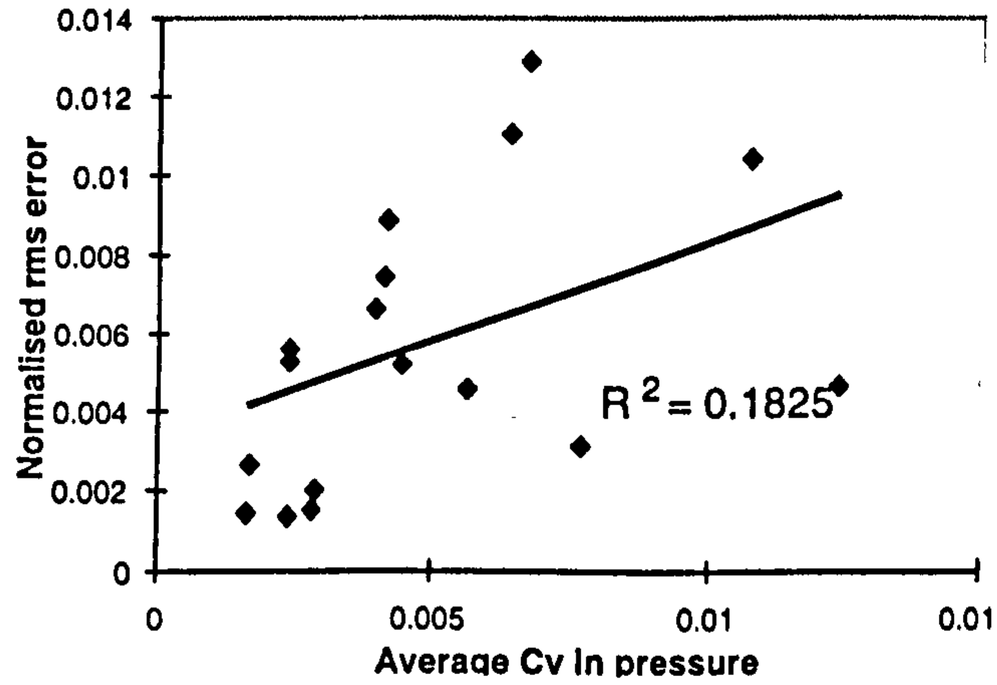

Figure 9a: Normalised rms error vs. C_v in pressure

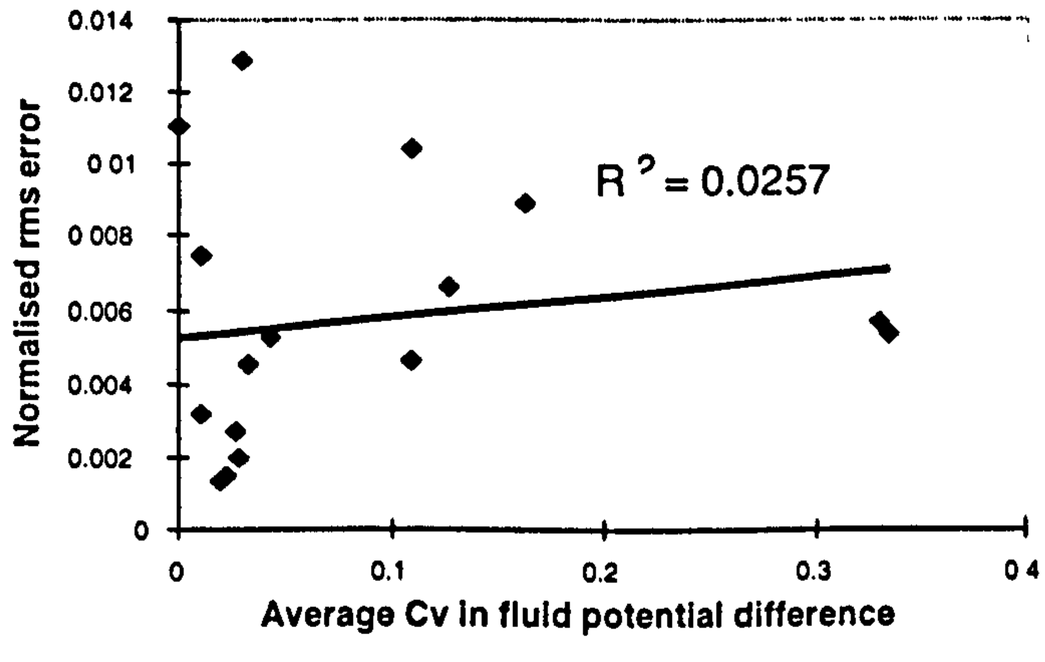

Figure 9b: Normalised rms error vs. C_v in fluid potential difference

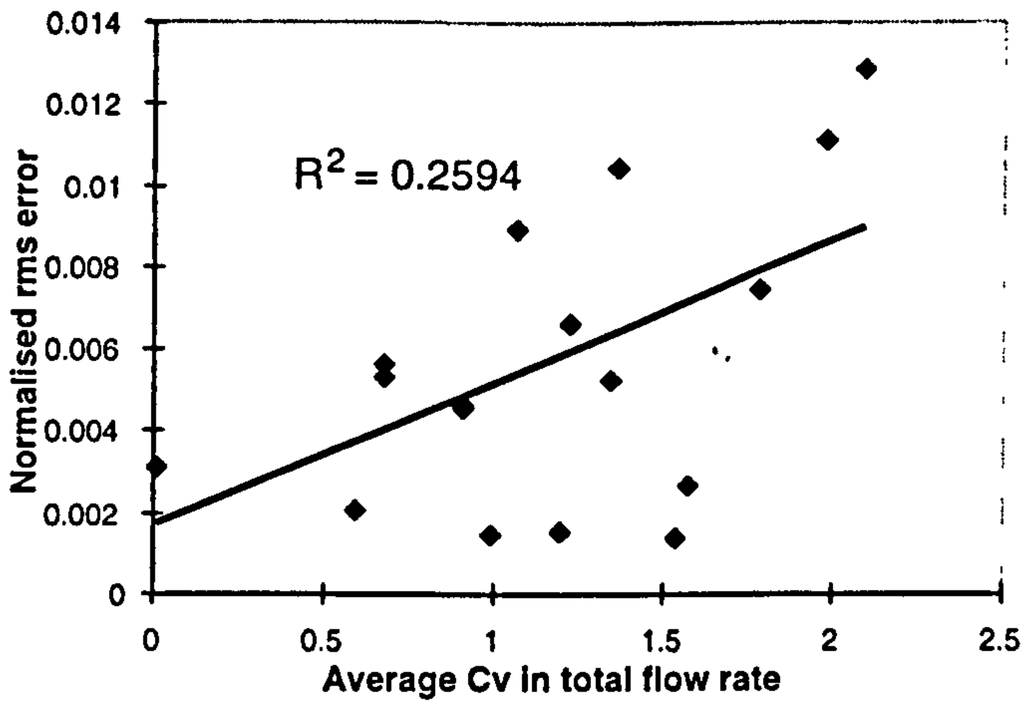

Figure 9c: Normalised rms error vs. C_v in total flow rate

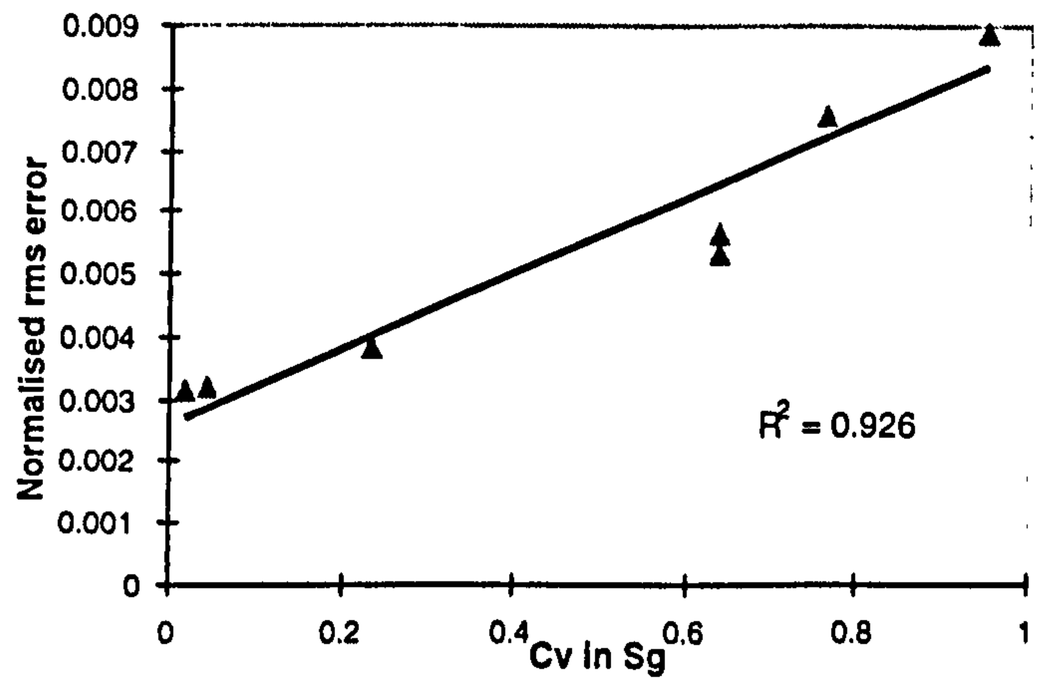

Figure 10a: Normalised rms error vs. C_v in gas saturation, S_g (Homogenous models)

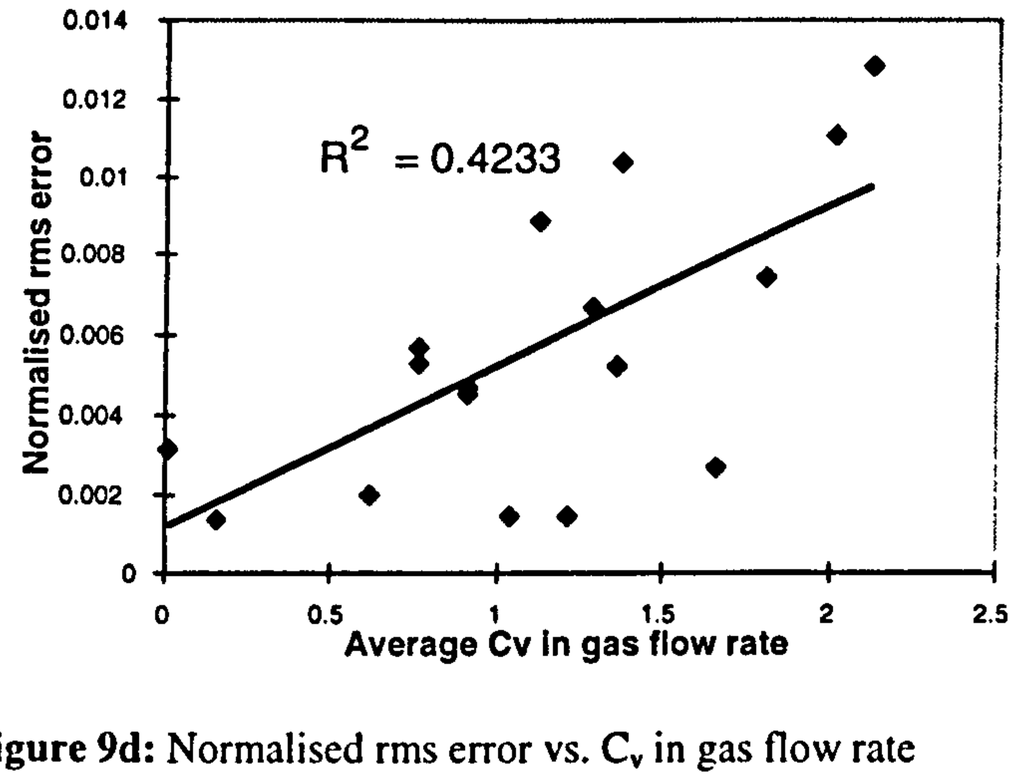

Figure 9d: Normalised rms error vs. C_v in gas flow rate

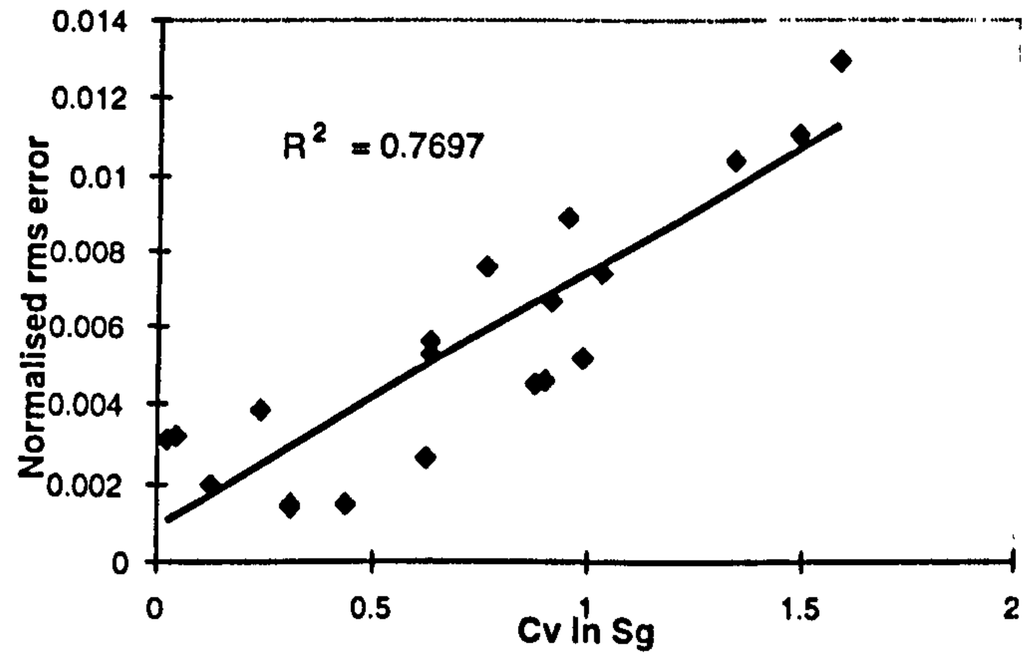

Figure 10b: Normalised rms error vs. C_v in gas saturation (All models)

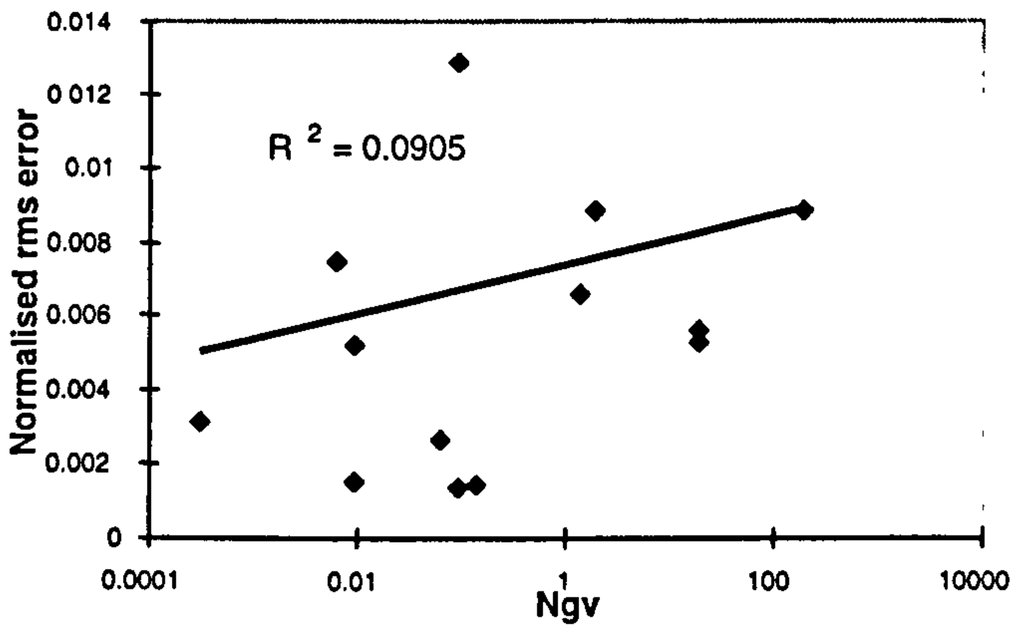

Figure 9e: Normalised rms error vs. N_{gv}

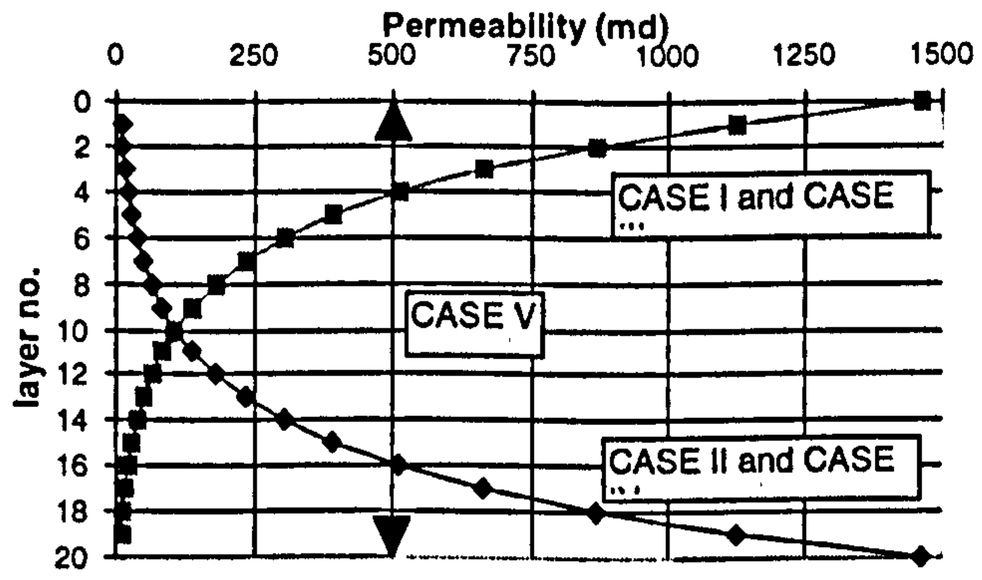

Figure 11: Permeability distributions for Case I to Case V

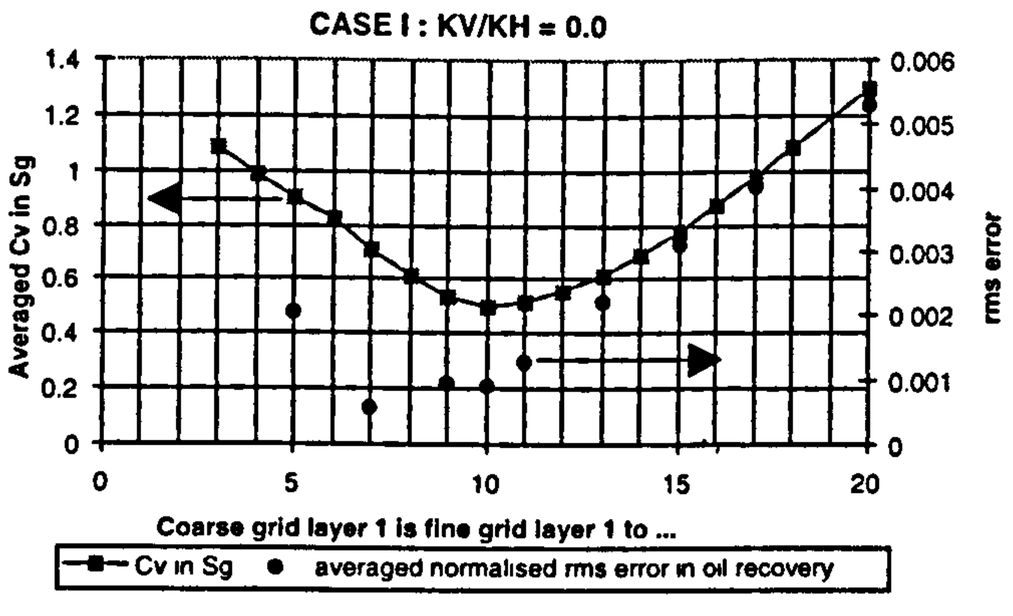

Figure 12a: Averaged C_v in S_g and averaged normalised rms error vs. coarsening scheme (CASE I)

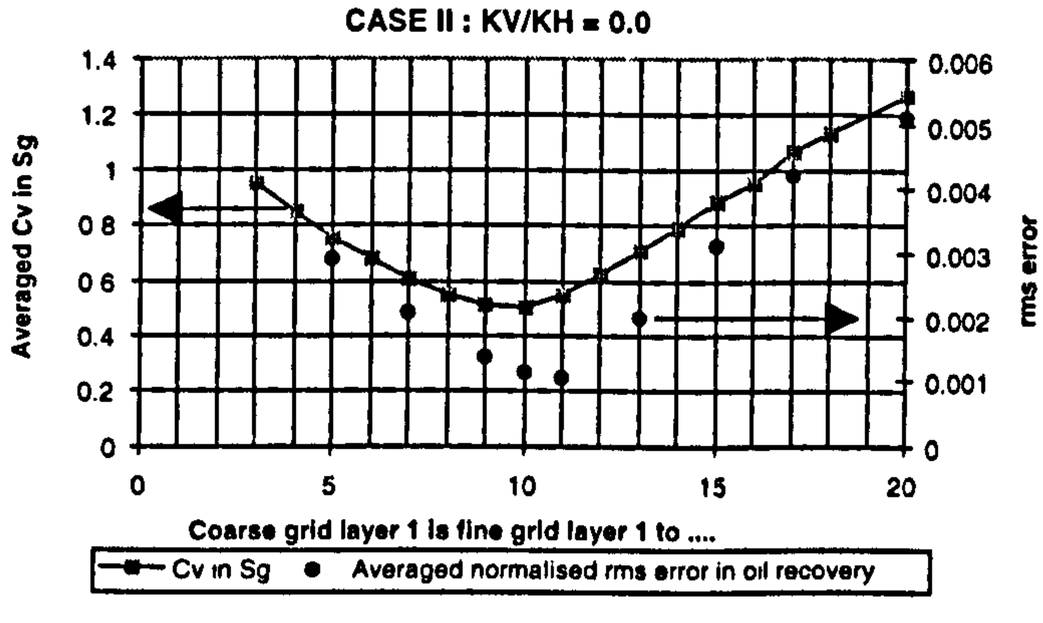

Figure 13a: Averaged C_v in S_g and averaged normalised rms error vs. coarsening scheme (CASE II)

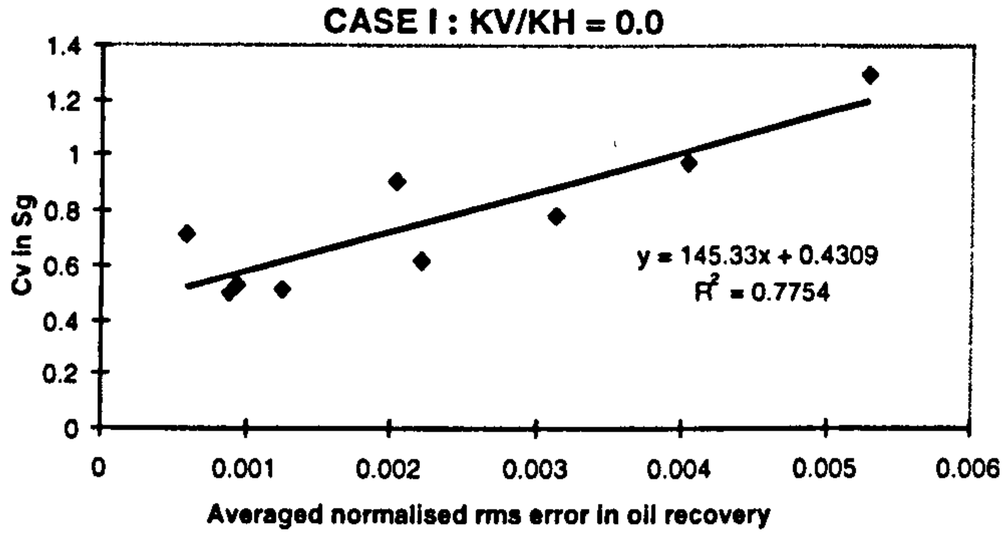

Figure 12b: Averaged C_v in S_g vs. averaged normalised rms error in oil recovery (CASE I)

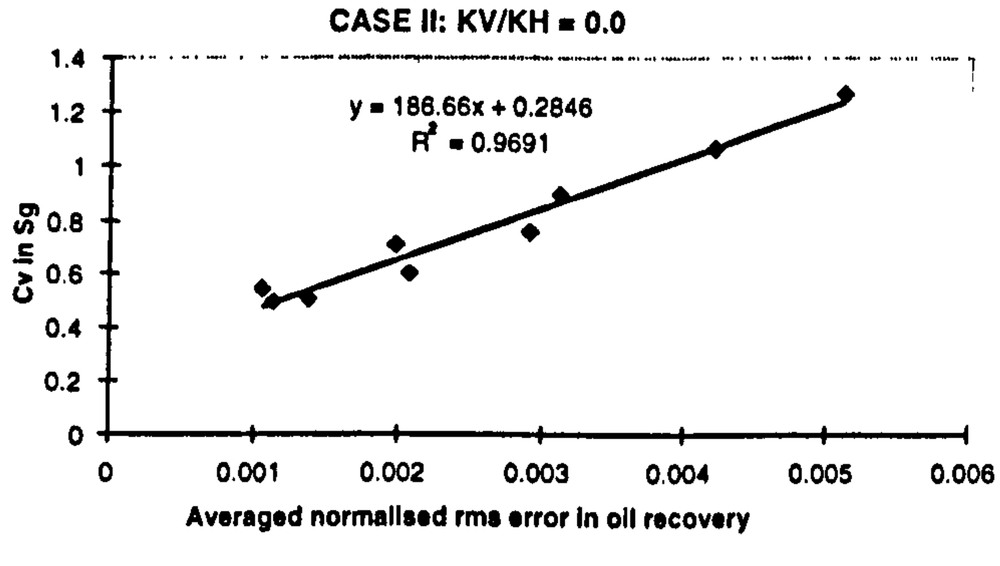

Figure 13b: Averaged C_v in S_g vs. averaged normalised rms error in oil recovery (CASE II)

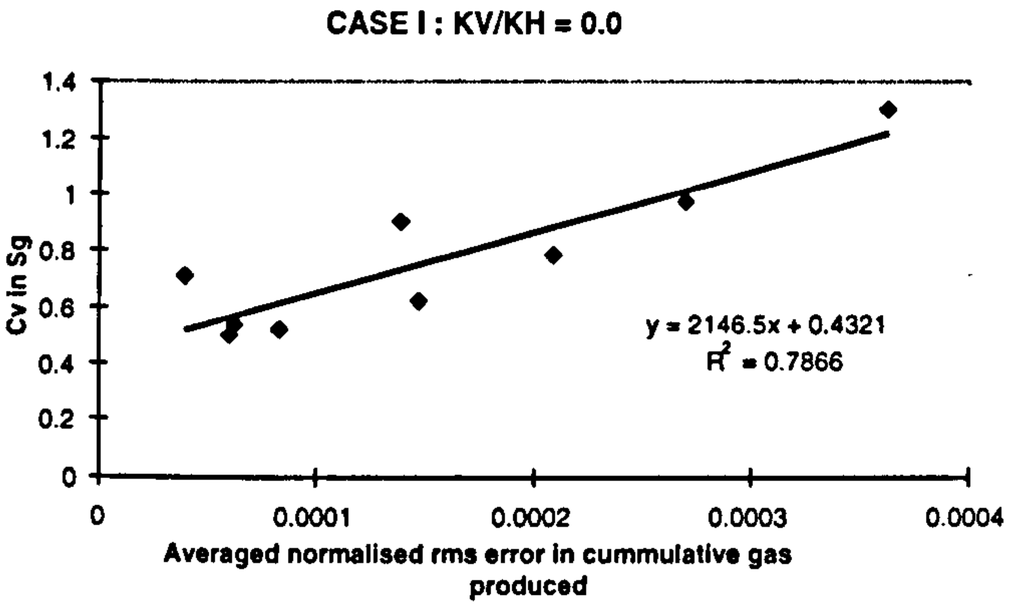

Figure 12c: Averaged C_v in S_g vs. averaged normalised rms error in cumulative gas produced (CASE I)

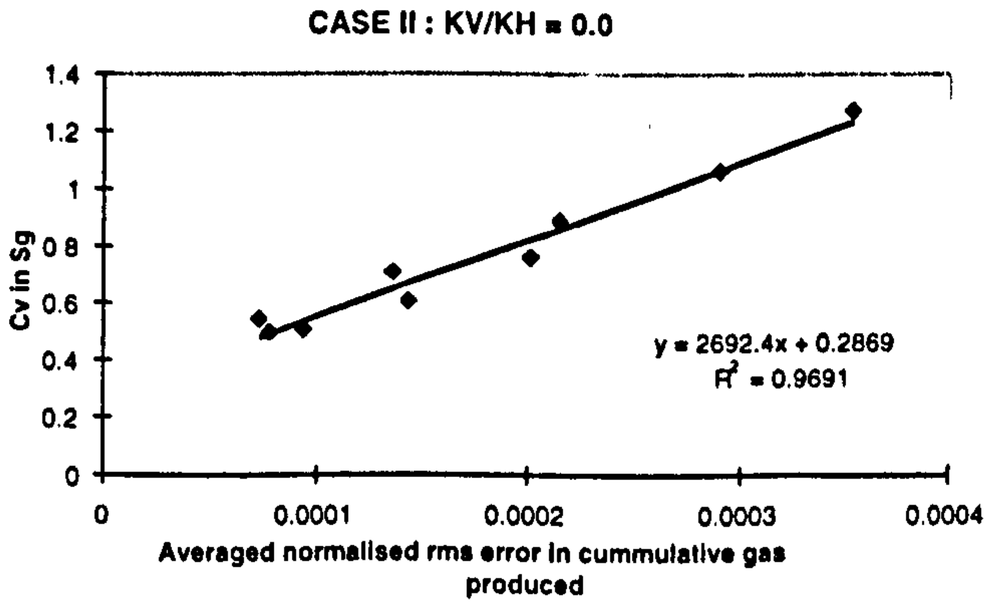

Figure 13c: Averaged C_v in S_g vs. averaged normalised rms error in cumulative gas produced (CASE II)

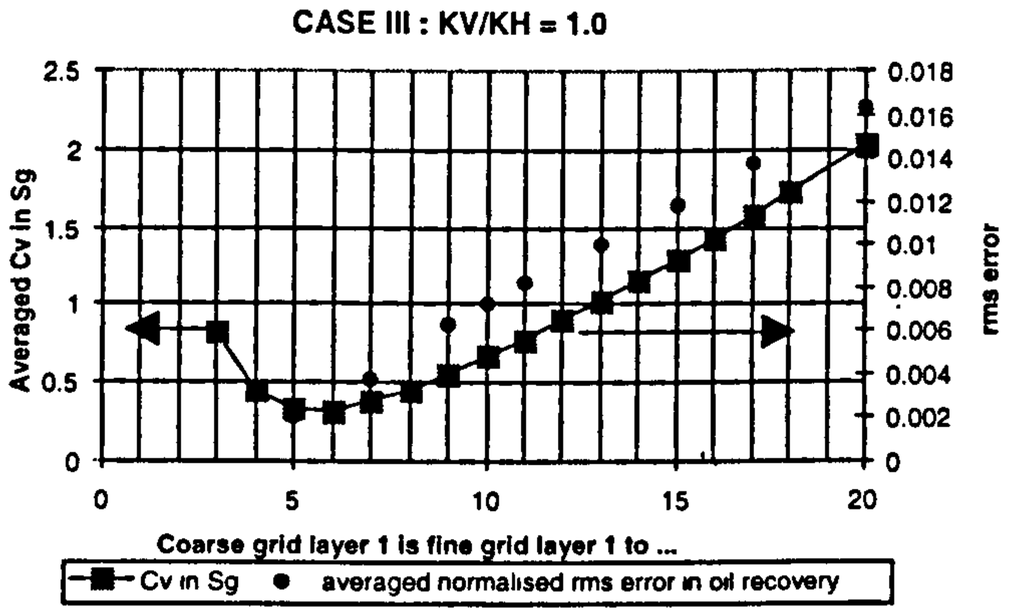

Figure 14a: Averaged C_v in S_g and averaged normalised rms error vs. coarsening scheme (CASE III)

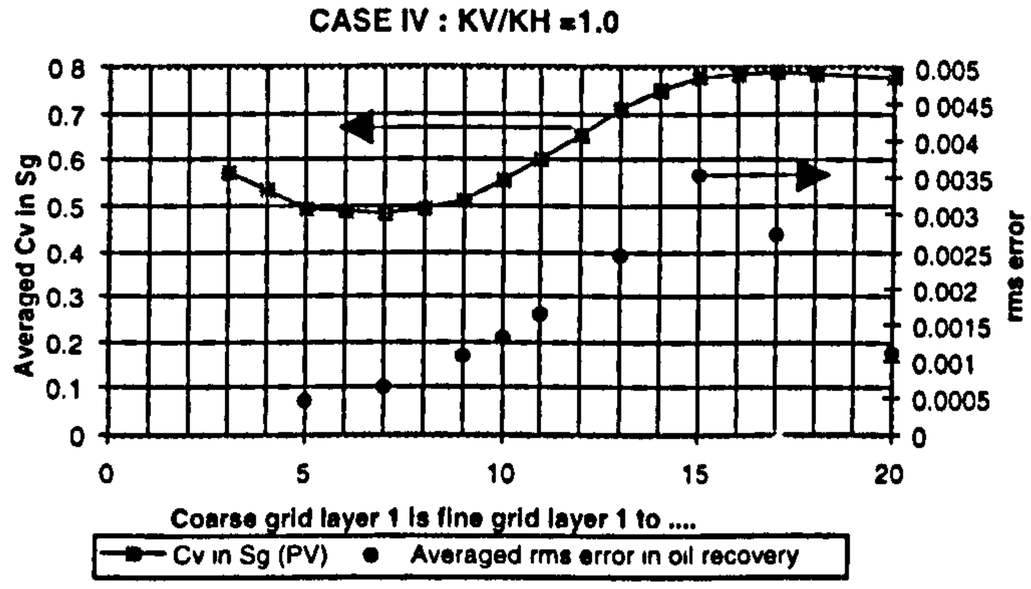

Figure 15a: Averaged C_v in S_g and averaged normalised rms error vs. coarsening scheme (CASE IV)

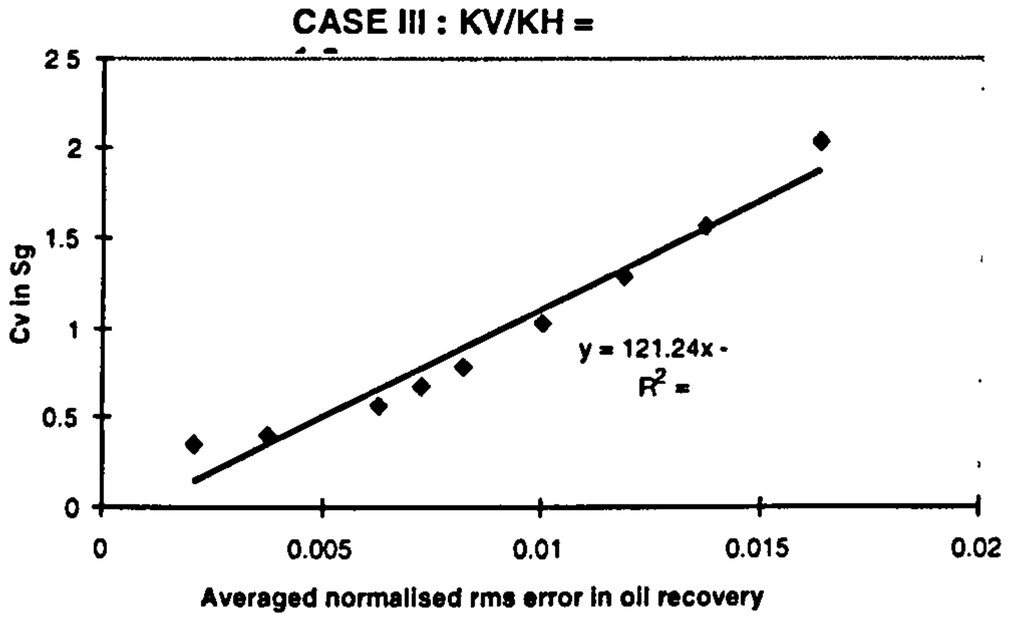

Figure 14b: Averaged C_v in S_g vs. averaged normalised rms error in oil recovery (CASE III)

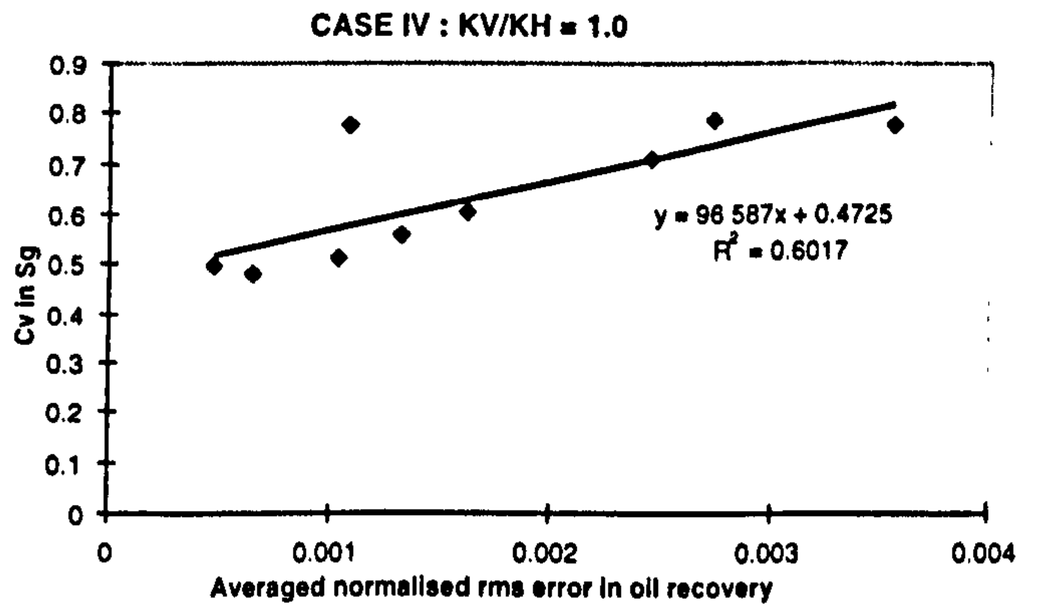

Figure 15b: Averaged C_v in S_g vs. averaged normalised rms error in oil recovery (CASE IV)

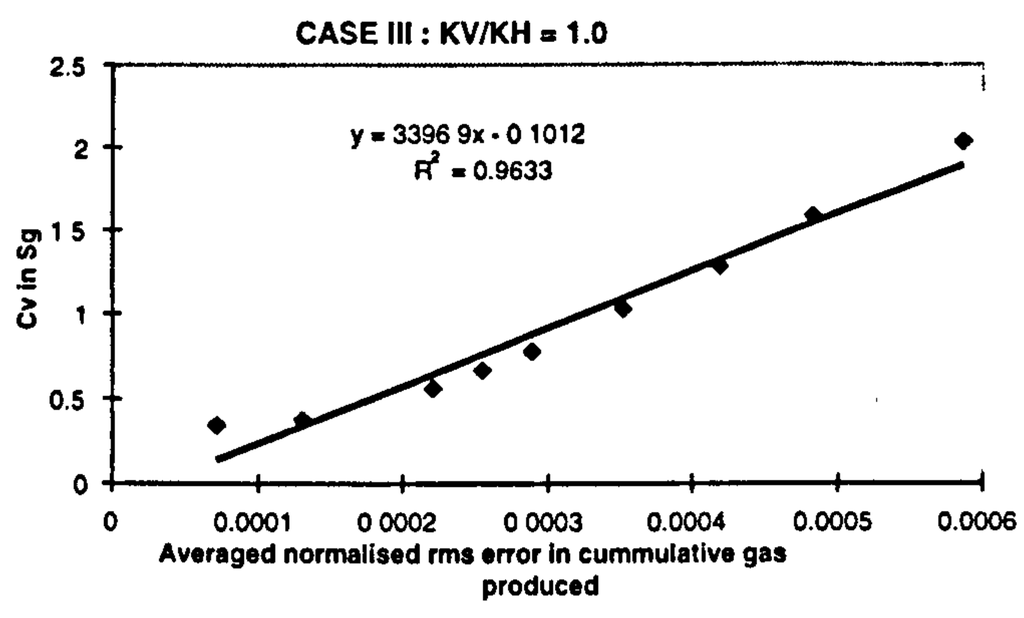

Figure 14c: Averaged C_v in S_g vs. averaged normalised rms error in cumulative gas produced (CASE III)

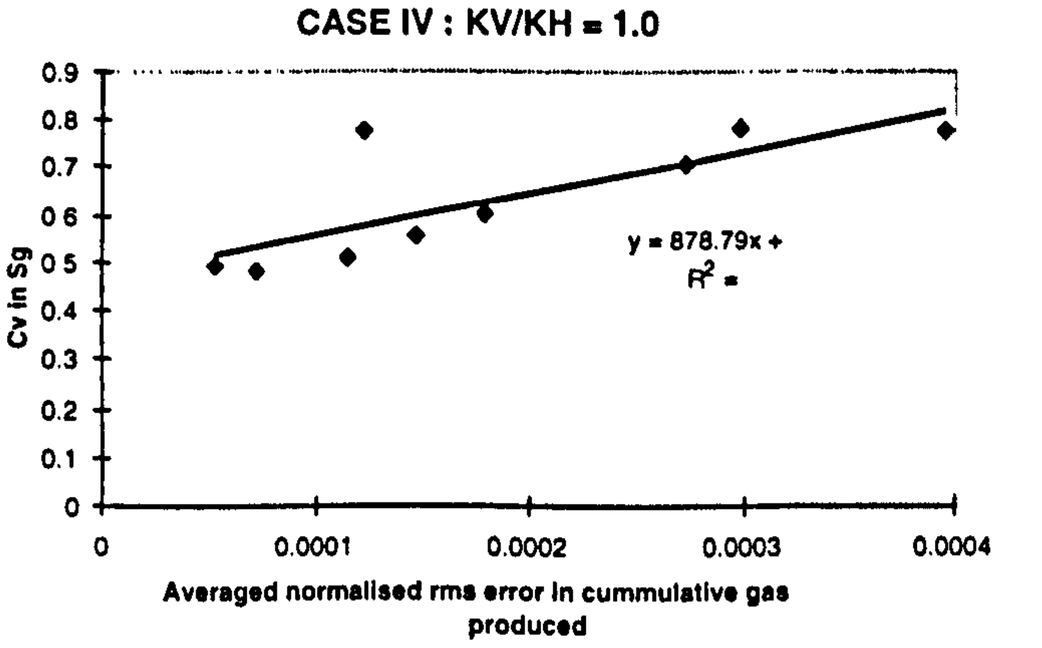

Figure 15c: Averaged C_v in S_g vs. averaged normalised rms error in cumulative gas produced (CASE IV)

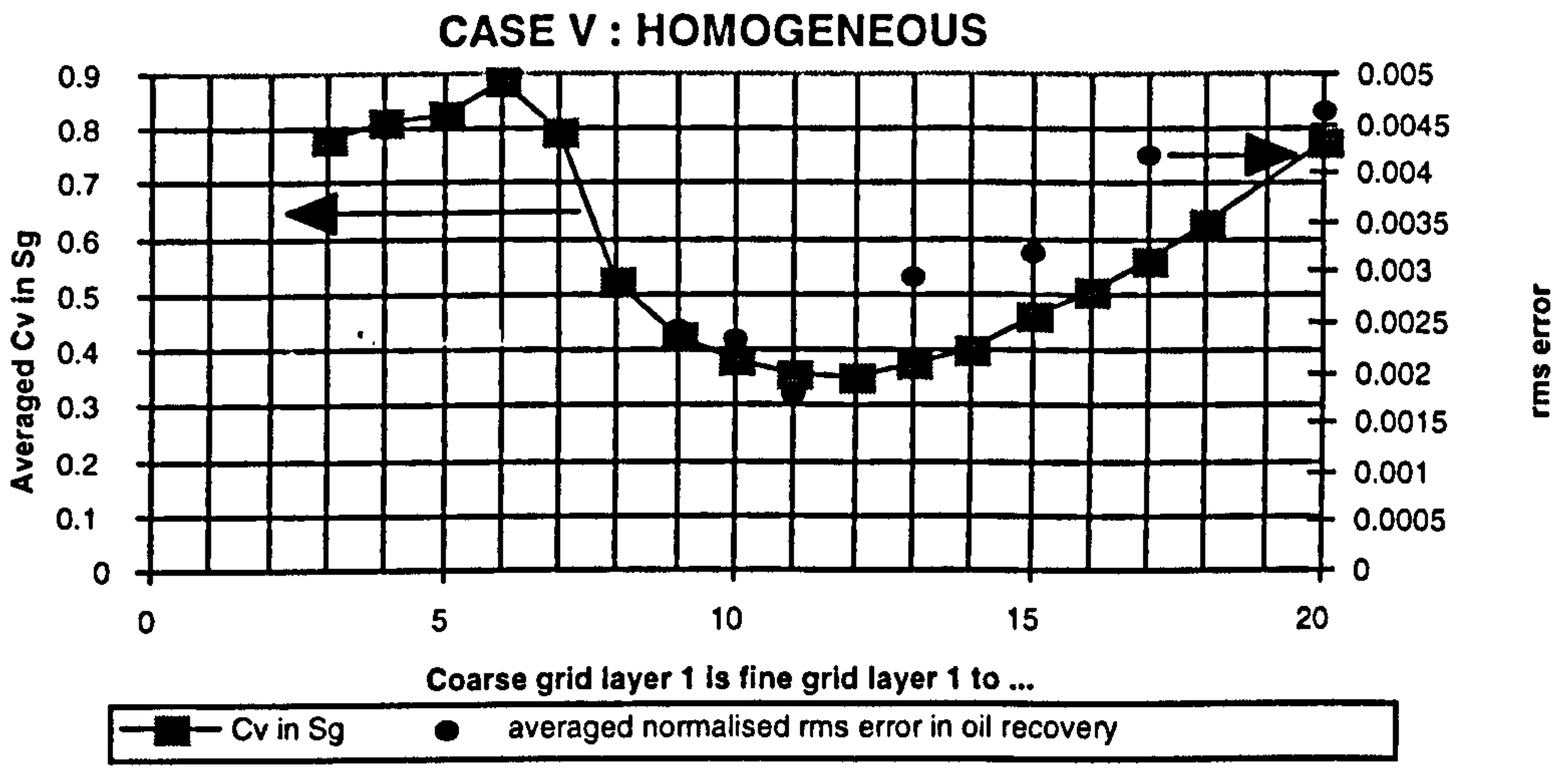

Figure 16a: Averaged C_v in S_g and averaged normalised rms error vs. coarsening scheme (CASE V)

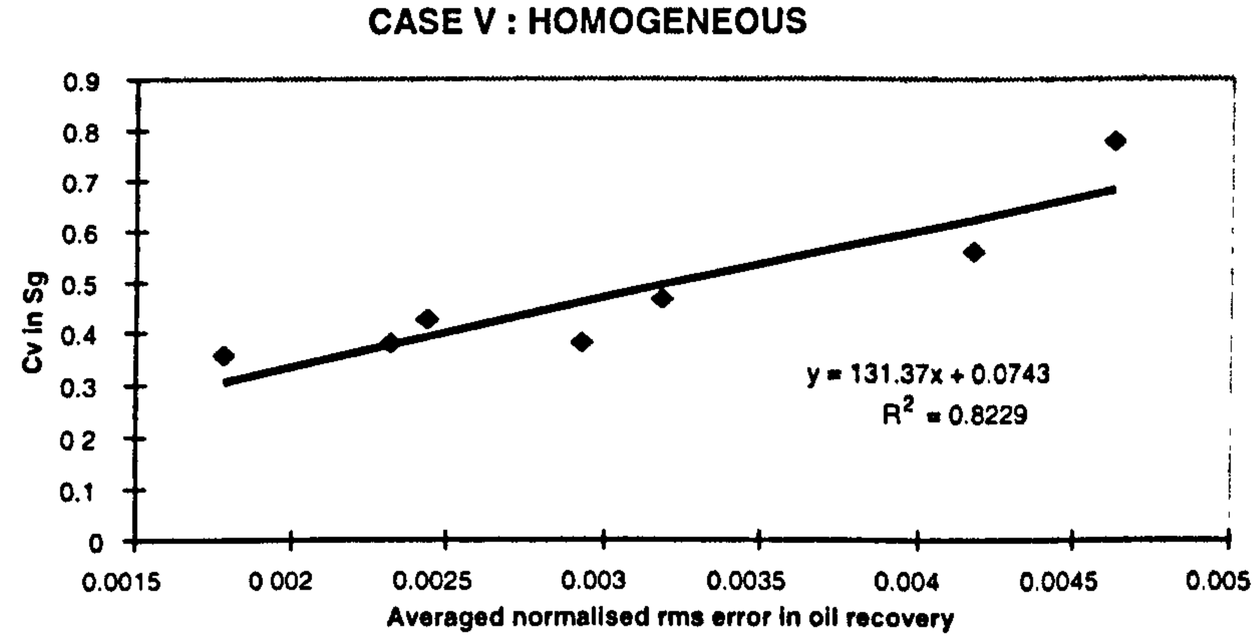

Figure 16b: Averaged C_v in S_g vs. averaged normalised rms error in oil recovery (CASE V)

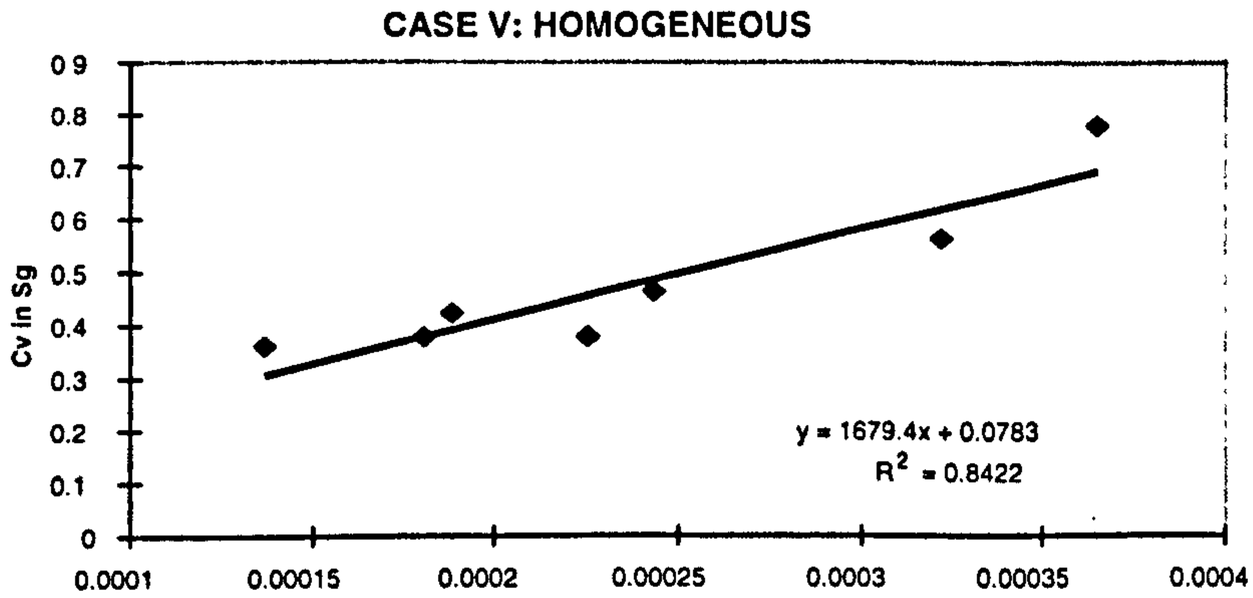

Figure 16c: Averaged C_v in S_g vs. averaged normalised rms error in cumulative gas produced (CASE V)

SPE 59452

Upscaling Immiscible Gas Displacements: Quantitative Use of Fine Grid Flow Data in Grid Coarsening Schemes

N.H. Darman, SPE, Petronas Research and Heriot-Watt University, L.J. Durlofsky, SPE, Chevron Petroleum Technology Company and Stanford University, K.S. Sorbie, SPE, and G.E. Pickup, SPE, Heriot-Watt University

This paper was prepared for presentation at the 2000 SPE Asia Pacific Conference on Integrated Modelling for Asset Management held in Yokohama, Japan, 25–26 April 2000.

Abstract

Grid coarsening schemes based on the quantitative use of fine scale two-phase flow information are presented and assessed. The basic approach is motivated from a volume average analysis of the fine scale saturation equation including gravitational effects. Extensive results for layered systems are presented. It is shown that coarse grid simulation error correlates closely with specific sub-grid quantities involving higher moments of fine grid variables, which can be computed from the fine scale simulations. By forming a coarse grid that minimises the appropriate sub-grid quantity, optimal coarse scale descriptions can be generated. The overall approach is shown to be applicable to coarse scale descriptions using either rock or pseudo relative permeability curves. The accuracy of the coarse grid calculations is, however, significantly better when pseudo functions are used. The method is applied to determine the optimal number and configuration of coarse grid layers in more general cases and it is shown that coarse grid results do not always improve as the number of coarse layers is increased.

Introduction

In modern reservoir characterisation, the spatial resolution that may be incorporated into geological models often exceeds the computational capabilities of fluid flow simulators by a significant margin. Therefore, some level of upscaling must be applied to the fine scale geological models before they can be used for practical flow calculations. This upscaling may be a simple block averaging of the single-phase permeability or it may involve the application of a complex upscaling procedure. When the degree of upscaling is very large, the use of a dynamic technique, which may involve the generation of upscaled or pseudo relative permeabilities, is generally required.

Several such upscaling methods have been developed and described in the literature; e.g. the Kyte and Berry[1], Stone[2], Vertical Equilibrium (VE)[3] and TW[4,a] methods. Hewett and coworkers have also suggested approaches based on streamline methods[5,6]. In general, all of these dynamic methods (except VE) involve some procedure for using the fine grid flows to generate modified pseudo relative permeability and capillary pressure curves at the coarse block scale.

When successfully applied, these pseudo functions will accurately incorporate the interaction between small-scale multi-phase fluid flow and heterogeneity, as well as correcting for the numerical dispersion in the coarse grid models. The principal metric is that the upscaling method provides a coarse-scale flow model that accurately reproduces the results (recovery profiles, breakthrough times, etc.) computed using the fine grid model. Pseudo functions do have costs and limitations associated with them, however, and these must be considered when such an approach is applied. Pseudo relative permeabilities may be subject to so-called process dependence, meaning the coarse scale pseudo functions vary with varying global boundary conditions. This in turn can result in a lack of robustness in the coarse scale model. In addition, when pseudo functions are generated through the simulation of a global fine scale flow problem, the computational requirements can be excessive in some cases.

In recent work, Darman et al.[4] have described a new pseudo generation scheme known as the transmissibility weighted (TW) method.[a] This was found to be particularly suitable for upscaling immiscible gas processes where large adverse mobility ratios and high gravity numbers are commonly encountered. It was also found that the error in the coarse grid model predictions (relative to the reference fine

[a] This method was originally referred to as the TPW method (Transmissibility–Potential-Weighted) but, since the potential is non-unique, we now use transmissibility weighting only. Numerically, the TW method gives virtually identical results to those in Ref. 4.

grid results) correlated closely with the sub-grid variability in the gas saturation. This variability was expressed as the coefficient of variation in the gas saturation, which we refer to as the C_v in S_g (this quantity is computed as the pore volume average of the C_v[b] in each of the coarse grid blocks, over all the calculated time steps). Because of the close correlation between the coarse grid error and the C_v in S_g, Darman et al.[4] were able to approximately minimise the coarse grid simulation error by choosing the coarse grid that minimises the C_v in S_g. This result forms the basis for a new grid coarsening scheme.

This method differs from conventional coarsening schemes in that it takes into account not only the static properties of the fine grid models but also the dynamic properties of the fine grid simulation runs. This in turn can lead to more accurate predictions of important quantities such as the recovery factor and gas-oil ratio when pseudo functions are applied. The idea of this coarsening method is to identify regions of the fine grid models where there is low variability of gas saturation, and to take such regions as the corresponding coarse grid blocks. As a result, the final composite coarse grid model may include both finely gridded and coarsely gridded regions.

This criterion (minimising the C_v in S_g), is not the only one that might be applied in developing the grid coarsening scheme. In previous work, Durlofsky[7,8] developed volume averaged saturation equations for viscous dominated immiscible displacements (i.e. gravity and capillary pressure effects were absent). There, it was shown that the coarse grid volume averaged equations contain terms involving higher moments of certain fine grid quantities. The specific higher moments that appear are the variance of saturation[c,d] (σ^2_S) and the velocity-saturation covariance[c] (σ_{vS}). Because these higher moments are not explicitly modelled in coarse grid simulations, it might be expected that coarse grid errors could be reduced by minimising the terms containing these higher moments. This could be accomplished by forming the coarse grid such that σ^2_S and σ_{vS} are minimised. This expectation is in fact quite consistent with previous results using a non-uniform coarsening procedure for viscous dominated displacements.[7]

There is clearly a close link between the numerical findings of Darman et al.[4] and the volume averaging results of Durlofsky[7] in that both have identified sub-grid variability in saturation as an important quantity to consider in forming the coarse grid. However, to more directly apply predictions from volume averaging to coarse scale simulations of immiscible gas displacements, it is necessary to introduce gravitational effects into the volume averaged saturation equation. This will then allow a direct comparison to be made between the theoretical predictions and the numerical experiments.

[b] The coefficient of variation, C_v, is equal to the standard deviation divided by the mean.
[c] Durlofsky used S_w instead of S_g.
[d] Note that the difference between σ^2_s and the C_v in S_g is that the C_v in S_g takes the square root of σ^2_s and then divides the number by the averaged saturation value for that particular coarse grid block.

Our intent in this paper is to explore the relationship between the volume averaged saturation equation and coarse scale numerical simulations for several model problems. We will also study the performance of coarse grid models developed using our new coarsening scheme in more general cases. This paper proceeds towards these goals as follows. We first introduce gravitational effects into the volume averaging procedure to allow us to assess the coarse scale numerical simulations in light of the volume averaged saturation equation. We consider many different aggregations of 20-layer systems to equivalent 2-layer systems and study the relationship of sub-grid variability to error in the coarse scale simulation results. We assess the use of both pseudo relative permeabilities and rock curves in these coarse scale simulations and determine which measure of sub-grid variability is most appropriate for use with each of these approaches. In the second part of the paper, we apply these findings to more general multi-layered cases (i.e. the coarse grid contains more than 2 layers). In addition, we apply our coarsening method in association with both the TW and Kyte and Berry methods to study the effect of using other pseudo generation methods with our coarsening technique. It is shown that the scheme continues to provide accurate coarse grid results in these more general cases.

Effects of Sub-Grid Quantities on Coarse Grid Error

The objective of this part of our study is to suggest a grid coarsening scheme which uses more than the static properties of the fine grid models, such as permeability distribution, net-to-gross ratio etc. Such a coarsening scheme should use the *dynamic* properties of the fine grid model such as the flood pattern, pressure and saturation distribution. It is hoped that this approach will result in more accurate predictions of important quantities such as total oil recovery and gas-oil ratio in coarse grid models. We proceed by first developing the volume averaged saturation equation and then discuss our numerical simulation results.

Coarse scale saturation equation. As indicated in the Introduction, the moments appearing in the averaged saturation equation for viscous dominated displacements are σ^2_S and σ_{vS}, defined as:

$$\sigma_S^2 = \langle S_g^2 \rangle - \langle S_g \rangle^2 = \overline{S'S'} = \langle S'S' \rangle \,, \tag{1}$$

$$\sigma_{vS} = \langle vS_g \rangle - \langle v \rangle \langle S_g \rangle = \overline{v'S'} = \langle v'S' \rangle \,, \tag{2}$$

where S_g or S (we use the two interchangeably) represents gas saturation, v represents the component of the total velocity in the dominant flow direction, the prime denotes a spatially fluctuating quantity and an overbar indicates a volume averaged quantity (see below). To determine the relevant moments for the case of immiscible gas displacement, for which gravitational effects are important, we must include the gravitational terms in the derivation of the volume averaged saturation equation.

To develop the volume averaged saturation equation with gravity effects included, we proceed as in Ref. 7. We express all fine grid quantities as the sum of a volume averaged or coarse grid component (designated by an overbar) and a fluctuating component (designated by a prime). Specifically, for any fine grid variable Φ, we write $\Phi(x,z)=\overline{\Phi}+\Phi'(x,z)$ (see Appendix). Capillary pressure and compressibility effects are neglected. The coarse scale saturation equation is then derived by inserting these expressions into the fine grid equation, volume averaging, and retaining terms involving products of two fluctuating quantities. Then, by expanding terms involving relative permeability and fractional flow around the average gas saturation $\overline{S}$ and again retaining only first order terms, we arrive at the volume averaged saturation equation. A detailed derivation is provided in the Appendix. The final form of the equation is as follows:

$$\frac{\partial\overline{S}}{\partial t}+\overline{\mathbf{v}}\cdot\nabla f(\overline{S})+\frac{1}{2}\overline{\mathbf{v}}\cdot\nabla\left\{f_{ss}(\overline{S})\overline{S'S'}\right\}+\nabla\cdot\left\{f_s(\overline{S})\overline{\mathbf{v}'S'}\right\}$$
$$-\frac{g\Delta\rho}{\mu_o}\nabla\cdot\left\{(\overline{\mathbf{k}}\eta(\overline{S})+\frac{1}{2}\eta_{ss}(\overline{S})\overline{\mathbf{k}}\,\overline{S'S'}+\eta_s(\overline{S})\overline{\mathbf{k}'S'})\cdot\mathbf{i}_z\right\}=0. \quad (3)$$

where the functions f and η are defined as:

$$f(S)=\frac{k_{rg}/\mu_g}{k_{rg}/\mu_g+k_{ro}/\mu_o}, \quad (4)$$

$$\eta(S)=k_{ro}f. \quad (5)$$

In Eqs. (3)-(5), t is time, $\mathbf{v}$ is the total Darcy velocity, $\Delta\rho=\rho_g-\rho_o$ (ρ_g is gas density and ρ_o is the oil density), g is gravitational acceleration (acting in the z-direction), μ_o is the oil viscosity, $\mathbf{k}$ is the local permeability tensor, $\mathbf{i}_z$ is the unit vector in the z-direction, k_{ro} is the relative permeability to oil, k_{rg} is the relative permeability to gas, and f_s, η_s, f_{ss} and η_{ss} are the first and second derivatives of f and η with respect to S_g.

There are several interesting aspects to Eq. (3). First, we note that the fine scale functions f and η appear explicitly in the coarse scale equation. These functions are not modified for use in the coarse scale models; i.e. the f and η have the same functional forms on both the fine and coarse scales. Second, the coarse scale equation is seen to contain three additional terms involving higher moments that account for the sub-grid effects. The moments that appear explicitly are $\overline{S'S'}$, $\overline{\mathbf{v}'S'}$ and $\overline{\mathbf{k}'S'}$, and these terms are always multiplied by derivatives of f or η. The moments appearing in the gravitational terms (the terms multiplied by $g\Delta\rho/\mu_o$) are $\overline{S'S'}$ and $\overline{\mathbf{k}'S'}$ only; $\overline{\mathbf{v}'S'}$ does not appear. From Eq. (3), we can determine the form of the error that will result from using rock curves (and neglecting the higher moment terms) on the coarse scale. Specifically, because such a scheme neglects all terms involving higher moments, the error can be expected to correlate with the magnitudes of the neglected terms, i.e. with $\overline{S'S'}$, $\overline{\mathbf{v}'S'}$ and $\overline{\mathbf{k}'S'}$.

Note that pseudo functions do not appear in Eqs. (3)-(5). Were we to use pseudo functions, the coarse scale equation would be of the same form as the fine grid equation but with upscaled (pseudo) parameters, computed from fine grid simulations, appearing in place of the fine scale f and η functions; i.e.

$$\frac{\partial\overline{S}}{\partial t}+\overline{\mathbf{v}}\cdot\nabla f^*(\overline{S})-\frac{g\Delta\rho}{\mu_o}\nabla\cdot(\eta^*(\overline{S})\overline{\mathbf{k}}\cdot\mathbf{i}_z)=0, \quad (6)$$

where the * superscript indicates functions derived from pseudo relative permeability. Comparing Eq. (6) with Eq. (3), we see that the pseudo functions attempt to capture sub-grid variability (which involves the higher moments $\overline{S'S'}$, $\overline{\mathbf{v}'S'}$ and $\overline{\mathbf{k}'S'}$) through use of coarse grid functions that depend on $\overline{S}$ only. Because the functional dependence of the pseudo functions is limited relative to the actual sub-grid effect (i.e. the pseudo functions depend on $\overline{S}$ only but the sub-grid effect additionally involves $\overline{S'S'}$, $\overline{\mathbf{v}'S'}$ and $\overline{\mathbf{k}'S'}$), this procedure will in general introduce some error. The magnitude of this error can be expected to correlate with the magnitude of the sub-grid terms themselves, i.e. with the higher moment terms.

Thus we see that the error using either the rock curves (and neglecting the higher order moment terms) or pseudo functions (where the pseudo functions approximately account for the sub-grid effects) will be related to the moments $\overline{S'S'}$, $\overline{\mathbf{v}'S'}$ and $\overline{\mathbf{k}'S'}$. However, because the pseudo functions are specifically introduced to capture the sub-grid effect, we expect that the error using pseudo functions will be considerably less than that using rock curves for the highly coarsened models that we will consider. Further, we also expect that the exact functional dependence of the coarse grid error on the higher moments will vary depending if we use rock curves or pseudo functions in the coarse grid model. We will test these speculations through detailed numerical calculations below.

We note that, in all the calculations below, fine grid simulations are required to compute the sub-grid quantities that will ultimately be used to determine the 'optimal' coarse grid structure. Thus, the need for a coarse scale description might be questioned in such cases; i.e. why do we need a coarse scale model if the fine scale result is already known. Because our intent in this paper is to understand the relationship between the accuracy of the coarse scale model and sub-grid terms, we are not particularly concerned with this issue here. However, before our method can be used in practice, we will need to establish that the grid structure (and the pseudo functions) determined from the 'base case' are applicable in other, similar problems as well. If this is indeed the case, then our coarse grid description will be more robust with respect to the global boundary conditions and could be quite useful in practice. We note finally that this issue is analogous to that surrounding the use of global fine scale simulations to compute coarse scale pseudo functions.

Description of the numerical models. Four cross sectional models with 100 × 1 × 20 fine grid blocks were used to compare the effectiveness of the sub-grid moments discussed above in different flow scenarios. The permeability trends for these four models are shown in Figure 1. Cases I and II were chosen to provide models with no cross flow between the fine grid layers. Cases III and IV were used to evaluate scenarios with free cross flow between the fine grid layers. The properties of the fine grid models are as follows:

Porosity,	$\phi = 0.2$;
Grid block sizes,	$\Delta x = \Delta y = \Delta z = 25$ ft or 7.63 m;
Viscosities,	$\mu_o = 10$ cp, $\mu_g = 0.1$ cp
Densities,	$\rho_o = 43.68$ lb/ft^3 or 700 kg/m^3,
	$\rho_g = 0.0624$ lb/ft^3 or 1.0 kg/m^3.

The fluids are assumed to be incompressible and immiscible. The rock relative permeabilities are power law curves as given by Guzman et al.[9]:

$$k_{ro} = ((1-S_g - S_{org} - S_{wc}) / (1 - S_{wc} - S_{org}))^{2.7},$$

$$k_{rg} = ((S_g - S_{gc}) / (1 - S_{gc} - S_{wc}))^{5.0}, \quad (7)$$

where S_{wc} = 0.15 (connate water saturation), S_{gc} = 0.05 (connate gas saturation) and S_{org} = 0.1 (residual oil to gas). Capillary pressure was assumed to be negligible in all cases, although the "rock" curves may be derived from a capillary equilibrium upscaling calculation when appropriate[10]. Gas was injected from an injector located at the left of the model and dead oil was produced from a well on the right of the model. Both wells were completed vertically throughout the model and the injection rate was set to give a frontal velocity of 0.3 m/d (about 1 ft/day).

Coarsening schemes. The four test cases described above (Cases I - IV) were run to establish the correlation between coarse grid error and C_v in S_g, C_v in vS, C_v in kS, $\overline{S'S'}$, $\overline{\mathbf{v}'S'}$ and $\overline{\mathbf{k}'S'}$. We note that C_v in vS and C_v in kS are defined analogously to C_v in S_g. We further note that we will subsequently refer to $\overline{S'S'}$, $\overline{\mathbf{v}'S'}$ and $\overline{\mathbf{k}'S'}$ as σ^2_S, σ_{vS} and σ_{kS}. In computing σ_{vS} and C_v in vS, we use the x-component of velocity; for σ_{kS} and C_v in kS, we use the z-component of absolute permeability. Error is computed as the normalised root mean square (rms) error in oil recovery factor. For each sub-grid quantity, we determine the coefficient of determination (R^2) between the sub-grid quantity and the coarse grid rms error in oil recovery factor. Three upscaling scenarios are considered:

1. The coarse grid models are run using the "rock" curves.
2. The coarse grid models are run with pseudo functions generated using the TW method.
3. The fine grid models are run using the coarse grid absolute permeabilities together with the rock relative permeabilities. This is done to quantify the effects of numerical dispersion in our models.

Our assessment proceeds as follows. For a given model, we first simulate the 20-layer fine grid model. We then consider the generation of equivalent 2-layer coarse grid models. With a 20-layer fine grid model, there are 19 different coarsening combinations that provide 2-layer models (plus one option for 2D → 1D). The possible coarsening schemes are listed in Table 1. In order to reduce the number of runs required, only coarsening options 5, 7, 9, 10, 11, 13, 15, 17 and 20 were considered. In the x-direction, we uniformly coarsen the 100 fine grid blocks to 20 coarse blocks. The dimensions of our coarse grid models are then 20 × 1 × 2.

Before each of these options was run, the values of the six sub-grid quantities were calculated based on the saturation, velocity and permeability distributions of the fine grid model. Each of the 2-layer coarse models was then run and the results were compared with the fine grid performance to quantify the error. The results for the four cases are discussed below.

Coarse grid models using rock curves. The results in Table 2 summarise the performance of each coarsening method (using rock curves) for each of the test cases. Figures 2a and 2b present graphically the performance for representative Case IV. In Cases I and II, $k_z = 0$, and hence gravitational effects are absent. The correlations between rms error and sub-grid quantities (R^2) for these cases are for the most part higher for σ_{vS} and σ^2_S ($\sigma_{kS} = 0$ in this case) than for C_v in vS and C_v in S_g. The high correlations observed for σ_{vS} and σ^2_S are consistent with previous results.[7,8]

The tendencies observed for Cases I and II are less apparent in Cases III and IV. In fact, Case III shows higher correlations with the C_v quantities than for the corresponding quantities computed in terms of σ. However, the differences are relatively slight (average R^2 of 0.97 versus 0.84). For Case IV, we observe the opposite behavior; namely, the error shows higher correlations with σ quantities than with C_v quantities. In this case, the differences in R^2 for the measures are more significant; 0.88 versus 0.51. Taken in total, we can conclude from Cases I-IV that the error in general correlates more closely with σ_{vS}, σ^2_S and σ_{kS}. Were we to use all three moments together, we could generate relationships between rms error and sub-grid quantities of greater R^2 than those in the Table 2.

Coarse grid models using pseudo functions. The procedure here is the same as that applied in the previous section except that the coarse grid models now use pseudo functions generated by the TW method. The results in Table 3 summarise the performance of the six sub-grid measures for each of the test cases and Figures 3a and 3b show the same results graphically for the representative Case IV. Several interesting observations emerge from these data.

Most notably, the magnitude of the error produced using the TW pseudo functions is less in all cases than that observed when using the rock curves directly. In fact, the error using pseudo relative permeabilities for any coarsening of the 20-layer system to a 2-layer coarse grid model is less than the error in the best case using rock curves. This is illustrated in Figure 4 for Case III (for which the rock curves are the least accurate of any of the four cases). The results in this figure clearly demonstrate the sensitivity of the coarse scale simulation results to the grid structure when rock curves are used. However, when pseudo functions are used, the magnitude of the error is much smaller. This might be expected, since the pseudo functions are computed for each specific grid from global fine scale simulations. This finding is consistent with the results of Wallstrom et al.[11] who found that the use of non-uniform coarsening methods[12] together with renormalised relative permeabilities[13] (computed from local fine scale problems) gave better results compared to the use of non-uniform coarsening alone.

Having demonstrated that the error using pseudo functions is relatively small, we now consider the correlations of this error with the C_v and σ quantities. A summary of these results is shown in Table 3. Although there are a few exceptions, errors using pseudo functions correlate more closely in general with the C_v quantities than with the σ quantities. This is most apparent for Case IV, for which the σ quantities display particularly low R^2 values. This observation is in contrast to the results using rock curves presented above.

The reason why the error correlates more closely with σ quantities when rock curves are used but more closely with C_v quantities when pseudo functions are used is not entirely clear. It is however quite reasonable that the precise forms of the sub-grid effects that best correlate with the error change when we go from rock curves to pseudo relative permeabilities. This is because pseudo functions are specifically designed to capture sub-grid effects, so the exact form of the error using pseudo functions would be expected to differ from that observed when sub-grid effects are not modelled at all. Further work will be required, however, to better understand these differences.

Fine grid models using coarse grid permeabilities and rock curves. As discussed in the Introduction, pseudo functions act both to capture the effects of sub-grid heterogeneity on the fluid flow and to correct for numerical dispersion. In this section, we evaluate and quantify the effects of numerical dispersion in our coarse grid models.

This is accomplished as follows. For each coarsening scheme, we make an additional run of fine grid models using coarse scale absolute permeability (defined over the same regions as in the coarse models) and the rock curve relative permeabilities. The difference in the results between these models and the coarse grid models using rock curves described above will reflect the effect of numerical dispersion. On the other hand, the difference between these models and the coarse-scale models using pseudo functions will quantify the effect of sub-grid heterogeneity on two-phase flow. Thus, from these results we can distinguish the extent to which the pseudo functions correct for numerical dispersion versus the degree to which they capture the effects of heterogeneity.

Detailed results comparing the errors due to numerical dispersion to the errors caused by using rock curves rather than pseudo functions are listed in Table 4. The results in Table 4 show quite clearly that numerical dispersion plays a relatively minor role in these test models. Most of the improvement is due to the ability of pseudo functions to capture the interactions between the small-scale multi-phase fluid flow and the heterogeneity of the porous media. This point is illustrated in Figure 5 for Case I (for the 2D → 1D coarsening scheme). From this figure, we see that there is only a slight difference between the performance of the coarse grid model using rock relative permeability curves and the fine grid model using the averaged absolute permeability and rock relative permeability curves. However, if we use pseudo functions in the coarse grid model, significant improvement is observed.

Application of the Non-uniform Coarsening Scheme in Multi-layered 2D → 2D Upscaling

In the previous section, we considered the coarsening of 20-layer (fine grid) models to 2-layer (coarse grid) models, using both rock curves and pseudo functions on the coarse scale. In this section, we consider coarsening these same 20-layer models to systems containing more than 2 layers. Our intent here is to determine if the coarsening approach used in the previous section applies equally to multi-layer systems. We consider only the use of pseudo functions at the coarse scale in this portion of the study.

The results of the previous section (Table 3) demonstrate, in general, reasonably good correlations of rms error with C_v in vS, C_v in S_g and, in cases involving gravitational effects, C_v in kS. The use of all three of these quantities together would probably provide the most accurate estimation of rms error. However, rather than form a correlation involving all three quantities, for present purposes we will simply use C_v in S_g to estimate error. We choose C_v in S_g because it is applicable in cases both with and without gravity and because it always provides at least a moderate coefficient of determination (minimum R^2 of 0.60 for the cases considered). In this section, we will test the conjecture that C_v in S_g can be used to correlate error in more general multi-layer cases.

Our approach here is to use C_v in S_g, determined from fine grid simulations, to guide the determination of the number of coarse grid layers as well as their configuration. We assess the applicability and accuracy of this approach through detailed numerical calculations. In order to investigate the compatibility of this coarsening scheme with other dynamic pseudo generation methods, both the TW and the Kyte and Berry methods are used.

Coarsening scheme. The same four test models described in the previous section were used for this purpose. A simple

computer programme was developed to determine every possible layering combination of the fine grid model, given the number of layers specified for the coarse grid model. Based on a single fine grid calculation, this program also calculated the corresponding C_v in S_g for each of the coarsening options and then sorted these values to obtain the maximum and the minimum. The number of possible coarsening options can be obtained using the following expression:

$$\text{No. of possible coarsening options} = \frac{(n-1)!}{(m-1)!(n-m)!}, \qquad (8)$$

where m is the number of the coarse grid layers and n is the number of the fine grid layers (in all of these cases, $n = 20$). It is clear from Eq. (8) that the number of possible coarsening options increases sharply (from both directions) toward a maximum at $m = 10$. Therefore, to reduce the total number of simulations, no attempt was made to verify the new coarsening method using more than seven layers in the coarse grid model. The results for all the test models are discussed below.

Discussion of the results. Tables 5 and 6 summarise the layer combinations that produce the minimum and the maximum C_v in S_g, respectively, for each of the test cases (for 2, 3 and 4 coarse grid layers). In these two tables, s1 denotes the number of the fine grid layer at the start of the first coarse grid layer, e1 denotes the number of the fine grid layer at the end of the first coarse grid layer, and so on. For comparative purposes, the gas saturation plots for all of the fine grid runs (Case I to Case IV) are shown in Figures 6a to 6d.

For Cases III and IV, where $k_v/k_h > 0$, no attempt was made to coarsen the fine grid models into 3-layer (or 5-layer) coarse models. This was because these coarsening schemes produce at least one coarse grid layer containing an even number of fine grid layers, but both pseudo generation methods require an odd number of layers in calculating pseudo functions in the vertical direction. Though the methods could be modified to handle these situations, the required averaging process may introduce an additional source of error. We note that in Cases I and II, where $k_v/k_h = 0$, pseudo functions are not required in the vertical direction, so coarse grids with even numbers of layers were considered.

Taking Case I as a representative case, we plot two figures to illustrate our findings (Figures 7a and 7b). In Figure 7a, we plot the average C_v in S_g together with the normalised rms error in oil recovery factor using the Kyte and Berry (KB) and the TW pseudo generation methods versus the number of coarse grid layers. This is shown using two examples of possible coarsening schemes. Specifically, we use the layer combinations that produce the maximum and the minimum values of C_v in S_g; i.e. the predicted worst and best layer combinations for upscaling. In Figure 7b, we plot the rms error calculated using both of the pseudo methods (KB and TW) versus their respective C_v in S_g for both of the coarsening options. Results for the other three cases are summarised and tabulated in Table 7. We now consider each case in more detail.

Case I, $k_v/k_h = 0.0$: This case was selected to show gas over-riding (Figure 6a) and no cross flow between the 20 fine grid layers. Figure 7a shows the C_v in S_g and the rms error versus the number of coarse grid layers for the best and worst grouping of layers in the coarse grid calculations. These results show that the performance of the pseudo functions does not necessarily improve as the number of the coarse grid layers is increased. The accuracy of both of the pseudo methods (KB and TW) in this 2D → 2D coarsening scheme will also depend on the configuration of the layering scheme adopted for the coarse grid models. For this particular case, the performance of the 2-layer coarse grid model using the layering scheme with the minimum value of C_v in S_g is far better than the 7-layer coarse grid model with the maximum value of C_v in S_g. The performance trend versus the number of coarse grid layers for both of the pseudo methods is very similar.

The results can be seen from another perspective as shown in Figure 7b where the rms error versus the C_v in S_g is plotted. This figure demonstrates that both of the pseudo methods produce errors that correlate directly with the calculated C_v in S_g. In this case, both of the pseudo methods produced an R^2 of more than 0.9; the TW method produces a slightly better R^2 (0.99) compared to the Kyte and Berry method ($R^2 = 0.91$). Therefore, we can conclude that this new dynamic grid coarsening scheme can be used in conjunction not only with the TW method but also with the Kyte and Berry method (with slightly less accuracy).

Case II, $k_v/k_h = 0.0$: This case shows gas under-running (Figure 6b) with no cross flow between the 20 fine grid layers. As above, the results indicate that the accuracy of the coarse grid model depends not only on the number of coarse grid layers but also on the configuration of the layering scheme. The actual values of the rms error calculated using the Kyte and Berry method are again quite comparable to those calculated using the TW method. Table 7 shows that the Kyte and Berry method produced an R^2 of about 0.74 (an acceptable number) compared to the TW method of 0.98. The results from this case are therefore consistent with our conclusions for Case I.

Case III, $k_v/k_h = 1.0$: This model is similar to Case I except that the k_v/k_h ratio is increased to unity. Therefore, gravity cross-flow will reinforce the tendency of the permeability distribution to segregate the injected gas from the reservoir fluid (oil). In this case, the performance of both of the pseudo methods follows a similar trend. The R^2 value of about 0.99 for both methods, as shown in Table 7, indicates again that C_v in S_g can provide reasonable estimates of rms error for both methods.

Case IV, $k_v/k_h = 1.0$: This is a difficult case because the flow here is controlled by the opposing effects of the permeability distribution (decreasing upward) and gravity segregation due to the large difference in fluid densities. The R^2 values for both of the methods are relatively low; for the TW method, $R^2 = 0.63$ and for the Kyte and Berry method, R^2

= 0.48. However, if we compare the performance of Case IV to that of Case III above (in terms of the rms error), we see that the overall results are actually better for Case IV. Refer to Table 4 for further detail, where the rms error in Case IV is seen to be a factor a 3-6 less than that for Case III (for the 2-layer coarse grid models). This occurs because the combined effect of the permeability distribution and the difference in fluid densities causes the front to be much more uniform in Case IV compared to Case III (see Figures 6c and 6d).

Summary and Conclusions

In this work, we studied the relationship between sub-grid effects and the accuracy of coarse scale simulation models for layered systems. The actual sub-grid measures considered represent higher moments of fine scale variables (C_v in S_g, C_v in vS, C_v in kS, σ^2_S, σ_{kS} and σ_{vS}) and derive from a volume averaging of the fine grid saturation equation. The coarse scale simulation results, taken in total, demonstrate that the volume averaging procedure can be used to model the form of the coarse grid error. Further, we showed that the coarse grid error can be minimised by designing the coarse grid models such that certain of these higher moments are minimised. The specific sub-grid measure that best correlated with the coarse grid error was shown to vary depending on whether rock curves or pseudo functions were used in the coarse grid model.

The use of pseudo functions together with the new grid coarsening scheme provides results of significantly better accuracy than does the use of rock curves alone for the cases considered. The effects of numerical dispersion in the coarse grid models were found to be relatively small, indicating that the effectiveness of the pseudo functions results from their ability to capture the effects of fine scale heterogeneity. It is not surprising that the pseudo functions provide accurate coarse grid results for the problems considered. This is because the pseudo functions were generated through the solution of a global fine grid problem and the global boundary conditions imposed on the coarse scale problem were identical to those for the fine scale problem. It would be of interest to assess the accuracy of the pseudo functions in other cases; e.g. for coarse grid boundary conditions that differ from those used on the fine grid or in the case where the pseudo functions are computed from local (rather than global) fine scale simulations.

We also demonstrated the applicability of the new grid coarsening scheme in more general cases, where we coarsened 20 layer systems to models containing more than 2 layers. For this portion of the study, both the TW and Kyte and Berry methods were considered. We showed that the accuracy of the coarse grid descriptions for these problems depended on both the number and configuration of the layers and that the coarse grid error continued to correlate with C_v in S_g (as in the 2-layer cases). The performance of the pseudo functions for these problems did not always improve as we increased the number of coarse grid layers. The results from this portion of the study suggest that a user could optimally select the number and configuration of the coarse scale layers from a single fine grid solution. This means that the various coarse grid models need not all be simulated to determine the optimum coarse grid representation.

In future work, we plan to apply our coarsening scheme to more general heterogeneous systems. We also hope to gauge the degree of process dependence of the coarse scale descriptions generated using this methodology. This will allow us to assess the applicability of the scheme to practical reservoir simulation problems.

Acknowledgements

The authors would like to acknowledge colleagues in the informal Heriot-Watt/Imperial College/BP Amoco Upscaling discussion group for many helpful discussions, particularly Peter King, Martin Blunt, Ann Muggeridge, Mike Christie, Jonathan Hastings and Karl Stephen.

Nomenclature

C_v	= coefficient of variation
f	= fractional flow of gas
f_s, f_{ss}	= first and second derivatives of f with respect to S_g
$\mathbf{i}_z$	= unit vector in the z-direction
$\mathbf{k}$	= permeability tensor
k_{rj}	= relative permeability of phase j (j = oil, gas)
R^2	= correlation coefficient
rms error	= normalised root mean square error in oil recovery factor
S, S_g	= gas saturation
S_{gc}	= critical gas saturation
S_{org}	= residual oil saturation relative to gas
S_{wc}	= connate water saturation
t	= time
$\mathbf{v}$	= total Darcy velocity
μ_j	= viscosity of phase j
ρ_j	= density of phase j
η	= oil relative permeability times fractional flow of gas
η_s, η_{ss}	= first and second derivatives of η with respect to S_g
σ^2_S	= variance of gas saturation
σ_{vS}	= covariance of velocity-gas saturation
σ_{kS}	= covariance of permeability-gas saturation
$< >$	= volume averaged property

Superscripts

*	= functions derived from pseudo relative permeability
'	= fluctuating property

Overbar

$\bar{}$	= volume averaged property (same as $< >$)

References

1. Kyte, J.R. and Berry, D.W.: "New Pseudo Functions to Control Numerical Dispersion", SPE J., pp 269-275, August 1975.

2. Stone, H.L.: "Rigorous Black Oil Pseudo Functions", SPE 21207, Proceedings of the 11th SPE Symposium on Reservoir Simulation, Anaheim, CA, 17-20 February 1991.
3. Coats, K.H., Dempsey J.R. and Henderson J.H.: "The Use of Vertical Equilibrium in Two-Dimension Simulation of Three-Dimensional Reservoir Performance", SPE J., March 1971.
4. Darman, N.H., Sorbie, K.S. and Pickup, G.E.: "The Development of Pseudo Functions for Gravity-Dominated Immiscible Gas Displacements", SPE 51941, Proceedings of the 15th SPE Reservoir Simulation Symposium, Houston, TX, 14-17 February 1999.
5. Hewett, T.A. and Archer, R.A.: "Scale-Averaged Effective Flow Properties for Coarse-Grid Reservoir Simulation", SPE 37988, Proceedings of the 14th SPE Reservoir Simulation Symposium, Dallas, TX, 8-11 June 1997.
6. Hewett, T.A. and Yamada, T.: "Theory for the Semi-Analytical Calculation of Oil Recovery and Effective Relative Permeabilities Using Streamtubes", Adv. Water Resources, 20, pp 279-292, 1997.
7. Durlofsky, L.J.: "Coarse Scale Models of Two Phase Flow in Heterogeneous Reservoirs: Volume Averaged Equations and their Relationship to Existing Upscaling Techniques", Computational Geosciences, 2, pp 73-92, 1998.
8. Durlofsky, L.J.: "Use of Higher Moments for the Description of Upscaled, Process Independent Relative Permeabilities", SPE J., December 1997.
9. Guzman, R.E., Giordano, D., Fayers, J., Godi, A. and Aziz, K.: "The Use of Dynamic Pseudo Functions in Reservoir Simulation", Presented at the 5th International Forum on Reservoir Simulation, Muscat, Oman, 10-14 December 1994.
10. Pickup, G.E. and Stephen, K.D.: "Steady-State Scale-up Methods", Presented at the 6th European Conference on the Mathematics of Oil Recovery, Peebles, Scotland, 8-11 September 1998.
11. Wallstrom, T.C., Hou, S., Christie, M.A., Durlofsky, L.J. and Sharp, D.H.: "Application of a New Two-Phase Upscaling Technique to Realistic Reservoir Cross Sections", SPE 51939, Proceedings of the 15th SPE Reservoir Simulation Symposium, Houston, TX, 14-17 February 1999.
12. Durlofsky, L.J., Jones, R.C. and Milliken, W.J.: "A Nonuniform Coarsening Approach for the Scale Up of Displacement Processes in Heterogeneous Porous Media", Adv. Water Resources, 20, pp 335-347, 1997.
13. Christie, M.A., Mansfield, M., King, P.R., Barker, J.W. and Culverwell, I.D.: "A Renormalisation-Based Upscaling Technique for WAG Floods in Heterogeneous Reservoirs", SPE 29127, Proceeding of the 13th SPE Reservoir Simulation Symposium, San Antonio, TX, 12-15 February 1995.

Appendix: Derivation of Averaged Saturation Equation with Gravitational Effects Included

We consider an incompressible two phase system of gas and oil. With gravitational effects included, the fine scale saturation equation can be written as:

$$\frac{\partial S}{\partial t}+\mathbf{v}\cdot\nabla f-\frac{g\Delta\rho}{\mu_o}\nabla\cdot(\eta\,\mathbf{k}\cdot\mathbf{i}_z)=0, \qquad \text{(A1)}$$

where all quantities are as defined in the Nomenclature.

In order to develop the volume averaged equations, we express the saturation, velocity and permeability in Eq. (A1) in terms of averaged and fluctuating quantities. Averages in this context are volume averages (area averages in two dimensions) over the fine grid region to be coarsened into a single coarse grid block. We define averaged and fluctuating quantities via:

$$\Phi(x,z)=\overline{\Phi}+\Phi'(x,z)\ , \qquad \text{(A2)}$$

where Φ represents any variable. The overbar indicates a volume averaged quantity (constant throughout the averaging region) and the prime denotes a spatially varying fluctuating quantity. The volume average in two dimensions is defined as

$$\overline{\Phi}=\frac{1}{A}\int_D\Phi(x,z)dA\ , \qquad \text{(A3)}$$

where D denotes the region within the coarse grid block and A is the area. Introducing the fine scale variables as the sum of averaged and fluctuating components into Eq. (A1) gives:

$$\begin{aligned}&\frac{\partial\overline{S}}{\partial t}+\frac{\partial S'}{\partial t}+\overline{\mathbf{v}}\cdot\nabla\overline{f}+\overline{\mathbf{v}}\cdot\nabla f'+\mathbf{v}'\cdot\nabla\overline{f}+\mathbf{v}'\cdot\nabla f'\\&-\frac{g\Delta\rho}{\mu_o}\nabla\cdot\left\{(\overline{\mathbf{k}}\,\overline{\eta}+\overline{\mathbf{k}}\eta'+\mathbf{k}'\overline{\eta}+\mathbf{k}'\eta')\cdot\mathbf{i}_z\right\}=0\ .\end{aligned} \qquad \text{(A4)}$$

Averaging Eq. (A4), and noting that averages of singly primed terms are zero, gives the equation for $\overline{S}$,

$$\frac{\partial\overline{S}}{\partial t}+\overline{\mathbf{v}}\cdot\nabla\overline{f}+\overline{\mathbf{v}'\cdot\nabla f'}-\frac{g\Delta\rho}{\mu_o}\nabla\cdot\left\{(\overline{\mathbf{k}}\,\overline{\eta}+\overline{\mathbf{k}'\eta'})\cdot\mathbf{i}_z\right\}=0. \qquad \text{(A5)}$$

We wish to express the averaged terms involving f and η in terms of $\overline{S'S'}$, $\overline{\mathbf{v}'S'}$ and $\overline{\mathbf{k}'S'}$. We proceed by expanding $f(S)$ in a Taylor series about $\overline{S}$; i.e.

$$f(S)\approx f(\overline{S})+f_s(\overline{S})(S-\overline{S})+\frac{1}{2}f_{ss}(\overline{S})(S-\overline{S})^2+... \qquad \text{(A6)}$$

where $f_s(\overline{S})=df/dS$ evaluated at $\overline{S}$ and $f_{ss}(\overline{S})=d^2f/dS^2$ evaluated at $\overline{S}$. Now, neglecting higher order terms, identifying $S'=S-\overline{S}$, and averaging, we can obtain the following expression for $\overline{f}$:

$$\overline{f}\approx f(\overline{S})+\frac{1}{2}f_{ss}(\overline{S})\overline{S'S'}\ . \qquad \text{(A7)}$$

Similarly, f' can be computed as

$$f'\approx f_s(\overline{S})S'+\frac{1}{2}f_{ss}(\overline{S})(S'S'-\overline{S'S'})\ . \qquad \text{(A8)}$$

From Eq. (A8), we can approximate $\overline{\mathbf{v}'f'}$ as:

$$\overline{\mathbf{v}'f'}\approx f_s(\overline{S})\overline{\mathbf{v}'S'}+\frac{1}{2}f_{ss}(\overline{S})\overline{\mathbf{v}'S'S'}\ . \qquad \text{(A9)}$$

We can express $\bar{\eta}$ using a similar approach. This allows us to write:

$$\bar{\eta} \approx \eta(\bar{S}) + \frac{1}{2}\eta_{ss}(\bar{S})\overline{S'S'}, \tag{A10}$$

$$\eta' \approx \eta_s(\bar{S})S' + \frac{1}{2}\eta_{ss}(\bar{S})(S'S' - \overline{S'S'}) \; . \tag{A11}$$

Introducing the above expressions into the averaged saturation equation (A5) and retaining terms to first order in fluctuating quantities (i.e. we neglect terms involving the products of three fluctuating quantities) gives the following equation:

$$\begin{aligned} &\frac{\partial \bar{S}}{\partial t} + \bar{\mathbf{v}} \cdot \nabla f(\bar{S}) + \frac{1}{2}\bar{\mathbf{v}} \cdot \nabla\left\{f_{ss}(\bar{S})\overline{S'S'}\right\} + \nabla \cdot \left\{f_s(\bar{S})\overline{\mathbf{v}'S'}\right\} \\ &- \frac{g\Delta\rho}{\mu_o}\nabla \cdot \left\{(\bar{\mathbf{k}}\eta(\bar{S}) + \frac{1}{2}\eta_{ss}(\bar{S})\bar{\mathbf{k}}\,\overline{S'S'} + \eta_s(\bar{S})\overline{\mathbf{k}'S'}) \cdot \mathbf{i}_z\right\} = 0. \end{aligned} \tag{A12}$$

This equation, identical to Eq. (3) in the main text, is the desired result; i.e. the averaged saturation equation expressed in terms of the moments $\overline{S'S'}$, $\overline{\mathbf{v}'S'}$ and $\overline{\mathbf{k}'S'}$.

Option	Coarse grid layer 1 is from fine grid :	Coarse grid layer 2 is from fine grid :
1	Layer 1 through 1	layer 2 through 20
:	:	:
19	Layer 1 through 19	layer 20 through 20
20	Fine grid layer 1 through 20	

Table 1: Possible options in 20-layer → 2-layer coarsening.

Cases	σ^2_s	σ_{vs}	σ_{ks}	C_v in S_g	C_v in vS	C_v in kS
Case I	0.9899	0.9406	-	0.4848	0.9583	-
Case II	0.6447	0.9099	-	0.3965	0.3600	-
Case III	0.8161	0.8109	0.9058	0.9856	0.9755	0.9547
Case IV	0.8254	0.8711	0.9503	0.5176	0.6474	0.3776
Average	**0.8190**	**0.8831**	**0.9281**	**0.5961**	**0.7353**	**0.6662**

Table 2: Coefficient of determination (R^2) between rms error and sub-grid quantities using rock curves in the coarse grid models.

Cases	σ^2_s	σ_{vs}	σ_{ks}	C_v in S_g	C_v in vS	C_v in kS
Case I	0.8757	0.6792	-	0.7754	0.9518	-
Case II	0.8774	0.3723	-	0.9691	0.8883	-
Case III	0.8725	0.8673	0.9470	0.9604	0.9443	0.9127
Case IV	0.2274	0.0001	0.0451	0.6017	0.3975	0.7059
Average	**0.7133**	**0.4797**	**0.4961**	**0.8267**	**0.7955**	**0.8093**

Table 3: Coefficient of determination (R^2) between rms error and sub-grid quantities using pseudo functions in the coarse grid models.

Coarsening options		5	7	9	11	13	15	17	20
Coarse grid with rock curve	Case I	6.23e-3	9.38e-3	1.87e-2	3.08e-2	4.46e-2	5.95e-2	7.49e-2	9.80e-2
	Case II	5.50e-2	4.10e-2	2.83e-2	1.74e-2	9.53e-3	1.23e-2	3.35e-2	9.16e-2
	Case III	6.45e-2	8.66e-2	1.11e-1	1.38e-1	1.65e-1	1.94e-1	2.23e-1	2.67e-1
	Case IV	2.23e-2	1.83e-2	1.59e-2	1.58e-2	1.85e-2	2.39e-2	3.19e-2	3.33e-2
Coarse grid with pseudo functions	Case I	2.04e-3	5.91e-4	9.34e-4	1.26e-3	2.21e-3	3.12e-3	4.03e-3	5.29e-3
	Case II	2.91e-3	2.08e-3	1.37e-3	1.06e-3	1.99e-3	3.12e-3	4.20e-3	5.11e-3
	Case III	2.07e-3	3.77e-3	6.28e-3	8.20e-3	1.00e-2	1.19e-2	1.37e-2	1.64e-2
	Case IV	4.69e-4	6.56e-4	1.05e-3	1.62e-3	2.46e-3	3.56e-3	2.74e-3	1.09e-3
Fine grid with averaged absolute permeability	Case I	9.13e-3	1.05e-2	2.00e-2	3.24e-2	4.64e-2	6.14e-2	7.70e-2	1.00e-1
	Case II	5.67e-2	4.26e-2	2.96e-2	1.84e-2	1.06e-2	1.55e-2	3.77e-2	9.40e-2
	Case III	5.47e-2	7.93e-2	1.07e-1	1.36e-1	1.65e-1	1.95e-1	2.25e-1	2.71e-1
	Case IV	1.93e-2	1.38e-2	1.15e-2	1.50e-2	2.17e-2	2.78e-2	2.96e-2	3.49e-2
Effect of numerical dispersion (absolute %)	Case I	29.00	10.51	6.58	5.04	4.00	3.17	2.87	2.58
	Case II	3.08	3.74	4.40	5.37	11.10	20.41	11.19	2.67
	Case III	15.61	8.81	4.54	1.71	0.006	0.70	1.00	1.75
	Case IV	13.41	25.24	29.58	5.71	14.29	13.86	7.81	4.52
Effect of sub-grid heterogeneity on 2-phase flow (absolute %)	Case I	71.00	89.49	93.42	94.96	96.00	96.83	97.13	97.42
	Case II	96.92	96.26	95.60	94.63	88.90	79.59	88.81	97.33
	Case III	84.39	91.19	95.46	98.29	99.94	93.30	99.00	98.25
	Case IV	86.59	74.76	70.42	94.29	85.71	86.14	92.19	95.48

Table 4: Rms error and quantification of effects of using pseudo functions for all the test cases

	2-layer coarse grid models				3-layer coarse grid models						4-layer coarse grid models							
	s1	e1	s2	e2	s1	e1	s2	e2	s3	e3	s1	e1	s2	e2	s3	e3	s4	e4
Case I	1	9	10	20	1	4	5	10	11	20	1	3	4	7	8	11	12	20
Case II	1	8	9	20	1	6	7	11	12	20	1	5	6	9	10	13	14	20
Case III	1	5	6	20	-	-	-	-	-	-	1	3	4	4	5	7	8	20
Case IV	1	5	6	20	-	-	-	-	-	-	1	1	2	4	5	9	10	20

Table 5: The best coarsening options (configurations that produce the minimum C_v in S_g)

	2-layer coarse grid models				3-layer coarse grid models						4-layer coarse grid models							
	s1	e1	s2	e2	s1	e1	s2	e2	s3	e3	s1	e1	s2	e2	s3	e3	s4	e4
Case I	1	19	20	20	1	18	19	19	20	20	1	17	18	18	19	19	20	20
Case II	1	19	20	20	1	18	19	19	20	20	1	17	18	18	19	19	20	20
Case III	1	19	20	20	-	-	-	-	-	-	1	17	18	18	19	19	20	20
Case IV	1	17	18	20	-	-	-	-	-	-	1	17	18	18	19	19	20	20

Table 6: The worst coarsening options (configurations that produce the maximum C_v in S_g)

Cases	Kyte and Berry	TW
Case I	0.9145	0.9873
Case II	0.7392	0.9843
Case III	0.9897	0.9916
Case IV	0.4763	0.6297

Table 7: The R^2 of rms error vs. C_v in S_g for Case I through Case IV

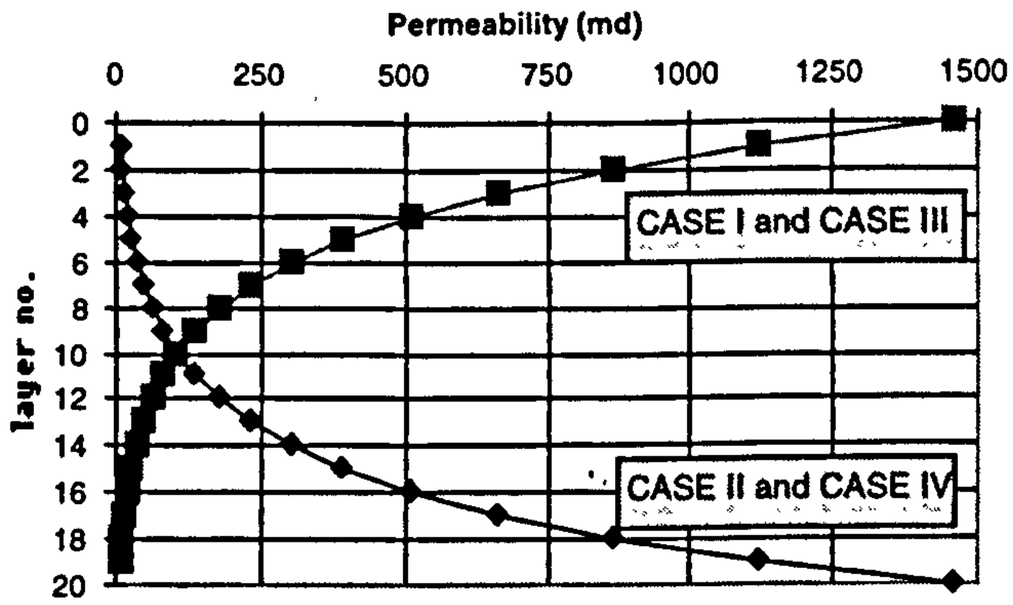

Figure 1: Permeability distributions for Case I to Case IV.

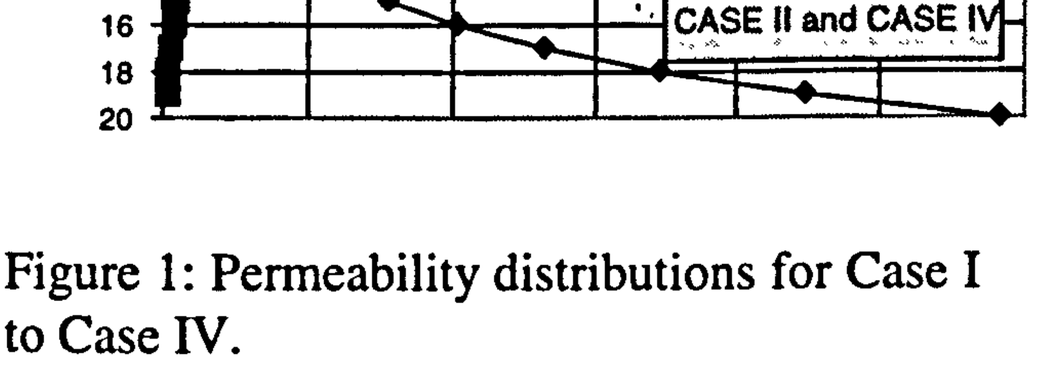

Figure 2a: Fluctuating moments in the form of σ vs. rms error (CaseIV, using rock curves)

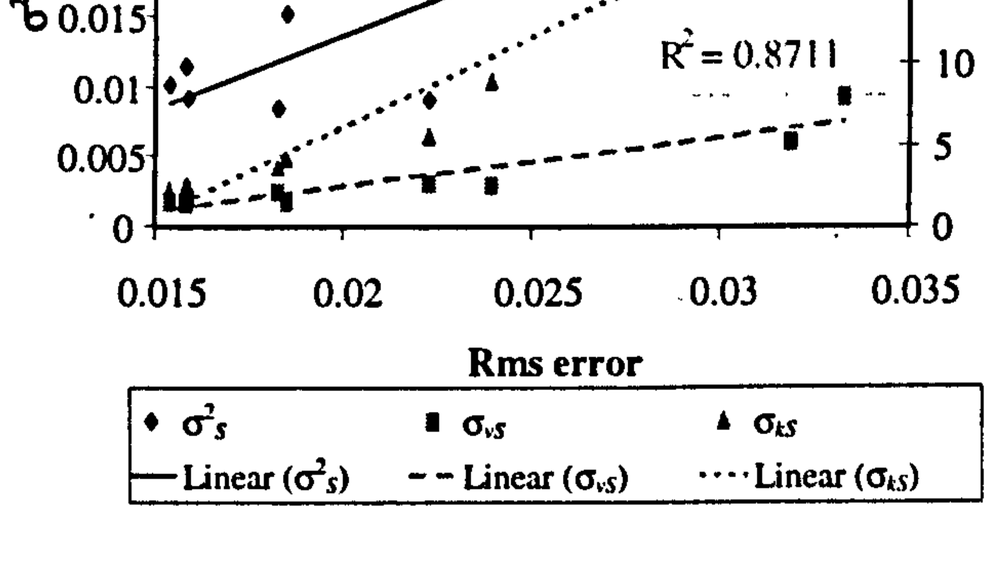

Figure 2b: Fluctuating moments in the form of C_v vs. rms error (Case IV, using rock curves)

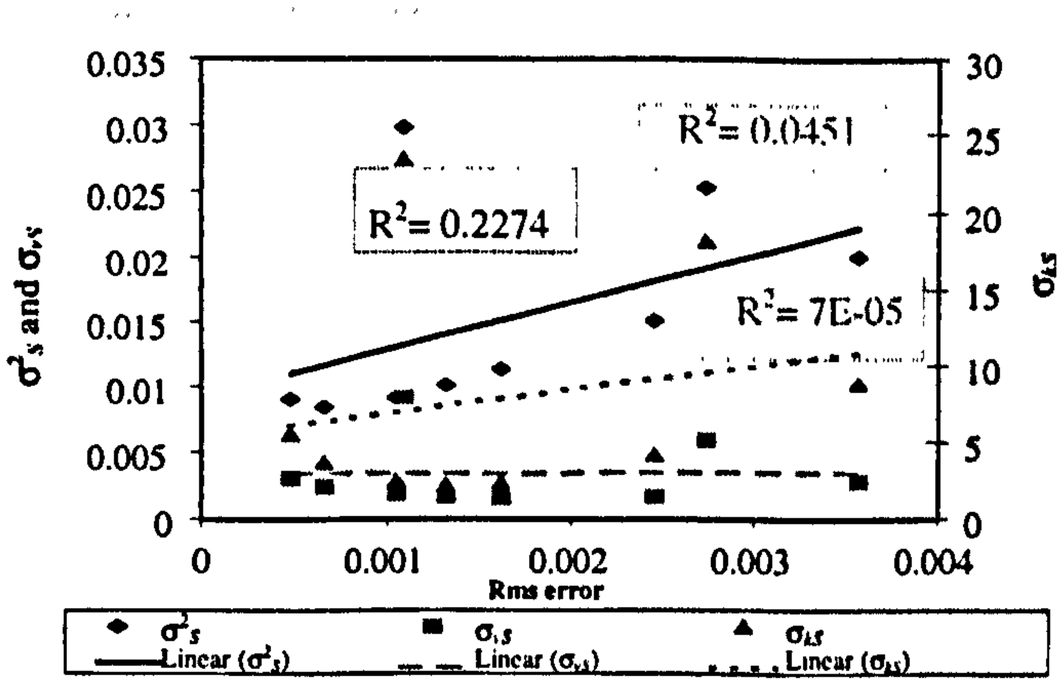

Figure 3a: Fluctuating moments in the form of σ vs. rms error (Case IV, using pseudo)

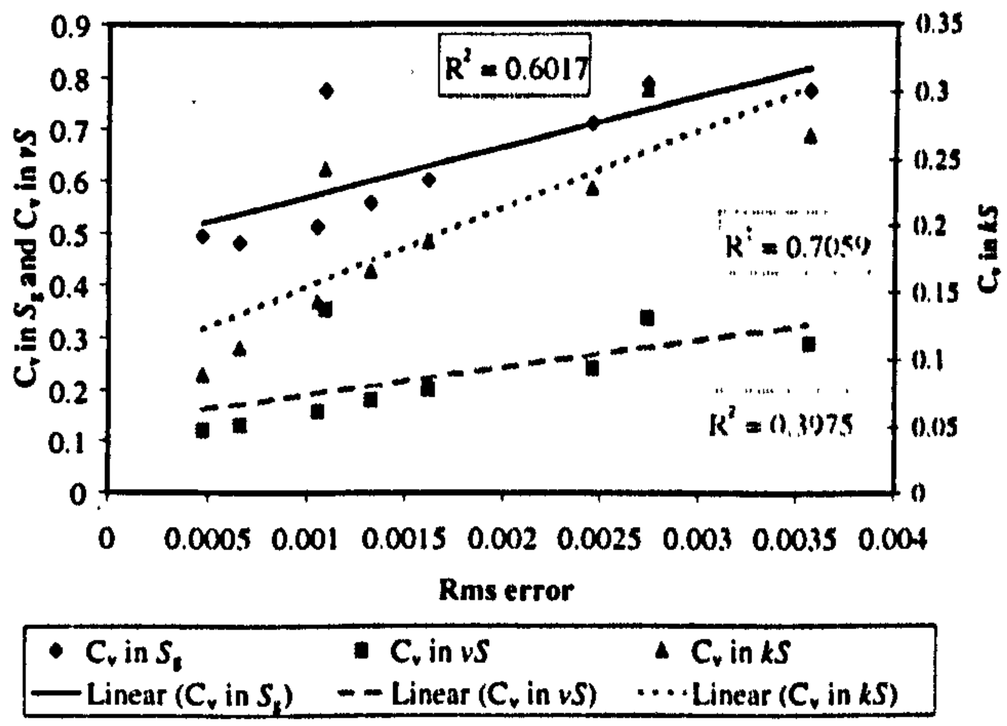

Figure 3b: Fluctuating moments in the form of C_v vs. rms error (Case IV, using pseudo)

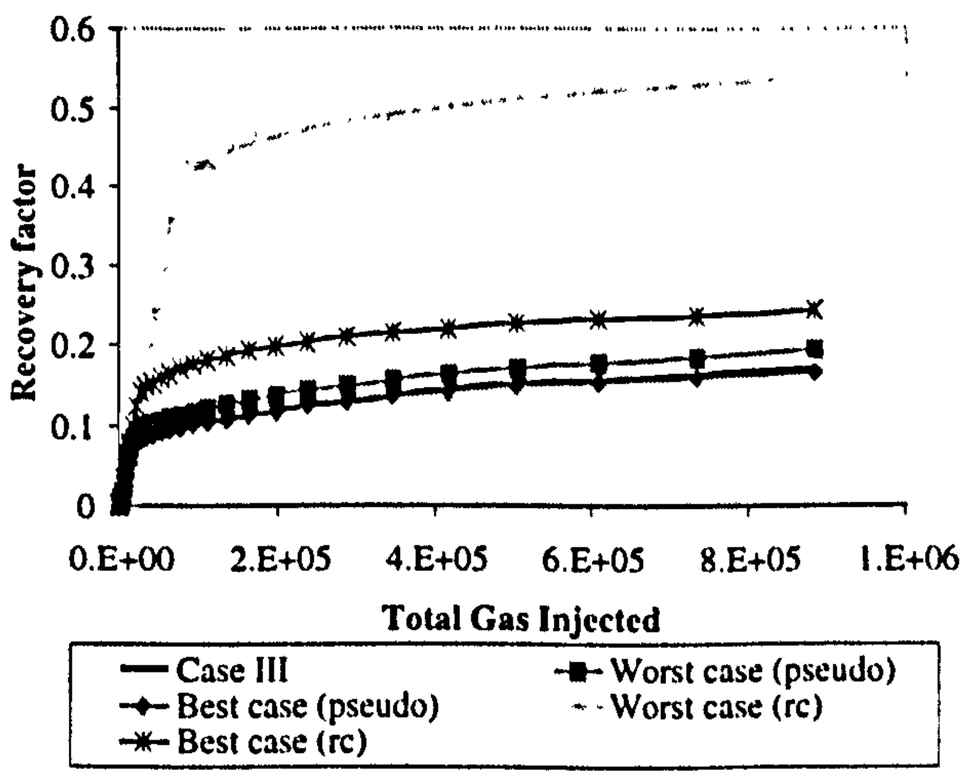

Figure 4: Oil recovery factor vs. total gas injected for Case III.

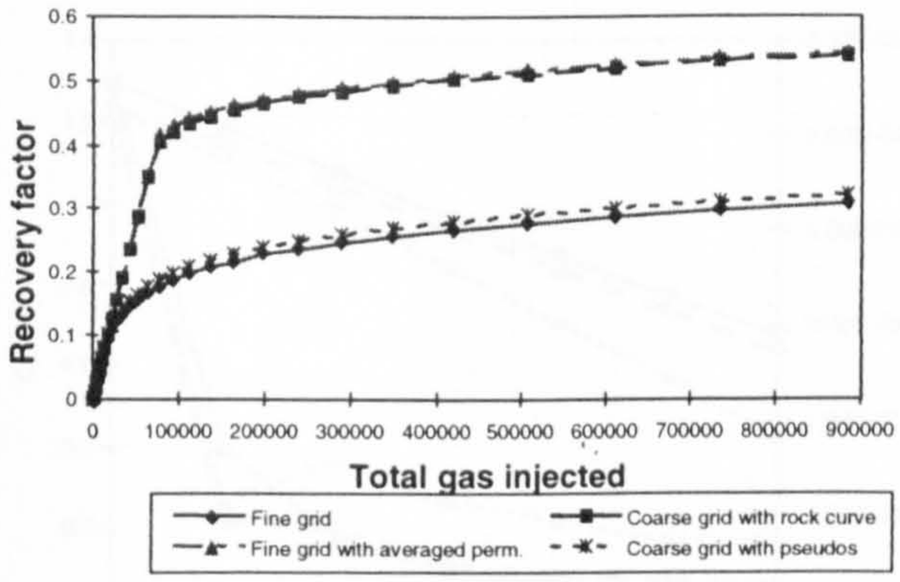

Figure 5: Recovery factor vs. total gas injected for Case I.

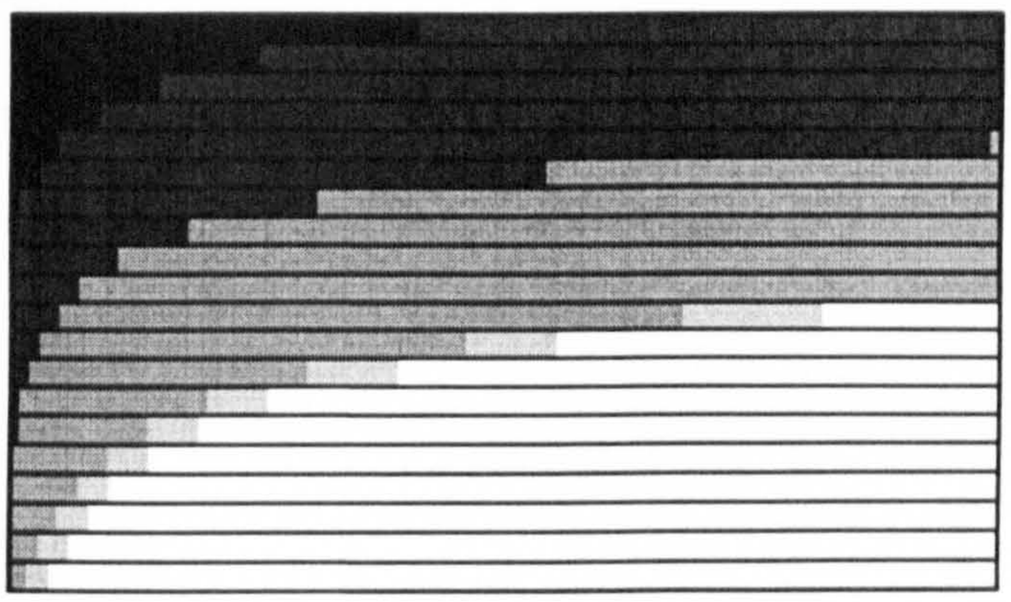

Figure 6a: Gas saturation plot at 4 PVI (Case I)

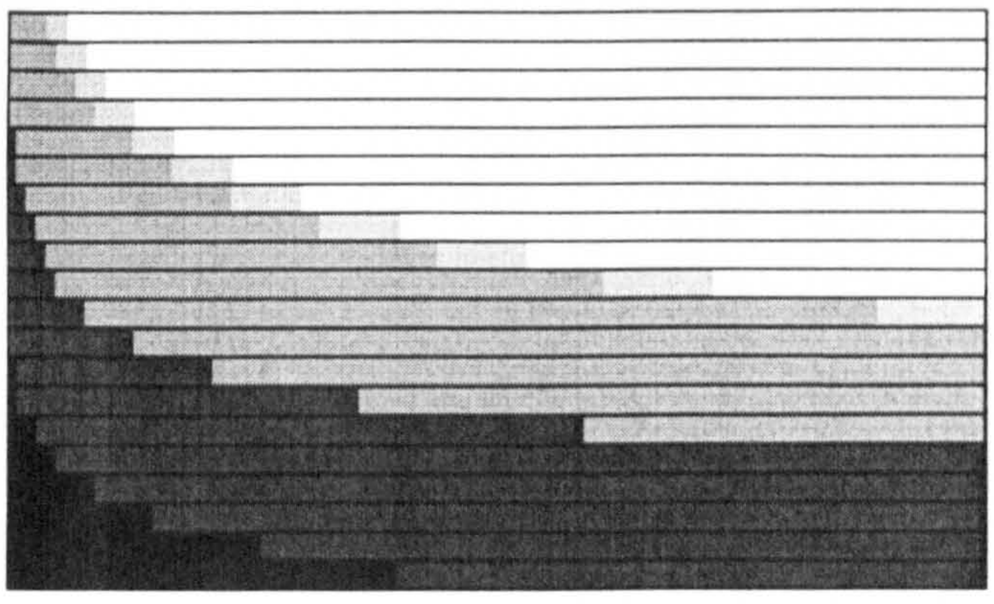

Figure 6b: Gas saturation plot at 4 PVI (Case II)

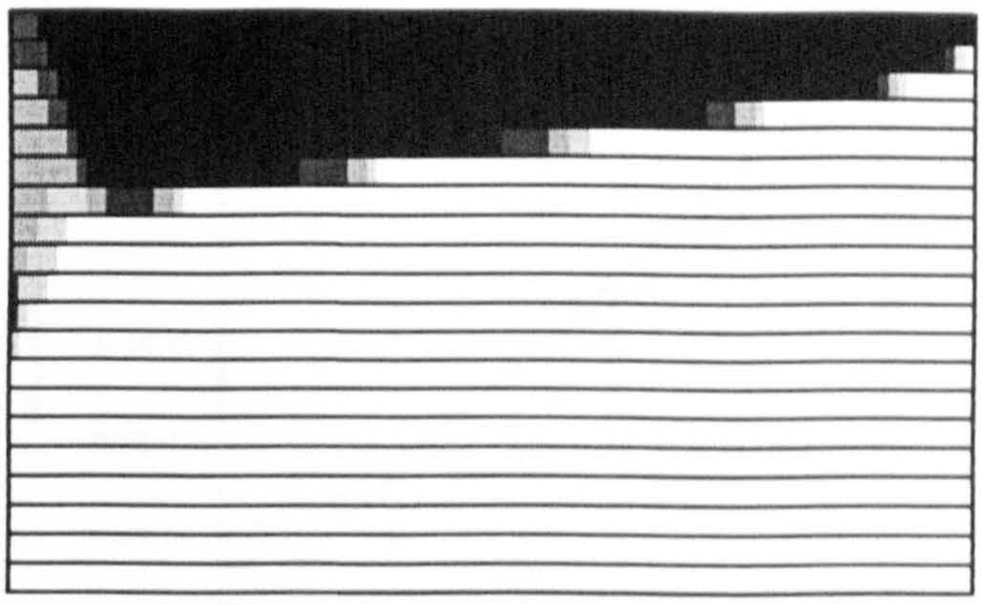

Figure 6c: Gas saturation plot at 4 PVI (Case III)

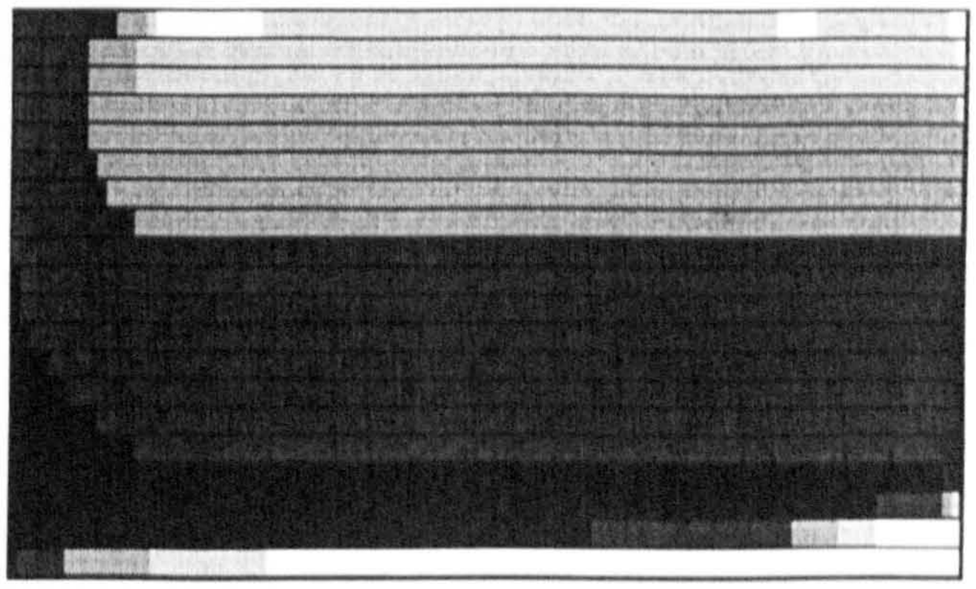

Figure 6d: Gas saturation plot at 4 PVI (Case IV)

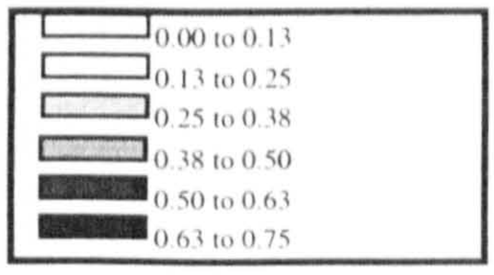

Saturation index for Figures 6a to 6d.

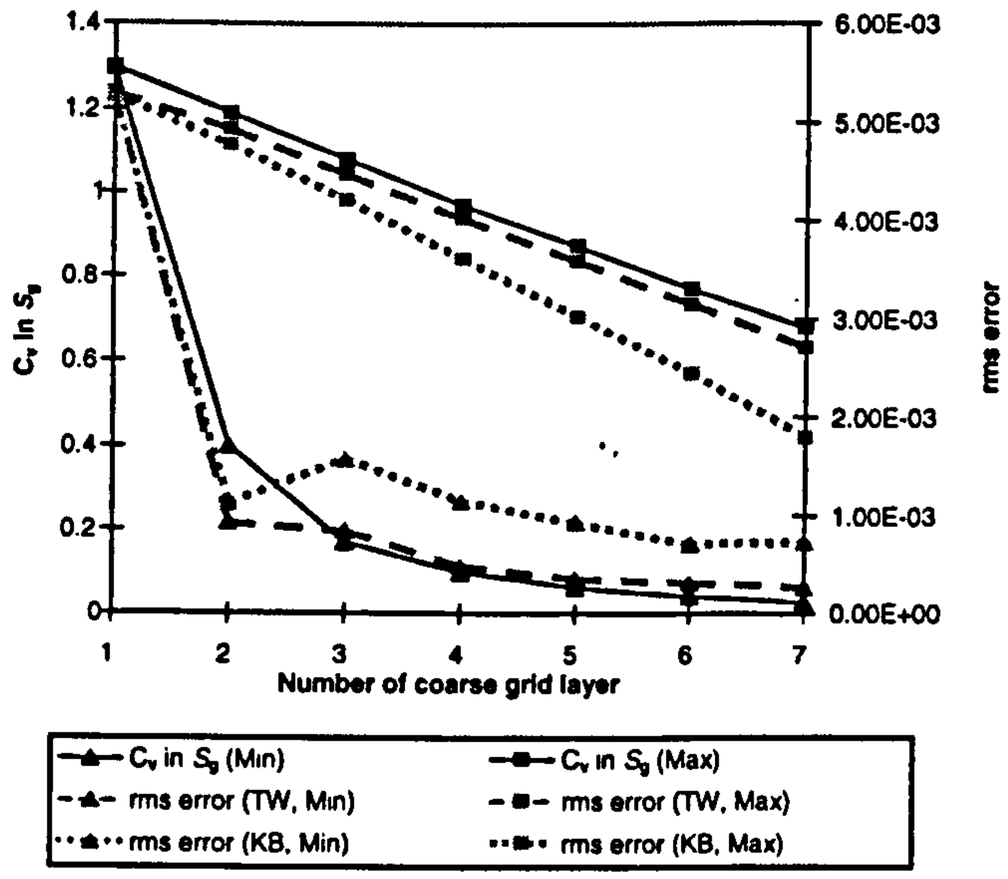

Figure 7a: C_v in S_g and rms error vs. no. of coarse grid layers (Case I)

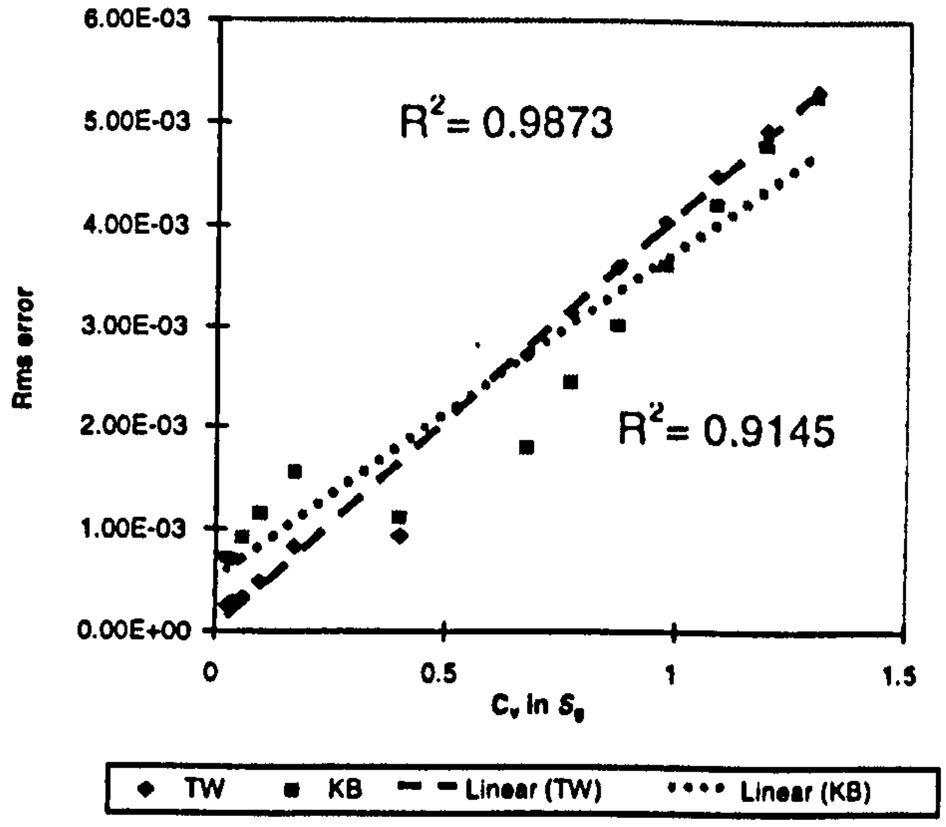

Figure 7b: Rms error vs. C_v in S_g (Case I)

APPENDIX III

PROGRAM PSEUDO

```
C ***************************************************************
C        THIS PROGRAM WILL CALCULATE PSEUDO FUNCTIONS FOR EVERY
C            COARSE GRIDBLOCKS KNOWING THE COARSENING SCHEME.
C
C           THERE ARE FOUR PSEUDO METHODS THAT ARE AVAILABLE:
C              1. THE ORIGINAL TPW METHOD
C              2. THE MODIFIED TW METHOD
C              3. THE PORE VOLUME WEIGHTED METHOD
C              4. THE HEWETT AND ARCHER METHOD
C
C  TO KNOW THE COARSENING SCHEME PLEASE RUN THE COARSENING.EXE FILE
C                          (APPENDIX IV)
C
C
C                    BY : NASIR HAJI DARMAN
C           HERIOT-WATT UNIVERSITY / PETRONAS RESEARCH
C
C                  LAST UPDATE : 20 / 1 / 2000
C***************************************************************


IMPLICIT NONE


INTEGER Z,XDIMF,YDIMF,ZDIMF,NCOL,TGBF,A,B,C,SK
INTEGER XDIMC,YDIMC,ZDIMC,TGBC,NN,JJ,N,ZZ
INTEGER I,J,K,N,P,PP,TS,L,OPT,TSTEP,SKIPLINE
INTEGER XDIMF1,YDIMF1,ZDIMF1,XDIMC1,YDIMC1,ZDIMC1
INTEGER TSTEP1,TGBF1,OPT1,NAS,NAS1,OPT2,NOY

REAL TEMP1,TEMP2,TEMP3,TEMP4,TEMP5,TEMP6,TEMP7,TEMP8,TEMP9
REAL OILVISCBAR,GASVISCBAR,GRA,TEMP10,TEMP11,TEMP12,TEMP13

PARAMETER (XDIMF1=200,YDIMF1=50,ZDIMF1=50)
PARAMETER (XDIMC=100,YDINC=50, ZDIMC=50)
PARAMETER (TSTEP1=30,TGBF1=500000)

INTEGER LIMLX(XDIMC1+1,YDIMC1+1,ZDIMC1+1)
INTEGER LIMHX(XDIMC1+1,YDIMC1+1,ZDIMC1+1)
INTEGER LIMLY(XDIMC1+1,YDIMC1+1,ZDIMC1+1)
INTEGER LIMHY(XDIMC1+1,YDIMC1+1,ZDIMC1+1)
INTEGER LIMLZ(XDIMC1+1,YDIMC1+1,ZDIMC1+1)
INTEGER LIMHZ(XDIMC1+1,YDIMC1+1,ZDIMC1+1)
INTEGER CCX(XDIMC1+1,YDIMC1+1,ZDIMC1+1)
INTEGER CCY(XDIMC1+1,YDIMC1+1,ZDIMC1+1)
INTEGER CCZ(XDIMC1+1,YDIMC1+1,ZDIMC1+1)
INTEGER SCHEME(0:ZDIMC1)

REAL PRESS(0:TSTEP1+1,TGBF1+1)
REAL PRESM(0:TSTEP1+1,XDIMF1+1,YDIMF1+1,ZDIMF1+1)
REAL SGASS(0:TSTEP1+1,TGBF1+1)
REAL SGASM(0:TSTEP1+1,XDIMF1+1,YDIMF1+1,ZDIMF1+1)
REAL FLOOILIPS(0:TSTEP1+1,TGBF1+1)
REAL FLOOILIPM(0:TSTEP1+1,XDIMF1+1,YDIMF1+1,ZDIMF1+1)
REAL FLOGASIPS(0:TSTEP1+1,TGBF1+1)
REAL FLOGASIPM(0:TSTEP1+1,XDIMF1+1,YDIMF1+1,ZDIMF1+1)
REAL FLOOILJPS(0:TSTEP1+1,TGBF1+1)
REAL FLOOILJPM(0:TSTEP1+1,XDIMF1+1,YDIMF1+1,ZDIMF1+1)
REAL FLOGASJPS(0:TSTEP1+1,TGBF1+1)
REAL FLOGASJPM(0:TSTEP1+1,XDIMF1+1,YDIMF1+1,ZDIMF1+1)
REAL FLOOILKPS(0:TSTEP1+1,TGBF1+1)
REAL FLOOILKPM(0:TSTEP1+1,XDIMF1+1,YDIMF1+1,ZDIMF1+1)
REAL FLOGASKPS(0:TSTEP1+1,TGBF1+1)
REAL FLOGASKPM(0:TSTEP1+1,XDIMF1+1,YDIMF1+1,ZDIMF1+1)
REAL FIPOILS(0:TSTEP1+1,TGBF1+1)
REAL FIPOILM(0:TSTEP1+1,XDIMF1+1,YDIMF1+1,ZDIMF1+1)
REAL FIPGASS(0:TSTEP1+1,TGBF1+1)
REAL FIPGASM(0:TSTEP1+1,XDIMF1+1,YDIMF1+1,ZDIMF1+1)
REAL OILPOTNS(0:TSTEP1+1,TGBF1+1)
REAL OILPOTNM(0:TSTEP1+1,XDIMF1+1,YDIMF1+1,ZDIMF1+1)
REAL OILVISCS(0:TSTEP1+1,TGBF1+1)
REAL OILVISCM(0:TSTEP1+1,XDIMF1+1,YDIMF1+1,ZDIMF1+1)
REAL GASPOTNS(0:TSTEP1+1,TGBF1+1)
REAL GASPOTNM(0:TSTEP1+1,XDIMF1+1,YDIMF1+1,ZDIMF1+1)
REAL GASVISCS(0:TSTEP1+1,TGBF1+1)
REAL GASVISCM(0:TSTEP1+1,XDIMF1+1,YDIMF1+1,ZDIMF1+1)
REAL POTCORRS(0:TSTEP1+1,TGBF1+1)
REAL POTCORRM(0:TSTEP1+1,XDIMF1+1,YDIMF1+1,ZDIMF1+1)
REAL KROS(0:TSTEP1+1,TGBF1+1)
REAL KROM(0:TSTEP1+1,XDIMF1+1,YDIMF1+1,ZDIMF1+1)
REAL KRGS(0:TSTEP1+1,TGBF1+1)
REAL KRGM(0:TSTEP1+1,XDIMF1+1,YDIMF1+1,ZDIMF1+1)
REAL PVS(TGBF1+1) ,PVM(XDIMF1+1, YDIMF1+1,ZDIMF1+1)
REAL DXS(TGBF1+1) ,DXM(XDIMF1+1, YDIMF1+1,ZDIMF1+1)
REAL DYS(TGBF1+1) ,DYM(XDIMF1+1, YDIMF1+1,ZDIMF1+1)
REAL DZS(TGBF1+1) ,DZM(XDIMF1+1, YDIMF1+1,ZDIMF1+1)
REAL PERMXS(TGBF1+1) ,PERMXM(XDIMF1+1, YDIMF1+1,ZDIMF1+1)
```

```
REAL PERMYS(TGBF1+1) ,PERMYM(XDIMF1+1, YDIMF1+1,ZDIMF1+1)
REAL PERMZS(TGBF1+1) ,PERMZM(XDIMF1+1, YDIMF1+1,ZDIMF1+1)
REAL MULTXS(TGBF1+1) ,MULTXM(XDIMF1+1, YDIMF1+1,ZDIMF1+1)
REAL MULTYS(TGBF1+1) ,MULTYM(XDIMF1+1, YDIMF1+1,ZDIMF1+1)
REAL MULTZS(TGBF1+1) ,MULTZM(XDIMF1+1, YDIMF1+1,ZDIMF1+1)
REAL POROS(TGBF1+1) ,POROM(XDIMF1+1, YDIMF1+1,ZDIMF1+1)
REAL NTGS(TGBF1+1) ,NTGM(XDIMF1+1, YDIMF1+1,ZDIMF1+1)
REAL TOPSS(TGBF1+1) ,TOPSM(XDIMF1+1, YDIMF1+1,ZDIMF1+1)
REAL DEPTHS(TGBF1+1) ,DEPTHM(XDIMF1+1, YDIMF1+1,ZDIMF1+1)
REAL TRANXS(TGBF1+1) ,TRANXM(XDIMF1+1, YDIMF1+1,ZDIMF1+1)
REAL TRANYS(TGBF1+1) ,TRANYM(XDIMF1+1, YDIMF1+1,ZDIMF1+1)
REAL TRANZS(TGBF1+1) ,TRANZM(XDIMF1+1, YDIMF1+1,ZDIMF1+1)

REAL TRANXBARS(TGBF1),TRANYBARS(TGBF1),TRANZBARS(TGBF1)
REAL TRANXBARM(XDIMF1+1, YDIMF1+1,ZDIMF1+1)
REAL TRANYBARM(XDIMF1+1, YDIMF1+1,ZDIMF1+1)
REAL SUMPV(XDIMC1+1,YDIMC1+1,ZDIMC1+1)
REAL SUMSGPV(0:TSTEP1+1,XDIMC1+1,YDIMC1+1,ZDIMC1+1)
REAL QOBARX(0:TSTEP1+1,XDIMC1+1,YDIMC1+1,ZDIMC1+1)
REAL QOBARY(0:TSTEP1+1,XDIMC1+1,YDIMC1+1,ZDIMC1+1)
REAL QOBARZ(0:TSTEP1+1,XDIMC1+1,YDIMC1+1,ZDIMC1+1)
REAL SGASBAR(0:TSTEP1+1,XDIMC1+1,YDIMC1+1,ZDIMC1+1)
REAL TEMPGASBAR(0:TSTEP1+1,XDIMC1+1,YDIMC1+1,ZDIMC1+1)
REAL QGBARX(0:TSTEP1+1,XDIMC1+1,YDIMC1+1,ZDIMC1+1)
REAL QGBARY(0:TSTEP1+1,XDIMC1+1,YDIMC1+1,ZDIMC1+1)
REAL QGBARZ(0:TSTEP1+1,XDIMC1+1,YDIMC1+1,ZDIMC1+1)
REAL TRANZBARM(XDIMF1+1, YDIMF1+1,ZDIMF1+1)

REAL SUMOILPOTNX(0:TSTEP1+1,XDIMC1+1,YDIMC1+1,ZDIMC1+1)
REAL SUMGASPOTNX(0:TSTEP1+1,XDIMC1+1,YDIMC1+1,ZDIMC1+1)
REAL SUMOILPOTNY(0:TSTEP1+1,XDIMC1+1,YDIMC1+1,ZDIMC1+1)
REAL SUMGASPOTNY(0:TSTEP1+1,XDIMC1+1,YDIMC1+1,ZDIMC1+1)
REAL SUMOILPOTNZ(0:TSTEP1+1,XDIMC1+1,YDIMC1+1,ZDIMC1+1)
REAL SUMGASPOTNZ(0:TSTEP1+1,XDIMC1+1,YDIMC1+1,ZDIMC1+1)
REAL SUMOILPOTNPX(0:TSTEP1+1,XDIMC1+1,YDIMC1+1,ZDIMC1+1)
REAL SUMGASPOTNPX(0:TSTEP1+1,XDIMC1+1,YDIMC1+1,ZDIMC1+1)
REAL SUMOILPOTNPY(0:TSTEP1+1,XDIMC1+1,YDIMC1+1,ZDIMC1+1)
REAL SUMGASPOTNPY(0:TSTEP1+1,XDIMC1+1,YDIMC1+1,ZDIMC1+1)
REAL SUMOILPOTNPZ(0:TSTEP1+1,XDIMC1+1,YDIMC1+1,ZDIMC1+1)
REAL SUMGASPOTNPZ(0:TSTEP1+1,XDIMC1+1,YDIMC1+1,ZDIMC1+1)
REAL DPOTOILLX(0:TSTEP1+1,XDIMF1+1,YDIMF1+1,ZDIMF1+1)
REAL DPOTGASLX(0:TSTEP1+1,XDIMF1+1,YDIMF1+1,ZDIMF1+1)
REAL DPOTOILLY(0:TSTEP1+1,XDIMF1+1,YDIMF1+1,ZDIMF1+1)
REAL DPOTGASLY(0:TSTEP1+1,XDIMF1+1,YDIMF1+1,ZDIMF1+1)
REAL DPOTOILLZ(0:TSTEP1+1,XDIMF1+1,YDIMF1+1,ZDIMF1+1)
REAL DPOTGASLZ(0:TSTEP1+1,XDIMF1+1,YDIMF1+1,ZDIMF1+1)

REAL DPOTOILNASX(0:TSTEP1+1,XDIMC1+1,YDIMC1+1,ZDIMC1+1)
REAL DPOTGASNASX(0:TSTEP1+1,XDIMC1+1,YDIMC1+1,ZDIMC1+1)
REAL DPOTOILNASY(0:TSTEP1+1,XDIMC1+1,YDIMC1+1,ZDIMC1+1)
REAL DPOTGASNASY(0:TSTEP1+1,XDIMC1+1,YDIMC1+1,ZDIMC1+1)
REAL DPOTOILNASZ(0:TSTEP1+1,XDIMC1+1,YDIMC1+1,ZDIMC1+1)
REAL DPOTGASNASZ(0:TSTEP1+1,XDIMC1+1,YDIMC1+1,ZDIMC1+1)
REAL KROBARNASX(0:TSTEP1+1,XDIMC1+1,YDIMC1+1,ZDIMC1+1)
REAL KRGBARNASX(0:TSTEP1+1,XDIMC1+1,YDIMC1+1,ZDIMC1+1)
REAL KROBARNASY(0:TSTEP1+1,XDIMC1+1,YDIMC1+1,ZDIMC1+1)
REAL KRGBARNASY(0:TSTEP1+1,XDIMC1+1,YDIMC1+1,ZDIMC1+1)
REAL KROBARNASZ(0:TSTEP1+1,XDIMC1+1,YDIMC1+1,ZDIMC1+1)
REAL KRGBARNASZ(0:TSTEP1+1,XDIMC1+1,YDIMC1+1,ZDIMC1+1)

REAL QOBARXM(0:TSTEP1+1,XDIMC1+1,YDIMC1+1,ZDIMC1+1)
REAL QGBARXM(0:TSTEP1+1,XDIMC1+1,YDIMC1+1,ZDIMC1+1)
REAL QOBARYM(0:TSTEP1+1,XDIMC1+1,YDIMC1+1,ZDIMC1+1)
REAL QGBARYM(0:TSTEP1+1,XDIMC1+1,YDIMC1+1,ZDIMC1+1)
REAL QOBARZM(0:TSTEP1+1,XDIMC1+1,YDIMC1+1,ZDIMC1+1)
REAL QGBARZM(0:TSTEP1+1,XDIMC1+1,YDIMC1+1,ZDIMC1+1)
REAL KROBARNASXM(0:TSTEP1+1,XDIMC1+1,YDIMC1+1,ZDIMC1+1)
REAL KRGBARNASXM(0:TSTEP1+1,XDIMC1+1,YDIMC1+1,ZDIMC1+1)
REAL KROBARNASYM(0:TSTEP1+1,XDIMC1+1,YDIMC1+1,ZDIMC1+1)
REAL KRGBARNASYM(0:TSTEP1+1,XDIMC1+1,YDIMC1+1,ZDIMC1+1)
REAL KROBARNASZM(0:TSTEP1+1,XDIMC1+1,YDIMC1+1,ZDIMC1+1)
REAL KRGBARNASZM(0:TSTEP1+1,XDIMC1+1,YDIMC1+1,ZDIMC1+1)

REAL TEMPXOIL(0:TSTEP1+1,XDIMC1+1,YDIMC1+1,ZDIMC1+1)
REAL TEMPXGAS(0:TSTEP1+1,XDIMC1+1,YDIMC1+1,ZDIMC1+1)
REAL TEMPYOIL(0:TSTEP1+1,XDIMC1+1,YDIMC1+1,ZDIMC1+1)
REAL TEMPYGAS(0:TSTEP1+1,XDIMC1+1,YDIMC1+1,ZDIMC1+1)
REAL TEMPZOIL(0:TSTEP1+1,XDIMC1+1,YDIMC1+1,ZDIMC1+1)
REAL TEMPZGAS(0:TSTEP1+1,XDIMC1+1,YDIMC1+1,ZDIMC1+1)
REAL DPOTOILNASXM(0:TSTEP1+1,XDIMC1+1,YDIMC1+1,ZDIMC1+1)
REAL DPOTGASNASXM(0:TSTEP1+1,XDIMC1+1,YDIMC1+1,ZDIMC1+1)
REAL DPOTOILNASYM(0:TSTEP1+1,XDIMC1+1,YDIMC1+1,ZDIMC1+1)
REAL DPOTGASNASYM(0:TSTEP1+1,XDIMC1+1,YDIMC1+1,ZDIMC1+1)
REAL DPOTOILNASZM(0:TSTEP1+1,XDIMC1+1,YDIMC1+1,ZDIMC1+1)
REAL DPOTGASNASZM(0:TSTEP1+1,XDIMC1+1,YDIMC1+1,ZDIMC1+1)
REAL DPOTOILLXM(0:TSTEP1+1,XDIMF1+1,YDIMF1+1,ZDIMF1+1)
REAL DPOTGASLXM(0:TSTEP1+1,XDIMF1+1,YDIMF1+1,ZDIMF1+1)
REAL DPOTOILLYM(0:TSTEP1+1,XDIMF1+1,YDIMF1+1,ZDIMF1+1)
REAL DPOTGASLYM(0:TSTEP1+1,XDIMF1+1,YDIMF1+1,ZDIMF1+1)
REAL DPOTOILLZM(0:TSTEP1+1,XDIMF1+1,YDIMF1+1,ZDIMF1+1)
REAL DPOTGASLZM(0:TSTEP1+1,XDIMF1+1,YDIMF1+1,ZDIMF1+1)
REAL SUMOILPOTNPXM(0:TSTEP1+1,XDIMC1+1,YDIMC1+1,ZDIMC1+1)
REAL SUMGASPOTNPXM(0:TSTEP1+1,XDIMC1+1,YDIMC1+1,ZDIMC1+1)
REAL SUMOILPOTNPYM(0:TSTEP1+1,XDIMC1+1,YDIMC1+1,ZDIMC1+1)
REAL SUMGASPOTNPYM(0:TSTEP1+1,XDIMC1+1,YDIMC1+1,ZDIMC1+1)
REAL SUMOILPOTNPZM(0:TSTEP1+1,XDIMC1+1,YDIMC1+1,ZDIMC1+1)
REAL SUMGASPOTNPZM(0:TSTEP1+1,XDIMC1+1,YDIMC1+1,ZDIMC1+1)

REAL OILWEIGHTX(0:TSTEP1+1,XDIMF1+1,YDIMF1+1,ZDIMF1+1)
REAL OILWEIGHTY(0:TSTEP1+1,XDIMF1+1,YDIMF1+1,ZDIMF1+1)
REAL OILWEIGHTZ(0:TSTEP1+1,XDIMF1+1,YDIMF1+1,ZDIMF1+1)
REAL GASWEIGHTX(0:TSTEP1+1,XDIMF1+1,YDIMF1+1,ZDIMF1+1)
REAL GASWEIGHTY(0:TSTEP1+1,XDIMF1+1,YDIMF1+1,ZDIMF1+1)
REAL GASWEIGHTZ(0:TSTEP1+1,XDIMF1+1,YDIMF1+1,ZDIMF1+1)
```

```
      REAL SOGCRS(TGBF1),SGLS(TGBF1),SGCRS(TGBF1),SGUS(TGBF1)
      REAL SOGCRM(XDIMF1+1, YDIMF1+1,ZDIMF1+1)
      REAL SGLM(XDIMF1+1, YDIMF1+1,ZDIMF1+1)
      REAL SGCRM(XDIMF1+1, YDIMF1+1,ZDIMF1+1)
      REAL SGUM(XDIMF1+1, YDIMF1+1,ZDIMF1+1)

      REAL KROMIN,KROMAX,KRGMIN,KRGMAX,DELTAHX,DELTADEN,RHOGHX
      REAL DELTAHY,RHOGHY,DELTAHZ,RHOGHZ

C     ************ SECTION 1: FILE NAMING **********************
C
C     FILE NO. 2 : IS THE FINE GRID RESTART FILE (FORMATTED,
C                  UNIFIED)
C     FILE NO. 3 : IS THE FINE GRID INIT FILE WITH MODIFICATION TO
C                  INCLUDE COARSE GRID TRANSMISSIBILITY (FORMATTED,
C                  UNIFIED)
C     FILE NO. 8 : IS THE OUTPUT FILE

      OPEN (2,FILE='CASE2.FUNRST')
      OPEN (3,FILE='CASE2.FINITMOD')
      OPEN (8,FILE='CASE2.RELPERM')


C      *********** SECTION 2: USER DEFINE DATA ******************

C      XDIMF : FINE GRID X DIMENSION
C      YDIMF : FINE GRID Y DIMENSION
C      ZDIMF : FINE GRID Z DIMENSION
C
C      XDIMC : COARSE GRID X DIMENSION
C      YDIMC : COARSE GRID Y DIMENSION
C
C      OILVISCBAR : AVERAGE OIL VISCOSITY (REAL NUMBER)
C      GASVISCBAR : AVERAGE GAS VISCOSITY (REAL NUMBER)
C
C      TSTEP    : MAXIMUM TIMESTEP NUMBER IN ECLIPSE RUN
C      SKIPLINE : NUMBER OF LINE TO BE SKIP IN *.FUNRST FILE BEFORE
C                 KEYWORD PRESSURE (96 FOR ECLIPSE VERSION 97A OR
C                 92 FOR ECLIPSE VERSION 98A OUTPUTS
C      DELTADEN : DIFFERENCE IN DENSITY (KG/M3)
C
C      KROMIN   : MINIMUM VALUE OF OIL RELATIVE PERMEABILITY
C                 (ROCK CURVE)
C      KROMAX   : MAXIMUM VALUE OF OIL RELATIVE PERMEABILITY
C                 (ROCK CURVE)
C      KRGMIN   : MINIMUM VALUE OF GAS RELATIVE PERMEABILITY
C                 (ROCK CURVE)
C      KRGMAX   : MAXIMUM VALUE OF GAS RELATIVE PERMEABILITY
C                 (ROCK CURVE)

      XDIMF = 200
      YDIMF = 1
      ZDIMF = 10

      XDIMC = 40
      YDIMC = 1

      OILVISCBAR = 1.0
      GASVISCBAR = 0.10

      DELTADEN = 699
      TSTEP = 30
      SKIPLINE = 92

      KROMIN = 0.0
      KROMAX = 1.0
      KRGMIN = 0.0
      KRGMAX = 1.0

C     *************** SECTION 3: CALCULATION OPTIONS *********

      NCOL = 4
      GRA = 9.81

      PRINT *
      PRINT *, ************************************************
      PRINT *, "PLEASE INPUT YOUR SELECTION OF WEIGHTING FACTOR"
      PRINT *, "   TYPE 1 FOR ORIGINAL TRANS AND POTENTIAL (TPW)"
      PRINT *, "   TYPE 2 FOR TRANSMISSIBILITY (TW)"
      PRINT *, "   TYPE 3 FOR PORE VOLUME"
      PRINT *, "   TYPE 4 FOR HEWEET & ARCHER METHOD"
      PRINT *, ************************************************
      READ(*,*) OPT
      PRINT *
      PRINT *
      PRINT *, ************************************************
      PRINT *, "END-POINT SCALING OPTION IN YOUR FINE GRID MODEL?"
      PRINT *, "   TYPE 1 FOR NO"
      PRINT *, "   TYPE 2 FOR YES"
      PRINT *, ************************************************
      READ(*,*) OPT1
      PRINT *
      PRINT *
      PRINT *, ************************************************
      PRINT *, "IS IT A 3D MODEL OR 2D CROSS SECTIONAL MODEL?"
      PRINT *, "   TYPE 1 FOR NO  (2D CROSS-SECTIONAL MODEL)"
      PRINT *, "   TYPE 2 FOR YES (3D MODEL)"
      PRINT *, ************************************************
      READ(*,*) OPT2
      PRINT *
```

```
C       **** SECTION 4: LAYERING SCHEMES AND MODEL DIMENSION *****

        SCHEME(0) = 0

        PRINT *,"TYPE NUMBER OF COARSE GRID LAYER?"
        READ (*,*) ZDIMC

        ZZ = 0

        DO 10 I = 1,ZDIMC


  20    IF (I .EQ. ZDIMC) THEN
        PRINT *,"HIGHER Z-LIMIT FOR COARSE LAYER",I," MUST BE",ZDIMF
        SCHEME(I) = ZDIMF
        GO TO 10
        ENDIF

        IF (ZZ .EQ. 99999) THEN
        SCHEME(I) = (ZDIMF-ZDIMC+I)
        GOTO 10
        ELSE
        PRINT *,"INPUT HIGHER Z-LIMIT FOR COARSE LAYER =",I
        READ (*,*)    SCHEME(I)
        ENDIF

        IF (SCHEME(I) .EQ. (ZDIMF-ZDIMC+I)) THEN
        PRINT *, "I KNOW HOW TO CALCULATE THE REST ... THANKS"
        PRINT *
        SCHEME(I) = (ZDIMF-ZDIMC+I)
        ZZ = 99999
        GOTO 10
        ENDIF

        IF (SCHEME(I) .LE. SCHEME(I-1)) THEN
        PRINT *, "THIS LAYER IS NOT POSSIBLE ! .. TRY AGAIN"
        PRINT *
        GOTO 20
        ENDIF

        IF (SCHEME(I) .GT. (ZDIMF-ZDIMC+I)) THEN
        PRINT *, "THIS LAYER IS NOT POSSIBLE ! .. TRY AGAIN"
        PRINT *
        GOTO 20
        ENDIF


        PRINT *

  10    CONTINUE
```

```
        PRINT *
        PRINT *,"**** YOUR SELECTED COARSENING SCHEME ****"
        PRINT *,"****      FOR CONFIRMATION ONLY       ****"
        PRINT *

        DO 30 I = 1,ZDIMC
        PRINT *,"COARSE LAYER",I," IS FROM FINE LAYER",SCHEME(I-1)+1,
     *  " TO FINE LAYER", SCHEME(I)
  30     CONTINUE

         PRINT *
         PRINT *,"*******************************"
         PRINT *

      TGBF = XDIMF*YDIMF*ZDIMF
      TGBC = XDIMC*YDIMC*ZDIMC

      DO 40 K = 1,ZDIMC
      DO 50 J = 1,YDIMC
      DO 60 I = 1,XDIMC

      LIMLX(I,J,K) = 1 + ((I-1)*XDIMF/XDIMC)
      LIMLY(I,J,K) = 1 + ((J-1)*YDIMF/YDIMC)
      LIMLZ(I,J,K) = SCHEME(K-1)+1
      LIMHX(I,J,K) = (XDIMF/XDIMC) + ((I-1)*XDIMF/XDIMC)
      LIMHY(I,J,K) = (YDIMF/YDIMC) + ((J-1)*YDIMF/YDIMC)
      LIMHZ(I,J,K) = SCHEME(K)

        CCX(I,J,K) = (LIMLX(I,J,K) +LIMHX(I,J,K))/2
        CCY(I,J,K) = (LIMLY(I,J,K) +LIMHY(I,J,K))/2
        CCZ(I,J,K) = (LIMLZ(I,J,K) +LIMHZ(I,J,K))/2


  60    CONTINUE
  50    CONTINUE
  40    CONTINUE

C       ******* SECTION 5: READING STATIC DATA FROM INIT FILE ****

        PRINT *
        PRINT *,'READING STATIC DATA'
        PRINT *,'*******************'
        PRINT *

        DO 70 I=1,SKIPLINE-2
        READ (3,*)
  70    CONTINUE

        READ (3,*)
        DO 80 N = 1,TGBF,NCOL
        READ (3,3000) PVS(N),PVS(N+1),PVS(N+2),
      * PVS(N+3)
```

```
80    CONTINUE


      READ (3,*)
      DO 90 N = 1,TGBF,NCOL
      READ (3,3000) DXS(N),DXS(N+1),DXS(N+2),
     * DXS(N+3)
90    CONTINUE

      READ (3,*)
      DO 100 N = 1,TGBF,NCOL
      READ (3,3000) DYS(N),DYS(N+1),DYS(N+2),
     * DYS(N+3)
100   CONTINUE

      READ (3,*)
      DO 110 N = 1,TGBF,NCOL
      READ (3,3000) DZS(N),DZS(N+1),DZS(N+2),
     * DZS(N+3)
110   CONTINUE

      READ (3,*)
      DO 120 N = 1,TGBF,NCOL
      READ (3,3000) PERMXS(N),PERMXS(N+1),PERMXS(N+2),
     * PERMXS(N+3)
120   CONTINUE

      READ (3,*)
      DO 130 N = 1,TGBF,NCOL
      READ (3,3000) PERMYS(N),PERMYS(N+1),PERMYS(N+2),
     * PERMYS(N+3)
130   CONTINUE

      READ (3,*)
      DO 140 N = 1,TGBF,NCOL
      READ (3,3000) PERMZS(N),PERMZS(N+1),PERMZS(N+2),
     * PERMZS(N+3)
140   CONTINUE

      READ (3,*)
      DO 150 N = 1,TGBF,NCOL
      READ (3,3000) MULTXS(N),MULTXS(N+1),MULTXS(N+2),
     * MULTXS(N+3)
150   CONTINUE

      READ (3,*)
      DO 160 N = 1,TGBF,NCOL
      READ (3,3000) MULTYS(N),MULTYS(N+1),MULTYS(N+2),
     * MULTYS(N+3)
160   CONTINUE

      READ (3,*)
      DO 170 N = 1,TGBF,NCOL
      READ (3,3000) MULTZS(N),MULTZS(N+1),MULTZS(N+2),
     * MULTZS(N+3)
170   CONTINUE

      READ (3,*)
      DO 180 N = 1,TGBF,NCOL
      READ (3,3000) POROS(N),POROS(N+1),POROS(N+2),
     * POROS(N+3)
180   CONTINUE

      READ (3,*)
      DO 190 N = 1,TGBF,NCOL
      READ (3,3000) NTGS(N),NTGS(N+1),NTGS(N+2),
     * NTGS(N+3)
190   CONTINUE

      READ (3,*)
      DO 200 N = 1,TGBF,NCOL
      READ (3,3000) TOPSS(N),TOPSS(N+1),TOPSS(N+2),
     * TOPSS(N+3)
200   CONTINUE

      READ (3,*)
      DO 210 N = 1,TGBF,NCOL
      READ (3,3000) DEPTHS(N),DEPTHS(N+1),DEPTHS(N+2),
     * DEPTHS(N+3)
210   CONTINUE

      READ (3,*)
      DO 220 N = 1,TGBF,NCOL
      READ (3,3000) TRANXS(N),TRANXS(N+1),TRANXS(N+2),
     * TRANXS(N+3)
220   CONTINUE

      READ (3,*)
      DO 230 N = 1,TGBF,NCOL
      READ (3,3000) TRANYS(N),TRANYS(N+1),TRANYS(N+2),
     * TRANYS(N+3)
230   CONTINUE

      READ (3,*)
      DO 240 N = 1,TGBF,NCOL
      READ (3,3000) TRANZS(N),TRANZS(N+1),TRANZS(N+2),
     * TRANZS(N+3)
240   CONTINUE

      READ (3,*)
      DO 250 N = 1,TGBC,NCOL
      READ (3,3000) TRANXBARS(N),TRANXBARS(N+1),TRANXBARS(N+2),
     * TRANXBARS(N+3)
250   CONTINUE
```

```
      READ (3,*)
      READ (3,*)
      DO 260 N = 1,TGBC,NCOL
      READ (3,3000) TRANYBARS(N),TRANYBARS(N+1),TRANYBARS(N+2),
     * TRANYBARS(N+3)
260   CONTINUE

      READ (3,*)
      READ (3,*)
      DO 270 N = 1,TGBC,NCOL
      READ (3,3000) TRANZBARS(N),TRANZBARS(N+1),TRANZBARS(N+2),
     * TRANZBARS(N+3)
270   CONTINUE

      IF (OPT1 .EQ. 1) THEN
      GOTO  275
      ENDIF

      READ (3,*)
      READ (3,*)

       DO 271 N = 1,TGBC,NCOL
      READ (3,3000) SOGCRS(N),SOGCRS(N+1),SOGCRS(N+2),
     * SOGCRS(N+3)
271   CONTINUE

      READ (3,*)
      READ (3,*)

       DO 272 N = 1,TGBC,NCOL
      READ (3,3000) SGLS(N),SGLS(N+1),SGLS(N+2),
     * SGLS(N+3)
272   CONTINUE

      READ (3,*)
      READ (3,*)

       DO 273 N = 1,TGBC,NCOL
      READ (3,3000) SGCRS(N),SGCRS(N+1),SGCRS(N+2),
     * SGCRS(N+3)
273   CONTINUE

      READ (3,*)
      READ (3,*)

       DO 274 N = 1,TGBC,NCOL
      READ (3,3000) SGUS(N),SGUS(N+1),SGUS(N+2),
     * SGUS(N+3)
274   CONTINUE
```

```
275   PRINT *

C     *** SECTION 6: CONVERTING STATIC DATA ********
C     ***      TO X-Y-Z DIMENSION ARRAY      ********

        DO 280 K=1,ZDIMF
        DO 290 J=1,YDIMF
        DO 300 I=1,XDIMF

          PP=I+(J*XDIMF-XDIMF)+(K*(XDIMF*YDIMF)-(XDIMF*YDIMF))

          PVM(I,J,K) = PVS(PP)
          DXM(I,J,K) = DXS(PP)
          DYM(I,J,K) = DYS(PP)
          DZM(I,J,K) = DZS(PP)
          PERMXM(I,J,K) = PERMXS(PP)
          PERMYM(I,J,K) = PERMYS(PP)
          PERMZM(I,J,K) = PERMZS(PP)
          MULTXM(I,J,K) = MULTXS(PP)
          MULTYM(I,J,K) = MULTYS(PP)
          MULTZM(I,J,K) = MULTZS(PP)
          POROM(I,J,K) = POROS(PP)
          NTGM(I,J,K) = NTGS(PP)
          TOPSM(I,J,K) = TOPSS(PP)
          DEPTHM(I,J,K) = DEPTHS(PP)
          TRANXM(I,J,K) = TRANXS(PP)
          TRANYM(I,J,K) = TRANYS(PP)
          TRANZM(I,J,K) = TRANZS(PP)

300           CONTINUE
290           CONTINUE
280           CONTINUE


      DO 310 K=1,ZDIMC
      DO 320 J=1,YDIMC
      DO 330 I=1,XDIMC

        PP=I+(J*XDIMC-XDIMC)+(K*(XDIMC*YDIMC)-(XDIMC*YDIMC))

        TRANXBARM(I,J,K) = TRANXBARS(PP)
        TRANYBARM(I,J,K) = TRANYBARS(PP)
        TRANZBARM(I,J,K) = TRANZBARS(PP)

        IF (OPT1 .EQ. 1) THEN
        GOTO 330
        ELSE
        SOGCRM(I,J,K) = SOGCRS(PP)
        SGLM(I,J,K) = SGLS(PP)
        SGCRM(I,J,K) = SGCRS(PP)
        SGUM(I,J,K) = SGUS(PP)
        ENDIF
```

```
 330          CONTINUE
 320          CONTINUE
 310          CONTINUE


          PRINT *,'FINISH READING STATIC DATA'
          PRINT *

C     ***** SECTION 7 : READING DYNAMIC DATA FROM UNRST FILE ****

       PRINT *
       PRINT *,'READING DYNAMIC DATA'
       PRINT *,'**********************'
       PRINT *

       DO 340 Z = 0,TSTEP

       READ (2,*)
       READ (2,2000) TS

        PRINT *,'READING TIMESTEP NO           ',TS

       DO 350 I=1,SKIPLINE
       READ (2,*)
 350   CONTINUE

       DO 360 N = 1,TGBF,NCOL
       READ (2,1600) PRESS(Z,N),PRESS(Z,N+1),PRESS(Z,N+2),
     * PRESS(Z,N+3)
 360   CONTINUE

       READ (2,*)
       DO 370 N = 1,TGBF,NCOL
       READ (2,1600) SGASS(Z,N),SGASS(Z,N+1),SGASS(Z,N+2),
     * SGASS(Z,N+3)
 370   CONTINUE

       READ (2,*)
       DO 380 N = 1,TGBF,NCOL
       READ (2,1600) FLOOILIPS(Z,N),FLOOILIPS(Z,N+1),
     * FLOOILIPS(Z,N+2),FLOOILIPS(Z,N+3)
 380   CONTINUE

       READ (2,*)
       DO 390 N = 1,TGBF,NCOL
       READ (2,1600) FLOGASIPS(Z,N),FLOGASIPS(Z,N+1),
     * FLOGASIPS(Z,N+2),FLOGASIPS(Z,N+3)
 390   CONTINUE


       IF (YDIMF .GT. 1) THEN

       READ (2,*)
       DO 391 N = 1,TGBF,NCOL
       READ (2,1600) FLOOILJPS(Z,N),FLOOILJPS(Z,N+1),
     * FLOOILJPS(Z,N+2),FLOOILJPS(Z,N+3)
 391   CONTINUE

       READ (2,*)
       DO 392 N = 1,TGBF,NCOL
       READ (2,1600) FLOGASJPS(Z,N),FLOGASJPS(Z,N+1),
     * FLOGASJPS(Z,N+2),FLOGASJPS(Z,N+3)
 392   CONTINUE

       ENDIF

       IF (ZDIMF .GT. 1) THEN

       READ (2,*)
       DO 400 N = 1,TGBF,NCOL
       READ (2,1600) FLOOILKPS(Z,N),FLOOILKPS(Z,N+1),
     * FLOOILKPS(Z,N+2),FLOOILKPS(Z,N+3)
 400   CONTINUE

       READ (2,*)
       DO 410 N = 1,TGBF,NCOL
       READ (2,1600) FLOGASKPS(Z,N),FLOGASKPS(Z,N+1),
     * FLOGASKPS(Z,N+2),FLOGASKPS(Z,N+3)
 410   CONTINUE

       ENDIF

       READ (2,*)
       DO 420 N = 1,TGBF,NCOL
       READ (2,1600) FIPOILS(Z,N),FIPOILS(Z,N+1),
     * FIPOILS(Z,N+2),FIPOILS(Z,N+3)
 420   CONTINUE

       READ (2,*)
       DO 430 N = 1,TGBF,NCOL
       READ (2,1600) FIPGASS(Z,N),FIPGASS(Z,N+1),
     * FIPGASS(Z,N+2),FIPGASS(Z,N+3)
 430   CONTINUE

       READ (2,*)
       DO 440 N = 1,TGBF,NCOL
       READ (2,1600) OILPOTNS(Z,N),OILPOTNS(Z,N+1),
     * OILPOTNS(Z,N+2),OILPOTNS(Z,N+3)
 440   CONTINUE

       READ (2,*)
       DO 450 N = 1,TGBF,NCOL
       READ (2,1600) OILVISCS(Z,N),OILVISCS(Z,N+1),
```

```
     * OILVISCS(Z,N+2),OILVISCS(Z,N+3)
450    CONTINUE

       READ (2,*)
       DO 460 N = 1,TGBF,NCOL
       READ (2,1600) GASPOTNS(Z,N),GASPOTNS(Z,N+1),
     * GASPOTNS(Z,N+2),GASPOTNS(Z,N+3)
460    CONTINUE

       READ (2,*)
       DO 470 N = 1,TGBF,NCOL
       READ (2,1600) GASVISCS(Z,N),GASVISCS(Z,N+1),
     * GASVISCS(Z,N+2),GASVISCS(Z,N+3)
470    CONTINUE

       READ (2,*)
       DO 480 N = 1,TGBF,NCOL
       READ (2,1600) POTCORRS(Z,N),POTCORRS(Z,N+1),
     * POTCORRS(Z,N+2),POTCORRS(Z,N+3)
480    CONTINUE

       READ (2,*)
       DO 490 N = 1,TGBF,NCOL
       READ (2,1600) KROS(Z,N),KROS(Z,N+1),
     * KROS(Z,N+2),KROS(Z,N+3)
490    CONTINUE

       READ (2,*)
       DO 500 N = 1,TGBF,NCOL
       READ (2,1600) KRGS(Z,N),KRGS(Z,N+1),
     * KRGS(Z,N+2),KRGS(Z,N+3)
500    CONTINUE

       READ (2,*)

        PRINT *,'FINISH READING TIMESTEP NO    ',TS
        PRINT *

 340     CONTINUE


C      *** SECTION 8 : CONVERTING DYNAMIC DATA ********
C      ***       TO X-Y-Z DIMENSION ARRAY      ********


       DO 510 Z=0,TSTEP
       DO 520 K=1,ZDIMF
       DO 530 J=1,YDIMF
       DO 540 I=1,XDIMF

          P=I+(J*XDIMF-XDIMF)+(K*(XDIMF*YDIMF)-(XDIMF*YDIMF))
          PRESM(Z,I,J,K) = PRESS(Z,P)
          SGASM(Z,I,J,K) = SGASS(Z,P)
          FLOOILIPM(Z,I,J,K) = FLOOILIPS(Z,P)
          FLOGASIPM(Z,I,J,K) = FLOGASIPS(Z,P)
          FLOOILJPM(Z,I,J,K) = FLOOILJPS(Z,P)
          FLOGASJPM(Z,I,J,K) = FLOGASJPS(Z,P)
          FLOOILKPM(Z,I,J,K) = FLOOILKPS(Z,P)
          FLOGASKPM(Z,I,J,K) = FLOGASKPS(Z,P)
          FIPOILM(Z,I,J,K) = FIPOILS(Z,P)
          FIPGASM(Z,I,J,K) = FIPGASS(Z,P)
          OILPOTNM(Z,I,J,K) = OILPOTNS(Z,P)
          OILVISCM(Z,I,J,K) = OILVISCS(Z,P)
          GASPOTNM(Z,I,J,K) = GASPOTNS(Z,P)
          GASVISCM(Z,I,J,K) = GASVISCS(Z,P)
          POTCORRM(Z,I,J,K) = POTCORRS(Z,P)
          KROM(Z,I,J,K) = KROS(Z,P)
          KRGM(Z,I,J,K) = KRGS(Z,P)

          IF (SGASM(Z,I,J,K) .LT. 0) THEN
             SGASM(Z,I,J,K) = 0
           ENDIF

540          CONTINUE
530          CONTINUE
520          CONTINUE
510          CONTINUE

       PRINT *
       PRINT *,'*****************************'
       PRINT *,'FINISH READING ALL THE DATA'
       PRINT *,'*****************************'
       PRINT *

C  ****** SECTION 9: SELECTION OF THE WEIGHTING FACTOR ******


       IF (OPT .EQ. 1) THEN
       WRITE (8,*) "WILL USE THE ORIGINAL TPW METHOD"

       DO 541 Z=0,TSTEP
       DO 542 K=1,ZDIMF
       DO 543 J=1,YDIMF
       DO 544 I=1,XDIMF

       OILWEIGHTX(Z,I,J,K) = OILPOTNM(Z,I,J,K)*TRANXM(I,J,K)
       GASWEIGHTX(Z,I,J,K) = GASPOTNM(Z,I,J,K)*TRANXM(I,J,K)
       OILWEIGHTY(Z,I,J,K) = OILPOTNM(Z,I,J,K)*TRANYM(I,J,K)
       GASWEIGHTY(Z,I,J,K) = GASPOTNM(Z,I,J,K)*TRANYM(I,J,K)
       OILWEIGHTZ(Z,I,J,K) = OILPOTNM(Z,I,J,K)*TRANZM(I,J,K)
       GASWEIGHTZ(Z,I,J,K) = GASPOTNM(Z,I,J,K)*TRANZM(I,J,K)

 544     CONTINUE
 543     CONTINUE
```

```
542     CONTINUE
541     CONTINUE

        ENDIF


        IF (OPT .EQ. 2) THEN
        WRITE (8,*) "WILL USE TRANSMISSIBILITY WEIGHTING "

        DO 545 Z=0,TSTEP
        DO 546 K=1,ZDIMF
        DO 547 J=1,YDIMF
        DO 548 I=1,XDIMF

        OILWEIGHTX(Z,I,J,K) = TRANXM(I,J,K)
        GASWEIGHTX(Z,I,J,K) = TRANXM(I,J,K)
        OILWEIGHTY(Z,I,J,K) = TRANYM(I,J,K)
        GASWEIGHTY(Z,I,J,K) = TRANYM(I,J,K)
        OILWEIGHTZ(Z,I,J,K) = TRANZM(I,J,K)
        GASWEIGHTZ(Z,I,J,K) = TRANZM(I,J,K)

548     CONTINUE
547     CONTINUE
546     CONTINUE
545     CONTINUE

        ENDIF


        IF (OPT .EQ. 3) THEN
        WRITE (8,*) "WILL USE PORE VOLUME WEIGHTING "

        DO 549 Z=0,TSTEP
        DO 550 K=1,ZDIMF
        DO 551 J=1,YDIMF
        DO 552 I=1,XDIMF

        OILWEIGHTX(Z,I,J,K) = PVM(I,J,K)
        GASWEIGHTX(Z,I,J,K) = PVM(I,J,K)
        OILWEIGHTY(Z,I,J,K) = PVM(I,J,K)
        GASWEIGHTY(Z,I,J,K) = PVM(I,J,K)
        OILWEIGHTZ(Z,I,J,K) = PVM(I,J,K)
        GASWEIGHTZ(Z,I,J,K) = PVM(I,J,K)

552     CONTINUE
551     CONTINUE
550     CONTINUE
549     CONTINUE

        ENDIF
```

```
C  *******     SECTION 10: SUMMATION OF PORE VOLUME ********

        DO 555 C = 1,ZDIMC
        DO 560 B = 1,YDIMC
        DO 570 A = 1,XDIMC

        DO 580 K = LIMLZ(A,B,C),LIMHZ(A,B,C)
        DO 590 J = LIMLY(A,B,C),LIMHY(A,B,C)
        DO 600 I = LIMLX(A,B,C),LIMHX(A,B,C)

        SUMPV(A,B,C) = PVM(I,J,K) + SUMPV(A,B,C)

600     CONTINUE
590     CONTINUE
580     CONTINUE
570     CONTINUE
560     CONTINUE
555     CONTINUE


C  *****  SECTION 11: SUMMATION OF PORE VOLUME TIMES SGAS *****

        DO 610 Z = 0,TSTEP

        DO 620 C = 1,ZDIMC
        DO 630 B = 1,YDIMC
        DO 640 A = 1,XDIMC

        DO 650 K = LIMLZ(A,B,C),LIMHZ(A,B,C)
        DO 660 J = LIMLY(A,B,C),LIMHY(A,B,C)
        DO 670 I = LIMLX(A,B,C),LIMHX(A,B,C)

        IF (SGASM(Z,I,J,K) .LT. 0) THEN
        SGASM(Z,I,J,K) = 0
        ENDIF

        SUMSGPV(Z,A,B,C) = (SGASM(Z,I,J,K) * PVM(I,J,K)) +
     *  SUMSGPV(Z,A,B,C)

670     CONTINUE
660     CONTINUE
650     CONTINUE
640     CONTINUE
630     CONTINUE
620     CONTINUE
610     CONTINUE


C  ******** SECTION 12: CALCULATION OF AVERAGE SGAS **********
```

```
      DO 680 Z = 0,TSTEP

      DO 690 C = 1,ZDIMC
      DO 700 B = 1,YDIMC
      DO 710 A = 1,XDIMC

      SGASBAR(Z,A,B,C) = SUMSGPV(Z,A,B,C)/SUMPV(A,B,C)

710   CONTINUE
700   CONTINUE
690   CONTINUE
680   CONTINUE


C  ****** SECTION 13: CALCULATION OF AVERAGED FLOW RATE ******

      DO 720 Z = 0,TSTEP

      DO 730 C = 1,ZDIMC
      DO 740 B = 1,YDIMC
      DO 750 A = 1,XDIMC

      DO 760 K = LIMLZ(A,B,C),LIMHZ(A,B,C)
      DO 770 J = LIMLY(A,B,C),LIMHY(A,B,C)
      DO 780 I = LIMHX(A,B,C),LIMHX(A,B,C)

      QOBARX(Z,A,B,C) = FLOOILIPM(Z,I,J,K) + QOBARX(Z,A,B,C)
      QGBARX(Z,A,B,C) = FLOGASIPM(Z,I,J,K) + QGBARX(Z,A,B,C)

780   CONTINUE
770   CONTINUE
760   CONTINUE
750   CONTINUE
740   CONTINUE
730   CONTINUE
720   CONTINUE


      DO 781 Z = 0,TSTEP

      DO 782 C = 1,ZDIMC
      DO 783 B = 1,YDIMC
      DO 784 A = 1,XDIMC

      DO 785 K = LIMLZ(A,B,C),LIMHZ(A,B,C)
      DO 786 J = LIMHY(A,B,C),LIMHY(A,B,C)
      DO 787 I = LIMLX(A,B,C),LIMHX(A,B,C)

      QOBARY(Z,A,B,C) = FLOOILJPM(Z,I,J,K) + QOBARY(Z,A,B,C)
      QGBARY(Z,A,B,C) = FLOGASJPM(Z,I,J,K) + QGBARY(Z,A,B,C)

787   CONTINUE
786   CONTINUE
785   CONTINUE
784   CONTINUE
783   CONTINUE
782   CONTINUE
781   CONTINUE


      DO 790 Z = 0,TSTEP

      DO 800 C = 1,ZDIMC
      DO 810 B = 1,YDIMC
      DO 820 A = 1,XDIMC

      DO 830 K = LIMHZ(A,B,C),LIMHZ(A,B,C)
      DO 840 J = LIMLY(A,B,C),LIMHY(A,B,C)
      DO 850 I = LIMLX(A,B,C),LIMHX(A,B,C)

      QOBARZ(Z,A,B,C) = FLOOILKPM(Z,I,J,K) + QOBARZ(Z,A,B,C)
      QGBARZ(Z,A,B,C) = FLOGASKPM(Z,I,J,K) + QGBARZ(Z,A,B,C)

850   CONTINUE
840   CONTINUE
830   CONTINUE
820   CONTINUE
810   CONTINUE
800   CONTINUE
790   CONTINUE


C  ***** SECTION 14: CALCULATING REVERSED FLOW RATE ********

      DO 860 Z = 0,TSTEP

      DO 870 C = 1,ZDIMC
      DO 880 B = 1,YDIMC
      DO 890 A = 1,XDIMC

      IF (QOBARX(Z,A,B,C) .LT. 0) THEN
      TEMPXOIL(Z,A,B,C) = QOBARX(Z,A,B,C)
      QOBARX(Z,A,B,C) = 0
      QOBARXM(Z,A+1,B,C) = TEMPXOIL(Z,A,B,C) * -1
      ELSE
      QOBARXM(Z,A+1,B,C) = 0
      ENDIF

      IF (QGBARX(Z,A,B,C) .LT. 0) THEN
      TEMPXGAS(Z,A,B,C) = QGBARX(Z,A,B,C)
      QGBARX(Z,A,B,C) = 0
      QGBARXM(Z,A+1,B,C) = TEMPXGAS(Z,A,B,C) * -1
      ELSE
      QGBARXM(Z,A+1,B,C) = 0
```

```
      ENDIF


      IF (QOBARY(Z,A,B,C) .LT. 0) THEN
      TEMPYOIL(Z,A,B,C) = QOBARY(Z,A,B,C)
      QOBARY(Z,A,B,C) = 0
      QOBARYM(Z,A,B+1,C) = TEMPYOIL(Z,A,B,C) * -1
      ELSE
      QOBARYM(Z,A,B+1,C) = 0
      ENDIF

      IF (QGBARY(Z,A,B,C) .LT. 0) THEN
      TEMPYGAS(Z,A,B,C) = QGBARY(Z,A,B,C)
      QGBARY(Z,A,B,C) = 0
      QGBARYM(Z,A,B+1,C) = TEMPYGAS(Z,A,B,C) * -1
      ELSE
      QGBARYM(Z,A,B+1,C) = 0
      ENDIF


      IF (QOBARZ(Z,A,B,C) .LT. 0) THEN
      TEMPZOIL(Z,A,B,C) = QOBARZ(Z,A,B,C)
      QOBARZ(Z,A,B,C) = 0
      QOBARZM(Z,A,B,C+1) = TEMPZOIL(Z,A,B,C) * -1
      ELSE
      QOBARZM(Z,A,B,C+1) = 0
      ENDIF

      IF (QGBARZ(Z,A,B,C) .LT. 0) THEN
      TEMPZGAS(Z,A,B,C) = QGBARZ(Z,A,B,C)
      QGBARZ(Z,A,B,C) = 0
      QGBARZM(Z,A,B,C+1) = TEMPZGAS(Z,A,B,C) * -1
      ELSE
      QGBARZM(Z,A,B,C+1) = 0
      ENDIF

890   CONTINUE
880   CONTINUE
870   CONTINUE
860   CONTINUE


C  ********** SECTION 15: CALCULATION OF DELTA POTENTIAL *********

C ************ SECTION 15A: X DIRECTION ************

      DO 900 Z = 0,TSTEP

      DO 910 C = 1,ZDIMC
      DO 920 B = 1,YDIMC
      DO 930 A = 1,XDIMC

      DO 940 K = LIMLZ(A,B,C),LIMHZ(A,B,C)
      DO 950 J = LIMLY(A,B,C),LIMHY(A,B,C)
      DO 960 I = CCX(A,B,C),CCX(A,B,C)


      DPOTOILLX(Z,I,J,K)=OILPOTNM(Z,I,J,K)
     *  -OILPOTNM(Z,CCX(A+1,B,C),J,K)

      DPOTGASLX(Z,I,J,K)=GASPOTNM(Z,I,J,K)
     *  -GASPOTNM(Z,CCX(A+1,B,C),J,K)

     DPOTOILLXM(Z,I,J,K)=OILPOTNM(Z,I,J,K)
     *  -OILPOTNM(Z,CCX(A-1,B,C),J,K)

     DPOTGASLXM(Z,I,J,K)=GASPOTNM(Z,I,J,K)
     *  -GASPOTNM(Z,CCX(A-1,B,C),J,K)


      SUMOILPOTNX(Z,A,B,C) = (OILWEIGHTX(Z,I,J,K))
     *   + SUMOILPOTNX(Z,A,B,C)

      SUMGASPOTNX(Z,A,B,C) = (GASWEIGHTX(Z,I,J,K))
     *   + SUMGASPOTNX(Z,A,B,C)


960   CONTINUE
950   CONTINUE
940   CONTINUE
930   CONTINUE
920   CONTINUE
910   CONTINUE
900   CONTINUE


      DO 970  Z = 0,TSTEP

      DO 980  C = 1,ZDIMC
      DO 990  B = 1,YDIMC
      DO 1000 A = 1,XDIMC

      DO 1010 K = LIMLZ(A,B,C),LIMHZ(A,B,C)
      DO 1020 J = LIMLY(A,B,C),LIMHY(A,B,C)
      DO 1030 I = CCX(A,B,C),CCX(A,B,C)


      SUMOILPOTNPX(Z,A,B,C) = (OILWEIGHTX(Z,I,J,K)
     *   * DPOTOILLX(Z,I,J,K)) +  SUMOILPOTNPX(Z,A,B,C)


      SUMGASPOTNPX(Z,A,B,C) = (GASWEIGHTX(Z,I,J,K)
     *   * DPOTGASLX(Z,I,J,K)) +  SUMGASPOTNPX(Z,A,B,C)
```

```
      SUMOILPOTNPXM(Z,A,B,C) = (OILWEIGHTX(Z,I,J,K)
     *   * DPOTOILLXM(Z,I,J,K)) +  SUMOILPOTNPXM(Z,A,B,C)


      SUMGASPOTNPXM(Z,A,B,C) = (GASWEIGHTX(Z,I,J,K)
     *   * DPOTGASLXM(Z,I,J,K)) +  SUMGASPOTNPXM(Z,A,B,C)


1030     CONTINUE
1020     CONTINUE
1010     CONTINUE
1000     CONTINUE
990      CONTINUE
980      CONTINUE
970      CONTINUE


C ************ SECTION 15B: Y DIRECTION ***************************

      DO 901 Z = 0,TSTEP

      DO 902 C = 1,ZDIMC
      DO 903 B = 1,YDIMC
      DO 904 A = 1,XDIMC

      DO 905 K = LIMLZ(A,B,C),LIMHZ(A,B,C)
      DO 906 J = CCY(A,B,C),CCY(A,B,C)
      DO 907 I = LIMLX(A,B,C),LIMHX(A,B,C)


      DPOTOILLY(Z,I,J,K)=OILPOTNM(Z,I,J,K)
     *  -OILPOTNM(Z,I,CCY(A,B+1,C),K)

      DPOTGASLY(Z,I,J,K)=GASPOTNM(Z,I,J,K)
     *  -GASPOTNM(Z,I,CCY(A,B+1,C),K)

     DPOTOILLYM(Z,I,J,K)=OILPOTNM(Z,I,J,K)
     *  -OILPOTNM(Z,I,CCY(A,B-1,C),K)

     DPOTGASLYM(Z,I,J,K)=GASPOTNM(Z,I,J,K)
     *  -GASPOTNM(Z,I,CCY(A,B-1,C),K)


      SUMOILPOTNY(Z,A,B,C) = (OILWEIGHTY(Z,I,J,K))
     *   +  SUMOILPOTNY(Z,A,B,C)

      SUMGASPOTNY(Z,A,B,C) = (GASWEIGHTY(Z,I,J,K))
     *   +  SUMGASPOTNY(Z,A,B,C)


907      CONTINUE
906      CONTINUE
905      CONTINUE
904      CONTINUE
903      CONTINUE
902      CONTINUE
901      CONTINUE


      DO 911  Z = 0,TSTEP

      DO 912  C = 1,ZDIMC
      DO 913  B = 1,YDIMC
      DO 914  A = 1,XDIMC

      DO 915  K = LIMLZ(A,B,C),LIMHZ(A,B,C)
      DO 916  J = CCY(A,B,C),CCY(A,B,C)
      DO 917  I = LIMLX(A,B,C),LIMHX(A,B,C)


      SUMOILPOTNPY(Z,A,B,C) = (OILWEIGHTY(Z,I,J,K)
     *   * DPOTOILLY(Z,I,J,K)) +  SUMOILPOTNPY(Z,A,B,C)


      SUMGASPOTNPY(Z,A,B,C) = (GASWEIGHTY(Z,I,J,K)
     *   * DPOTGASLY(Z,I,J,K)) +  SUMGASPOTNPY(Z,A,B,C)


      SUMOILPOTNPYM(Z,A,B,C) = (OILWEIGHTY(Z,I,J,K)
     *   * DPOTOILLYM(Z,I,J,K)) +  SUMOILPOTNPYM(Z,A,B,C)


      SUMGASPOTNPYM(Z,A,B,C) = (GASWEIGHTY(Z,I,J,K)
     *   * DPOTGASLYM(Z,I,J,K)) +  SUMGASPOTNPYM(Z,A,B,C)


917      CONTINUE
916      CONTINUE
915      CONTINUE
914      CONTINUE
913      CONTINUE
912      CONTINUE
911      CONTINUE


C ************ SECTION 15C: Z DIRECTION ***********************
C   *****   SECTION 15C1: EVEN LAYERS AVERAGING  ****

      DO 1031 Z = 0,TSTEP

      DO 1032 C = 1,ZDIMC
```

```
      DO 1033 B = 1,YDIMC
      DO 1034 A = 1,XDIMC

       IF ((((LIMHZ(A,B,C) + LIMLZ(A,B,C))/2)*2) .EQ.
     *  (LIMHZ(A,B,C) + LIMLZ(A,B,C))) THEN

       GOTO 1034

       ELSE

      DO 1035 K = CCZ(A,B,C),CCZ(A,B,C)
      DO 1036 J = LIMLY(A,B,C),LIMHY(A,B,C)
      DO 1037 I = LIMLX(A,B,C),LIMHX(A,B,C)


       TRANZM(I,J,K)      = (TRANZM(I,J,K)+TRANZM(I,J,K+1))/2
       OILPOTNM(Z,I,J,K) = (OILPOTNM(Z,I,J,K)+OILPOTNM(Z,I,J,K+1))/2
       GASPOTNM(Z,I,J,K) = (GASPOTNM(Z,I,J,K)+GASPOTNM(Z,I,J,K+1))/2

1037    CONTINUE
1036    CONTINUE
1035    CONTINUE

       ENDIF

1034    CONTINUE
1033    CONTINUE
1032    CONTINUE
1031    CONTINUE

C    *****   SECTION 15C2: DELTA POTENTIAL (Z-DIRECTION) ****


      DO 1040 Z = 0,TSTEP

      DO 1050 C = 1,ZDIMC
      DO 1060 B = 1,YDIMC
      DO 1070 A = 1,XDIMC

      DO 1080 K = CCZ(A,B,C),CCZ(A,B,C)
      DO 1090 J = LIMLY(A,B,C),LIMHY(A,B,C)
      DO 1100 I = LIMLX(A,B,C),LIMHX(A,B,C)

      DPOTOILLZ(Z,I,J,K)=OILPOTNM(Z,I,J,K)
     *  -OILPOTNM(Z,I,J,CCZ(A,B,C+1))

      DPOTGASLZ(Z,I,J,K)=GASPOTNM(Z,I,J,K)
     *  -GASPOTNM(Z,I,J,CCZ(A,B,C+1))

      DPOTOILLZM(Z,I,J,K)=OILPOTNM(Z,I,J,K)
     *  -OILPOTNM(Z,I,J,CCZ(A,B,C-1))

      DPOTGASLZM(Z,I,J,K)=GASPOTNM(Z,I,J,K)
     *  -GASPOTNM(Z,I,J,CCZ(A,B,C-1))


      SUMOILPOTNZ(Z,A,B,C) = (OILWEIGHTZ(Z,I,J,K))
     *  + SUMOILPOTNZ(Z,A,B,C)

      SUMGASPOTNZ(Z,A,B,C) = (GASWEIGHTZ(Z,I,J,K))
     *  + SUMGASPOTNZ(Z,A,B,C)


1100    CONTINUE
1090    CONTINUE
1080    CONTINUE
1070    CONTINUE
1060    CONTINUE
1050    CONTINUE
1040    CONTINUE


      DO 1101 Z = 0,TSTEP

      DO 1110 C = 1,ZDIMC
      DO 1120 B = 1,YDIMC
      DO 1130 A = 1,XDIMC

      DO 1140 K = CCZ(A,B,C),CCZ(A,B,C)
      DO 1150 J = LIMLY(A,B,C),LIMHY(A,B,C)
      DO 1160 I = LIMLX(A,B,C),LIMHX(A,B,C)


      SUMOILPOTNPZ(Z,A,B,C) = (OILWEIGHTZ(Z,I,J,K)
     *  * DPOTOILLZ(Z,I,J,K)) +  SUMOILPOTNPZ(Z,A,B,C)

      SUMGASPOTNPZ(Z,A,B,C) = (GASWEIGHTZ(Z,I,J,K)
     *  * DPOTGASLZ(Z,I,J,K))+  SUMGASPOTNPZ(Z,A,B,C)

      SUMOILPOTNPZM(Z,A,B,C) = (OILWEIGHTZ(Z,I,J,K)
     *  * DPOTOILLZM(Z,I,J,K)) +  SUMOILPOTNPZM(Z,A,B,C)

      SUMGASPOTNPZM(Z,A,B,C) = (GASWEIGHTZ(Z,I,J,K)
     *  * DPOTGASLZM(Z,I,J,K))+  SUMGASPOTNPZM(Z,A,B,C)


1160    CONTINUE
1150    CONTINUE
1140    CONTINUE
1130    CONTINUE
1120    CONTINUE
1110    CONTINUE
1101    CONTINUE
```

```
C ********* SECTION 15D: AVERAGED DELTA POTENTIAL ******

      DO 1170 Z = 0,TSTEP

      DO 1180 C = 1,ZDIMC
      DO 1190 B = 1,YDIMC
      DO 1200 A = 1,XDIMC

      DPOTOILNASX(Z,A,B,C) = SUMOILPOTNPX(Z,A,B,C)
     *  /SUMOILPOTNX(Z,A,B,C)

      DPOTGASNASX(Z,A,B,C) = SUMGASPOTNPX(Z,A,B,C)
     *  /SUMGASPOTNX(Z,A,B,C)

       DPOTOILNASY(Z,A,B,C) = SUMOILPOTNPY(Z,A,B,C)
     *  /SUMOILPOTNY(Z,A,B,C)

      DPOTGASNASY(Z,A,B,C) = SUMGASPOTNPY(Z,A,B,C)
     *  /SUMGASPOTNY(Z,A,B,C)

      DPOTOILNASZ(Z,A,B,C) = SUMOILPOTNPZ(Z,A,B,C)
     *  /SUMOILPOTNZ(Z,A,B,C)

      DPOTGASNASZ(Z,A,B,C) = SUMGASPOTNPZ(Z,A,B,C)
     *  /SUMGASPOTNZ(Z,A,B,C)

      DPOTOILNASXM(Z,A,B,C) = SUMOILPOTNPXM(Z,A,B,C)
     *  /SUMOILPOTNX(Z,A,B,C)

      DPOTGASNASXM(Z,A,B,C) = SUMGASPOTNPXM(Z,A,B,C)
     *  /SUMGASPOTNX(Z,A,B,C)

      DPOTOILNASYM(Z,A,B,C) = SUMOILPOTNPYM(Z,A,B,C)
     *  /SUMOILPOTNY(Z,A,B,C)

      DPOTGASNASYM(Z,A,B,C) = SUMGASPOTNPYM(Z,A,B,C)
     *  /SUMGASPOTNY(Z,A,B,C)

      DPOTOILNASZM(Z,A,B,C) = SUMOILPOTNPZM(Z,A,B,C)
     *  /SUMOILPOTNZ(Z,A,B,C)

      DPOTGASNASZM(Z,A,B,C) = SUMGASPOTNPZM(Z,A,B,C)
     *  /SUMGASPOTNZ(Z,A,B,C)


1200   CONTINUE
1190   CONTINUE
1180   CONTINUE
1170   CONTINUE
```

```
C *** SECTION 15 E: CALCULATION FOR HEWETT & ARCHER METHOD *****
C                   **** Assume Uniform Dipping ******

      IF (XDIMC .EQ. 1) THEN
      DELTAHX = 0
      ELSE
      DELTAHX= DEPTHM(CCX(2,1,1),CCY(1,1,1),CCZ(1,1,1))-
     *         DEPTHM(CCX(1,1,1),CCY(1,1,1),CCZ(1,1,1))
      ENDIF

      IF (YDIMC .EQ. 1) THEN
      DELTAHY = 0
      ELSE
      DELTAHY= DEPTHM(CCX(1,1,1),CCY(1,2,1),CCZ(1,1,1))-
     *         DEPTHM(CCX(1,1,1),CCY(1,1,1),CCZ(1,1,1))
      ENDIF

      IF (ZDIMC .EQ. 1) THEN
      DELTAHZ = 0
      ELSE
      DELTAHZ= DEPTHM(CCX(1,1,1),CCY(1,1,1),CCZ(1,1,2))-
     *         DEPTHM(CCX(1,1,1),CCY(1,1,1),CCZ(1,1,1))
      ENDIF

      RHOGHX = (DELTADEN*GRA*DELTAHX)/100000
      RHOGHY = (DELTADEN*GRA*DELTAHY)/100000
      RHOGHZ = (DELTADEN*GRA*DELTAHZ)/100000

      IF (OPT .EQ. 4) THEN
      WRITE (8,*) "WILL USE HEWEET & ARCHER METHOD"
      ENDIF

      IF (OPT .EQ. 4 ) THEN

      DO 1201 Z = 0,TSTEP

      DO 1202 C = 1,ZDIMC
      DO 1203 B = 1,YDIMC
      DO 1204 A = 1,XDIMC

      DO 1205 K = CCZ(A,B,C),CCZ(A,B,C)
      DO 1206 J = CCY(A,B,C),CCY(A,B,C)
      DO 1207 I = CCX(A,B,C),CCX(A,B,C)

      DPOTOILNASX(Z,A,B,C)=OILPOTNM(Z,I,J,K)
     *-OILPOTNM(Z,CCX(A+1,B,C),J,K)

      DPOTOILNASXM(Z,A,B,C)=OILPOTNM(Z,I,J,K)
     *-OILPOTNM(Z,CCX(A-1,B,C),J,K)
```

```
      DPOTOILNASY(Z,A,B,C)=OILPOTNM(Z,I,J,K)
     *  -OILPOTNM(Z,I,CCY(A,B+1,C),K)

      DPOTOILNASYM(Z,A,B,C)=OILPOTNM(Z,I,J,K)
     *  -OILPOTNM(Z,I,CCY(A,B-1,C),K)

      DPOTOILNASZ(Z,A,B,C)=OILPOTNM(Z,I,J,K)
     *  -OILPOTNM(Z,I,J,CCZ(A,B,C+1))

      DPOTOILNASZM(Z,A,B,C)=OILPOTNM(Z,I,J,K)
     *  -OILPOTNM(Z,I,J,CCZ(A,B,C-1))

      DPOTGASNASX(Z,A,B,C)=DPOTOILNASX(Z,A,B,C) - RHOGHX
      DPOTGASNASXM(Z,A,B,C)=DPOTOILNASXM(Z,A,B,C) + RHOGHX

      DPOTGASNASY(Z,A,B,C)=DPOTOILNASY(Z,A,B,C) - RHOGHY
      DPOTGASNASYM(Z,A,B,C)=DPOTOILNASYM(Z,A,B,C) + RHOGHY

      DPOTGASNASZ(Z,A,B,C)=DPOTOILNASZ(Z,A,B,C) - RHOGHZ
      DPOTGASNASZM(Z,A,B,C)=DPOTOILNASZM(Z,A,B,C) + RHOGHZ


 1207   CONTINUE
 1206   CONTINUE
 1205   CONTINUE
 1204   CONTINUE
 1203   CONTINUE
 1202   CONTINUE
 1201   CONTINUE

        END IF

C ********** SECTION 16: CALCULATION OF PSEUDO RELPERM ************
C ************* SECTION 16 A: X-DIRECTION *****************

        DO 1210 Z = 0,TSTEP

        DO 1220 C = 1,ZDIMC
        DO 1230 B = 1,YDIMC
        DO 1240 A = 1,XDIMC

        IF (QOBARXM(Z,A,B,C) .GT. 0) THEN
        KROBARNASX(Z,A-1,B,C) = 0
        KROBARNASXM(Z,A,B,C)= QOBARXM(Z,A,B,C)*OILVISCBAR
     *   /(TRANXBARM(A-1,B,C)*DPOTOILNASXM(Z,A,B,C))
         ELSE
        KROBARNASX(Z,A-1,B,C)=QOBARX(Z,A-1,B,C)*OILVISCBAR
     *   /(TRANXBARM(A-1,B,C)*DPOTOILNASX(Z,A-1,B,C))
         KROBARNASXM(Z,A,B,C) =0
         ENDIF


        IF (QOBARX(Z,A,B,C) .GT. 0) THEN
        KROBARNASXM(Z,A+1,B,C) = 0
        KROBARNASX(Z,A,B,C)= QOBARX(Z,A,B,C)*OILVISCBAR
     *   /(TRANXBARM(A,B,C)*DPOTOILNASX(Z,A,B,C))
         ELSE
        KROBARNASXM(Z,A+1,B,C)=QOBARXM(Z,A+1,B,C)*OILVISCBAR
     *   /(TRANXBARM(A,B,C)*DPOTOILNASXM(Z,A+1,B,C))
         KROBARNASX(Z,A,B,C) =0
         ENDIF


        IF (QGBARXM(Z,A,B,C) .GT. 0) THEN
        KRGBARNASX(Z,A-1,B,C) = 0
        KRGBARNASXM(Z,A,B,C)= QGBARXM(Z,A,B,C)*GASVISCBAR
     *   /(TRANXBARM(A-1,B,C)*DPOTGASNASXM(Z,A,B,C))
         ELSE
        KRGBARNASX(Z,A-1,B,C)=QGBARX(Z,A-1,B,C)*GASVISCBAR
     *   /(TRANXBARM(A-1,B,C)*DPOTGASNASX(Z,A-1,B,C))
         KRGBARNASXM(Z,A,B,C) =0
         ENDIF


        IF (QGBARX(Z,A,B,C) .GT. 0) THEN
        KRGBARNASXM(Z,A+1,B,C) = 0
        KRGBARNASX(Z,A,B,C)= QGBARX(Z,A,B,C)*GASVISCBAR
     *   /(TRANXBARM(A,B,C)*DPOTGASNASX(Z,A,B,C))
         ELSE
        KRGBARNASXM(Z,A+1,B,C)=QGBARXM(Z,A+1,B,C)*GASVISCBAR
     *   /(TRANXBARM(A,B,C)*DPOTGASNASXM(Z,A+1,B,C))
         KRGBARNASX(Z,A,B,C) =0
         ENDIF


C ************** SECTION 16 B: Y-DIRECTION *****************

        IF (QOBARYM(Z,A,B,C) .GT. 0) THEN
        KROBARNASY(Z,A,B-1,C) = 0
        KROBARNASYM(Z,A,B,C)= QOBARYM(Z,A,B,C)*OILVISCBAR
     *   /(TRANYBARM(A,B-1,C)*DPOTOILNASYM(Z,A,B,C))
         ELSE
        KROBARNASY(Z,A,B-1,C)=QOBARY(Z,A,B-1,C)*OILVISCBAR
     *   /(TRANYBARM(A,B-1,C)*DPOTOILNASY(Z,A,B-1,C))
         KROBARNASYM(Z,A,B,C) =0
         ENDIF

        IF (QOBARY(Z,A,B,C) .GT. 0) THEN
        KROBARNASYM(Z,A,B+1,C) = 0
        KROBARNASY(Z,A,B,C)= QOBARY(Z,A,B,C)*OILVISCBAR
     *   /(TRANYBARM(A,B,C)*DPOTOILNASY(Z,A,B,C))
```

```
      ELSE
     KROBARNASYM(Z,A,B+1,C)=QOBARYM(Z,A,B+1,C)*OILVISCBAR
     *  /(TRANYBARM(A,B,C)*DPOTOILNASYM(Z,A,B+1,C))
      KROBARNASY(Z,A,B,C) =0
      ENDIF

     IF (QGBARYM(Z,A,B,C) .GT. 0) THEN
     KRGBARNASY(Z,A,B-1,C) = 0
     KRGBARNASYM(Z,A,B,C)= QGBARYM(Z,A,B,C)*GASVISCBAR
     *  /(TRANYBARM(A,B-1,C)*DPOTGASNASYM(Z,A,B,C))
      ELSE
     KRGBARNASY(Z,A,B-1,C)=QGBARY(Z,A,B-1,C)*GASVISCBAR
     *  /(TRANYBARM(A,B-1,C)*DPOTGASNASY(Z,A,B-1,C))
      KRGBARNASYM(Z,A,B,C) =0
      ENDIF

     IF (QGBARY(Z,A,B,C) .GT. 0) THEN
     KRGBARNASYM(Z,A,B+1,C) = 0
     KRGBARNASY(Z,A,B,C)= QGBARY(Z,A,B,C)*GASVISCBAR
     *  /(TRANYBARM(A,B,C)*DPOTGASNASY(Z,A,B,C))
      ELSE
     KRGBARNASYM(Z,A,B+1,C)=QGBARYM(Z,A,B+1,C)*GASVISCBAR
     *  /(TRANYBARM(A,B,C)*DPOTGASNASYM(Z,A,B+1,C))
      KRGBARNASY(Z,A,B,C) =0
      ENDIF

C ************** SECTION 16 C: Z-DIRECTION *****************

     IF (QOBARZM(Z,A,B,C) .GT. 0) THEN
     KROBARNASZ(Z,A,B,C-1) = 0
     KROBARNASZM(Z,A,B,C)= QOBARZM(Z,A,B,C)*OILVISCBAR
     *  /(TRANZBARM(A,B,C-1)*DPOTOILNASZM(Z,A,B,C))
      ELSE
     KROBARNASZ(Z,A,B,C-1)=QOBARZ(Z,A,B,C-1)*OILVISCBAR
     *  /(TRANZBARM(A,B,C-1)*DPOTOILNASZ(Z,A,B,C-1))
      KROBARNASZM(Z,A,B,C) =0
      ENDIF

     IF (QOBARZ(Z,A,B,C) .GT. 0) THEN
     KROBARNASZM(Z,A,B,C+1) = 0
     KROBARNASZ(Z,A,B,C)= QOBARX(Z,A,B,C)*OILVISCBAR
     *  /(TRANZBARM(A,B,C)*DPOTOILNASZ(Z,A,B,C))
      ELSE
     KROBARNASZM(Z,A,B,C+1)=QOBARZM(Z,A,B,C+1)*OILVISCBAR
     *  /(TRANZBARM(A,B,C)*DPOTOILNASZM(Z,A,B,C+1))
      KROBARNASZ(Z,A,B,C) =0
      ENDIF

     IF (QGBARZM(Z,A,B,C) .GT. 0) THEN
     KRGBARNASZ(Z,A,B,C-1) = 0
     KRGBARNASZM(Z,A,B,C)= QGBARZM(Z,A,B,C)*GASVISCBAR
     *  /(TRANZBARM(A,B,C-1)*DPOTGASNASZM(Z,A,B,C))
      ELSE
     KRGBARNASZ(Z,A,B,C-1)=QGBARZ(Z,A,B,C-1)*GASVISCBAR
     *  /(TRANZBARM(A,B,C-1)*DPOTGASNASZ(Z,A,B,C-1))
      KRGBARNASZM(Z,A,B,C) =0
      ENDIF

     IF (QGBARZ(Z,A,B,C) .GT. 0) THEN
     KRGBARNASZM(Z,A,B,C+1) = 0
     KRGBARNASZ(Z,A,B,C)= QGBARZ(Z,A,B,C)*GASVISCBAR
     *  /(TRANZBARM(A,B,C)*DPOTGASNASZ(Z,A,B,C))
      ELSE
     KRGBARNASZM(Z,A,B,C+1)=QGBARZM(Z,A,B,C+1)*GASVISCBAR
     *  /(TRANZBARM(A,B,C)*DPOTGASNASZM(Z,A,B,C+1))
      KRGBARNASZ(Z,A,B,C) =0
      ENDIF


1240  CONTINUE
1230  CONTINUE
1220  CONTINUE
1210  CONTINUE


C     ****** SECTION 17: PRINTING THE RESULTS ***************
C     ****** SECTION 17 A: INITIALISATION ********************

      NAS = 0
      NAS1 = 0

      DO 1250 Z = 0,0

      DO 1260 C = 1,ZDIMC
      DO 1270 B = 1,YDIMC
      DO 1280 A = 1,XDIMC

       KRGBARNASX(Z,A,B,C) = KRGMIN
       KROBARNASX(Z,A,B,C) = KROMAX
       KRGBARNASXM(Z,A,B,C) = KRGMIN
       KROBARNASXM(Z,A,B,C) = KROMAX

       KRGBARNASY(Z,A,B,C) = KRGMIN
       KROBARNASY(Z,A,B,C) = KROMAX
       KRGBARNASYM(Z,A,B,C) = KRGMIN
       KROBARNASYM(Z,A,B,C) = KROMAX

       KRGBARNASZ(Z,A,B,C) = KRGMIN
       KROBARNASZ(Z,A,B,C) = KROMAX
       KRGBARNASZM(Z,A,B,C) = KRGMIN
       KROBARNASZM(Z,A,B,C) = KROMAX

       KRGBARNASX(Z+TSTEP,A,B,C) = KRGMAX
       KROBARNASX(Z+TSTEP,A,B,C) = KROMIN
```

```
          KRGBARNASXM(Z+TSTEP,A,B,C) = KRGMAX
          KROBARNASXM(Z+TSTEP,A,B,C) = KROMIN

          KRGBARNASY(Z+TSTEP,A,B,C) = KRGMAX
          KROBARNASY(Z+TSTEP,A,B,C) = KROMIN
          KRGBARNASYM(Z+TSTEP,A,B,C) = KRGMAX
          KROBARNASYM(Z+TSTEP,A,B,C) = KROMIN

          KRGBARNASZ(Z+TSTEP,A,B,C) = KRGMAX
          KROBARNASZ(Z+TSTEP,A,B,C) = KROMIN
          KRGBARNASZM(Z+TSTEP,A,B,C) = KRGMAX
          KROBARNASZM(Z+TSTEP,A,B,C) = KROMIN

          SGASBAR(Z+TSTEP,A,B,C) = 0.85

1280      CONTINUE
1270      CONTINUE
1260      CONTINUE
1250      CONTINUE


C  *************** SECTION 17 B: SORTING ****************

          DO 1290 C = 1,ZDIMC
          DO 1300 B = 1,YDIMC
          DO 1310 A = 1,XDIMC
          DO 1320 Z = 0,TSTEP

IF (SGASBAR(Z,A,B,C) .LT.  0.00001) THEN
SGASBAR(Z,A,B,C) = 0.0
 ENDIF

NN = TSTEP - 1
DO 1330 K = 1,NN
JJ= TSTEP-1
DO 1340 L =1,JJ

 IF (SGASBAR(L,A,B,C) .LE. SGASBAR(L+1,A,B,C)) GO TO 1340

  TEMP1 = SGASBAR(L,A,B,C)
  TEMP2 = KROBARNASX(L,A,B,C)
  TEMP3 = KRGBARNASX(L,A,B,C)
  TEMP4 = KROBARNASZ(L,A,B,C)
  TEMP5 = KRGBARNASZ(L,A,B,C)
  TEMP6 = KROBARNASXM(L,A,B,C)
  TEMP7 = KRGBARNASXM(L,A,B,C)
  TEMP8 = KROBARNASZM(L,A,B,C)
  TEMP9 = KRGBARNASZM(L,A,B,C)
  TEMP10 = KROBARNASY(L,A,B,C)
  TEMP11 = KRGBARNASY(L,A,B,C)
  TEMP12 = KROBARNASYM(L,A,B,C)
  TEMP13 = KRGBARNASYM(L,A,B,C)

SGASBAR(L,A,B,C) = SGASBAR(L+1,A,B,C)
KROBARNASX(L,A,B,C) = KROBARNASX(L+1,A,B,C)
KRGBARNASX(L,A,B,C) = KRGBARNASX(L+1,A,B,C)
KROBARNASY(L,A,B,C) = KROBARNASX(L+1,A,B,C)
KRGBARNASY(L,A,B,C) = KRGBARNASX(L+1,A,B,C)
KROBARNASZ(L,A,B,C) = KROBARNASZ(L+1,A,B,C)
KRGBARNASZ(L,A,B,C) = KRGBARNASZ(L+1,A,B,C)
KROBARNASXM(L,A,B,C) = KROBARNASXM(L+1,A,B,C)
KRGBARNASXM(L,A,B,C) = KRGBARNASXM(L+1,A,B,C)
KROBARNASYM(L,A,B,C) = KROBARNASXM(L+1,A,B,C)
KRGBARNASYM(L,A,B,C) = KRGBARNASXM(L+1,A,B,C)
KROBARNASZM(L,A,B,C) = KROBARNASZM(L+1,A,B,C)
KRGBARNASZM(L,A,B,C) = KRGBARNASZM(L+1,A,B,C)

 SGASBAR(L+1,A,B,C) = TEMP1
 KROBARNASX(L+1,A,B,C) = TEMP2
 KRGBARNASX(L+1,A,B,C) = TEMP3
 KROBARNASZ(L+1,A,B,C) = TEMP4
 KRGBARNASZ(L+1,A,B,C) = TEMP5
 KROBARNASXM(L+1,A,B,C) = TEMP6
 KRGBARNASXM(L+1,A,B,C) = TEMP7
 KROBARNASZM(L+1,A,B,C) = TEMP8
 KRGBARNASZM(L+1,A,B,C) = TEMP9
 KROBARNASY(L+1,A,B,C) = TEMP10
 KRGBARNASY(L+1,A,B,C) = TEMP11
 KROBARNASYM(L+1,A,B,C) = TEMP12
 KRGBARNASYM(L+1,A,B,C) = TEMP13

1340      CONTINUE
1330      CONTINUE
1320      CONTINUE
1310      CONTINUE
1300      CONTINUE
1290      CONTINUE


C  ********* SECTION 17 C: PRINTING X-PLUS DIRECTION *************

          DO 1350 C = 1,ZDIMC
          DO 1360 B = 1,YDIMC
          DO 1370 A = 1,XDIMC
          DO 1380 Z = 0,TSTEP

          IF (Z .GT. 0) THEN
            IF (KRGBARNASX(Z,A,B,C) .LT. 0) THEN
              KRGBARNASX(Z,A,B,C) = 0.0
            ENDIF
            IF (KROBARNASX(Z,A,B,C) .LT. 0) THEN
              KROBARNASX(Z,A,B,C) = 0.0
            ENDIF
```

```
      ENDIF

      IF (A .EQ. XDIMC) THEN
      CALL RCURVE
      WRITE (8,*)
      WRITE (8,*) '/','  BLOCK',A,B,C,' X PLUS-DIRECTION (RCURVE)'
      WRITE (8,*)
      GOTO 1370
      ENDIF


C  ********* SECTION 17 C1: X-PLUS END POINT SCALING ***********

      IF (OPT1 .EQ. 2) THEN
      TEMPGASBAR(Z,A,B,C) = SGASBAR(Z,A,B,C)
      SGASBAR(Z,A,B,C) = (SGASBAR(Z,A,B,C)-SGCRM(A,B,C))/
     *                   ((1-SOGCRM(A,B,C))-SGCRM(A,B,C))

      IF (SGASBAR(Z,A,B,C) .LT. 0) THEN
      GOTO 1381
      ELSE
      NAS = NAS + 1
      ENDIF

      IF (NAS .EQ. 1) THEN
      WRITE (8,4000) 0,KRGMIN,KROMAX,0
      ENDIF

      IF (SGASBAR(Z,A,B,C) .GT. 1) THEN
      NAS1 = NAS1 + 1
      ENDIF

      IF (NAS1 .EQ. 1) THEN
      WRITE (8,4000) 1.0000,KRGMAX,KROMIN,0
      GOTO 1381
      ENDIF

      ENDIF

      IF (Z .GT. 0) THEN
      IF (SGASBAR(Z,A,B,C) .EQ. 0) THEN
      GOTO 1381

      ENDIF
      ENDIF


      IF ((KRGBARNASX(Z,A,B,C) + KROBARNASX(Z,A,B,C)) .EQ. 0 )THEN
      GOTO 1381
      ENDIF

      DO 8001 SK = 1,TSTEP

      IF (Z .GE. 1) THEN
      IF (Z - SK .GE. 0) THEN
      IF (SGASBAR(Z,A,B,C)- SGASBAR(Z-SK,A,B,C) .LE. 0.0001) THEN
      GOTO 1381
      ENDIF
      ENDIF
      ENDIF
8001  CONTINUE

      IF (SGASBAR(Z,A,B,C) .GT. 1) THEN
      GOTO 1381
      ENDIF


      WRITE (8,4000) SGASBAR(Z,A,B,C),KRGBARNASX(Z,A,B,C),
     * KROBARNASX(Z,A,B,C),0

1381  IF (Z .EQ. (TSTEP-1)) THEN
      IF (SGASBAR(Z,A,B,C) .LT. 0.75) THE :
      WRITE (8,4000) 0.75000,0.51291,0.00000,0.00000
      WRITE (8,4000) 0.77500,0.61128,0.00000,0.00000
      WRITE (8,4000) 0.80000,0.72420,0.00000,0.00000
      WRITE (8,4000) 0.82500,0.85321,0.00000,0.00000
      ENDIF
      ENDIF

1380  CONTINUE
      WRITE (8,*)
      WRITE (8,*) '/',' BLOCK',A,B,C,' X PLUS-DIRECTION'
      WRITE (8,*)

      NAS = 0
      NAS1 = 0

1370  CONTINUE
1360  CONTINUE
1350  CONTINUE


C  ************ SECTION 17 D: X - MINUS DIRECTION **************

      IF (ZDIMC .EQ. 1) THEN
      IF (YDIMC .EQ. 1) THEN
      GOTO 1511
      ENDIF
      ENDIF

      NAS = 0
      NAS1 = 0

      DO 1390 C = 1,ZDIMC
```

```
      DO 1400 B = 1,YDIMC
      DO 1410 A = 1,XDIMC
      DO 1420 Z = 0,TSTEP

      IF (Z .GT. 0) THEN
      IF (KRGBARNASXM(Z,A,B,C) .LT. 0) THEN
      KRGBARNASXM(Z,A,B,C) = 0.0
      ENDIF
      IF (KROBARNASXM(Z,A,B,C) .LT. 0) THEN
      KROBARNASXM(Z,A,B,C) = 0.0
      ENDIF
        ENDIF

      IF (A .EQ. 1) THEN
      CALL RCURVE
      WRITE (8,*)
      WRITE (8,*) '/','  BLOCK',A,B,C,' X MINUS-DIRECTION (RCURVE)'
      WRITE (8,*)
      GOTO 1410
      ENDIF


C  ****** SECTION 17 D1: X-MINUS  END POINT SCALING ***************

      IF (OPT1 .EQ. 2) THEN
      SGASBAR(Z,A,B,C) = TEMPGASBAR(Z,A,B,C)
      SGASBAR(Z,A,B,C) = (SGASBAR(Z,A,B,C)-SGCRM(A,B,C))/
     *                   ((1-SOGCRM(A,B,C))-SGCRM(A,B,C))

      IF (SGASBAR(Z,A,B,C) .LT. 0) THEN
      GOTO 1421
      ELSE
      NAS = NAS + 1
      ENDIF

      IF (NAS .EQ. 1) THEN
      WRITE (8,4000) 0,KRGMIN,KROMAX,0
      ENDIF

      IF (SGASBAR(Z,A,B,C) .GT. 1) THEN
      NAS1 = NAS1 + 1
      ENDIF

      IF (NAS1 .EQ. 1) THEN
      WRITE (8,4000) 1.0000,KRGMAX,KROMIN,0
      GOTO 1421
      ENDIF

      ENDIF

      IF (Z .GT. 0) THEN
      IF (SGASBAR(Z,A,B,C) .EQ. 0) THEN
      GOTO 1421

      ENDIF
      ENDIF

      IF ((KRGBARNASXM(Z,A,B,C) + KROBARNASXM(Z,A,B,C)) .EQ. 0 )THEN
      GOTO 1421
      ENDIF

      DO 8002 SK = 1,TSTEP
      IF (Z .GE. 1) THEN
      IF (Z- SK .GE. 0) THEN
      IF (SGASBAR(Z,A,B,C)- SGASBAR(Z-SK,A,B,C) .LE. 0.0001) THEN
      GOTO 1421
      ENDIF
      ENDIF
      ENDIF
8002  CONTINUE

      IF (SGASBAR(Z,A,B,C) .GT. 1) THEN
      GOTO 1421
      ENDIF

      )
        WRITE (8,4000) SGASBAR(Z,A,B,C),KRGBARNASXM(Z,A,B,C),
     *  KROBARNASXM(Z,A,B,C),0

1421  IF (Z .EQ. (TSTEP-1)) THEN
      IF (SGASBAR(Z,A,B,C) .LT. 0.75) THEN
      WRITE (8,4000) 0.75000,0.51291,0.00000,0.00000
      WRITE (8,4000) 0.77500,0.61128,0.00000,0.00000
      WRITE (8,4000) 0.80000,0.72420,0.00000,0.00000
      WRITE (8,4000) 0.82500,0.85321,0.00000,0.00000
      ENDIF
      ENDIF

1420  CONTINUE

      WRITE (8,*)
      WRITE (8,*) '/',' BLOCK',A,B,C,' X MINUS-DIRECTION'
      WRITE (8,*)

      NAS = 0
      NAS1 = 0

1410  CONTINUE
1400  CONTINUE
1390  CONTINUE


C  ********* SECTION 17 E: PRINTING Y-PLUS DIRECTION *************

      IF (YDIMC .GT. 1 ) THEN
```

```
      DO 1351 C = 1,ZDIMC
      DO 1352 B = 1,YDIMC
      DO 1353 A = 1,XDIMC
      DO 1354 Z = 0,TSTEP

      IF (Z .GT. 0) THEN
        IF (KRGBARNASY(Z,A,B,C) .LT. 0) THEN
          KRGBARNASY(Z,A,B,C) = 0.0
        ENDIF
        IF (KROBARNASY(Z,A,B,C) .LT. 0) THEN
          KROBARNASY(Z,A,B,C) = 0.0
        ENDIF
      ENDIF

      IF (B .EQ. YDIMC) THEN
      CALL RCURVE
      WRITE (8,*)
      WRITE (8,*) '/','  BLOCK',A,B,C,' Y PLUS-DIRECTION (RCURVE)'
      WRITE (8,*)
      GOTO 1353
      ENDIF

C  ********* SECTION 17 E1: Y-PLUS END POINT SCALING ***********
      IF (OPT1 .EQ. 2) THEN
      TEMPGASBAR(Z,A,B,C) = SGASBAR(Z,A,B,C)
      SGASBAR(Z,A,B,C) = (SGASBAR(Z,A,B,C)-SGCRM(A,B,C))/
     *                   ((1-SOGCRM(A,B,C))-SGCRM(A,B,C))

      IF (SGASBAR(Z,A,B,C) .LT. 0) THEN
      GOTO 1355
      ELSE
      NAS = NAS + 1
      ENDIF

      IF (NAS .EQ. 1) THEN
      WRITE (8,4000) 0,KRGMIN,KROMAX,0
      ENDIF

      IF (SGASBAR(Z,A,B,C) .GT. 1) THEN
      NAS1 = NAS1 + 1
      ENDIF

      IF (NAS1 .EQ. 1) THEN
      WRITE (8,4000) 1.0000,KRGMAX,KROMIN,0
      GOTO 1355
      ENDIF

      ENDIF

      IF (Z .GT. 0) THEN
      IF (SGASBAR(Z,A,B,C) .EQ. 0) THEN
      GOTO 1355

      ENDIF
      ENDIF


      IF ((KRGBARNASY(Z,A,B,C) + KROBARNASY(Z,A,B,C)) .EQ. 0 )THEN
      GOTO 1355
      ENDIF

      DO 1356 SK = 1,TSTEP
      IF (Z .GE. 1) THEN
      IF (Z - SK .GE. 0) THEN
      IF (SGASBAR(Z,A,B,C)- SGASBAR(Z-SK,A,B,C) .LE. 0.0001) THEN
      GOTO 1355
      ENDIF
      ENDIF
      ENDIF
1356  CONTINUE

      IF (SGASBAR(Z,A,B,C) .GT. 1) THEN
      GOTO 1355
      ENDIF

      WRITE (8,4000) SGASBAR(Z,A,B,C),KRGBARNASY(Z,A,B,C),
     *KROBARNASY(Z,A,B,C),0

1355  IF (Z .EQ. (TSTEP-1)) THEN
      IF (SGASBAR(Z,A,B,C) .LT. 0.75) THEN
      WRITE (8,4000) 0.75000,0.51291,0.00000,0.00000
      WRITE (8,4000) 0.77500,0.61128,0.00000,0.00000
      WRITE (8,4000) 0.80000,0.72420,0.00000,0.00000
      WRITE (8,4000) 0.82500,0.85321,0.00000,0.00000
      ENDIF
      ENDIF

1354  CONTINUE

      WRITE (8,*)
      WRITE (8,*) '/','  BLOCK',A,B,C,' Y PLUS-DIRECTION'
      WRITE (8,*)

      NAS = 0
      NAS1 = 0

1353  CONTINUE
1352  CONTINUE
1351  CONTINUE
```

```
C  ************ SECTION 17 F: Y - MINUS DIRECTION ***************

        NAS = 0
        NAS1 = 0

        DO 1361 C = 1,ZDIMC
        DO 1362 B = 1,YDIMC
        DO 1363 A = 1,XDIMC
        DO 1364 Z = 0,TSTEP

        IF (Z .GT. 0) THEN
        IF (KRGBARNASYM(Z,A,B,C) .LT. 0) THEN
        KRGBARNASYM(Z,A,B,C) = 0.0
        ENDIF
        IF (KROBARNASYM(Z,A,B,C) .LT. 0) THEN
        KROBARNASYM(Z,A,B,C) = 0.0
        ENDIF
        ENDIF

        IF (B .EQ. 1) THEN
        CALL RCURVE
        WRITE (8,*)
        WRITE (8,*) '/','  BLOCK',A,B,C,' Y MINUS-DIRECTION (RCURVE)'
        WRITE (8,*)
        GOTO 1363
        ENDIF

C  ****** SECTION 17 F1: Y-MINUS  END POINT SCALING ***************

        IF (OPT1 .EQ. 2) THEN
        SGASBAR(Z,A,B,C) = TEMPGASBAR(Z,A,B,C)
        SGASBAR(Z,A,B,C) = (SGASBAR(Z,A,B,C)-SGCRM(A,B,C))/
     *                     ((1-SOGCRM(A,B,C))-SGCRM(A,B,C))

        IF (SGASBAR(Z,A,B,C) .LT. 0) THEN
        GOTO 1365
        ELSE
        NAS = NAS + 1
        ENDIF

        IF (NAS .EQ. 1) THEN
        WRITE (8,4000) 0,KRGMIN,KROMAX,0
        ENDIF

        IF (SGASBAR(Z,A,B,C) .GT. 1) THEN
        NAS1 = NAS1 + 1
        ENDIF

        IF (NAS1 .EQ. 1) THEN
        WRITE (8,4000) 1.0000,KRGMAX,KROMIN,0
        GOTO 1365
        ENDIF

        ENDIF

        IF (Z .GT. 0) THEN
        IF (SGASBAR(Z,A,B,C) .EQ. 0) THEN
        GOTO 1365

        ENDIF
        ENDIF

        IF ((KRGBARNASYM(Z,A,B,C) + KROBARNASYM(Z,A,B,C)) .EQ. 0 )THEN
        GOTO 1365
        ENDIF

        DO 1366 SK = 1,TSTEP
        IF (Z .GE. 1) THEN
        IF (Z- SK .GE. 0) THEN
        IF (SGASBAR(Z,A,B,C)- SGASBAR(Z-SK,A,B,C) .LE. 0.0001) THEN
        GOTO 1365
        ENDIF
        ENDIF
        ENDIF
1366    CONTINUE

        IF (SGASBAR(Z,A,B,C) .GT. 1) THEN
        GOTO 1365
        ENDIF

        WRITE (8,4000) SGASBAR(Z,A,B,C),KRGBARNASYM(Z,A,B,C),
     *  KROBARNASYM(Z,A,B,C),0

1365    IF (Z .EQ. (TSTEP-1)) THEN
        IF (SGASBAR(Z,A,B,C) .LT. 0.75) THEN
        WRITE (8,4000) 0.75000,0.51291,0.00000,0.00000
        WRITE (8,4000) 0.77500,0.61128,0.00000,0.00000
        WRITE (8,4000) 0.80000,0.72420,0.00000,0.00000
        WRITE (8,4000) 0.82500,0.85321,0.00000,0.00000
        ENDIF
        ENDIF

1364    CONTINUE

        WRITE (8,*)
        WRITE (8,*) '/','  BLOCK',A,B,C,' Y MINUS-DIRECTION'
        WRITE (8,*)

        NAS = 0
        NAS1 = 0
```

```
1363      CONTINUE
1362      CONTINUE
1361      CONTINUE

          ENDIF

C  ************ SECTION 17G : Z - PLUS DIRECTION ***************

          IF (ZDIMC .GT. 1) THEN

          NAS = 0
          NAS1 = 0

          DO 1430 C = 1,ZDIMC
          DO 1440 B = 1,YDIMC
          DO 1450 A = 1,XDIMC
          DO 1460 Z = 0,TSTEP

          IF (Z .GT. 0) THEN
          IF (KRGBARNASZ(Z,A,B,C) .LT. 0) THEN
          KRGBARNASZ(Z,A,B,C) = 0.0
          ENDIF
          IF (KROBARNASZ(Z,A,B,C) .LT. 0) THEN
          KROBARNASZ(Z,A,B,C) = 0.0
          ENDIF
          ENDIF

          IF (C .EQ. ZDIMC) THEN
          CALL RCURVE
          WRITE (8,*)
          WRITE (8,*) '/','  BLOCK',A,B,C,' Z PLUS - DIRECTION (RCURVE)'
          WRITE (8,*)
          GOTO 1450
          ENDIF


C  ***** SECTION 17 G1: Z-PLUS  END POINT SCALING ******************

          IF (OPT1 .EQ. 2) THEN
          SGASBAR(Z,A,B,C) = TEMPGASBAR(Z,A,B,C)
          SGASBAR(Z,A,B,C) = (SGASBAR(Z,A,B,C)-SGCRM(A,B,C))/
     *                       ((1-SOGCRM(A,B,C))-SGCRM(A,B,C))

          IF (SGASBAR(Z,A,B,C) .LT. 0) THEN
          GOTO 1461
          ELSE
          NAS = NAS + 1
          ENDIF

          IF (NAS .EQ. 1) THEN
          WRITE (8,4000) 0,KRGMIN,KROMAX,0
          ENDIF

          IF (SGASBAR(Z,A,B,C) .GT. 1) THEN
          NAS1 = NAS1 + 1
          ENDIF

          IF (NAS1 .EQ. 1) THEN
          WRITE (8,4000) 1.0000,KRGMAX,KROMIN,0
          GOTO 1461
          ENDIF

          ENDIF

          IF (Z .GT. 0) THEN
          IF (SGASBAR(Z,A,B,C) .EQ. 0) THEN
          GOTO 1461
          ENDIF
          ENDIF

          IF ((KRGBARNASZ(Z,A,B,C)+KROBARNASZ(Z,A,B,C)) .EQ. 0 )THEN
          GOTO 1461
          ENDIF


          DO 8003 SK = 1,TSTEP
          IF (Z .GE. 1) THEN
          IF (Z-SK .GE. 0) THEN
          IF (SGASBAR(Z,A,B,C)- SGASBAR(Z-SK,A,B,C) .LE. 0.0001) THEN
          GOTO 1461
          ENDIF
          ENDIF
          ENDIF
8003      CONTINUE


          IF (SGASBAR(Z,A,B,C) .GT. 1) THEN
          GOTO 1461
          ENDIF

          WRITE (8,4000) SGASBAR(Z,A,B,C),KRGBARNASZ(Z,A,B,C),
     *    KROBARNASZ(Z,A,B,C),0

1461      IF (Z .EQ. (TSTEP-1)) THEN
          IF (SGASBAR(Z,A,B,C) .LT. 0.75) THEN
          WRITE (8,4000) 0.75000,0.51291,0.00000,0.00000
          WRITE (8,4000) 0.77500,0.61128,0.00000,0.00000
          WRITE (8,4000) 0.80000,0.72420,0.00000,0.00000
          WRITE (8,4000) 0.82500,0.85321,0.00000,0.00000
          ENDIF
          ENDIF
```

```
1460        CONTINUE

        WRITE (8,*)
        WRITE (8,*) '/','  BLOCK',A,B,C,' Z PLUS - DIRECTION'
        WRITE (8,*)

        NAS=0
        NAS1=0

1450    CONTINUE
1440    CONTINUE
1430    CONTINUE


C  ************ SECTION 17 H: Z - MINUS DIRECTION ***************

        NAS=0
        NAS1=0

        DO 1470 C = 1,ZDIMC
        DO 1480 B = 1,YDIMC
        DO 1490 A = 1,XDIMC
        DO 1500 Z = 0,TSTEP

        IF (Z .GT. 0) THEN
        IF (KRGBARNASZM(Z,A,B,C) .LT. 0) THEN
        KRGBARNASZM(Z,A,B,C) = 0.0
        ENDIF
        IF (KROBARNASZM(Z,A,B,C) .LT. 0) THEN
        KROBARNASZM(Z,A,B,C) = 0.0
        ENDIF
        ENDIF

        IF (C .EQ. 1) THEN
        CALL RCURVE
        WRITE (8,*)
        WRITE (8,*) '/','  BLOCK',A,B,C,' Z MINUS - DIRECTION (RCURVE)'
        WRITE (8,*)

        GOTO 1490
        ENDIF

C  ****** SECTION 17 H1 :  END POINT SCALING ***********************

        IF (OPT1 .EQ. 2) THEN
        SGASBAR(Z,A,B,C) = TEMPGASBAR(Z,A,B,C)
        SGASBAR(Z,A,B,C) = (SGASBAR(Z,A,B,C)-SGCRM(A,B,C))/
     *                     ((1-SOGCRM(A,B,C))-SGCRM(A,B,C))

        IF (SGASBAR(Z,A,B,C) .LT. 0) THEN
        GOTO 1501
        ELSE
        NAS = NAS + 1
        ENDIF

        IF (NAS .EQ. 1) THEN
        WRITE (8,4000) 0,KRGMIN,KROMAX,0
        ENDIF

        IF (SGASBAR(Z,A,B,C) .GT. 1) THEN
        NAS1 = NAS1 + 1
        ENDIF

        IF (NAS1 .EQ. 1) THEN
        WRITE (8,4000) 1.0000,KRGMAX,KROMIN,0
        GOTO 1501
        ENDIF

        ENDIF

        IF (Z .GT. 0) THEN
        IF (SGASBAR(Z,A,B,C) .EQ. 0) THEN
        GOTO 1501

        ENDIF
        ENDIF

        IF ((KRGBARNASZM(Z,A,B,C)+KROBARNASZM(Z,A,B,C)) .EQ. 0 )THEN
        GOTO 1501
        ENDIF

        DO 8004 SK = 1,TSTEP
        IF (Z .GE. 1) THEN
        IF (Z-SK .GE. 0) THEN
        IF (SGASBAR(Z,A,B,C)- SGASBAR(Z-SK,A,B,C) .LE. 0.0001) THEN
        GOTO 1501
        ENDIF
        ENDIF
        ENDIF
8004    CONTINUE


        IF (SGASBAR(Z,A,B,C) .GT. 1) THEN
        GOTO 1501
        ENDIF

        WRITE (8,4000) SGASBAR(Z,A,B,C),KRGBARNASZM(Z,A,B,C),
     *  KROBARNASZM(Z,A,B,C),0

1501    IF (Z .EQ. (TSTEP-1)) THEN
        IF (SGASBAR(Z,A,B,C) .LT. 0.75) THEN
        WRITE (8,4000) 0.75000,0.51291,0.00000,0.00000
        WRITE (8,4000) 0.77500,0.61128,0.00000,0.00000
        WRITE (8,4000) 0.80000,0.72420,0.00000,0.00000
```

```
        WRITE (8,4000) 0.82500,0.85321,0.00000,0.00000
        ENDIF
        ENDIF

 1500       CONTINUE

        WRITE (8,*)
        WRITE (8,*) '/',' BLOCK',A,B,C,' Z MINUS - DIRECTION'
        WRITE (8,*)

        NAS=0
        NAS1=0

 1490   CONTINUE
 1480   CONTINUE
 1470   CONTINUE

        ENDIF

C ********** SECTION 18: PRINTING REGION KEYWORD **************

 1511   PRINT *

        WRITE (8,*)'REGIONS'
        WRITE (8,*)'SATNUM'

        DO 1510 C = 1,ZDIMC*XDIMC*YDIMC,10

        IF (C .EQ. ZDIMC*XDIMC*YDIMC)THEN
        WRITE (8,6000) C
        GOTO 1510
        ELSEIF (C+1 .EQ. ZDIMC*XDIMC*YDIMC) THEN
        WRITE (8,6000) C,C+1
        GOTO 1510
        ELSEIF (C+2 .EQ. ZDIMC*XDIMC*YDIMC) THEN
        WRITE (8,6000) C,C+1,C+2
        GOTO 1510
        ELSEIF (C+3 .EQ. ZDIMC*XDIMC*YDIMC) THEN
        WRITE (8,6000) C,C+1,C+2,C+3
        GOTO 1510
        ELSEIF (C+4 .EQ. ZDIMC*XDIMC*YDIMC) THEN
        WRITE (8,6000) C,C+1,C+2,C+3,C+4
        GOTO 1510
        ELSEIF (C+5 .EQ. ZDIMC*XDIMC*YDIMC) THEN
        WRITE (8,6000) C,C+1,C+2,C+3,C+4,C+5
        GOTO 1510
        ELSEIF (C+6 .EQ. ZDIMC*XDIMC*YDIMC) THEN
        WRITE (8,6000) C,C+1,C+2,C+3,C+4,C+5,C+6
        GOTO 1510
        ELSEIF (C+7 .EQ. ZDIMC*XDIMC*YDIMC) THEN
        WRITE (8,6000) C,C+1,C+2,C+3,C+4,C+5,C+6,C+7
        GOTO 1510
        ELSEIF (C+8 .EQ. ZDIMC*XDIMC*YDIMC) THEN
        WRITE (8,6000) C,C+1,C+2,C+3,C+4,C+5,C+6,C+7,C+8
        GOTO 1510
        ELSEIF (C+8 .EQ. ZDIMC*XDIMC*YDIMC) THEN
        WRITE (8,6000) C,C+1,C+2,C+3,C+4,C+5,C+6,C+7,C+8
        GOTO 1510
        ELSE
        WRITE (8,6000) C,C+1,C+2,C+3,C+4,C+5,C+6,C+7,C+8,C+9

        ENDIF

 1510   CONTINUE
        WRITE (8,*) '/'

C       ******** SECTION 18 A: KRNUMX ************************

        IF (YDIMC .EQ. 1) THEN
        IF (ZDIMC .EQ. 1) THEN
        GOTO 1553
        ENDIF
        ENDIF

        WRITE (8,*)''
        WRITE (8,*)''
        WRITE (8,*)'KRNUMX'

        DO 1520 C = 1,ZDIMC*XDIMC*YDIMC,10

        IF (C .EQ. ZDIMC*XDIMC*YDIMC)THEN
        WRITE (8,6000) C
        GOTO 1520
        ELSEIF (C+1 .EQ. ZDIMC*XDIMC*YDIMC) THEN
        WRITE (8,6000) C,C+1
        GOTO 1520
        ELSEIF (C+2 .EQ. ZDIMC*XDIMC*YDIMC) THEN
        WRITE (8,6000) C,C+1,C+2
        GOTO 1520
        ELSEIF (C+3 .EQ. ZDIMC*XDIMC*YDIMC) THEN
        WRITE (8,6000) C,C+1,C+2,C+3
        GOTO 1520
        ELSEIF (C+4 .EQ. ZDIMC*XDIMC*YDIMC) THEN
        WRITE (8,6000) C,C+1,C+2,C+3,C+4
        GOTO 1520
        ELSEIF (C+5 .EQ. ZDIMC*XDIMC*YDIMC) THEN
        WRITE (8,6000) C,C+1,C+2,C+3,C+4,C+5
        GOTO 1520
        ELSEIF (C+6 .EQ. ZDIMC*XDIMC*YDIMC) THEN
        WRITE (8,6000) C,C+1,C+2,C+3,C+4,C+5,C+6
        GOTO 1520
        ELSEIF (C+7 .EQ. ZDIMC*XDIMC*YDIMC) THEN
        WRITE (8,6000) C,C+1,C+2,C+3,C+4,C+5,C+6,C+7
        GOTO 1520
        ELSEIF (C+8 .EQ. ZDIMC*XDIMC*YDIMC) THEN
        WRITE (8,6000) C,C+1,C+2,C+3,C+4,C+5,C+6,C+7,C+8
```

```
      GOTO 1520
       ELSE
      WRITE (8,6000) C,C+1,C+2,C+3,C+4,C+5,C+6,C+7,C+8,C+9
       ENDIF
1520   CONTINUE
      WRITE (8,*) '/'


C     ******** SECTION 18 B: KRNUMX- ************************

      WRITE (8,*)''
      WRITE (8,*)''
      WRITE (8,*)'KRNUMX-'

      DO 1530 C = ZDIMC*XDIMC*YDIMC+1,ZDIMC*XDIMC*YDIMC*2,10

      IF (C .EQ. ZDIMC*XDIMC*YDIMC*2)THEN
      WRITE (8,6000) C
      GOTO 1530
      ELSEIF (C+1 .EQ. ZDIMC*XDIMC*YDIMC*2) THEN
      WRITE (8,6000) C,C+1
      GOTO 1530
      ELSEIF (C+2 .EQ. ZDIMC*XDIMC*YDIMC*2) THEN
      WRITE (8,6000) C,C+1,C+2
      GOTO 1530
      ELSEIF (C+3 .EQ. ZDIMC*XDIMC*YDIMC*2) THEN
      WRITE (8,6000) C,C+1,C+2,C+3
      GOTO 1530
      ELSEIF (C+4 .EQ. ZDIMC*XDIMC*YDIMC*2) THEN
      WRITE (8,6000) C,C+1,C+2,C+3,C+4
      GOTO 1530
      ELSEIF (C+5 .EQ. ZDIMC*XDIMC*YDIMC*2) THEN
      WRITE (8,6000) C,C+1,C+2,C+3,C+4,C+5
      GOTO 1530
      ELSEIF (C+6 .EQ. ZDIMC*XDIMC*YDIMC*2) THEN
      WRITE (8,6000) C,C+1,C+2,C+3,C+4,C+5,C+6
      GOTO 1530
      ELSEIF (C+7 .EQ. ZDIMC*XDIMC*YDIMC*2) THEN
      WRITE (8,6000) C,C+1,C+2,C+3,C+4,C+5,C+6,C+7
      GOTO 1530
      ELSEIF (C+8 .EQ. ZDIMC*XDIMC*YDIMC*2) THEN
      WRITE (8,6000) C,C+1,C+2,C+3,C+4,C+5,C+6,C+7,C+8
      GOTO 1530
       ELSE

        WRITE (8,6000) C,C+1,C+2,C+3,C+4,C+5,C+6,C+7,C+8,C+9
        ENDIF

1530   CONTINUE
      WRITE (8,*) '/'


C     ******** SECTION 18 C: KRNUMY ************************

      IF (YDIMC .GT. 1) THEN

      WRITE (8,*)''
      WRITE (8,*)''
      WRITE (8,*)'KRNUMY'

      DO 1541 C = (ZDIMC*XDIMC*YDIMC*2)+1,ZDIMC*XDIMC*YDIMC*3,10

      IF (C .EQ. ZDIMC*XDIMC*YDIMC*3)THEN
      WRITE (8,6000) C
      GOTO 1541
      ELSEIF (C+1 .EQ. ZDIMC*XDIMC*YDIMC*3) THEN
      WRITE (8,6000) C,C+1
      GOTO 1541
      ELSEIF (C+2 .EQ. ZDIMC*XDIMC*YDIMC*3) THEN
      WRITE (8,6000) C,C+1,C+2
      GOTO 1541
      ELSEIF (C+3 .EQ. ZDIMC*XDIMC*YDIMC*3) THEN
      WRITE (8,6000) C,C+1,C+2,C+3
      GOTO 1541
      ELSEIF (C+4 .EQ. ZDIMC*XDIMC*YDIMC*3) THEN
      WRITE (8,6000) C,C+1,C+2,C+3,C+4
      GOTO 1541
      ELSEIF (C+5 .EQ. ZDIMC*XDIMC*YDIMC*3) THEN
      WRITE (8,6000) C,C+1,C+2,C+3,C+4,C+5
      GOTO 1541
      ELSEIF (C+6 .EQ. ZDIMC*XDIMC*YDIMC*3) THEN
      WRITE (8,6000) C,C+1,C+2,C+3,C+4,C+5,C+6
      GOTO 1541
      ELSEIF (C+7 .EQ. ZDIMC*XDIMC*YDIMC*3) THEN
      WRITE (8,6000) C,C+1,C+2,C+3,C+4,C+5,C+6,C+7
      GOTO 1541
      ELSEIF (C+8 .EQ. ZDIMC*XDIMC*YDIMC*3) THEN
      WRITE (8,6000) C,C+1,C+2,C+3,C+4,C+5,C+6,C+7,C+8
      GOTO 1541
       ELSE

      WRITE (8,6000) C,C+1,C+2,C+3,C+4,C+5,C+6,C+7,C+8,C+9
      ENDIF
1541   CONTINUE
      WRITE (8,*) '/'


C     ******** SECTION 18 D: KRNUMY- ************************

      WRITE (8,*)''
      WRITE (8,*)''
      WRITE (8,*)'KRNUMY-'

      DO 1542 C = (ZDIMC*XDIMC*YDIMC*3)+1,ZDIMC*XDIMC*YDIMC*4,10
```

```
      IF (C .EQ. ZDIMC*XDIMC*YDIMC*4)THEN
      WRITE (8,6000) C
      GOTO 1542
      ELSEIF (C+1 .EQ. ZDIMC*XDIMC*YDIMC*4) THEN
      WRITE (8,6000) C,C+1
      GOTO 1542
      ELSEIF (C+2 .EQ. ZDIMC*XDIMC*YDIMC*4) THEN
      WRITE (8,6000) C,C+1,C+2
      GOTO 1542
      ELSEIF (C+3 .EQ. ZDIMC*XDIMC*YDIMC*4) THEN
      WRITE (8,6000) C,C+1,C+2,C+3
      GOTO 1542
      ELSEIF (C+4 .EQ. ZDIMC*XDIMC*YDIMC*4) THEN
      WRITE (8,6000) C,C+1,C+2,C+3,C+4
      GOTO 1542
      ELSEIF (C+5 .EQ. ZDIMC*XDIMC*YDIMC*4) THEN
      WRITE (8,6000) C,C+1,C+2,C+3,C+4,C+5
      GOTO 1542
      ELSEIF (C+6 .EQ. ZDIMC*XDIMC*YDIMC*4) THEN
      WRITE (8,6000) C,C+1,C+2,C+3,C+4,C+5,C+6
      GOTO 1542
      ELSEIF (C+7 .EQ. ZDIMC*XDIMC*YDIMC*4) THEN
      WRITE (8,6000) C,C+1,C+2,C+3,C+4,C+5,C+6,C+7
      GOTO 1542
      ELSEIF (C+8 .EQ. ZDIMC*XDIMC*YDIMC*4) THEN
      WRITE (8,6000) C,C+1,C+2,C+3,C+4,C+5,C+6,C+7,C+8
      GOTO 1542
      ELSE


      WRITE (8,6000) C,C+1,C+2,C+3,C+4,C+5,C+6,C+7,C+8,C+9
      ENDIF
 1542 CONTINUE
      WRITE (8,*) '/'

      ELSE
      NOY = 1
      ENDIF


C     ******** SECTION 18 E: KRNUMZ *************************

      IF (ZDIMC .EQ. 1) THEN
      GOTO 1553
      END IF


      IF (NOY .EQ. 1) THEN


      WRITE (8,*)''
      WRITE (8,*)''
      WRITE (8,*)'KRNUMZ'

      DO 1540 C = (ZDIMC*XDIMC*YDIMC*2)+1,ZDIMC*XDIMC*YDIMC*3,10

      IF (C .EQ. ZDIMC*XDIMC*YDIMC*3)THEN
      WRITE (8,6000) C
      GOTO 1540
      ELSEIF (C+1 .EQ. ZDIMC*XDIMC*YDIMC*3) THEN
      WRITE (8,6000) C,C+1
      GOTO 1540
      ELSEIF (C+2 .EQ. ZDIMC*XDIMC*YDIMC*3) THEN
      WRITE (8,6000) C,C+1,C+2
      GOTO 1540
      ELSEIF (C+3 .EQ. ZDIMC*XDIMC*YDIMC*3) THEN
      WRITE (8,6000) C,C+1,C+2,C+3
      GOTO 1540
      ELSEIF (C+4 .EQ. ZDIMC*XDIMC*YDIMC*3) THEN
      WRITE (8,6000) C,C+1,C+2,C+3,C+4
      GOTO 1540
      ELSEIF (C+5 .EQ. ZDIMC*XDIMC*YDIMC*3) THEN
      WRITE (8,6000) C,C+1,C+2,C+3,C+4,C+5
      GOTO 1540
      ELSEIF (C+6 .EQ. ZDIMC*XDIMC*YDIMC*3) THEN
      WRITE (8,6000) C,C+1,C+2,C+3,C+4,C+5,C+6
      GOTO 1540
      ELSEIF (C+7 .EQ. ZDIMC*XDIMC*YDIMC*3) THEN
      WRITE (8,6000) C,C+1,C+2,C+3,C+4,C+5,C+6,C+7
      GOTO 1540
      ELSEIF (C+8 .EQ. ZDIMC*XDIMC*YDIMC*3) THEN
      WRITE (8,6000) C,C+1,C+2,C+3,C+4,C+5,C+6,C+7,C+8
      GOTO 1540
       ELSE



      WRITE (8,6000) C,C+1,C+2,C+3,C+4,C+5,C+6,C+7,C+8,C+9
      ENDIF
 1540  CONTINUE
      WRITE (8,*) '/'


C     ******** SECTION 18 F: KRNUMZ- *************************

      WRITE (8,*)''
      WRITE (8,*)''
      WRITE (8,*)'KRNUMZ-'

      DO 1550 C = (ZDIMC*XDIMC*YDIMC*3)+1,ZDIMC*XDIMC*YDIMC*4,10

      IF (C .EQ. ZDIMC*XDIMC*YDIMC*4)THEN
      WRITE (8,6000) C
```

```
GOTO 1550
ELSEIF (C+1 .EQ. ZDIMC*XDIMC*YDIMC*4) THEN
WRITE (8,6000) C,C+1
GOTO 1550
ELSEIF (C+2 .EQ. ZDIMC*XDIMC*YDIMC*4) THEN
WRITE (8,6000) C,C+1,C+2
GOTO 1550
ELSEIF (C+3 .EQ. ZDIMC*XDIMC*YDIMC*4) THEN
WRITE (8,6000) C,C+1,C+2,C+3
GOTO 1550
ELSEIF (C+4 .EQ. ZDIMC*XDIMC*YDIMC*4) THEN
WRITE (8,6000) C,C+1,C+2,C+3,C+4
GOTO 1550
ELSEIF (C+5 .EQ. ZDIMC*XDIMC*YDIMC*4) THEN
WRITE (8,6000) C,C+1,C+2,C+3,C+4,C+5
GOTO 1550
ELSEIF (C+6 .EQ. ZDIMC*XDIMC*YDIMC*4) THEN
WRITE (8,6000) C,C+1,C+2,C+3,C+4,C+5,C+6
GOTO 1550
ELSEIF (C+7 .EQ. ZDIMC*XDIMC*YDIMC*4) THEN
WRITE (8,6000) C,C+1,C+2,C+3,C+4,C+5,C+6,C+7
GOTO 1550
ELSEIF (C+8 .EQ. ZDIMC*XDIMC*YDIMC*4) THEN
WRITE (8,6000) C,C+1,C+2,C+3,C+4,C+5,C+6,C+7,C+8
GOTO 1550
ELSE

      WRITE (8,6000) C,C+1,C+2,C+3,C+4,C+5,C+6,C+7,C+8,C+9
      ENDIF
1550  CONTINUE
      WRITE (8,*) '/'

      ELSE

      WRITE (8,*)''
      WRITE (8,*)''
      WRITE (8,*)'KRNUMZ'

      DO 1551 C = (ZDIMC*XDIMC*YDIMC*4)+1,ZDIMC*XDIMC*YDIMC*5,10

      IF (C .EQ. ZDIMC*XDIMC*YDIMC*5)THEN
      WRITE (8,6000) C
      GOTO 1551
      ELSEIF (C+1 .EQ. ZDIMC*XDIMC*YDIMC*5) THEN
      WRITE (8,6000) C,C+1
      GOTO 1551
      ELSEIF (C+2 .EQ. ZDIMC*XDIMC*YDIMC*5) THEN
      WRITE (8,6000) C,C+1,C+2
      GOTO 1551
      ELSEIF (C+3 .EQ. ZDIMC*XDIMC*YDIMC*5) THEN
      WRITE (8,6000) C,C+1,C+2,C+3
      GOTO 1551
      ELSEIF (C+4 .EQ. ZDIMC*XDIMC*YDIMC*5) THEN
      WRITE (8,6000) C,C+1,C+2,C+3,C+4
      GOTO 1551
      ELSEIF (C+5 .EQ. ZDIMC*XDIMC*YDIMC*5) THEN
      WRITE (8,6000) C,C+1,C+2,C+3,C+4,C+5
      GOTO 1551
      ELSEIF (C+6 .EQ. ZDIMC*XDIMC*YDIMC*5) THEN
      WRITE (8,6000) C,C+1,C+2,C+3,C+4,C+5,C+6
      GOTO 1551
      ELSEIF (C+7 .EQ. ZDIMC*XDIMC*YDIMC*5) THEN
      WRITE (8,6000) C,C+1,C+2,C+3,C+4,C+5,C+6,C+7
      GOTO 1551
      ELSEIF (C+8 .EQ. ZDIMC*XDIMC*YDIMC*5) THEN
      WRITE (8,6000) C,C+1,C+2,C+3,C+4,C+5,C+6,C+7,C+8
      GOTO 1551
       ELSE

      WRITE (8,6000) C,C+1,C+2,C+3,C+4,C+5,C+6,C+7,C+8,C+9
      ENDIF
1551  CONTINUE
      WRITE (8,*) '/'

      WRITE (8,*)''
      WRITE (8,*)''
      WRITE (8,*)'KRNUMZ-'

      DO 1552 C = (ZDIMC*XDIMC*YDIMC*5)+1,ZDIMC*XDIMC*YDIMC*6,10

      IF (C .EQ. ZDIMC*XDIMC*YDIMC*6)THEN
      WRITE (8,6000) C
      GOTO 1552
      ELSEIF (C+1 .EQ. ZDIMC*XDIMC*YDIMC*6) THEN
      WRITE (8,6000) C,C+1
      GOTO 1552
      ELSEIF (C+2 .EQ. ZDIMC*XDIMC*YDIMC*6) THEN
      WRITE (8,6000) C,C+1,C+2
      GOTO 1552
      ELSEIF (C+3 .EQ. ZDIMC*XDIMC*YDIMC*6) THEN
      WRITE (8,6000) C,C+1,C+2,C+3
      GOTO 1552
      ELSEIF (C+4 .EQ. ZDIMC*XDIMC*YDIMC*6) THEN
      WRITE (8,6000) C,C+1,C+2,C+3,C+4
      GOTO 1552
      ELSEIF (C+5 .EQ. ZDIMC*XDIMC*YDIMC*6) THEN
      WRITE (8,6000) C,C+1,C+2,C+3,C+4,C+5
      GOTO 1552
      ELSEIF (C+6 .EQ. ZDIMC*XDIMC*YDIMC*6) THEN
      WRITE (8,6000) C,C+1,C+2,C+3,C+4,C+5,C+6
      GOTO 1552
      ELSEIF (C+7 .EQ. ZDIMC*XDIMC*YDIMC*6) THEN
      WRITE (8,6000) C,C+1,C+2,C+3,C+4,C+5,C+6,C+7
```

```
      GOTO 1552
      ELSEIF (C+8 .EQ. ZDIMC*XDIMC*YDIMC*6) THEN
      WRITE (8,6000) C,C+1,C+2,C+3,C+4,C+5,C+6,C+7,C+8
      GOTO 1552
      ELSE


      WRITE (8,6000) C,C+1,C+2,C+3,C+4,C+5,C+6,C+7,C+8,C+9
      ENDIF
 1552 CONTINUE
      WRITE (8,*) '/'

      END IF

 1553 PRINT *

1600  FORMAT (4E17.0)
2000  FORMAT (I12)
3000  FORMAT (4E17.0)
4000  FORMAT (E15.5,'    ',E15.5,'    ',E15.5,'    ',E15.5)
5000  FORMAT (E15.4,'  ',E15.4,'  ',E15.4,'  ',E15.4,'  ',E15.4)
6000  FORMAT (10I5)
8000  FORMAT (E15.5,' ',E15.5,' ',E15.5,' ',E15.5,' ',I2,'  ****')

       PRINT *
       PRINT *,'**************************'
       PRINT *,'PROGRAM STOP SUCCESSFULLY'
       PRINT *,'**************************'
       STOP
       END


SUBROUTINE RCURVE


WRITE (8,7000) 0.000000,0.000000,1.000000,0.000000
WRITE (8,7000) 0.025000,0.000000,0.912530,0.000000
WRITE (8,7000) 0.050000,0.000000,0.830041,0.000000
WRITE (8,7000) 0.075000,0.000000,0.752410,0.000000
WRITE (8,7000) 0.100000,0.000001,0.679518,0.000000
WRITE (8,7000) 0.125000,0.000007,0.611238,0.000000
WRITE (8,7000) 0.150000,0.000031,0.547448,0.000000
WRITE (8,7000) 0.175000,0.000093,0.488020,0.000000
WRITE (8,7000) 0.200000,0.000232,0.432827,0.000000
WRITE (8,7000) 0.225000,0.000501,0.381737,0.000000
WRITE (8,7000) 0.250000,0.000977,0.334621,0.000000
WRITE (8,7000) 0.275000,0.001760,0.291345,0.000000
WRITE (8,7000) 0.300000,0.002980,0.251773,0.000000
WRITE (8,7000) 0.325000,0.004800,0.215767,0.000000
WRITE (8,7000) 0.350000,0.007416,0.183188,0.000000
WRITE (8,7000) 0.375000,0.011065,0.153893,0.000000
WRITE (8,7000) 0.400000,0.016028,0.127737,0.000000
WRITE (8,7000) 0.425000,0.022631,0.104573,0.000000
WRITE (8,7000) 0.450000,0.031250,0.084248,0.000000
WRITE (8,7000) 0.475000,0.042315,0.066609,0.000000
WRITE (8,7000) 0.500000,0.056314,0.051496,0.000000
WRITE (8,7000) 0.525000,0.073794,0.038746,0.000000
WRITE (8,7000) 0.550000,0.095367,0.028191,0.000000
WRITE (8,7000) 0.575000,0.121716,0.019658,0.000000
WRITE (8,7000) 0.600000,0.153590,0.012965,0.000000
WRITE (8,7000) 0.625000,0.191818,0.007925,0.000000
WRITE (8,7000) 0.650000,0.237305,0.004338,0.000000
WRITE (8,7000) 0.675000,0.291038,0.001995,0.000000
WRITE (8,7000) 0.700000,0.354093,0.000668,0.000000
WRITE (8,7000) 0.725000,0.427631,0.000103,0.000000
WRITE (8,7000) 0.750000,0.512909,0.000000,0.000000
WRITE (8,7000) 0.775000,0.611280,0.000000,0.000000
WRITE (8,7000) 0.800000,0.724196,0.000000,0.000000
WRITE (8,7000) 0.825000,0.853215,0.000000,0.000000
WRITE (8,7000) 0.850000,1.000000,0.000000,0.000000

7000   FORMAT (E15.5,'    ',E15.5,'    ',E15.5,'    ',E15.5)

RETURN
END
```

APPENDIX IV

PROGRAM COARSENING

```
C ***************************************************************
C     THIS PROGRAM WILL CALCULATE FINE GRID FLUCTUATING MOMENTS
C   FOR EVERY POSSIBLE COMBINATIONS OF COARSE GRID BLOCKS AND THEN
C   PROPOSE THE  BEST COARSENING SCHEMES FOR THE COARSE GRID MODEL
C
C
C                    BY : NASIR HAJI DARMAN
C             HERIOT-WATT UNIVERSITY / PETRONAS RESEARCH
C
C                    LAST UPDATE : 23 / 1 / 2000
C***************************************************************

      IMPLICIT NONE

      CHARACTER*20 FN1

      INTEGER GET_LEN

INTEGER ZDIMF,ZDIMC,ROW,COL
INTEGER XDIMF,XDIMC,YDIMF,YDIMC,TSTEP,SKIPLINE
INTEGER NCOL,A,B,C,NFCX,NFCY,N,Z,I,J,K,MAX,MIN,XXX
INTEGER XDIMF1,YDIMF1,ZDIMF1,  XDIMC1,YDIMC1,ZDIMC1
INTEGER TSTEP1,POSSOPTS1,TGBF1,OPT,OPT1,II

REAL PROD1,TOTPV,DZ,DY,GRA

PARAMETER (XDIMF1=100,YDIMF1=1,ZDIMF1=20,XDIMC1=20,YDIMC1=1)
PARAMETER (ZDIMC1=2,TSTEP1=30,POSSOPTS1=450000)
PARAMETER (TGBF1=2000)

INTEGER MAXOPTION(ZDIMC1+1)
INTEGER FROM(ZDIMC1+1,POSSOPTS1+1,ZDIMC1+1)
INTEGER TO(ZDIMC1+1,POSSOPTS1+1,ZDIMC1+1)
INTEGER CCX(XDIMC1+1,YDIMC1+1,ZDIMC1+1)
INTEGER CCY(XDIMC1+1,YDIMC1+1,ZDIMC1+1)
INTEGER CCZ(XDIMC1+1,YDIMC1+1,ZDIMC1+1)
INTEGER LIMLX(XDIMC1+1,YDIMC1+1,ZDIMC1+1)
INTEGER LIMHX(XDIMC1+1,YDIMC1+1,ZDIMC1+1)
INTEGER LIMLY(XDIMC1+1,YDIMC1+1,ZDIMC1+1)
INTEGER LIMHY(XDIMC1+1,YDIMC1+1,ZDIMC1+1)
INTEGER LIMLZ(XDIMC1+1,YDIMC1+1,ZDIMC1+1)
INTEGER LIMHZ(XDIMC1+1,YDIMC1+1,ZDIMC1+1)
INTEGER MINXVAL(XDIMC1+1,YDIMC1+1,ZDIMC1+1)
INTEGER MAXXVAL(XDIMC1+1,YDIMC1+1,ZDIMC1+1)
INTEGER BESTDIM(ZDIMC1+1),WORSTDIM(ZDIMC1+1)
INTEGER LOCATOR(POSSOPTS1+1)

REAL DUMMY(POSSOPTS1+1),DUMMY1(POSSOPTS1+1)

REAL SGASM(0:TSTEP1+1,XDIMF1+1,YDIMF1+1,ZDIMF1+1)
REAL FLOOILIPM(0:TSTEP1+1,XDIMF1+1,YDIMF1+1,ZDIMF1+1)
REAL FLOGASIPM(0:TSTEP1+1,XDIMF1+1,YDIMF1+1,ZDIMF1+1)
REAL FLOOILKPM(0:TSTEP1+1,XDIMF1+1,YDIMF1+1,ZDIMF1+1)
REAL FLOGASKPM(0:TSTEP1+1,XDIMF1+1,YDIMF1+1,ZDIMF1+1)
REAL OILPOTNM(0:TSTEP1+1,XDIMF1+1,YDIMF1+1,ZDIMF1+1)
REAL GASPOTNM(0:TSTEP1+1,XDIMF1+1,YDIMF1+1,ZDIMF1+1)
REAL PRESM(0:TSTEP1+1,XDIMF1+1,YDIMF1+1,ZDIMF1+1)
REAL PERMZM(XDIMF1+1, YDIMF1+1,ZDIMF1+1)
REAL PVM(XDIMF1+1, YDIMF1+1,ZDIMF1+1)
REAL TRANXM(XDIMF1+1, YDIMF1+1,ZDIMF1+1)
REAL TRANYM(XDIMF1+1, YDIMF1+1,ZDIMF1+1)
REAL TRANZM(XDIMF1+1, YDIMF1+1,ZDIMF1+1)

REAL AVECX(ZDIMC1+1,POSSOPTS1+1)
REAL SUMPV(XDIMC1+1,YDIMC1+1,ZDIMC1+1)
REAL CV(0:TSTEP1+1,XDIMC1+1,YDIMC1+1,ZDIMC1+1)
REAL VARIANCE(0:TSTEP1+1,XDIMC1+1,YDIMC1+1,ZDIMC1+1)
REAL MEAN(0:TSTEP1+1,XDIMC1+1,YDIMC1+1,ZDIMC1+1)
REAL AVECV(ZDIMC1+1)

REAL AA(0:TSTEP1+1,XDIMC1+1,YDIMC1+1,ZDIMC1+1)
REAL BB(0:TSTEP1+1,XDIMC1+1,YDIMC1+1,ZDIMC1+1)
REAL CC(0:TSTEP1+1,XDIMC1+1,YDIMC1+1,ZDIMC1+1)
REAL DD(0:TSTEP1+1,XDIMC1+1,YDIMC1+1,ZDIMC1+1)
REAL EE(0:TSTEP1+1,XDIMC1+1,YDIMC1+1,ZDIMC1+1)
REAL FF(0:TSTEP1+1,XDIMC1+1,YDIMC1+1,ZDIMC1+1)
REAL GG(0:TSTEP1+1,XDIMC1+1,YDIMC1+1,ZDIMC1+1)
REAL HH(0:TSTEP1+1,XDIMC1+1,YDIMC1+1,ZDIMC1+1)
REAL PAR1(0:TSTEP1+1,XDIMC1+1,YDIMC1+1,ZDIMC1+1)
REAL PAR2(0:TSTEP1+1,XDIMC1+1,YDIMC1+1,ZDIMC1+1)
REAL PAR3(0:TSTEP1+1,XDIMC1+1,YDIMC1+1,ZDIMC1+1)
REAL PAR4(0:TSTEP1+1,XDIMC1+1,YDIMC1+1,ZDIMC1+1)
REAL PAR5(0:TSTEP1+1,XDIMC1+1,YDIMC1+1,ZDIMC1+1)
REAL PAR6(0:TSTEP1+1,XDIMC1+1,YDIMC1+1,ZDIMC1+1)
REAL PAR7(0:TSTEP1+1,XDIMC1+1,YDIMC1+1,ZDIMC1+1)
REAL PAR8(0:TSTEP1+1,XDIMC1+1,YDIMC1+1,ZDIMC1+1)
```

```
      REAL TOTCV(ZDIMC1+1)
      REAL LOW(ZDIMC1+1)
      REAL HIGH(ZDIMC1+1)
      REAL PURATA(ZDIMC1+1)

C      ************** SECTION 1: USER DEFINE DATA ****************

C      XDIMF : FINE GRID X DIMENSION
C      YDIMF : FINE GRID Y DIMENSION
C      ZDIMF : FINE GRID Z DIMENSION
C
C      XDIMC : COARSE GRID X DIMENSION
C      YDIMC : COARSE GRID Y DIMENSION
C
C      MAX : MAXIMUM COARSE GRID LAYER IN THE ANALYSIS
C      MIN : MINIMUM COARSE GRID LAYER IN THE ANALYSIS
C
C      TSTEP: NUMBER OF TIMESTEP IN ECLIPSE RUN

      XDIMF = 100
      YDIMF = 1
      ZDIMF = 20

      XDIMC = 20
      YDIMC = 1

      MIN = 1
      MAX = 2

      TSTEP = 30

      DZ = 7.62
      DY = 7.62


C      ************ SECTION 2: SETTING THE CONSTANT ***************

C      SKIPLINE = 96 FOR ECLIPSE VERSION 97A AND 92 FOR 98A
C      NCOL = NUMBER OF COLUMN IN THE ECLIPSE FILE
C      GRA = GRAVITY CONSTANT

      SKIPLINE = 92
      NCOL = 4
      GRA = 9.81

C      *************** SECTION 3:  FILE NAMING ******************

      PRINT *,"YOUR INPUT FILE NAME (.FUNRST, .FINIT)"
      PRINT *,"*****************************************"
      PRINT *
      READ (*,2000) FN1

I = 20
DO WHILE (FN1(I:I) .EQ. ' ' .AND. I .GT. 0)
I=I-1
END DO
GET_LEN = I

OPEN (3,FILE=FN1(1:GET_LEN)//'.FUNRST')
OPEN (4,FILE=FN1(1:GET_LEN)//'.FINIT')

PRINT *
PRINT *, "*****************************************************"
PRINT *, "PLEASE INPUT YOUR COARSENING STRATEGY                 "
PRINT *, "1 FOR ALL POSSIBLE LAYER COMBINATIONS                 "
PRINT *, "2 FOR COMBINATIONS THAT PRODUCE ODD LAYERS ONLY       "
PRINT *, "*****************************************************"
READ(*,*) OPT1
PRINT *

PRINT *
PRINT *, "*****************************************************"
PRINT *, "PLEASE SELECT YOUR SUB-GR D VARIABLE PARAMETER        "
PRINT *, "1 FOR VARIANCE IN GAS SATURATION                      "
PRINT *, "2 FOR VARIANCE IN PRESSURE                            "
PRINT *, "3 FOR COVARIANCE IN GAS SATURATION TIMES VELOCITY     "
PRINT *, "4 FOR COVARIANCE IN ABS. PERM TIMES GAS SATURATION    "
PRINT *, "5 FOR CV IN GAS SATURATION TIMES VELOCITY             "
PRINT *, "6 FOR CV IN ABS. PERMS TIMES GAS SATURATION           "
PRINT *, "7 FOR CV IN GAS SATURATION                            "
PRINT *, "*****************************************************"
READ(*,*) OPT
PRINT *

IF (OPT .EQ. 1) THEN
OPEN (2,FILE=FN1(1:GET_LEN)//'.VARSG')
WRITE (2,*) 'WILL USE VARIANCE IN SATURATION'
WRITE (2,*) '*******************************'
WRITE (2,*)

ELSE IF (OPT .EQ. 2) THEN
OPEN (2,FILE=FN1(1:GET_LEN)//'.VARPRES')
WRITE (2,*) 'WILL USE VARIANCE IN PRESSURE'
WRITE (2,*) '*****************************'
WRITE (2,*)

ELSE IF (OPT .EQ. 3) THEN
OPEN (2,FILE=FN1(1:GET_LEN)//'.COVARSGV')
WRITE (2,*) 'WILL USE COVARIANCE IN SATURATION TIMES VELOCITY'
WRITE (2,*) '************************************************'
WRITE (2,*)

ELSE  IF (OPT .EQ. 4) THEN
OPEN (2,FILE=FN1(1:GET_LEN)//'.COVARSGK')
```

```
      WRITE (2,*) 'WILL USE COVARIANCE IN SATURATION TIMES ABS. PERM'
      WRITE (2,*) '************************************************'
      WRITE (2,*)

      ELSE  IF (OPT .EQ. 5) THEN
      OPEN (2,FILE=FN1(1:GET_LEN)//'.CVSGV')
      WRITE (2,*) 'WILL USE CV IN SATURATION TIMES VELOCITY'
      WRITE (2,*) '****************************************'
      WRITE (2,*)

      ELSE   IF (OPT .EQ. 6) THEN
      OPEN (2,FILE=FN1(1:GET_LEN)//'.CVKSG')
      WRITE (2,*) 'WILL USE CV IN SATURATION TIMES ABS. PERM'
      WRITE (2,*) '****************************************'
      WRITE (2,*)

      ELSE   IF (OPT .EQ. 7) THEN
      OPEN (2,FILE=FN1(1:GET_LEN)//'.CVSG')
      WRITE (2,*) 'WILL USE CV IN SATURATION'
      WRITE (2,*) '*************************'
      WRITE (2,*)

      ENDIF

      IF (OPT1 .EQ. 1) THEN
      WRITE (2,*) "WILL USE ALL POSSIBLE LAYER COMBINATIONS "
      WRITE (2,*) "****************************************"
      WRITE (2,*)
       ELSE
       WRITE (2,*)"WILL USE COMBINATIONS THAT PRODUCE ODD LAYERS ONLY"
       WRITE (2,*)"*************************************************"
       WRITE (2,*)
       ENDIF

C      ************* SECTION 4: CALLING SUB LAYER ********************
C
C      THIS SUBROUTINE WILL CALCULATE EVERY POSSIBLE COMBINATIONS
C      OF THE COARSE GRID LAYERS
C

       CALL LAYER(ZDIMF,ZDIMC,ROW,COL,FROM,TO,MAXOPTION,MAX,MIN)


C      ************* SECTION 5: CALLING SUB READRST *****************
C
C      THIS SUBROUTINE WILL READ THE FINE GRID INFORMATION FROM ECLIPSE
C      *.FUNRST AND *.FINIT FILES
C

       CALL READRST(XDIMF,YDIMF,ZDIMF,NCOL,SGASM,
     * FLOOILIPM,FLOGASIPM,FLOOILKPM,FLOGASKPM,
     * SKIPLINE,OILPOTNM,GASPOTNM,
     * TSTEP,PVM,TRANXM,TRANYM,TRANZM,PRESM,PERMZM)

C      ****** SECTION 6: X AND Y COARSE GRID BOUNDARY  *******

       NFCX = XDIMF/XDIMC
       NFCY = YDIMF/YDIMC
       N=0

       DO 610 ZDIMC = MIN,MAX

       PRINT *,"PLEASE WAIT...."
       PRINT *,"CALCULATING SUB-GRID VALUES FOR CG = ",ZDIMC
       PRINT *

       DO 620 ROW = 1,MAXOPTION(ZDIMC)
       DO 630 C = 1,ZDIMC
       DO 640 B = 1,YDIMC
       DO 650 A = 1,XDIMC

       LIMHY(A,0,C) = 0
       LIMHX(0,B,C) = 0

       LIMLX(A,B,C) = LIMHX(A-1,B,C)+1
       LIMHX(A,B,C) = LIMLX(A,B,C) + NFCX - 1

       LIMLY(A,B,C) = LIMHY(A,B-1,C)+1
       LIMHY(A,B,C) = LIMLY(A,B,C) + NFCY - 1

       LIMLZ(A,B,C) = FROM(ZDIMC,ROW,C)
       LIMHZ(A,B,C) = TO(ZDIMC,ROW,C)

       CCX(A,B,C) = (LIMLX(A,B,C)+LIMHX(A,B,C))/2

       CCY(A,B,C) = (LIMLY(A,B,C)+LIMHY(A,B,C))/2

       CCZ(A,B,C) = (LIMLZ(A,B,C)+LIMHZ(A,B,C))/2

650    CONTINUE
640    CONTINUE
630    CONTINUE

C      ********* SECTION 7: SUB-GRID VALUES CALCULATION *********

       DO 701 C = 1,ZDIMC
       DO 702 B = 1,YDIMC
       DO 703 A = 1,XDIMC

       IF ( OPT .EQ. 5 ) THEN
       MINXVAL(A,B,C) = LIMLX(A,B,C)
       MAXXVAL(A,B,C) = LIMHX(A,B,C)

       ELSE IF ( OPT .EQ. 6 ) THEN
```

```
      MINXVAL(A,B,C) = LIMLX(A,B,C)
      MAXXVAL(A,B,C) = LIMHX(A,B,C)

      ELSE IF ( OPT .EQ. 7 ) THEN
      MINXVAL(A,B,C) = CCX(A,B,C)
      MAXXVAL(A,B,C) = CCX(A,B,C)

      ELSE
      MINXVAL(A,B,C) = LIMHX(A,B,C)
      MAXXVAL(A,B,C) = LIMHX(A,B,C)

      ENDIF

  703 CONTINUE
  702 CONTINUE
  701 CONTINUE

      N = 0

      DO 705 Z = 0,TSTEP
      DO 710 C = 1,ZDIMC
      DO 715 B = 1,YDIMC
      DO 720 A = 1,XDIMC
      DO 725 K = LIMLZ(A,B,C),LIMHZ(A,B,C)
      DO 730 I = MINXVAL(A,B,C),MAXXVAL(A,B,C)

      N = N + 1
      AA(Z,A,B,C) = (SGASM(Z,I,B,K)**2) + AA(Z,A,B,C)
      BB(Z,A,B,C) = SGASM(Z,I,B,K) + BB(Z,A,B,C)
      CC(Z,A,B,C) = (PRESM(Z,I,B,K)**2) + CC(Z,A,B,C)
      DD(Z,A,B,C) = PRESM(Z,I,B,K) + DD(Z,A,B,C)

      EE(Z,A,B,C) = (((FLOOILIPM(Z,I,B,K) / (DY*DZ))
     * +(FLOGASIPM(Z,I,B,K) / (DY*DZ)))
     * *SGASM(Z,I,B,K)) + EE(Z,A,B,C)

      FF(Z,A,B,C) = ((FLOOILIPM(Z,I,B,K) / (DY*DZ))
     * +(FLOGASIPM(Z,I,B,K) / (DY*DZ)))
     *  + FF(Z,A,B,C)

      GG(Z,A,B,C) = (PERMZM(I,B,K)*SGASM(Z,I,B,K))+GG(Z,A,B,C)

      HH(Z,A,B,C) = (PERMZM(I,B,K))+HH(Z,A,B,C)


  730 CONTINUE
  725 CONTINUE


       PAR1(Z,A,B,C) = AA(Z,A,B,C) / N
       PAR2(Z,A,B,C) = BB(Z,A,B,C) / N
       PAR3(Z,A,B,C) = CC(Z,A,B,C) / N
       PAR4(Z,A,B,C) = DD(Z,A,B,C) / N
       PAR5(Z,A,B,C) = EE(Z,A,B,C) / N
       PAR6(Z,A,B,C) = FF(Z,A,B,C) / N
       PAR7(Z,A,B,C) = GG(Z,A,B,C) / N
       PAR8(Z,A,B,C) = HH(Z,A,B,C) / N

       IF (OPT .EQ. 1) THEN

           IF (PAR1(Z,A,B,C) .LT. (PAR2(Z,A,B,C))**2) THEN
              VARIANCE(Z,A,B,C) = 0
              GOTO 731
           ENDIF

        VARIANCE(Z,A,B,C) = PAR1(Z,A,B,C) - (PAR2(Z,A,B,C))**2

       ENDIF

       IF (OPT .EQ. 2) THEN

          IF (PAR3(Z,A,B,C) .LT. (PAR4(Z,A,B,C))**2) THEN
             VARIANCE(Z,A,B,C) = 0
             GOTO 731
          ENDIF

        VARIANCE(Z,A,B,C)  = PAR3(Z,A,B,C) - (PAR4(Z,A,B,C))**2

      ENDIF

       IF (OPT .EQ. 3) THEN

         IF (PAR5(Z,A,B,C) .LT. (PAR6(Z,A,B,C)*PAR2(Z,A,B,C))) THEN
           VARIANCE(Z,A,B,C) = 0
           GOTO 731
         ENDIF

        VARIANCE(Z,A,B,C)  = PAR5(Z,A,B,C) -
     *  (PAR6(Z,A,B,C)*PAR2(Z,A,B,C))

       ENDIF

       IF (OPT .EQ. 4) THEN

        IF (PAR7(Z,A,B,C) .LT. (PAR8(Z,A,B,C)*PAR2(Z,A,B,C))) THEN
          VARIANCE(Z,A,B,C) = 0
          GOTO 731
        ENDIF

        VARIANCE(Z,A,B,C)  = PAR7(Z,A,B,C) -
     *  (PAR8(Z,A,B,C)*PAR2(Z,A,B,C))

       ENDIF
```

```
      IF (OPT .EQ. 5) THEN

       IF (PAR5(Z,A,B,C) .LT. (PAR6(Z,A,B,C)*PAR2(Z,A,B,C))) THEN
         VARIANCE(Z,A,B,C) = 0
         GOTO 731
       ENDIF

       IF (PAR5(Z,A,B,C) .EQ. 0) THEN
         VARIANCE(Z,A,B,C) = 0
         GOTO 731
       ENDIF

       VARIANCE(Z,A,B,C)  = (PAR5(Z,A,B,C) -
     *  (PAR6(Z,A,B,C)*PAR2(Z,A,B,C))) / PAR5(Z,A,B,C)

      ENDIF


     IF (OPT .EQ. 6) THEN

      IF (PAR7(Z,A,B,C) .LT. (PAR8(Z,A,B,C)*PAR2(Z,A,B,C))) THEN
        VARIANCE(Z,A,B,C) = 0
        GOTO 731
       ENDIF

      IF (PAR7(Z,A,B,C) .EQ. 0) THEN
        VARIANCE(Z,A,B,C) = 0
        GOTO 731
      ENDIF

       VARIANCE(Z,A,B,C)  = (PAR7(Z,A,B,C) -
     *  (PAR8(Z,A,B,C)*PAR2(Z,A,B,C))) / PAR7(Z,A,B,C)

     ENDIF


      IF (OPT .EQ. 7) THEN

       IF (PAR1(Z,A,B,C) .LT. (PAR2(Z,A,B,C))**2) THEN
         VARIANCE(Z,A,B,C) = 0
         GOTO 731
       ENDIF

       IF (PAR2(Z,A,B,C) .EQ. 0 ) THEN
         VARIANCE(Z,A,B,C) = 0
         GOTO 731
       ENDIF

     VARIANCE(Z,A,B,C) = ((PAR1(Z,A,B,C) - (PAR2(Z,A,B,C))**2)**0.5)
     *  /PAR2(Z,A,B,C)

      ENDIF
```

```
731     IF (N .EQ. 1) THEN
        VARIANCE(Z,A,B,C) = 0
        ENDIF

        CV(Z,A,B,C) = VARIANCE(Z,A,B,C)

        N = 0

720     CONTINUE
715     CONTINUE
710     CONTINUE
705     CONTINUE

C  *******    CALCULATE PORE VOLUME FOR EACH COARSE GB ************

        DO 735 C = 1,ZDIMC
        DO 740 B = 1,YDIMC
        DO 745 A = 1,XDIMC

        DO 750 K = LIMLZ(A,B,C),LIMHZ(A,B,C)
        DO 755 J = LIMLY(A,B,C),LIMHY(A,B,C)
        DO 760 I = LIMLX(A,B,C),LIMHX(A,B,C)

        SUMPV(A,B,C) = PVM(I,J,K) + SUMPV(A,B,C)

760     CONTINUE
755     CONTINUE
750     CONTINUE
745     CONTINUE
740     CONTINUE
735     CONTINUE

C  ******* CALCULATE CV AND PORE VOLUME FOR EACH COARSE LAYER ****

        N = 0

        DO 765 C = 1,ZDIMC
        DO 770 Z = 1,TSTEP-1
        DO 775 B = 1,YDIMC
        DO 780 A = 2,XDIMC-1

        N= N+1

          DUMMY(C) = (CV(Z,A,B,C)) + DUMMY(C)

780     CONTINUE
775     CONTINUE
770     CONTINUE

          AVECV(C) = DUMMY(C) / N
```

```
765    CONTINUE

       N = 0

       DO 781 C = 1,ZDIMC
       DO 782 B = 1,YDIMC
       DO 783 A = 2,XDIMC-1
       N= N+1

         DUMMY1(C) = SUMPV(A,B,C) + DUMMY1(C)

783    CONTINUE
782    CONTINUE
781    CONTINUE

       DO 785 C = 1, ZDIMC

       PROD1 = (AVECV(C) * DUMMY1(C)) + PROD1

       TOTPV = DUMMY1(C) + TOTPV


785    CONTINUE

       AVECX(ZDIMC,ROW) = PROD1/TOTPV

       DO 790 Z = 1,TSTEP
       DO 791 C = 1,ZDIMC
       DO 792 B = 1,YDIMC
       DO 793 A = 1,XDIMC

         TOTPV = 0
         DUMMY1(C) = 0
         SUMPV(A,B,C) = 0

         PROD1 =0
         AVECV(C) = 0
         DUMMY(C) = 0
         CV(Z,A,B,C)= 0
         AA(Z,A,B,C)= 0
         BB(Z,A,B,C)= 0
         CC(Z,A,B,C)= 0
         DD(Z,A,B,C)= 0
         EE(Z,A,B,C)= 0
         FF(Z,A,B,C)= 0
         GG(Z,A,B,C)= 0
         HH(Z,A,B,C)= 0
         PAR1(Z,A,B,C)= 0
         PAR2(Z,A,B,C)= 0
         PAR3(Z,A,B,C)= 0
         PAR4(Z,A,B,C)= 0
         PAR5(Z,A,B,C)= 0
         PAR6(Z,A,B,C)= 0
         PAR7(Z,A,B,C)= 0
         PAR8(Z,A,B,C)= 0
         MEAN(Z,A,B,C)= 0
         VARIANCE(Z,A,B,C)= 0

793    CONTINUE
792    CONTINUE
791    CONTINUE
790    CONTINUE


620    CONTINUE
610    CONTINUE

C  ** SECTION 8: TO FIND MEAN,MAX,MIN OF THE CV FOR ALL OPTIONS **

       N = 0

       DO 800 ZDIMC = MIN,MAX

        HIGH(ZDIMC) = AVECX(ZDIMC,1)
        LOW(ZDIMC) =  AVECX(ZDIMC,1)

       DO 810 ROW = 1,MAXOPTION(ZDIMC)

        IF (OPT1 .EQ. 1) THEN
         GOTO 807
        ELSE

        DO 811 C = 1,ZDIMC

         LOCATOR(C) = TO(ZDIMC,ROW,C)- FROM(ZDIMC,ROW,C)

         IF (LOCATOR(C) .EQ. 0) THEN
           GOTO 805
         ELSE

         IF (((LOCATOR(C)/2)*2).EQ. LOCATOR(C)) THEN
           GOTO 805
         ELSE
           GOTO 810

       ENDIF
       ENDIF

805    IF (C .EQ. ZDIMC) THEN
         GOTO 806
       ELSE
         GOTO 811
```

```
       ENDIF

 811   CONTINUE


 806    XXX=1
       ENDIF


 807   N= N+1

       TOTCV(ZDIMC) = AVECX(ZDIMC,ROW) +TOTCV(ZDIMC)

       IF (LOW(ZDIMC) .GE. AVECX(ZDIMC,ROW)) THEN
         LOW(ZDIMC) = AVECX(ZDIMC,ROW)
         BESTDIM(ZDIMC) = ROW
       ENDIF

       IF (HIGH(ZDIMC) .LE. AVECX(ZDIMC,ROW)) THEN
         HIGH(ZDIMC) = AVECX(ZDIMC,ROW)
         WORSTDIM(ZDIMC) = ROW
       ENDIF

 810   CONTINUE

        PURATA(ZDIMC) = TOTCV(ZDIMC) / N

        WRITE (2,1000) ZDIMC,LOW(ZDIMC),HIGH(ZDIMC),PURATA(ZDIMC),
     *    BESTDIM(ZDIMC),WORSTDIM(ZDIMC)

        N=0

 800    CONTINUE

          WRITE (2,*)
          WRITE (2,*)

        DO 820 ZDIMC = MIN,MAX

       ROW = BESTDIM(ZDIMC)

       WRITE (2,*)"BEST OPTION FOR CG LAYER =",ZDIMC," IS OPTION =",ROW
       WRITE (2,*)"*************************************************"

       DO 830 II = 1,ZDIMC
         WRITE (2,*)  FROM(ZDIMC,ROW,II),TO(ZDIMC,ROW,II)
 830   CONTINUE

       WRITE (2,*)

 820   CONTINUE
```



```
          WRITE (2,*)
          WRITE (2,*)

       DO 831 ZDIMC = MIN,MAX

       ROW = WORSTDIM(ZDIMC)
       WRITE (2,*)"WORST OPTION FOR CG LAYER =",ZDIMC," IS OPTION =",ROW
       WRITE (2,*)"*************************************************"

       DO 832 II = 1,ZDIMC
        WRITE (2,*)  FROM(ZDIMC,ROW,II),TO(ZDIMC,ROW,II)
 832   CONTINUE

       WRITE (2,*)

 831   CONTINUE

          WRITE (2,*)
          WRITE (2,*)

C      ************  SECTION 9: PRINTING  ************************

       DO 900 ZDIMC = MIN,MAX

       DO 910 ROW = 1,MAXOPTION(ZDIMC)

       IF ((ABS(AVECX(ZDIMC,ROW) - AVECX(ZDIMC,ROW-1))).LT.0.001) THEN
       GO TO 910
       ENDIF

          WRITE (2,*) ZDIMC,ROW,AVECX(ZDIMC,ROW)

 910   CONTINUE
 900   CONTINUE

       DO 920 ZDIMC = MIN,MAX
       PRINT *,"COARSE GRID LAYER =  ",ZDIMC
       PRINT *,"POSSIBLE COARSENING SCHEME = ",MAXOPTION(ZDIMC)
       PRINT *,"*************************************"

 920   CONTINUE


        PRINT *
        PRINT *,"************************"
        PRINT *, "RUN STOP SUCCESSFULLY"
        PRINT *,"************************"

 1000  FORMAT (I4,6X,E10.5,3X,E10.5,3X,E10.5,3X,I4,3X,I6)
 2000  FORMAT (A15)
       STOP
       END
```

```
C   ******************** SUBROUTINE LAYER ***************************
C
C  THIS SUBROUTINE WILL CALCULATE EVERY POSSIBLE LAYER COMBINATIONS
C                       FOR THE COARSE GRID MODEL
C
C

      SUBROUTINE LAYER(ZDIMF,ZDIMC,ROW,COL,FROM,TO,MAXOPTION,MAX,MIN)

      IMPLICIT NONE

      INTEGER XDIMF1,YDIMF1,ZDIMF1, XDIMC1,YDIMC1,ZDIMC1,TGBF1
      INTEGER TSTEP1,POSSOPTS1
      INTEGER ZDIMF,ZDIMC,ROW,COL
      INTEGER FORCOL,BAKCOL,DUMMY,X,MAX,MIN

      PARAMETER (XDIMF1=100,YDIMF1=1,ZDIMF1=20,XDIMC1=20,YDIMC1=1)
      PARAMETER (ZDIMC1=2,TSTEP1=30,POSSOPTS1=450000)
      PARAMETER (TGBF1=2000)

      INTEGER MAXOPTION(ZDIMC1+1)
      INTEGER FROM(ZDIMC1+1,POSSOPTS1+1,ZDIMC1+1)
      INTEGER TO(ZDIMC1+1,POSSOPTS1+1,ZDIMC1+1)

      DO 1 ZDIMC = MIN,MAX
      PRINT *,"SPLITING THE LAYER. CG  =  ", ZDIMC
      PRINT *
      ROW = 1
      COL = ZDIMC

      FROM(ZDIMC,ROW,COL)=ZDIMC

      TO(ZDIMC,ROW,COL)=ZDIMF

      IF (ZDIMC .EQ. 1) THEN
        MAXOPTION(ZDIMC) = 1
        GOTO 1
      ENDIF

10    COL = COL -1

      IF (COL .LT. 1) THEN
        GOTO 20
      ENDIF

      TO(ZDIMC,ROW,COL) = FROM(ZDIMC,ROW,COL+1)-1
      FROM(ZDIMC,ROW,COL) = TO(ZDIMC,ROW,COL)
      FROM(ZDIMC,ROW,1) = 1

      GOTO 10

20    ROW = ROW + 1
      COL = ZDIMC

      FROM(ZDIMC,ROW,COL)=(FROM(ZDIMC,ROW-1,COL))+1
      TO(ZDIMC,ROW,COL) = ZDIMF

      DO 30 COL = COL-1,1,-1

      TO(ZDIMC,ROW,COL) = (FROM(ZDIMC,ROW,COL+1))-1
      FROM(ZDIMC,ROW,COL)= FROM(ZDIMC,ROW-1,COL)
      FROM(ZDIMC,ROW,1) =1

30    CONTINUE

40    IF (TO(ZDIMC,ROW,1) .GT. (ZDIMF-ZDIMC+1)) THEN

      GOTO 350
      ENDIF

      DO 50 COL = 1,ZDIMC

      IF (FROM(ZDIMC,ROW,COL) .GT. (ZDIMF-ZDIMC+COL)) THEN
        GOTO 60
      ENDIF

 50   CONTINUE

      GOTO 20

60    COL = COL - 1

      DUMMY=COL

      FROM(ZDIMC,ROW,COL)=(FROM(ZDIMC,ROW-1,COL))+1

      TO(ZDIMC,ROW,COL) = FROM(ZDIMC,ROW,COL)

      FORCOL = ZDIMC-COL
      BAKCOL = COL - 1

      IF (BAKCOL .LE. 0) THEN

        COL = 1
        FROM(ZDIMC,ROW,1) =1
        TO(ZDIMC,ROW,COL) = (FROM(ZDIMC,ROW,COL+1))-1

      ENDIF

       DO 70 X = 1,FORCOL,1
       COL = DUMMY + X
```

```
      IF (COL .LT. ZDIMC) THEN

        FROM(ZDIMC,ROW,COL)=(TO(ZDIMC,ROW,COL-1))+1
        TO(ZDIMC,ROW,COL)=FROM(ZDIMC,ROW,COL)

      ENDIF

      IF (COL .EQ. ZDIMC) THEN

      FROM(ZDIMC,ROW,COL)=(TO(ZDIMC,ROW,COL-1))+1
      TO(ZDIMC,ROW,ZDIMC) = ZDIMF

      ENDIF

70    CONTINUE

      COL=DUMMY

      DO 80 X = 1,BAKCOL
      COL = DUMMY - X

      IF (COL .GT. 1) THEN

        TO(ZDIMC,ROW,COL)=(FROM(ZDIMC,ROW,COL+1))-1
        FROM(ZDIMC,ROW,COL)= FROM(ZDIMC,ROW-1,COL)

      ENDIF

      IF (COL .LE. 1) THEN

        COL = 1
        FROM(ZDIMC,ROW,1) =1
        TO(ZDIMC,ROW,COL) = (FROM(ZDIMC,ROW,COL+1))-1

      ENDIF

80    CONTINUE

      GOTO 40

350   MAXOPTION(ZDIMC)= ROW-1


1     CONTINUE


      RETURN
      END

C     ********************* SUBROUTINE READRST ****************************
C           THIS SUBROUTINE WILL READ ECLIPSE RESTART AND INIT FILE
C
      SUBROUTINE READRST(XDIMF,YDIMF,ZDIMF,NCOL,SGASM,
     * FLOOILIPM,FLOGASIPM,FLOOILKPM,FLOGASKPM,
     * SKIPLINE,OILPOTNM,GASPOTNM,
     * TSTEP,PVM,TRANXM,TRANYM,TRANZM,PRESM,PERMZM)

      IMPLICIT NONE

      INTEGER XDIMF,YDIMF,ZDIMF,TSTEP,SKIPLINE,NCOL,TGBF
      INTEGER Z,TS,I,N,K,J,P,PP
      INTEGER XDIMF1,YDIMF1,ZDIMF1, XDIMC1,YDIMC1,ZDIMC1
      INTEGER TSTEP1,POSSOPTS1,TGBF1

      PARAMETER (XDIMF1=100,YDIMF1=1,ZDIMF1=20,XDIMC1=20,YDIMC1=1)
      PARAMETER (ZDIMC1=2,TSTEP1=30,POSSOPTS1=450000)
      PARAMETER (TGBF1=2000)

      REAL PRESS(0:TSTEP1+1,TGBF1+1)
      REAL PRESM(0:TSTEP1+1,XDIMF1+1,YDIMF1+1,ZDIMF1+1)
      REAL SGASS(0:TSTEP1+1,TGBF1+1)
      REAL SGASM(0:TSTEP1+1,XDIMF1+1,YDIMF1+1,ZDIMF1+1)
      REAL FLOOILIPS(0:TSTEP1+1,TGBF1+1)
      REAL FLOOILIPM(0:TSTEP1+1,XDIMF1+1,YDIMF1+1,ZDIMF1+1)
      REAL FLOGASIPS(0:TSTEP1+1,TGBF1+1)
      REAL FLOGASIPM(0:TSTEP1+1,XDIMF1+1,YDIMF1+1,ZDIMF1+1)
      REAL FLOOILKPS(0:TSTEP1+1,TGBF1+1)
      REAL FLOOILKPM(0:TSTEP1+1,XDIMF1+1,YDIMF1+1,ZDIMF1+1)
      REAL FLOGASKPS(0:TSTEP1+1,TGBF1+1)
      REAL FLOGASKPM(0:TSTEP1+1,XDIMF1+1,YDIMF1+1,ZDIMF1+1)
      REAL FIPOILS(0:TSTEP1+1,TGBF1+1)
      REAL FIPOILM(0:TSTEP1+1,XDIMF1+1,YDIMF1+1,ZDIMF1+1)
      REAL FIPGASS(0:TSTEP1+1,TGBF1+1)
      REAL FIPGASM(0:TSTEP1+1,XDIMF1+1,YDIMF1+1,ZDIMF1+1)
      REAL OILPOTNS(0:TSTEP1+1,TGBF1+1)
      REAL OILPOTNM(0:TSTEP1+1,XDIMF1+1,YDIMF1+1,ZDIMF1+1)
      REAL OILVISCS(0:TSTEP1+1,TGBF1+1)
      REAL OILVISCM(0:TSTEP1+1,XDIMF1+1,YDIMF1+1,ZDIMF1+1)
      REAL GASPOTNS(0:TSTEP1+1,TGBF1+1)
      REAL GASPOTNM(0:TSTEP1+1,XDIMF1+1,YDIMF1+1,ZDIMF1+1)
      REAL GASVISCS(0:TSTEP1+1,TGBF1+1)
      REAL GASVISCM(0:TSTEP1+1,XDIMF1+1,YDIMF1+1,ZDIMF1+1)
      REAL POTCORRS(0:TSTEP1+1,TGBF1+1)
      REAL POTCORRM(0:TSTEP1+1,XDIMF1+1,YDIMF1+1,ZDIMF1+1)
      REAL KROS(0:TSTEP1+1,TGBF1+1)
      REAL KROM(0:TSTEP1+1,XDIMF1+1,YDIMF1+1,ZDIMF1+1)
      REAL KRGS(0:TSTEP1+1,TGBF1+1)
      REAL KRGM(0:TSTEP1+1,XDIMF1+1,YDIMF1+1,ZDIMF1+1)


      REAL PVS(TGBF1+1)
      REAL PVM(XDIMF1+1, YDIMF1+1,ZDIMF1+1)
```

```
      REAL DXS(TGBF1+1)
      REAL DXM(XDIMF1+1, YDIMF1+1,ZDIMF1+1)
      REAL DYS(TGBF1+1)
      REAL DYM(XDIMF1+1, YDIMF1+1,ZDIMF1+1)
      REAL DZS(TGBF1+1)
      REAL DZM(XDIMF1+1, YDIMF1+1,ZDIMF1+1)
      REAL PERMXS(TGBF1+1)
      REAL PERMXM(XDIMF1+1, YDIMF1+1,ZDIMF1+1)
      REAL PERMYS(TGBF1+1)
      REAL PERMYM(XDIMF1+1, YDIMF1+1,ZDIMF1+1)
      REAL PERMZS(TGBF1+1)
      REAL PERMZM(XDIMF1+1, YDIMF1+1,ZDIMF1+1)
      REAL MULTXS(TGBF1+1)
      REAL MULTXM(XDIMF1+1, YDIMF1+1,ZDIMF1+1)
      REAL MULTYS(TGBF1+1)
      REAL MULTYM(XDIMF1+1, YDIMF1+1,ZDIMF1+1)
      REAL MULTZS(TGBF1+1)
      REAL MULTZM(XDIMF1+1, YDIMF1+1,ZDIMF1+1)
      REAL POROS(TGBF1+1)
      REAL POROM(XDIMF1+1, YDIMF1+1,ZDIMF1+1)
      REAL NTGS(TGBF1+1)
      REAL NTGM(XDIMF1+1, YDIMF1+1,ZDIMF1+1)
      REAL TOPSS(TGBF1+1)
      REAL TOPSM(XDIMF1+1, YDIMF1+1,ZDIMF1+1)
      REAL DEPTHS(TGBF1+1)
      REAL DEPTHM(XDIMF1+1, YDIMF1+1,ZDIMF1+1)
      REAL TRANXS(TGBF1+1)
      REAL TRANXM(XDIMF1+1, YDIMF1+1,ZDIMF1+1)
      REAL TRANYS(TGBF1+1)
      REAL TRANYM(XDIMF1+1, YDIMF1+1,ZDIMF1+1)
      REAL TRANZS(TGBF1+1)
      REAL TRANZM(XDIMF1+1, YDIMF1+1,ZDIMF1+1)

      TGBF = XDIMF*YDIMF*ZDIMF

      PRINT *
      PRINT *,'READING STATIC DATA'
      PRINT *,'********************'
      PRINT *
      DO 19 I=1,SKIPLINE-2
      READ (4,*)
19    CONTINUE

      READ (4,*)

      DO 20 N = 1,TGBF,NCOL
      READ (4,3000) PVS(N),PVS(N+1),PVS(N+2),
     * PVS(N+3)
20    CONTINUE

      READ (4,*)

      DO 30 N = 1,TGBF,NCOL
      READ (4,3000) DXS(N),DXS(N+1),DXS(N+2),
     * DXS(N+3)
30    CONTINUE

      READ (4,*)

      DO 40 N = 1,TGBF,NCOL
      READ (4,3000) DYS(N),DYS(N+1),DYS(N+2),
     * DYS(N+3)
40    CONTINUE

      READ (4,*)

      DO 50 N = 1,TGBF,NCOL
      READ (4,3000) DZS(N),DZS(N+1),DZS(N+2),
     * DZS(N+3)
50    CONTINUE

      READ (4,*)

      DO 60 N = 1,TGBF,NCOL
      READ (4,3000) PERMXS(N),PERMXS(N+1),PERMXS(N+2),
     * PERMXS(N+3)
60    CONTINUE

      READ (4,*)

      DO 70 N = 1,TGBF,NCOL
      READ (4,3000) PERMYS(N),PERMYS(N+1),PERMYS(N+2),
     * PERMYS(N+3)
70    CONTINUE

      READ (4,*)

      DO 80 N = 1,TGBF,NCOL
      READ (4,3000) PERMZS(N),PERMZS(N+1),PERMZS(N+2),
     * PERMZS(N+3)
80    CONTINUE

      READ (4,*)

      DO 90 N = 1,TGBF,NCOL
      READ (4,3000) MULTXS(N),MULTXS(N+1),MULTXS(N+2),
     * MULTXS(N+3)
90    CONTINUE

      READ (4,*)

      DO 100 N = 1,TGBF,NCOL
      READ (4,3000) MULTYS(N),MULTYS(N+1),MULTYS(N+2),
     * MULTYS(N+3)
```

```
100   CONTINUE

      READ (4,*)

      DO 110 N = 1,TGBF,NCOL
      READ (4,3000) MULTZS(N),MULTZS(N+1),MULTZS(N+2),
     * MULTZS(N+3)
110    CONTINUE

      READ (4,*)

      DO 120 N = 1,TGBF,NCOL
      READ (4,3000) POROS(N),POROS(N+1),POROS(N+2),
     * POROS(N+3)
120    CONTINUE

      READ (4,*)

      DO 130 N = 1,TGBF,NCOL
      READ (4,3000) NTGS(N),NTGS(N+1),NTGS(N+2),
     * NTGS(N+3)
130   CONTINUE

      READ (4,*)

      DO 140 N = 1,TGBF,NCOL
      READ (4,3000) TOPSS(N),TOPSS(N+1),TOPSS(N+2),
     * TOPSS(N+3)
140    CONTINUE

      READ (4,*)

      DO 150 N = 1,TGBF,NCOL
      READ (4,3000) DEPTHS(N),DEPTHS(N+1),DEPTHS(N+2),
     * DEPTHS(N+3)
150    CONTINUE

      READ (4,*)

      DO 160 N = 1,TGBF,NCOL
      READ (4,3000) TRANXS(N),TRANXS(N+1),TRANXS(N+2),
     * TRANXS(N+3)
160    CONTINUE

      READ (4,*)

      DO 170 N = 1,TGBF,NCOL
      READ (4,3000) TRANYS(N),TRANYS(N+1),TRANYS(N+2),
     * TRANYS(N+3)
170    CONTINUE

      READ (4,*)

      DO 180 N = 1,TGBF,NCOL
      READ (4,3000) TRANZS(N),TRANZS(N+1),TRANZS(N+2),
     * TRANZS(N+3)
180    CONTINUE

C     ***       CONVERTING STATIC DATA        ********
C     ***      TO X-Y-Z DIMENSION ARRAY       ********

        DO 190 K=1,ZDIMF
        DO 200 J=1,YDIMF
        DO 210 I=1,XDIMF

          PP=I+(J*XDIMF-XDIMF)+(K*(XDIMF*YDIMF)-(XDIMF*YDIMF))

          PVM(I,J,K) = PVS(PP)
          DXM(I,J,K) = DXS(PP)
          DYM(I,J,K) = DYS(PP)
          DZM(I,J,K) = DZS(PP)
          PERMXM(I,J,K) = PERMXS(PP)
          PERMYM(I,J,K) = PERMYS(PP)
          PERMZM(I,J,K) = PERMZS(PP)
          MULTXM(I,J,K) = MULTXS(PP)
          MULTYM(I,J,K) = MULTYS(PP)
          MULTZM(I,J,K) = MULTZS(PP)
          POROM(I,J,K) = POROS(PP)
          NTGM(I,J,K) = NTGS(PP)
          TOPSM(I,J,K) = TOPSS(PP)
          DEPTHM(I,J,K) = DEPTHS(PP)
          TRANXM(I,J,K) = TRANXS(PP)
          TRANYM(I,J,K) = TRANYS(PP)
          TRANZM(I,J,K) = TRANZS(PP)

210           CONTINUE
200           CONTINUE
190           CONTINUE

          PRINT *,'FINISH READING STATIC DATA'
          PRINT *

      PRINT *
      PRINT *,'READING DYNAMIC DATA'
      PRINT *,'********************'
      PRINT *

      DO 220 Z = 0,TSTEP

      READ (3,*)
      READ (3,2000) TS

       PRINT *,'READING TIMESTEP NO          ',TS
```

```
      DO 230 I=1,SKIPLINE
      READ (3,*)
230   CONTINUE

      DO 240 N = 1,TGBF,NCOL
      READ (3,1000) PRESS(Z,N),PRESS(Z,N+1),PRESS(Z,N+2),
     * PRESS(Z,N+3)
240   CONTINUE

      READ (3,*)

      DO 250 N = 1,TGBF,NCOL
      READ (3,1000) SGASS(Z,N),SGASS(Z,N+1),SGASS(Z,N+2),
     * SGASS(Z,N+3)
250   CONTINUE

      READ (3,*)

      DO 260 N = 1,TGBF,NCOL
      READ (3,1000) FLOOILIPS(Z,N),FLOOILIPS(Z,N+1),
     * FLOOILIPS(Z,N+2),FLOOILIPS(Z,N+3)
260   CONTINUE

      READ (3,*)

      DO 270 N = 1,TGBF,NCOL
      READ (3,1000) FLOGASIPS(Z,N),FLOGASIPS(Z,N+1),
     * FLOGASIPS(Z,N+2),FLOGASIPS(Z,N+3)
270   CONTINUE

      READ (3,*)

      DO 280 N = 1,TGBF,NCOL
      READ (3,1000) FLOOILKPS(Z,N),FLOOILKPS(Z,N+1),
     * FLOOILKPS(Z,N+2),FLOOILKPS(Z,N+3)
280   CONTINUE

      READ (3,*)

      DO 290 N = 1,TGBF,NCOL
      READ (3,1000) FLOGASKPS(Z,N),FLOGASKPS(Z,N+1),
     * FLOGASKPS(Z,N+2),FLOGASKPS(Z,N+3)
290   CONTINUE

      READ (3,*)

      DO 300 N = 1,TGBF,NCOL
      READ (3,1000) FIPOILS(Z,N),FIPOILS(Z,N+1),
     * FIPOILS(Z,N+2),FIPOILS(Z,N+3)
300   CONTINUE

      READ (3,*)

      DO 310 N = 1,TGBF,NCOL
      READ (3,1000) FIPGASS(Z,N),FIPGASS(Z,N+1),
     * FIPGASS(Z,N+2),FIPGASS(Z,N+3)
310   CONTINUE

      READ (3,*)

      DO 320 N = 1,TGBF,NCOL
      READ (3,1000) OILPOTNS(Z,N),OILPOTNS(Z,N+1),
     * OILPOTNS(Z,N+2),OILPOTNS(Z,N+3)
320   CONTINUE

      READ (3,*)

      DO 330 N = 1,TGBF,NCOL
      READ (3,1000) OILVISCS(Z,N),OILVISCS(Z,N+1),
     * OILVISCS(Z,N+2),OILVISCS(Z,N+3)
330   CONTINUE

      READ (3,*)

      DO 340 N = 1,TGBF,NCOL
      READ (3,1000) GASPOTNS(Z,N),GASPOTNS(Z,N+1),
     * GASPOTNS(Z,N+2),GASPOTNS(Z,N+3)
340   CONTINUE

      READ (3,*)

      DO 350 N = 1,TGBF,NCOL
      READ (3,1000) GASVISCS(Z,N),GASVISCS(Z,N+1),
     * GASVISCS(Z,N+2),GASVISCS(Z,N+3)
350   CONTINUE

      READ (3,*)

      DO 360 N = 1,TGBF,NCOL
      READ (3,1000) POTCORRS(Z,N),POTCORRS(Z,N+1),
     * POTCORRS(Z,N+2),POTCORRS(Z,N+3)
360   CONTINUE

      READ (3,*)

      DO 370 N = 1,TGBF,NCOL
      READ (3,1000) KROS(Z,N),KROS(Z,N+1),
     * KROS(Z,N+2),KROS(Z,N+3)
370   CONTINUE

      READ (3,*)
      DO 380 N = 1,TGBF,NCOL
      READ (3,1000) KRGS(Z,N),KRGS(Z,N+1),
     * KRGS(Z,N+2),KRGS(Z,N+3)
```

```
 380   CONTINUE

       READ (3,*)

        PRINT *,'FINISH READING TIMESTEP NO    ',TS
        PRINT *

 220   CONTINUE

C      ***       CONVERTING DYNAMIC DATA        ********
C      ***      TO X-Y-Z DIMENSION ARRAY       ********

       DO 390 Z=0,TSTEP
       DO 391 K=1,ZDIMF
       DO 392 J=1,YDIMF
       DO 393 I=1,XDIMF

          P=I+(J*XDIMF-XDIMF)+(K*(XDIMF*YDIMF)-(XDIMF*YDIMF))
          PRESM(Z,I,J,K) = PRESS(Z,P)
          SGASM(Z,I,J,K) = SGASS(Z,P)
          FLOOILIPM(Z,I,J,K) = FLOOILIPS(Z,P)
          FLOGASIPM(Z,I,J,K) = FLOGASIPS(Z,P)
          FLOOILKPM(Z,I,J,K) = FLOOILKPS(Z,P)
          FLOGASKPM(Z,I,J,K) = FLOGASKPS(Z,P)
          FIPOILM(Z,I,J,K) = FIPOILS(Z,P)
          FIPGASM(Z,I,J,K) = FIPGASS(Z,P)
          OILPOTNM(Z,I,J,K) = OILPOTNS(Z,P)
          OILVISCM(Z,I,J,K) = OILVISCS(Z,P)
          GASPOTNM(Z,I,J,K) = GASPOTNS(Z,P)
          GASVISCM(Z,I,J,K) = GASVISCS(Z,P)
          POTCORRM(Z,I,J,K) = POTCORRS(Z,P)
          KROM(Z,I,J,K) = KROS(Z,P)
          KRGM(Z,I,J,K) = KRGS(Z,P)

          IF (SGASM(Z,I,J,K) .LT. 0) THEN
          SGASM(Z,I,J,K) = 0
          ENDIF
 393          CONTINUE
 392          CONTINUE
 391          CONTINUE
 390          CONTINUE

          WRITE (2,*)
          WRITE (2,*) "NO C.LAY    MIN          MAX          AVE"
          WRITE (2,*) "--------    ---          ---          ---"

C ***************************************************************
C ***************************************************************

        PRINT *
        PRINT *,'*****************************'
        PRINT *,'FINISH READING ALL THE DATA'
        PRINT *,'*****************************'
        PRINT *

 1000   FORMAT (4E17.0)
 2000   FORMAT (I12)
 3000   FORMAT (4E17.0)
        RETURN
        END
```